ASSESSMENT OF SANDBAG DIKE PERFORMANCE

BY

TIMOTHY JOHN KRAHN

A Thesis submitted to
the Faculty of Graduate Studies
In Partial Fulfillment of the Requirements for the Degree of

MASTER OF SCIENCE

Department of Civil Engineering
University of Manitoba
Winnipeg, Manitoba

Assessment of Sandbag Dike Performance

BY

Timothy John Krahn

A Thesis/Practicum submitted to the Faculty of Graduate Studies of The University of Manitoba in partial fulfillment of the requirement of the degree

Of

MASTER OF SCIENCE

ABSTRACT

This thesis examines the interface friction characteristics and full-scale testing of sandbag dikes under simulated flood conditions. A laboratory testing program and a full-scale testing program have been conducted to assess the performance of sandbag structures built according to the City of Winnipeg's 1997 design template.

The laboratory testing program consists of large-scale and bench-scale direct shear tests on soil-geosynthetic, grass-geosynthetic, and geosynthetic-geosynthetic interfaces representing the material interfaces that exist in sandbag dikes. The large-scale shear apparatus used has a 1.0 m^2 interface area, which minimizes edge effects on the interaction between the surfaces being tested. Bench-scale direct shear tests using a typical direct shear apparatus are also conducted for comparison with the large-scale results.

The full-scale testing program is conducted in a modular test facility built at the University of Manitoba. The sandbag dikes are instrumented and monitored internally and externally for horizontal and vertical deformation, pore pressure, total stress changes, and leakage rates during all stages of loading and failure.

The results of the laboratory testing program are summarized using interpreted Mohr-Coulomb failure parameters to quantify the cohesive and frictional characteristics for each interface. The results of the full-scale testing program are summarized with respect to stability and seepage rates measured for a given dike height and geometry. The importance of the results with respect to understanding the behaviour of these important flood protection structures is presented.

ACKNOWLEDGEMENTS

I would like to thank my advisor, Dr. James Blatz for his support and guidance throughout the course of this research program. His approachability and flexible management techniques have served me well and he has taught me many lessons about professionalism and goals that are above and beyond any curriculum requirements.

I would also like to thank my colleagues in the Geotech grad lab: Greg Siemens, Deni Priyanto, Dr. Grant Ferguson, Lee Peters, Kate Franklin, David Anderson, Luke Novy, Yadav Pathak, German Ciro, Wisam Abdul-Rizaq, Vivek Bhardwaj, Alex Man and Neil Privat. It has been a great pleasure and learning experience to work with all of these people, as well as with Winnipeg's professional Geotechnical community.

Thanks to Kerry Lynch and Narong Piamsalee for their technical support in and around the Geotech labs at the University of Manitoba.

Thanks also to all at Bathurst Clarabut Geotechnical Testing who helped me get started with real lab work in the spring of 2003. Pete Clarabut and Dr. Richard Bathurst provided expertise and equipment that was absolutely invaluable for this research.

Sincere and heartfelt thanks go out to all and everyone who helped move equipment and sandbags around during the full-scale research in the summer of 2004. Jared Baldwin and Paul Klassen deserve especially notable gratitude, as without these two particular summer students this research would not have gone as far or as smoothly as it did. A warm thanks also to the grad students in the Hydraulics lab, who were there whenever I needed a few thousand extra sandbags moved around.

The author would like to acknowledge financial support from the City of Winnipeg, the Province of Manitoba and the Government of Canada through the Secondary Diking Enhancements Program.

Finally I would like to thank Dalila Seckar for her support and encouragement throughout this research program. Thanks for your patience and insight and for always being there.

'	feet
"	inches
Alt	Alternative
ASCE	American Society of Civil Engineers
ASTM	American Society for Testing and Materials
B	Bench-scale Direct Shear Test
BCGT	Bathurst Clarabut Geotechnical Testing
BH	Bird's Hill
c	Cohesion Intercept (Mohr-Coulomb Shear Strength Parameter)
c'	Effective Stress Cohesion Intercept
CGSB	Canadian General Standards Board
CS	Campbell Scientific
D/A	Data Acquisition
DEM	Digital Elevation Model
DS	Direct Shear
EMO	Emergency Measures Organization
HD	Heavy Duty
HRTF	Hydraulics Research and Testing Facility
L	Large-scale Direct Shear Test
LLDPE	Linear Low Density Polyethylene
LVDT	Linear Variable Differential Transformer
m	metre
min	minute
mm	millimetre
NSF	National Science Foundation
°F	Degrees Fahrenheit
PES	Polyethylene Sheet
psi	pounds per square inch
PVC	Poly Vinyl Chloride
RMC	Royal Military College of Canada
Sat.	Saturated
SWRB	Storm Water Retention Basin
USACE	United States Army Corps of Engineers
WSFPP	Woven Slit Film Polypropylene
WWD	Water and Waste Department
ϕ	Friction Angle (Mohr-Coulomb Shear Strength Parameter)
ϕ'	Effective Stress Friction Angle
θ	Angle Between Major Principal Plane and Plane of Shearing Failure
σ_1'	Effective Major Principal Stress
σ_3'	Effective Minor Principal Stress
σ_f	Normal Stress on a Soil Mass
σ_f'	Effective Normal Stress
τ_f	Shear Strength of a Soil Mass

1 Introduction

1.1 General Overview

Manitoba's Red River valley has flood characteristics that are dominated by its geological history as part of the glacial Lake Agassiz basin. The valley has little relief in the north-south axis, covering the 877 kilometres between Wahpeton, North Dakota and Lake Winnipeg with a drop of only 70 metres. That works out to a slope of approximately 8 centimetres per kilometre. The valley contains the confluence of the Red and Assiniboine Rivers called the Forks, which is located in downtown Winnipeg. The Red River watershed stretches from North Dakota in the south to Hudson's Bay in the north, covering an area of 125,285 square kilometres. The Assiniboine River watershed extends from the Alberta border in the west to northwestern Ontario in the east, with a total area of 164,438 square kilometres. Given these hydrological characteristics, it is no surprise that flooding is a regular occurrence for residents in the Red River Valley.

Sandbag dikes have been used as temporary flood protection measures in Red River Valley floods during the past century. The most recent and notable flood took place in the spring of 1997. As the Red River rose and communities upstream fought the flood, the City of Winnipeg initiated emergency response measures to ensure adequate safety against flooding for the citizens of Winnipeg and their property. As part of the flood protection effort, thousands of volunteers assisted with the construction of sandbag dikes. It is estimated that 150,000 volunteer days of work contributed to the flood fighting efforts.

The City of Winnipeg Water and Waste Department and Public Works Department ensured adequate materials and resources were available for construction of these secondary dikes. City crews and volunteers filled an estimated eight million sandbags in

total. Volunteer training on how to construct sandbag structures took place on site. City of Winnipeg staff was available to assist with dike building instruction where needed.

The rapidly-built sandbag dikes performed with varying levels of success. A plan for around the clock inspection of all permanent and temporary dikes was implemented to identify any problem areas prior to failure. Before the river crested, 33 two-person teams patrolled and monitored the dikes on a 24-hour basis. The monitoring teams were supported by on-call survey crews, geotechnical engineers, and military personnel to respond to any concerns regarding integrity of the structures. The dike patrols looked for anything from minor seepage to major dike breaches. At the time there was considerable anxiety caused by reports of leakage through and under structures, and also of distortional movements noted at some dike locations.

The importance of secondary dikes as part of the City's flood protection system as well as some of the uncertainties surrounding their construction and behaviour are easily identified in major floods. The flood of 1997 was a maximum design event for Winnipeg's flood protection system (Rob Kenyon, personal communication, June 9, 2005). Statistically, 1997 has been identified as a one in ninety year event. This experience and the subsequent analysis point out the need for higher flood protection levels for the City of Winnipeg. This means that higher primary and secondary dikes will be required in the future when a comparable or larger flood occurs.

The secondary diking enhancement program has been operating since the flood of 1997 to provide increased flood protection to an elevation appropriate to ensure adequate protection for future floods. However, it is recognized that permanent clay dikes cannot be continuous because of access, sight-line, property and slope stability issues. It is in

these areas that temporary flood protection infrastructure such as sandbags will continue to be necessary.

In summary, it is recognized that sandbag dikes are not a permanent protection measure. Although permanent facilities are being constructed at various locations throughout the City under the Canada-Manitoba-City of Winnipeg Secondary Diking Enhancements Agreement, sandbag dikes will continue to be an integral part of flood protection for all sites outside the Primary Diking System in the City of Winnipeg. Any improvements to understanding the behaviour of these structures to better define construction procedures and height restrictions will benefit the City and its citizens in future flood diversion efforts.

1.2 Hypothesis and Objectives

The behaviour of sandbag structures under lateral hydraulic loading is not well documented scientifically. This research program starts with the investigation of the interface qualities of each surface and material found in a sandbag dike using direct shear tests at both large- and bench-scales. The data from these direct shear tests is summarized as a set of Mohr-Coulomb shear strength parameters. These parameters are used to predict failure modes and behaviour under flood loading using available numerical modelling tools and fundamental soil mechanics. Finally, full-scale tests of sandbag structures under simulated flood conditions are conducted to verify the predicted behaviour and monitor actual structures under known loading conditions.

Objectives of Testing Program:

a) To quantitatively assess the stability of sandbag structures of varying heights constructed according to the design cross-section developed by the City of Winnipeg (Figure 1).

b) To develop a measure of reliability for the existing method of construction and to identify height limits based on acceptable probabilities of failure.

c) To evaluate new design cross-sections and/or methods of construction, if necessary.

The results of this research will provide a basis for evaluating new methods and materials (sandbags or other products) for dike structures in the future.

1.3 General Description of Experimental Testing and Numerical Simulations

The best method for assessing the stability of sandbag structures is to undertake full-scale model tests to monitor the performance of these structures under simulated flood loading conditions. Unfortunately, due to the cost and length of time required to undertake these large experiments, it has not been economically practical to explore every proposed cross-section and construction method. That being said, this research project has progressed in three phases which have optimized the value of a limited number of full-scale tests and have produced a set of data which can be used for a more comprehensive study of sandbag structure designs.

The first phase of the interface shear testing was carried out in Kingston, Ontario under the supervision of the Geo-Engineering Centre at Queen's-Royal Military College (RMC) using a large-scale direct shear apparatus (1 m by 1 m) to quantify the frictional characteristics and sliding behaviour of the sandbag material. This specialized equipment enabled the testing of the pure interface friction as a function of the overburden pressure (dike height) as well as the sandbag to sandbag and sandbag to sod interface properties.

The second phase of the testing was to undertake bench-scale laboratory tests on the interface shear properties between the bag materials and the in-isolation properties of the sand in the bags. The in-isolation testing is conducted at the University of Manitoba Geotechnical Laboratory using existing soil testing equipment to characterize the load and deformation behaviour of both the sand material and individual bags.

The third phase of the research program consisted of the design and construction of five full-scale sandbag dike structures. Each of these plane-strain sandbag dikes (24 feet (7.31 m) long and between 6 and 10 feet (1.83 and 3.05 m) tall) were constructed and loaded to failure by hydraulic loading simulating flood conditions. The models were constructed at the University of Manitoba using a three sided flume to maintain controlled hydraulic loading conditions. Four of the dikes were constructed using the design methodology outlined by the City of Winnipeg (Figure 1) for constructing temporary sandbag dikes. Each dike was instrumented during construction and during all stages of loading prior to collapse. Sensors placed within and outside of each structure monitored displacement of internal and outer sandbags, seepage through the structure, vertical displacement of the structure at selected points, sliding between selected sandbags, vertical and horizontal pressures at the base and midpoints in the dikes, and hydraulic loading during all stages of testing. The deformed geometry and collapse mechanism was monitored by onsite staff and recorded using a video camera. The testing facility was built adjacent to the East SmartPark storm water retention basin (SWRB) to provide a catchment for water released during anticipated failure of the full-scale dikes. Water for the tests was provided via the fire hydrant system running along Innovation Drive, ensuring adequate flow to simulate flood loading conditions.

A benefit of testing the sandbag structures at full-scale was that the dikes are constructed on native grass consistent with typical construction conditions experienced

during floods. However, a number of known construction and loading factors have been ignored in this study to simplify the interpretation of the results. For example, the application of lateral loads at the water surface due to floating ice and debris has not been examined. Another factor that was not examined is the frozen or mid-thaw ground condition that may occur during construction, which would be expected to influence the interface behaviour between the bags and the ground surface. It is important to note that the facility has been designed and constructed in a modular fashion so that additional research beyond the scope of this project can be conducted in the future to examine the influence of important considerations ignored in this first step.

Finally, an analysis of the research program uses the results from the three stages of testing (large- and bench-scale shear and full-scale field tests) to build a set of data which can be used to analyze the performance of sandbag structure configurations. In order to develop rational analytical techniques for examining the behaviour of sandbag dikes we must first have an understanding of the physics of how they behave at both operating and failure conditions.

1.4 Organization of Thesis

The thesis is organized as follows: Chapter 2 presents a background of sandbag dike use in the City of Winnipeg, a literature review of relevant research and theories important to understanding this thesis, and a summary of new developments in temporary flood protection that may be relevant to stakeholders. Chapter 3 is a description of the materials, procedures and equipment used to test the interface friction properties of the surfaces present in a sandbag dike as well as the results of the large- and bench-scale direct shear tests. Chapter 4 discusses the equipment and procedure used to conduct the full-scale sandbag dike field tests as well as the results of these

tests. Chapter 5 is a discussion and analysis of the results of all of the full-scale testing conducted. Chapter 6 is a comparison of several notable sandbag dikes tested with respect to height, geometry, construction method, materials and quality. Chapter 7 presents conclusions and recommendations for further work in the future.

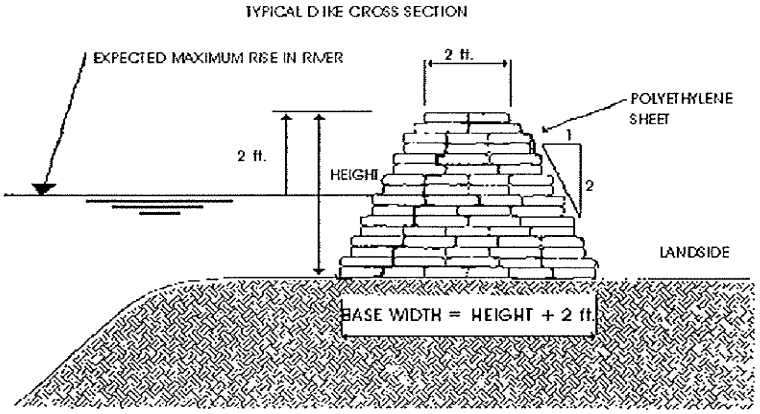

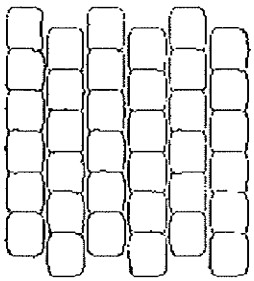

PLAN OF LAYER

HEIGHT	BASE WIDTH
1.0	3.0
2.0	4.0
3.0	5.0
4.0	6.0

ALL DIMENSIONS IN FEET

METHOD OF LAPPING SANDBAGS

- Base area of sand bag dike should be clear of snow or ice prior to commencing.
- Leave at least 8 feet between a dike and buildings. The base of the dike should be 2 feet wider than the ultimate height of the dike, E.G. Height = 4 ft., base = 6 ft.. Every second layer of sand bags should be set back 1/4 of a sand bag width, both on the river side and the land side of the dike, giving it a step-like appearance. The top of the dike should be 2 feet wide.
- The bottom layer of bags on the river side will run parallel with the river.
- Sand bags are to be tamped firmly into place.
- It is recommended that 6 mil polyethylene sheets in 10 foot wide rolls be used as water proofing on the river side of the dike. The polyethylene sheet should be placed loosely against the sand bag dike during construction with a protective layer of sand bags placed on the river side as indicated in the figure.
- Have extra sand bags on hand to strengthen any weak spots in the dike.
- If untied bags are used, the top, or unfilled portion of the sack should be stretched lengthwise and the next bag laid on top of it. This method is known as lapping as indicated in the figure. It is not necessary to tie sacks. Untied bags should be filled to half full.

Figure 1 – City of Winnipeg Sandbag Dike Template (1997).

2 Literature Review

2.1 Introduction

Sandbag dikes have been used as temporary flood protection measures all over the world. This is both due to availability of the bags in consistent sizes and large numbers as a result of textile manufacturing progress during and after the industrial revolution, and to the range of materials that can be used to fill these bags. Sandbag dikes have been used extensively for flood protection and diversion in the Red River Valley since the turn of the century.

A review of the literature has been conducted in order to present previous research that is relevant to the assessment of sandbag dike performance. The review is divided into sections including: Soilbag Reinforced Embankment Stability Considerations, Compaction and Settling of Granular Materials by Wetting, Interface Behaviour between Soils and Geosynthetics, Direct Shear Testing on Interfaces, and Large-scale Testing of Reinforced Embankments.

Alternatives to sandbag dikes for temporary flood protection have been developed by both the private and public sectors in recent years. A summary of some of the most promising technologies is presented.

2.1.1 The Red River Valley and Sandbag Dikes

The shallow average slope of 8 centimetres for every kilometre along the Red River between Wahpeton and Lake Winnipeg guarantees relatively slow headwaters in a flood situation. This means that flood protection personnel have a longer warning time in the Red River valley than in other steeper watersheds. Hydrological models have been developed and refined in combination with digital elevation models (DEMs) to yield

increasingly accurate crest predictions. Manitoba Conservation has made its DEM available to the general public via an internet website (http://geoapp.gov.mb.ca/website/rrvfp/mainFrame.htm). The site allows any user to assess the elevation of flood protection that is required at their property given the latest crest prediction.

The low slope of the valley has given the Red a meandering path, which means that there are long riverbanks requiring protection, which is of particular concern when the river flows within town or city limits. These riverbanks are of varying height and slope, and many of them are not suitable for supporting the size of permanent earthen dike required to guarantee flood protection in an extreme flood year. Property rights, accessibility and aesthetic issues as well as economic constraints mean that temporary flood protection systems will always be necessary in the City of Winnipeg.

The storability of sandbags, their use for many municipal activities in non-flood situations as well as the availability of large amounts of sand and gravel in the Bird's Hill area to the north of the city make sandbag dikes the standard for temporary flood protection in Winnipeg.

Since the flood of 1950, people in the Red River valley have relied on sandbag dikes to bring their permanent flood protection systems up to the necessary elevation to keep their property safe. These temporary structures have performed with varying degrees of success, and the experience gained from several extreme flood events has lead to the template that the City of Winnipeg used as a guide during the flood of 1997.

2.1.2 History of Winnipeg's Sandbag Dike Design Development

According to City engineer Aurele Delaurier, (personal communication, October 6, 2004) the City of Winnipeg's sandbag dike cross-section was initially developed in 1996 after the Water and Waste Department (WWD) took over responsibility of secondary dike protection from the City Districts that were dissolved in 1995. From an initial review of information from the Districts, WWD determined that no technical memorandum on sandbag dikes or a cross-section template existed. However, information was found from the files of District 6 on sandbag counts, dike lengths and heights for properties protected during the 1979 flood. WWD staff back-calculated a dike cross-section based on the 1979 flood protection data. This cross section was then used by the City to protect properties for the 1996 flood, where levels were comparable to that of the 1979 flood.

2.1.3 Other Published Sandbag Dike Templates

2.1.3.1 United States Army Corps of Engineers (USACE)

Figure 2.1 is a reproduction of the current USACE sandbag dike template and sandbag ring dike template for surrounding sand boils. As part of their instruction package, the USACE also provides the following instructions:

> "SANDBAG DIKES The sandbag dike should not be considered as a primary flood barrier. The main objections to their use are that the materials (bags and sand) are quite costly; they require a tremendous amount of manpower; and are time consuming to construct. Sandbag dikes should be used where a very low and relatively short barrier is required and earth fill would not be practicable, such as in the freeboard range along an arterial street. They are very useful in constricted areas such as around or very close to buildings, where rights-of-way would preclude using earth fill. They are also useful where temporary closure is required, such as roads and railroad tracks. A polyethylene seepage barrier should be incorporated into the sandbag structure. The poly must be on the riverward slope and

brought up immediately behind the outermost layer of bags. The poly should or, at best, lapped under the sandbags for anchorage. See plate 1 for recommended practices in sandbag dike construction.

A few points to be aware of in sandbag construction are:
1) sand, or predominantly sandy or gravelly material should be used;
2) extremely fine, clean sand, such as washed mortar sand, should be avoided;
3) bags should be ½ full;
4) bags should be lapped when placing;
5) bags should be tamped tightly in place;
6) the base width should be wide enough to resist the head at high water.

Sandbagging is also practical for raising a narrow levee, or when construction equipment cannot be used. Sandbag raises should be limited to 3 feet, if possible."

It is worth noting that the USACE doesn't recommend using sandbags for flood diversion efforts requiring more than three feet of elevation increase. This is a considerably more conservative design than the City of Winnipeg's 1997 template. The USACE templates do not appear to have been updated since World War II.

2.1.3.2 Manitoba Emergency Measures Organization (EMO)

Figure 2.2 is a reproduction of the current Manitoba EMO sandbag dike template. It is essentially the same as the USACE template in geometry and height recommendations. The Manitoba EMO website where the template is made available to the public does have a link to the City of Winnipeg's website, and includes a table with some estimates of the number of bags necessary of dike required to protect 100 linear feet at three different heights.

2.1.4 Stability Considerations for Sandbag Structures

The observed failure mechanism in sandbag dikes in the Red River Valley is the formation of a slip surface along the interface between the sandbags themselves. Failure does not generally occur through the bags, as the interface shear strength between the

materials is lower than the tension strength of the bag material. In failed dikes built on regular sod, the slip surface generally daylights above the base of the dike, indicating that the weakest interface is within the dike itself and not between the dike and its foundation (Ken Skaftfeld, personal communication, June 7, 2005).

Base sliding is a failure mechanism that is considered to be important by both the USACE and EMO design templates described above. Both the USACE and EMO templates advocate the installation of a key trench to prevent the dike from translating under lateral hydraulic loading. This technique generally requires heavy equipment during spring in the Red River Valley due to frozen soil conditions, and therefore is rarely undertaken. Base sliding has generally not been observed to be the critical failure mode for sandbag dikes built in the Red River Valley.

As a first step in quantifying the stability of sandbag structures, an investigation of the interface properties of the materials used in their construction must be completed.

2.2 Review of Relevant Literature

2.2.1 Soilbag Reinforced Embankment Stability Considerations

Matsuoka, Liu and Yamaguchi (2001) conducted tests on soilbags for the purpose of earth reinforcement of slopes and below footings. They varied both the material inside and making up the bags, and tested them in laboratory and in-situ conditions. Their laboratory tests were compression tests in both a confined and unconfined testing apparatus. The confined tests were conducted on a two-dimensional model made of aluminium rods to simulate a cohesionless soil mass and paper sheets to simulate bags containing the soil. The unconfined tests consisted of full size soilbags placed in a loading frame and compressed to failure. The size of bag used in the unconfined tests was 40 cm x 40 cm x 10 cm. The materials used to make the bags were polyethylene,

polypropylene and another polyethylene treated to resist photo-degradation from ultra-violet wavelengths in sunlight. The materials used to fill the bags were two sizes of crushed stone, coal ash, shirash and volcanic ash. The fill materials were tested in both wet and dry conditions.

The results of their laboratory tests showed that the compressive load the filled bags were able to sustain was between 10 and 40 times the load that the individual bags were able to sustain in tension. This non-linear increase in strength between the individual components and the system they are made into is consistent with the observations of soil-geotextile strengths made in the literature.

The in-situ applications of soilbag reinforcement tested by Matsuoka et al. (2001) were in a retaining wall and in pre-stressing micropile foundations. In both cases the soilbag reinforcement was found to be both effective and economically beneficial.

Allan, Komar and Hart (2003) present a test case where sand filled geotextile bags are used as the core material of an artificial dune built to protect a state park in Oregon. The artificial dune acts as a wave barrier in support of a dynamic cobble beach that acts as an energy dissipater on the park's ocean coast. The authors report that the artificial dune is a success after three winters of operation which included several over-topping storm events, although the need for regular maintenance is noted.

Finch (1939) reports the use of an earth-cement mixture in sacks being used as a revetment on a river bank at Fort Sam Houston, Texas. The context of the use of the earth filled sacks is as an emergency measure, with the erosion of the river bank threatening the foundations of the post headquarters. The effectiveness and economy (both in terms of timeliness and monetary cost) of the method is noted.

2.2.2 Compaction and Settling of Granular Materials by Wetting

In engineering terms, the strength of a cohesionless soil material is dependant on its grain size distribution, moisture content and density. Kerr (1978) points out that there is a general increase in soil strength with decreasing water content and with increasing density. Further, he notes that increasing density generally increases elasticity and decreases compressibility.

Increased bearing capacity, control of settlements and decreased permeability are the goals of compaction in this discussion. Similarly, when a sandbag dike is built according to the city of Winnipeg design, compaction is achieved during construction by the persons involved via physically walking on each successive course of bags and tamping them down with their feet and hands.

Figure 2.3 is an illustration of a cross-section of soil particles in both a loose and a compacted state. The area of the soil particles is equal in both of the cross-sections, but the area in the dashed line surrounding the soil particles is smaller in the compacted configuration than in the loose configuration.

According to Kerr (1978), the main mechanism of compaction in cohesionless soils is the re-orientation of soil particles from a lower initial density to a configuration with a higher overall density. In cohesionless soils the major resistance to re-orientation is friction between the particles. The friction between the particles is affected by the moisture content of the soil. Between the completely dry state and the lower limit moisture content for compaction, capillary tension increases, the inter-particle friction increases and the density of the soil decreases. Between the lower limit and optimum moisture contents for compaction, capillary tension decreases and the density of the soil increases.

Compactive efforts result in decreased density at moisture contents above the optimum for compaction.

Kerr (1978) also notes the difference in the behaviour of soils compacted at moisture contents on either side of optimum. For a cohesionless soil compacted on the dry side of optimum, settlement may occur after saturation due to a re-orientation of the soil structure.

Laba (1983) noted that compaction of trench back-fill by water jetting was impeded by cases where insufficient drainage was present. In these cases, the tests yielded lower densities and higher moisture contents in the same fill materials than in cases where good drainage was assured.

The American Society of Civil Engineers (ASCE), St. Louis section, Report on Backfilling in Public Rights-of-way (1968) notes that compaction by jetting, ponding or flooding is normally successful in non-cohesive, coarse grained soils that are freely draining.

2.2.3 Interface Behaviour between Soils and Geosynthetics

Koerner (1998) lists a number of families of geosynthetics in his design text, including geotextiles, geogrids, geonets, geomembranes, geosynthetic clay liners, geopipe, geocomposites and geo-others. They are made primarily of polymers synthesized from petroleum, but are also made of fibreglass, rubber, jute, bamboo and other natural materials. Generally a geosynthetic is employed to reinforce a soil mass, enhance filtration, form a flow barrier or retardant, or enhance drainage.

For the purposes of this research, geotextiles and geomembranes are the two geosynthetics that are relevant, although testing methods and research results from

studies on other types of geosynthetics are also relevant in terms of stress-strain and frictional behaviour.

The shear strength of a soil-geosynthetic interface is related to the confining pressure, the grain-size distribution, shape and hardness of the soil particles, the roughness and elasticity of the geosynthetic, the water content and density of the mass and the strain rate used in the testing apparatus. Investigations of the interface shear characteristics between soils and geosynthetics and between geosynthetics and geosynthetics are commonly carried out using direct shear, pull-out or inclined plane testing apparatus.

The direct shear apparatus consists of a rigid box split into upper and lower halves. One of the halves is held fast laterally and the other half is able to translate horizontally at a known strain rate. A normal stress can be applied to the material being tested, generally on the half of the box that is held fast laterally. In most direct shear apparatus the half of the box restrained from horizontal movement is allowed to move vertically in order to reduce the boundary effects on the stress distributions in the soil mass being tested. The strain rate, horizontal and vertical displacements, and loads are all monitored throughout the test, and the load-displacement data is used to calculate stress-strain relationships which are in turn used to calculate Mohr-Coulomb failure parameters.

The pull-out apparatus consists of a split box similar to the direct shear apparatus, but both halves of the box are held rigidly. A pull-out mechanism that moves at a controlled rate is attached to a geosynthetic sample that is installed inside a soil mass or attached to a support strata with the soil or other geosynthetic to be sheared installed against it. Normal stress is applied to the whole mass being tested, and a load cell or proving ring measures the force required to pull the geosynthetic out of the box at the set strain rate.

Load-displacement data are collected and similar calculations to those conducted for the direct shear tests are carried out.

The inclined plane apparatus is a modified direct shear test that is capable of operating at a range of inclinations to simulate shearing on an inclined surface.

In tests conducted on three different sands and their interface with a single non-woven needle punched geotextile, Kalumba and Scheele (1999) found that the interface shear strength of a given soil-geotextile tested in a direct shear device was lower than the shear strength of the soil tested alone at the same confining pressure. This is to be expected, since the resisting volume in a soil-geosynthetic interface test is best described as an area, i.e. without depth above and below the shear plane, while the resisting volume in a soil shear test has some depth both above and below the shearing plane. The residual shear strength (at relatively large strains) is about the same for both soil-geotextile and soil tests.

Kalumba and Scheele (1999) repeated their direct shear tests using a pull-out apparatus in order to establish the stress distribution and strain behaviour of the geotextile at known confining pressures. They determined that the skin friction distribution had its maximum at the pull-out end, then sharply declined over approximately 1/3 of the length of the geotextile, then gradually went to zero over the remaining 2/3 of the geotextile. The pull-out tests generally showed lower interface shear friction angles than the direct shear tests, but significantly higher adhesion values.

Lopes, Lopes and Lopes (2001) list the interaction mechanisms at the soil-geogrid interface as (i) skin friction over the planar geogrid surface; (ii) soil-soil friction through the geogrid apertures; and (iii) passive resistance of the geogrid bearing members. Their

tests on six geosynthetic materials and two cohesionless soils in an inclined plane shear apparatus also provided insight into the interaction mechanisms between the soils and geomembranes and geotextiles.

The primary interaction mechanism at the soil-geotextile interface is skin friction between the soil particles and the geotextile. This mechanism is also the primary interaction between soil-geomembrane interfaces. The shear strength of the soil-geomembrane interface tends to be slightly higher than the shear strength of a soil-geotextile given the same soil and testing conditions when comparing a smooth geomembrane and a woven geotextile. This is due to the soil particles ploughing into the relatively soft geomembrane surface, where they slide over the harder more porous woven geotextile.

O'Rourke, Druschel and Netravali (1990) reported similar findings in a summary of over 450 direct shear tests on sand-polymer interfaces. They found that interface frictional strength increased with soil density and decreased with hardness of the polymer being tested.

In terms of the effect of test method and geosynthetic orientation, Lopes et al. (2001) found that soil-geotextile and soil-geomembrane interface shear values were least affected of the materials in their inclined plane shear testing program.

2.2.4 Direct Shear Testing on Interfaces

The literature shows that early reports of testing the frictional relationship between a soil and a geotextile using a direct shear device when Collios, et al (1980) presented a paper at the American Society of Civil Engineers (ASCE) National Convention in Portland, Oregon. The importance of understanding and quantifying the shear strength of soil-geotextile interfaces in cases where the geotextile is not being used as reinforcement is

noted. This is especially important where this interface can form a slip surface inside an earth mass, as in the case of a sandbag dike.

The American Society for Testing and Materials (ASTM) established its standard test method for determining the coefficient of soil and geosynthetic or geosynthetic and geosynthetic friction by the direct shear method in 1992, and this method was reapproved in 1998. The ASTM standard describes the test method as a performance test for determining the coefficient of friction between soil and geosynthetic or geosynthetic and geosynthetic. The coefficient of friction is a summary quantity of total measured sliding resistance that may be a combination of sliding, rolling, interlocking of soil particles and geosynthetic surfaces and shear strain within the geosynthetic specimen, ASTM (2000). Each of the direct shear interface tests conducted for this research was carried out in general accordance with this standard.

Bove (1990) cites Richardson and Koerner for demonstrating analytically that the tensile stress applied to a geosynthetic component in a multi-layer system is more dependant on the differences in the shear resistance of the layers above and below than on the magnitude of the normal stress originally applied to the whole system. Richardson and Koerner develop a clear relationship between system stability and interface shear resistance.

2.2.4.1 Effect of Equipment and Scale on the Accuracy of the Direct Shear Test Method

Bove (1990) refers to the use of larger than conventional direct shear devices for the testing of geosynthetic-soil interfaces. Devices with shear boxes of 300 mm x 300 mm (as opposed to 100 mm x 100 mm) are cited as being more accurate due to the larger

specimen area available for evaluating shear failure. The ASTM standard recommends 300 mm as the minimum horizontal shear box dimension for these tests.

Criley and Saint John (1997) conducted a series of direct shear tests on similar materials using identical equipment and methods in order to analyse the variability of results obtained in determining soil-geosynthetic interface friction characteristics by the ASTM method. They note that the adhesion, or apparent cohesion, component of the shear strength had the greatest variability throughout their tests, and that the overall variability between tests decreased as the applied normal stress increased. In general, they recommend repeated tests using a standardized test method carried out by experienced personnel on properly calibrated equipment to improve reproducibility and accuracy. Their tests were carried out on a 300 mm x 300 mm direct shear apparatus, and no mention of the effect of scale was made in the paper.

Jewell and Wroth (1987) assert that boundary conditions are affected by the scale of a direct shear test, and recommend a ratio of shear box length to average particle size in the range of 50 to 300 in order to achieve acceptable test accuracy.

Tan, Chew, and Wong (1998) used a ring shear test apparatus in their soil-geotextile frictional testing in order to overcome the limited displacement capacities of a conventional bench-scale direct shear apparatus. They found that for displacements between 3 and 14 mm, the boundary conditions of a conventional 100 mm by 100 mm direct shear box dominated the test and affected the results to an unacceptable degree.

It follows that increasing the scale of the direct shear apparatus used will increase the accuracy of interface friction test results.

2.2.4.2 *Mohr-Coulomb Shear Strength Parameters from Direct Shear Tests*

Mohr-Coulomb failure criteria are commonly used to quantitatively evaluate shear strength in soils and geosynthetics. The stability of any given soil mass is directly related to the mean shear strength of the soil. Equation 2.1 is Coulomb's expression of the shear strength (τ_f) of a soil mass in a given plane as a linear function of the stress normal (σ_f) to that plane at the same point in the soil mass;

$$\tau_f = c + \sigma_f \tan\phi, \tag{2.1}$$

where c and ϕ are the Mohr-Coulomb shear strength parameters cohesion intercept and friction angle, respectively. As cited in Craig (1998), Karl Terzaghi asserted that the shear stress in a soil can only be resisted by the skeleton of solid particles that make up the soil mass, and that this resistance is dependant on the effective stress normal to the shear plane in question. Equation 2.2 is a modification of 2.1, taking Terzaghi's concept of effective stress into account;

$$\tau_f = c' + \sigma'_f \tan\phi', \tag{2.2}$$

where c' and ϕ' are the shear strength parameters in terms of effective stress. Equation 2.2 produces a straight line when plotted with shear stress on a y-axis versus normal stress on an x-axis. This line represents a failure envelope for a set of effective major and minor principal stresses σ'_1 and σ'_3, as shown in Figure 2.4; compressive stress being taken as positive. The line is tangent to a Mohr circle defining the stresses at a particular failure point which is shown having the coordinates τ_f and σ'_f. Equations 2.3 and 2.4 give these shear and normal stresses;

$$\tau_f = \frac{1}{2}(\sigma'_1 - \sigma'_3)\sin 2\theta, \tag{2.3}$$

$$\sigma'_f = \frac{1}{2}(\sigma'_1+\sigma'_3)+\frac{1}{2}(\sigma'_1-\sigma'_3)\cos 2\theta, \qquad (2.4)$$

where θ is the angle between the major principal plane and the plane of shearing failure. By familiar geometrical relations it can be shown that;

$$\theta = 45^o + \frac{\phi'}{2}. \qquad (2.5)$$

The Mohr-Coulomb failure criteria as laid out here describes a linear approximation of a failure envelope running along a common tangent as described by equation 2.2 (Craig, 1998).

2.2.5 Large-scale Testing of Reinforced Embankments

Large-scale testing is instinctively recognised as a more accurate means of observing the behaviour of civil engineering structures than bench-scale testing. The ability of a sample on the order of 1/10th the scale of in-situ elements to reproduce actual behaviours is suspect. However, budgetary constraints frequently curtail attempts to conduct large- or full-scale tests on structures such as reinforced embankments. It should be noted that in cases where the structure is of high importance, such as hydroelectric dams, centrifuge studies are often undertaken to overcome the negative effects of under-scaled testing.

Blatz and Bathurst (2003) conducted tests on three large-scale embankments loaded vertically near their crest at the Royal Military College of Canada (RMC) retaining wall test facility. Two of the test embankments were built with geosynthetic reinforcement and one was not. All of the embankments were heavily instrumented in order to precisely define the failure surface and behaviour of the materials during all phases of loading up to and including failure. The embankment monitoring data served to verify predicted failure modes and slip surface locations. The testing and analysis conducted illustrated

the importance of using high quality values for the characterisation of the mobilisation of the tensile load in the geosynthetic reinforcement as well as the peak shear resistance of the soil in order to ensure high quality predictions of the footing's bearing capacity.

Hanson, Cook and Hahn (2000) presented preliminary results of a large-scale testing program on earthen embankments under sustained overtopping hydraulic loading. The test embankments were three homogeneous sections built from different soil materials. They were each 2.3 m in height and 7.3 m in width, with 1V:3H slopes on both the wet and dry sides. The embankments were pre-loaded to 1.2 m of water on the day before the test, and then overtopped and monitored for erosion and downstream flow rate at a known input flow rate. The test embankments were not reinforced with minimal vegetation on their surfaces. The preliminary test results show that plastic clay soils are more stable and erosion resistant under sustained overtop hydraulic loads than silty sands.

Juran and Christopher (1989) conducted laboratory tests on a set of reduced scale geosynthetic reinforced retaining walls to describe the failure modes of two types of geosynthetic reinforcement. They found that woven polyester reinforced retaining walls failed by sliding along slip surfaces defined by the plane where the geosynthetic was installed, or by excessive deformation of the face of the wall. Plastic grid reinforced retaining walls failed by rupture of the grid along a slip surface within the soil mass.

2.2.6 Temporary Flood Protection Alternatives to Sandbag Dikes

In recent years both the public and private sectors have been working to develop alternatives to the sandbag dike for temporary flood protection. These alternative

designs range widely in cost, adaptability and basic strategy, but their performances are all measured against sandbag dikes.

Duncan, Mitchell, Lovern, and Coffey (1997) published a literature review of historical techniques, commercial products and current military and professional practise for innovative flood protection concepts with the purpose of evaluation for further research and investigation. They held a workshop to consult with experts in the field of flood protection in order to develop a short list of candidates from the innovative flood protection concepts found in the aforementioned review.

All of the flood protection concepts were initially divided into two broad groups, temporary and permanent techniques; although some systems fell into both categories. A system of grading was developed to help in the evaluation and ranking of each flood protection system.

The top ranked temporary flood protection systems as evaluated by the workshop attendees were: 1. Jersey highway barriers, 2. Water-filled geomembrane barriers, and 3. Deep cellular confinement systems, Duncan et al. (1997). Figures 2.5, 2.6 and 2.7 show the three systems in the same order that they are listed here.

Biggar and Masala (1998) reviewed the work done by Duncan et al. (1997) and prepared a technology overview of alternative flood protection systems for the Alberta Transportation and Utilities Disaster Services Branch. Their objective was to evaluate innovative alternative flood protection technologies against the benchmark of sandbag dikes. In comparison to sandbags, the new technology was to be more easily installed and removed, sufficiently stable against sliding and overturning, resistant to seepage both through and beneath, flexible in use outside of flood protection, and cost effective.

Their specific evaluation criteria were as follows: stability with regard to base sliding as well as overturning, seepage both below and through the barrier, induced loading on the soil beneath the structure, ability to fix and/or strengthen the system when in use, adaptability to different and/or changing terrain conditions, modularity, time required for installation and removal, simplicity of construction, labour required, equipment for transport and installation, site preparation and operating space requirements, initial investment cost, storage requirements, durability in use and versatility, installation and removal costs, and training and supervision requirements.

These criteria were evaluated based on data available from manufacturers as well as trips to the towns of Peace River and Pincher Creek, both in Alberta. These sites were selected as examples of relatively slow moving, ice-jam susceptible flood areas and much faster 'flash' flood prone areas, respectively.

Based on these criteria and discussions with municipal employees, a list of systems that merit further study was produced. The list consisted of: 1. Inflatable (water or air) tubular geomembranes; 2. Cellular (gabion-like) structures; 3. Fixed post-and-lagging systems; and 4. Jersey highway barriers. It should be noted that item 2 on this list corresponds to item 3 on the list published by Duncan et al. (1997). That is to say, deep cellular confinement systems are equivalent to cellular (gabion-like) structures.

Biggar and Masala (1998) made some key observations in their study of temporary flood protection techniques. In general, continuous structures outperformed segmented ones, as they are better able to deal with corners and variations in terrain. Also, systems with a sealing component in their design outperformed those relying on available on-site materials and the construction skill of the people assembling the system. Additionally,

using different techniques along different stretches of the same flood prone area demands compatibility between each consecutive system.

They noted that, as long as the construction of the system is completed according to the intended design, seepage characteristics will be dominated by interface properties between the flood protection structure and the ground that it is built on. Further, rigid structures are prone to increased seepage when base conditions change, where flexible structures can adapt to changing base conditions.

Biggar and Masala (1998) concluded that simple constructability and basic design are better than complex systems requiring specialized equipment and trained personnel, and that each municipality will have to base its flood protection plan on a careful assessment of its own geography as well as the flood protection plan of neighbouring municipalities.

2.2.6.1 Alternative techniques used in the Red River valley

Several of the aforementioned technologies, as well as some other unique systems, have been proposed for flood protection in the Red River valley.

Manitoba Hydro has elected to use a water-filled geomembrane system to protect its transformer stations in areas at risk of flooding. The transformer sites (notably the one at Letellier) are well suited to this system, as they have a relatively level topography as well as adequate storage space for the geomembrane tubes, fuel and pumps that are required. Logistically, the utility is able to send teams of two or three trained people to each transformer station and can expect these sites to be protected to a known flood elevation within a days notice.

At this point there have not been any reports of use of deep cellular or gabion-like structures for flood prevention in the Red River valley. These structures may be

appropriate for areas where there is adequate access and bearing capacity for the heavy equipment required to make their construction efficient and economical in terms of time.

During the spring of 1997, 1 m^3 sandbags were used along some of the secondary dikes within the City of Winnipeg as well as in the construction of the 'Z-dike' protecting the South-west quadrant of the City (Ken Skaftfeld, personal communication, June 8, 2005). These 'super-bags' required front-end loaders to be moved and placed, and therefore their constructability could be considered equivalent to the that of the deep cellular or gabion-like systems mentioned above.

Several private citizens have built foundation systems surrounding their properties in order to facilitate modular wall systems that can be relatively quickly assembled when the threat of flooding is apparent. These systems are similar to the post-and-lagging structures studied by Biggar and Masala (1998). They are temporary in the sense that their configuration as a flood protection structure is not the same as their non-flood configuration. They incorporate a permanent foundation system which must be installed ahead of time. It is extremely unlikely that these foundations could be set up properly during a spring flood event in the Red River valley. The ground on which the foundations must bear will be frozen and the heavy equipment required to overcome these conditions will likely be occupied with other aspects of the flood protection effort. The applicability and economy of these types of flood protection strategies is strongly site dependant and must be determined well in advance by the appropriate stakeholders.

These select situations where flood protection alternatives have been chosen all have unique factors that influenced the respective stakeholders decisions. Both the private citizens mentioned and the electrical utility are concerned with isolating a single site from

the flood waters. This is a containment strategy, and should not be confused with a diversion strategy.

In the case of a municipality that is responsible for long stretches of riverbank or ring dikes that require additional height, the more comprehensive point of view of diversion is necessary. Municipalities must also consider their neighbour's strategies in order to assure that there is continuity in the flood protection system at their borders. The public bodies responsible for protecting both citizens and their property must adopt the mentality of considering and accounting for the weakest link within their jurisdiction, and they must realize that the floodwaters cannot be stopped; only redirected on their journey across the watershed to the ocean.

2.2.7 Justification of Large-scale Direct Shear Interface and Full-scale Sandbag Structure Testing Program

This review of the literature reveals a lack of scientific investigation of the properties of sandbag materials and sandbag structures as they are commonly used for temporary flood protection measures. The materials used to make these structures are common and well known individually, but their characteristics as discrete block structures built on sod and loaded hydraulically have not been documented.

Direct shear tests have been shown to be an effective way to characterise the interface shear strengths of soil-geosynthetic and geosynthetic-geosynthetic interfaces, and the benefits of increased scale in these tests has been demonstrated. Large-scale tests on reinforced embankments have been carried out to verify the ability of various design models to accurately predict bearing capacities and failure modes under vertical loading. Full-scale tests have been conducted on unreinforced embankments under hydraulic

loading, but these tests have focussed on the flow rate and erosion caused by sustained overtop conditions.

Therefore, to quantify the stability and seepage characteristics of sandbag structures built according to the City of Winnipeg's 1997 design template, this research must be undertaken. The interface shear qualities of the materials making up the structures as well as the unique behaviour of the sandbags themselves need to be tested at an appropriate scale to adequately model actual loading conditions in an apparatus capable of quantifiably measuring these characteristics. These data need to be used to design and carry out full-scale tests of sandbag structures under simulated flood conditions in order to verify the accuracy of the design models used and to provide baseline data on the deformation, seepage and failure characteristics of these structures.

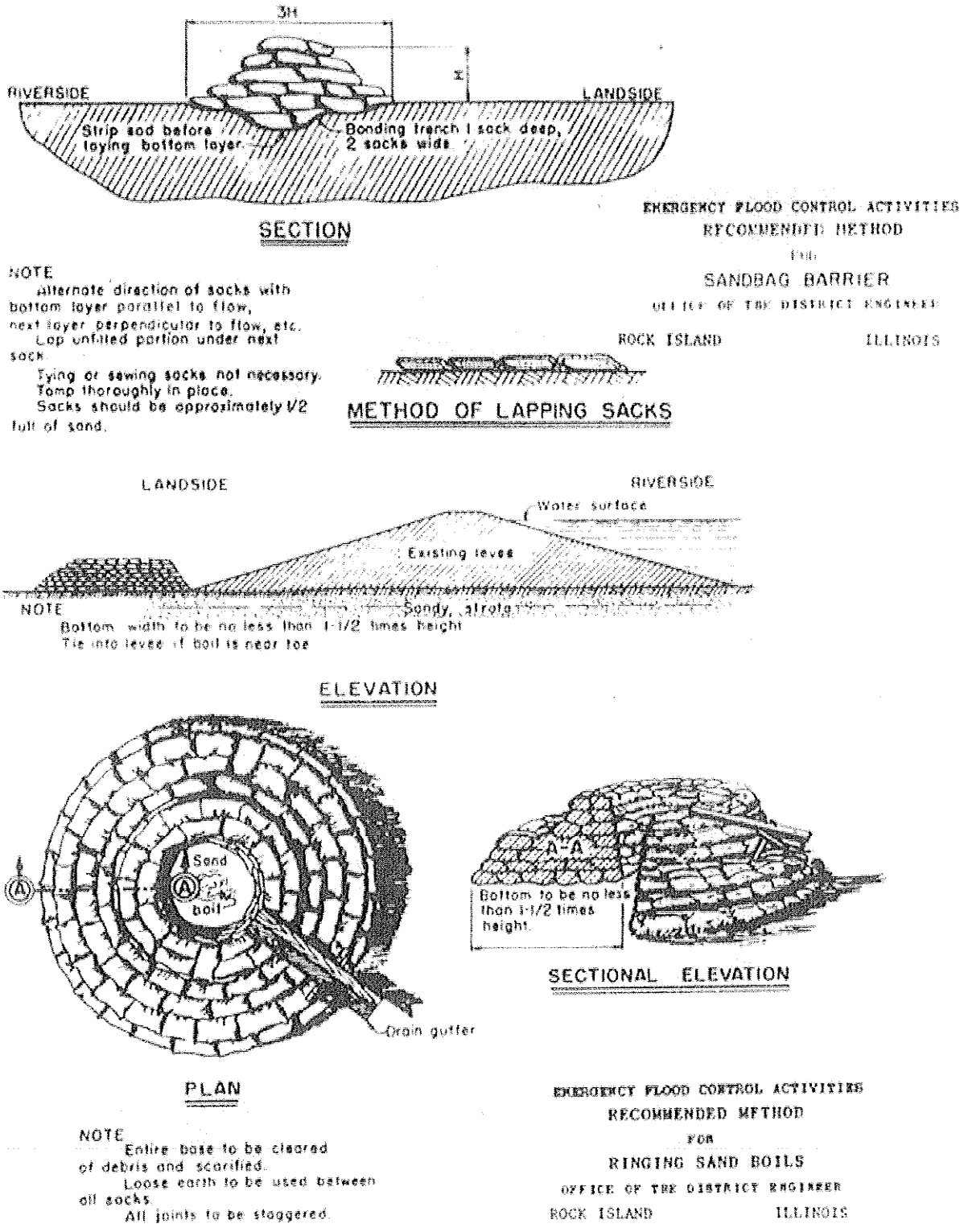

Figure 2.1 – USACE Sandbag Dike and Sand Boil Ring Dike Template.
(after: http://www.mvr.usace.army.mil/PA_brochure16813/PA16813_01.htm)

Guidelines for Sand Bag Dike Construction

How to Fill and Lap Sand Bags

- Strip sod before placing bottom layer. Bonding trench is 1 sack deep by 2 sacks wide.
- Sacks should be half full of clay, sand or silt.
- Lap unfilled portion of sack under next sack.
- Tying or sewing of sacks is not necessary.
- Tamp sacks thoroughly in place.
- Alternate direction of sacks with bottom layer (i.e. bottom layer lengthwise with dike, next layer crosswise).

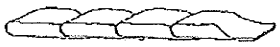

Bags Required for 100 Linear Feet of Dike

Height	Bags Required
1 foot	600
2 feet	2,000
3 feet	3,400

Stacking Sand Bags

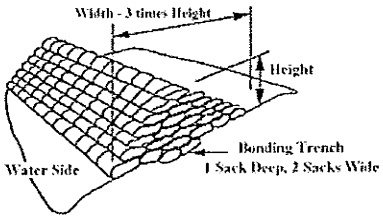

Sealing the Dike

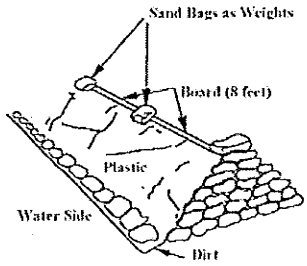

Disclaimer: This document provides only basic information that may be insufficient in addressing all your concerns about sandbag dike construction. We suggest you contact your local municipal authorities for additional information and guidance.

More Information

- City of Winnipeg: Building a Dike

Figure 2.2 – Manitoba Emergency Measures Organization Sandbag Dike Template. (after: http://www.gov.mb.ca/itm/emo/pubinfo/dyke.html).

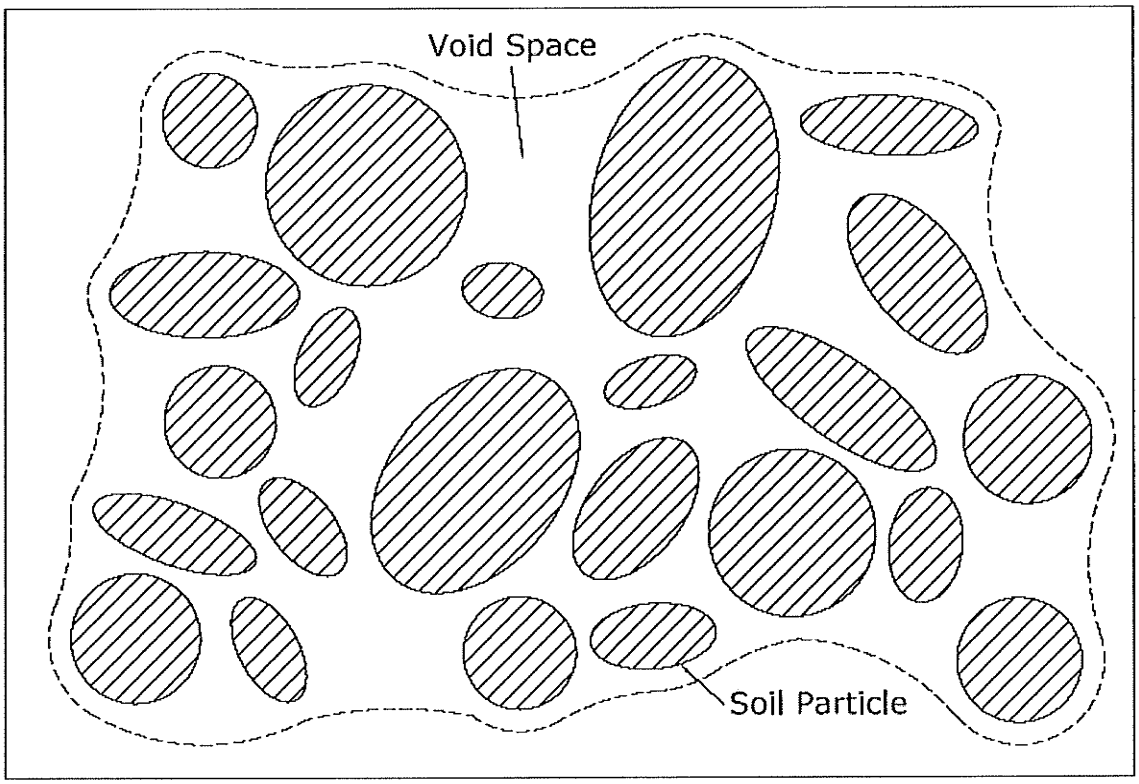

Soil Particles in a Loose Configuration

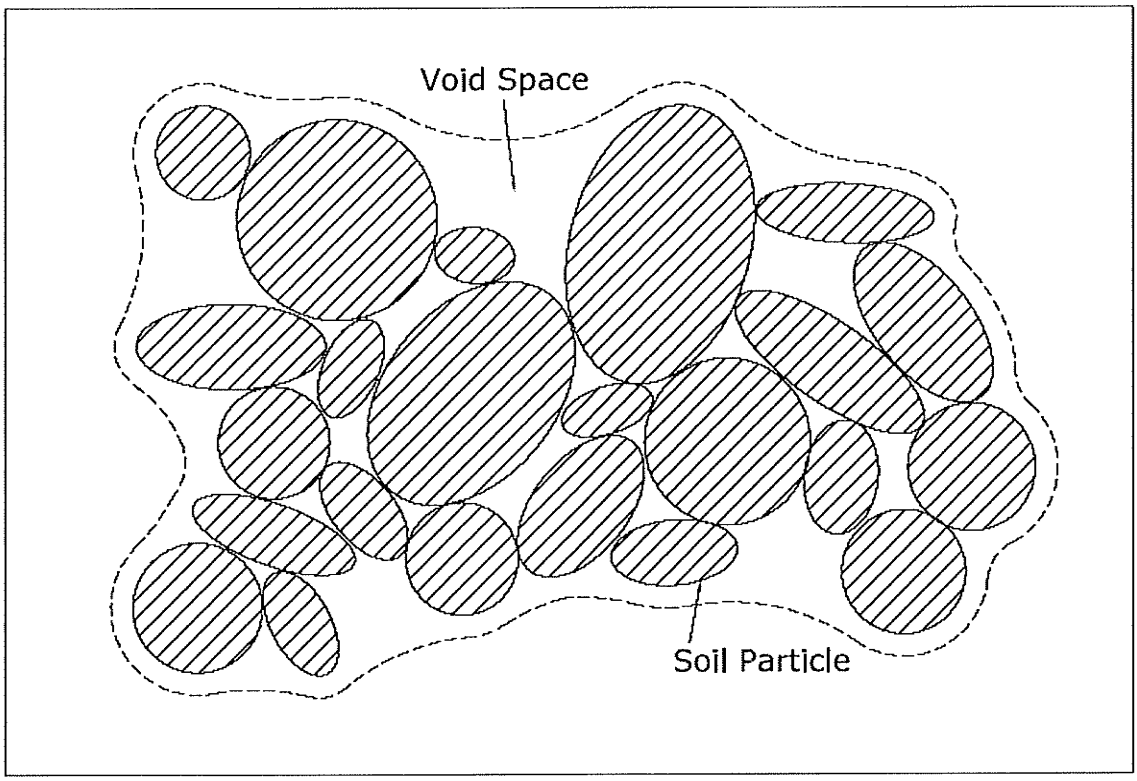

Soil Particles in a Compacted Configuration

Figure 2.3 – Cross-sections of Similar Soil Particles at Two Levels of Compaction.

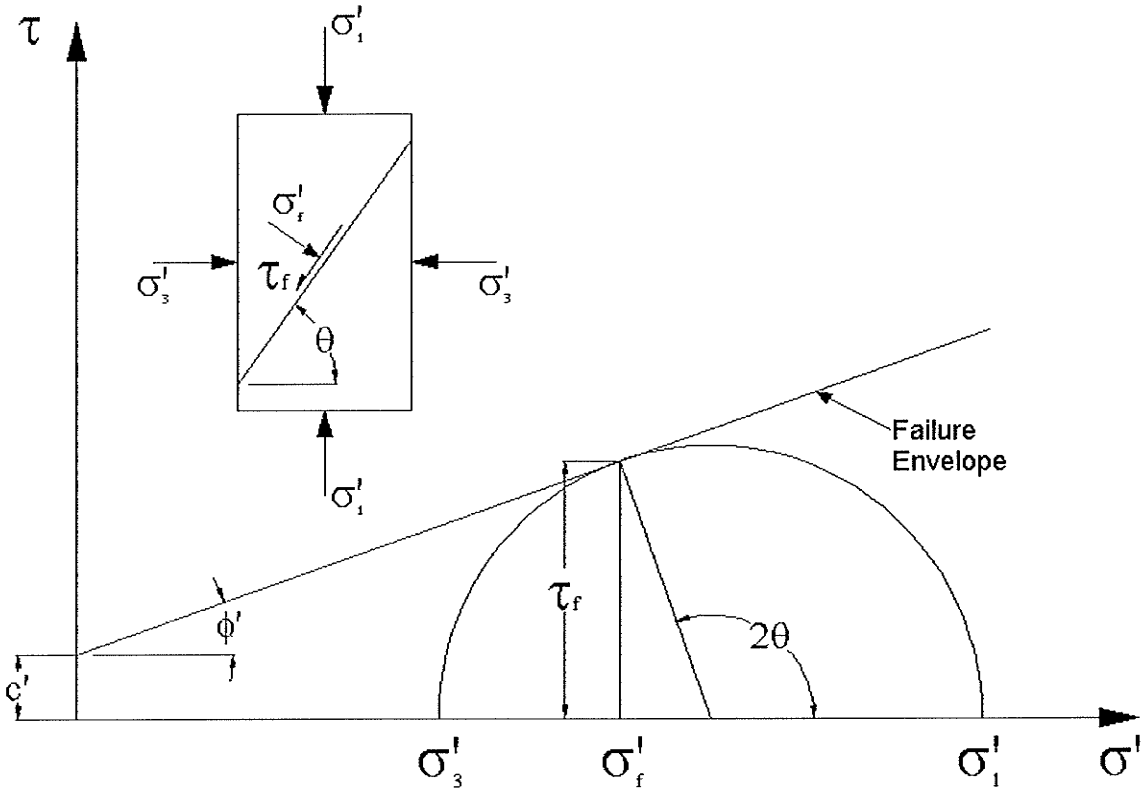

Figure 2.4 – Mohr-Coulomb Failure Envelope, after Craig (1998).

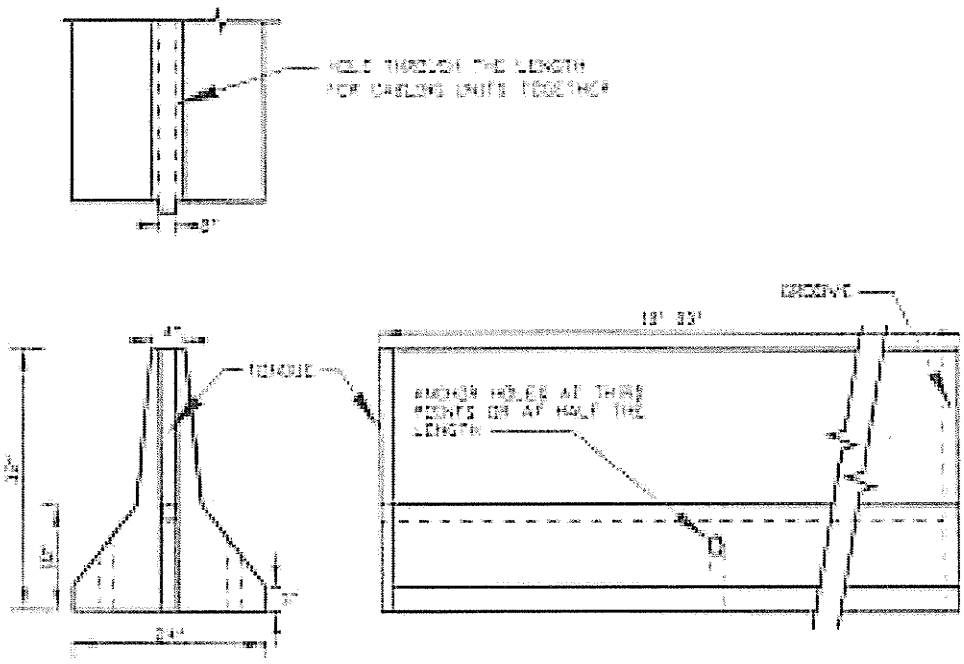

Single Jersey Barriers

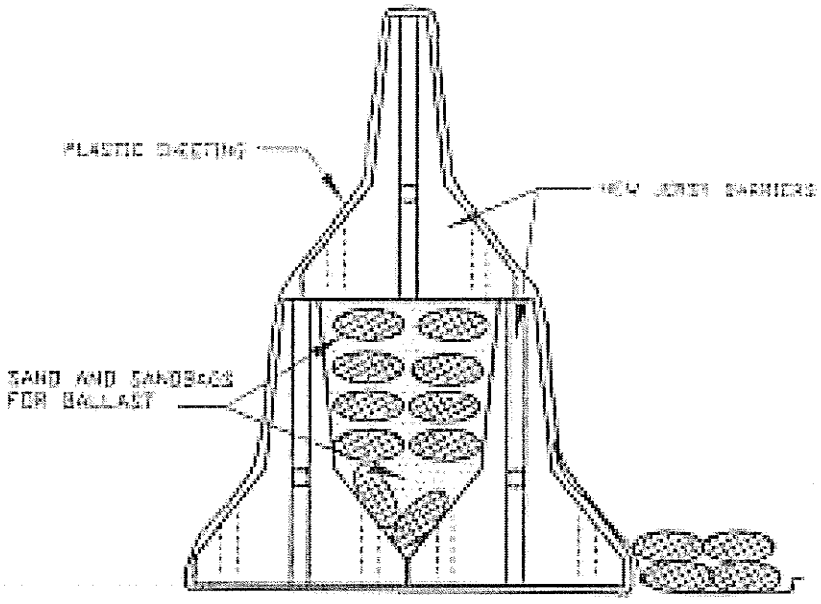

Stacked Jersey Barriers

Source: Turk and Torrey, Figs. 3-6 and 3-8

Figure 2.5 – Jersey Highway Barriers (after Duncan et al. p. 40)

Strong Points:

Can be emptied and reused
Portable
Very expedient if water and tube easily available
Double tube water barrier can be used to further reduce gradient at the factor of safety against sliding
Can be pumped with air and floated to site
Limited required manpower - 2 men can easily place
Works well on hard surfaces (concrete, asphalt)
Holes can be easily patched, even when filled with water
Interlocking collars for connecting adjacent sections (Aquabarrier)
Some systems have permanently attached seepage blanket (NOAQ)

Problems:

Expensive initial cost
May have anchoring problems on intermediate sections of the tube
Will not work on all saturated foundation soils
Weak seams have been a problem
Base width to height of retained water is large (~3)

Sketch:

Source: www.aquabarrier.com

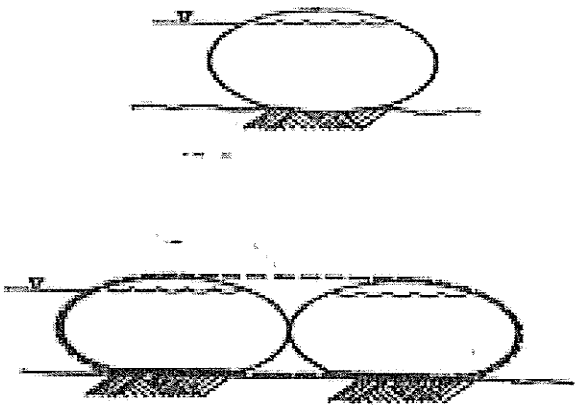

Single and Double Tube Water Barriers

Source: Turk and Torrey, Fig 3-10

Figure 2.6 – Water-filled Geomembrane Tubes (after Duncan et al. p.46)

Problems: Labor intensive and need on-site fill
Toppling can be an issue during filling due to its high height:base width ratio
Difficult to fill under saturated foundation soil conditions due to access required for construction equipment
Systems requiring filling with varying gradations of soil for a filtering action (Marine Cells) may be too complicated for average worker in a flood fight situation

Sketch:

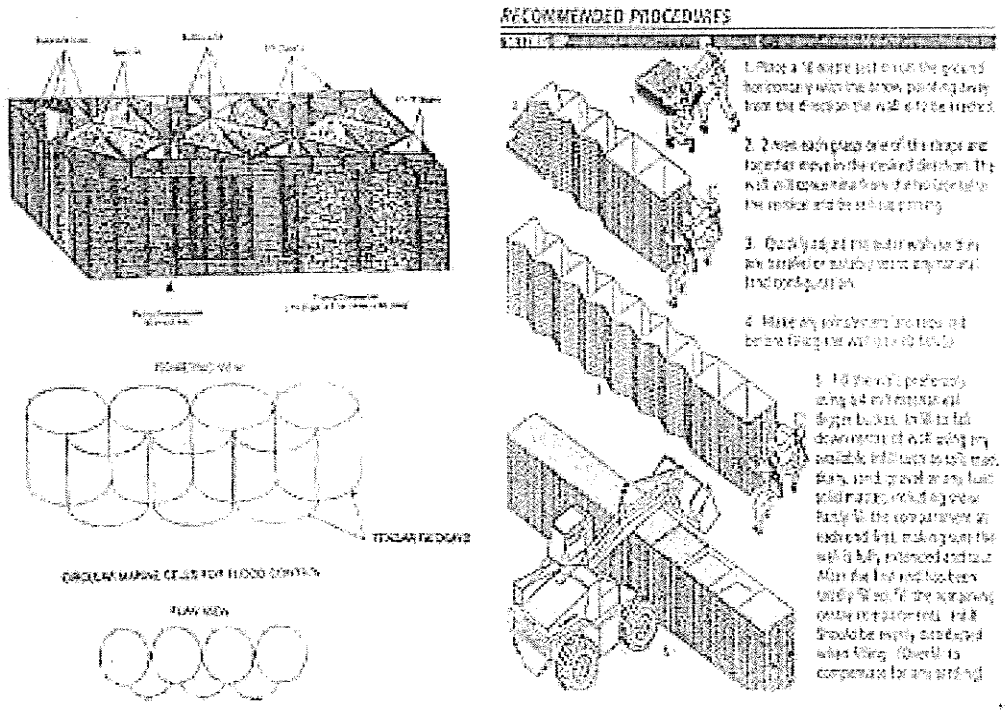

Marine Cells

Concertainer®

Source: Torrey and Davidson, Figs. 2-11 and 2-12

Figure 2.7 – Deep Cellular Confinement System (after Duncan et al. p. 30)

3 Characterisation and Laboratory Testing of Materials

3.1 Introduction

The laboratory testing component of this research project included in-isolation testing conducted at the University of Manitoba and the GeoEngineering Centre at Queen's-RMC in Kingston, Ontario. The testing examined the materials and interfaces present in sandbag dikes constructed according to the city of Winnipeg's 1997 template. The tests include interface shear, direct shear, grain-size analysis and a test of the densification of granular materials by wetting.

The interface and direct shear tests were conducted at both large- and bench-scales. Large-scale direct shear tests were conducted at the laboratories of Bathurst Clarabut Geotechnical Testing (BCGT) in cooperation with the GeoEngineering Centre at Queen's-RMC. The testing period was from June 9th to the 27th, 2003. These facilities were made available by Dr. Richard Bathurst, who also provided advice and expertise on test set-up and data analysis. The tests were supervised by Mr. Peter Clarabut, BCGT manager and the principal designer of the large-scale direct shear apparatus that was used. Figure 3.1 is a photograph of the large-scale direct shear apparatus at the BCGT laboratories.

The bench-scale direct shear tests were conducted at the University of Manitoba's geotechnical laboratories. The testing period was from October, 2003 to December, 2004. Figure 3.2 is a photograph of both of the bench-scale direct shear apparatus that were used along with their data acquisition systems.

Grain-size analysis and densification of granular material by wetting tests were conducted at the University of Manitoba's geotechnical laboratories.

3.2 Materials used in Sandbag Dikes Built in Winnipeg

Typical sandbags utilized by the City of Winnipeg are made up of woven slit film polypropylene (WSFPP) material sewn into bags and filled with granular sand. Polyethylene sheeting (PES) is incorporated as a flow barrier by weaving it in between the bags on the side of the dike nearest to the flood water. Dikes are constructed on the grass covered soil along riverbanks, parks and lawns in flood prone areas. The foundation is often snow and ice covered during spring flooding conditions in Manitoba; however this consideration has not been examined in this project.

3.2.1 Polyethylene Sheeting (PES)

There were two types of PES used in these tests. One was CGSB standard 6 mil vapour barrier polyethylene sheeting and the other was 'heavy-duty' polyethylene sheeting. Both are commonly available at building material supply stores, but the CGSB rated PES is manufactured to a published standard. It is guaranteed to be a minimum 6 mil in thickness, while the 'heavy-duty' PES is sold with no guaranteed consistency or minimum thickness. No appreciable difference in frictional characteristics between the two grades of PES was made evident in these tests.

3.2.2 Woven Slit Film Polypropylene (WSFPP)

The WSFPP bags used by the City of Winnipeg for sandbag dikes are purchased in bulk, usually in bundles of 1000. The current suppliers of these products are located in mainland China, and use several manufacturing plants to fill their orders. The bags are generally made out of ends and scraps left over from larger, more valuable textile products. This means that there is generally limited information and consistency of material properties available for these bags.

All of the bags used in the laboratory testing portion of this project were from the same batch and behaved in a relatively uniform manner in the shear devices. The 1 m^2 sheets used for the large-scale tests were obtained from the WSFPP used to bundle the bags for shipping. The local distributor for the City of Winnipeg's Public Works department indicated that it was common practice for the manufacturer to use the same materials for packaging in the case of products like sandbags. Visual inspection of samples taken from the bags and the packing WSFPP did not reveal any visual differences aside from overall dimension.

It is also common practice for the manufacturers to treat the WSFPP with a surfactant to reduce static electricity as a result of the rubbing that occurs during shipping and handling. Tests were conducted on the WSFPP both in its original (out of the bundle) condition, and after scrubbing the material to remove the surfactant.

3.2.3 Granular Material (Sand)

The granular material used in City of Winnipeg sandbag dikes is taken from a large esker deposit in the Bird's Hill area north-east of the city limits. For the purposes of this project it is assumed that this material is representative of the sand that is used in any given flood event.

The granular material used for the large-scale direct shear tests conducted for this research was supplied by the Royal Military College (RMC). Two types of sand used for testing at RMC were considered; 'sweet' sand and 'medium' sand.

The granular material used in the bench-scale direct shear tests conducted for this research was from the Bird's Hill deposit. It was supplied by the City of Winnipeg public works department, taken from their supply piles.

3.2.3.1 Grain-size Analysis of Granular Material

Sieve tests were conducted on two types of RMC sand and the Bird's Hill sand for comparison of their grain-size distributions. Figure 3.3 is a summary of the sieve tests. The grain size analysis tests were conducted in general accordance with ASTM D 422 – 63 (1998). The results of the grain-size distribution analysis of the three sands were compared to determine which of the RMC sands were most appropriate for the shear and interface friction testing in the large-scale direct shear box.

Based on the comparison of the sieve tests, the RMC sweet sand was chosen for the large-scale direct shear testing. The sweet sand has a broader grain-size distribution, the upper and lower bounds encompassing the grain-size distribution of the Bird's Hill sand.

3.2.3.2 Densification of Granular Material by Wetting

Tests were conducted on Bird's Hill sand to measure changes to volume and density caused by wetting of samples of granular material having an initially known volume and density. This is of special significance with respect to sandbag structures built as temporary flood protection. These structures are built without heavy equipment, and are only subject to the compactive effort of the people carrying and placing the sandbags. As temporary flood protection, the principal load placed on the structures is hydrostatic. This load is generally applied from one side at a relatively slow rate and then held for a time before slowly dropping off. The total loading period may be up to four weeks, and the structure is likely to experience some precipitation during this time as well.

The loss of available freeboard in sandbag structures during loading has been observed in the field during flood events before and including 1997. This has often been attributed to changes or inaccuracies in flood elevation predictions. However, measurements and

observations made during the full-scale testing program of this research indicate that densification by wetting is a major cause of height loss in sandbag structures. This loss of height results in the loss of the available freeboard which is necessary to keep the dikes stable and reliable under wind and debris loading.

The effect of densification by wetting on full-scale sandbag structures is outlined in chapter 5 of this thesis. The following section of this chapter is a description of the bench-scale test devised to quantify the effects of densification by wetting on a volume of sand with a known initial density.

3.2.3.2.1 Test set-up and Apparatus

The test consisted of partially filling a 5 gallon plastic pail with sand by pouring it from a known height. The weight of the sand was measured immediately after pouring, taking care not to reduce the volume by vibrating or bumping the container. The volume of the sand in the container was measured by reading the depth from the top of the container to the sand at thirteen separate points, using a template to insure a consistent pattern and distribution of measurement points. Holes were drilled in the bottom of the pail to ensure free draining conditions for the tests. A piece of WSFPP was cut to fit into the bottom of the pail to prevent grains of sand from falling through the holes. Figure 3.4 is a photograph of the test apparatus and set-up, and Figure 3.5 is a photograph of the template used to keep the measurements consistent.

The heights used for pouring the sand were between 77 cm and 151 cm. This resulted in different initial densities for comparable volumes of sand. The first test was conducted without smoothing the surface of the sand after pouring. Measurements to the top of the sand were made from the top of the pail at 10 locations, but these locations were randomly chosen and could not be exactly replicated. The disparity between each of the

initial measurements lead to the implementation of a plywood template fitted over the top of the pail. The template had 13 marked measuring locations in order to improve repeatability. In the four subsequent tests the dry (ambient humidity of lab) sand was also smoothed gently to ensure a more level surface for the measurements. This combination of smoothing and the use of the template explain the differences in densification values measured in trial one compared with trials 2 through 5.

After measuring the weight and volume of the sand, it was wetted until ponding of one centimetre occurred over the highest point in the pail. The wetting was accomplished using a common garden watering can held so that the water was sprayed gently over the entire surface of the sand in the pail until the sand was completely saturated with 1 cm of water ponding on top. The watering can was consistently held at a height of 50 cm above the surface of the sand. This was done to both minimize and regulate the amount of densification occurring due to the initial impact of the water falling on the sand so that this factor was constant between each test.

The water was allowed to drain freely until no more was observed coming out of the holes in the bottom of the pail. The height of the sand in the pail was then recorded.

3.2.3.2.2 Summary of Densification of Granular Material by Wetting

Table 3.1 is a summary of the test data gathered in the densification tests. Figure 3.6 is

Table 3.1 – Densification of Sand by Wetting Data Summary

Test	Height of Pouring (cm)	H_i	H_f	ΔVolume (%)	ΔDensity (%)
1*	97 to 107	10.6	9.7	-9.2	10.1
2	77 to 87	7.8	7.5	-3.8	4.0
3	77 to 87	11.1	10.7	-4.2	4.4
4	139 to 151	10.5	10.2	-2.7	2.8
5	97 to 107	9.3	8.9	-4.7	5.0

* No smoothing or template were used in the first test

a plot of the change in density after wetting against the height that the sand was poured from in tests 2 through 5.

3.2.4 Sod

There are a large variety of plants and grasses present where sandbag dikes are built in the Red River valley. In the interests of simplicity, Kentucky blue-grass sod was chosen for the large-scale direct shear tests conducted for this research. This is believed to be the most common variety of sod found locally.

3.3 Direct-Shear Experimental Program

The sandbag dike cross-section detailed in Figure 1 includes a total of six distinct material interfaces; PES on PES, WSFPP on PES, WSFPP on WSFPP, WSFPP on sand, PES on sod and WSFPP on sod. A testing program to investigate the behaviour of these interfaces was implemented using both a large- and bench-scale direct shear apparatus. The large-scale direct shear apparatus allowed the testing of interfaces that are best described as exhibiting discrete block behaviour, such as the interface between filled sandbags and sod, as well as filled sandbags on filled sandbags. The bench-scale direct shear apparatus allowed testing of saturated material interfaces. A comparison of duplicate tests on interfaces at both scales is presented, along with summaries of both sets of tests.

3.3.1 Large-scale Direct Shear

One of the limitations in the use of traditional bench-scale direct shear apparatus is the domination of boundary effects on the data that is produced. This effect is reduced significantly by increasing the size of the direct shear apparatus. Another result of increasing the size of the direct shear apparatus is the capacity to test interfaces that are more than two-dimensional. These are typical in sandbag dike structures, and their

behaviour can be described as discrete blocks moving against each other. Each surface of the interfaces in the dikes can be tested in two dimensions using a direct shear apparatus, but use of the large-scale direct shear allows the testing of full-scale sandbags as well as surfaces with varying depth, such as sod.

3.3.1.1 *Equipment Description and Calibration*

The large-scale direct shear test apparatus used for the testing is a custom built device equipped with a 1 m^3 shear box that can be separated into four equal sections of 250 cm in height, each with a plan view cross-sectional area of 1 m^2. The principal shear plane was located at the 500 cm mark, as shown in Figure 3.7.

The apparatus is mobile so that it can be transported and used on-site. It is linked to a custom data acquisition system to control and monitor the normal stress, horizontal loading, vertical displacement, and horizontal displacement. The horizontal load and stroke is provided by a 222 kN hydraulic actuator. Figure 3.8 is a photograph of the normal loading platen in the upper half of the shear box of the apparatus.

To determine the basic friction angle and cohesion intercept of the large-scale direct shear box in the BCGT lab, several tests were conducted at known normal stresses with no additional shear resistance. The cohesion intercept and friction angle determined from these tests is presented in Figure 3.9. At the time when these tests were conducted, the equipment was quite new and a calibration of the linear variable differential transformers (lvdt) and the load cells had recently been completed in May of 2003. Due to time constraints, a verification calibration could not be conducted during the testing period from June 9th to the 27th. However, the apparatus was used extensively during the summer and the results of the next calibration conducted by

BCGT personnel following these tests confirmed the accuracy of the data presented here.

3.3.1.2 *Material Support & Interface Location*

This was the first time interface friction tests were conducted using this particular equipment. The bulk of the volume of the bottom shear box was taken up by constructing a crib out of 4 inch by 4 inch (89 mm by 89 mm nominal cross-section) dimensional lumber cut into 37.5 inch (95cm) lengths. Figure 3.10 is a photograph of the crib material, layout and orientation in the bottom shear box of the large-scale direct shear apparatus.

Sheets of 16 mm and 24 mm thick plywood were employed to hold the test materials. They were cut to just under 100cm square in order to fit into the shear box with minimal room to move horizontally. A minimum of three sheets were used for both the top and bottom interface supports to ensure that the interface remained relatively flat and continuous during tests. Figure 3.11 is a photograph of the plywood and test materials at the interface location in the large-scale direct shear apparatus. Sheet metal flashing of 1 mm nominal thickness was used as shim material to adjust the interface location so that it was appropriate for each normal stress applied.

The sheet materials tested (PES and WSFPP) were cut into 47.25 inch by 47.25 inch (1.2 m by 1.2 m) squares which were then trimmed at the corners and folded over the top of a designated plywood sheet and stapled onto the back of that sheet. Figure 3.12 is a photograph of the PES being attached to the plywood support sheet.

The discrete block interfaces tested were filled sandbags on sod and filled sandbags on filled sandbags. A sheet of plywood was customized to accept the sod by installing deck

screws in a 4" (100 mm) grid pattern, leaving the top ¼" (6 mm) of the screw head protruding from the sheet to hold the soil at the base of the sod. Figure 3.13 is a photograph of the sod in the bottom of the large-scale direct shear apparatus before a test. Figure 3.14 is a photograph of filled sandbags on sod with the top half of the large-scale direct shear box removed after shearing.

3.3.1.3 Normal Load Range and Shear Rate

The normal loads used for this research were selected based on a range of sandbag dike sizes used in previous flood protection efforts in the Red River Valley. The range of dike heights tested at full scale in this research program is from 6 to 10 feet (1.83 m to 3.05 m) at two foot (0.61 m) increments. To calculate the normal load range for the laboratory testing, we used a minimum dike height of 4 feet (1.22 m) and a maximum of 14 feet (4.27 m). The pressure at the bottom of the bags, calculated at the centre of the dike, using an estimated saturated weight for sand and bags of 20 kN/m^3, is 24.4 kPa for the smaller and 85.3 kPa for the larger dike.

Based on these calculations, a normal load range of 25 to 125 kPa was selected in order to bracket the range of operating normal stresses. Each set of the direct shear tests were conducted at three normal stresses; namely 25, 75 and 125 kPa.

A shear rate of 5 mm/min was used in the large-scale direct shear testing, which resulted in test durations of 1 hour to achieve 300 mm of horizontal displacement. As specified by ASTM D 3080, this is sufficiently slow to ensure that excess pore pressures are dissipated in cases where the sand was saturated. For consistency, this rate was used for all tests in this apparatus.

3.3.1.4 Testing Matrix

Table 3.2 outlines the test matrix for all interfaces and materials investigated using direct shear apparatus. The shaded cells marked with 'L' represent interfaces that were only tested in the large-scale direct shear apparatus. The shaded cells marked 'B & L' represent interfaces that were tested in both the large- and bench- scale direct shear apparatus.

Table 3.2 – Large-scale Direct Shear Testing Matrix

Test Materials	Dry PES	Dry WSFPP	Sand	Sat. PES	Sat. WSFPP	Scrubbed WSFPP	Sod	Filled Sandbags
Dry PES	B & L	B & L	B				L	
Dry WSFPP	B & L	B & L	B & L				L	
Sand	B	B & L	B					
Sat. PES				B	B	B		
Sat. WSFPP				B	B			
Scrubbed WSFPP				B		B		
Sod	L	L						L
Filled Sandbags							L	L

3.3.1.5 Plots of Test Data

The data gathered using the large-scale direct shear apparatus consists of horizontal and vertical load, as well as horizontal and vertical displacement. The horizontal (shear) and vertical (normal) loads are measured with load cells attached to the hydraulic rams that apply the force directly to the bottom half of the shear box and the top loading platen, respectively.

The raw load and displacement data are converted to stress and strain units following testing. Conversion from a load (force) unit to a stress (force/area) unit is accomplished by dividing the measured load by the area to which it is applied. In the case of the large-scale direct shear apparatus, the area is 1.0 m^2, so the load data can be read directly as a stress in kilo-Pascals (kPa). The displacement units (mm) can be converted to horizontal strains (%) by dividing the displacement at any given time in the test by the initial horizontal dimension of the specimen (mm/mm).

Figures 3.15 through 3.22 are plots of the direct shear stresses against horizontal strains at all of the applied normal stresses for each of the interfaces tested in the large-scale direct shear apparatus. The peak strain values at each normal stress chosen for analysis are indicated with arrows.

3.3.2 Bench-Scale Direct Shear

Bench-scale testing was carried out in order to compare the results of the large-scale direct shear tests with results from traditionally scaled apparatus. In addition to the set of comparison tests, saturated tests and tests on scrubbed WSFPP were conducted at the bench-scale.

3.3.2.1 Equipment Description & Calibration

The bench-scale direct shear apparatus used for these tests are Wykeham-Farrance units located in the University of Manitoba's geotechnical laboratories. The units are labelled DS #1 and DS #2. Both of these systems are driven by an electric motor through a gear-box and worm-gear driveshaft that allows a broad range of choices for strain rate. They are equipped with a load cell capable of measuring both tensile and compressive forces and two lvdts for horizontal and vertical displacements respectively.

The lvdts on these units are regularly calibrated for range and accuracy by checking their voltage output against displacements set by a standard gauge kit. The load cell is similarly tested for range and accuracy by checking its voltage output when known weights are applied. These instruments were calibrated before and after the bench-scale tests to ensure the accuracy of the data throughout the tests.

3.3.2.2 *Material Support & Interface Location*

The shear box used for this testing with the Wykeham-Farrance units is 60 mm square in plan, and divided into 25 mm halves. As with the large-scale apparatus, plywood was used to support the PES and WSFPP inside the shear box. The smaller scale of the bench-scale apparatus in comparison with the large-scale allowed the use of 6 mm nominal thickness plywood, cut into 59 mm x 59 mm squares. Shim materials used to provide the correct interface height were lexan, melamine, metal mesh and construction paper.

3.3.2.3 *Normal Load Range and Shear Rate*

The normal load range used for the bench-scale direct shear interface testing in this research is the same as the range used in the large-scale tests. Each interface was tested at 25, 75 and 125 kPa.

The shear rate for the bench-scale tests was scaled to correspond to the rate used in the large-scale tests. Converting the large-scale apparatus shear rate of 5 mm/min from displacement per time to shear strain per time yields 1.67 %/min. For the 60 mm bench-scale shear box, using this shear strain per time means a displacement per time rate of 0.30 mm/min. Values as close to that based on set gear selections available were used in the bench-scale tests.

3.3.2.4 Testing Matrix

Table 3.3 is the test matrix for interfaces investigated using the bench-scale shear apparatus. The shaded cells marked with 'B' represent interfaces that were only tested in the bench-scale direct shear apparatus. The shaded cells marked 'B & L' represent interfaces that were tested in both the large- and bench- scale direct shear apparatus.

Table 3.3 – Bench-scale Direct Shear Testing Matrix

Test Materials	Dry PES	Dry WSFPP	Sand	Sat. PES	Sat. WSFPP	Scrubbed WSFPP	Sod	Filled Sandbags
Dry PES	B & L	B & L	B				L	
Dry WSFPP	B & L	B & L	B & L				L	
Sand	B	B & L	B					
Sat. PES				B	B	B		
Sat. WSFPP				B	B			
Scrubbed WSFPP				B		B		
Sod	L	L						L
Filled Sandbags							L	L

3.3.2.5 Plots of Test Data

The data gathered using the bench-scale direct shear apparatus consists of horizontal (shear) load, as well as horizontal and vertical displacement. The horizontal load is measured with a load cell attached to the drive shaft that applies the force directly to the bottom half of the shear box by maintaining a constant displacement rate. The displacement rate is set by a variety of gears and motor speeds, as mentioned in 3.3.2.1.

Figures 3.23 through 3.33 are plots of the direct shear stresses against horizontal strains at all of the applied normal stresses for each of the interfaces tested in the bench-scale direct shear apparatus. The peak strain values at each normal stress chosen for analysis are indicated with arrows.

3.4 Interface Shear Data Analysis

The stress-strain data from the large-scale and bench-scale direct shear testing was analysed in order to produce a range of Mohr-Coulomb strength parameters for each interface tested. The parameters are a c' value in kPa, representing adhesion, or apparent cohesion intercept, and a ϕ' value in degrees, representing a friction angle or angle of shearing resistance. The parameters are determined by performing a linear regression through a set of three interface shear stresses, one for each normal stress tested. The ϕ' value is the angle of the slope of the linear regression and the c' value is the positive y-axis intercept from the regression. In cases where the y-axis intercept was negative, the regression was forced through the origin and the c' value becomes 0. The range of parameters for each interface includes values for peak, upper residual and lower residual shear strength.

3.4.1 Shear and Normal Stress Data Analysis

The stress-strain plots for each interface were examined in the light of field observations of the deformations and displacements of actual sandbag dikes under flood conditions in order to determine the appropriate strain level to use for analysis. The peak shear strength values were taken from the strain range from 0 to 3%. In most cases an obvious peak value was apparent on the plot, often in the 1 to 1 ½% strain range. The upper and lower residual strength values were taken from the strain range between 3 and 30%. For design purposes, the peak shear strength parameters are the most relevant, since

strains above 3% are likely to be accompanied by deformations leading to catastrophic failures in sandbag structures in flood conditions. However, it is useful for designers to have upper and lower residual shear strength values to compare with the peak values for each interface as an indication of which interface is critical and whether a different interface will become critical under higher strains.

The normal stress versus peak shear stress plots for the large-scale interface shear tests are presented in figures 3.34 through 3.42. The normal stress versus upper residual shear stress plots for the large-scale interface shear tests are presented in figures 3.43 through 3.49. The normal stress versus lower residual shear stress plots for the large-scale interface shear tests are presented in figures 3.50 through 3.57. The c', ϕ' and r^2 values from the linear regression are shown on each plot. Summary plots for each set of interface shear strength values are presented in figures 3.58 through 3.60.

The normal stress versus peak shear stress plots for the bench-scale interface shear tests are presented in figures 3.61 through 3.71. The normal stress versus upper residual shear stress plots for the bench-scale interface shear tests are presented in figures 3.72 through 3.82. The normal stress versus lower residual shear stress plots for the bench-scale interface shear tests are presented in figures 3.83 through 3.93. The c', ϕ' and r^2 values from the linear regression are shown on each plot. Summary plots for each set of interface shear strength values are presented in figures 3.94 through 3.96.

3.4.2 Mohr-Coulomb Interface Shear Parameter Summary

Table 3.4 is a summary of the Mohr-Coulomb interface shear parameters for the interfaces tested in the large-scale direct shear apparatus. The shaded cells represent interface shear tests that were conducted at both large- and bench-scales and are directly comparable.

Table 3.4 – Mohr-Coulomb Parameter Summary for Large-Scale Direct Shear Tests						
Interface Tested	Peak Shear Stress		Upper Residual Shear Stress		Lower Residual Shear Stress	
	c' (kPa)	ϕ' (°)	c' (kPa)	ϕ' (°)	c' (kPa)	ϕ' (°)
Dry HD PES on PES	0	16	3	16	3	14
Dry HD PES on WSFPP	4	15	3	13	3	12
Dry WSFPP on WSFPP	2	19	3	18	3	16
Dry RMC Sand on WSFPP	3	26	9	25	8	24
Dry HD PES on Sod	3	14	2	18	3	17
Dry WSFPP on Sod	5	21	6	26	8	23
Dry Sandbags on Sod	5	22	10	28	8	27
Dry Sandbags on Sandbags	6	25	11	34	8	33

Table 3.5 is a summary of the Mohr-Coulomb interface shear parameters for the interfaces tested in the bench-scale direct shear apparatus. Again, the shaded cells represent interface shear tests that were conducted at both large- and bench-scales and are directly comparable.

Table 3.5 – Mohr-Coulomb Parameter Summary for Bench-Scale Direct Shear Tests						
Interface Tested	Peak Shear Stress		Upper Residual Shear Stress		Lower Residual Shear Stress	
	c' (kPa)	ϕ' (°)	c' (kPa)	ϕ' (°)	c' (kPa)	ϕ' (°)
Dry CGSB PES on PES	0	10	2	8	1	8
Dry HD PES on PES	0	13	0	10	0	8
Dry CGSB PES on WSFPP	3	14	3	11	1	11
Dry WSFPP on WSFPP	0	18	5	19	3	17
Dry BH Sand on WSFPP	0	37	3	34	3	32
Dry BH Sand on CGSB PES	10	25	9	20	6	15
Saturated CGSB PES on PES	0	12	0	11	0	10
Saturated CGSB PES on WSFPP	1	10	1	11	0	10
Saturated WSFPP on WSFPP	0	21	1	25	3	18
Scrubbed WSFPP on CGSB	5	7	3	8	1	8

PES						
Scrubbed WSFPP on WSFPP	0	24	3	17	2	17

3.4.2.1 Comparison of Large- and Bench-Scale Mohr-Coulomb Parameters

The Mohr-Coulomb parameters for the three sheet material interfaces calculated from peak shear stresses in the bench-scale apparatus are noticeably lower than those calculated from the peak shear stresses measured in the large-scale apparatus. These are the interfaces between PES and PES, WSFPP and PES and WSFPP and WSFPP. However, for the interface between WSFPP and granular material, the bench-scale tests gave significantly higher values than the large-scale tests.

In both cases the impact of boundary conditions are the most likely cause of the differences between the two test scales. The bench-scale direct shear apparatus has a perimeter to surface area ratio of 24.4 cm to 37.21 cm^2, or 0.66 cm^{-1}. The large-scale direct shear apparatus has a perimeter to surface area ratio of 400 cm to 10,000 cm^2, or 0.04 cm^{-1}. The result of the higher ratio for the bench-scale tests is to under-represent the interface between sheet materials by minimising contact area and to over-represent the strength of granular materials by providing a relatively long perimeter for grains to lodge and stick. The reverse is true for the large-scale apparatus.

The over-estimation of shear strength for the sand on WSFPP interface in the bench-scale tests is of significance because this is the information most likely to be used by designers as bulk shear strength values for sandbag structures. The under-estimation of the sheet material interface shear strength by the bench-scale tests is also significant as it emphasizes effects of scale in the interpretation of direct-shear test results.

3.4.2.2 Sandbag and Sod Interface Mohr-Coulomb Parameters

The ability to test interfaces with greater depth in the large-scale direct shear apparatus provided insight into the importance of both the base conditions in a sandbag structure as well as the discrete block behaviour of the sandbags moving against themselves within these structures.

The interfaces between the sheet materials and the sod reveal that the PES is weaker of the two in terms of frictional resistance. Throughout the entire strain range tested, the WSFPP is stronger against itself than it is against sod.

The shear strengths measured in the interface test between filled sandbags and sod were higher than between WSFPP in a sheet and sod, but lower than between WSFPP in a sheet and sand. The interface between filled sandbags and filled sandbags was comparable in strength to the interface between sheet WSFPP and sand at peak shear stresses. However, at larger strains the sandbag on sandbag interface shear strength increased, which is due to the tendency of the sandbags to shift and bind against each other as they undergo increasing strains.

3.4.2.3 Saturated and Scrubbed WSFPP Mohr-Coulomb Parameters

Due to time constraints, two effects not tested in the large-scale direct shear apparatus were saturation of the interfaces with water and the roughening of the WSFPP and removal of the surfactant applied to the WSFPP by the manufacturer. These effects were investigated on the PES-WSFPP and WSFPP-WSFPP interfaces in the bench-scale direct shear apparatus.

The saturated PES on PES interface showed an increase in frictional strength over the dry PES on PES interface, as did the saturated WSFPP on WSFPP interface. The

saturated PES on WSFPP interface was significantly weaker than its dry counterpart. The scrubbed WSFPP was stronger against itself than both the saturated and dry intact WSFPP, but considerably weaker against PES.

3.4.2.4 Ranking the Shear Strengths of the Interfaces in Sandbag Structures

Table 3.6 presents the six distinct interfaces present in sandbag dikes that were listed at the beginning of this chapter in order of increasing frictional strength as measured using Mohr-Coulomb interface shear parameters.

Table 3.6 – Rank of Interface Shear Strengths present in Sandbag Structures

Interface	Rank	
PES on WSFPP	1	lowest strength
PES on PES	2	
PES on Sod	3	
WSFPP on Sod	4	
WSFPP on WSFPP	5	
WSFPP on Sand	6	highest strength

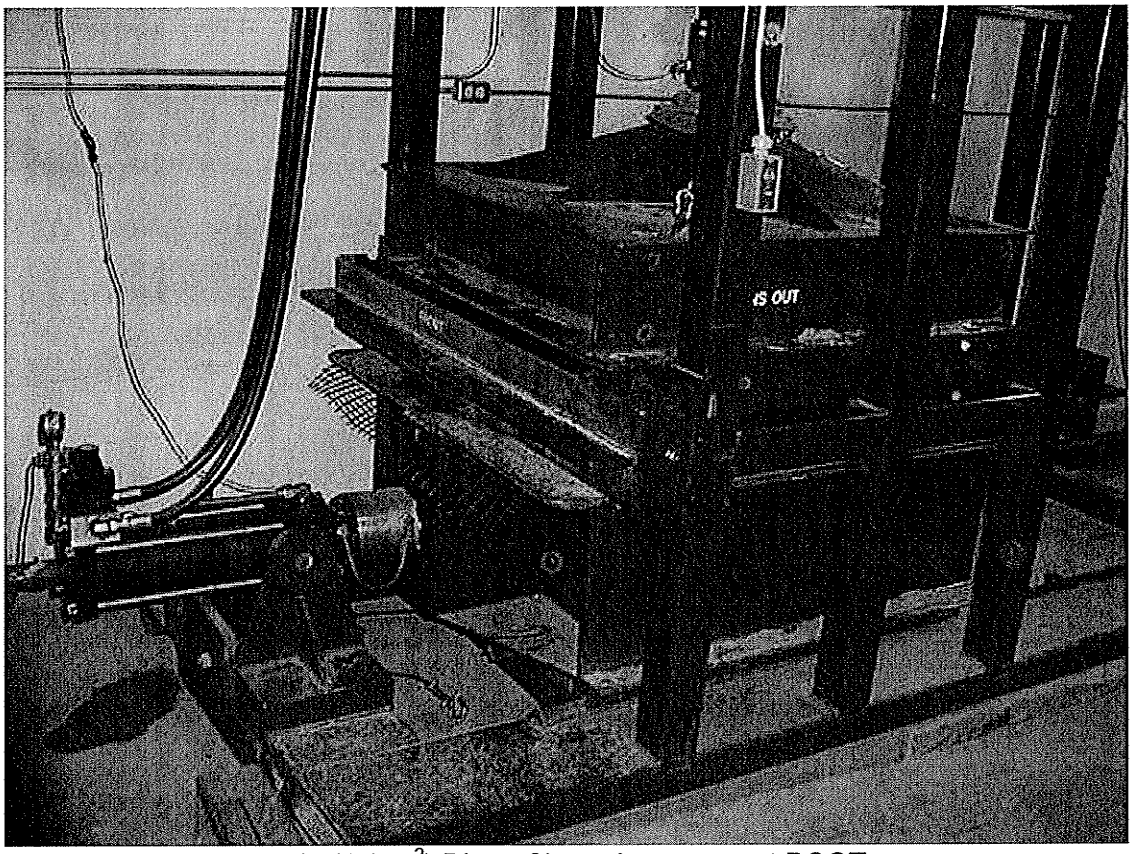

Figure 3.1 – Large-scale (1.0 m^2) Direct Shear Apparatus at BCGT.

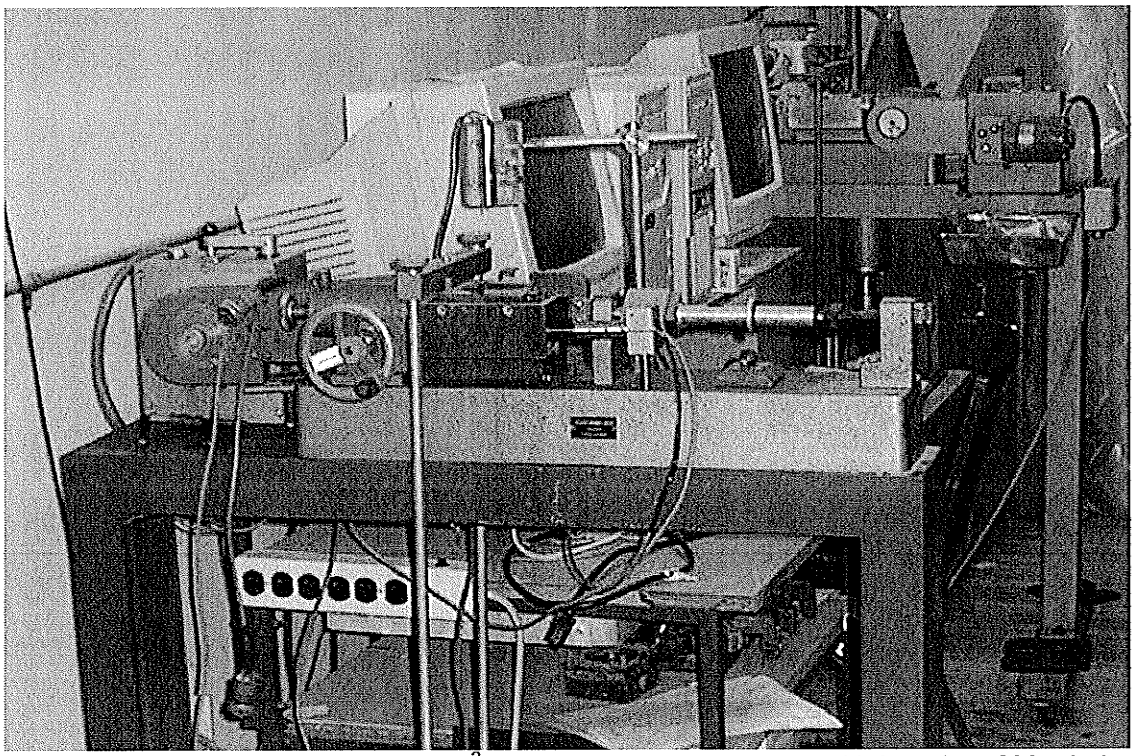

Figure 3.2 – Bench-scale (0.0035 m^2) Direct Shear Apparatus at University of Manitoba.

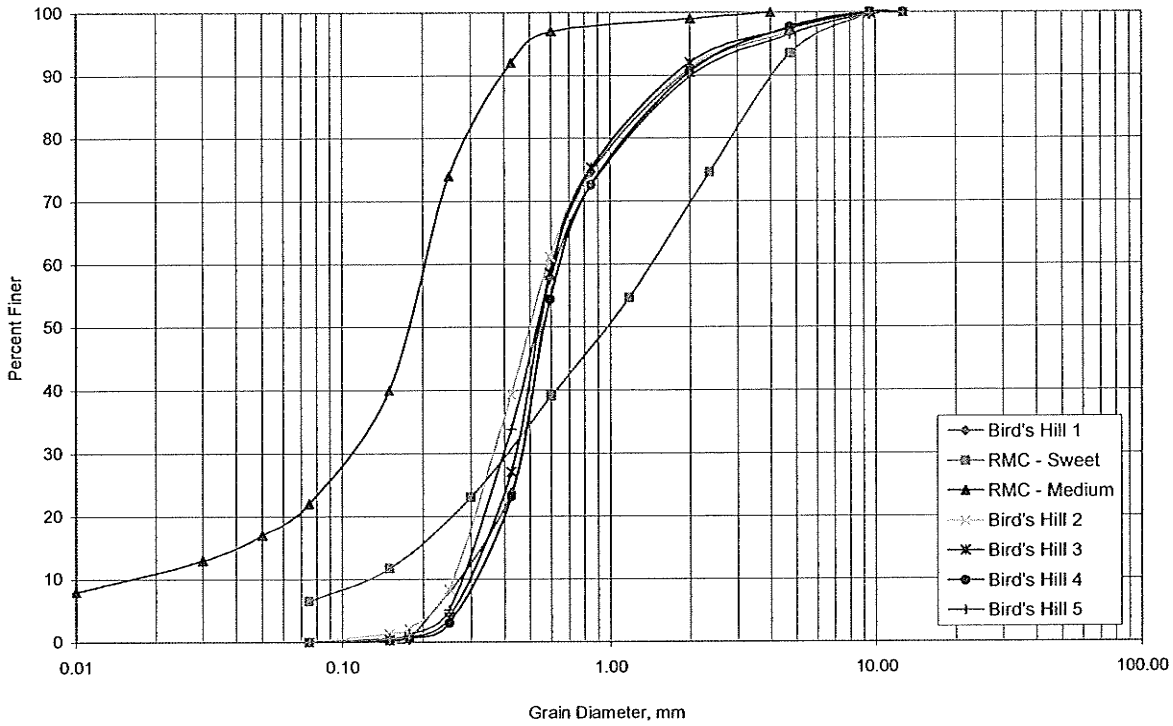

Figure 3.3 – Grain-size Distribution Curves for RMC and Bird's Hill Sands.

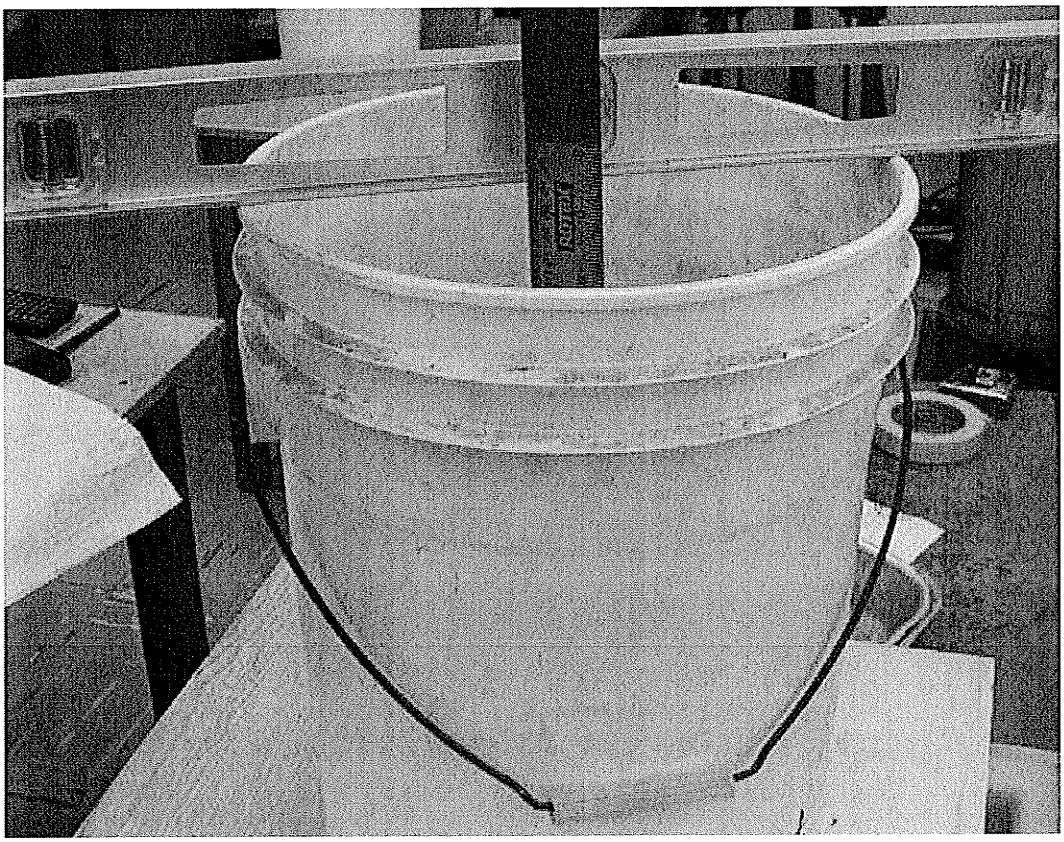

Figure 3.4 – Densification of Granular Materials due to Wetting Test Apparatus.

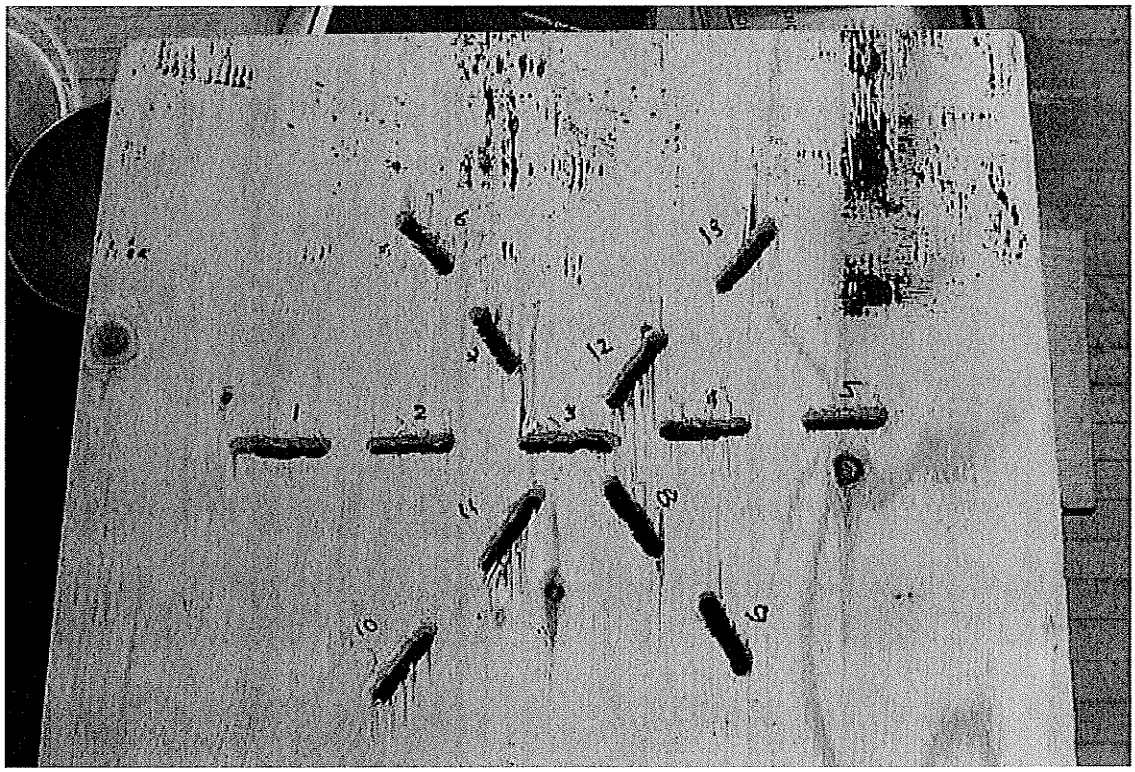

Figure 3.5 – Plywood Template for Consistent Measurement of Distance to Sand.

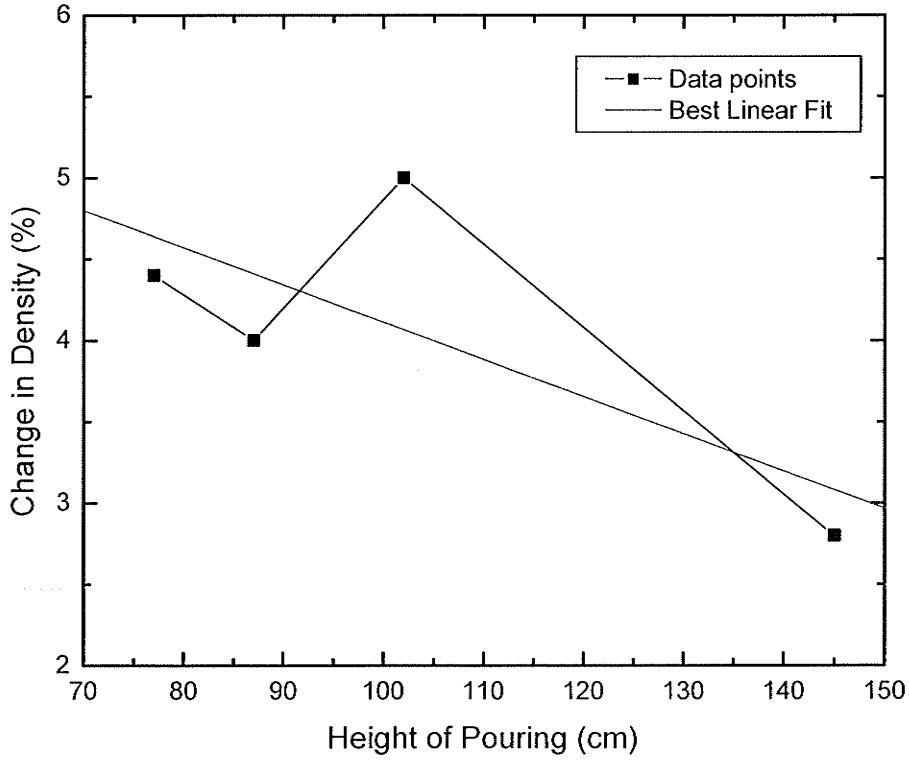

Figure 3.6 – Plot of Change in Density Against the Height of Pouring in the Densification by Wetting Tests.

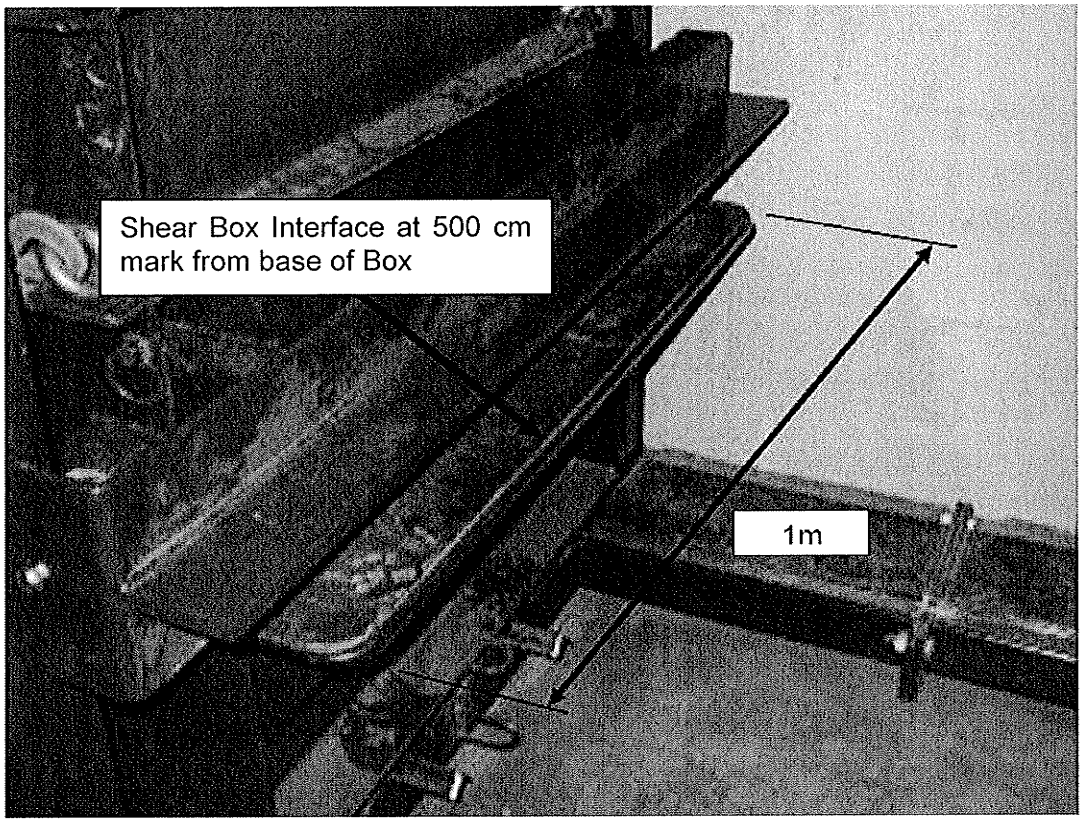

Figure 3.7 – Interface Location on Large-scale Direct Shear Apparatus.

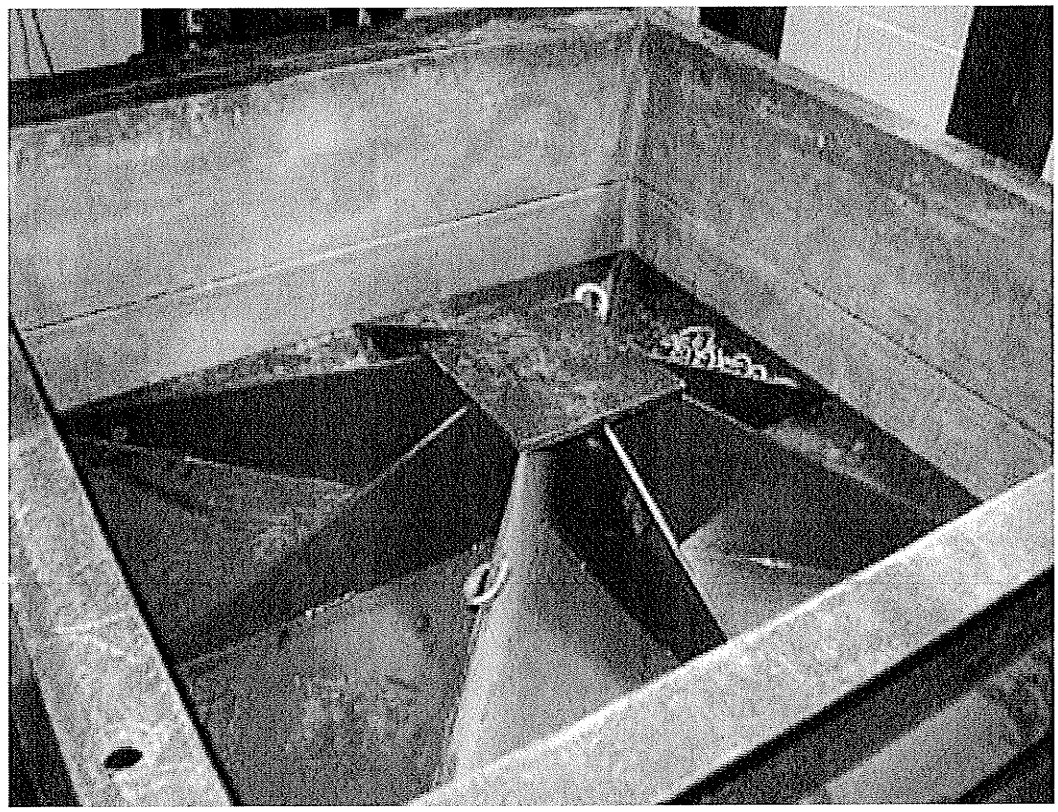

Figure 3.8 – Normal Loading Platen on Large-scale Direct Shear Apparatus.

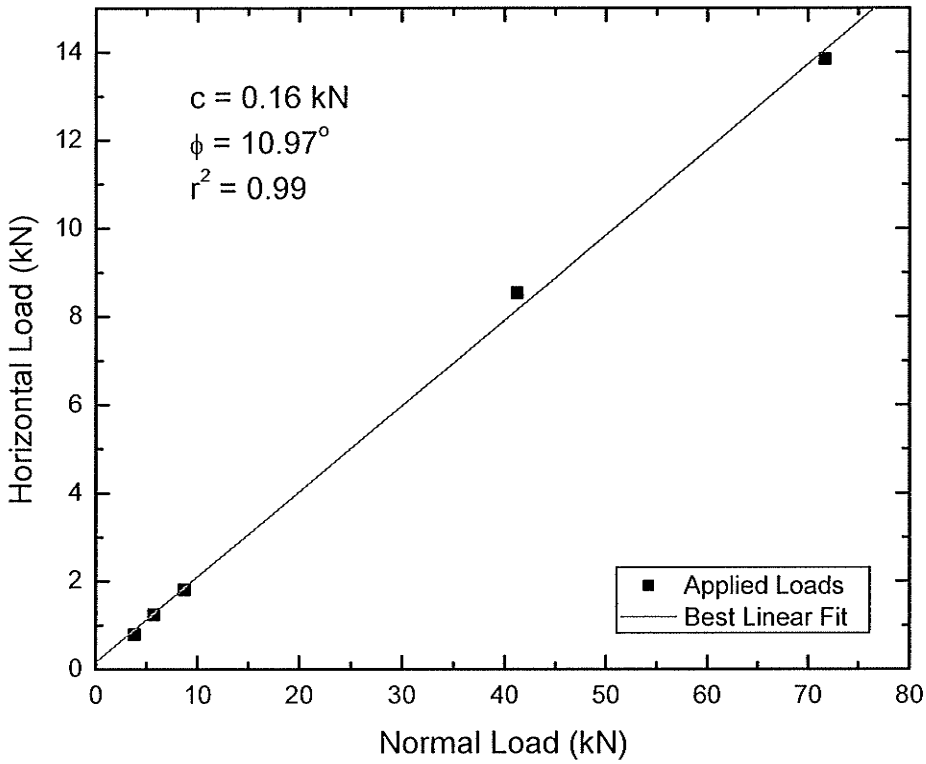

Figure 3.9 - Friction Angle and Cohesion Intercept for Large-scale Direct Shear Apparatus.

Figure 3.10 – Crib Support Material in Bottom of Large-scale Direct Shear Apparatus.

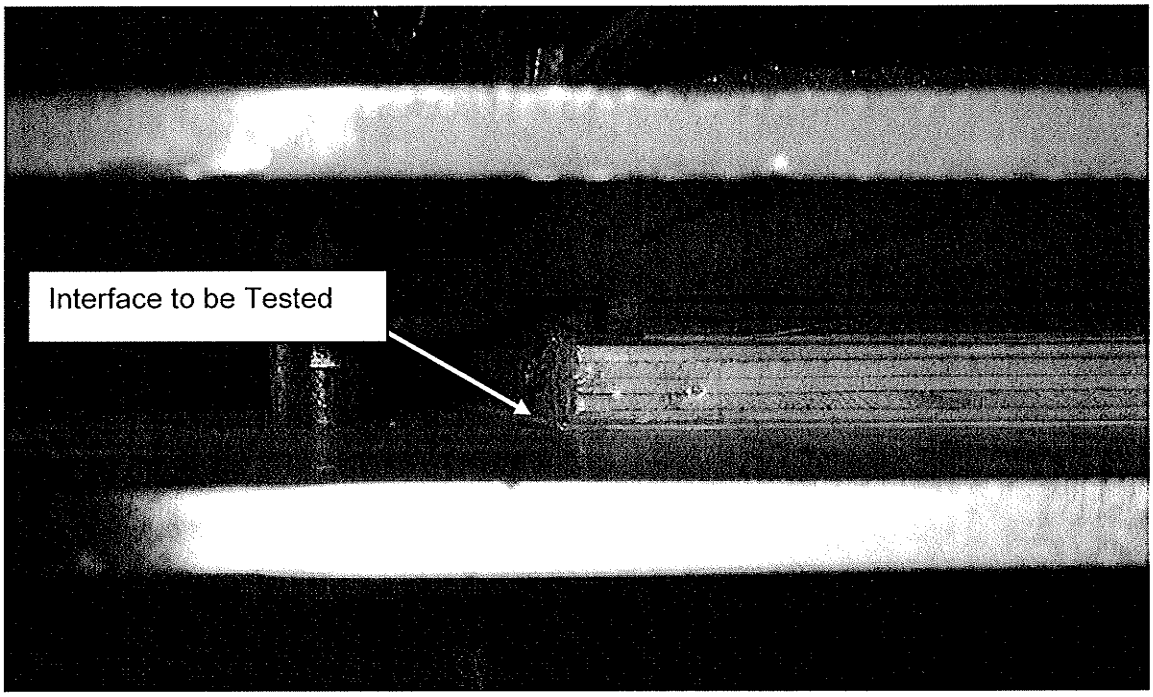

Figure 3.11 – Interface Location for PES on PES Testing in Large-scale Direct Shear Apparatus.

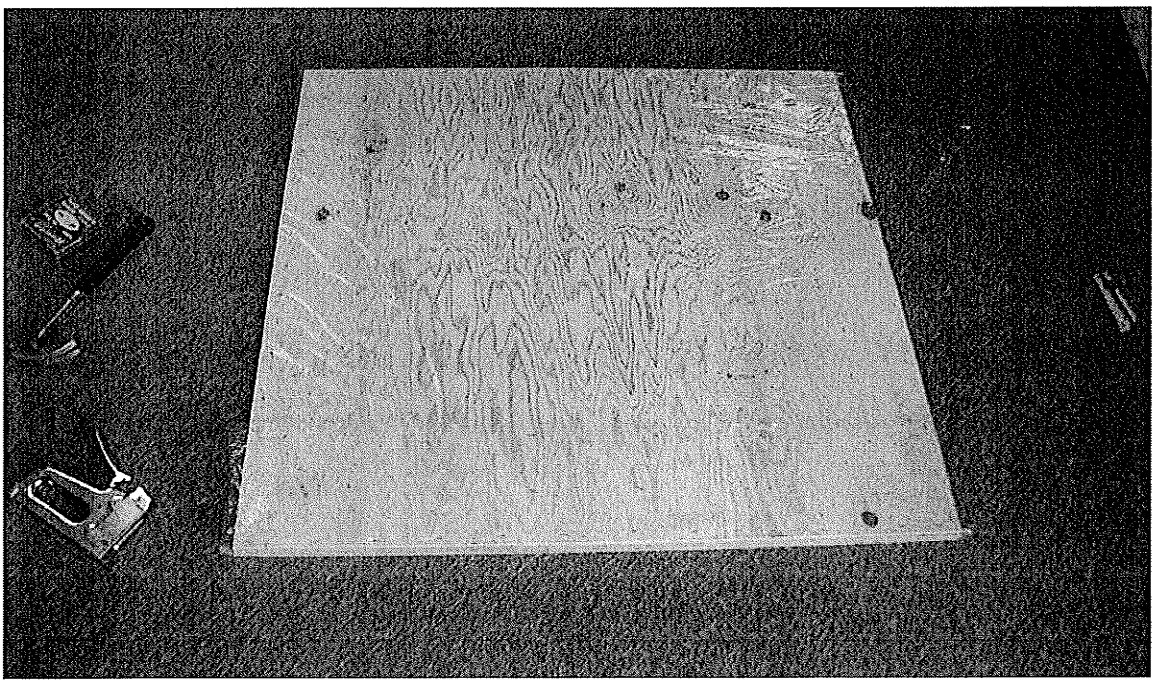

Figure 3.12 – Attachment of PES to Plywood Support for Interface Shear Testing in Large-scale Direct Shear Apparatus.

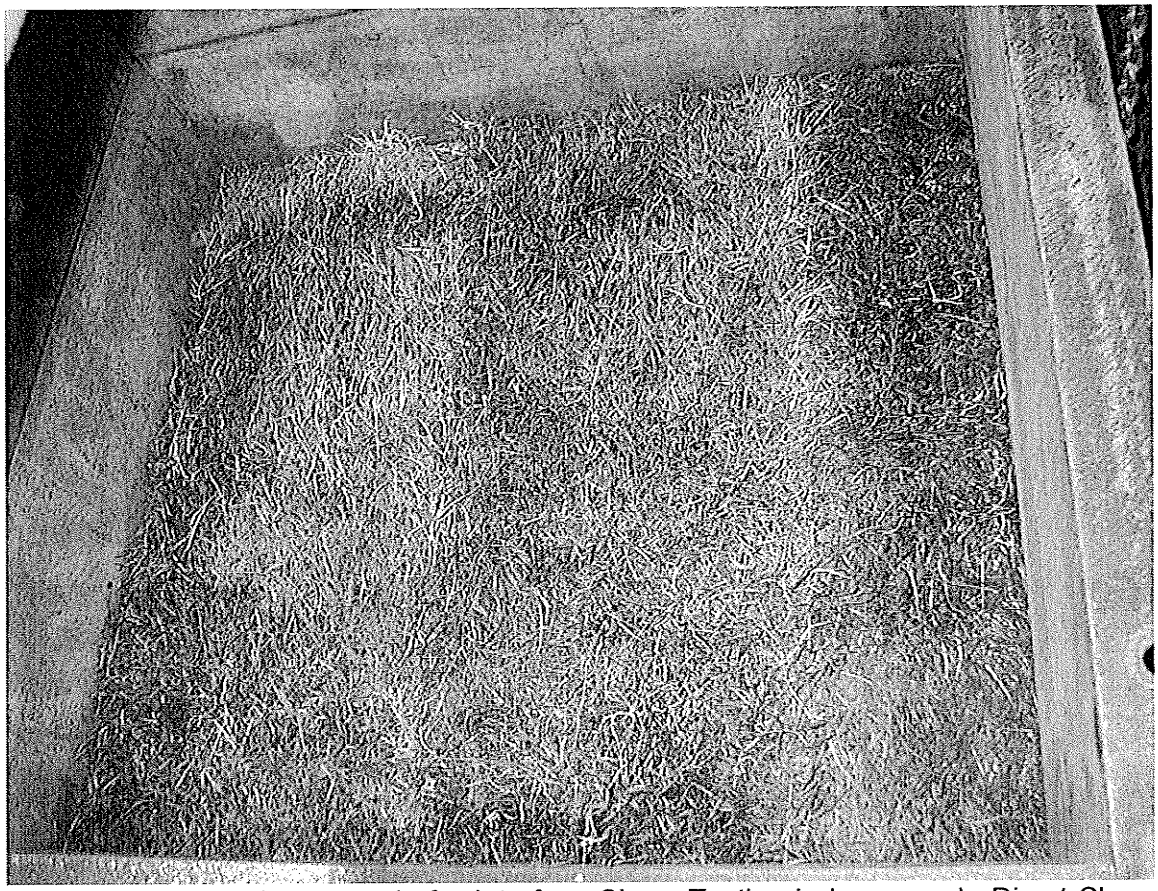

Figure 3.13 – Sod Layer ready for Interface Shear Testing in Large-scale Direct Shear Apparatus.

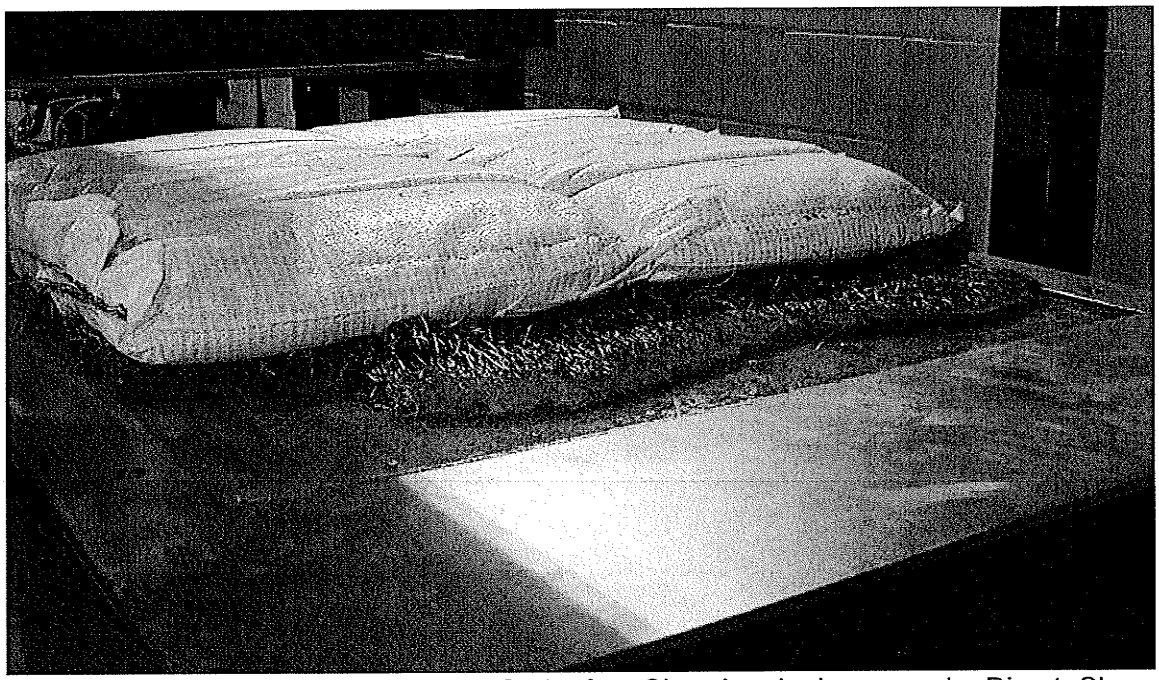

Figure 3.14 – Filled Sandbags on Sod after Shearing in Large-scale Direct Shear Apparatus.

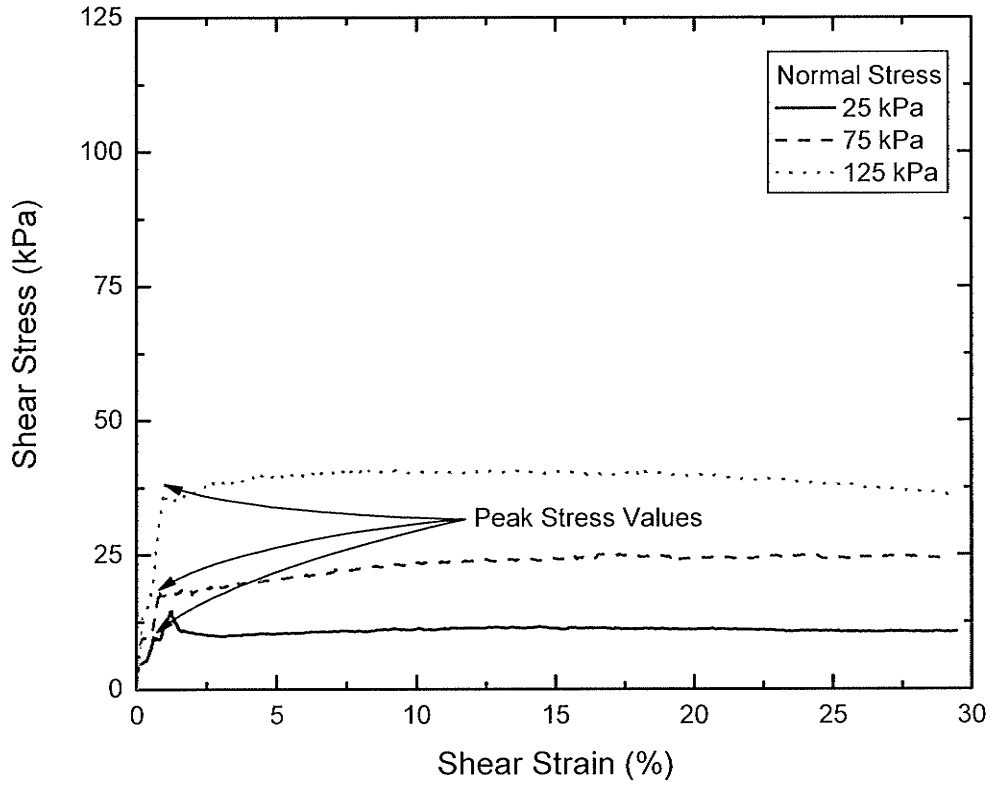

Figure 3.15 – Large-scale Direct Shear Stress versus Shear Strain for the Interface between Dry PES and Dry PES.

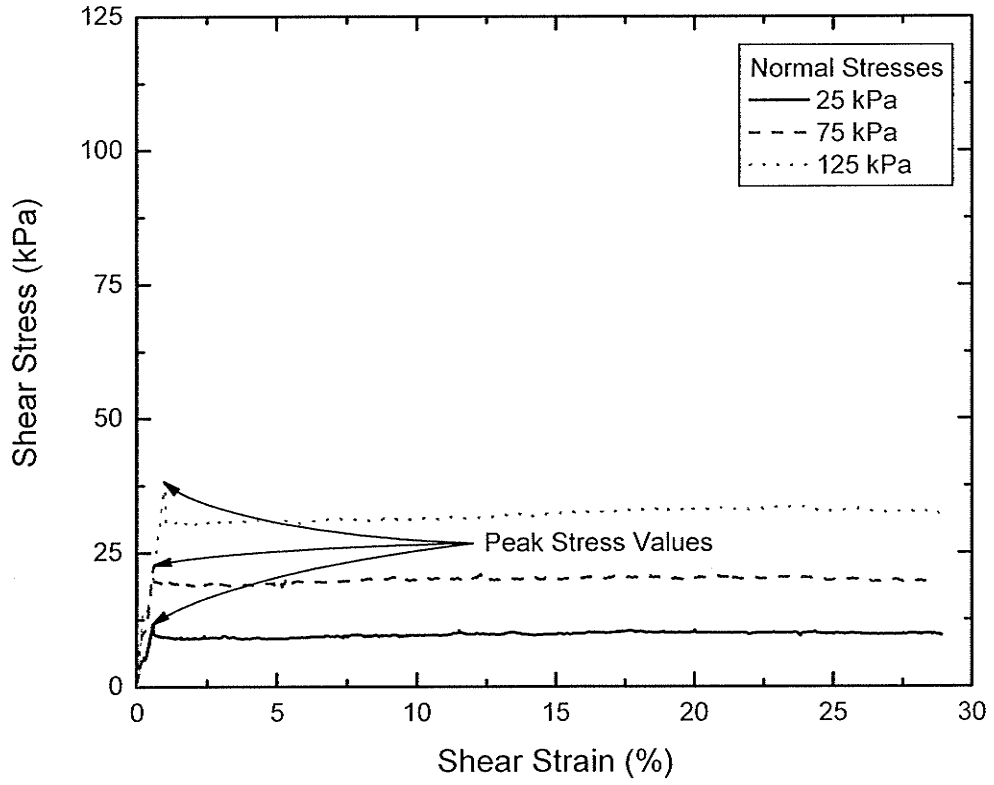

Figure 3.16 – Large-scale Direct Shear Stress versus Shear Strain for the Interface between Dry PES and Dry WSFPP.

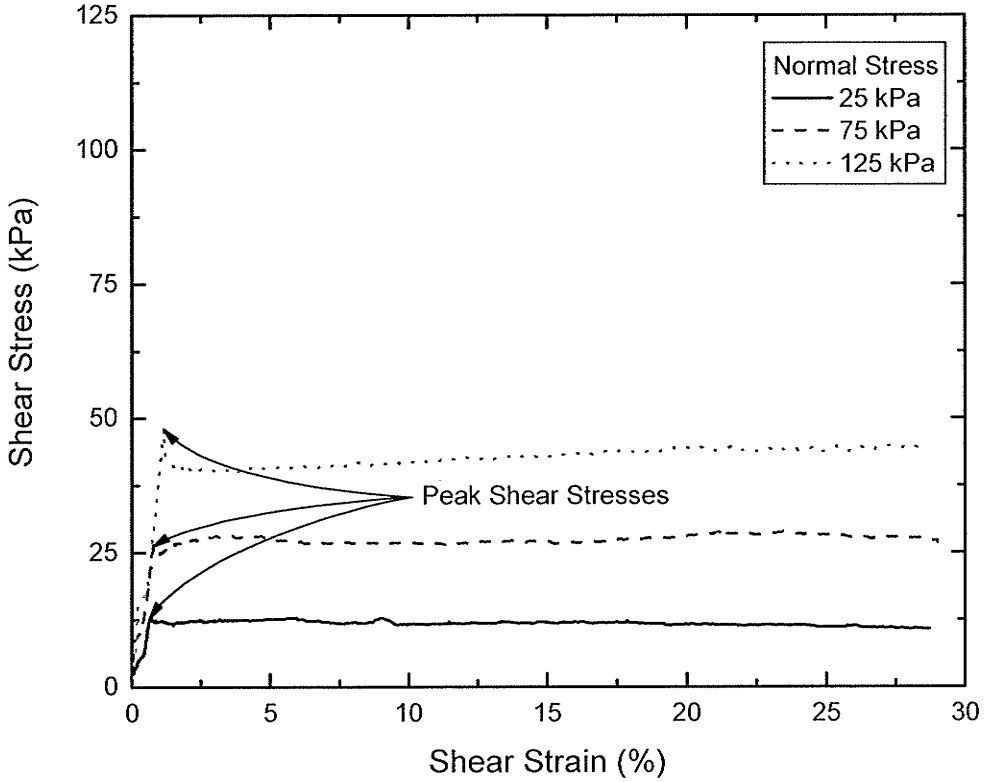

Figure 3.17 – Large-scale Direct Shear Stress versus Shear Strain for the Interface between Dry WSFPP and Dry WSFPP.

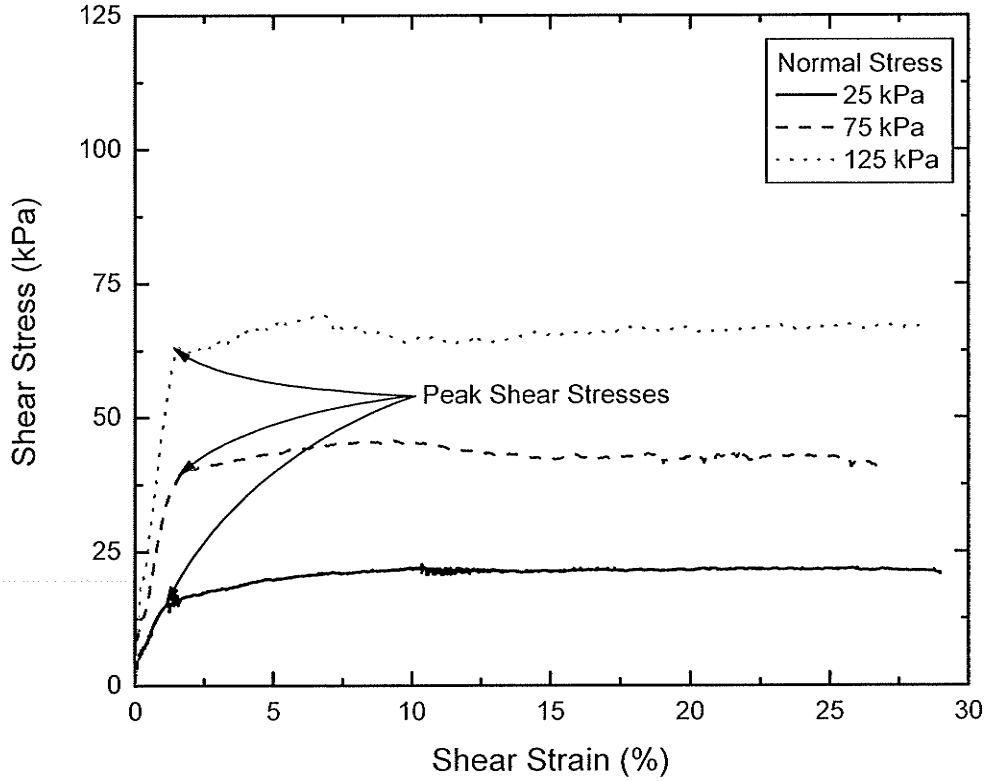

Figure 3.18 – Large-scale Direct Shear Stress versus Shear Strain for the Interface between Dry RMC Sweet Sand and Dry WSFPP.

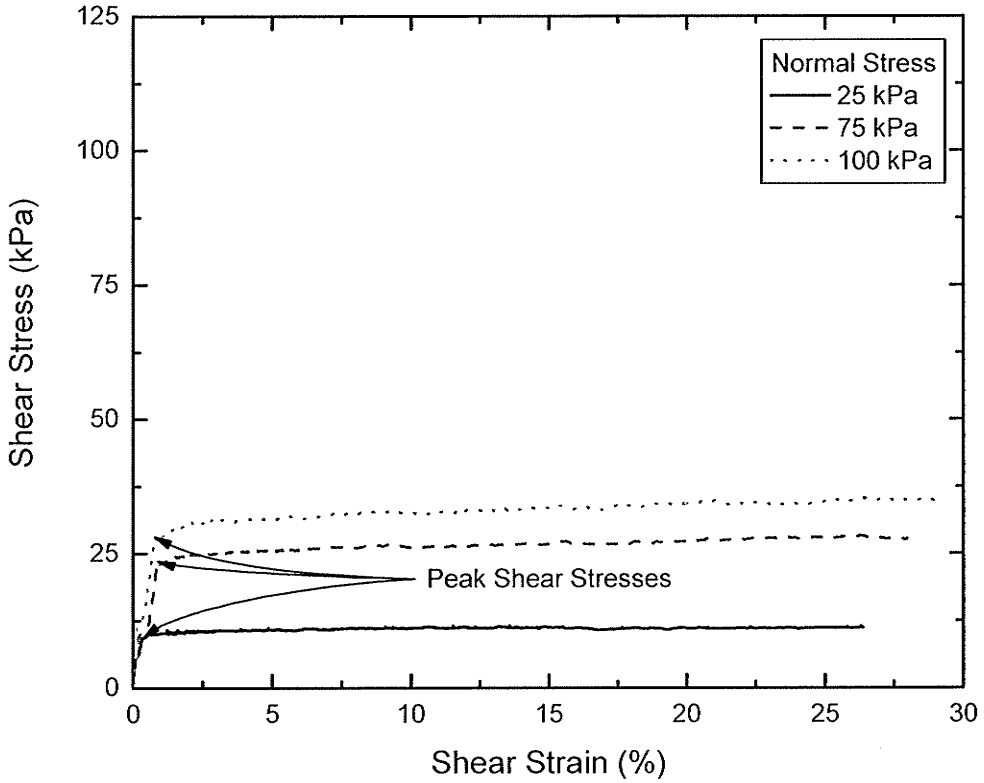

Figure 3.19 – Large-scale Direct Shear Stress versus Shear Strain for the Interface between Dry PES and Unsaturated Sod.

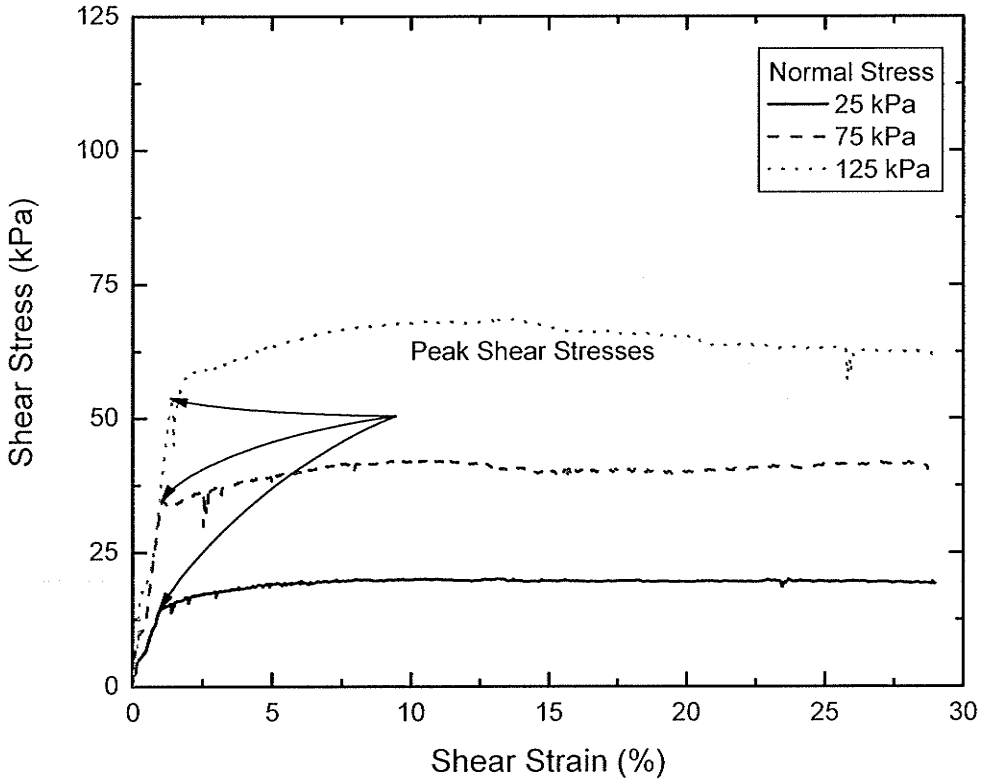

Figure 3.20 – Large-scale Direct Shear Stress versus Shear Strain for the Interface between Dry WSFPP and Unsaturated Sod.

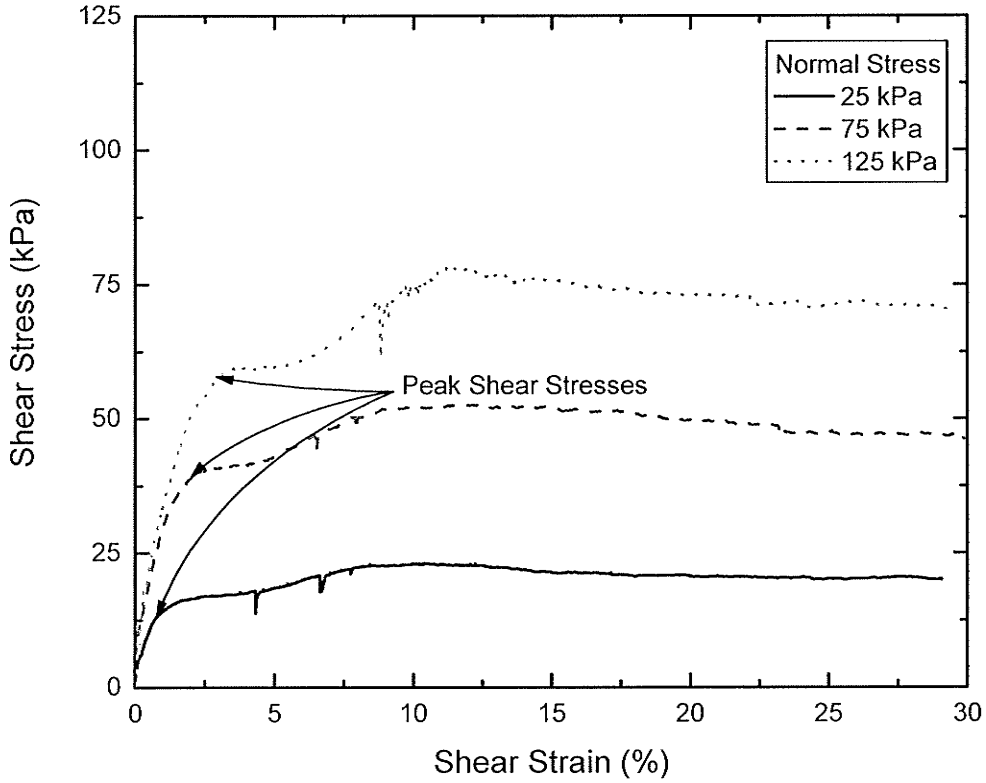

Figure 3.21 – Large-scale Direct Shear Stress versus Shear Strain for the Interface between Dry Filled Sandbags and Unsaturated Sod.

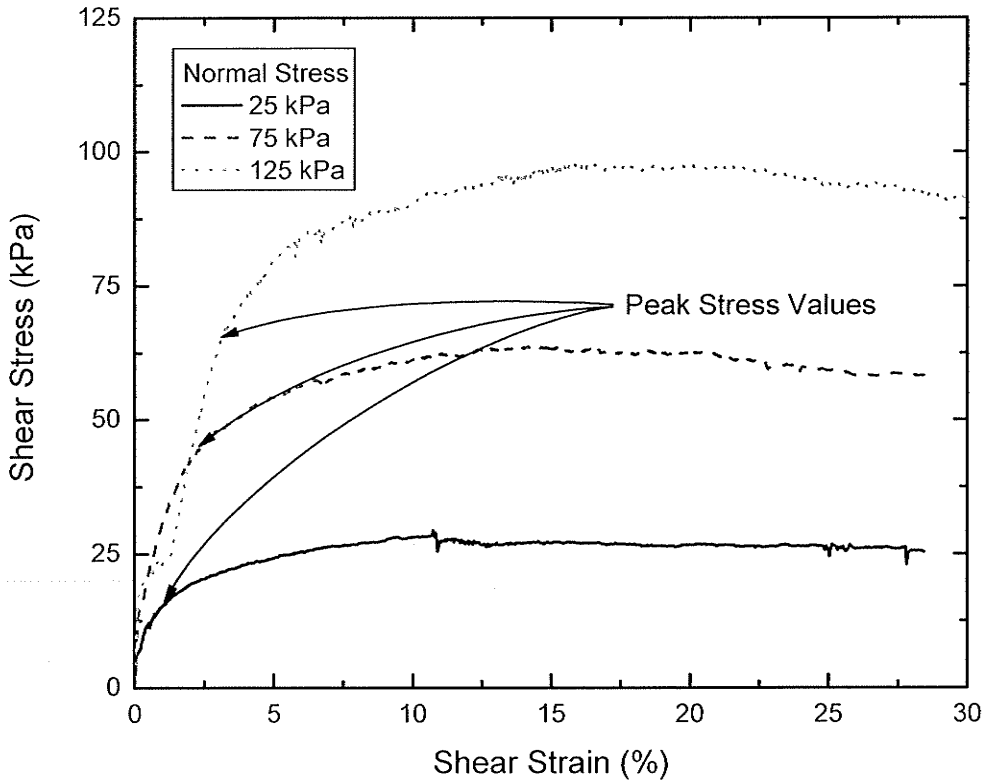

Figure 3.22 – Large-scale Direct Shear Stress versus Shear Strain for the Interface between Dry Filled Sandbags and Dry Filled Sandbags.

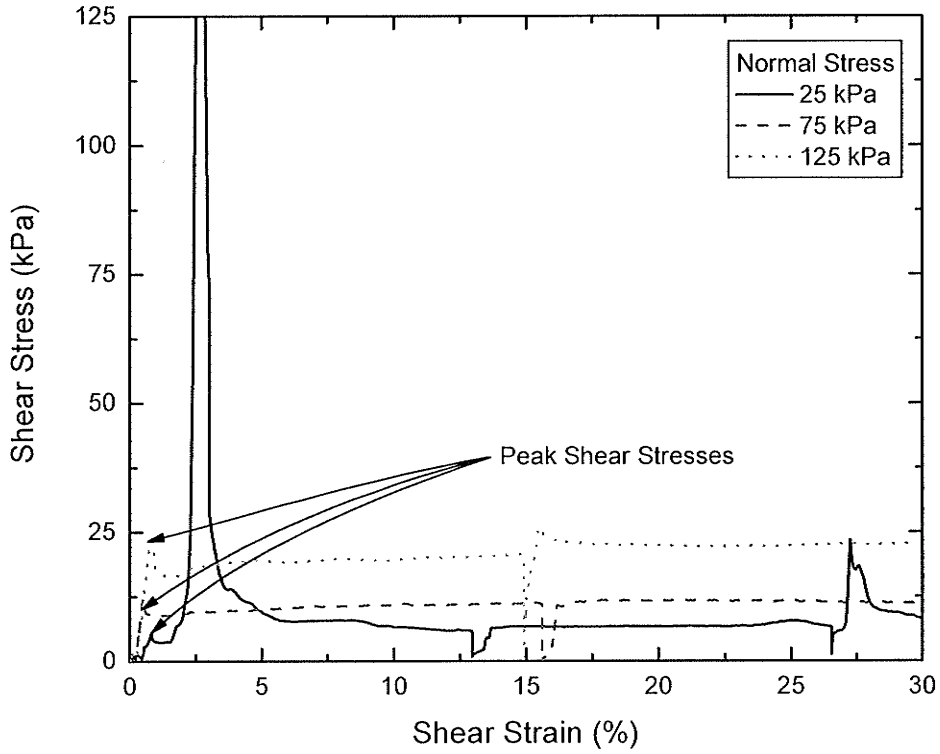

Figure 3.23 – Bench-scale Direct Shear Stress versus Shear Strain for the Interface between Dry CGSB PES and Dry CGSB PES.

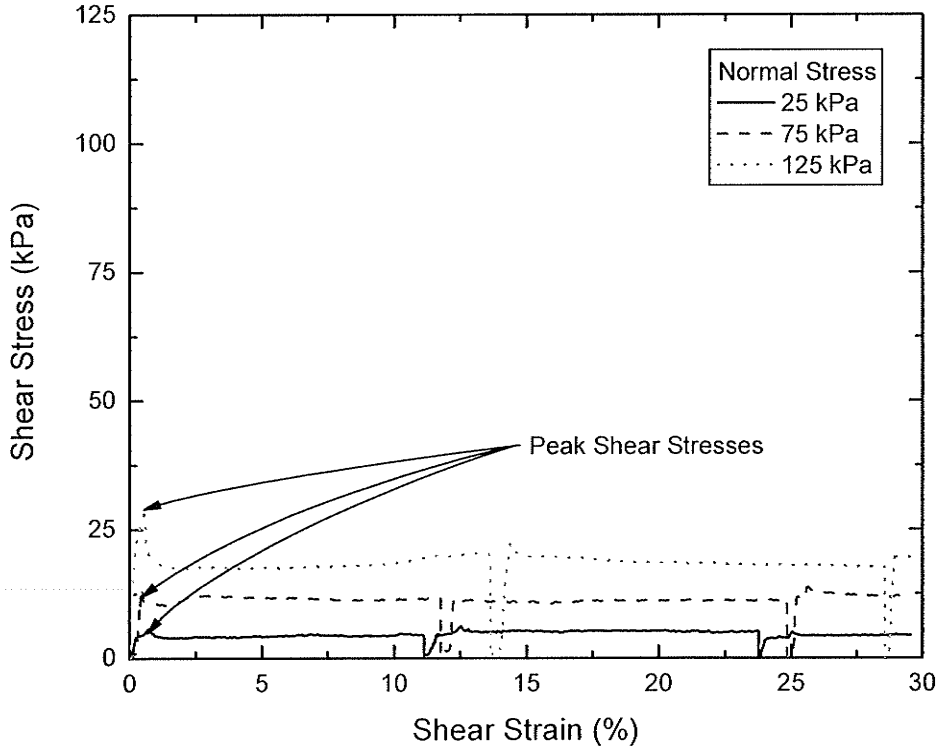

Figure 3.24 – Bench-scale Direct Shear Stress versus Shear Strain for the Interface between Dry HD PES and Dry HD PES.

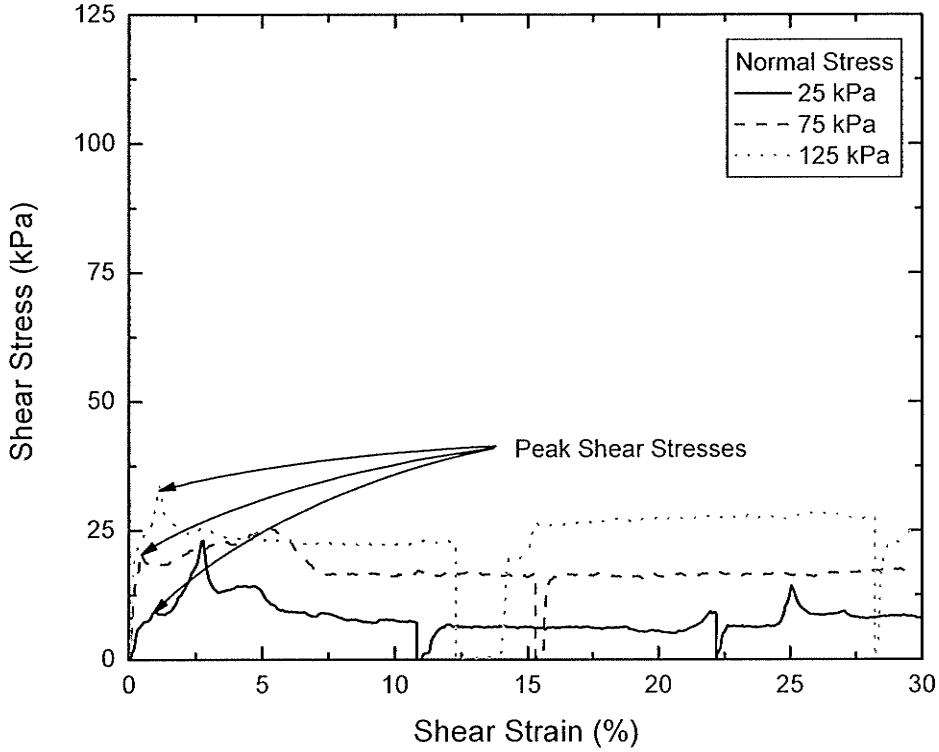

Figure 3.25 – Bench-scale Direct Shear Stress versus Shear Strain for the Interface between Dry CGSB PES and Dry WSFPP.

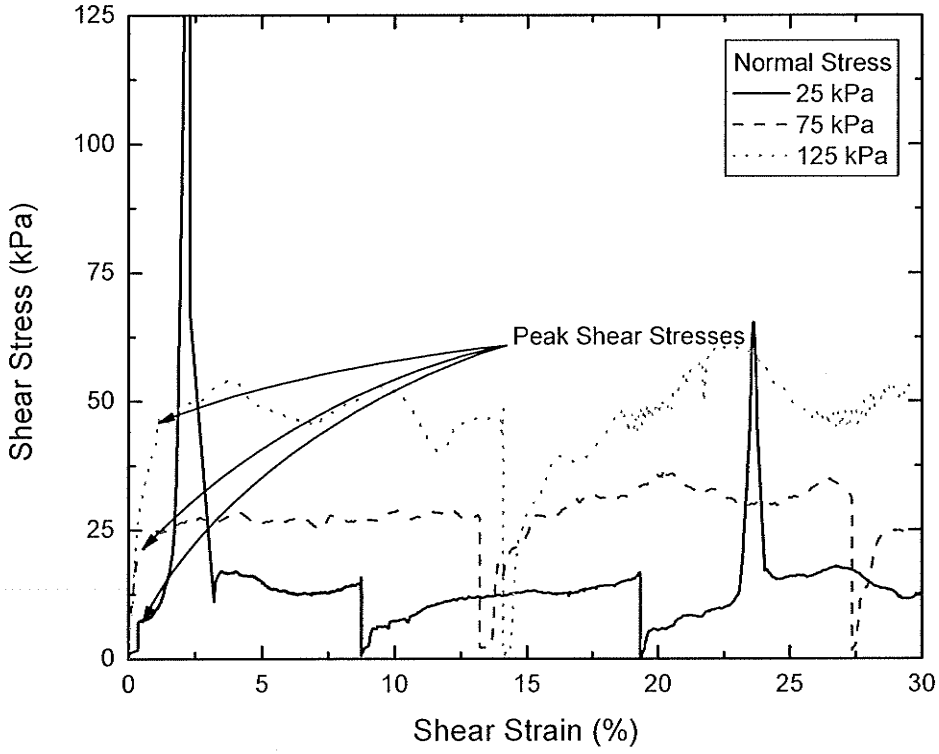

Figure 3.26 – Bench-scale Direct Shear Stress versus Shear Strain for the Interface between Dry WSFPP and Dry WSFPP.

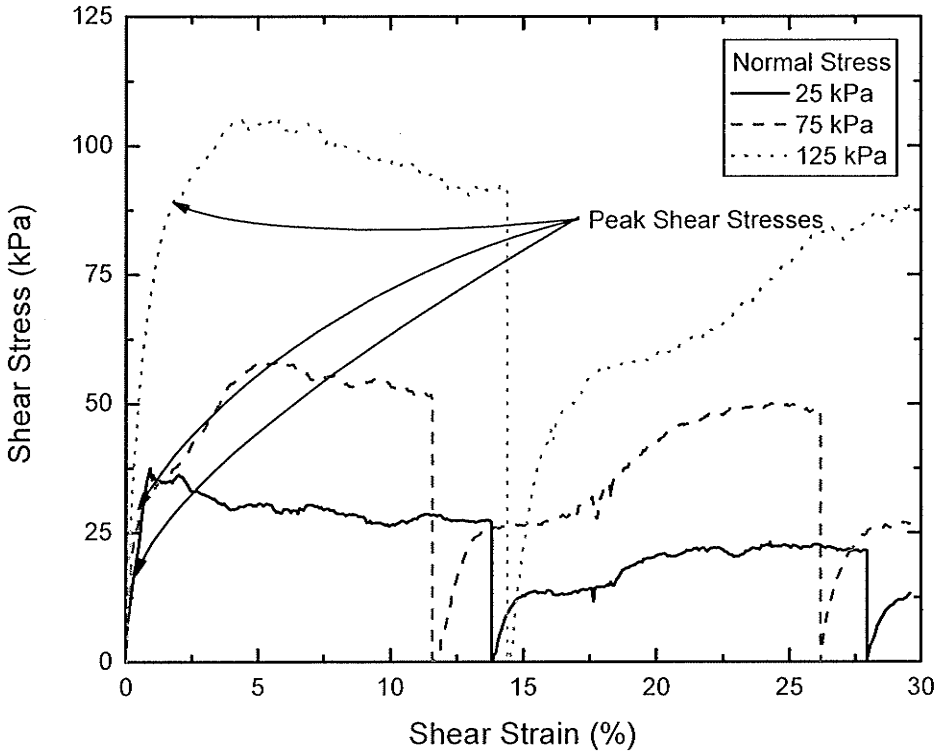

Figure 3.27 – Bench-scale Direct Shear Stress versus Shear Strain for the Interface between Dry Bird's Hill Sand and Dry WSFPP.

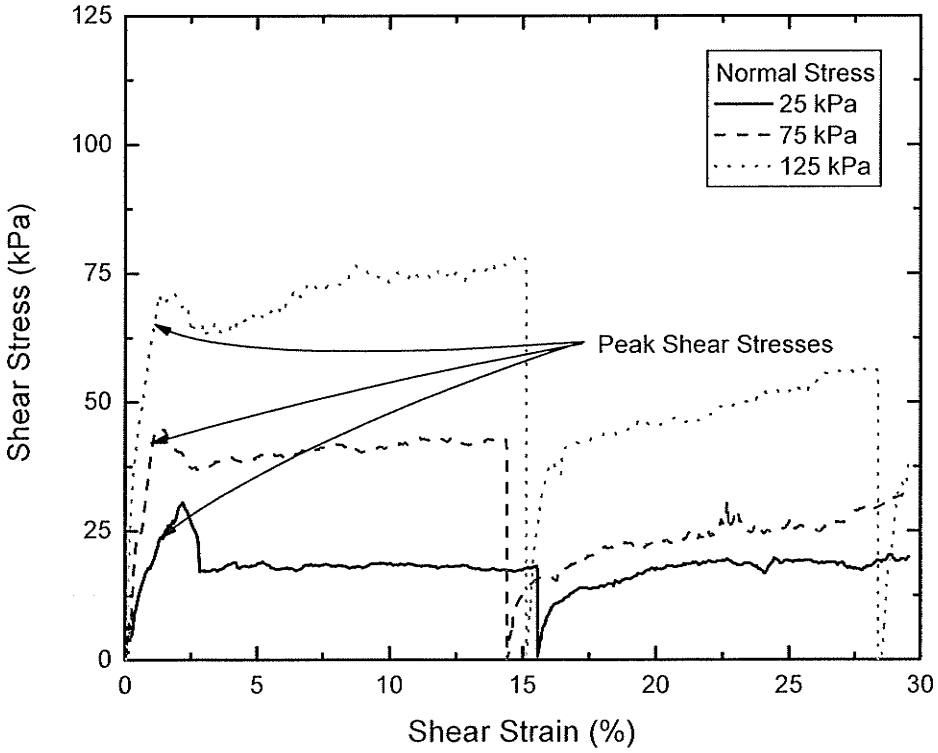

Figure 3.28 – Bench-scale Direct Shear Stress versus Shear Strain for the Interface between Dry Bird's Hill Sand and Dry CGSB PES.

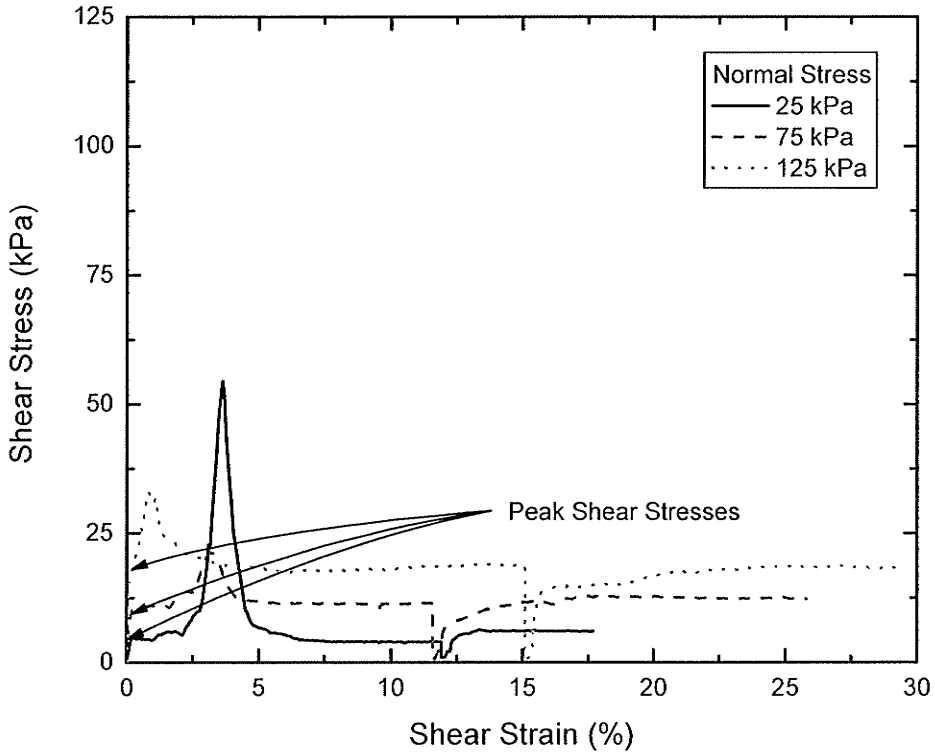

Figure 3.29 – Bench-scale Direct Shear Stress versus Shear Strain for the Interface between Saturated CGSB PES and Saturated CGSB PES.

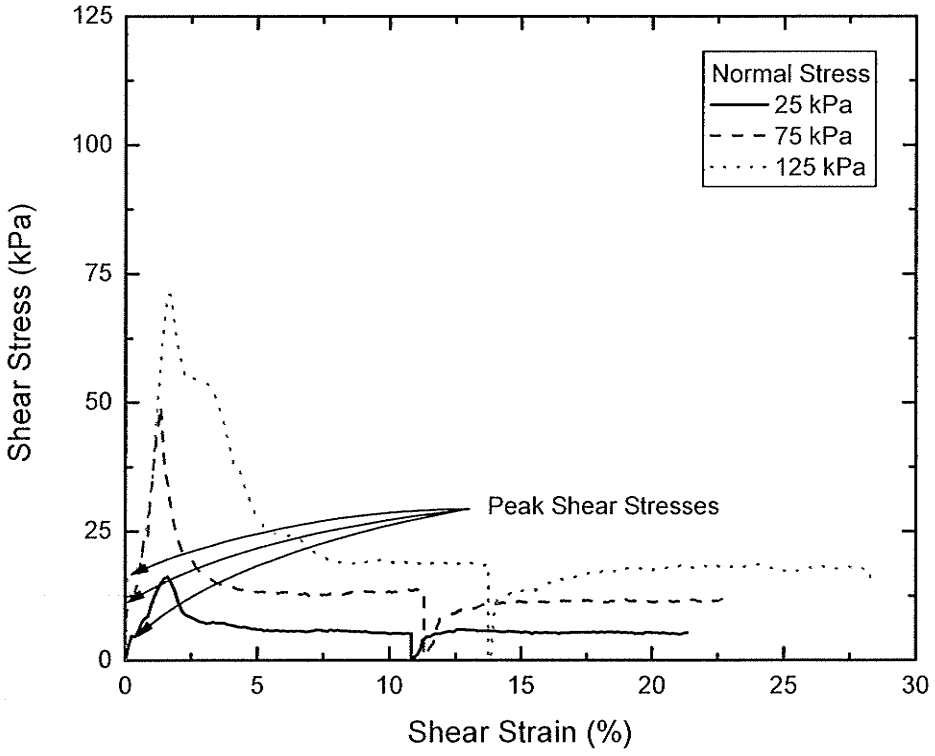

Figure 3.30 – Bench-scale Direct Shear Stress versus Shear Strain for the Interface between Saturated CGSB PES and Saturated WSFPP.

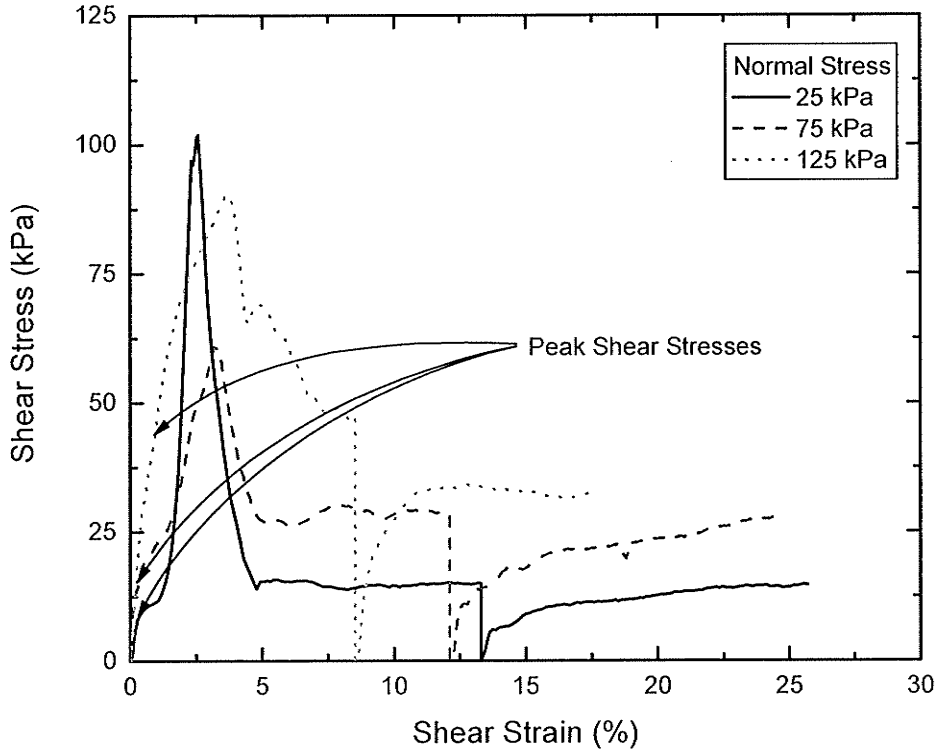

Figure 3.31 – Bench-scale Direct Shear Stress versus Shear Strain for the Interface between Saturated WSFPP and Saturated WSFPP.

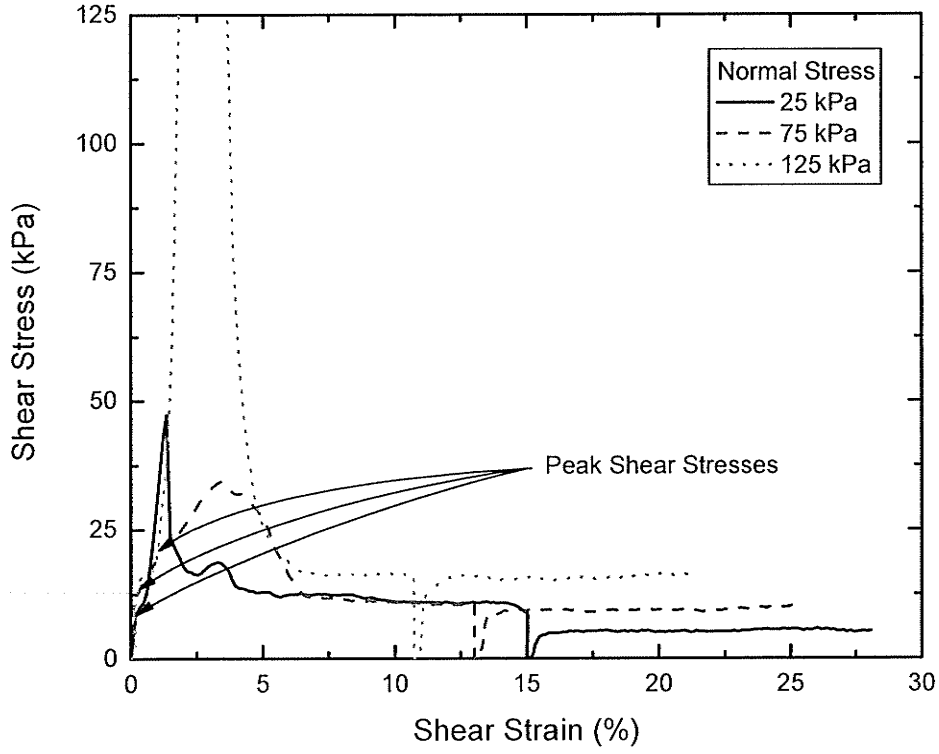

Figure 3.32 – Bench-scale Direct Shear Stress versus Shear Strain for the Interface between Scrubbed WSFPP and PES.

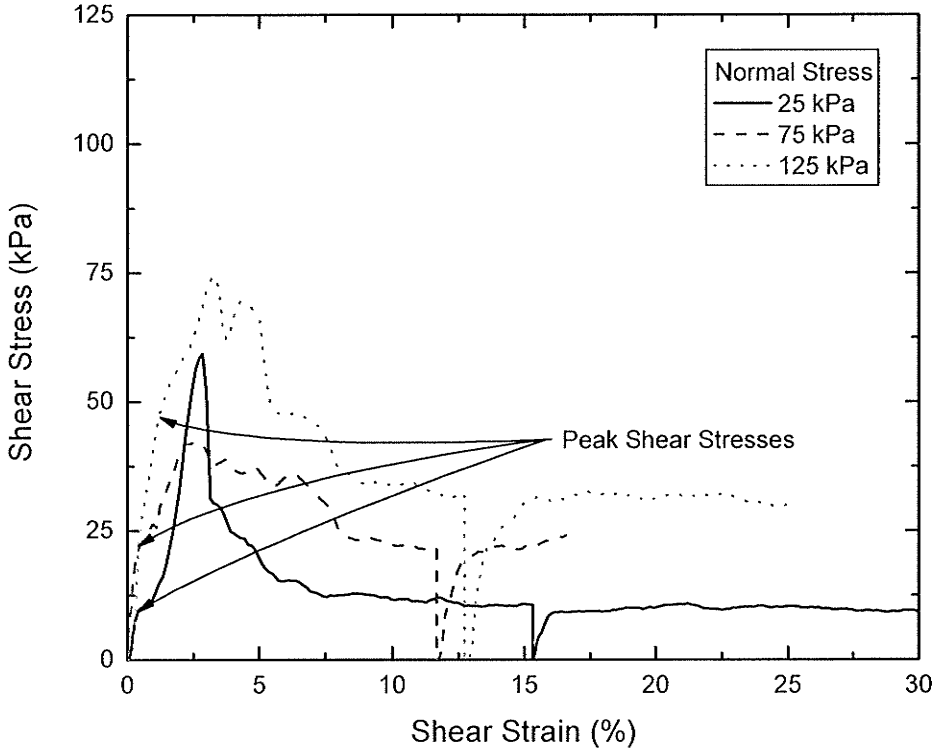

Figure 3.33 – Bench-scale Direct Shear Stress versus Shear Strain for the Interface between Scrubbed WSFPP and Scrubbed WSFPP.

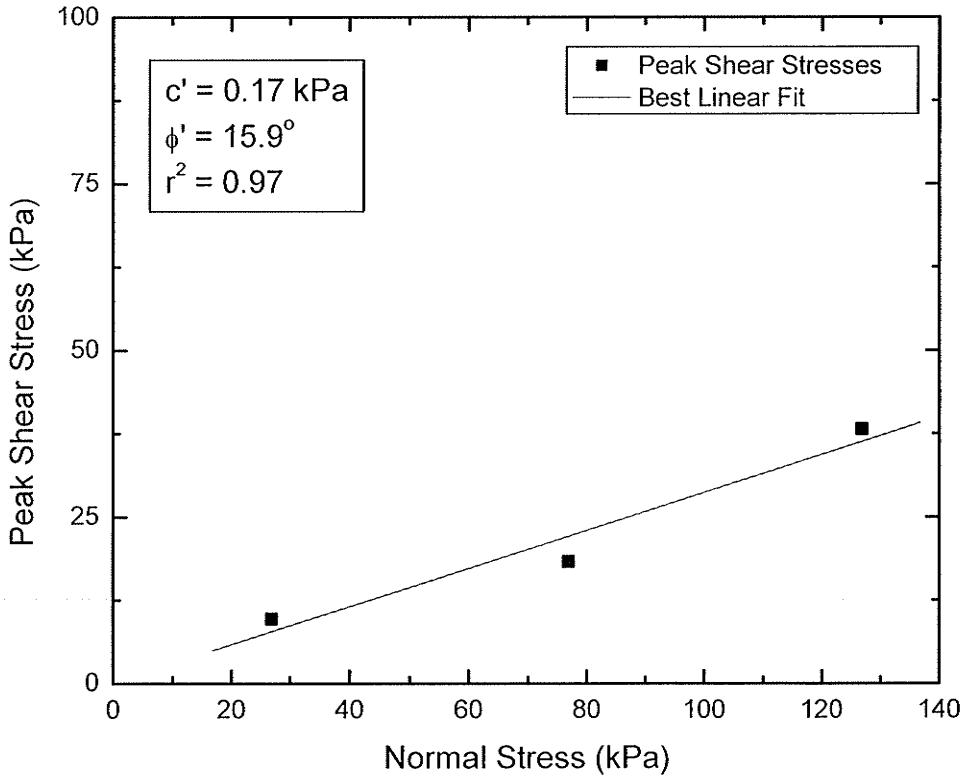

Figure 3.34 – Peak Shear Stress versus Normal Stress for dry HD PES on dry HD PES interface tested in Large-scale Direct Shear Apparatus.

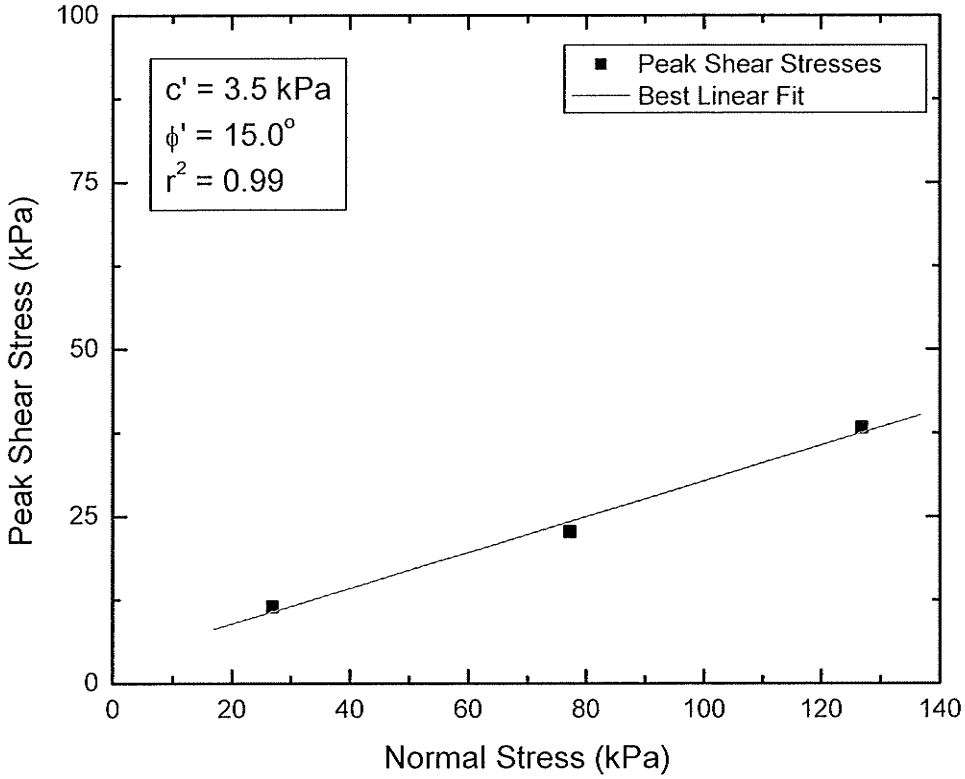

Figure 3.35 – Peak Shear Stress versus Normal Stress for dry HD PES on dry WSFPP interface tested in Large-scale Direct Shear Apparatus.

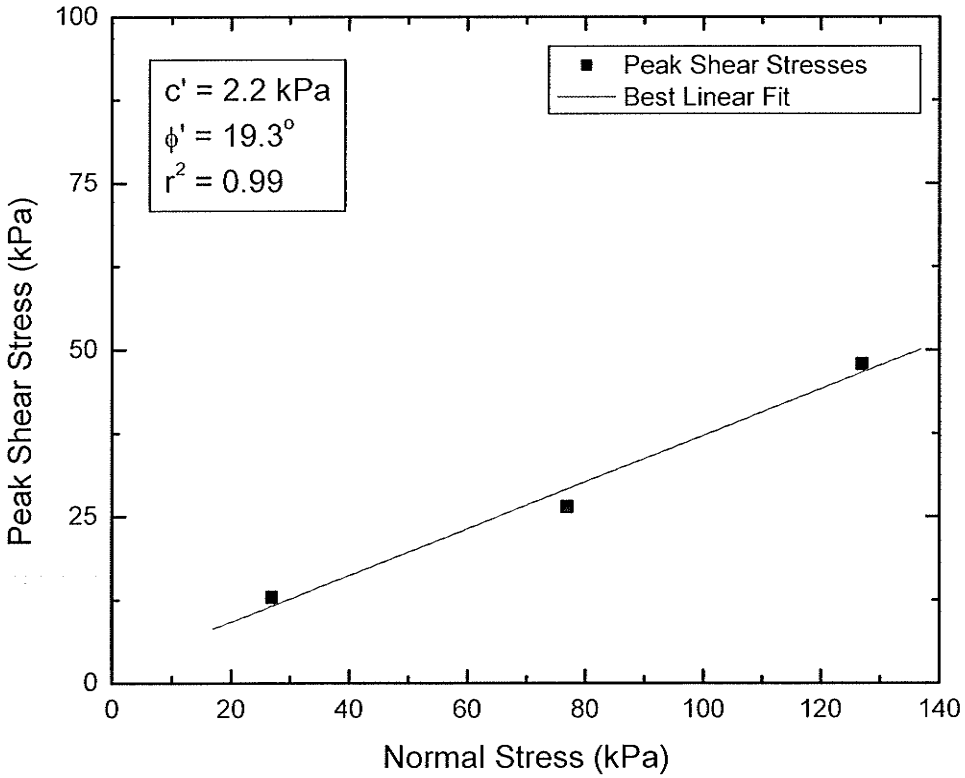

Figure 3.36 – Peak Shear Stress versus Normal Stress for dry WSFPP on dry WSFPP interface tested in Large-scale Direct Shear Apparatus.

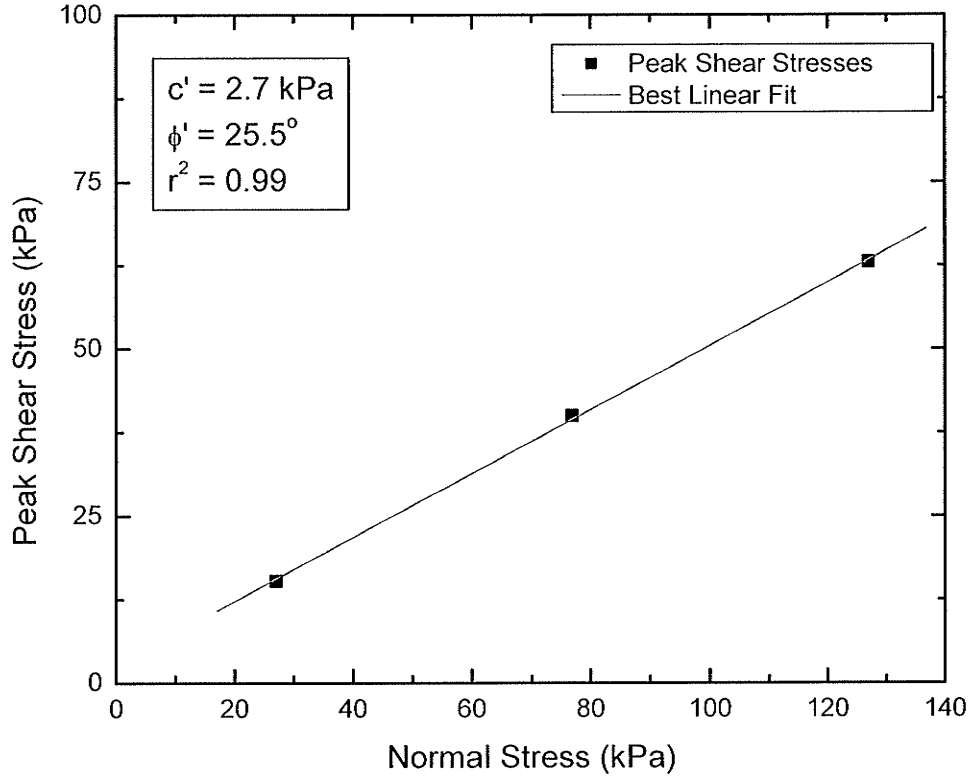

Figure 3.37 – Peak Shear Stress versus Normal Stress for RMC Sand on dry WSFPP interface tested in Large-scale Direct Shear Apparatus.

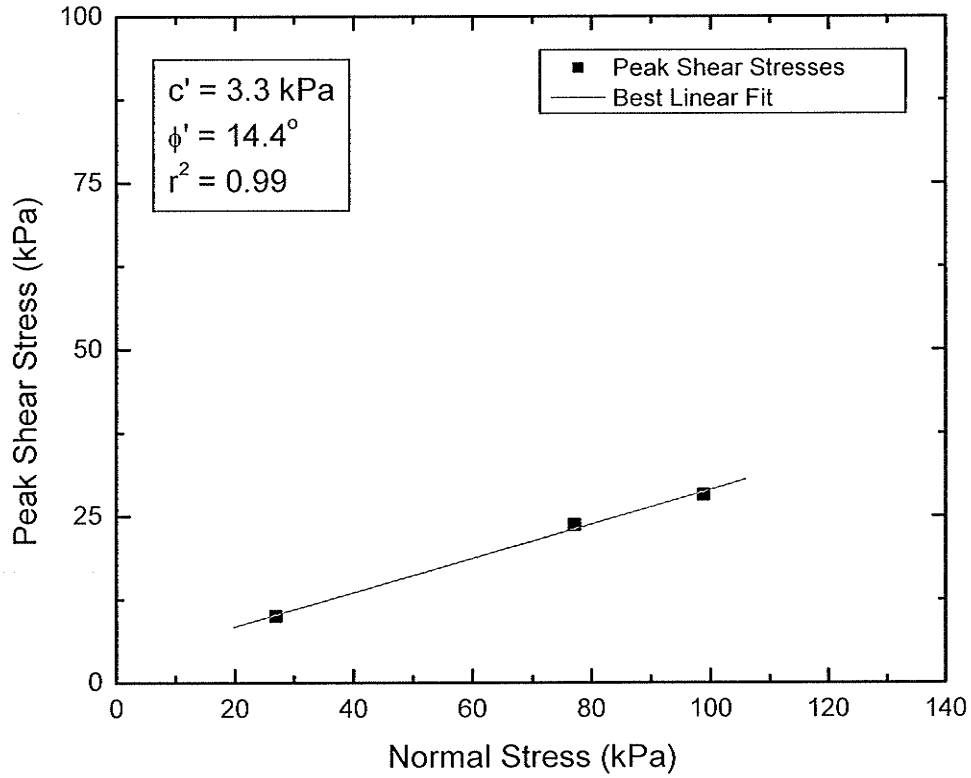

Figure 3.38 – Peak Shear Stress versus Normal Stress for dry HD PES on unsaturated Sod interface tested in Large-scale Direct Shear Apparatus.

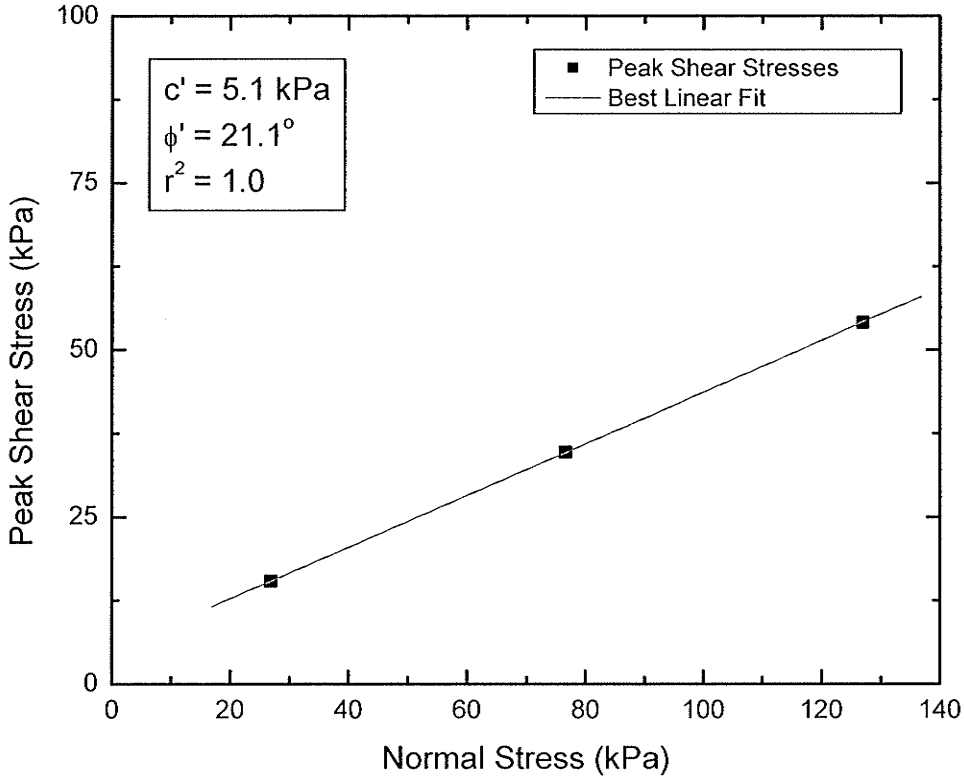

Figure 3.39 – Peak Shear Stress versus Normal Stress for dry WSFPP on unsaturated Sod interface tested in Large-scale Direct Shear Apparatus.

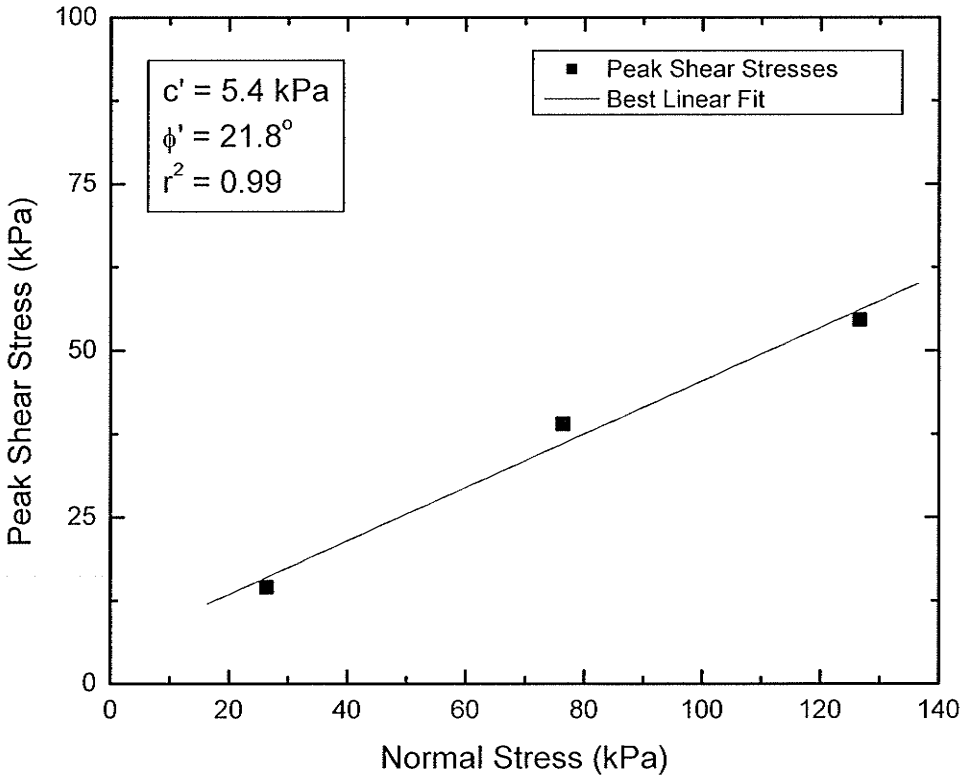

Figure 3.40 – Peak Shear Stress versus Normal Stress for filled Sandbags on unsaturated Sod interface tested in Large-scale Direct Shear Apparatus.

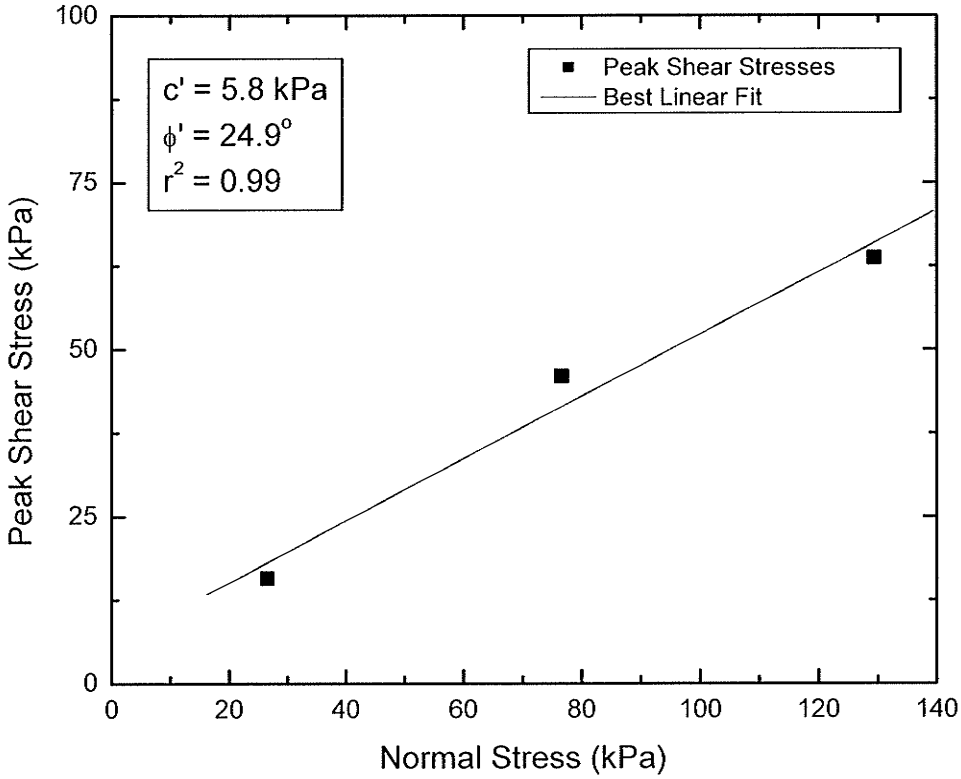

Figure 3.41 – Peak Shear Stress versus Normal Stress for filled Sandbags on filled Sandbags interface tested in Large-scale Direct Shear Apparatus.

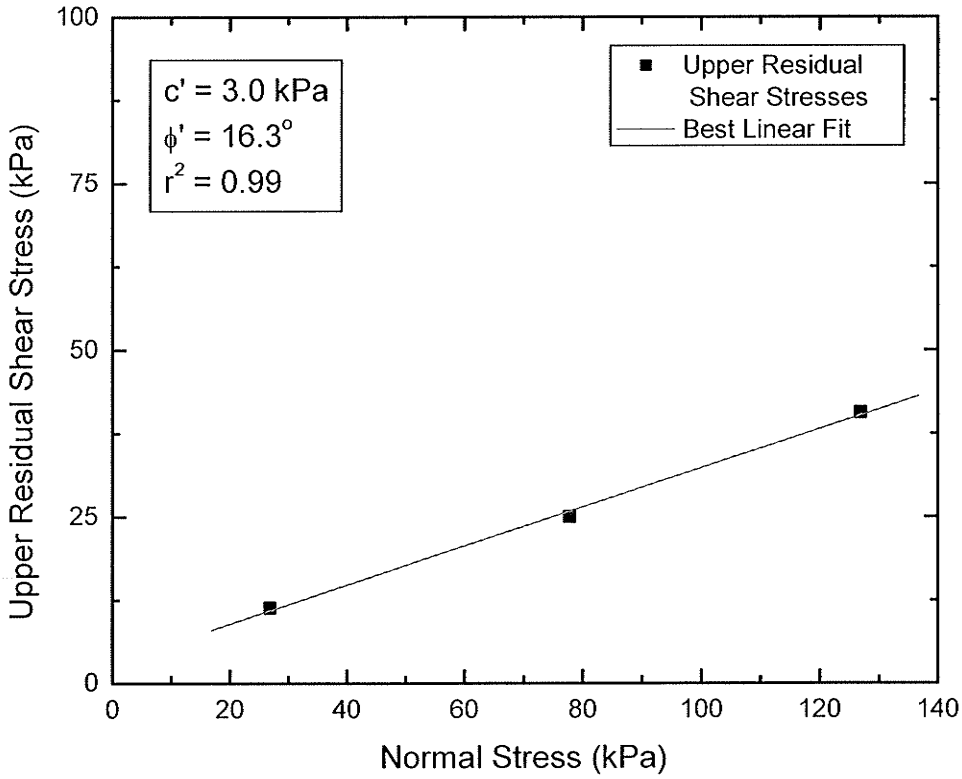

Figure 3.42 – Upper Residual Shear Stress versus Normal Stress for dry HD PES on dry HD PES interface tested in Large-scale Direct Shear Apparatus.

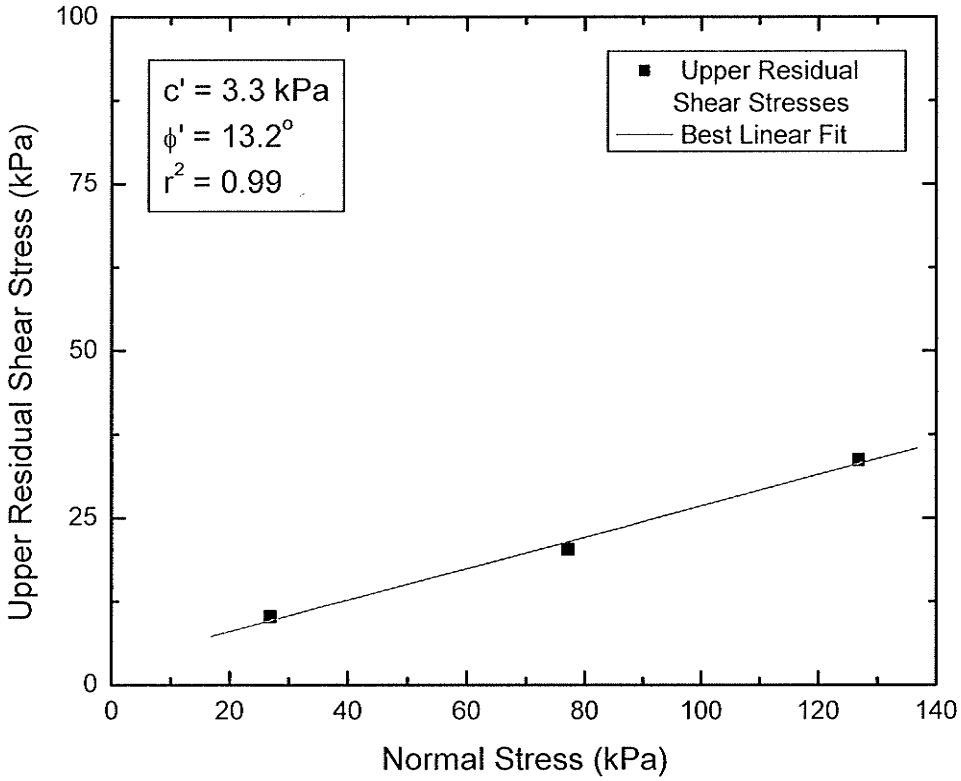

Figure 3.43 – Upper Residual Shear Stress versus Normal Stress for dry HD PES on dry WSFPP interface tested in Large-scale Direct Shear Apparatus.

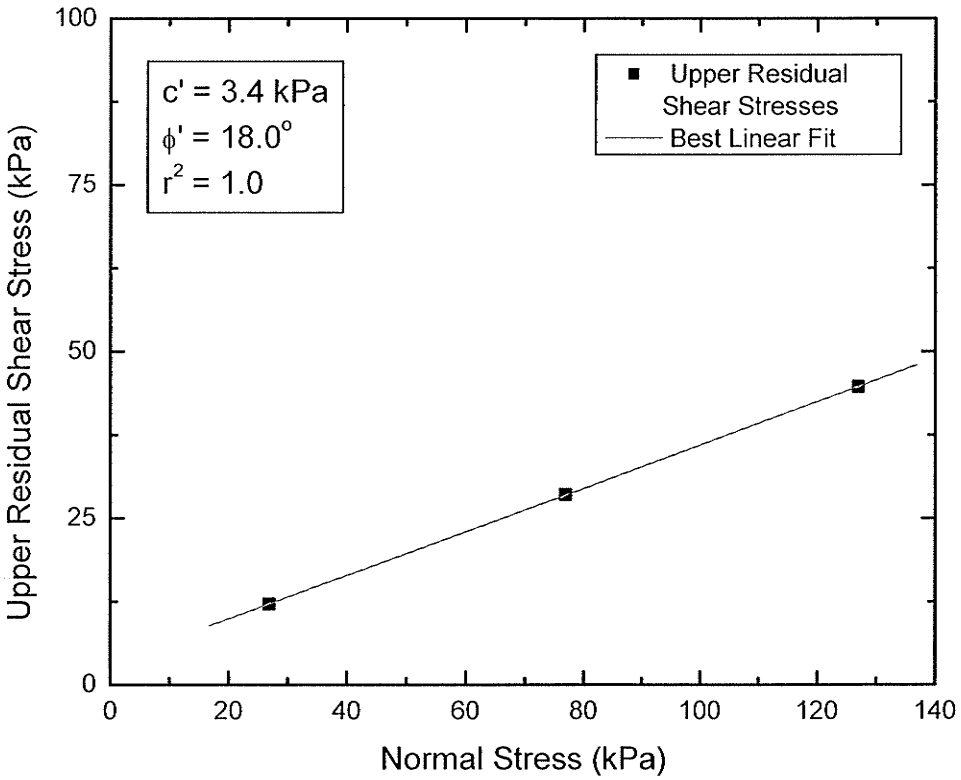

Figure 3.44 – Upper Residual Shear Stress versus Normal Stress for dry WSFPP on dry WSFPP interface tested in Large-scale Direct Shear Apparatus.

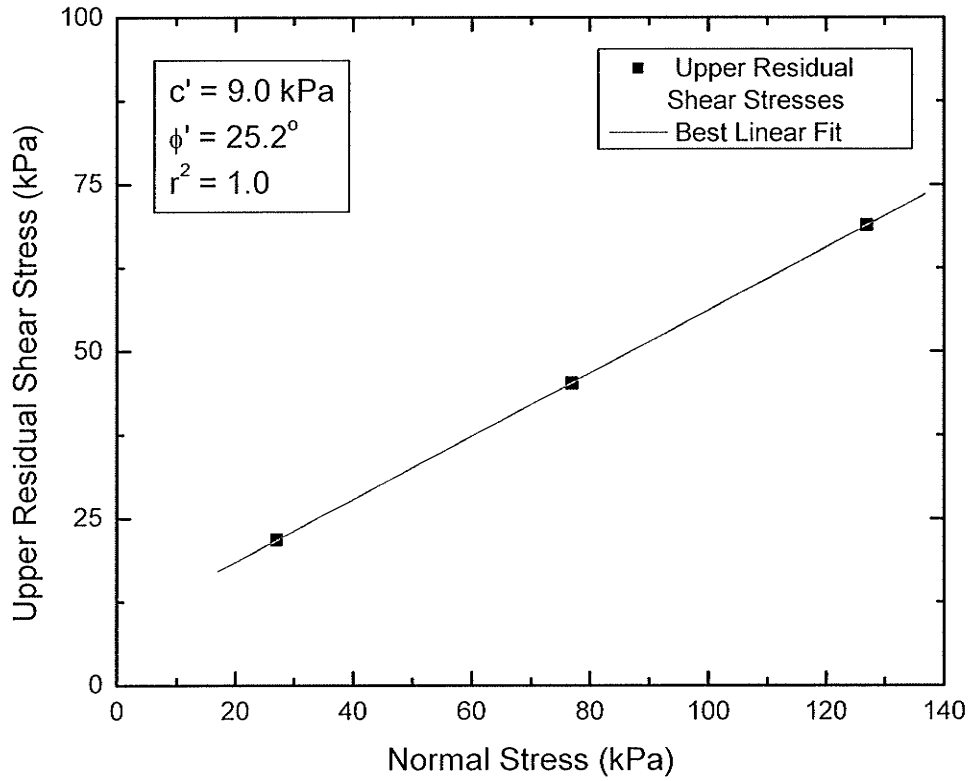

Figure 3.45 – Upper Residual Shear Stress versus Normal Stress for RMC Sand on dry WSFPP interface tested in Large-scale Direct Shear Apparatus.

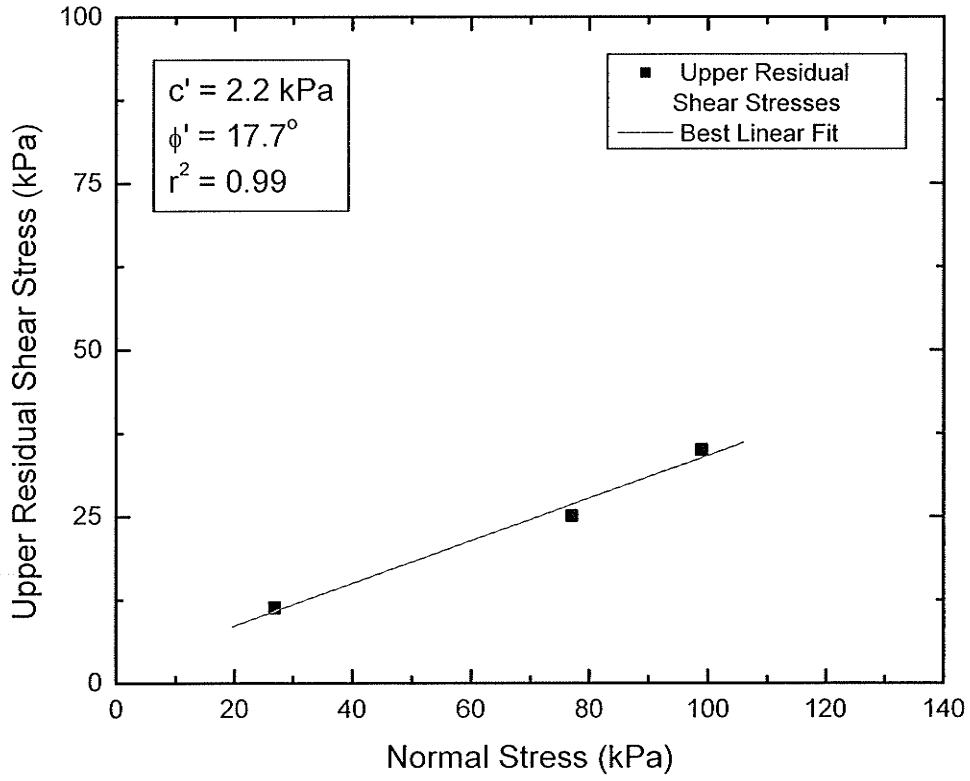

Figure 3.46 – Upper Residual Shear Stress versus Normal Stress for dry HD PES on unsaturated Sod interface tested in Large-scale Direct Shear Apparatus.

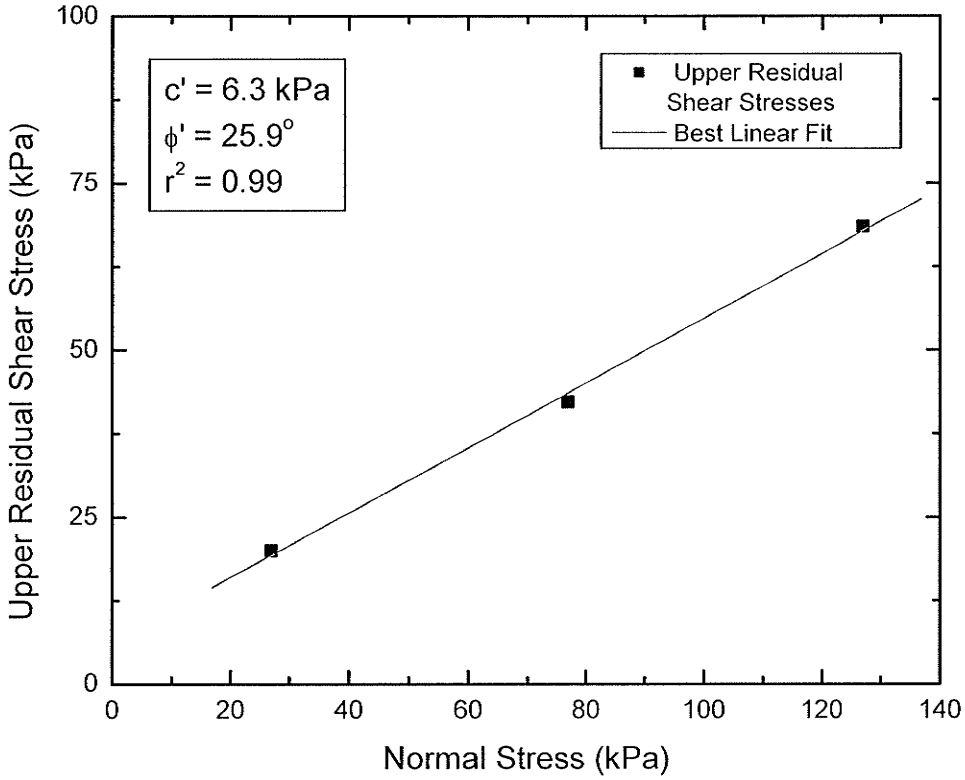

Figure 3.47 – Upper Residual Shear Stress versus Normal Stress for dry WSFPP on unsaturated Sod interface tested in Large-scale Direct Shear Apparatus.

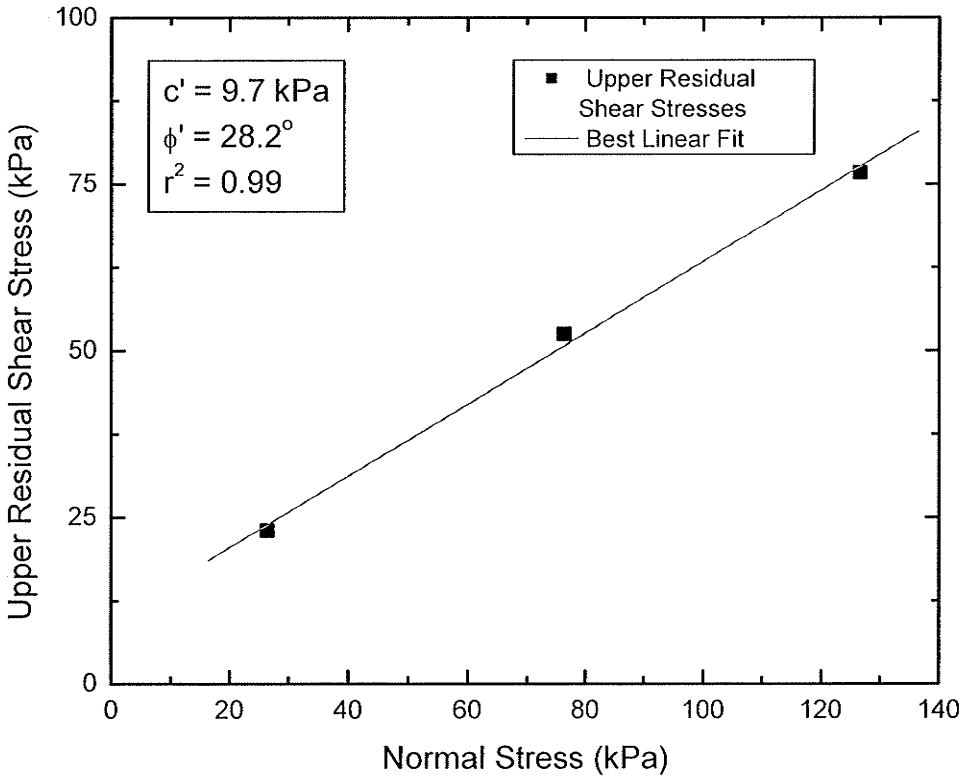

Figure 3.48 – Upper Residual Shear Stress versus Normal Stress for filled Sandbags on unsaturated Sod interface tested in Large-scale Direct Shear Apparatus.

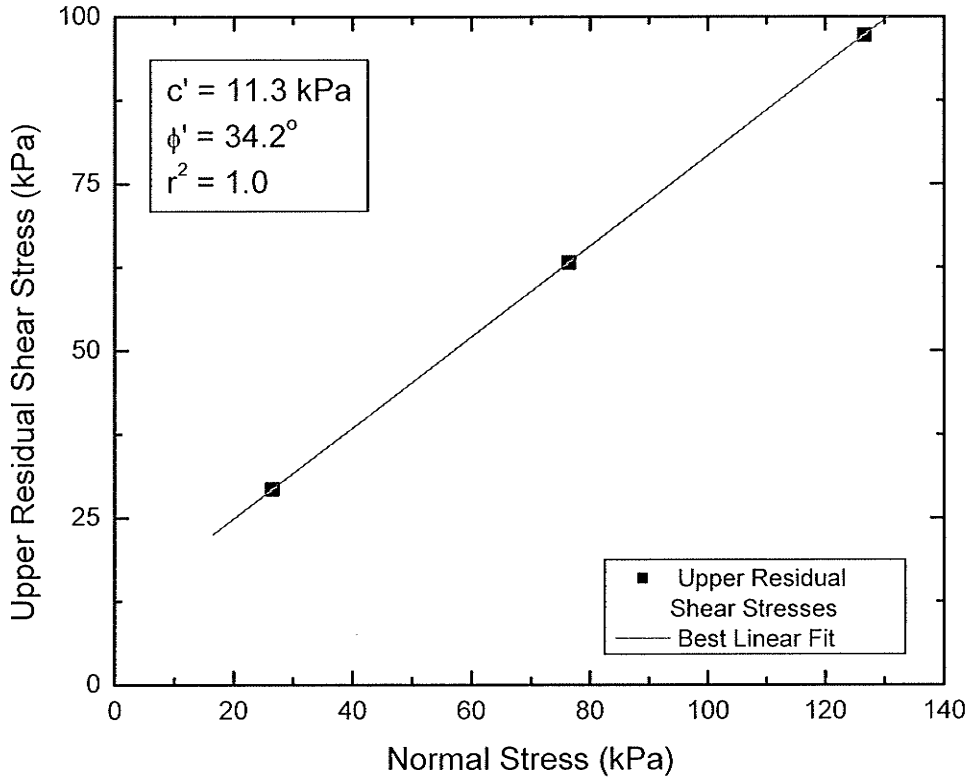

Figure 3.49 – Upper Residual Shear Stress versus Normal Stress for filled Sandbags on filled Sandbags interface tested in Large-scale Direct Shear Apparatus.

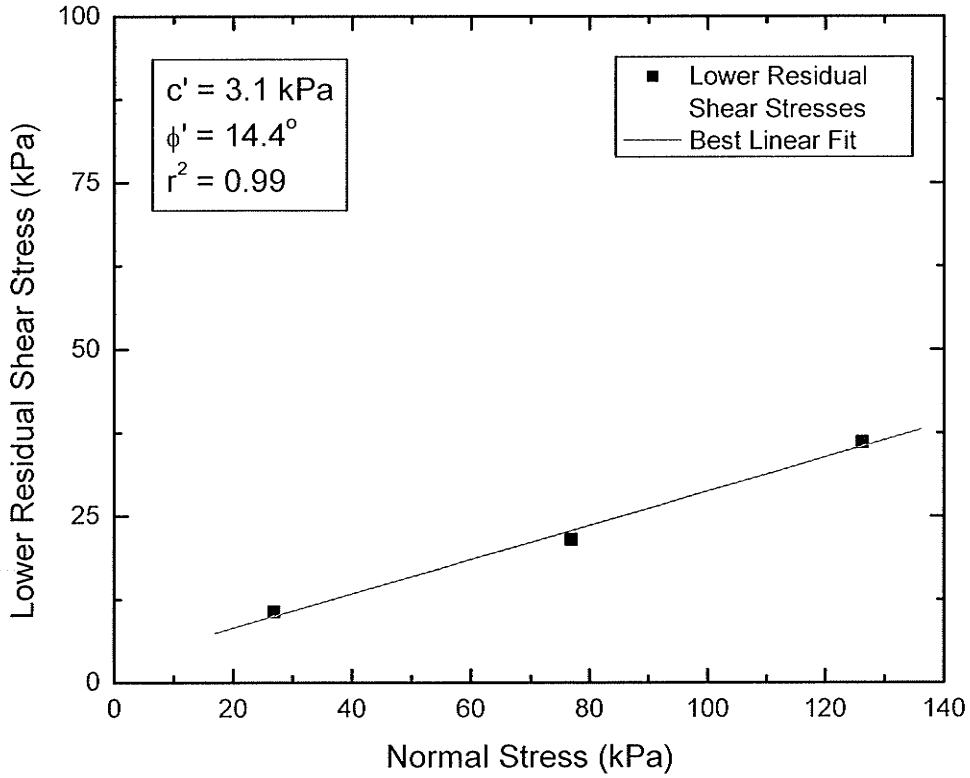

Figure 3.50 – Lower Residual Shear Stress versus Normal Stress for dry HD PES on dry HD PES interface tested in Large-scale Direct Shear Apparatus.

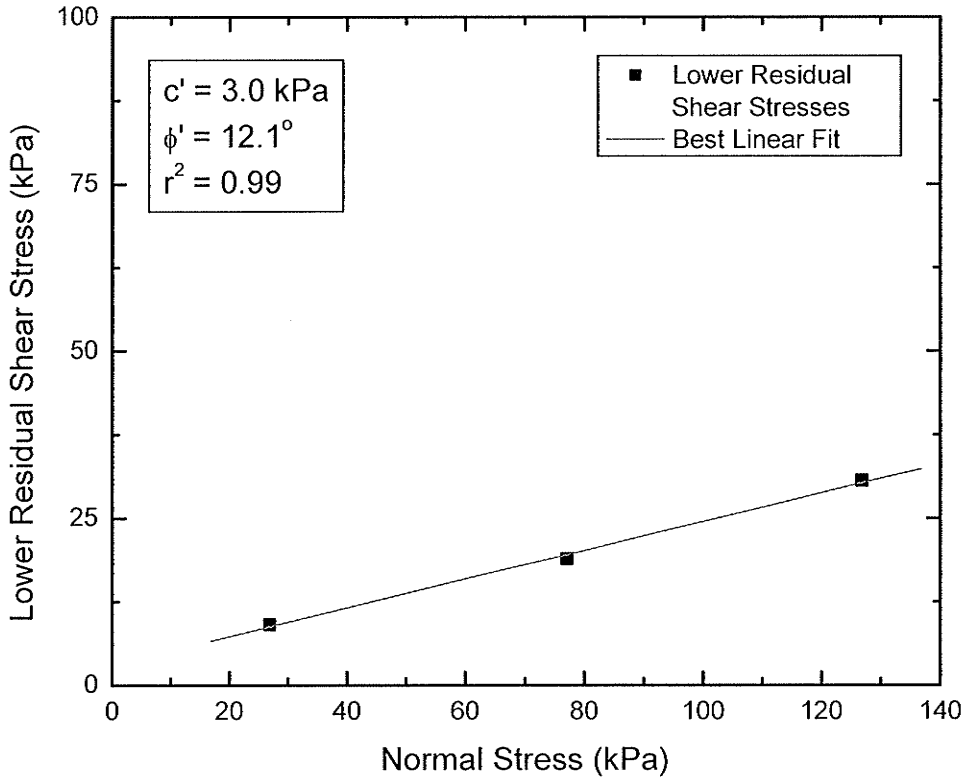

Figure 3.51 – Lower Residual Shear Stress versus Normal Stress for dry HD PES on dry WSFPP interface tested in Large-scale Direct Shear Apparatus.

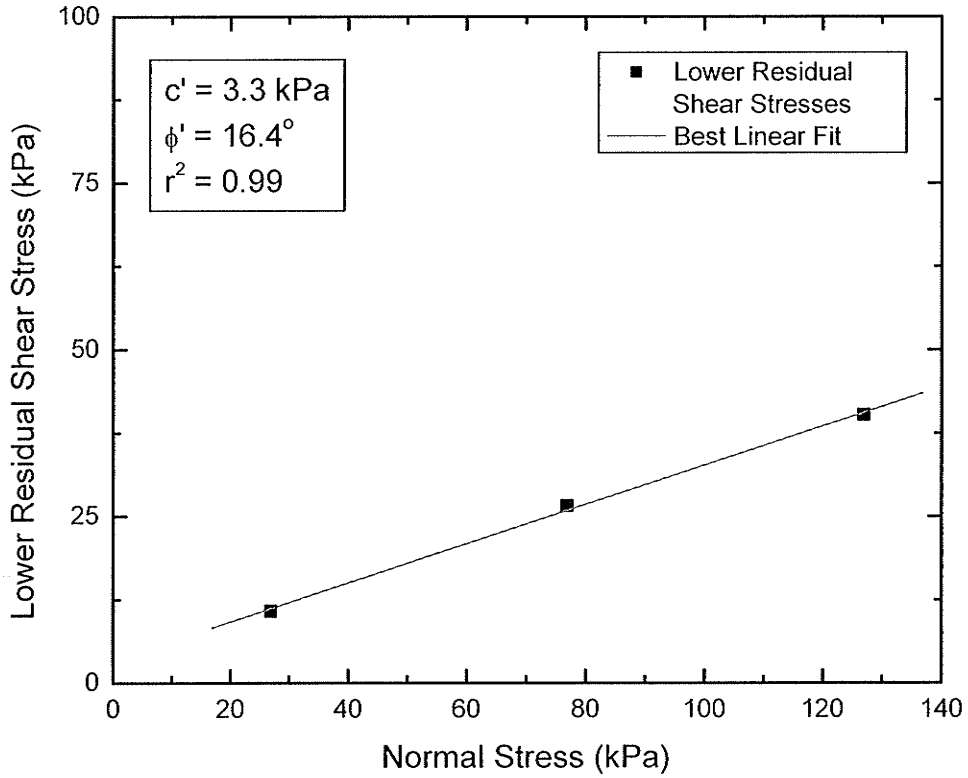

Figure 3.52 – Lower Residual Shear Stress versus Normal Stress for dry WSFPP on dry WSFPP interface tested in Large-scale Direct Shear Apparatus.

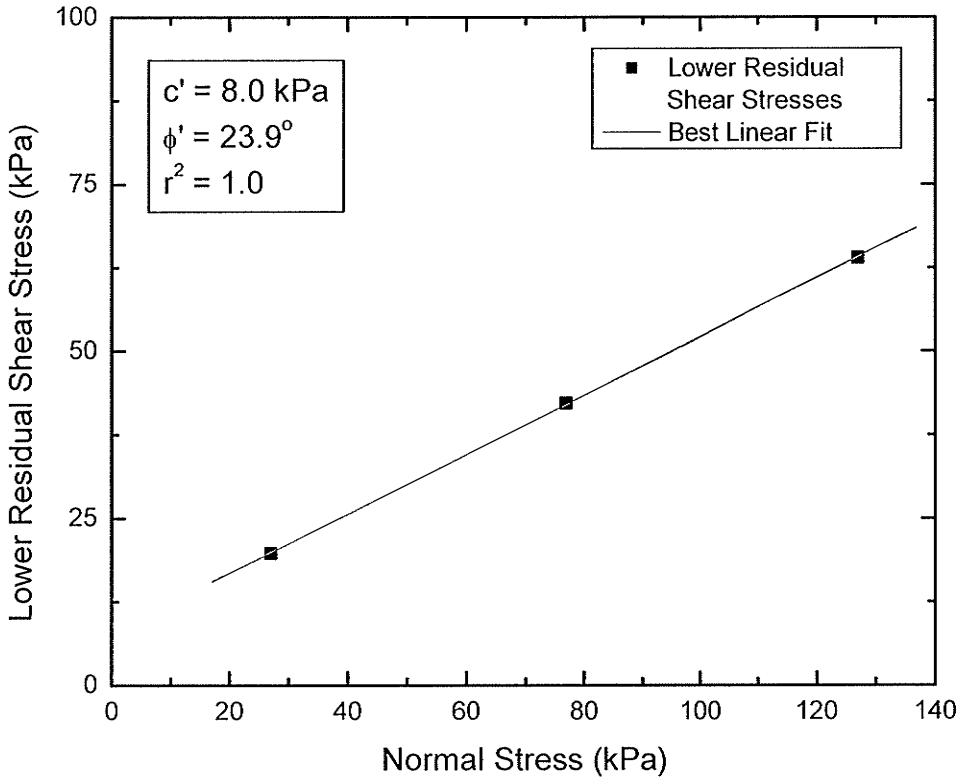

Figure 3.53 – Lower Residual Shear Stress versus Normal Stress for RMC Sand on dry WSFPP interface tested in Large-scale Direct Shear Apparatus.

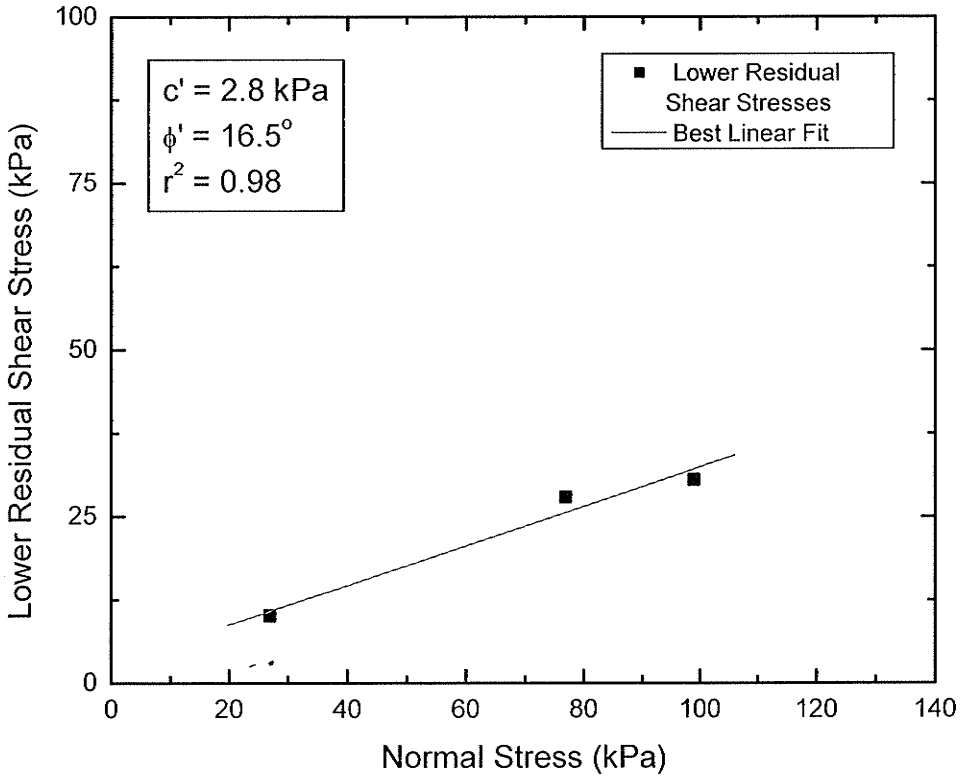

Figure 3.54 – Lower Residual Shear Stress versus Normal Stress for dry HD PES on unsaturated Sod interface tested in Large-scale Direct Shear Apparatus.

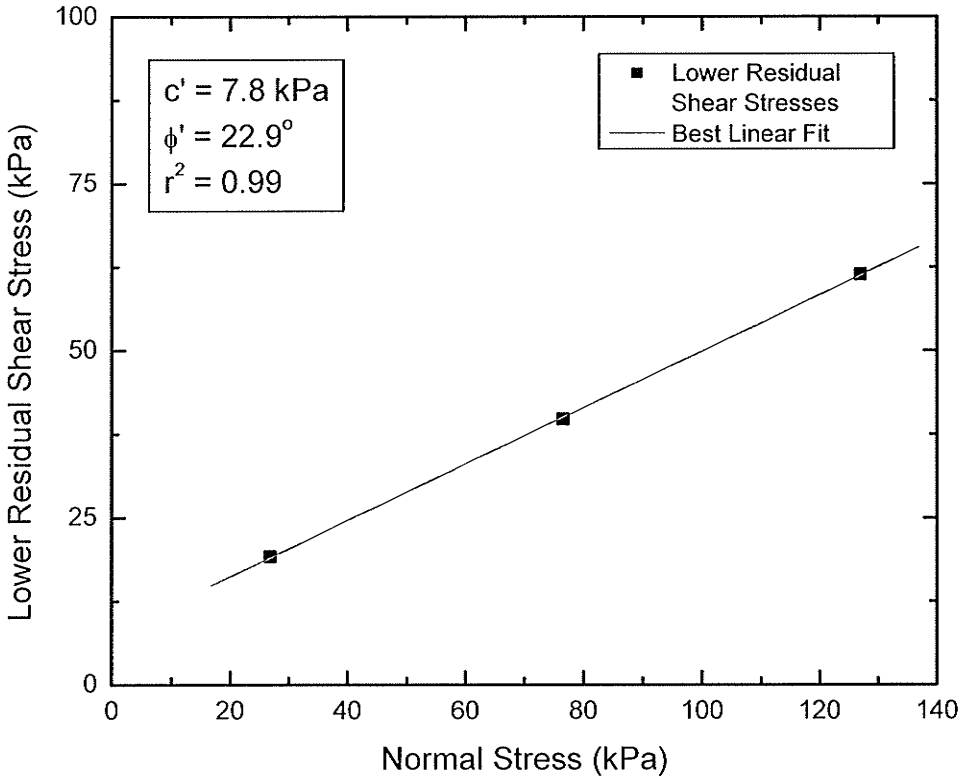

Figure 3.55 – Lower Residual Shear Stress versus Normal Stress for dry WSFPP on unsaturated Sod interface tested in Large-scale Direct Shear Apparatus.

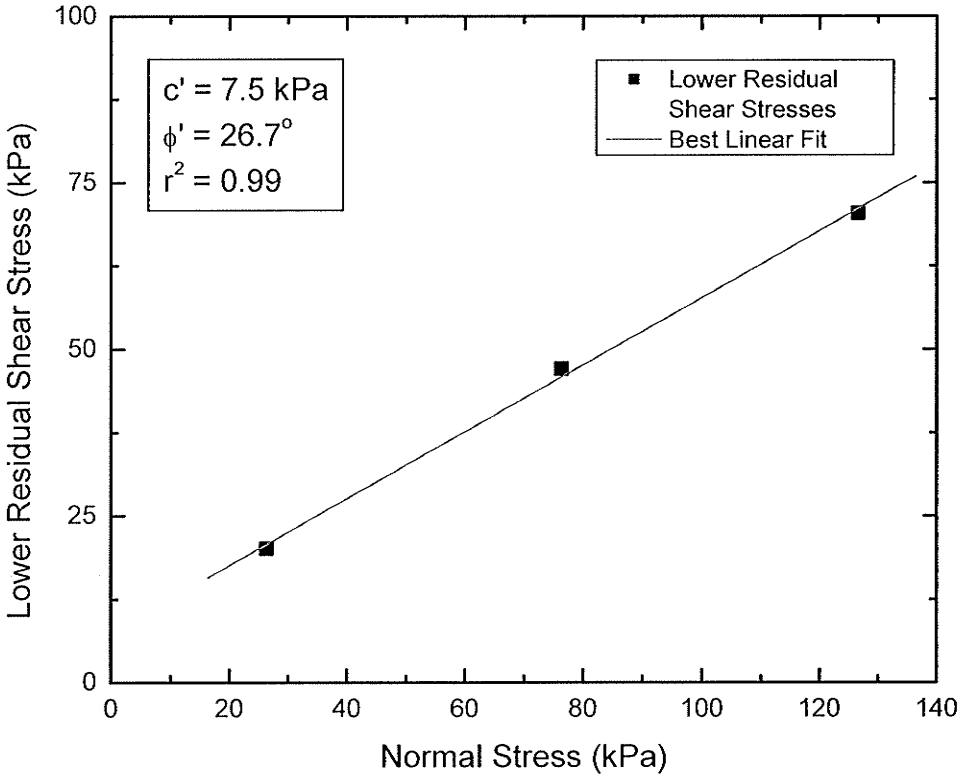

Figure 3.56 – Lower Residual Shear Stress versus Normal Stress for filled Sandbags on unsaturated Sod interface tested in Large-scale Direct Shear Apparatus.

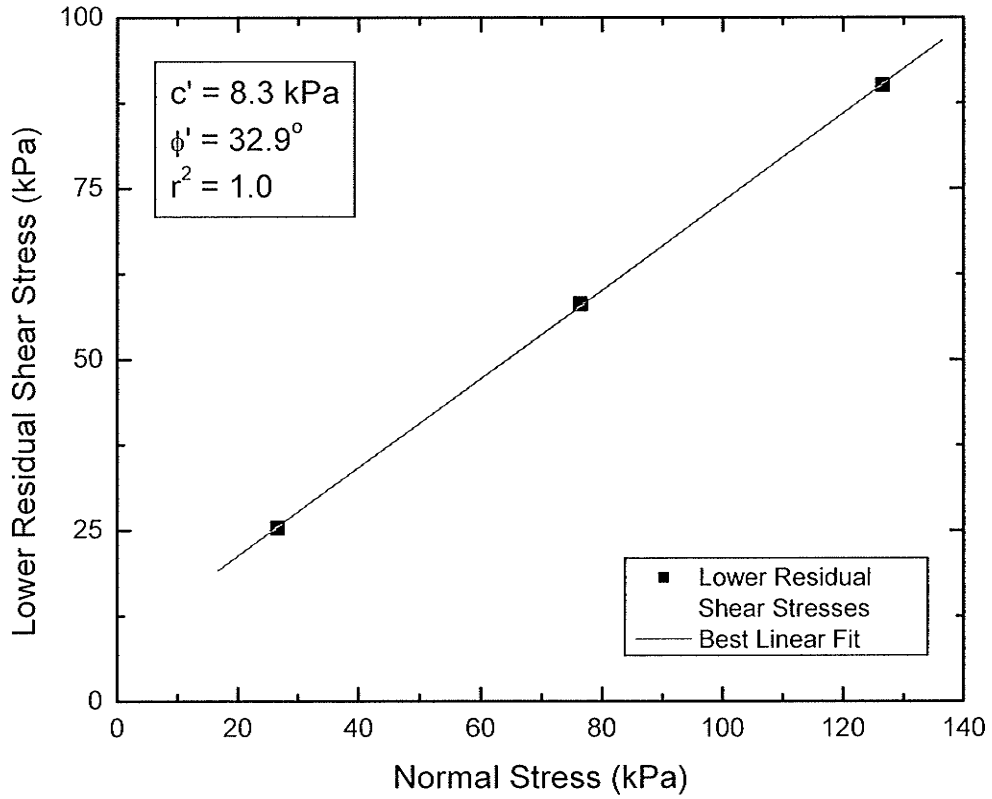

Figure 3.57 – Lower Residual Shear Stress versus Normal Stress for filled Sandbags on filled Sandbags interface tested in Large-scale Direct Shear Apparatus.

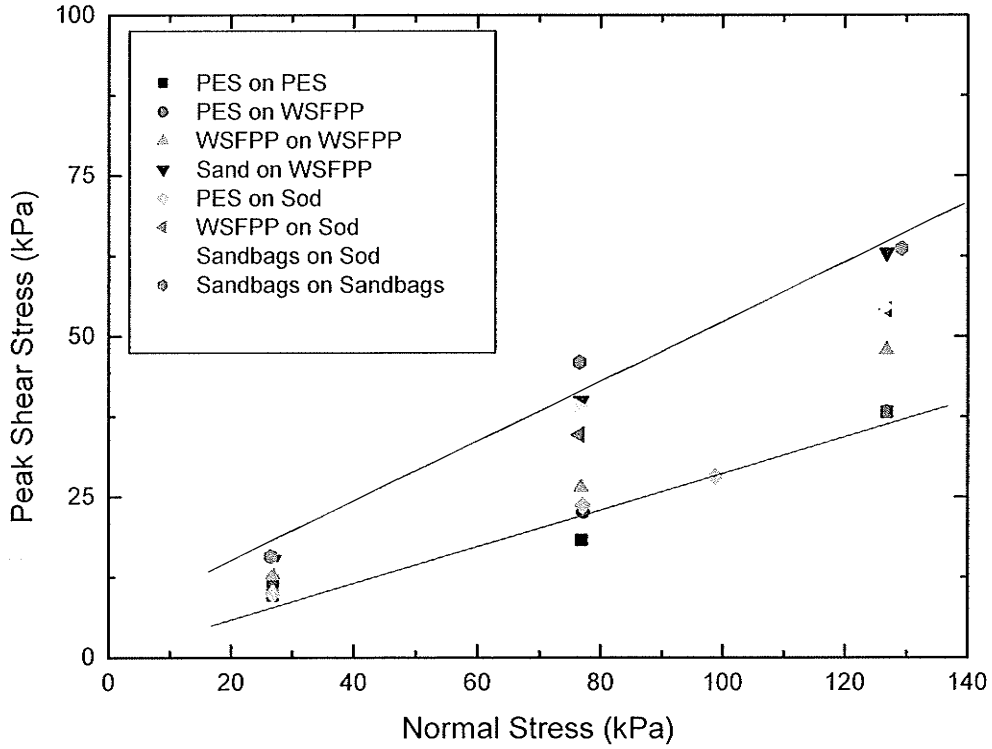

Figure 3.58 – Peak Shear Stress versus Normal Stress Summary for all interfaces tested in Large-scale Direct Shear Apparatus.

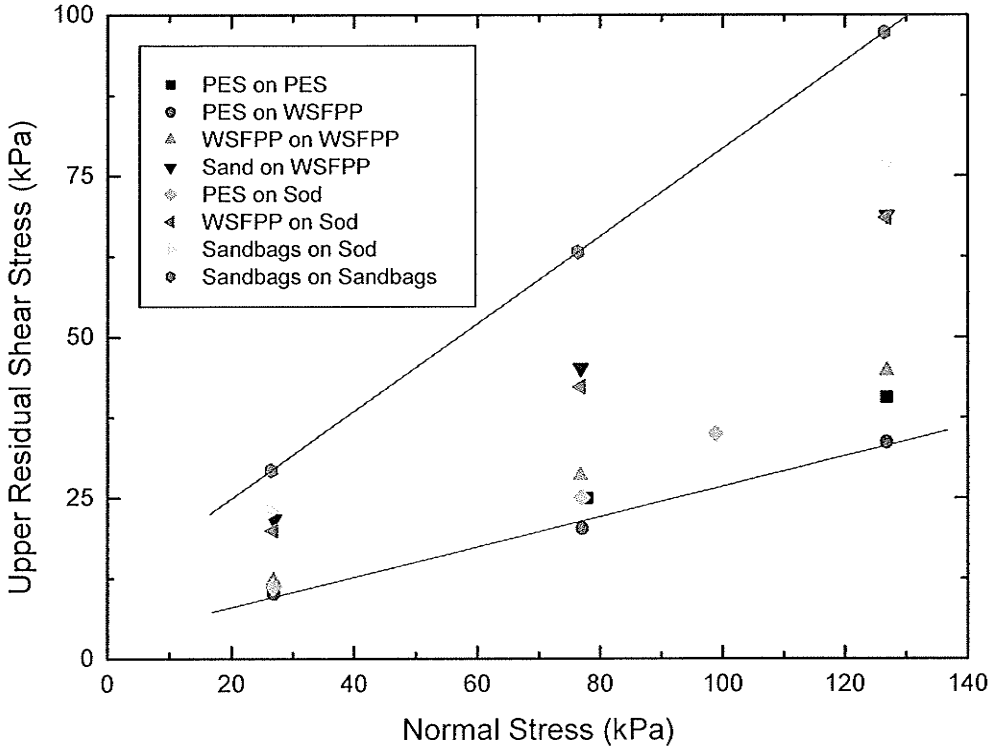

Figure 3.59 – Upper Residual Shear Stress versus Normal Stress Summary for all interfaces tested in Large-scale Direct Shear Apparatus.

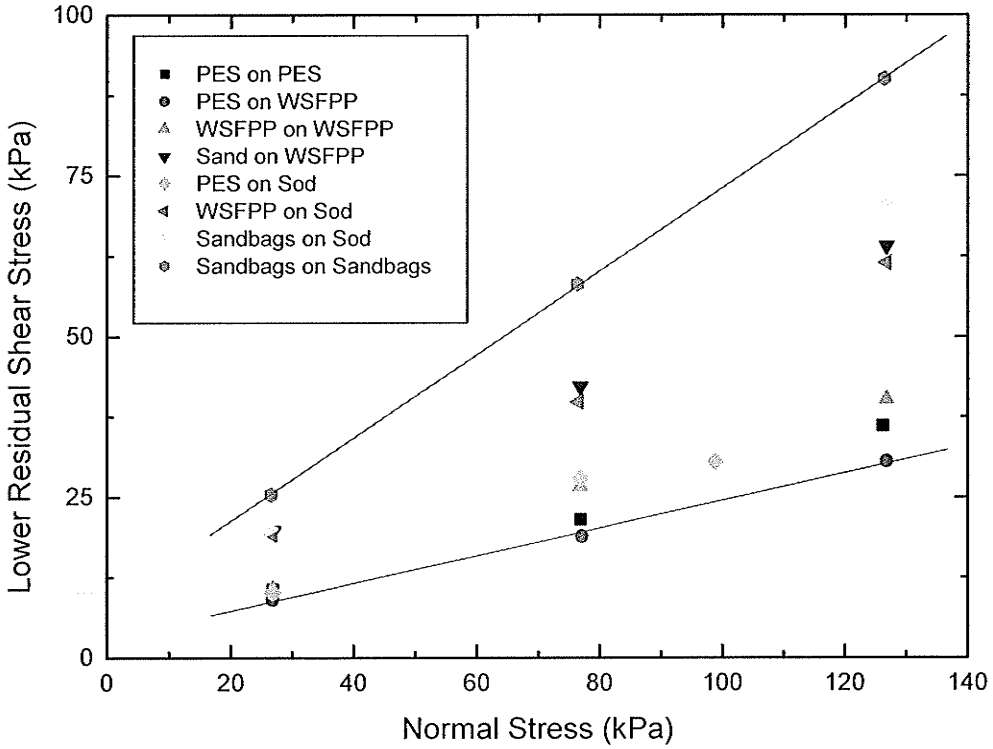

Figure 3.60 – Lower Residual Shear Stress versus Normal Stress Summary for all interfaces tested in Large-scale Direct Shear Apparatus.

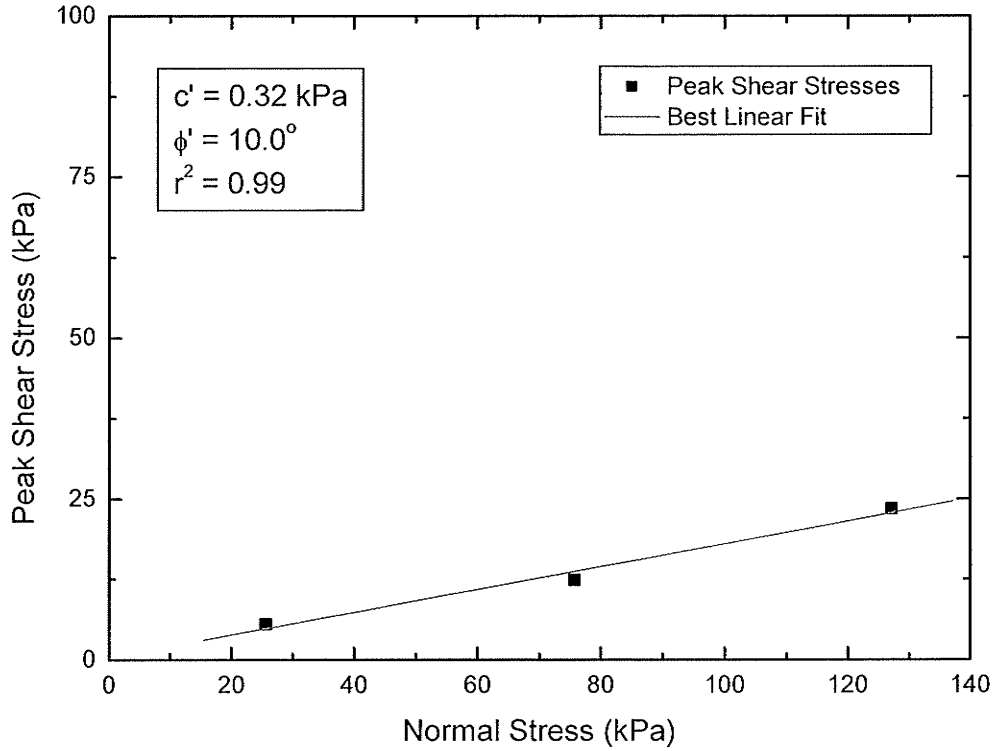

Figure 3.61 – Peak Shear Stress versus Normal Stress for dry CGSB PES on dry CGSB PES interface tested in Bench-scale Direct Shear Apparatus.

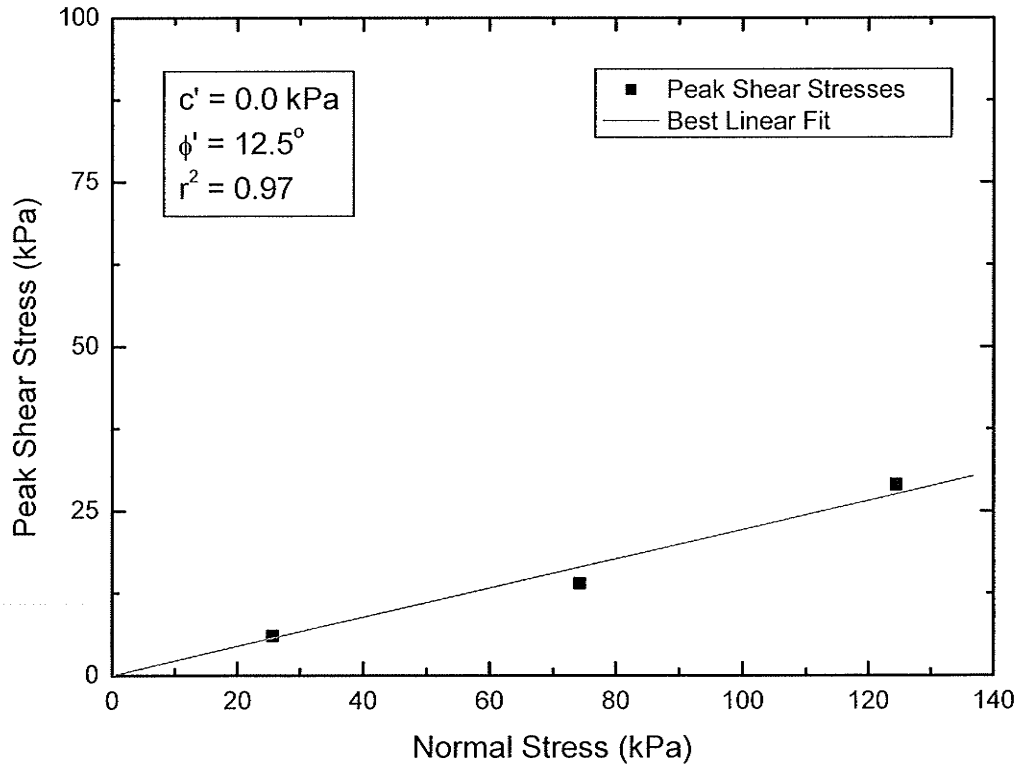

Figure 3.62 – Peak Shear Stress versus Normal Stress for dry HD PES on dry HD PES interface tested in Bench-scale Direct Shear Apparatus.

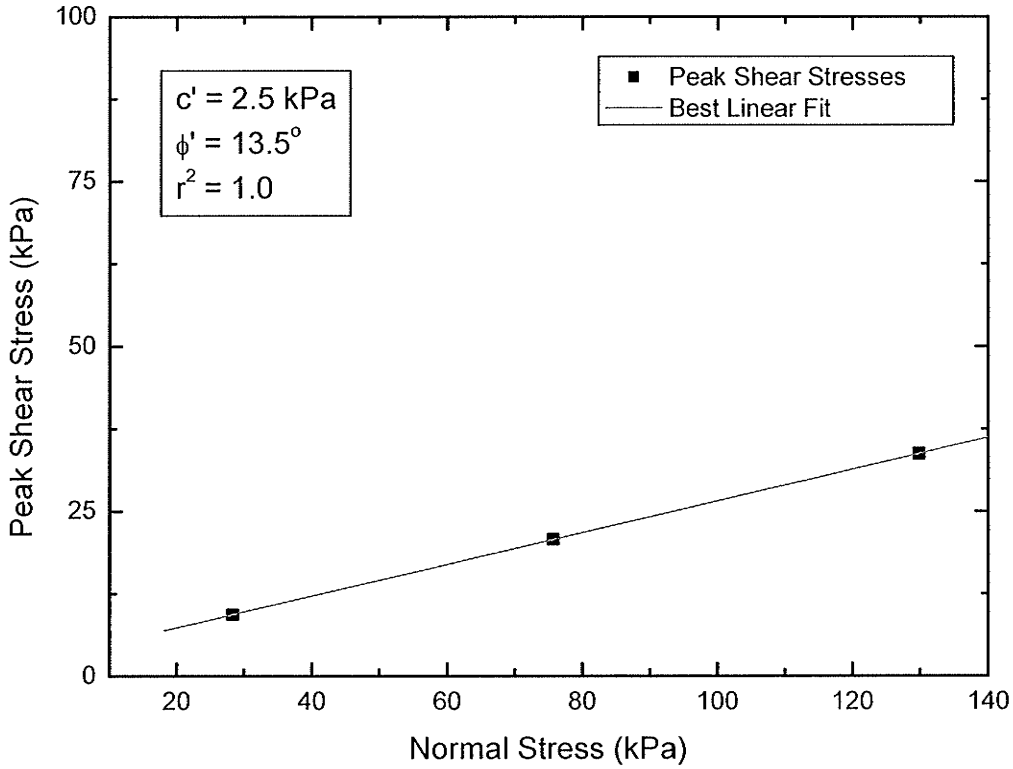

Figure 3.63 – Peak Shear Stress versus Normal Stress for dry CGSB PES on dry WSFPP interface tested in Bench-scale Direct Shear Apparatus.

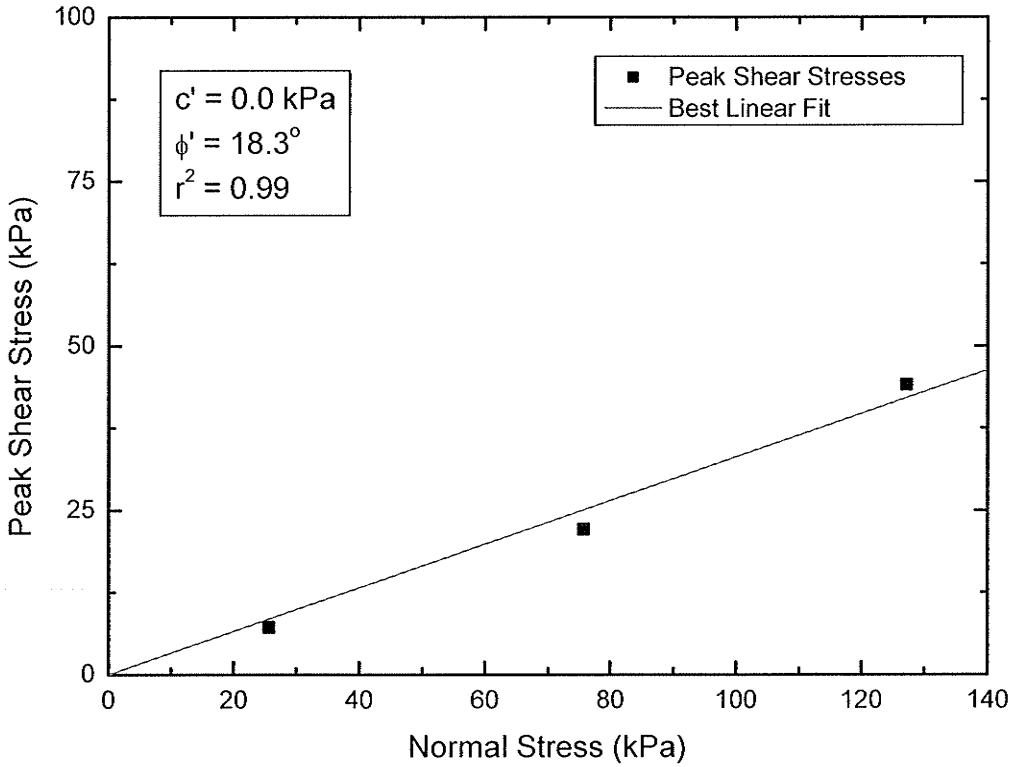

Figure 3.64 – Peak Shear Stress versus Normal Stress for dry WSFPP on dry WSFPP interface tested in Bench-scale Direct Shear Apparatus.

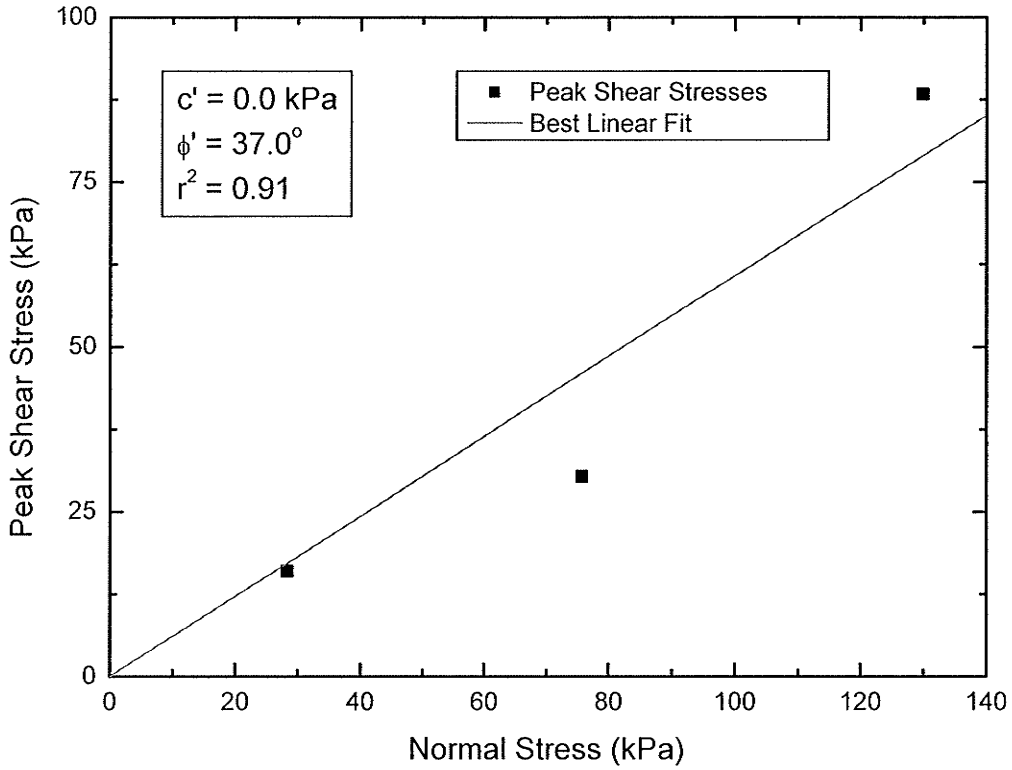

Figure 3.65 – Peak Shear Stress versus Normal Stress for dry Bird's Hill Sand on dry WSFPP interface tested in Bench-scale Direct Shear Apparatus.

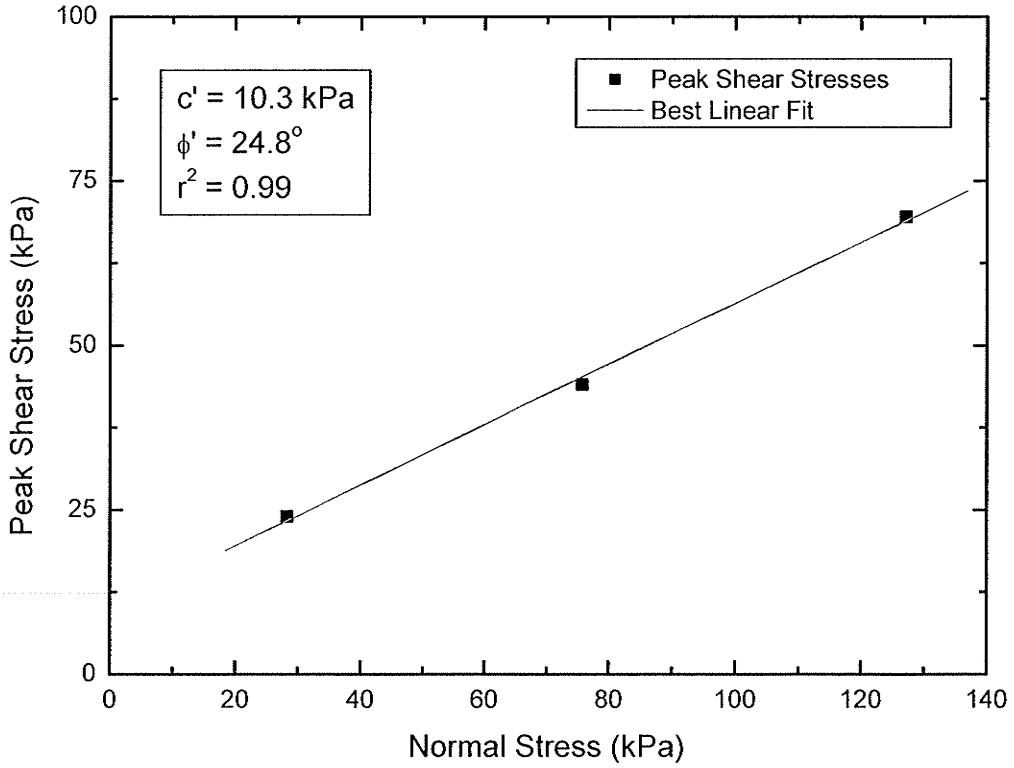

Figure 3.66 – Peak Shear Stress versus Normal Stress for dry Bird's Hill Sand on dry CGSB PES interface tested in Bench-scale Direct Shear Apparatus.

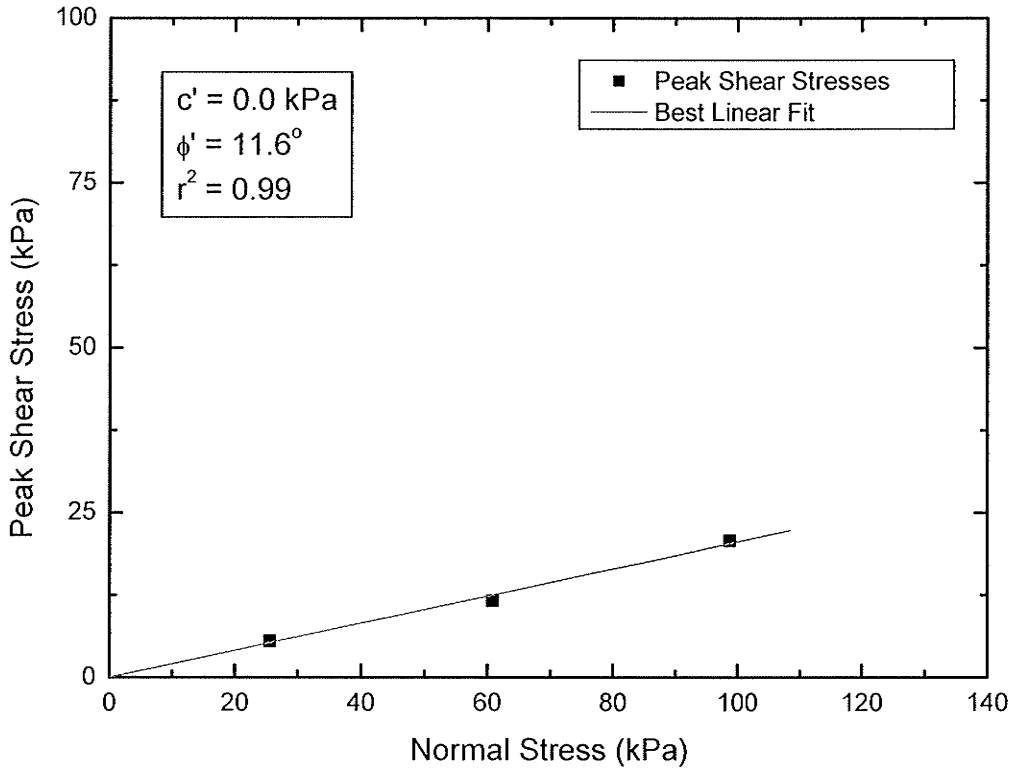

Figure 3.67 – Peak Shear Stress versus Normal Stress for Saturated CGSB PES on Saturated CGSB PES interface tested in Bench-scale Direct Shear Apparatus.

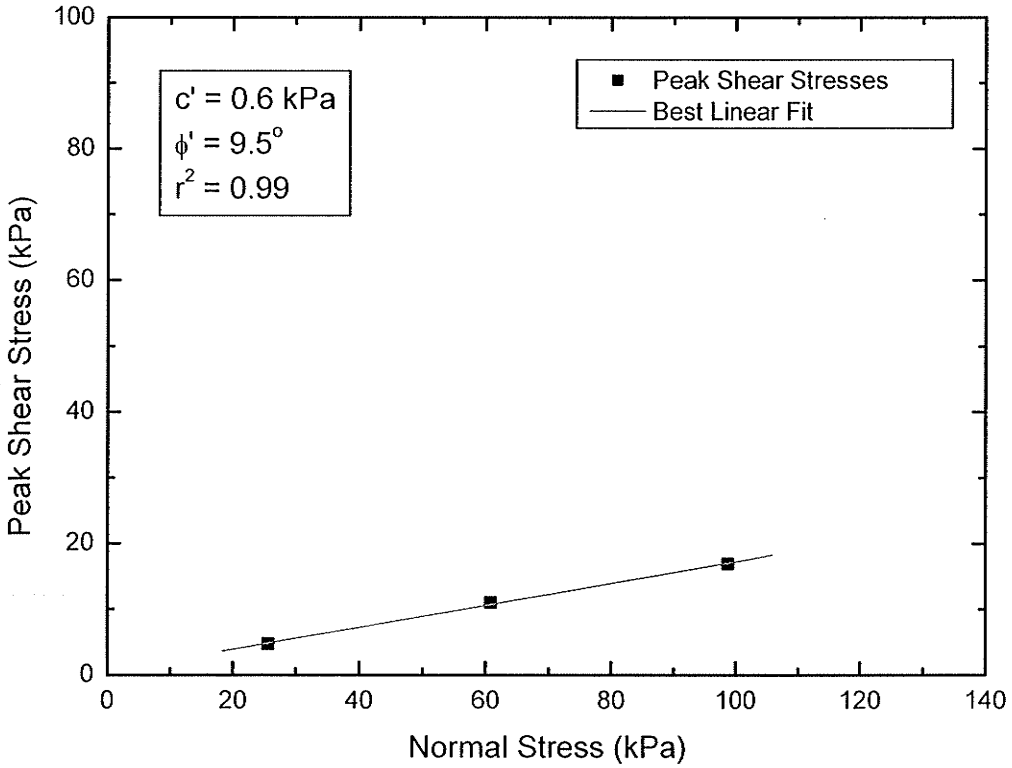

Figure 3.68 – Peak Shear Stress versus Normal Stress for Saturated CGSB PES on Saturated WSFPP interface tested in Bench-scale Direct Shear Apparatus.

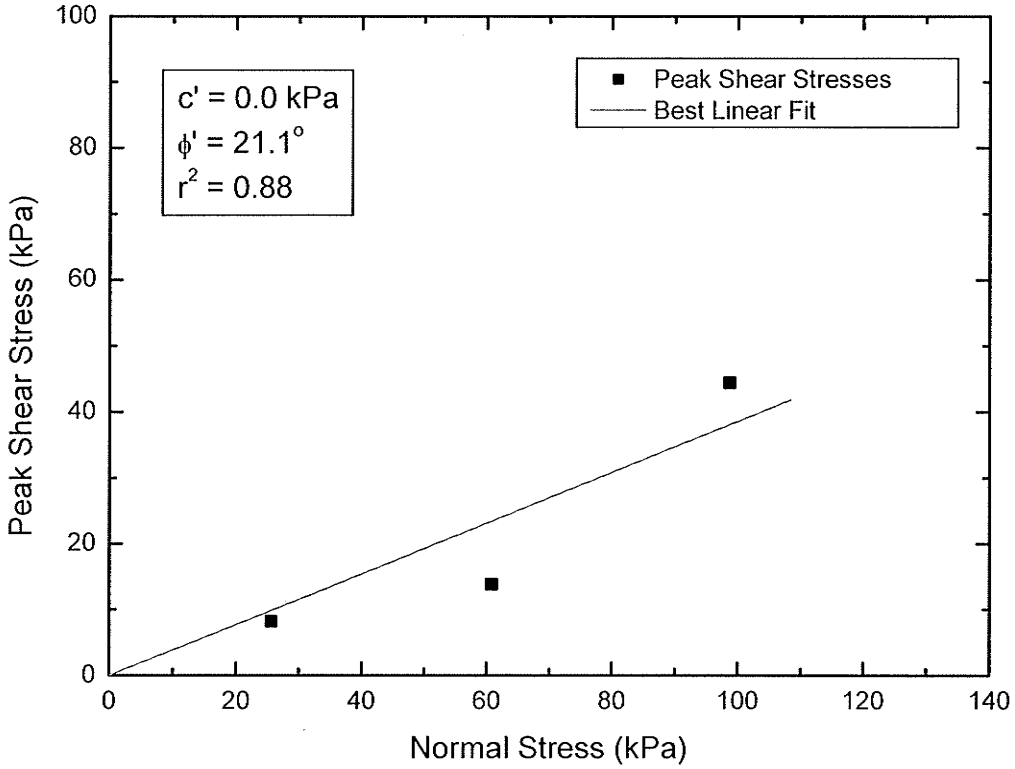

Figure 3.69 – Peak Shear Stress versus Normal Stress for Saturated WSFPP on Saturated WSFPP interface tested in Bench-scale Direct Shear Apparatus.

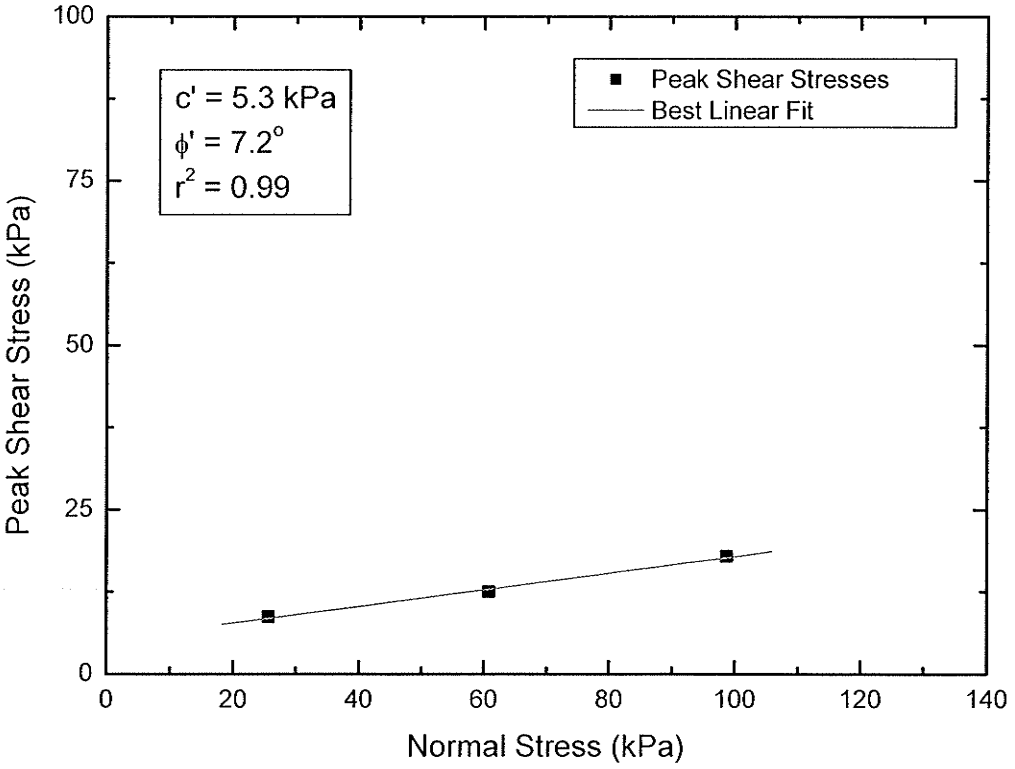

Figure 3.70 – Peak Shear Stress versus Normal Stress for Scrubbed WSFPP on CGSB PES interface tested in Bench-scale Direct Shear Apparatus.

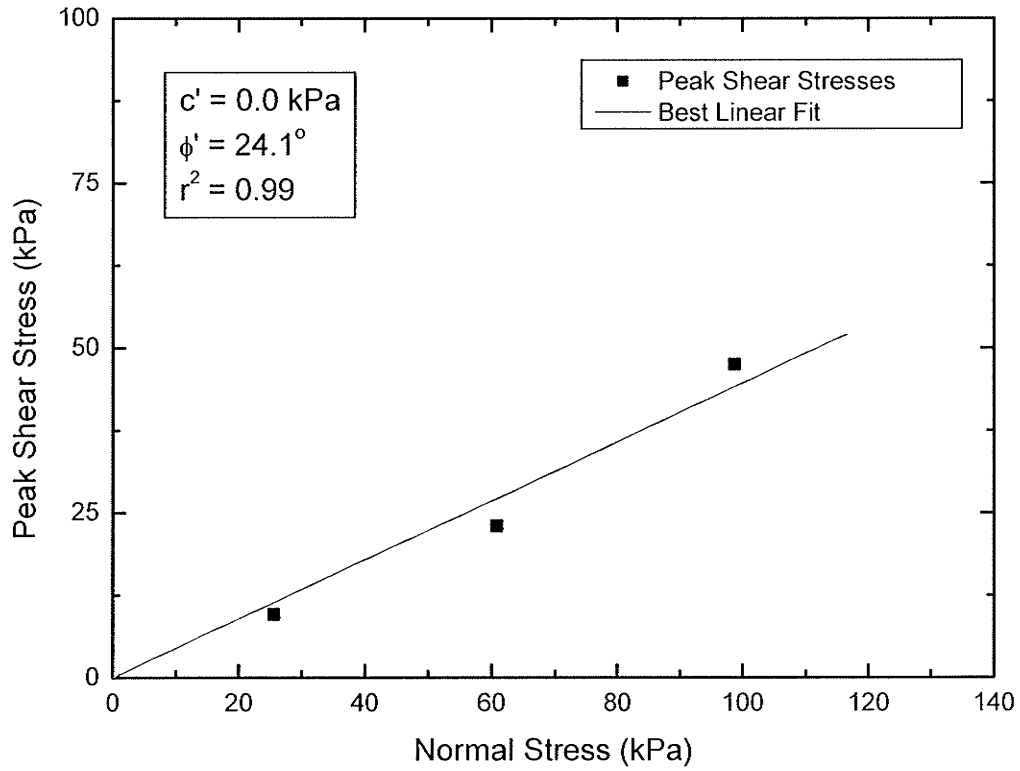

Figure 3.71 – Peak Shear Stress versus Normal Stress for Scrubbed WSFPP on Scrubbed WSFPP interface tested in Bench-scale Direct Shear Apparatus.

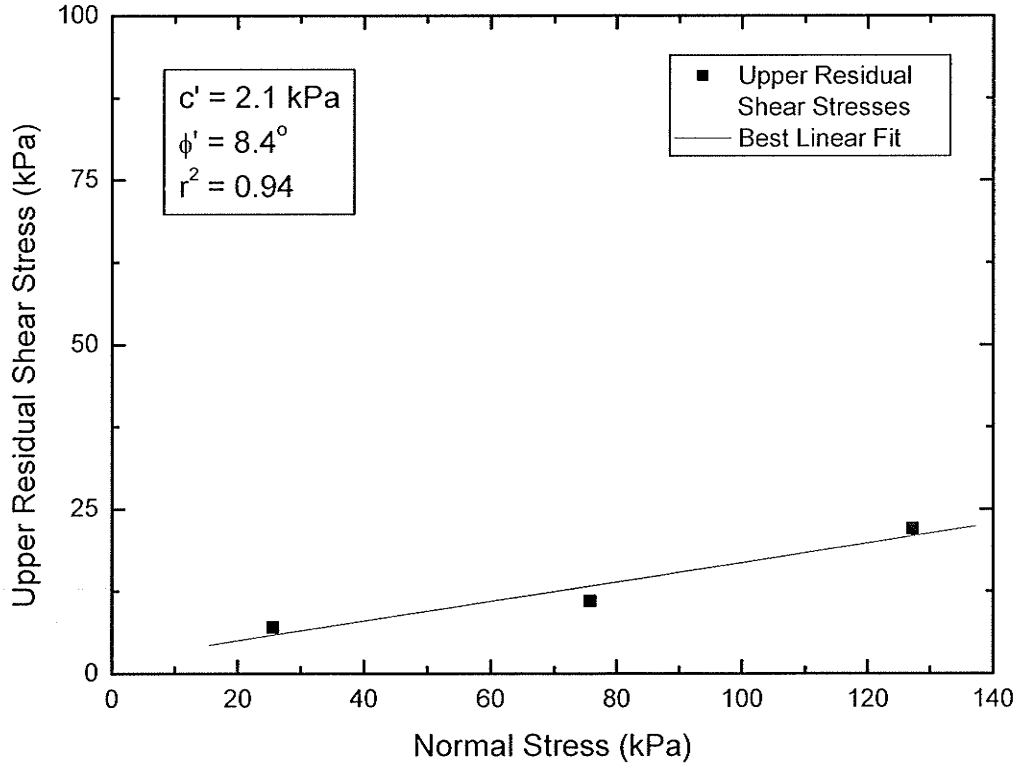

Figure 3.72 – Upper Residual Shear Stress versus Normal Stress for dry CGSB PES on dry CGSB PES interface tested in Bench-scale Direct Shear Apparatus.

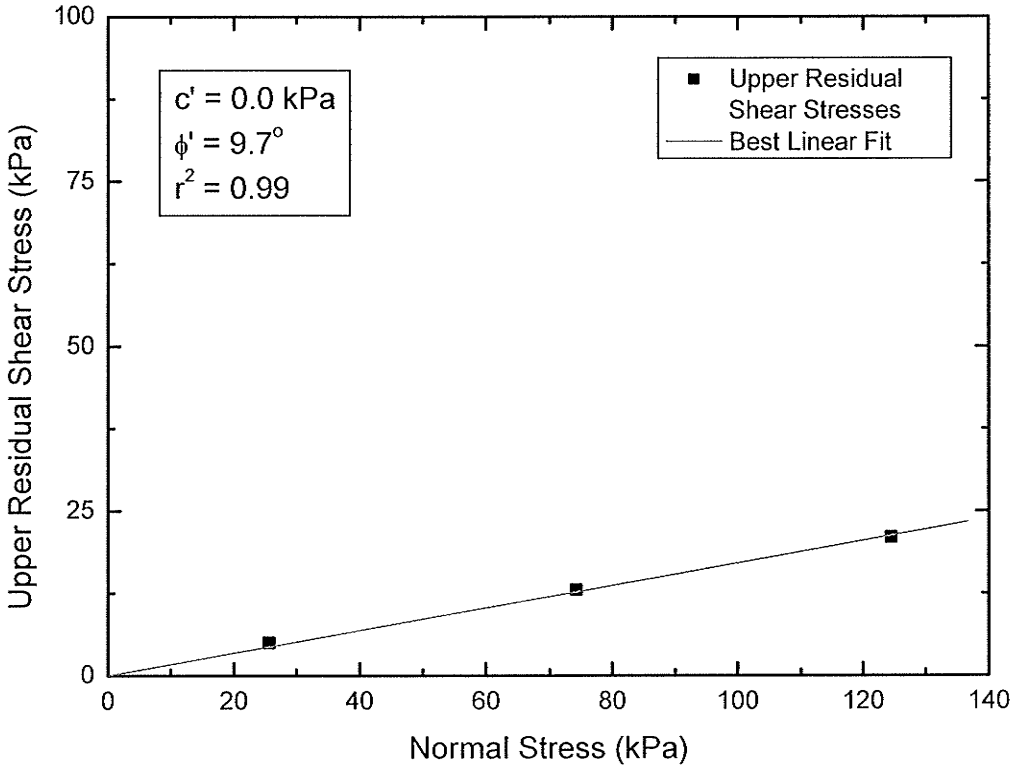

Figure 3.73 – Upper Residual Shear Stress versus Normal Stress for dry HD PES on dry HD PES interface tested in Bench-scale Direct Shear Apparatus.

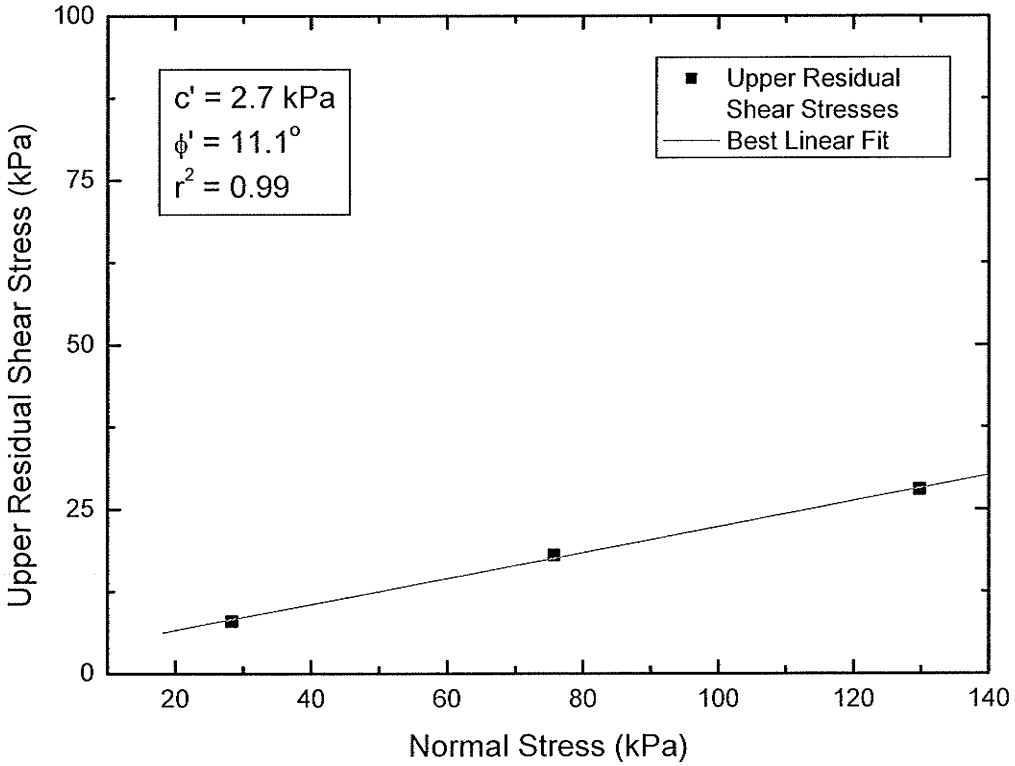

Figure 3.74 – Upper Residual Shear Stress versus Normal Stress for dry CGSB PES on dry WSFPP interface tested in Bench-scale Direct Shear Apparatus.

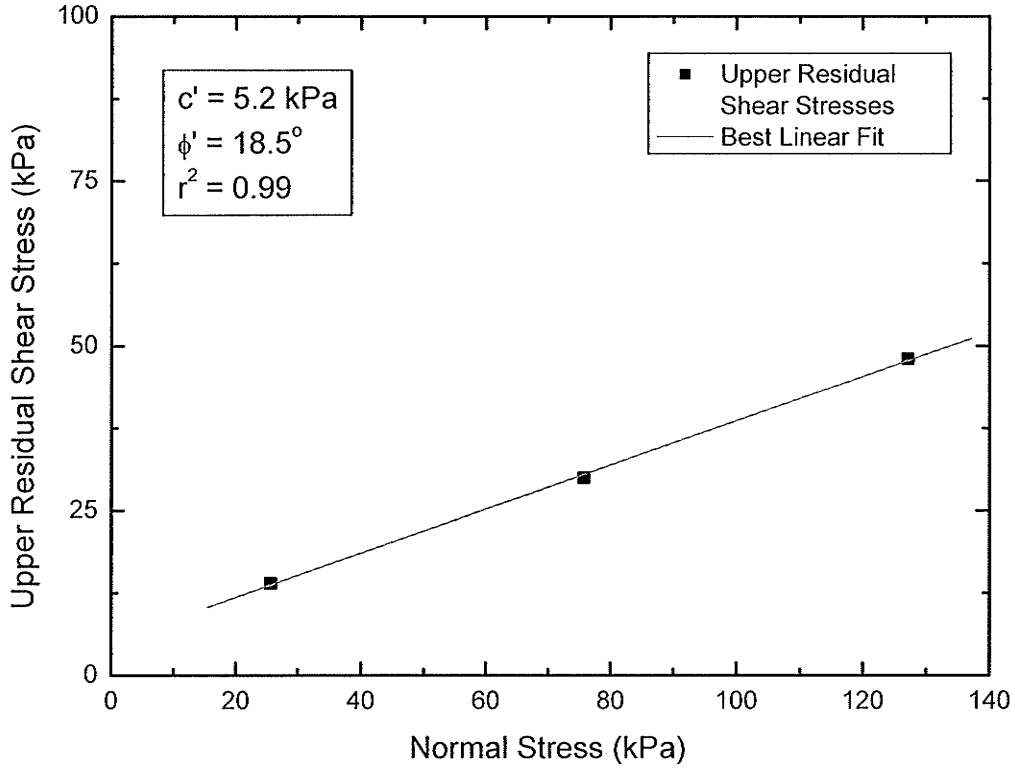

Figure 3.75 – Upper Residual Shear Stress versus Normal Stress for dry WSFPP on dry WSFPP interface tested in Bench-scale Direct Shear Apparatus.

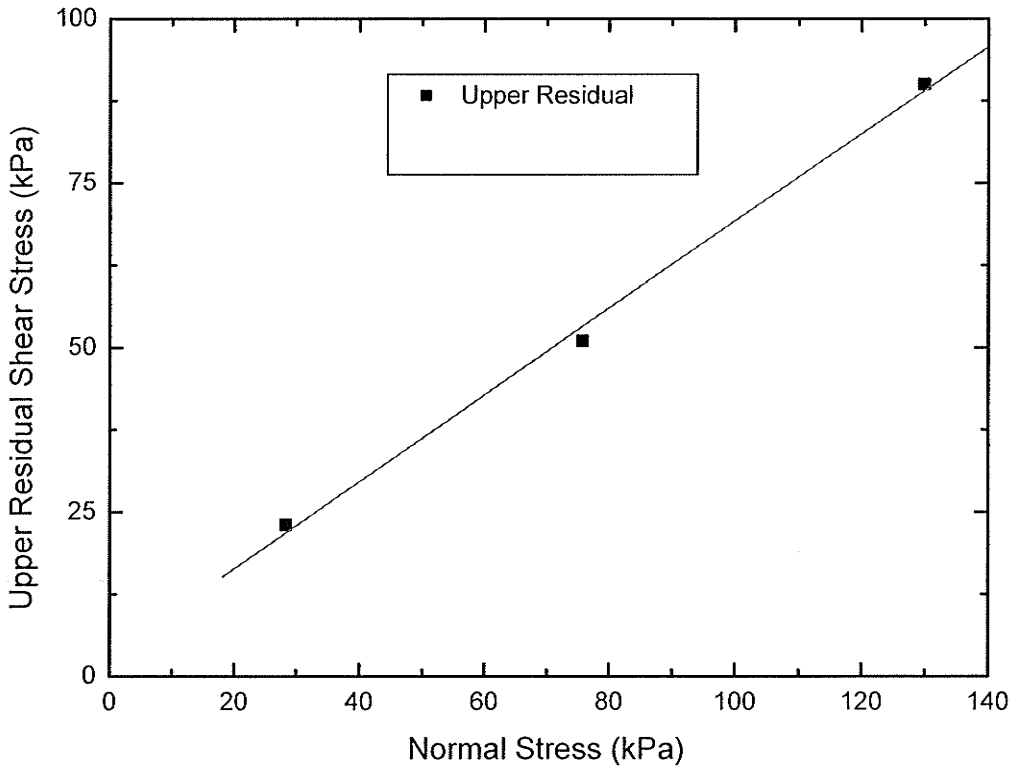

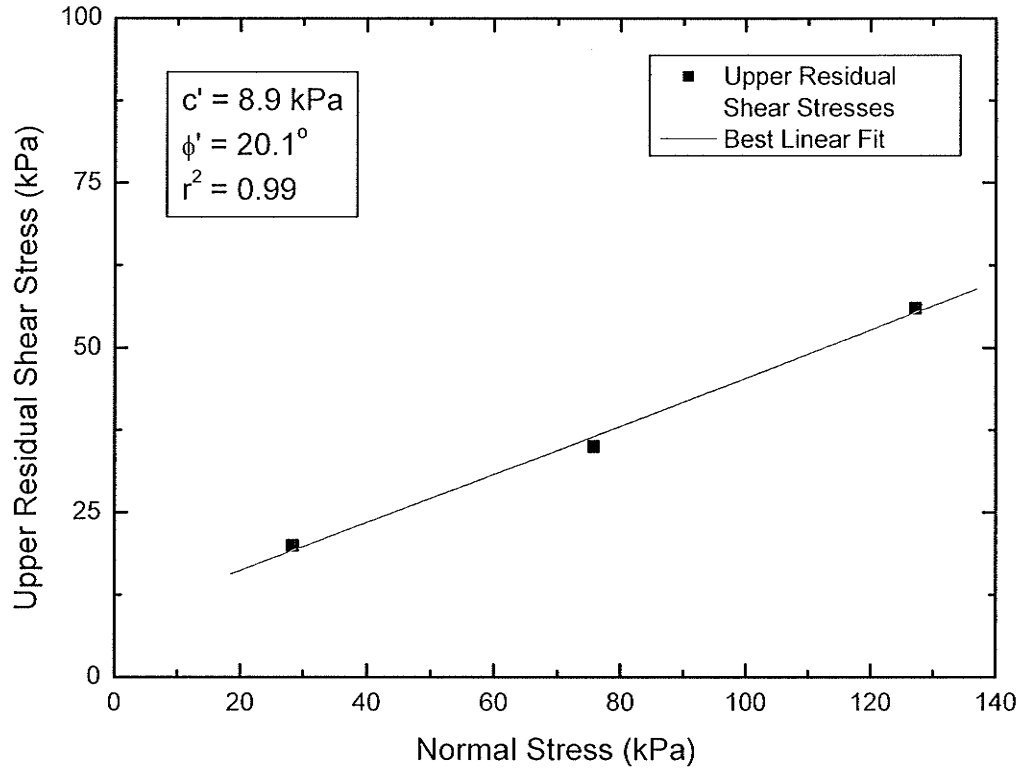

Figure 3.77 – Upper Residual Shear Stress versus Normal Stress for dry Bird's Hill Sand on dry CGSB PES interface tested in Bench-scale Direct Shear Apparatus.

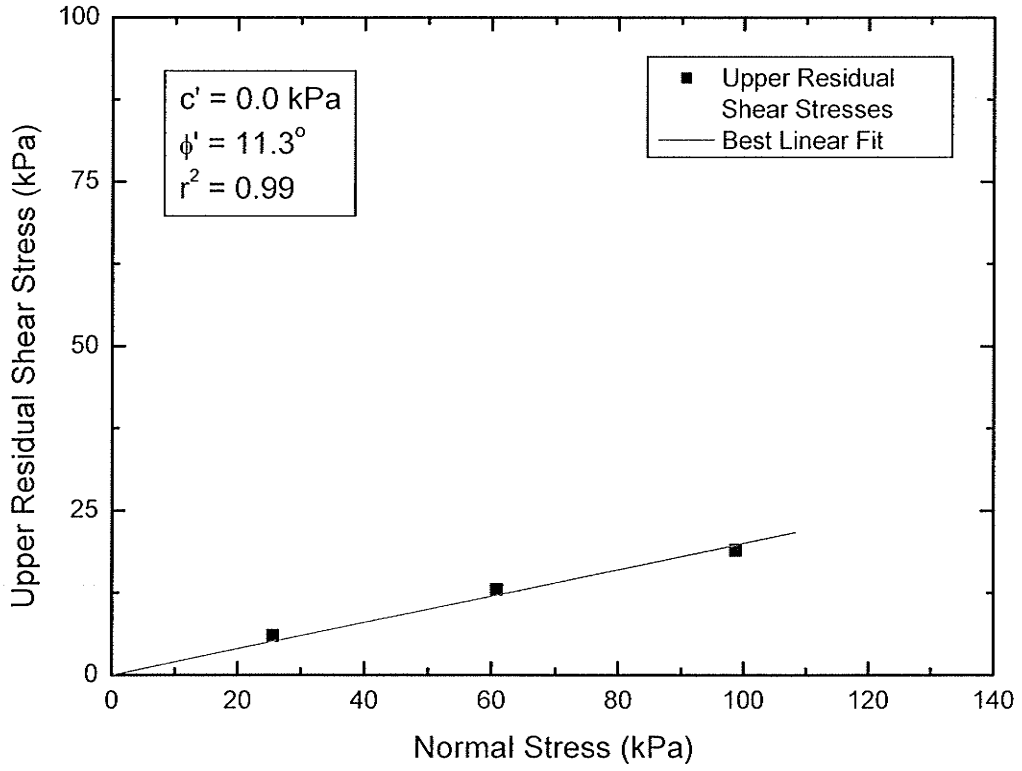

Figure 3.78 – Upper Residual Shear Stress versus Normal Stress for Saturated CGSB PES on Saturated CGSB PES interface tested in Bench-scale Direct Shear Apparatus.

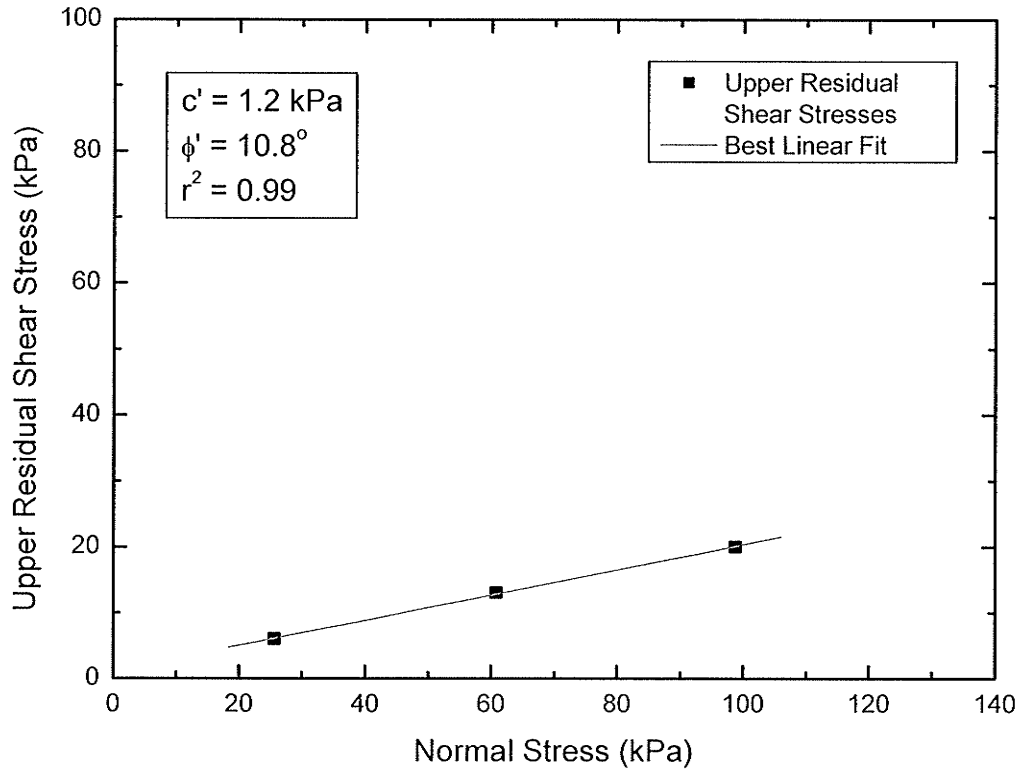

Figure 3.79 – Upper Residual Shear Stress versus Normal Stress for Saturated CGSB PES on Saturated WSFPP interface tested in Bench-scale Direct Shear Apparatus.

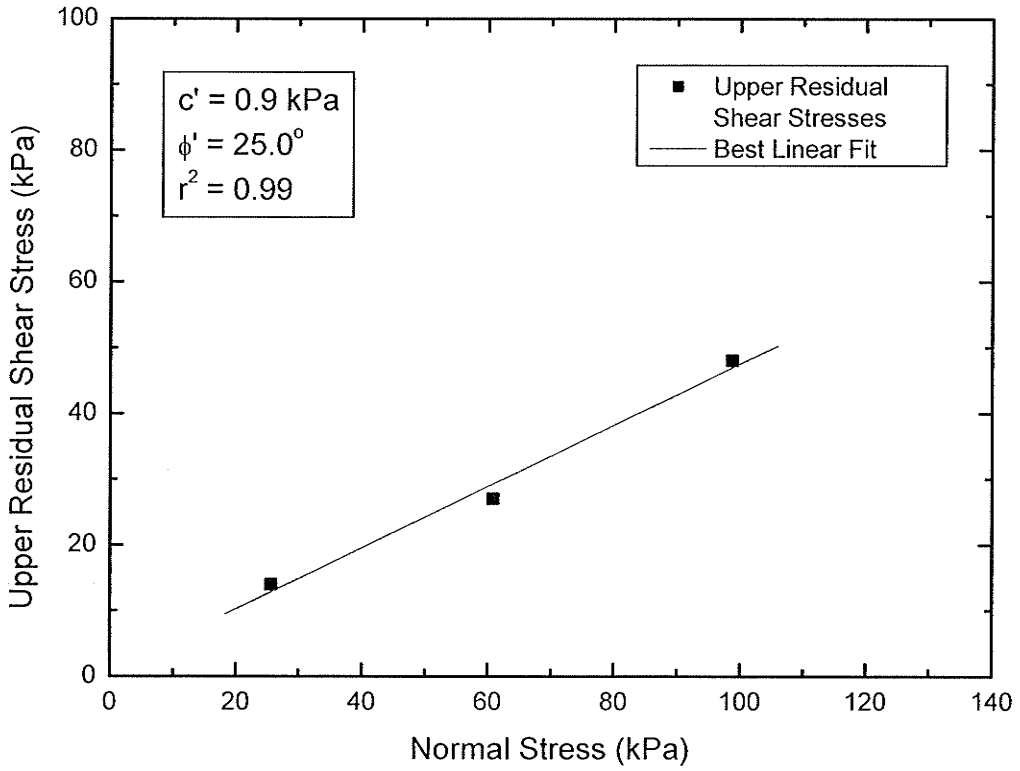

Figure 3.80 – Upper Residual Shear Stress versus Normal Stress for Saturated WSFPP on Saturated WSFPP interface tested in Bench-scale Direct Shear Apparatus.

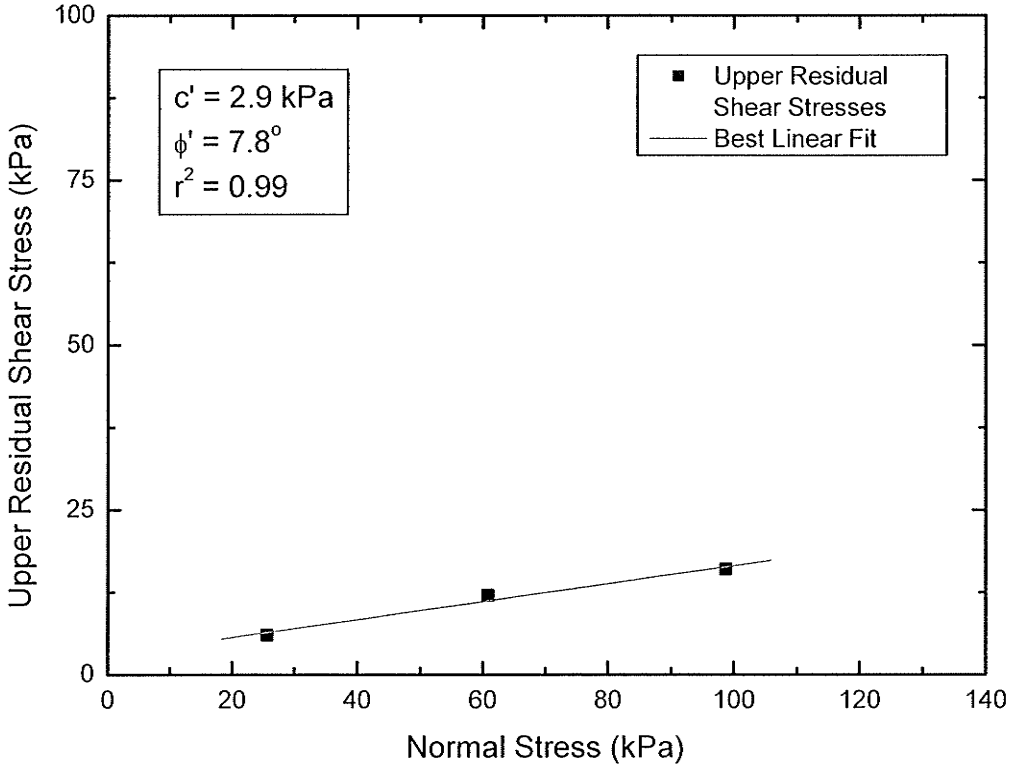

Figure 3.81 – Upper Residual Shear Stress versus Normal Stress for Scrubbed WSFPP on CGSB PES interface tested in Bench-scale Direct Shear Apparatus.

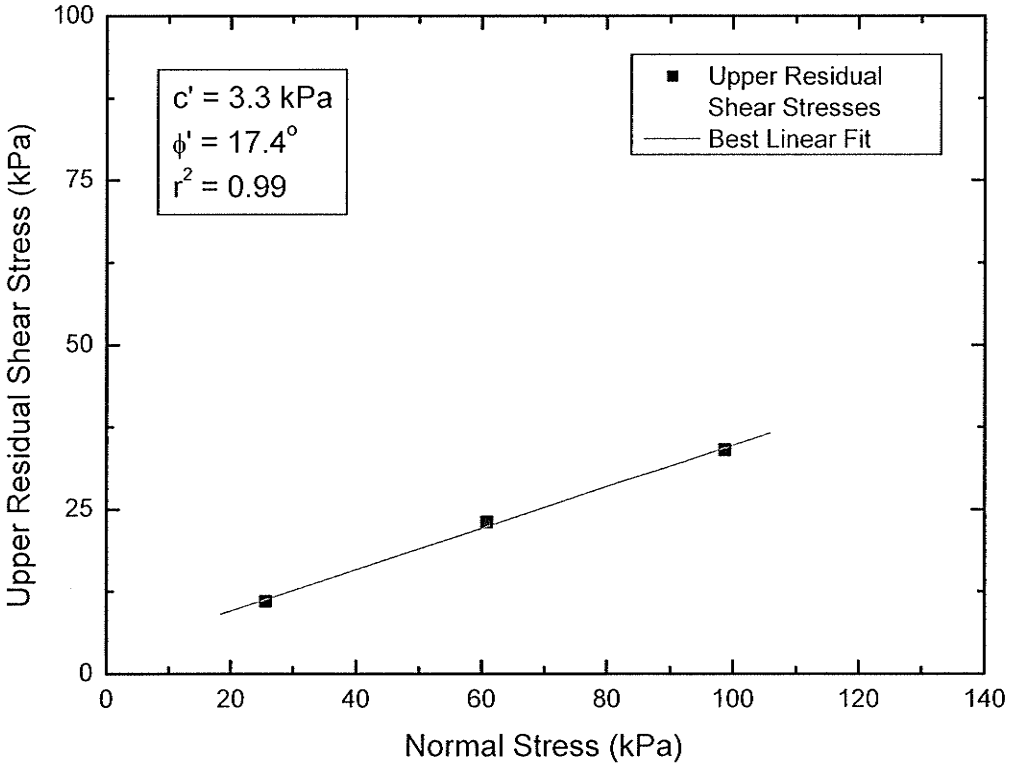

Figure 3.82 – Upper Residual Shear Stress versus Normal Stress for Scrubbed WSFPP on Scrubbed WSFPP interface tested in Bench-scale Direct Shear Apparatus.

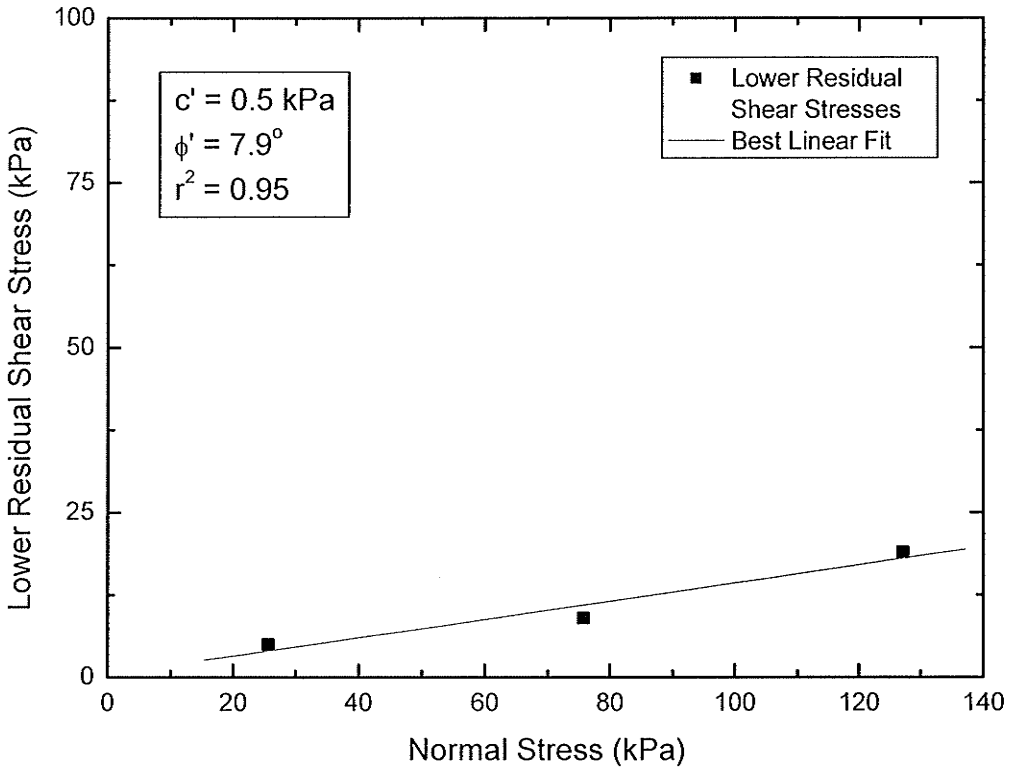

Figure 3.83 – Lower Residual Shear Stress versus Normal Stress for dry CGSB PES on dry CGSB PES interface tested in Bench-scale Direct Shear Apparatus.

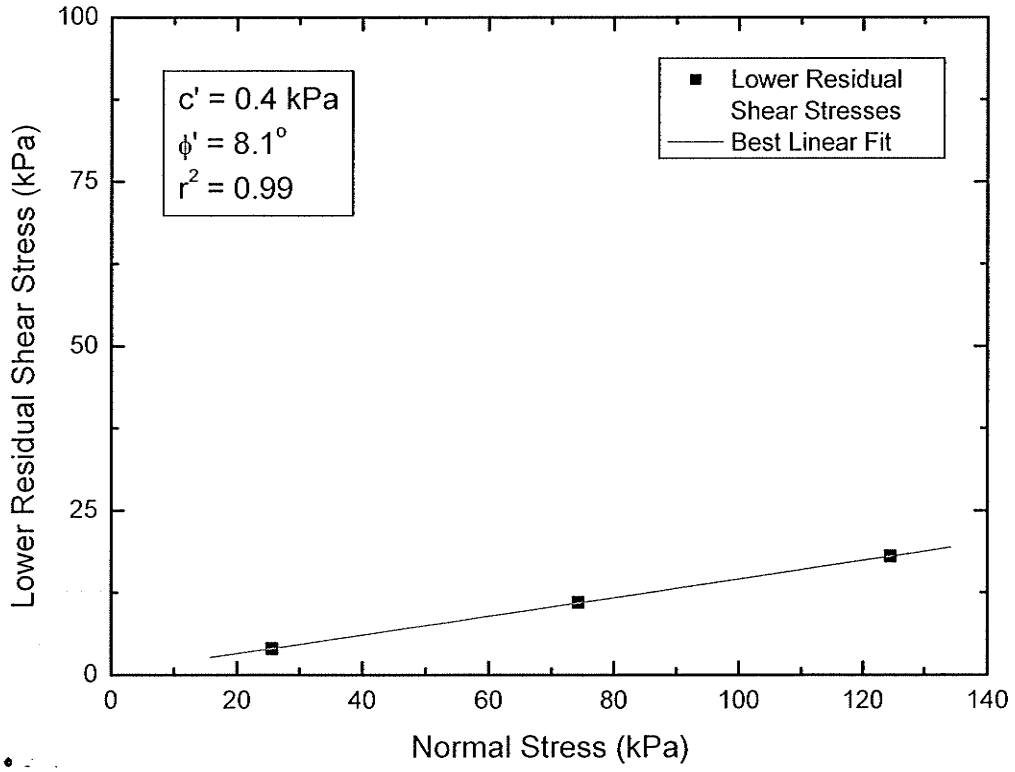

Figure 3.84 – Lower Residual Shear Stress versus Normal Stress for dry HD PES on dry HD PES interface tested in Bench-scale Direct Shear Apparatus.

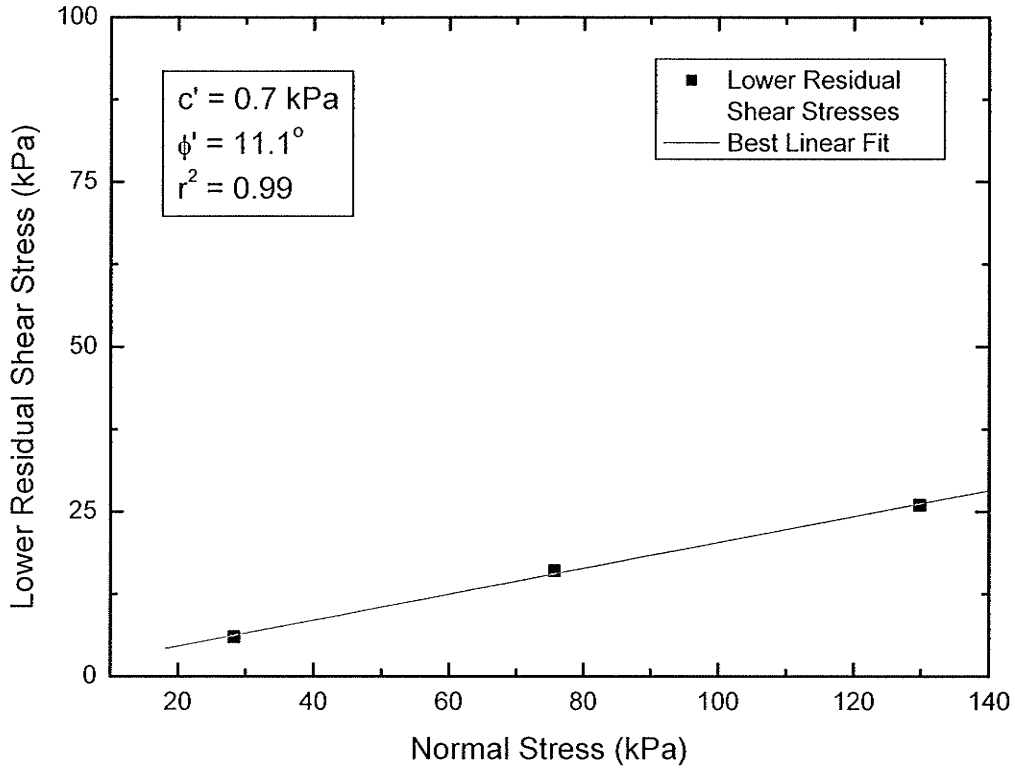

Figure 3.85 – Lower Residual Shear Stress versus Normal Stress for dry CGSB PES on dry WSFPP interface tested in Bench-scale Direct Shear Apparatus.

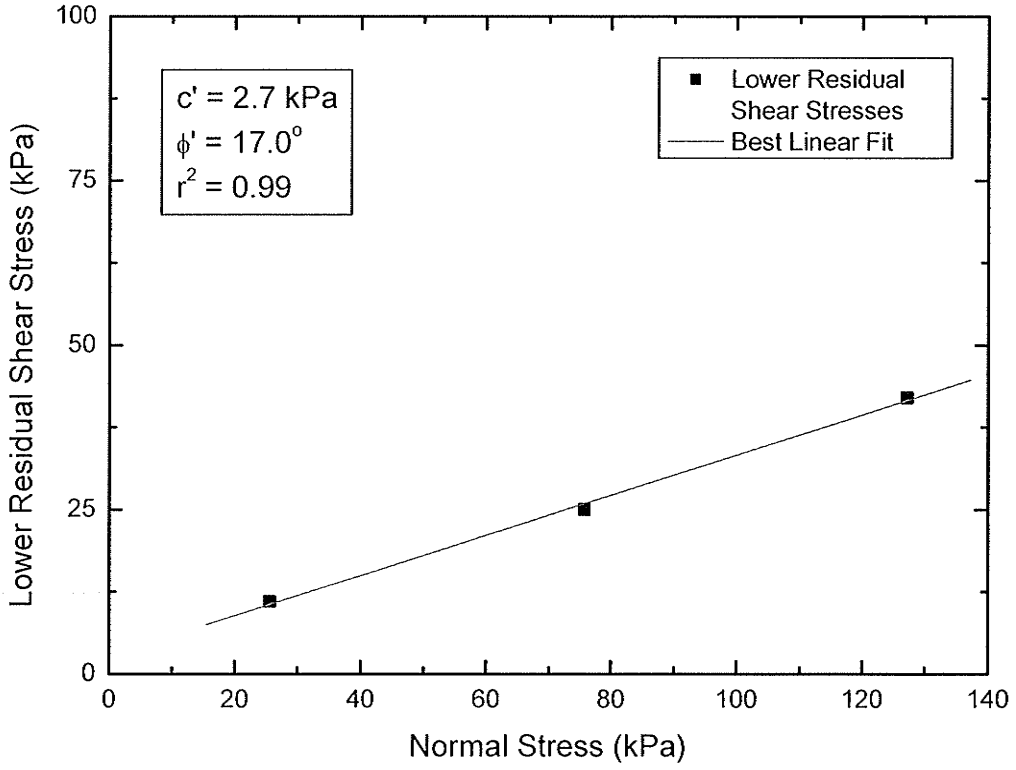

Figure 3.86 – Lower Residual Shear Stress versus Normal Stress for dry WSFPP on dry WSFPP interface tested in Bench-scale Direct Shear Apparatus.

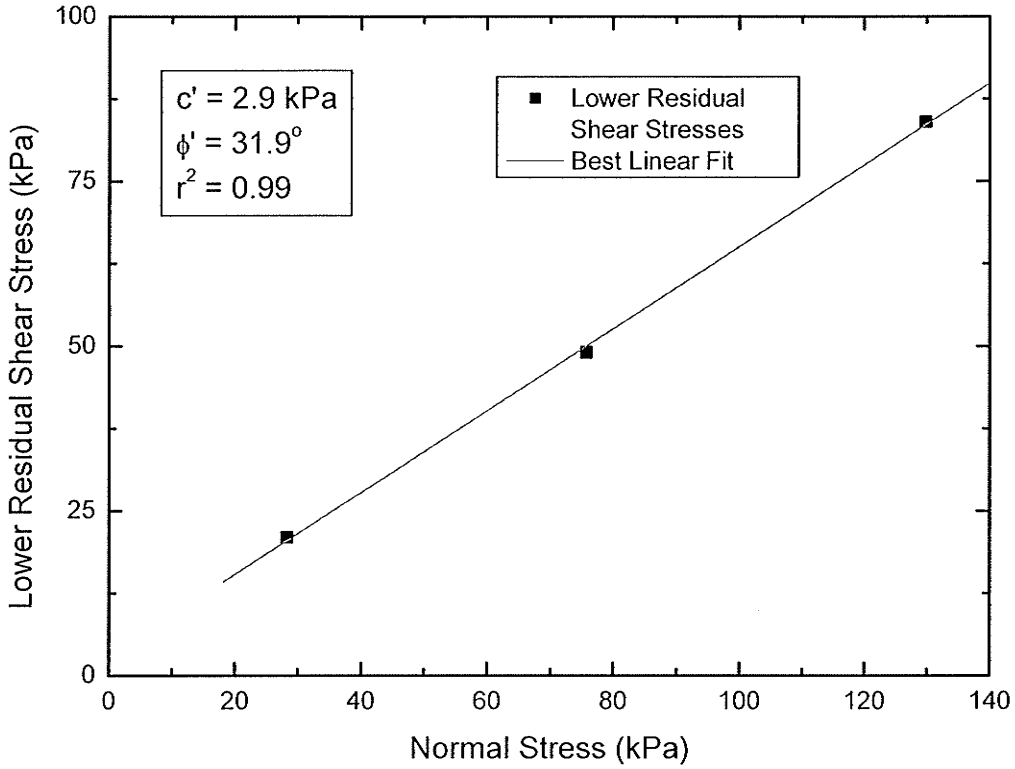

Figure 3.87 – Lower Residual Shear Stress versus Normal Stress for dry Bird's Hill Sand on dry WSFPP interface tested in Bench-scale Direct Shear Apparatus.

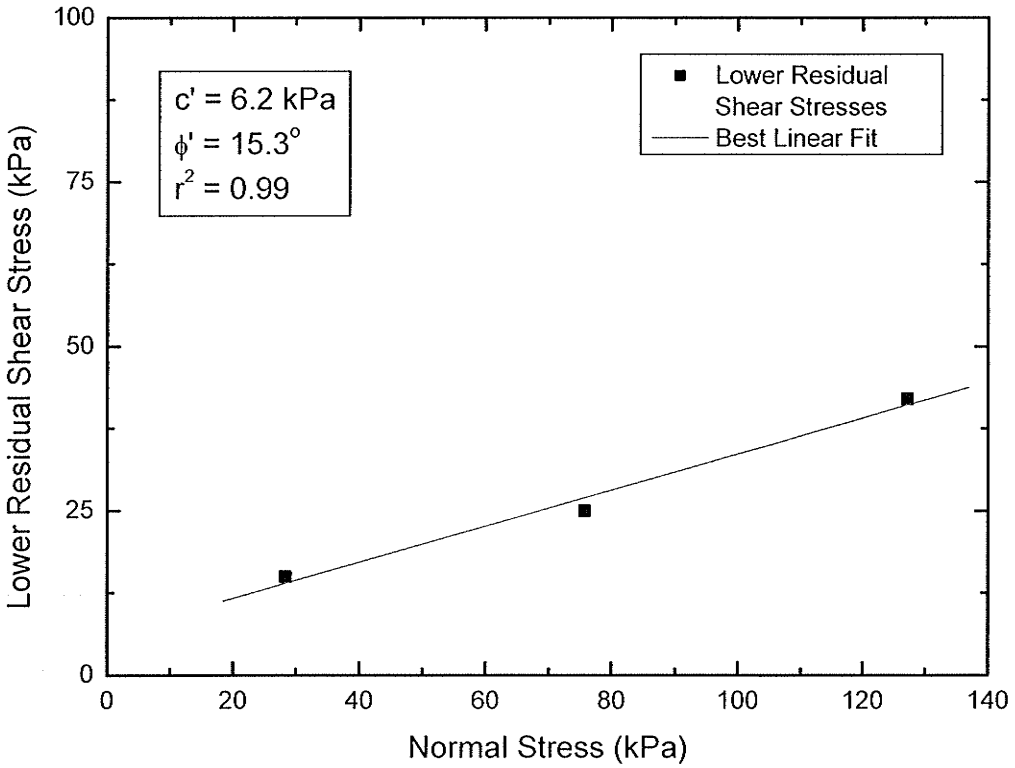

Figure 3.88 – Lower Residual Shear Stress versus Normal Stress for dry Bird's Hill Sand on dry CGSB PES interface tested in Bench-scale Direct Shear Apparatus.

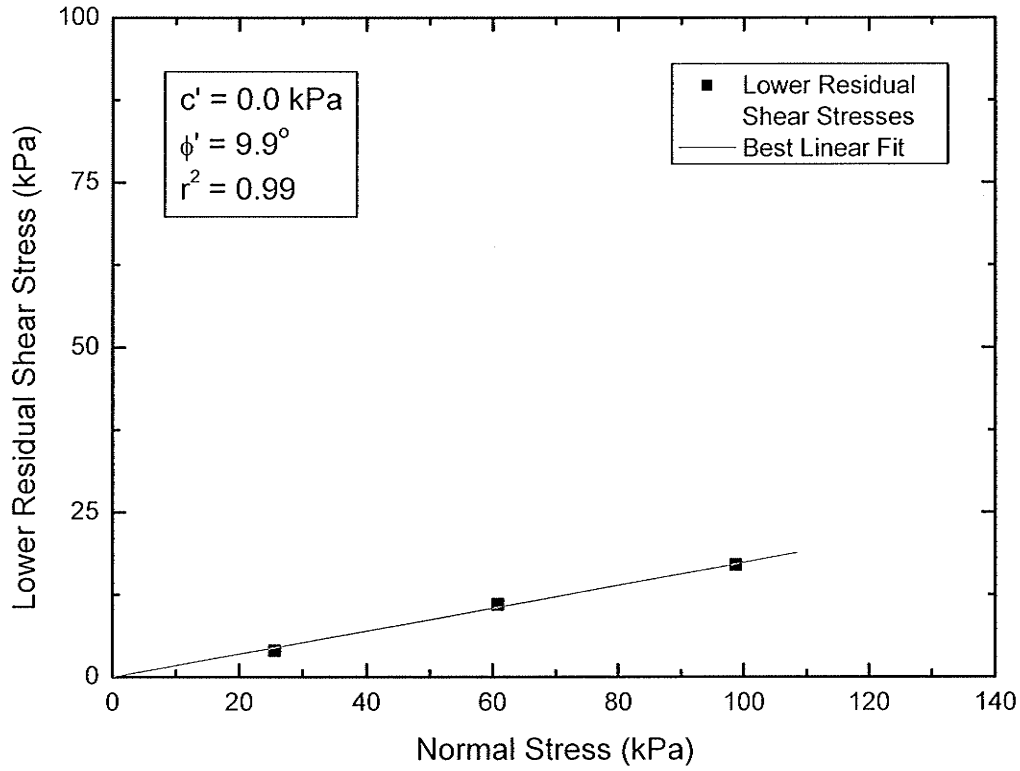

Figure 3.89 – Lower Residual Shear Stress versus Normal Stress for Saturated CGSB PES on Saturated CGSB PES interface tested in Bench-scale Direct Shear Apparatus.

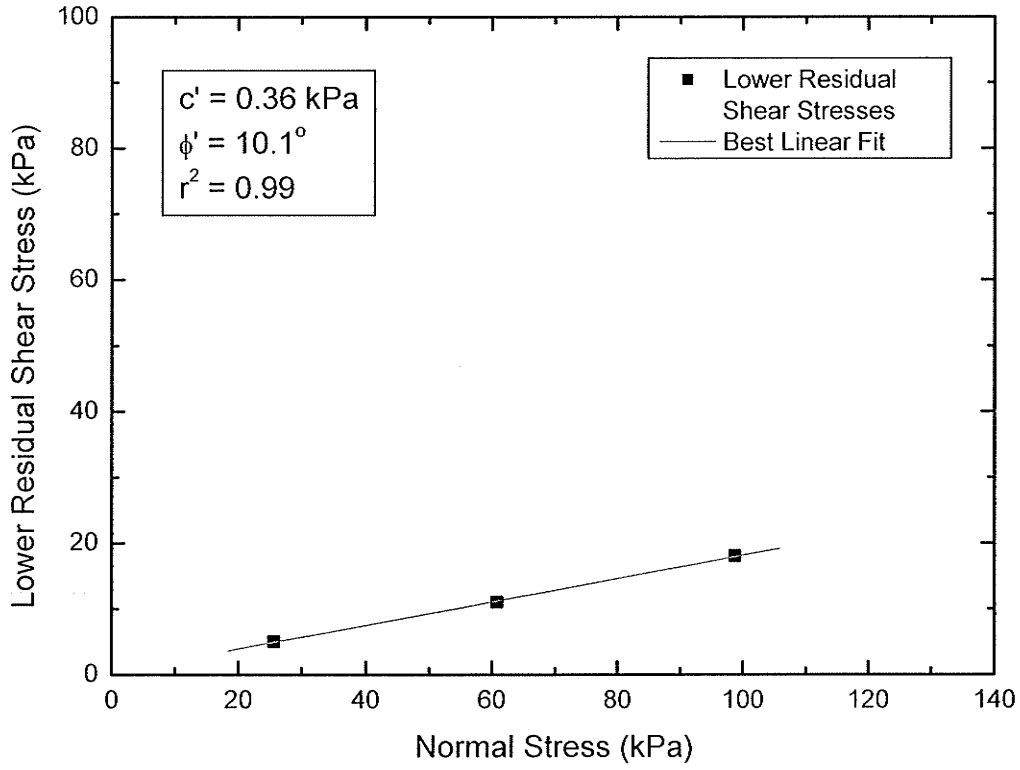

Figure 3.90 – Lower Residual Shear Stress versus Normal Stress for Saturated CGSB PES on Saturated WSFPP interface tested in Bench-scale Direct Shear Apparatus.

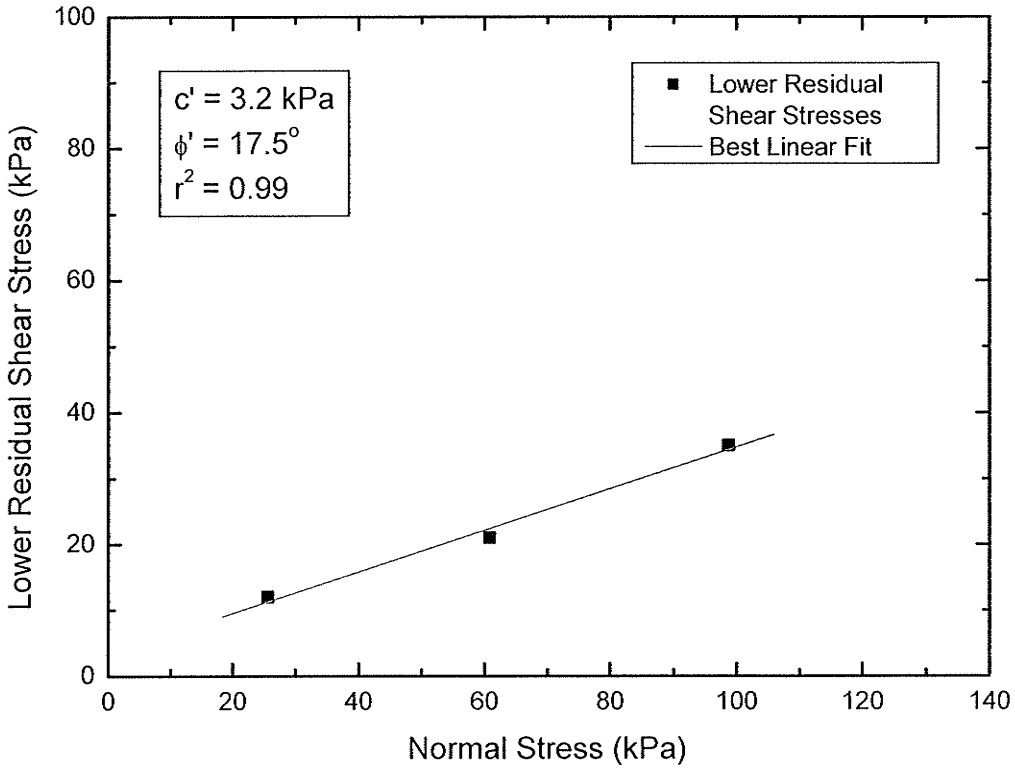

Figure 3.91 – Lower Residual Shear Stress versus Normal Stress for Saturated WSFPP on Saturated WSFPP interface tested in Bench-scale Direct Shear Apparatus.

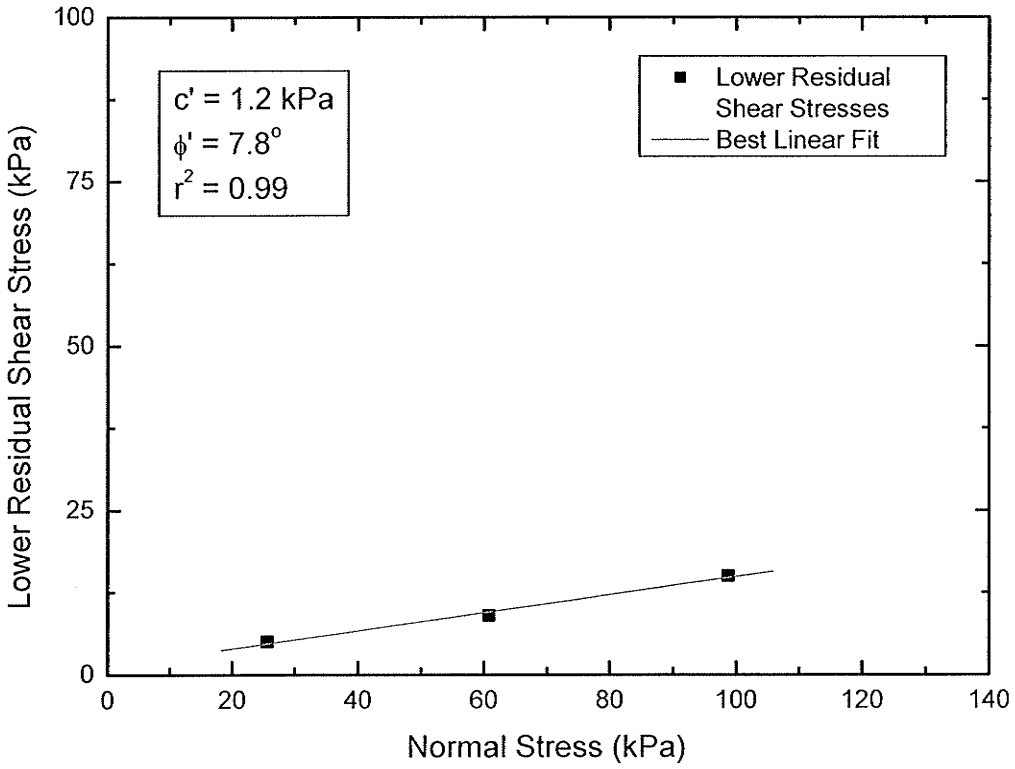

Figure 3.92 – Lower Residual Shear Stress versus Normal Stress for Scrubbed WSFPP on CGSB PES interface tested in Bench-scale Direct Shear Apparatus.

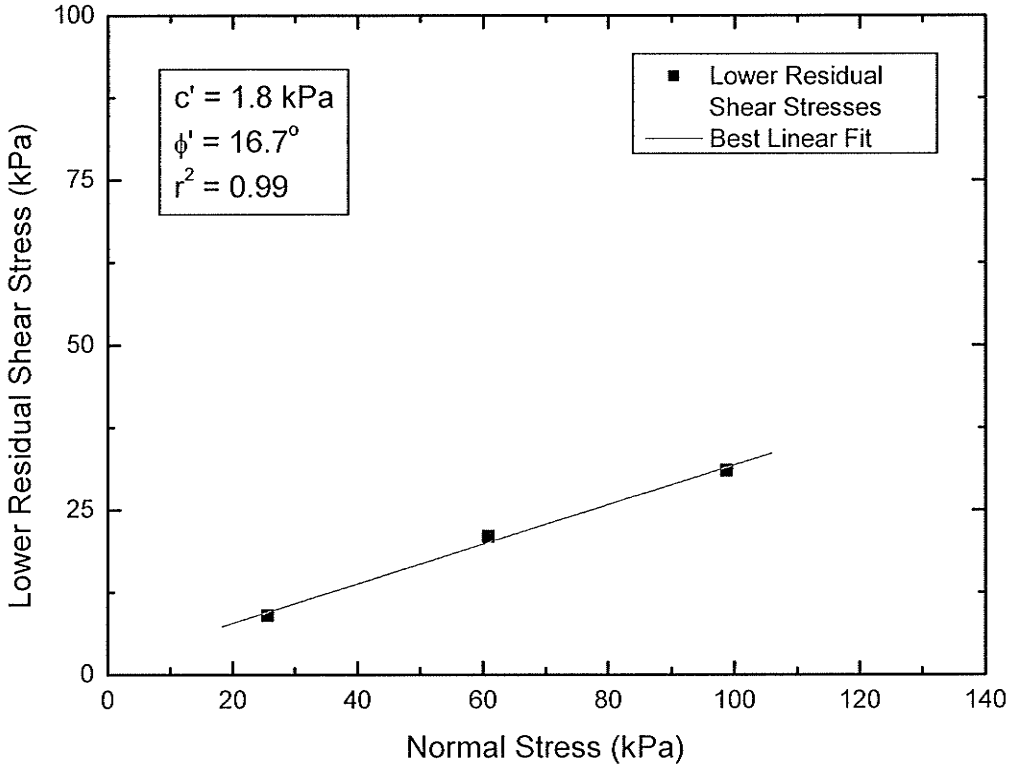

Figure 3.93 – Lower Residual Shear Stress versus Normal Stress for Scrubbed WSFPP on Scrubbed WSFPP interface tested in Bench-scale Direct Shear Apparatus.

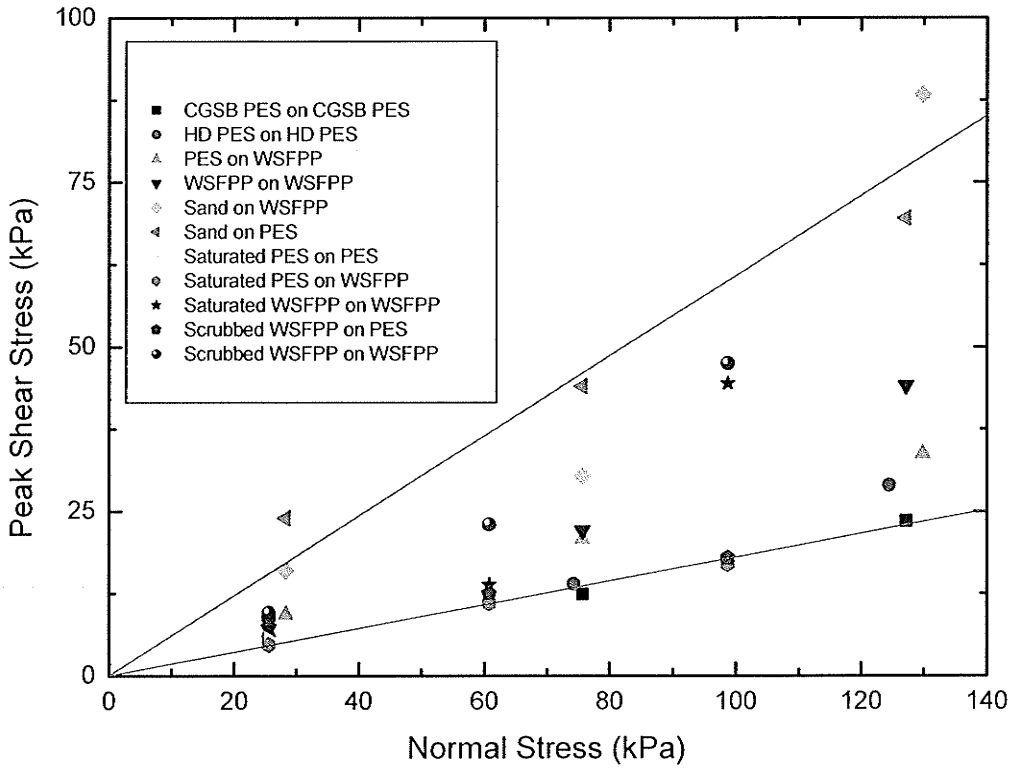

Figure 3.94 – Peak Shear Stress versus Normal Stress Summary for all interfaces tested in Bench-scale Direct Shear Apparatus.

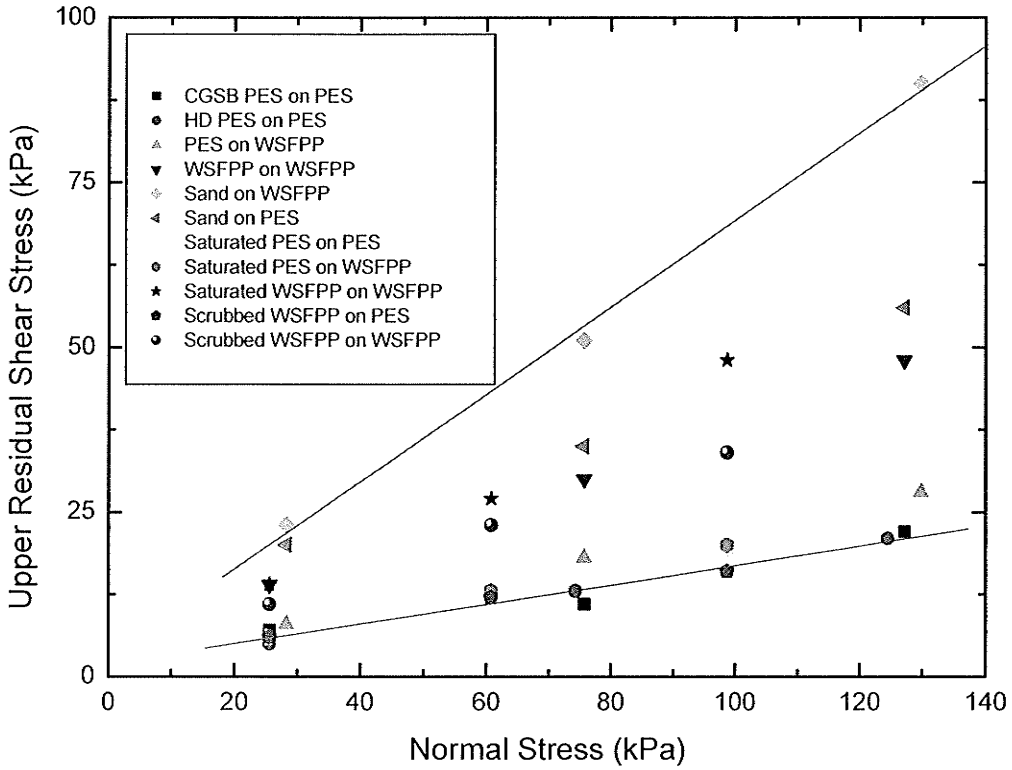

Figure 3.95 – Upper Residual Shear Stress versus Normal Stress Summary for all interfaces tested in Bench-scale Direct Shear Apparatus.

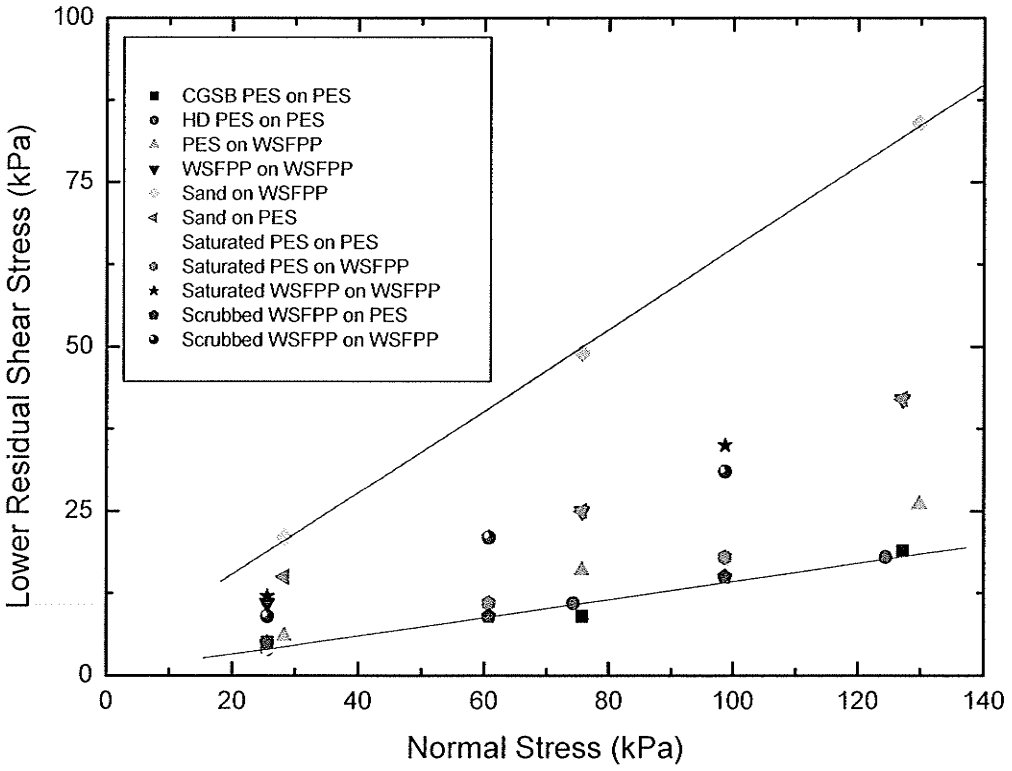

Figure 3.96 – Lower Residual Shear Stress versus Normal Stress Summary for all interfaces tested in Bench-scale Direct Shear Apparatus.

4 Full-Scale Testing of Sandbag Dikes

4.1 Introduction

The full-scale testing of sandbag dikes was undertaken in the summer of 2004. The facility was built in stages beginning with modular wall panels in April, 2004. Site preparation and erection of the flume was carried out in May and June, 2004. A grand opening was held at the site on June 16th, with representatives of all levels of government in attendance.

Ten tests on five dike types were carried out between July 7th and August 21st, 2004. In general, the testing program was a success. The requirements and milestones of the research proposal were all met or exceeded. The terms and conditions of use of the SmartPark property and SWRB were met, the facility has been disassembled and put into storage and the site has been remediated.

4.2 Test Apparatus Design and Construction

The full-scale test apparatus is a wooden flume 24 feet (7.32 m) in width, 16 feet (4.88 m) in depth and 16 feet (4.88 m) in height. It is a modular design consisting of basic panel units 4 feet (1.22 m) wide and 16 feet (4.88 m) long. These panels are constructed of 2 x 8 (39 mm x 190 mm nominal) dimension lumber framed at 1 foot (0.30 m) centres and sheeted with two layers of ½" (12.5 mm) plywood. All of the wood used in the construction of the panels is pressure treated lumber.

The flume is open on one side, and is supported horizontally by bracing designed as a modified truss system. Figure 4.1 is a plan view drawing and Figure 4.2 is an elevation view drawing of the flume and the bracing. The truss system is made of untreated SPF dimension lumber. All of the connections in the trusses as well as the connections

between the trusses and the walls are modified bolt connections. The majority of these connections are between four pieces of dimension lumber across the 2 inch (39 mm nominal) dimension. In order to increase the stiffness and shear resistance of these connections, the holes through the lumber are drilled at a 1.25 inch (32 mm) diameter, with a section of 1 inch (25 mm) inside diameter steel pipe inserted into the hole before installing the 0.75 inch (19 mm) diameter bolt.

4.2.1 Pre-assembly of panels and truss bracing

The panels were partially pre-assembled in the engineering laboratories at the University of Manitoba. One stud was left out to aid in attaching each panel to its neighbour, and only one sheet of the ½" (12.5 mm) plywood was installed.

Each member in the trusses for the bracing system were pre-cut and labelled for ease of construction on site. Sections of pipe were cut to length for the modified bolt connections.

4.2.2 Location and Construction of Flume

The full-scale testing facility was constructed on the north shore of the east storm water retention pond in SmartPark, on the south side of Innovation Drive. Figure 4.3 is a map of SmartPark with the project location labelled.

The site was surveyed to determine the best location for the flume. Considerations were local slope, proximity to the pond, the location of electrical service and the total length of fence that would be required to enclose the site. A development permit was obtained from the City of Winnipeg before any work was done at the site. Natural Gas, Electricity and Telephone utilities were contacted to determine if any of the earthworks that would

be necessary would interfere with buried cables or gas lines. The lines were marked out by a service person from Manitoba Hydro.

Reclaimed chain link fence from a decommissioned University of Manitoba Physical Plant compound was used to construct a fence around the site. The fence had two gates, one at the north-east corner and one on the south side. The fence was 8 feet (2.44 m) in height and was kept locked whenever the site was unattended.

Figure 4.4 is a photograph of the trench that was prepared to anchor the walls of the flume. The panels and truss braces were transported to site and erected as shown in Figures 4.5 through 4.8. The truss braces were anchored to the ground via 8 inch by 8 inch (190 mm by 190 mm nominal) dimension lumber salvaged from Physical Plant's supply of used parking posts.

A catwalk was made using engineered truss joists supplied by a local wood truss manufacturer. Along with a three-sided threaded steel rod bracing system, these joists provided stability for the top of the flume. The joists were attached to the flume using steel straps and deck screws to minimize deflections during loading and to provide ease of disassembly.

A seven foot high, four foot by four foot wide wooden shed was built to provide storage and shelter for the D/A system. The shed was equipped with a padlock for additional security.

Figure 4.9 is a photograph of the flume with the initial sandbag dike built inside, ready for testing.

4.2.3 Instrumentation

The full-scale tests are designed to monitor displacements, pressures and flow through the sandbag dike. Horizontal displacements are measured during tests using extending wire potentiometers. Vertical displacements are recorded by measuring selected positions before and after each test against benchmarks on the inside walls of the facility as well as surveying known points outside the test facility using a total station. Pore pressures through the dike are measured using vibrating wire piezometers. Changes in total pressure distribution through the dike are monitored using fluid-filled pressure plates. Seepage is monitored with a v-notch weir installed downstream of the dike. Water depth behind the dike is measured against a benchmark painted on the inside wall of the flume. Temperature is measured using a standard mercury thermometer.

4.2.3.1 Draw-wire Extensometers

The extending wire potentiometers used in the full-scale tests are Micro-Epsilon WPS-MK30 models. Three measurement ranges are used, specifically: 250 mm, 500 mm and 750 mm. Figure 4.10 is a reproduction of the manufacturer's photograph and schematic diagram of one of the units.

The extensometers are mounted on a sheet of plywood that is attached to the top centre of the north wall of the flume. The extensometer draw wire is run along a PVC channel with a stop system at the end of its safe stroke distance. The draw wires are then attached to metal cable which passes through a pulley mounted on a plywood plate that can be moved to accommodate different test configurations. The metal cables are attached to specific sandbags outfitted with grommets during dike construction by means of an angler's leader apparatus. This configuration provides a continuous link between the sandbag that is being monitored for horizontal translation as well as two fail-safes to

protect the extensometer from over-extension or sudden snap back. Figures 4.11 and 4.12 are photographs of the extensometer set-up. Fourteen extensometers in total were used; four 250 mm units, six 500 mm units and four 750 mm units.

The extensometers produce a voltage that varies with the amount that the wire is extended beyond the casing. The wires are spring-loaded and the signal is valid in both directions – extension and return. The extensometers are calibrated against a known distance and their output voltage is read with a Campbell Scientific CR23-X data acquisition (D/A) system. The D/A is connected to a laptop computer that records the incoming data in a spreadsheet.

4.2.3.2 Total Station

The total station used in these tests is a Topcon GTS-605AF, owned and operated by the Civil Engineering Department of the University of Manitoba. All of the readings were recorded manually in a standard surveyor's field book. Figures 4.13 and 4.14 are photographs of the prism and the total station being used during a test.

This survey equipment is used to measure set points on the dike face before and after each test. This data is recorded and stored manually in a field book to provide both redundancy and a comparison for the observed deformations and displacements that occur during each test.

4.2.3.3 Vibrating-wire Piezometers

The pore pressure measurements within the sandbag dikes are taken by vibrating-wire piezometers. The 10 GeoKon 4500S models are laid out at various heights and positions through the centre line of each sandbag dike, 9 within the dike itself, and 1 in a sheltered position under the catwalk. The sheltered unit measures ambient atmospheric pressure

and temperature which are used to calibrate the measurements of the piezometers installed inside the dike itself.

The output from the vibrating-wire piezometers is run through a Campbell Scientific CS-723X multiplexer that allows all of the piezometers to be read using a single channel of the CR-23X D/A. Figures 4.15 and 4.16 are photographs of the piezometers, multiplexer and D/A system.

4.2.3.4 Liquid-filled Pressure Plates

The pressure plates used to monitor changes in total pressure under the sandbag dikes are fluid filled metal disks connected to pressure gauges. Figure 4.17 is a photograph of a pressure plate and gauge. Measurements from the pressure plates are read manually from the gauges during tests.

4.2.3.5 V-notch Weir

The v-notch weir used to measure the flow rate through each sandbag dike is a plate aluminium weir provided by the University of Manitoba's Hydraulics Research and Testing Facility (HRTF). It is positioned downstream of the test facility and a known width of each sandbag dike is connected to a channel with the flume mounted at the channel's end. The collection system is lined with PES to prevent loss of water before measurement is completed. Figure 4.18 is a photograph of the weir and channel set-up. Up-stream water depth measurements from the weir are taken manually during tests.

4.2.3.6 Water Depth behind the Dike

Water depth during each test is monitored manually from the catwalk by an operator. Readings of depth from the base of the flume are taken along with the time. Figure 4.19 is a photograph of the scale painted onto the sides of the flume during one of the tests.

4.2.3.7 *Ambient Air Temperature*

The ambient air temperature was recorded manually during each test on two standard mercury thermometers located near the pressure plate gauges, one in the shade and one in the sun. These measurements were compared with the measurements recorded automatically by the piezometers.

4.3 Full-scale Experimental Program

4.3.1 Test Schedule

Table 4.1 is a schedule of all tests conducted in the full-scale testing facility. The test designation in the right hand column groups similar/comparable structures by letter.

Table 4.1 – Tests Conducted on Sandbag Dikes in Full-scale Facility

Date	Height	Configuration	Notes	Test
July 7	8' (2.44m)	City of Wpg	1.16 m maximum water depth	A1
July 14	8' (2.44m)	City of Wpg	Design depth held for ~40 min.	A2
July 23	10' (3.05m)	City of Wpg	Design depth held for ~110 min.	B1
July 28	10' (3.05m)	City of Wpg	Water over PES	B2
August 6	6' (1.83m)	City of Wpg	Design depth held for ~120 min.	C1
August 10	6' (1.83m)	City of Wpg	Dike overtopped intentionally	C2
August 11	6' (1.83m)	No PES	Dike built without PES	C3
August 17	6' (1.83m)	Alternative	1:1 slope on dry side	D1
August 18	6' (1.83m)	Alternative	1:1 slope dry side, no PES	D2
August 21	6' (1.83m)	City of Wpg	Built by volunteers	E

4.3.2 General Test Protocol

The procedure of building, instrumenting, measuring, filling and emptying the test facility was refined throughout the summer as further experience was gained. Key elements that were common to each test run are provided in the following sections.

4.3.2.1 Dike Profile Geometry

Outlines of the dike profile were marked on the walls of the facility and a line was marked along the ground between the front and back lines on each side using surveyor's spray marking paint. These marks helped ensure the geometry of the dike was consistent during the placing of the bags.

4.3.2.2 Monitoring Flume Wall Movement

One 500mm extensometer was mounted on the transformer box near the data & storage shed and attached to the back wall of the flume on the outside. The readings from this extensometer are used to account for the deflection of the wall outward under the load of the water.

4.3.2.3 Placement of Sandbags and PES Layer

The bags were placed and tamped by hand, one layer at a time. All bags were oriented parallel to the long wall of the facility to simulate being placed parallel to the flow of the flood waters as directed by the City of Winnipeg template. The PES was placed on the ground about 2 feet (0.61 m) from the first row of sandbags on the water side of the dike. The PES was placed under the first row of bags and subsequently interwoven into each layer (or lift) of bags, taking care to keep the PES from being exposed on the water side. At the same time the bags were interwoven on each side of the PES sufficiently to maintain stability of the bags on the wet side. Three to four lifts of bags were placed on the dry side, and then the PES was folded over and bags were placed on the wet side up to the same level as on the dry side. At all times a minimum of one bag was maintained between the water and the PES. The pattern generally repeated every three to four lifts where one row of bags was on the wet side of the PES, and then a lift where

two rows of bags were on the wet side. Figure 4.20 is a photograph of PES installation after four lifts of bags were placed in one of the test dike set-ups.

4.3.2.4 *Installation of Internal Instrumentation*

The instrumentation design for each test was established on a cross-section for each structure. The dimensions of this cross-section were generally followed during construction of each dike. The height and width of the dike were carefully monitored during construction and when the target height for each instrumentation layer was reached, instruments were installed in their selected position.

Vibrating wire piezometers and pressure plates were installed by labelling and placing each one in its prescribed place and then taking care that the label and connection to the D/A system or gauge set-up was correct. Figure 4.21 is a photograph showing installation of piezometers and pressure plates at the base level of one of the test dikes.

Extensometers were attached to individual bags which were each marked with surveyor's paint, as shown in Figure 4.22. A metal grommet was pre-installed on each bag in order to provide a place to attach the cable leader system for each draw-wire extensometer, as shown in Figure 4.23.

A majority of the extensometers in each test were attached to bags on the dry side of the PES. The cable leader and pulley system used for the attachment passed through the PES for each instrument. This was accomplished by poking an 18" (0.46 m) length of LLDPE plastic tubing (John Guest ¼" O.D. x 0.170" I.D. [NSF 51] [NSF 61] Max 230 psi at 70° F and Max 120 psi at 150° F) through the PES and sealing the PES-tube junction with acoustical sealant. The cable leader was then threaded through the tube and

attached to its designated bag. Figure 4.24 is a photograph of the lowest row of bags attached to extensometers in a typical dike set-up.

4.3.2.5 *Installation of External Instrumentation*

A v-notch weir was installed at the end of a plywood channel lined with PES. A funnel system made of plywood and lined with PES was installed between the dike and the channel to direct the water into the channel. The funnel system was lined with PES to minimize the amount of water lost to leakage and infiltration into the sod between the outer dike face and the weir. The distance across the front of the dike captured by the funnel system was recorded at the beginning of each test in order to be able to accurately calculate the seepage rate per unit length of each dike.

Gauges for the pressure plates were installed on the south end of the wall on the east side of the flume. During testing it was observed that the readings on the gauges were very sensitive to temperature and direct exposure to sunlight. A system of shading the gauges and the lines running from the plates to the gauges using plywood and tarps was developed. The shading system caused a marked reduction in the fluctuation of the readings on the gauges. Considerable difficulty was found in trying to calibrate the pressure plates. Following the first tests there was concern regarding how meaningful the data was in terms of pressure magnitude. The plates still proved useful in providing information regarding the relative increase and decrease in total pressures within each dike during the test and various loading increments.

A total station was set up facing the facility, between the dike and the SWRB, but off to one side so that the tripod was not directly in the line of any incidental water flowing from the flume into the SWRB.

Water depth readings were taken manually by an observer on the catwalk above the dike being tested. The depth gauge on the east wall of flume was marked using the same convention as a surveyor's rod, with its smallest increments at 10 cm (3.94"). Readings were taken at known time intervals which were coordinated with the clock on the computer collecting the information from the D/A system at the start of each test.

4.3.3 July 7, 8 foot (2.44 m) Test A1

The initial test in the facility was an 8 foot (2.44 m) sandbag dike built according to the City of Winnipeg's 1997 design template. The construction of the dike and the testing methodology followed the general protocol presented in 4.3.2, with the following additional notes.

Dike A1 was built in two stages. The initial bag placement for the dike started in the second week of June in order to demonstrate a cut-away detail at the facility's grand opening. Figure 4.25 is a photograph of the first bags for the dike in the facility being shown to some of the media and participants. Care was taken to ensure that the geometry of the dike was not compromised by this construction method, which was not followed in any of the other tests conducted during this research.

The piezometers, pressure plates and extensometers were installed in the dike according to the schematic on Figure 4.26.

The initial test was a first experience in terms of determining the water tightness of the flume as well as the input flow rate necessary to fill the test apparatus to the design depth of water for an 8 foot (2.44 m) dike. Due to a low input flow rate (2" diameter fire hose and line with a back-flow valve at the fire hydrant) and excessive leaks at the

corners of the flume, the maximum depth achieved in the initial test was 1.16 m (3.81 feet). The design depth for an 8 foot (2.44 m) dike is 6 feet (1.83 m).

The v-notch weir installation in the initial test was adequate to handle and measure the flow rate through the 8 foot (2.44 m) dike, but only because the design depth of water was not reached. It was apparent that the channel feeding the seepage water to the weir required widening, and this was noted for the following test. Figure 4.27 is a plot of water depth behind the dike and flow rate through the dike against time.

Table 4.2 is a summary of the relative changes in total pressure within the dike during test A1.

Table 4.2 – Pressure Plate Data – Total Pressure Changes during Test A1

Time (min)	Water Depth (m)	Plate 1	Plate 2	Plate 3	Plate 4	Plate 5	Plate 6
0	0	-	-	-	-	-	-
15	0.5	increasing	increasing	increasing	increasing	increasing	increasing
23	0.764	increasing	increasing	increasing	increasing	increasing	increasing
31	0.92	increasing	increasing	increasing	increasing	increasing	increasing
39	1.0	equal	equal	increasing	equal	increasing	increasing
67	1.1	increasing	increasing	increasing	increasing	increasing	increasing
87	1.16	increasing	decreasing	equal	equal	equal	increasing
111	1.11	decreasing	increasing	decreasing	increasing	decreasing	increasing

The extensometer and piezometer data from test A1 are summarised in sections in Figures 4.28 through 4.33 respectively, each figure summarising the data from an entire row of instrumentation.

4.3.4 July 14, 8 foot (2.44 m) Test A2

The second test in the facility was also an 8 foot (2.44 m) sandbag dike built according to the City of Winnipeg's 1997 design template. The construction of the dike and the test

method carried out followed the general protocol presented in 4.3.2, with the following additional notes.

The flow rate issues experienced in test A1 were dealt with by upgrading the water delivery hose to a full 3" line and eliminating the back-flow valve at the hydrant. The ability of this set-up to deliver water proved adequate for all of the subsequent tests run in the facility. Plumbing staff from The University of Manitoba's Physical Plant were present during the initial loading and final unloading of the dike to assure that no damage to the hydrant system would occur due to the sandbag dike testing activities.

A gap between the wall and the PES layer on the west side of the dike in test A2 was observed at the beginning of the test.

The piezometers, pressure plates and extensometers were installed in the dike according to the schematic on Figure 4.26.

Figure 4.34 is a plot of water depth behind the dike and flow rate through the dike against time. The design depth of 6 feet (1.85 m) was reached easily with the improved flow apparatus, and the input was regulated to keep the loading between 1.8 and 2.0 m for the majority of the test.

The channel feeding the v-notch weir was enlarged to accommodate the anticipated increase in flow, and this proved adequate for the flow rates in all of the subsequent tests. The funnel system leading up to the weir was modified to allow the leakage at the sides of the flume to pass by the weir in an effort to only measure the leakage through the dike itself. The edges of the funnel were moved 3 feet (0.9 m) in from each wall, so that the width of dike covered was reduced from 24 feet (7.3 m) to 18 feet (5.5 m).

Table 4.3 is a summary of the relative changes in total pressure within the dike during test A2.

Table 4.3 – Pressure Plate Data – Total Pressure Changes during Test A2

Time (min)	Water Depth (m)	Plate 1	Plate 2	Plate 3	Plate 4	Plate 5	Plate 6
0	0.28	-	-	-	-	-	-
8	0.85	increasing	decreasing	decreasing	decreasing	decreasing	decreasing
12	1.26	increasing	decreasing	decreasing	decreasing	decreasing	decreasing
17	1.5	increasing	decreasing	decreasing	decreasing	decreasing	decreasing
22	1.6	increasing	decreasing	increasing	increasing	decreasing	decreasing
32	1.82	increasing	decreasing	increasing	increasing	decreasing	decreasing
37	1.82	increasing	decreasing	increasing	increasing	decreasing	decreasing
41	1.84	increasing	decreasing	increasing	increasing	decreasing	decreasing
46	1.83	increasing	decreasing	increasing	increasing	decreasing	decreasing
51	1.82	increasing	decreasing	increasing	increasing	decreasing	decreasing
55	1.82	increasing	decreasing	increasing	increasing	decreasing	decreasing
60	1.9	increasing	decreasing	increasing	increasing	decreasing	decreasing
67	2.0	increasing	decreasing	increasing	increasing	decreasing	decreasing
75	2.07	increasing	decreasing	increasing	increasing	decreasing	decreasing
80	2.06	increasing	decreasing	increasing	increasing	decreasing	decreasing
86	1.2	increasing	decreasing	increasing	decreasing	decreasing	decreasing
90	1.05	decreasing	decreasing	increasing	decreasing	decreasing	decreasing
96	0.68	decreasing	decreasing	decreasing	decreasing	decreasing	decreasing

The extensometer and piezometer data from test A2 are summarised in sections in Figures 4.35 through 4.40 respectively, each figure summarising the data from an entire row of instrumentation.

4.3.5 July 23, 10 foot (3.05 m) Test B1

The third test in the facility was a 10 foot (3.05 m) sandbag dike built according to the City of Winnipeg's 1997 design template. The construction of the dike and the test method carried out followed the general protocol presented in 4.3.2, with the following additional notes.

The piezometers, pressure plates and extensometers were installed in the dike according to the schematic shown in Figure 4.41.

Figure 4.42 is a plot of water depth behind the dike and flow rate through the dike against time. The design depth of 8 feet (2.4 m) was reached in the first 20 minutes and the flow was maintained to keep the loading between 2.3 and 2.6 m for the majority of the test. The funnel system feeding the v-notch weir was set at 18 feet (5.5 m) for this test.

Table 4.4 is a summary of the relative changes in total pressure within the dike during test B1.

Table 4.4 – Pressure Plate Data – Total Pressure Changes during Test B1

Time (min)	Water Depth (m)	Plate 1	Plate 2	Plate 3	Plate 4	Plate 5	Plate 6
0	0	-	-	-	-	-	-
4	1.2	decreasing	increasing	decreasing	decreasing	decreasing	decreasing
10	2.0	increasing	increasing	increasing	decreasing	decreasing	decreasing
19	2.6	increasing	increasing	increasing	increasing	decreasing	increasing
35	2.39	increasing	increasing	decreasing	increasing	decreasing	increasing
42	2.46	increasing	increasing	decreasing	increasing	decreasing	increasing
54	2.5	increasing	increasing	decreasing	increasing	decreasing	increasing
72	2.61	increasing	increasing	decreasing	increasing	increasing	increasing
84	2.6	increasing	increasing	decreasing	increasing	increasing	increasing
111	2.5	increasing	increasing	decreasing	increasing	increasing	increasing
132	1.9	increasing	increasing	decreasing	increasing	increasing	increasing
143	0.8	increasing	increasing	decreasing	increasing	increasing	increasing

The extensometer and piezometer data from test B1 are summarised in sections in Figures 4.43 through 4.47 respectively, each figure summarising the data from an entire row of instrumentation.

4.3.6 July 28, 10 foot (3.05 m) Test B2

The fourth test in the facility was a 10 foot (3.05 m) sandbag dike built according to the city of Winnipeg's 1997 design template. The construction of the dike and the test method carried out followed the general protocol presented in 4.3.2, with the following notes.

The piezometers, pressure plates and extensometers were installed in the dike according to the schematic on Figure 4.41.

Figure 4.48 is a plot of water depth behind the dike against time. Test B2 was an attempt to overtop a 10 foot (3.05 m) dike, so the flow from the hydrant was turned as high as possible from the beginning of the test. There were no readings taken on the v-notch weir during test B2.

Table 4.5 is a summary of the relative changes in total pressure within the dike during test B2.

Table 4.5 – Pressure Plate Data – Total Pressure Changes during Test B2

Time (min)	Water Depth (m)	Plate 1	Plate 2	Plate 3	Plate 4	Plate 5	Plate 6
0	0	-	-	-	-	-	-
11	1.44	increasing	decreasing	decreasing	decreasing	decreasing	decreasing
18	2.11	increasing	increasing	decreasing	decreasing	decreasing	decreasing
28	2.58	increasing	increasing	decreasing	increasing	decreasing	decreasing
45	1.67	increasing	increasing	decreasing	decreasing	increasing	decreasing
56	0.9	increasing	increasing	decreasing	decreasing	increasing	decreasing

The extensometer and piezometer data from test B2 are summarised in sections in Figures 4.49 through 4.53 respectively, each figure summarising the data from an entire row of instrumentation.

4.3.7 August 6, 6 foot (1.83 m) Test C1

The fifth test in the facility was a 6 foot (1.85 m) sandbag dike built according to the City of Winnipeg's 1997 design template. The construction of the dike and the test method carried out followed the general protocol presented in 4.3.2, with the following additional notes.

The piezometers, pressure plates and extensometers were installed in the dike according to the schematic on Figure 4.54.

Figure 4.55 is a plot of water depth behind the dike and flow rate through the dike against time. Test C1 was a base-line test on a 6 foot (1.85 m) dike, which has a design water depth of 4 feet (1.22 m). The water depth was maintained between 1.2 and 1.5 m for the majority of the test. The funnel system feeding the v-notch weir was set at 18 feet (5.5 m) for this test.

Table 4.6 is a summary of the relative changes in total pressure within the dike during test C1.

Table 4.6 – Pressure Plate Data – Total Pressure Changes during Test C1

Time (min)	Water Depth (m)	Plate 1	Plate 2	Plate 3	Plate 4	Plate 5	Plate 6
10	0.15	-	-	-	-	-	-
15	0.75	decreasing	increasing	decreasing	decreasing	decreasing	increasing
31	1.36	increasing	increasing	decreasing	increasing	increasing	increasing
49	1.45	decreasing	decreasing	decreasing	increasing	increasing	increasing
60	1.36	decreasing	decreasing	decreasing	increasing	increasing	decreasing
75	1.41	decreasing	decreasing	decreasing	increasing	increasing	decreasing
96	1.33	decreasing	decreasing	equal	increasing	increasing	decreasing
113	1.47	increasing	decreasing	equal	increasing	increasing	increasing
122	1.6	decreasing	decreasing	equal	increasing	increasing	increasing
132	1.75	decreasing	decreasing	equal	increasing	increasing	increasing
137	1.74	increasing	decreasing	equal	increasing	increasing	increasing
147	1.68	increasing	decreasing	equal	increasing	increasing	decreasing
158	1.16	decreasing	decreasing	equal	increasing	increasing	decreasing

The extensometer and piezometer data from test C1 are summarised in sections in Figures 4.56 through 4.60 respectively, each figure summarising the data from an entire row of instrumentation.

4.3.8 August 10, 6 foot (1.83 m) Test C2

The sixth test in the facility was another 6 foot (1.85 m) sandbag dike built according to the City of Winnipeg's 1997 design template. The construction of the dike and the test method carried out followed the general protocol presented in 4.3.2, with the following additional notes.

The piezometers, pressure plates and extensometers were installed in the dike according to the schematic on Figure 4.54.

Figure 4.61 is a plot of the water depth behind the dike and flow rate through the dike against time. Test C2 was an overtop test, so the flow from the hydrant was turned as high as possible from the beginning of the test. The funnel system feeding the V-notch weir was set at 18 feet (5.5 m) for this test.

Table 4.7 is a summary of the relative changes in total pressure within the dike during test C2.

Table 4.7 – Pressure Plate Data – Total Pressure Changes during Test C2

Time (min)	Water Depth (m)	Plate 1	Plate 2	Plate 3	Plate 4	Plate 5	Plate 6
8	0	-	-	-	-	-	-
15	1.1	increasing	increasing	decreasing	increasing	decreasing	increasing
21	1.58	increasing	increasing	decreasing	increasing	decreasing	increasing
28	1.79	increasing	increasing	decreasing	increasing	decreasing	increasing
35	1.77	increasing	decreasing	decreasing	increasing	decreasing	increasing
44	1.74	increasing	decreasing	decreasing	increasing	decreasing	increasing
50	1.38	increasing	decreasing	decreasing	increasing	increasing	decreasing

The extensometer and piezometer data from test C2 are summarised in sections in figures 4.62 through 4.66 respectively, each figure summarising the data from an entire row of instrumentation.

4.3.9 August 11, 6 foot (1.83 m) Test C3

The seventh test in the facility was a 6 foot (1.85 m) sandbag dike built according to the City of Winnipeg's 1997 design template without the PES layer on the water side. The construction of the dike and the test method carried out followed the general protocol presented in 4.3.2, with the following additional notes.

The piezometers, pressure plates and extensometers were installed in the dike according to the schematic on Figure 4.54.

Figure 4.67 is a plot of the water depth behind the dike and flow rate through the dike against time. Test C3 was a test on a 6 foot (1.85 m) dike without PES. The water depth was raised at the same rate as the previous tests, but the dike was not able to sustain the load and design depth could not be maintained during this test. The funnel system feeding the v-notch weir was set at 18 feet (5.5 m) for this test.

Table 4.8 is a summary of the relative changes in total pressure within the dike during test C3.

Table 4.8 – Pressure Plate Data – Total Pressure Changes during Test C3

Time (min)	Water Depth (m)	Plate 1	Plate 2	Plate 3	Plate 4	Plate 5	Plate 6
10	0.28	-	-	-	-	-	-
19	1.31	increasing	decreasing	decreasing	increasing	increasing	increasing
24	1.48	increasing	decreasing	decreasing	increasing	increasing	increasing

The extensometer and piezometer data from test C3 are summarised in sections in Figures 4.68 through 4.72 respectively, each figure summarising the data from an entire row of instrumentation.

4.3.10 August 17, 6 foot (1.83 m) Test D1

The eighth test in the facility was a 6 foot (1.85 m) sandbag dike built according to the City of Winnipeg's 1997 design template on the wet side, but with a 1:1 slope on the dry side. Other than the change to the dry side geometry, the construction of the dike and the test method carried out followed the general protocol presented in 4.3.2, with the following additional notes.

The piezometers, pressure plates and extensometers were installed in the dike according to the schematic on Figure 4.73.

Figure 4.74 is a plot of the water depth behind the dike and flow rate through the dike against time. Test D1 was a baseline test on a 6 foot (1.85 m) dike with a modified geometry. The water depth was raised to the design depth of 4 feet (1.22 m) and maintained between 1.25 and 1.5 m during the majority of this test. The funnel system feeding the v-notch weir was set at 14 feet (4.27 m) for this test.

Table 4.9 is a summary of the relative changes in total pressure within the dike during test D1.

Table 4.9 – Pressure Plate Data – Total Pressure Changes during Test D1

Time (min)	Water Depth (m)	Plate 1	Plate 2	Plate 3	Plate 4	Plate 5	Plate 6
0	0	-	-	-	-	-	-
7	1.26	increasing	increasing	decreasing	increasing	increasing	increasing
17	1.57	increasing	increasing	increasing	increasing	increasing	increasing
37	1.52	increasing	increasing	increasing	increasing	increasing	increasing

47	1.51	increasing	increasing	decreasing	increasing	increasing	increasing
62	1.47	increasing	increasing	decreasing	increasing	increasing	increasing
80	1.68	increasing	increasing	increasing	increasing	increasing	increasing
97	1.01	increasing	increasing	decreasing	increasing	increasing	increasing

The extensometer and piezometer data from test D1 are summarised in sections in figures 4.75 through 4.79 respectively, each figure summarising the data from an entire row of instrumentation.

4.3.11 August 18, 6 foot (1.83 m) Test D2

The ninth test in the facility was a 6 foot (1.85 m) sandbag dike built according to the City of Winnipeg's 1997 design template on the wet side, but with a 1:1 slope on the dry side and without the PES layer. Other than the change to the dry side geometry and the lack of PES, the construction of the dike and the test method carried out followed the general protocol presented in 4.3.2, with the following additional notes.

The piezometers, pressure plates and extensometers were installed in the dike according to the schematic on Figure 4.73.

Figure 4.80 is a plot of the water depth behind the dike and flow rate through the dike against time. Test D2 was on a 6 foot (1.85 m) dike with a modified geometry and no PES layer. The water depth was raised to the design depth of 4 feet (1.22 m) and maintained between 1.25 and 1.5 m during the beginning of the test, and then raised to overtop levels for the final 2/3 of the test. The funnel system feeding the v-notch weir was set at 14 feet (4.27 m) for this test.

Table 4.10 is a summary of the relative changes in total pressure within the dike during test D2.

Table 4.10 – Pressure Plate Data – Total Pressure Changes during Test D2							
Time (min)	Water Depth (m)	Plate 1	Plate 2	Plate 3	Plate 4	Plate 5	Plate 6
5	0.64	-	-	-	-	-	-
15	1.5	increasing	decreasing	decreasing	decreasing	decreasing	decreasing
30	1.37	increasing	decreasing	decreasing	decreasing	decreasing	decreasing
37	1.6	increasing	decreasing	decreasing	decreasing	decreasing	decreasing
63	1.66	decreasing	decreasing	decreasing	decreasing	decreasing	decreasing
78	1.07	decreasing	decreasing	decreasing	decreasing	decreasing	decreasing

The extensometer and piezometer data from test D2 are summarised in sections in Figures 4.81 through 4.85 respectively, each figure summarising the data from an entire row of instrumentation.

4.3.12 August 21, 6 foot (1.83 m) Test E

The eleventh and final test in the facility was a 6 foot (1.85 m) sandbag dike built according to the city of Winnipeg's 1997 design template by a group of volunteers. The construction of the dike and the test method carried deviated from the general protocol presented in 4.3.2, as summarised in the following notes.

The volunteers were each given a paper copy of the City of Winnipeg's 1997 sandbag dike template along with a 5 minute verbal summary by the research team. One of the volunteers was appointed to act as the homeowner whose property was being protected by the dike, and this person was charged with overseeing and maintaining the quality of the dike construction. The researchers were involved only as members of the lines of people delivering bags, they did not place any bags or arrange any of the PES in the dike. The Manitoba EMO provided a safety officer for the test.

The piezometers, pressure plates and extensometers were installed in the dike according to the schematic on Figure 4.54. This internal instrumentation was installed during water breaks taken by the volunteer crew at the appropriate time intervals.

Figure 4.86 is a plot of the water depth behind the dike against time. Test E was a test on a 6 foot (1.85 m) dike, which has a design water depth of 4 feet (1.22 m). The water depth was raised to the design depth and maintained between 1.25 and 1.5 m during the beginning of the test, and then raised to overtop levels for the final 3/4 of the test. The funnel system and v-notch weir were not set up for this test.

Table 4.11 is a summary of the relative changes in total pressure within the dike during test E.

Table 4.11 – Pressure Plate Data – Total Pressure Changes during Test E

Time (min)	Water Depth (m)	Plate 1	Plate 2	Plate 3	Plate 4	Plate 5	Plate 6
8	0.65	-	-	-	-	-	-
16	1.48	increasing	decreasing	decreasing	increasing	increasing	decreasing
26	1.66	increasing	decreasing	decreasing	increasing	increasing	decreasing
34	1.75	increasing	decreasing	decreasing	increasing	increasing	decreasing
41	1.78	increasing	decreasing	decreasing	increasing	increasing	decreasing
49	1.8	increasing	decreasing	decreasing	increasing	increasing	increasing
55	1.75	increasing	decreasing	decreasing	increasing	increasing	increasing
57	1.56	increasing	decreasing	increasing	increasing	increasing	increasing
59	1.37	increasing	decreasing	increasing	increasing	increasing	increasing
61	1.18	increasing	decreasing	increasing	increasing	increasing	increasing
63	0.8	increasing	decreasing	increasing	decreasing	decreasing	increasing

The extensometer and piezometer data from test E are summarised in sections in Figures 4.87 through 4.91 respectively, each figure summarising the data from an entire row of instrumentation.

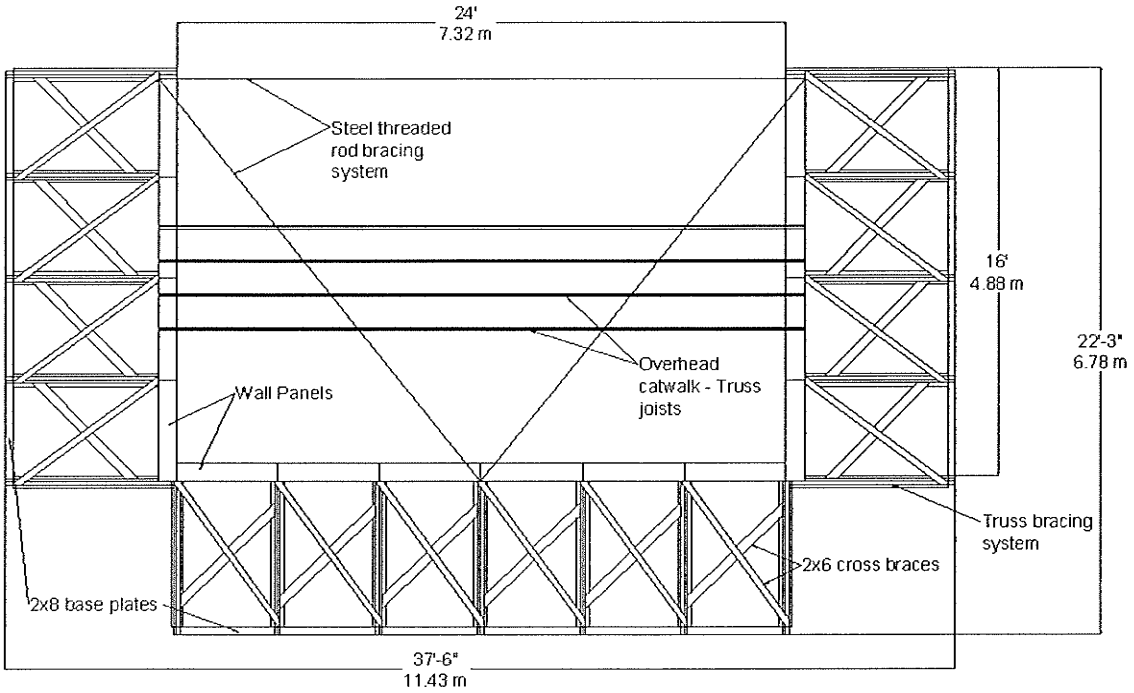

Figure 4.1 – Plan view Schematic of Flume showing Support Systems.

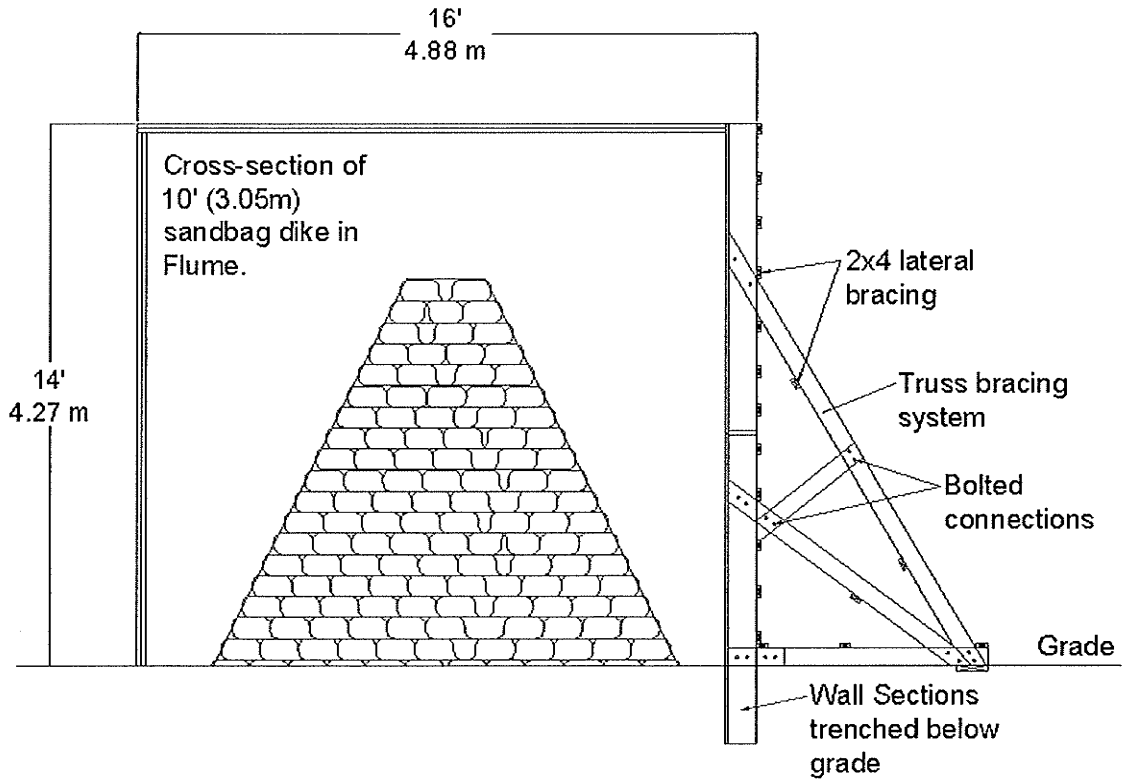

Figure 4.2 – Elevation view Schematic of Flume through North-South cross-section.

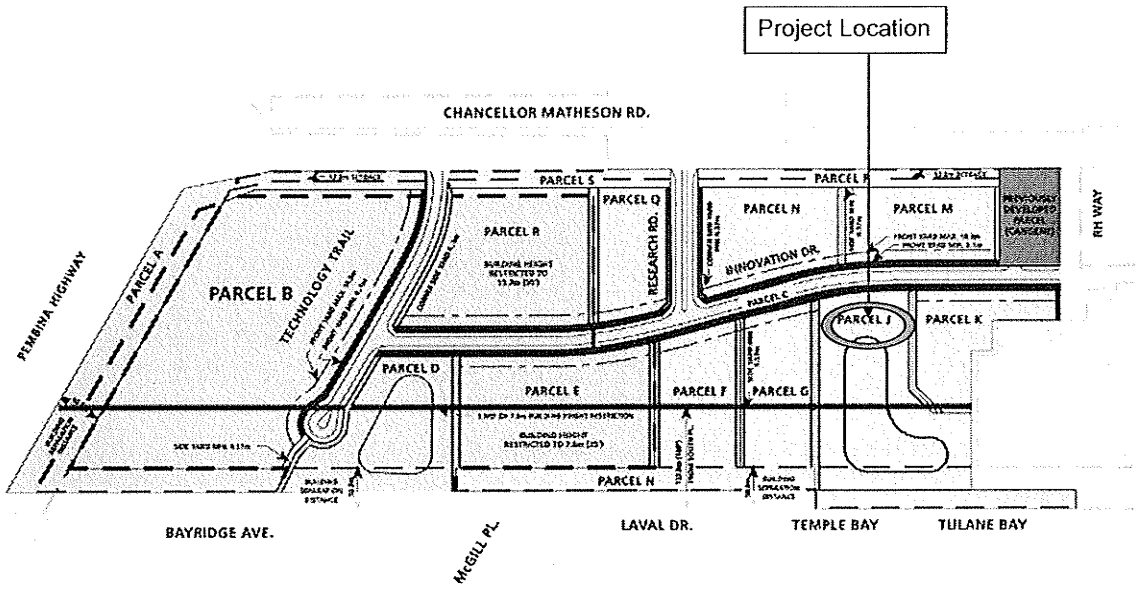

Figure 4.3 – Map of SmartPark showing location of Full-scale Testing Facility.

Figure 4.4 – Completed Trench Ready for Wall Assembly (View to the East).

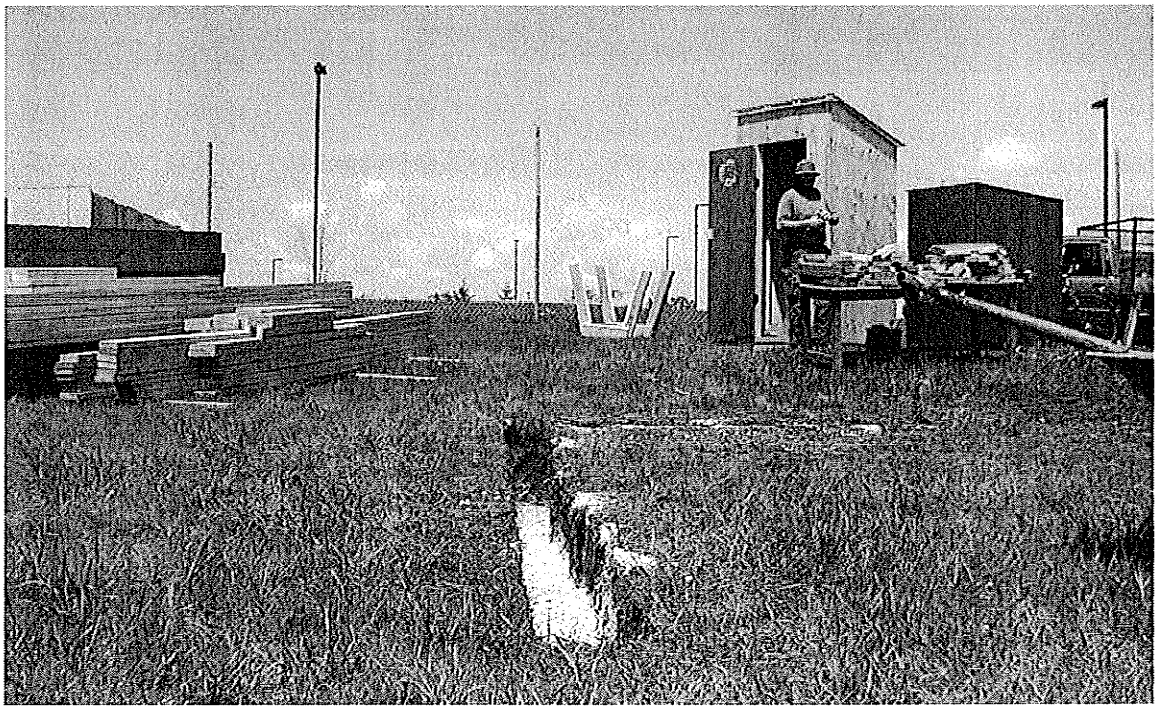

Figure 4.5 – Trench, Stacked Wall Panels, Lumber Pile and Storage/Data Shed (view to the North).

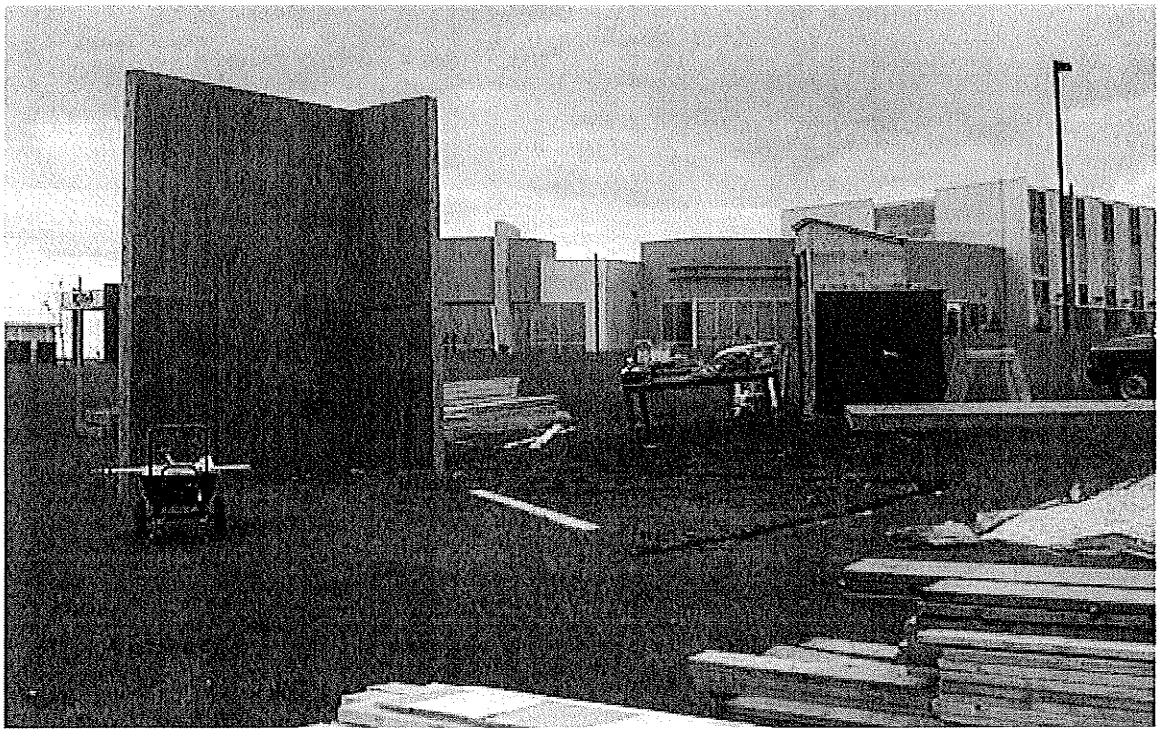

Figure 4.6 – Initial four Wall Panels erected and placed in Trench (view to the North West).

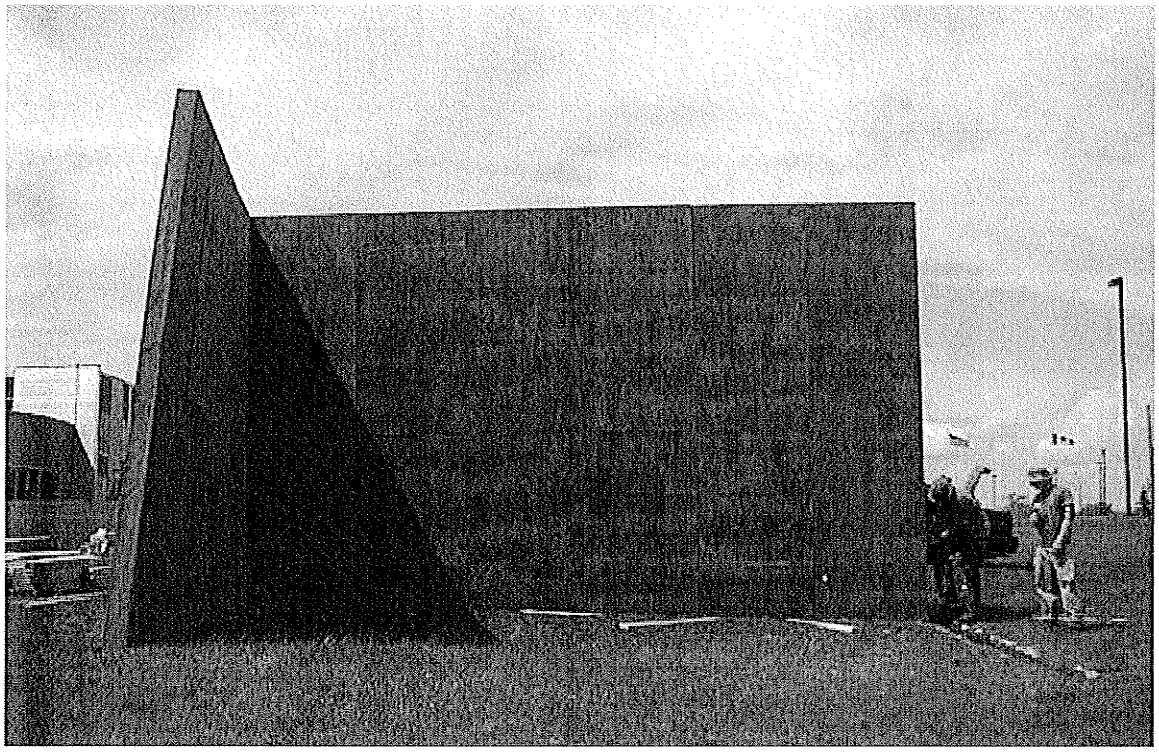

Figure 4.7 – North and West Wall Panels erected and placed in Trench (view to the North).

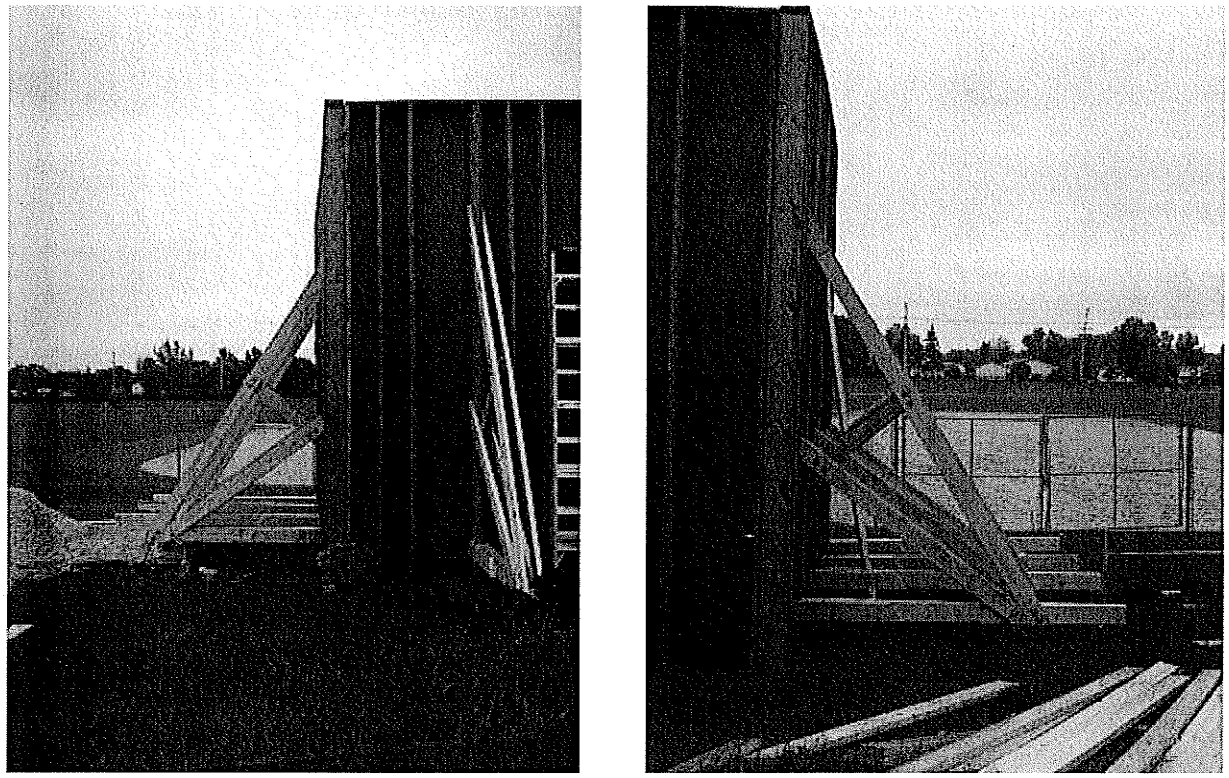

Figure 4.8 – East and West Truss bracing systems under construction (view to the South).

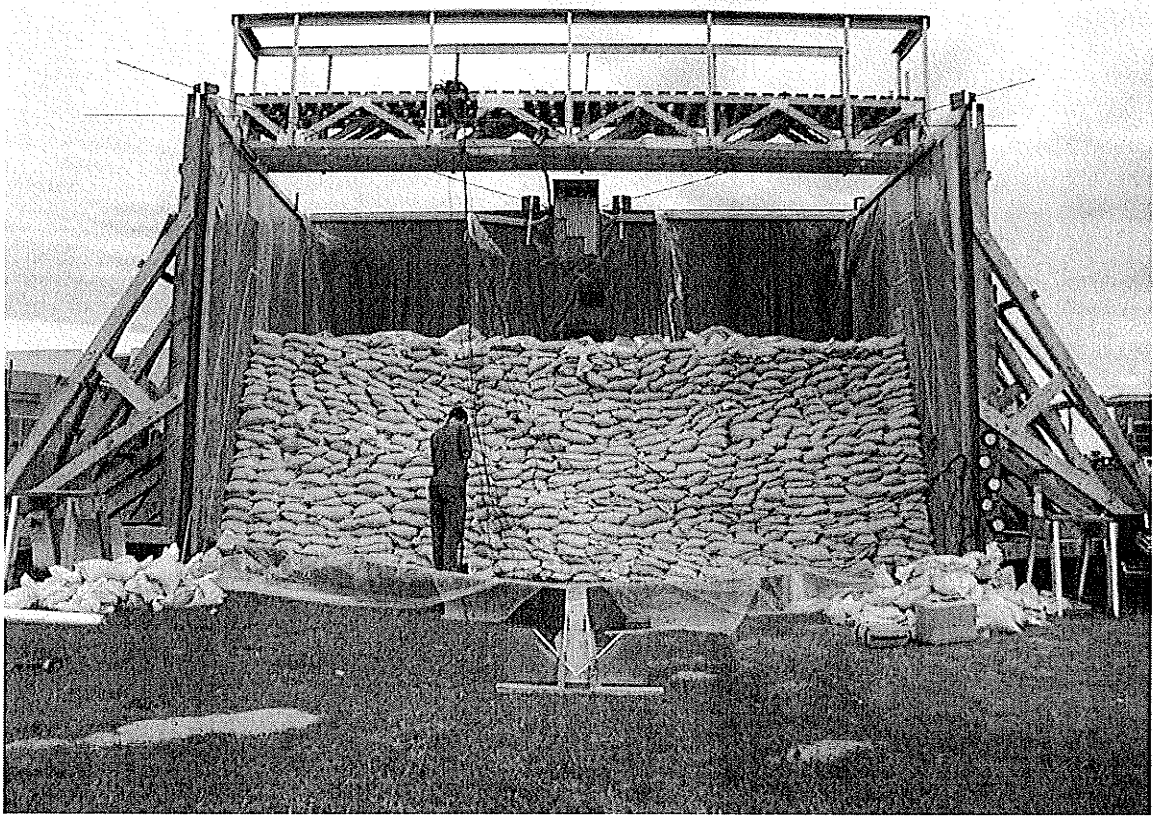

Figure 4.9 – Completed Flume with Initial Sandbag Dike ready for Testing (view to the North).

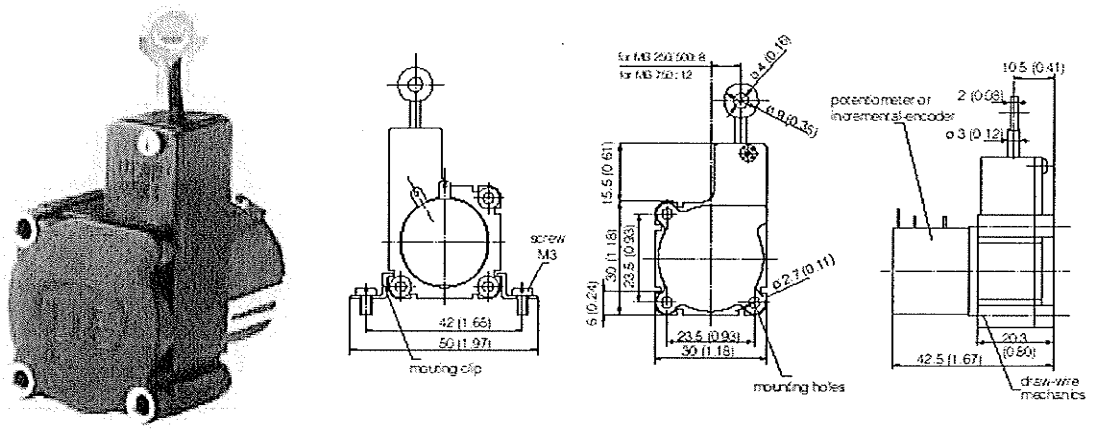

Figure 4.10 – Draw-wire Extensometers used in Full-scale Test Apparatus.

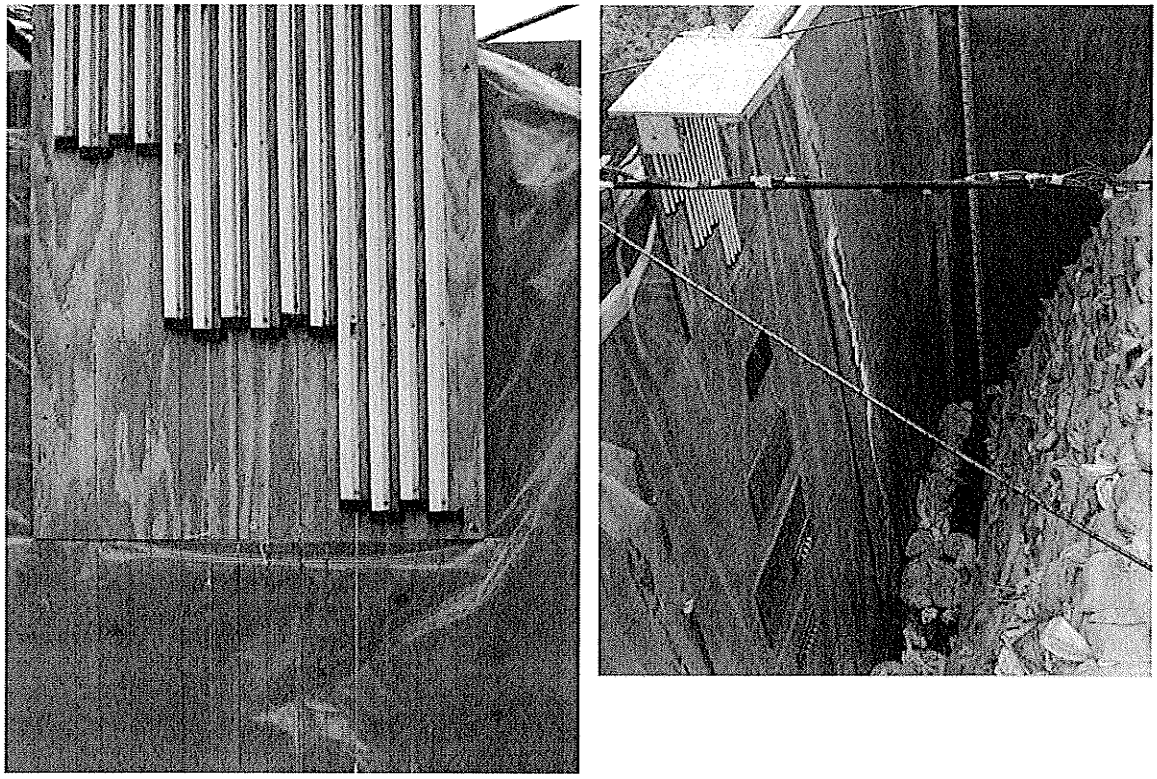

Figure 4.11 – Extensometer Board and Pulley system mounted on Flume Wall.

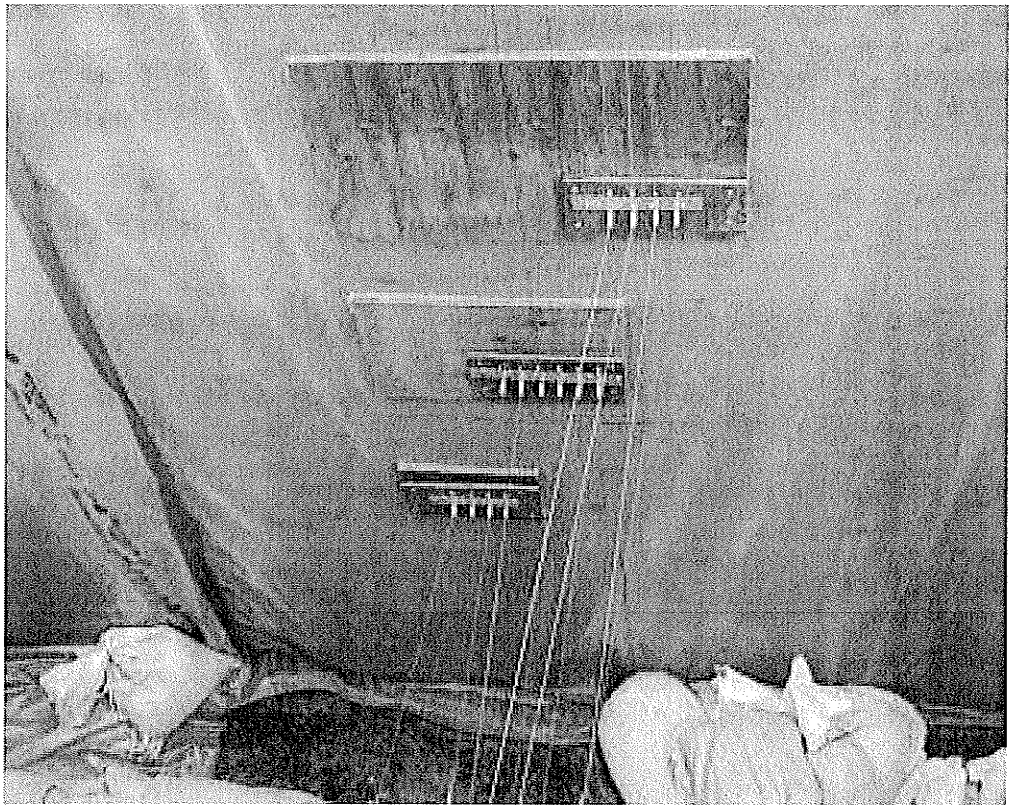

Figure 4.12 – Extensometer Pulley System mounted on Flume wall with Cables attaching to Sandbags in Dike (not shown – foreground).

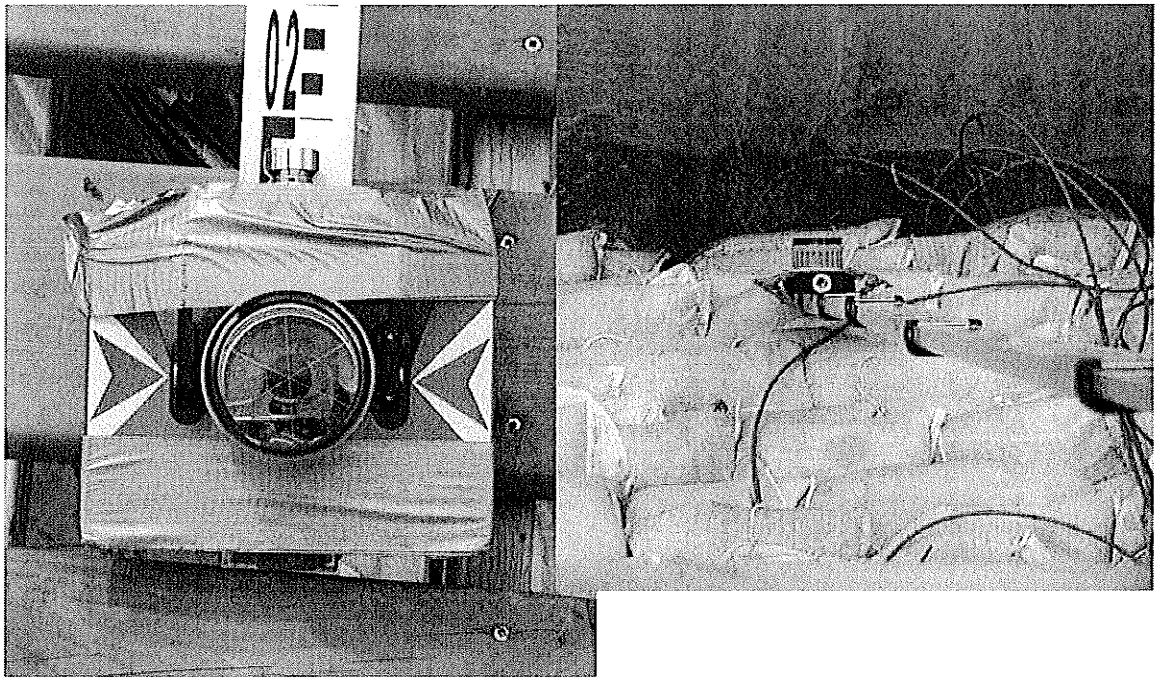

Figure 4.13 – Optical Survey Prism attached to base end of Survey Rod (left), and Prism being used to Survey Points on a Sandbag Dike (right).

Figure 4.14 – Total Station being used to Survey Points on Sandbag Dike.

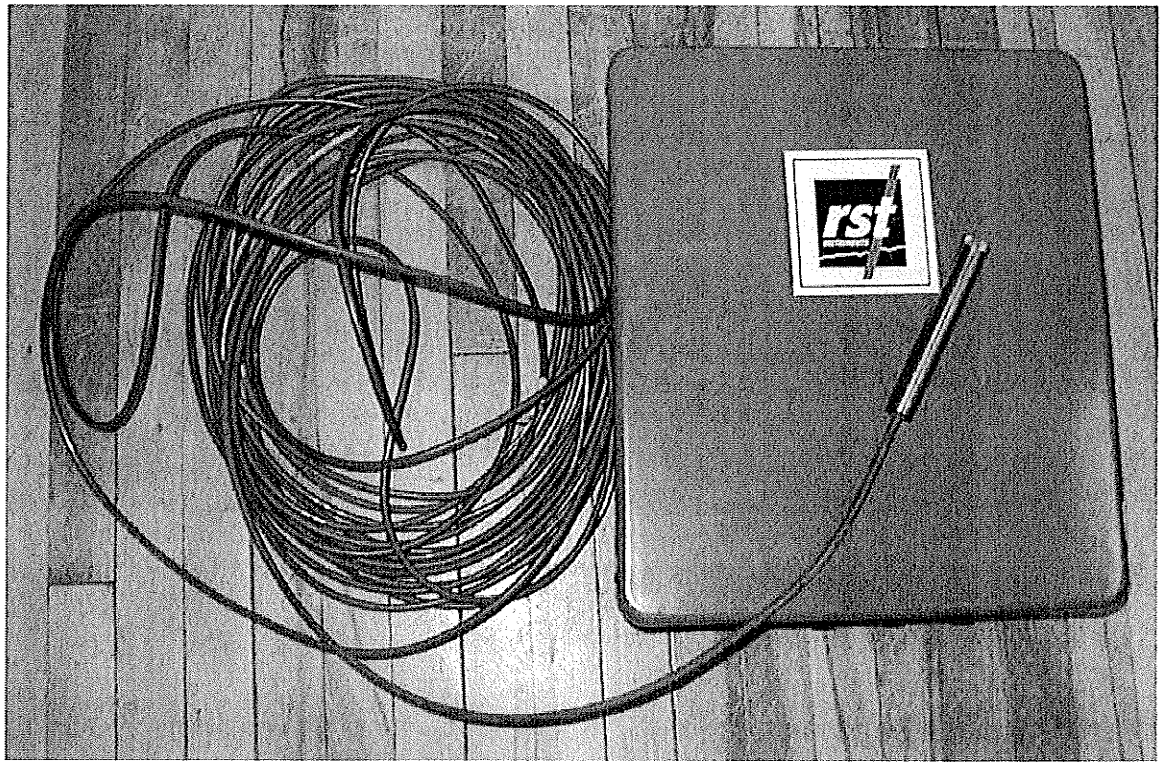

Figure 4.15 – GeoKon 4500S vibrating wire piezometer, cable and case.

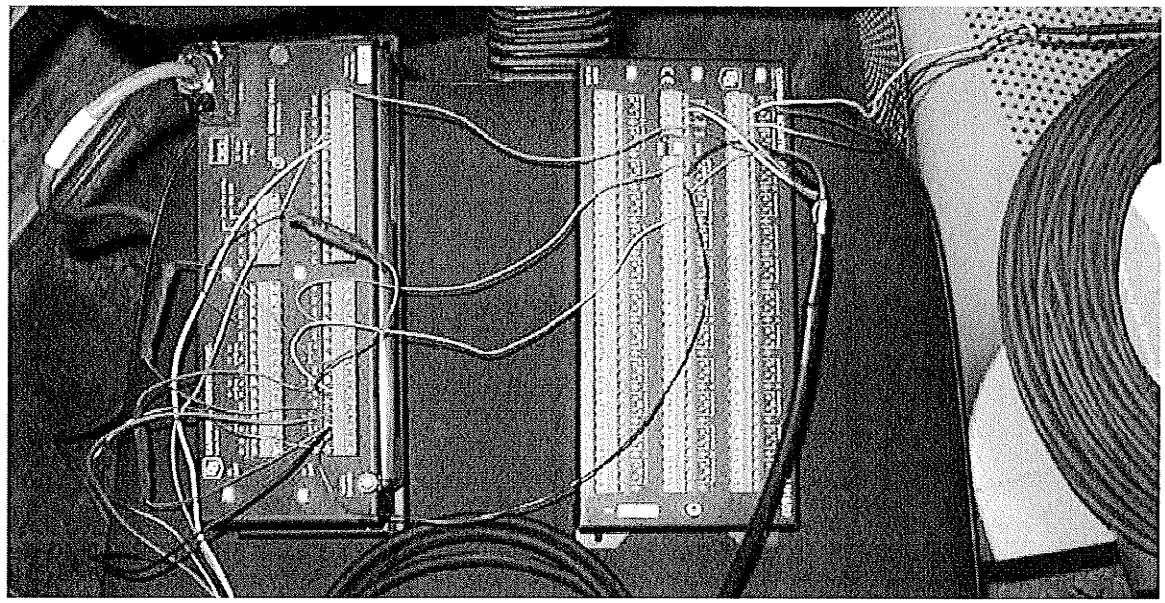

Figure 4.16 – CS 723X multiplexer (right) connected to CR23X I/O panel.

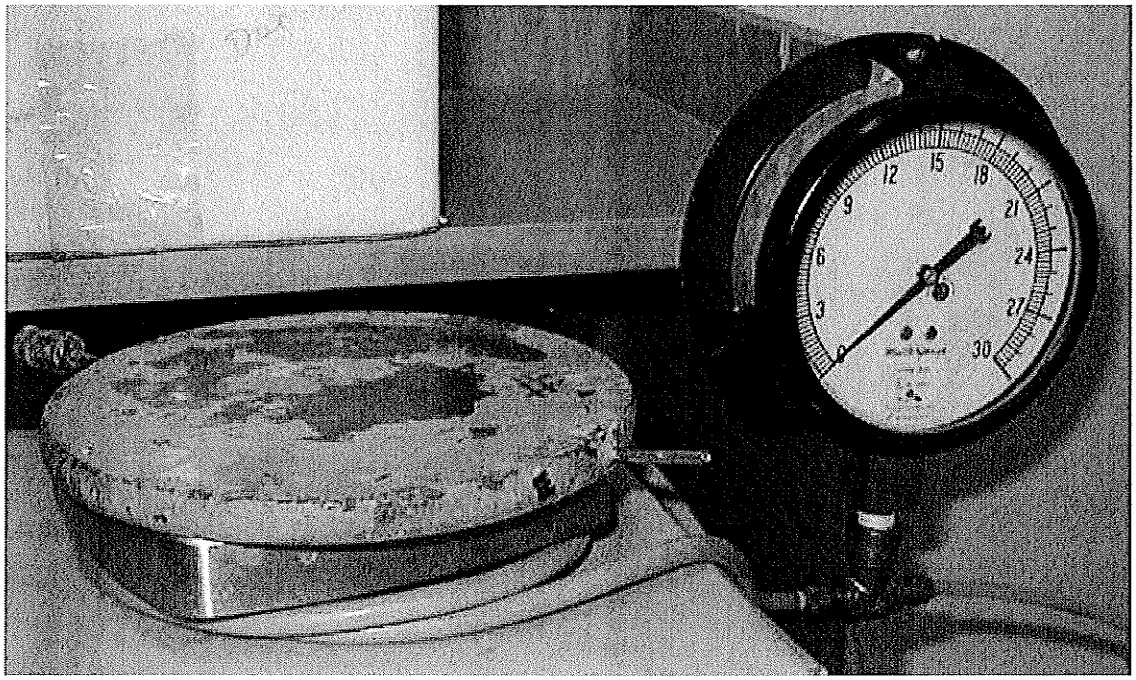

Figure 4.17 – Pressure Plate and Gauge.

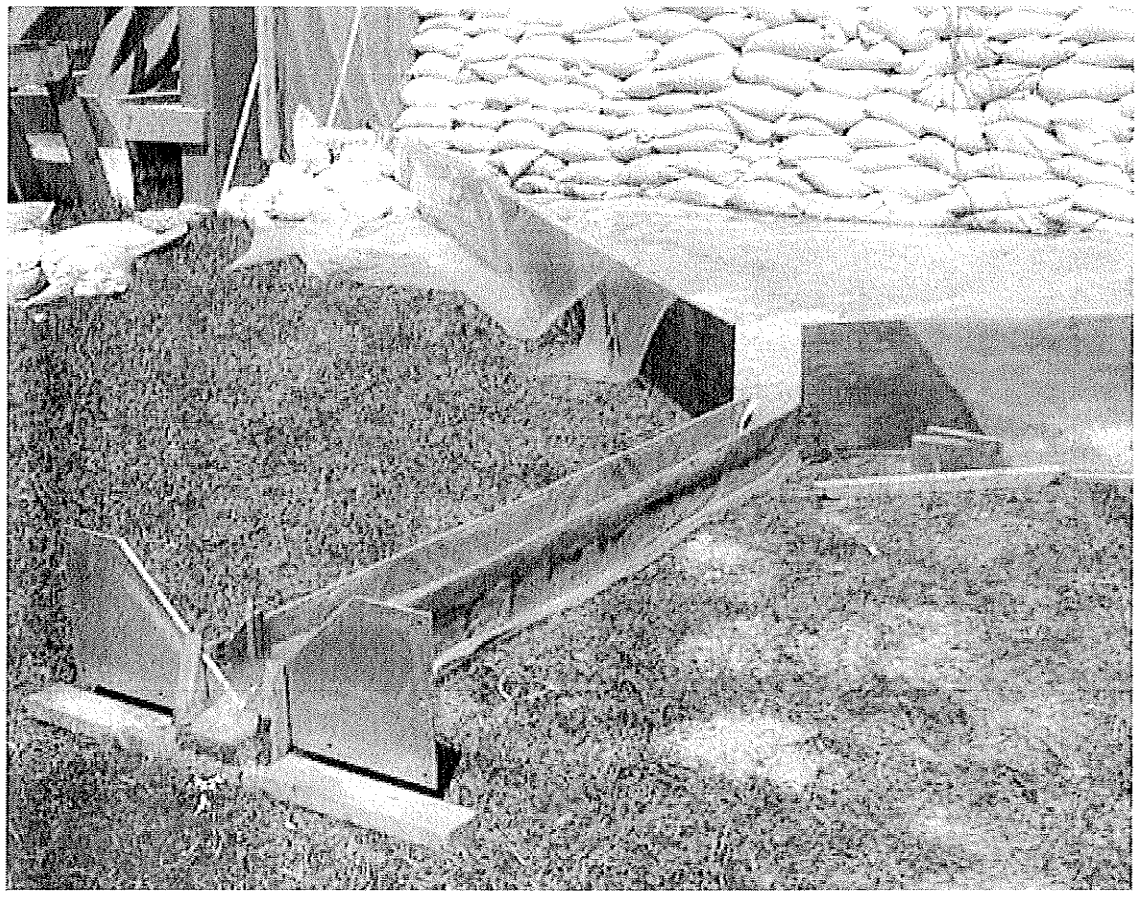

Figure 4.18 – V-notch Weir and Channel Operating during a Test.

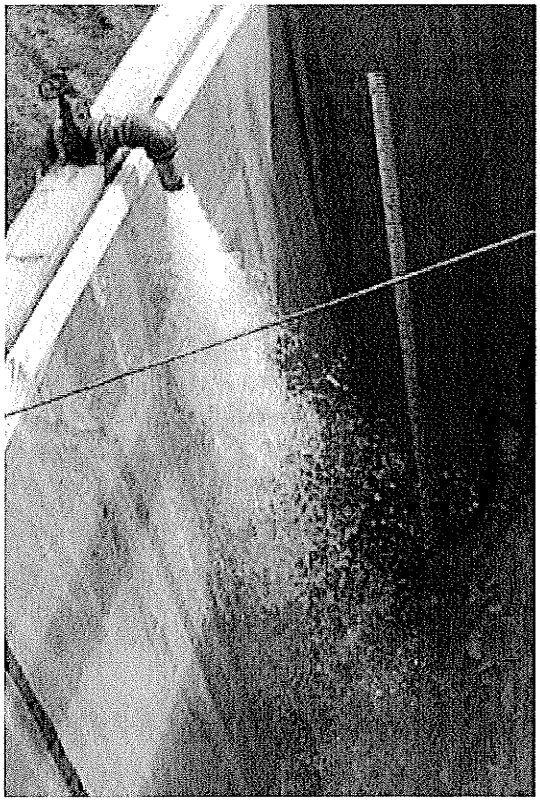

Figure 4.19 – Water Depth Measurement Gauge inside Flume during filling.

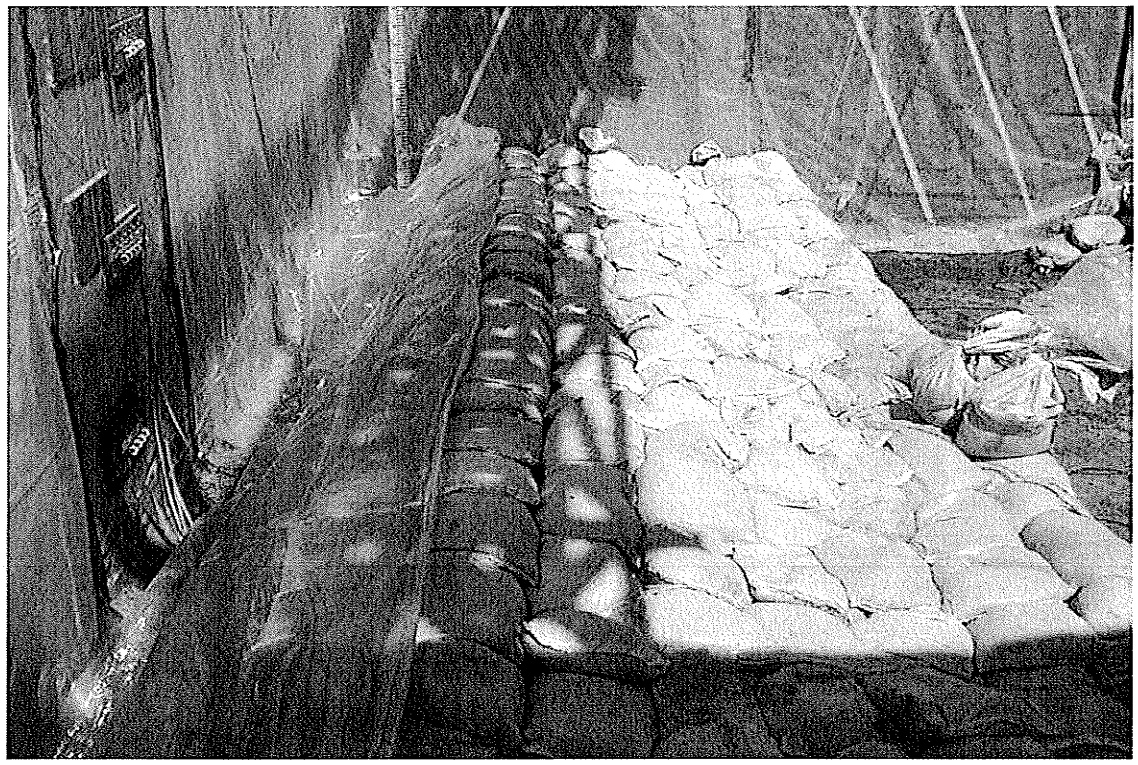

Figure 4.20 – Base Sandbag courses and PES installation during 6' dike C1 test set-up.

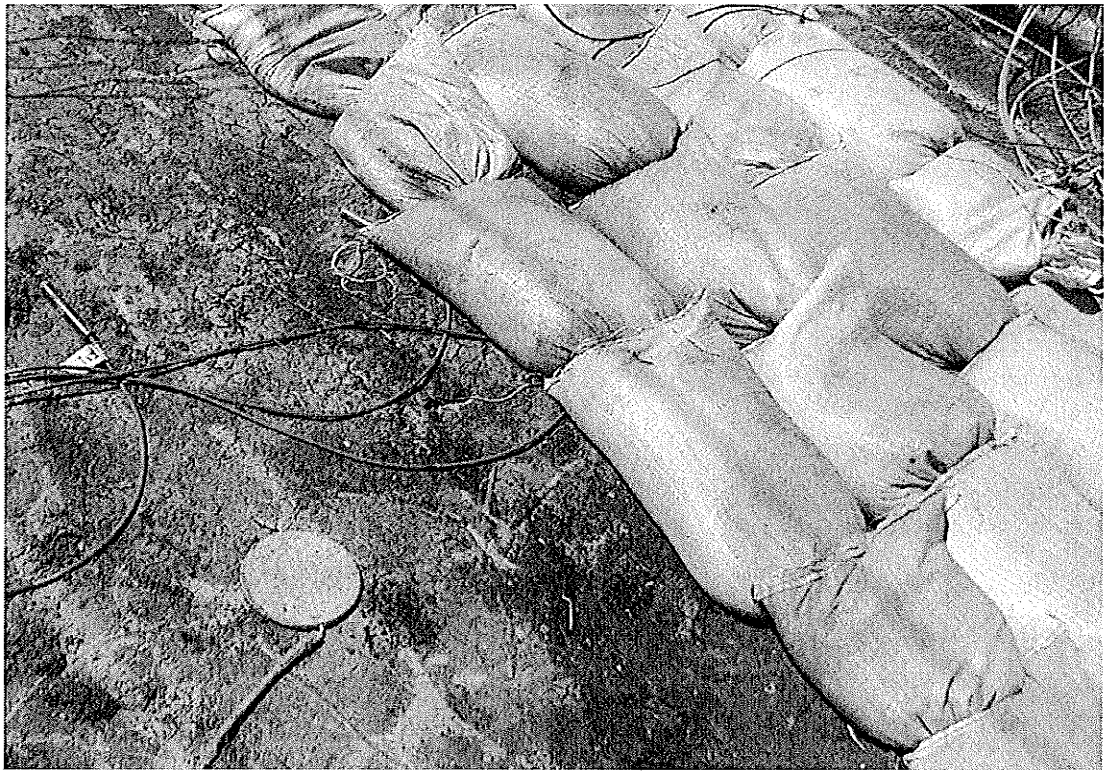

Figure 4.21 – Photograph of Piezometer and Pressure Plate Placement at Base Level during Preparation of 6' Dike C1.

Figure 4.22 – Photograph of Filled Sandbags Marked and Grommetted for Attachment to Extensometers.

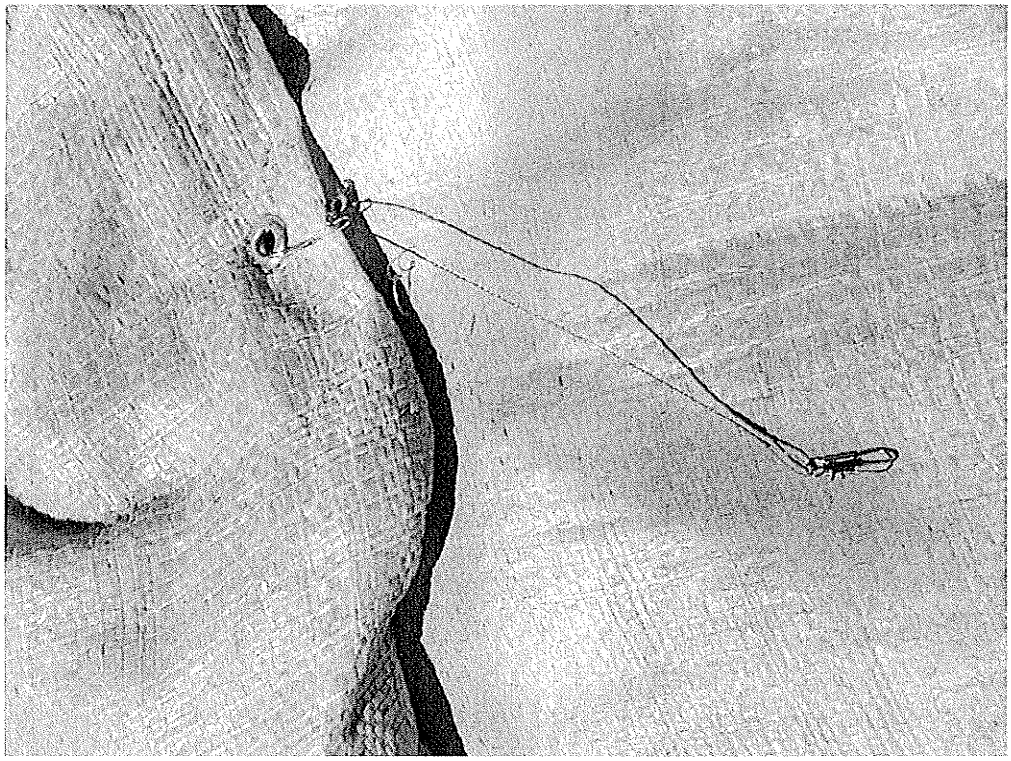

Figure 4.23 – Close-up Photograph of Grommet/Cable-leader System for Attachment to Extensometers.

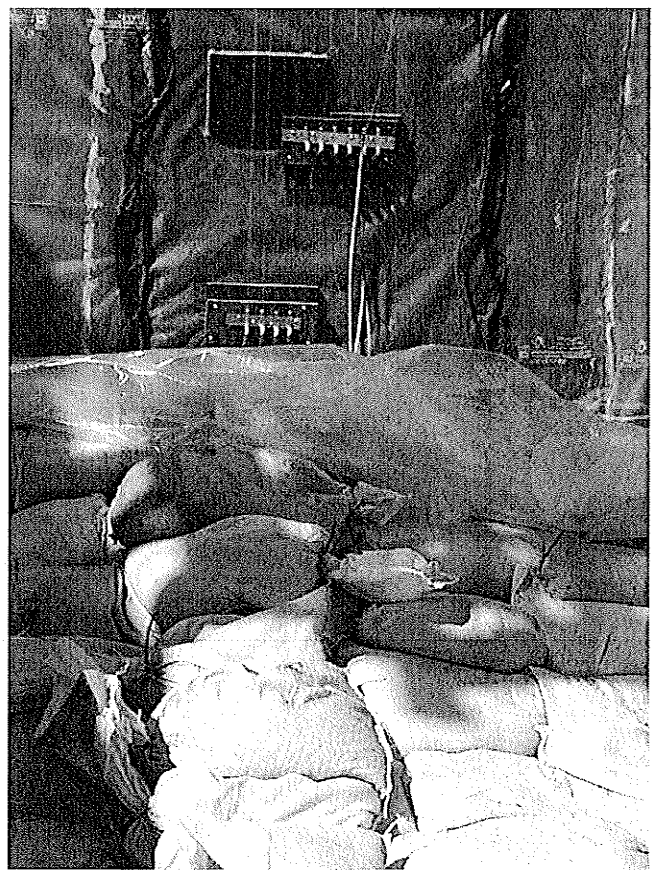

Figure 4.24 – Photograph of Bags Attached to Extensometer Cable/Pulley System.

Figure 4.25 – Media and Participants in Flume with initial Sandbags on Opening Day.

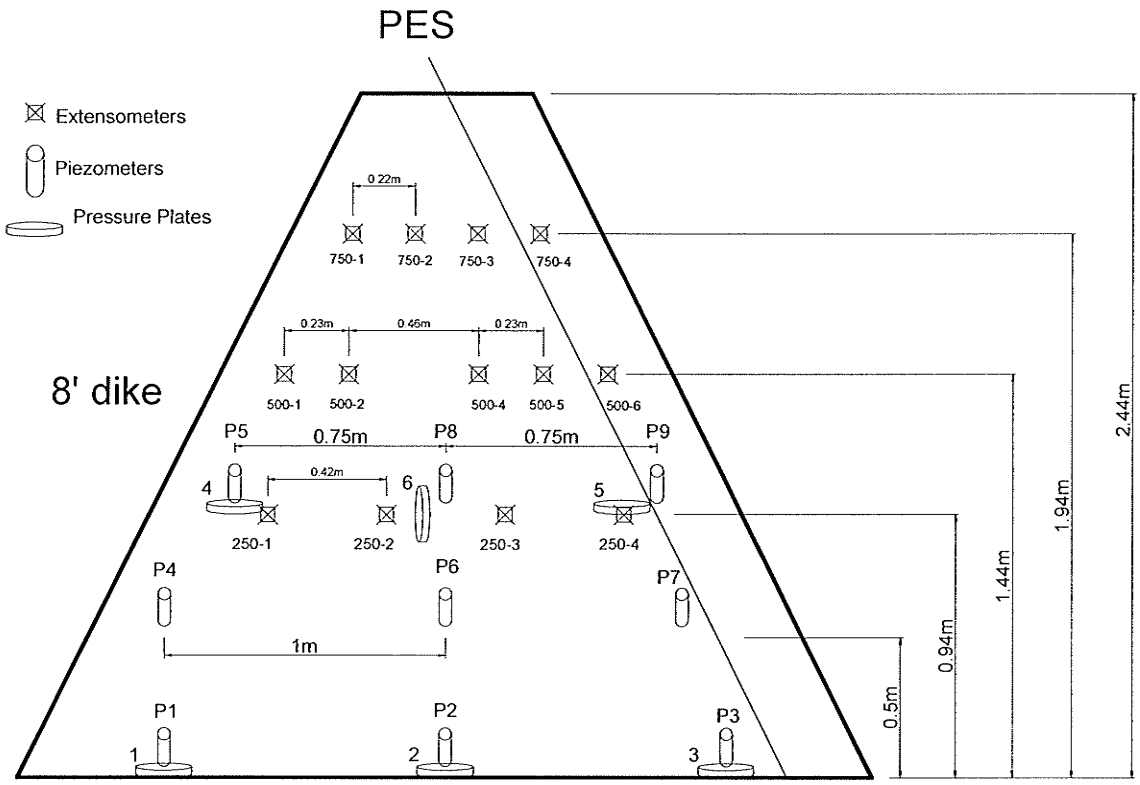

Figure 4.26 – Schematic of Internal Instrumentation Placement for Group A tests.

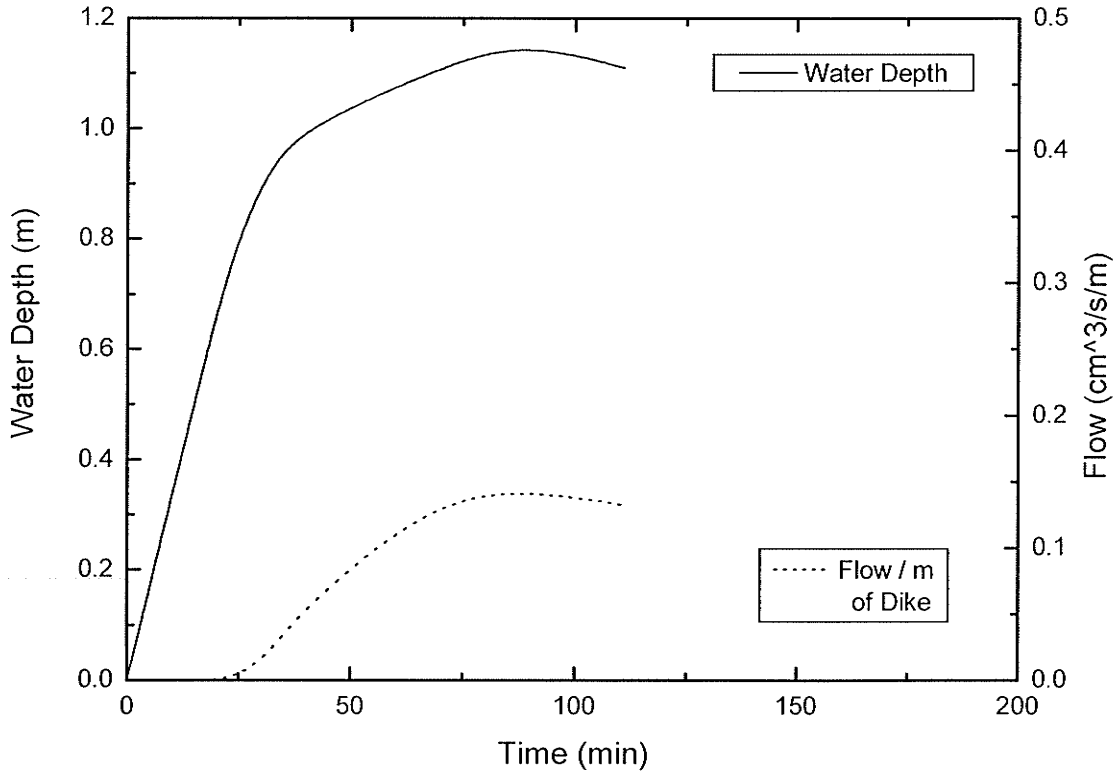

Figure 4.27 – Water Depth and Seepage through Dike A1, July 7, 2004.

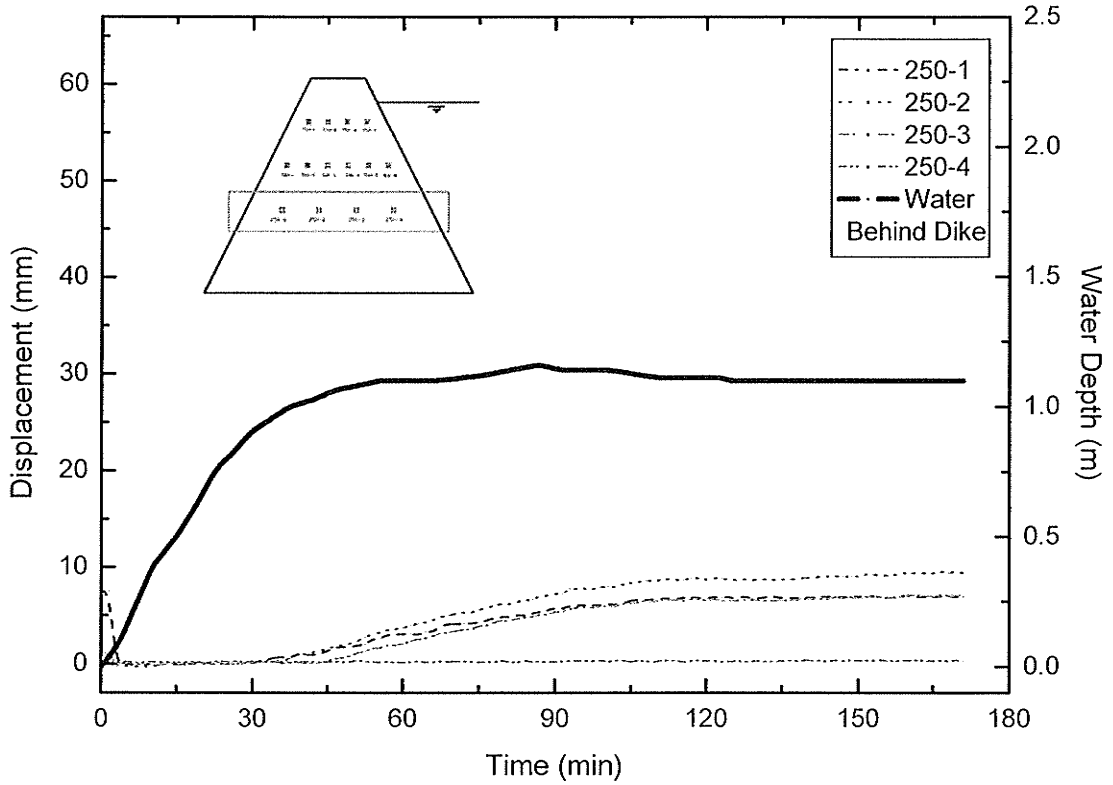

Figure 4.28 – Summary of Extensometers 0.94 m above base of Dike A1, Displacement and Water Depth vs. Time, July 7, 2004.

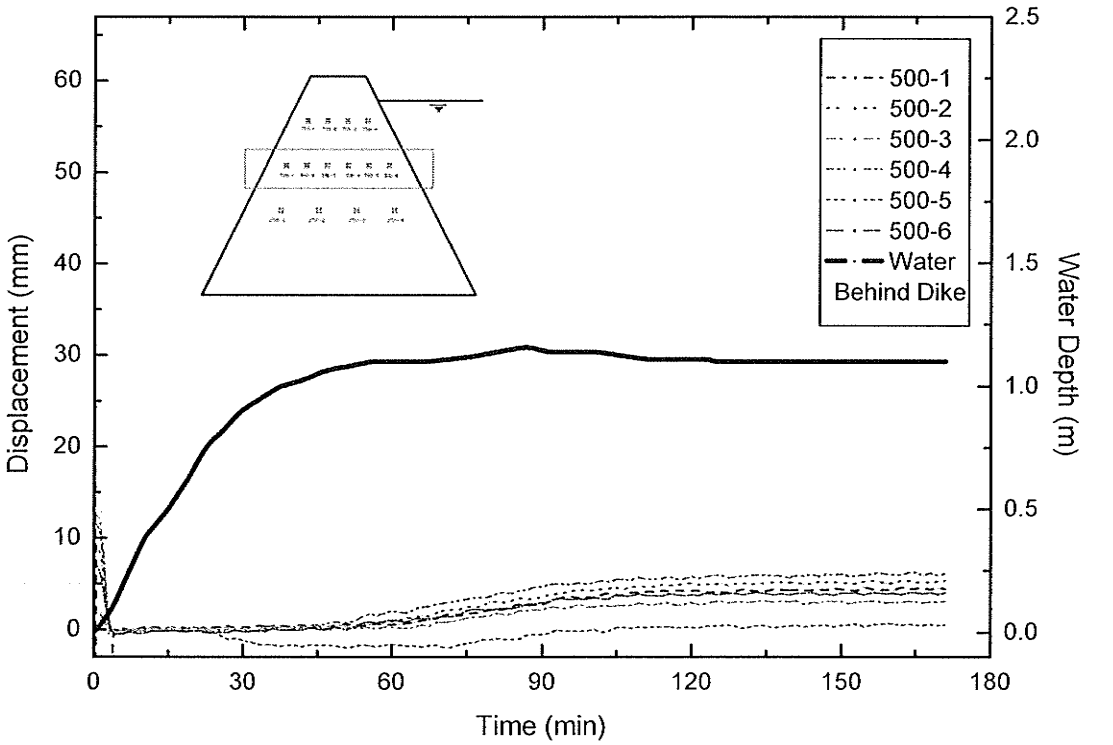

Figure 4.29 – Summary of Extensometers 1.4 m above base of Dike A1, Displacement and Water Depth vs. Time, July 7, 2004.

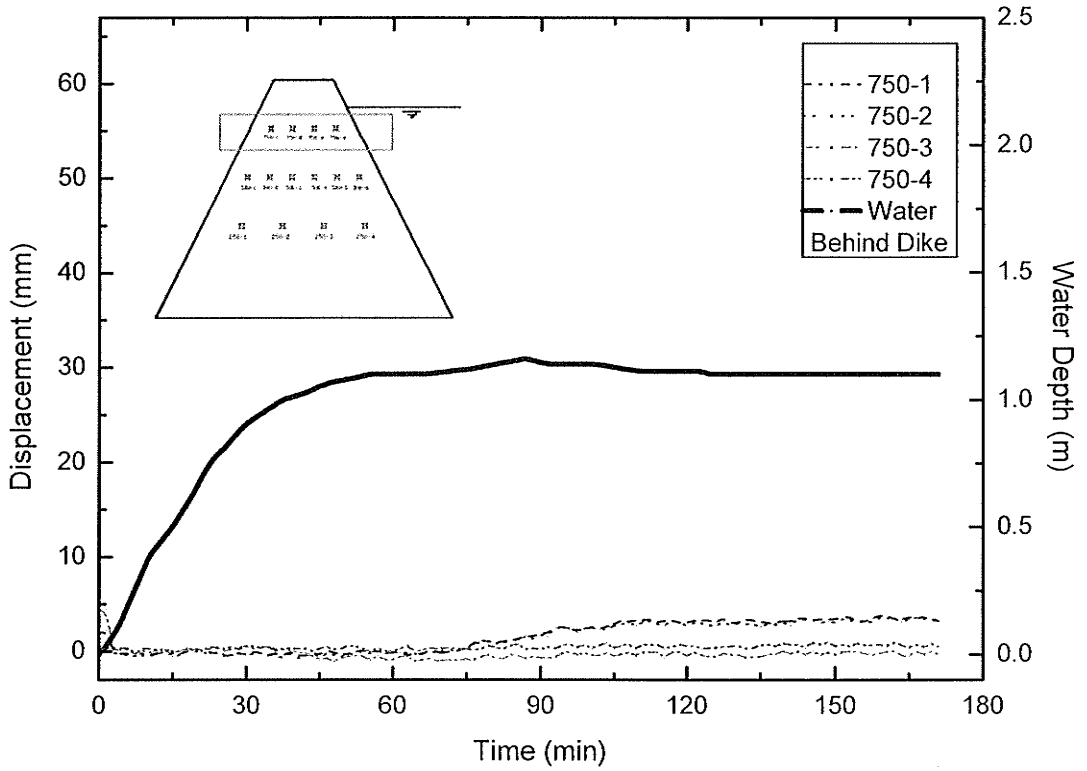

Figure 4.30 – Summary of Extensometers 1.94 m above base of Dike A1, Displacement and Water Depth vs. Time, July 7, 2004.

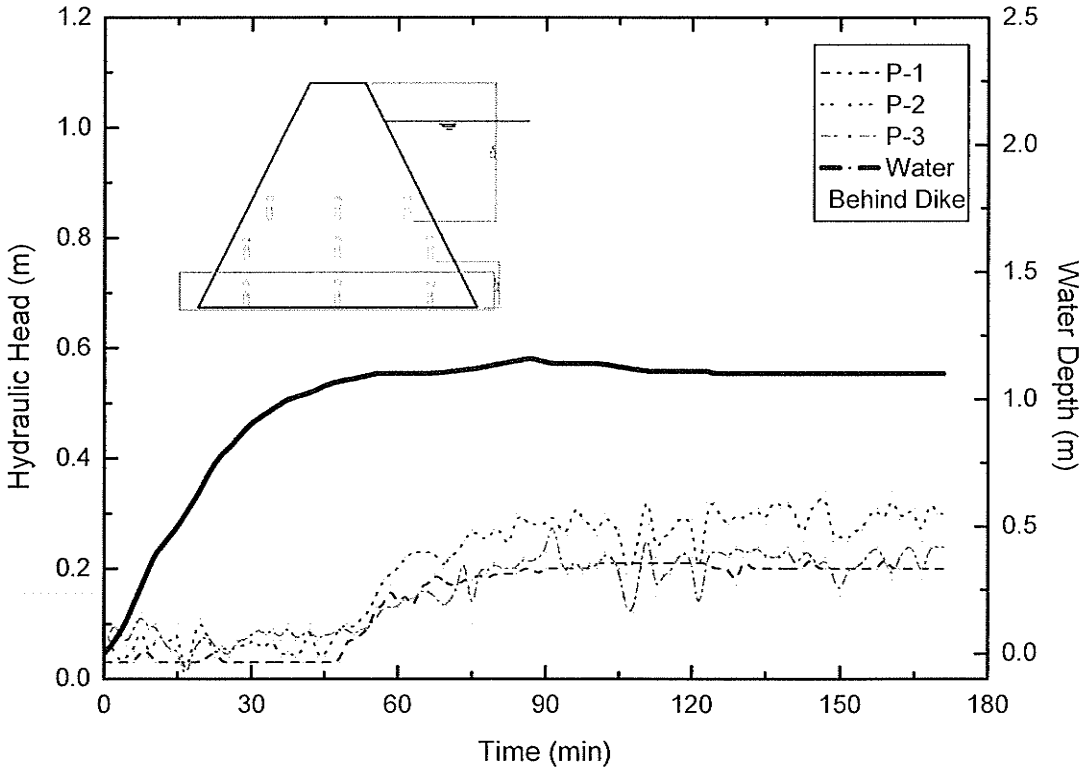

Figure 4.31 – Summary of Hydraulic Head readings by Piezometers at base of Dike A1, Time vs. Hydraulic Head, July 7, 2004.

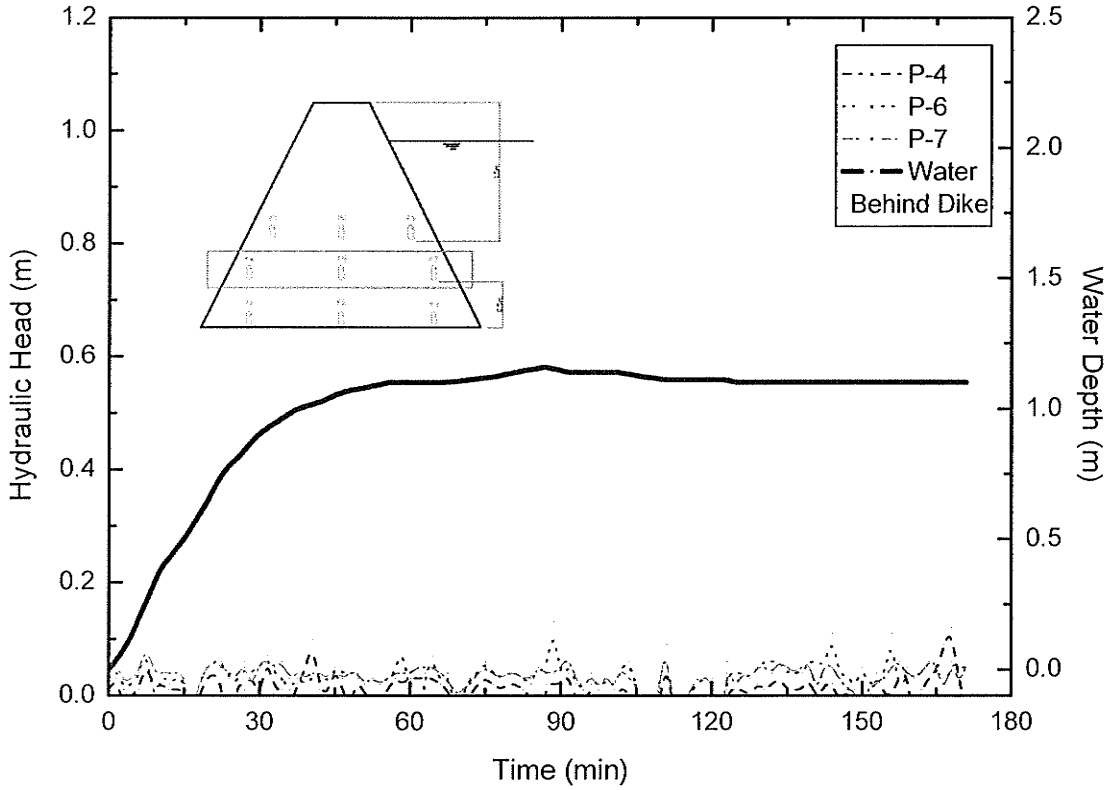

Figure 4.32 – Summary of Hydraulic Head readings by Piezometers 0.5 m above base of Dike A1, Time vs. Hydraulic Head, July 7, 2004.

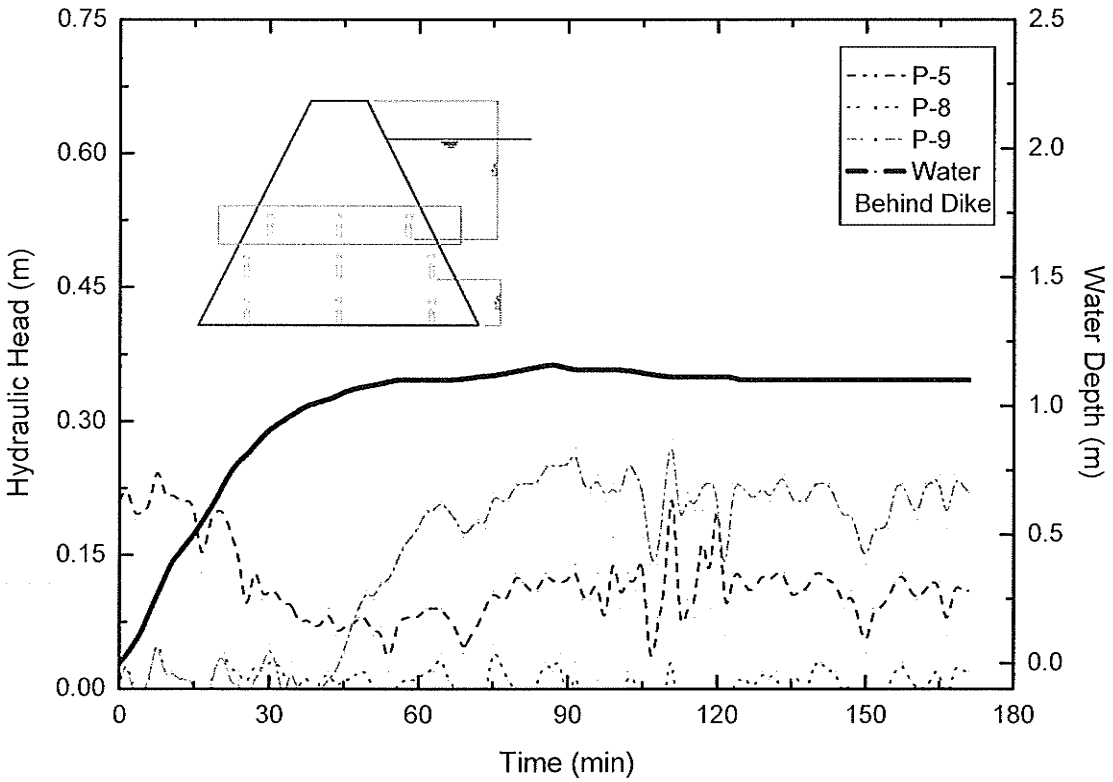

Figure 4.33 – Summary of Hydraulic Head readings by Piezometers 0.94 m above base of Dike A1, Time vs. Hydraulic Head, July 7, 2004.

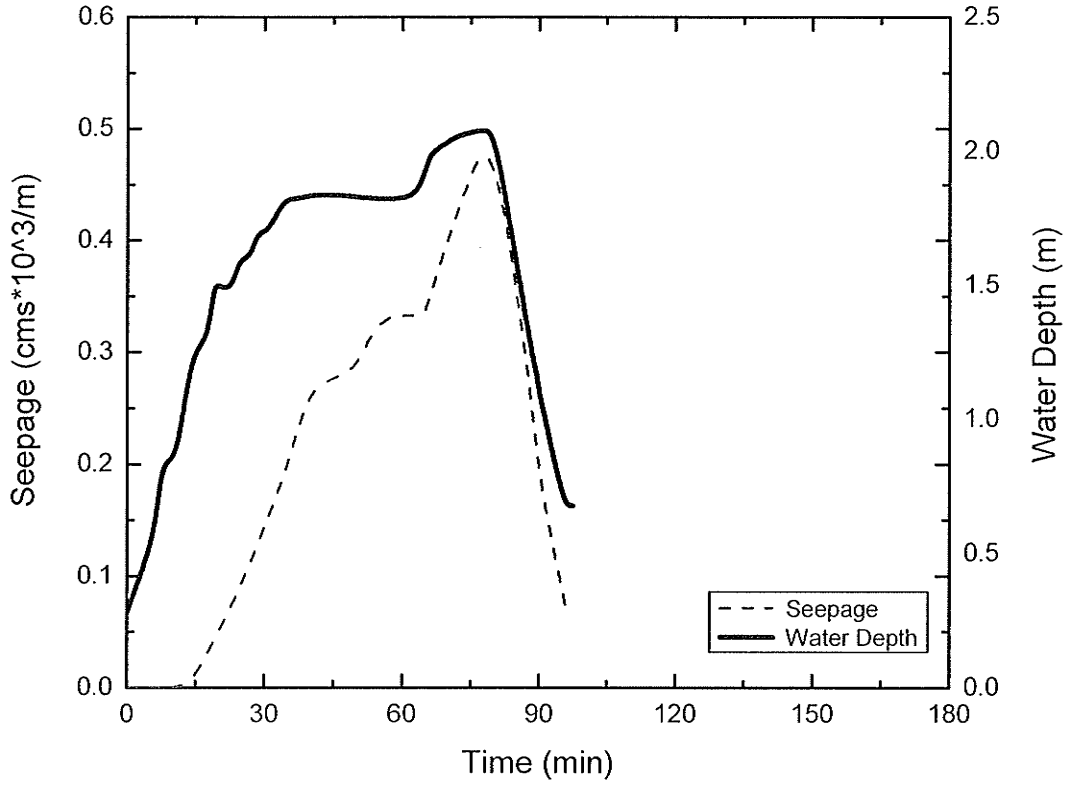

Figure 4.34 – Water Depth and Seepage through Dike A2, July 14, 2004.

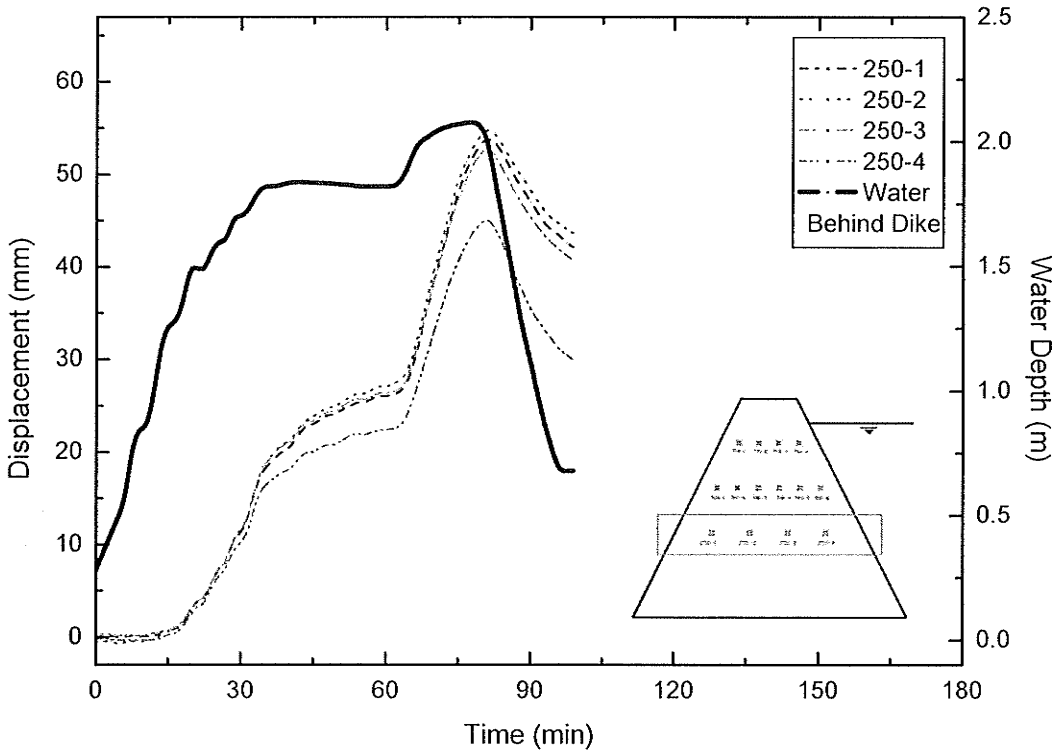

Figure 4.35 – Summary of Extensometers 0.94 m above base of Dike A2, Displacement and Water Depth vs. Time, July 14, 2004.

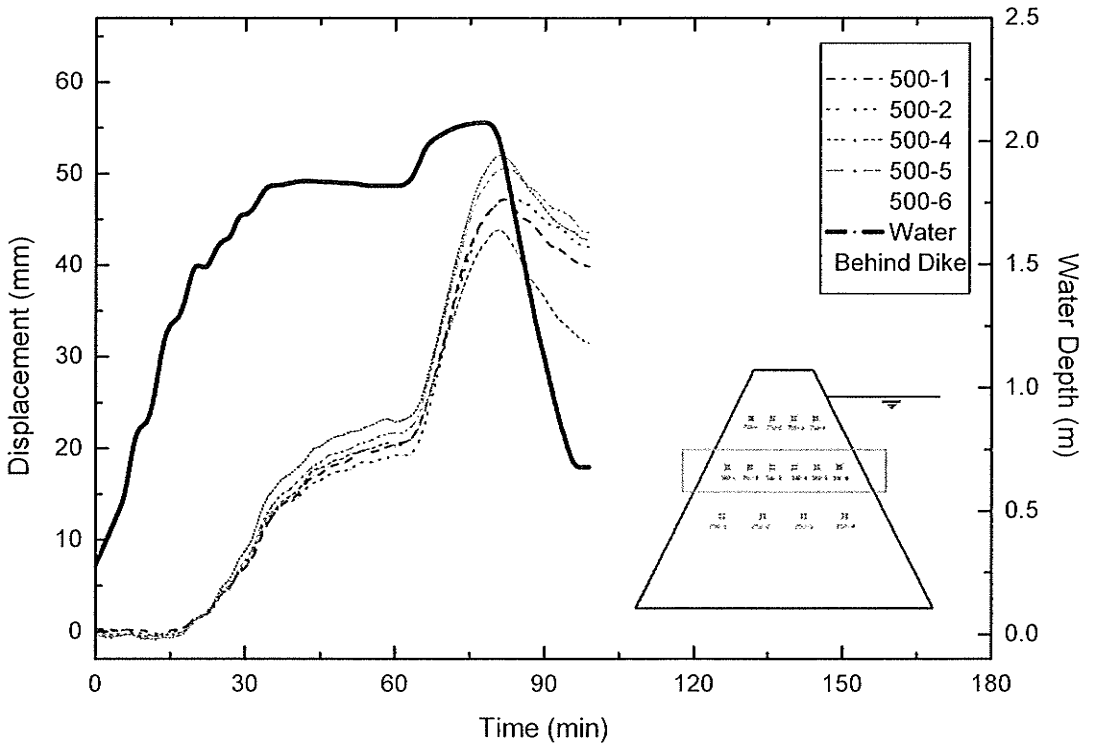

Figure 4.36 – Summary of Extensometers 1.4 m above base of Dike A2, Displacement and Water Depth vs. Time, July 14, 2004.

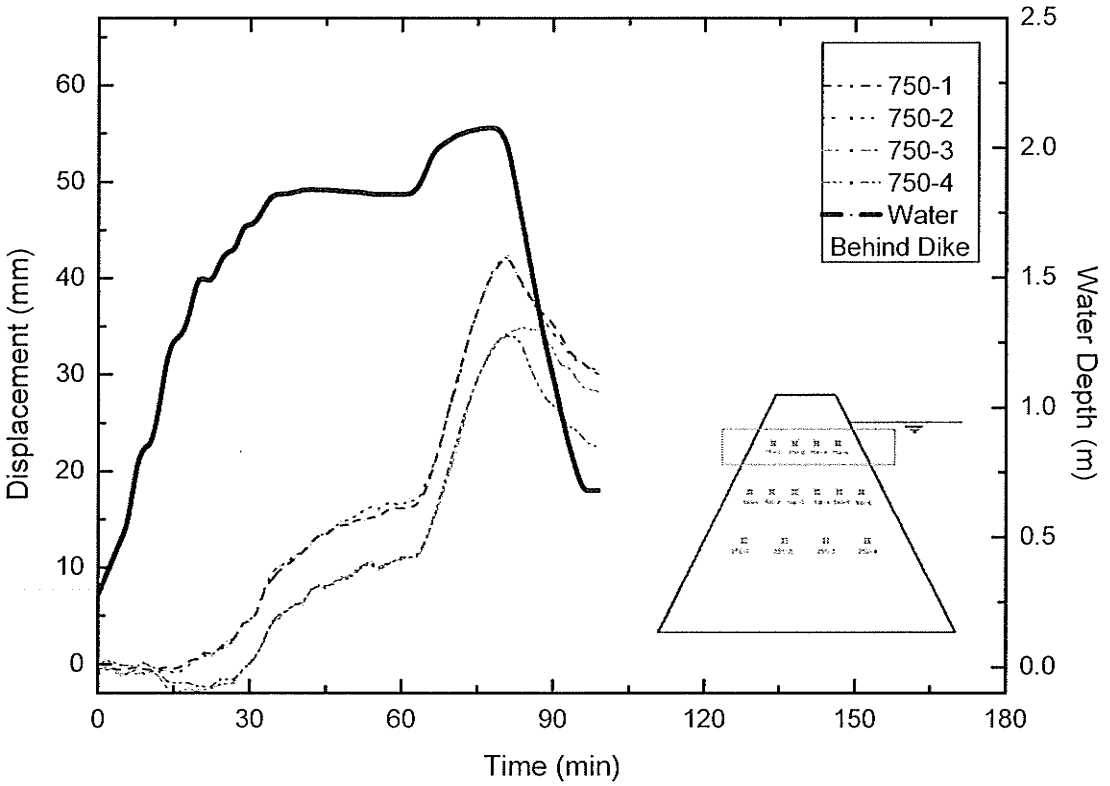

Figure 4.37 – Summary of Extensometers 1.94 m above base of Dike A2, Displacement and Water Depth vs. Time, July 14, 2004.

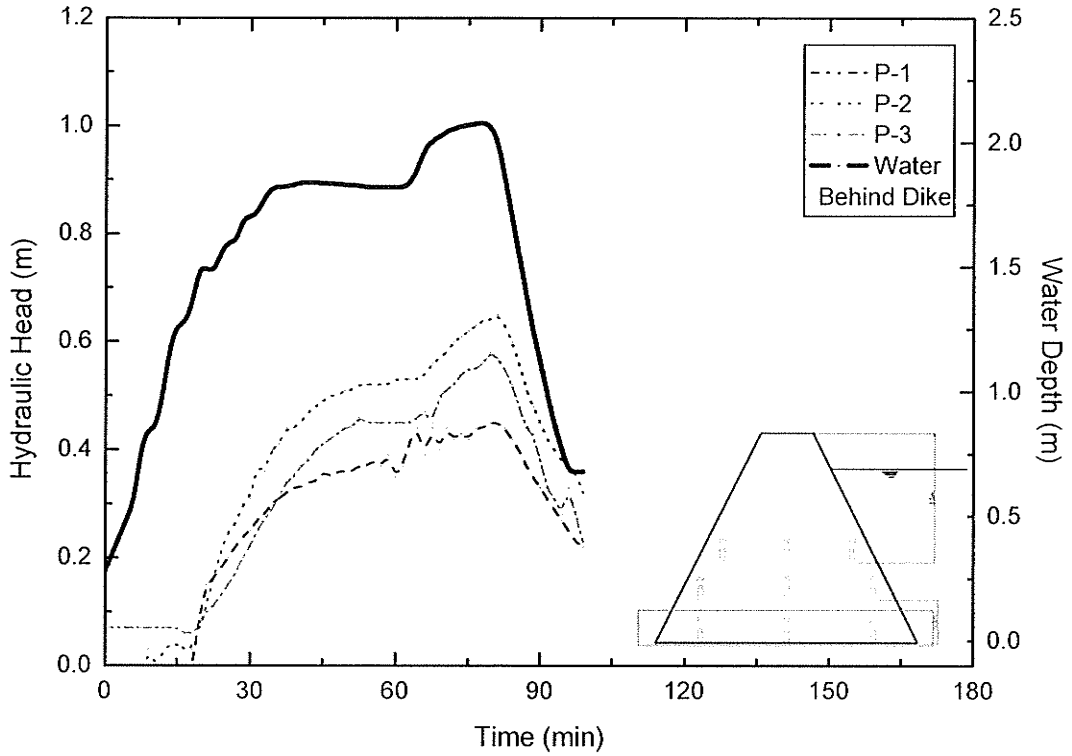

Figure 4.38 – Summary of Hydraulic Head readings by Piezometers at base of Dike A2, Time vs. Hydraulic Head, July 14, 2004.

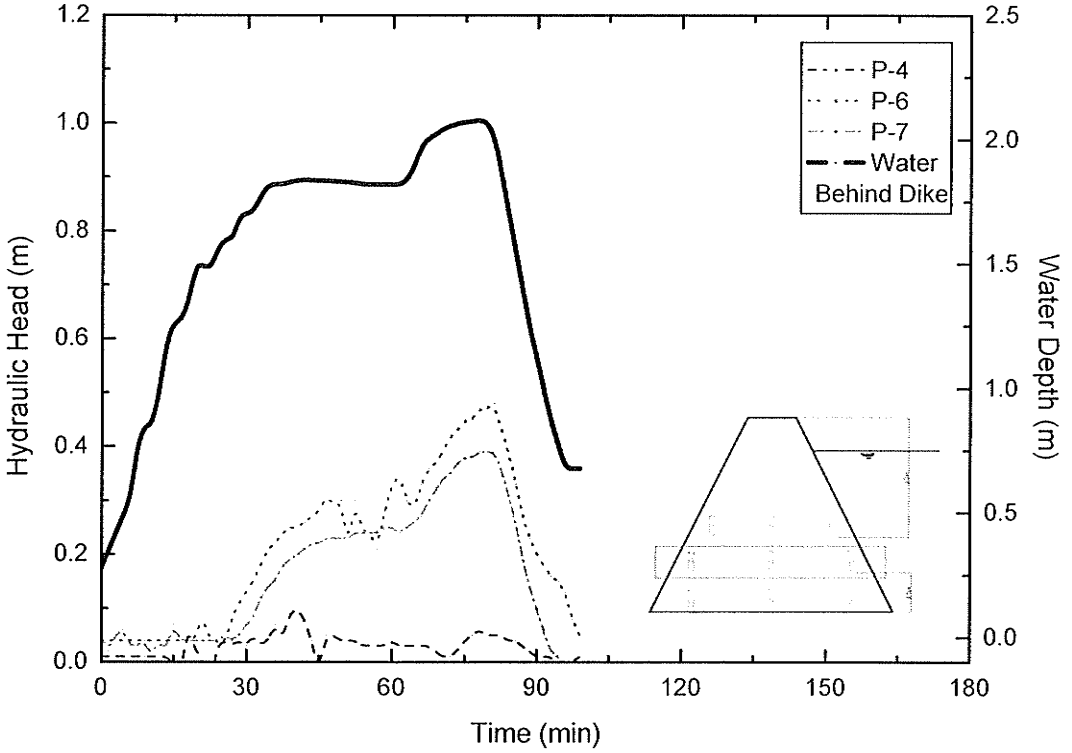

Figure 4.39 – Summary of Hydraulic Head readings by Piezometers 0.5 m above base of Dike A2, Time vs. Hydraulic Head, July 14, 2004.

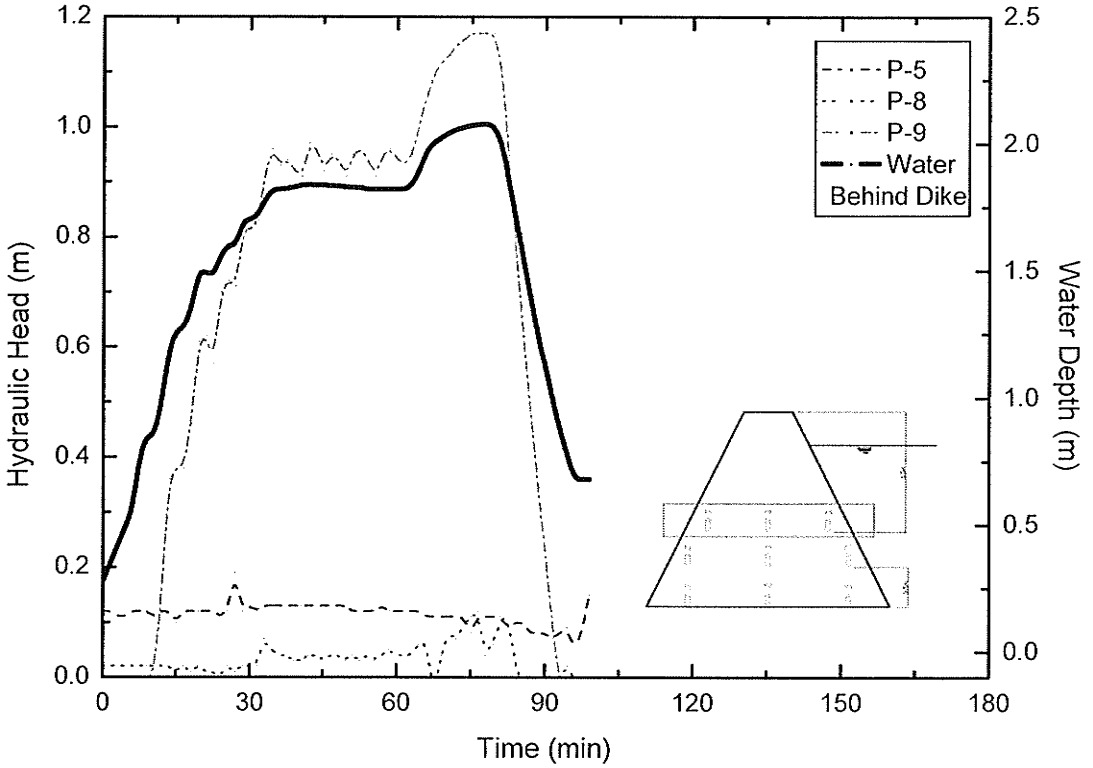

Figure 4.40 – Summary of Hydraulic Head readings by Piezometers 0.94 m above base of Dike A2, Time vs. Hydraulic Head, July 14, 2004.

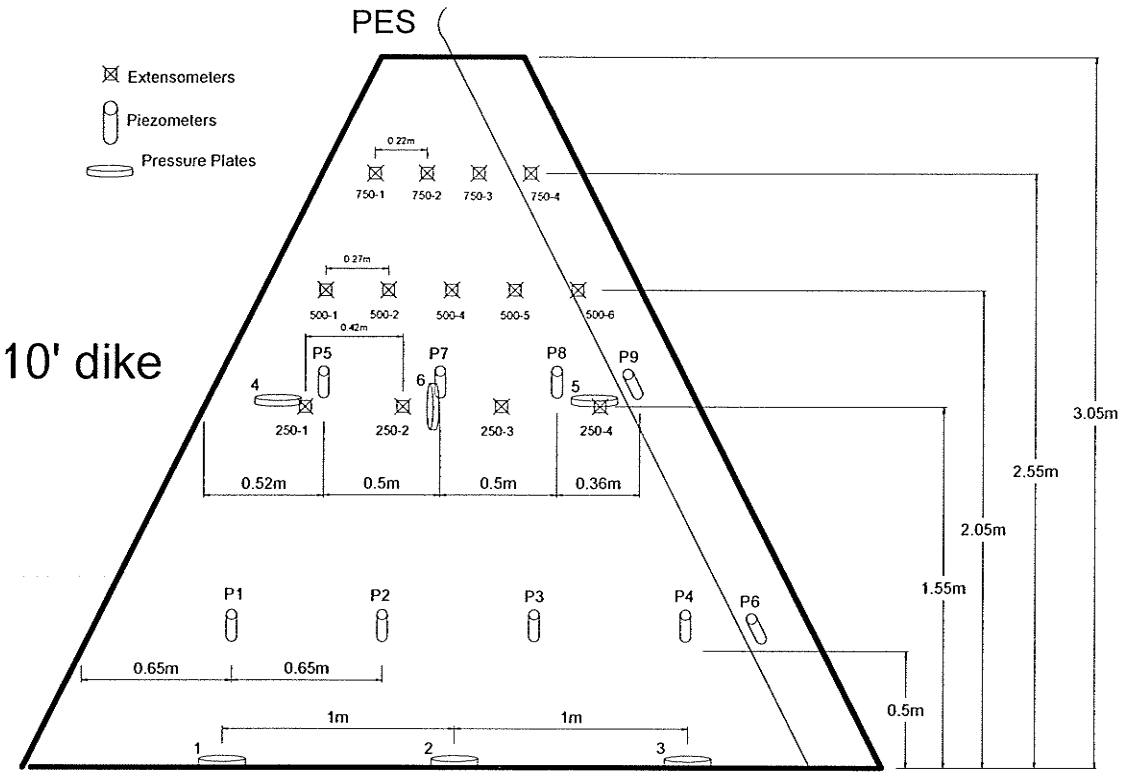

Figure 4.41 – Schematic of Internal Instrumentation Placement for Group B tests.

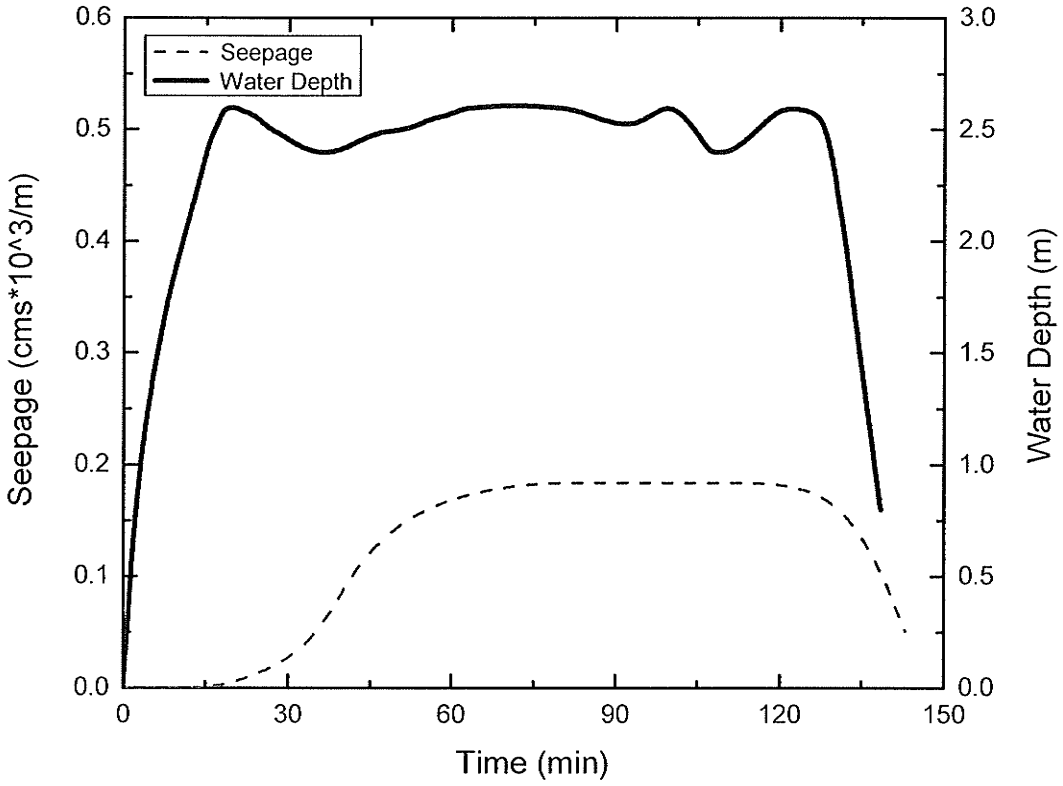

Figure 4.42 – Water Depth and Seepage through Dike B1, July 23, 2004.

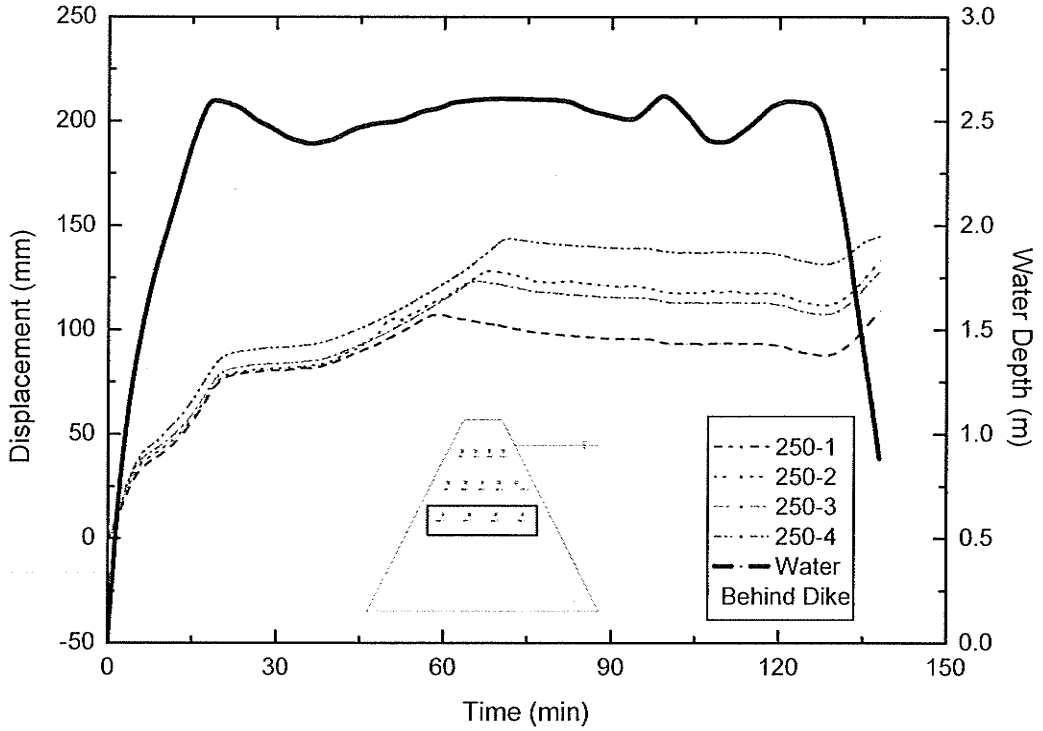

Figure 4.43 – Summary of Extensometers 1.55 m above base of Dike B1, Displacement and Water Depth vs. Time, July 23, 2004.

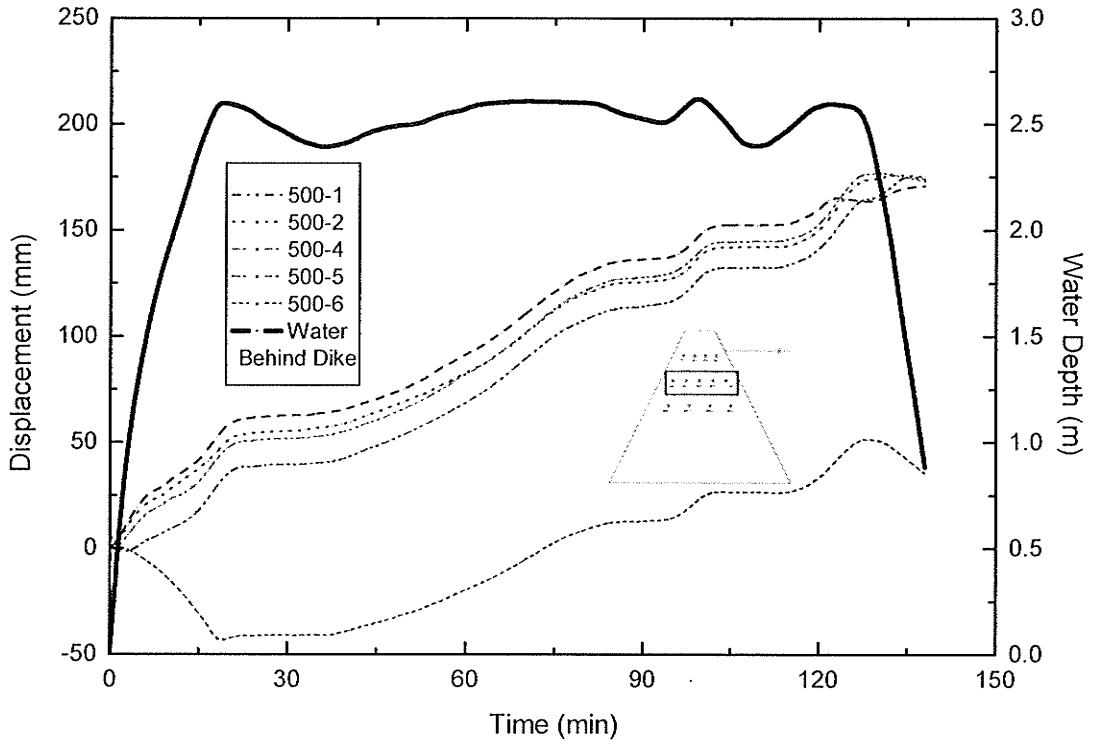

Figure 4.44 – Summary of Extensometers 2.05 m above base of Dike B1, Displacement and Water Depth vs. Time, July 23, 2004.

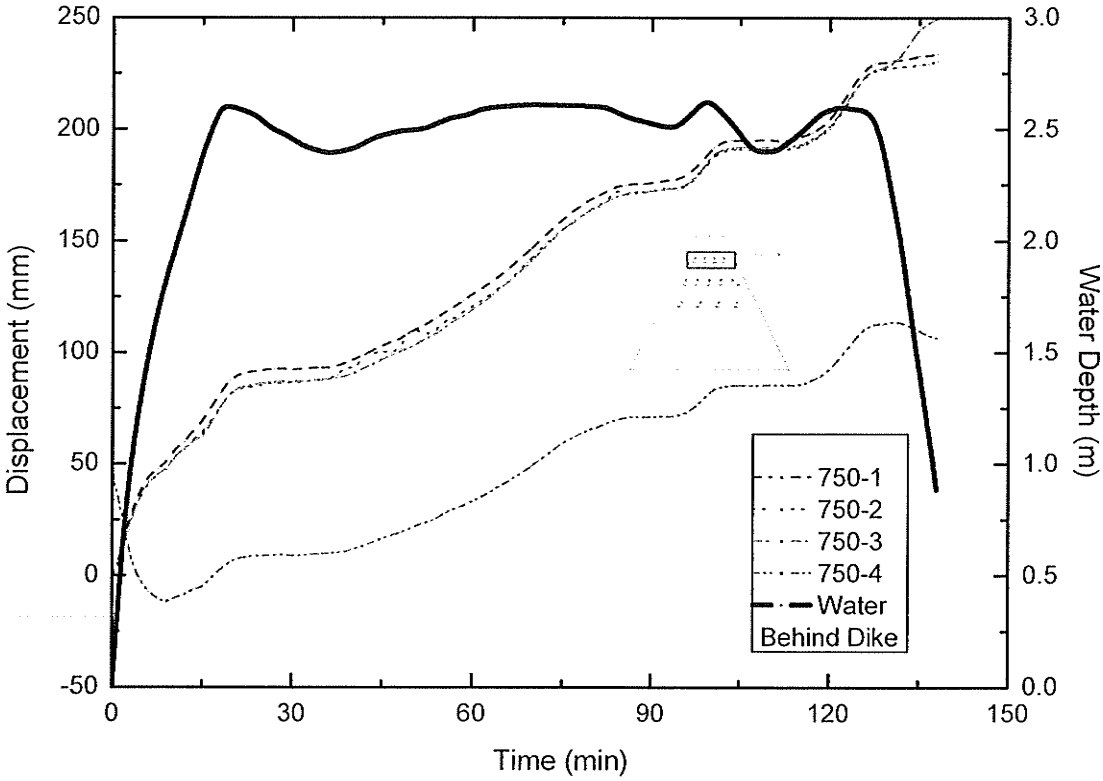

Figure 4.45 – Summary of Extensometers 2.55 m above base of Dike B1, Displacement and Water Depth vs. Time, July 23, 2004.

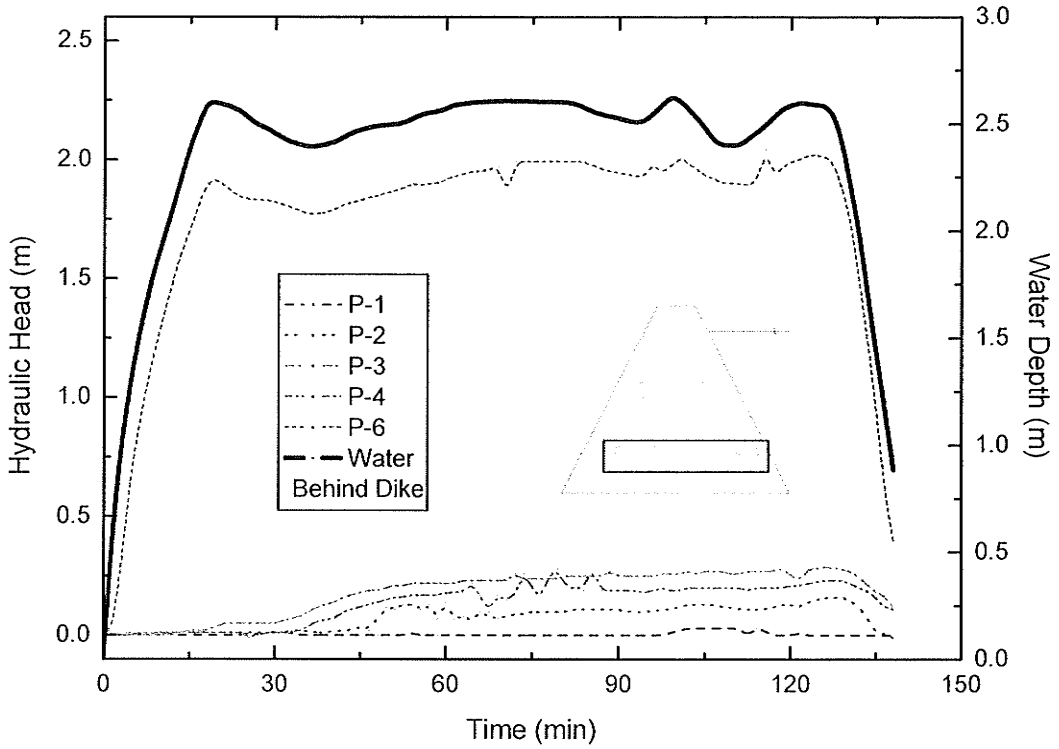

Figure 4.46 – Summary of Hydraulic Head readings by Piezometers 0.5 m above base of Dike B1, Time vs. Hydraulic Head, July 23, 2004.

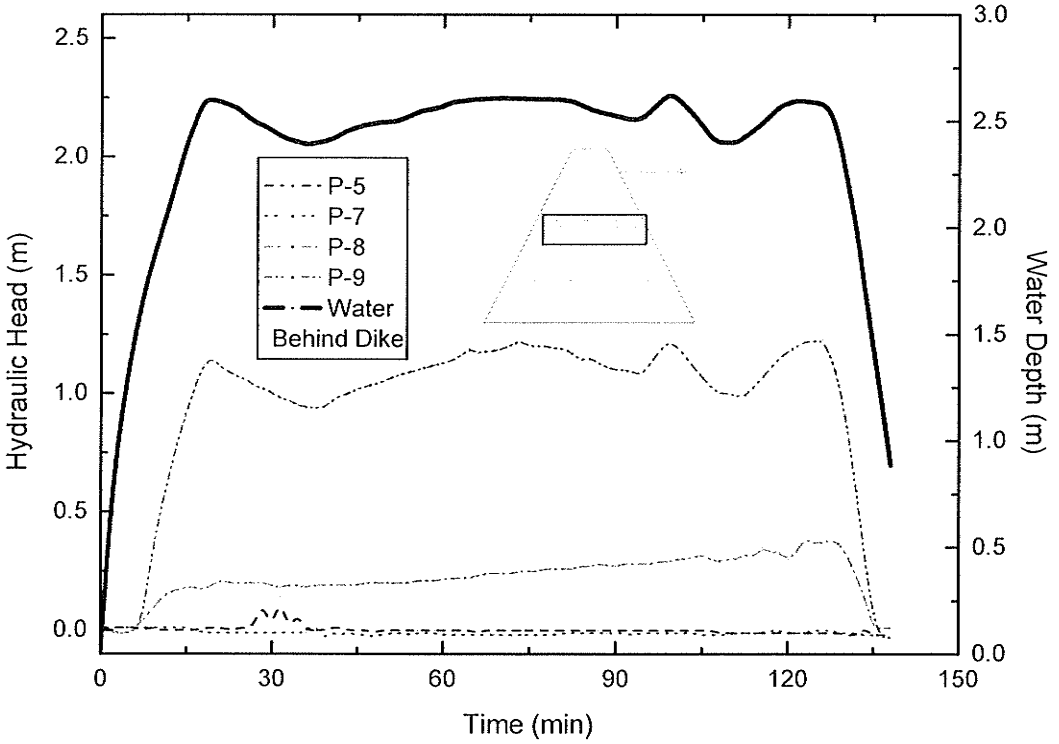

Figure 4.47 – Summary of Hydraulic Head readings by Piezometers 1.55 m above base of Dike B1, Time vs. Hydraulic Head, July 23, 2004.

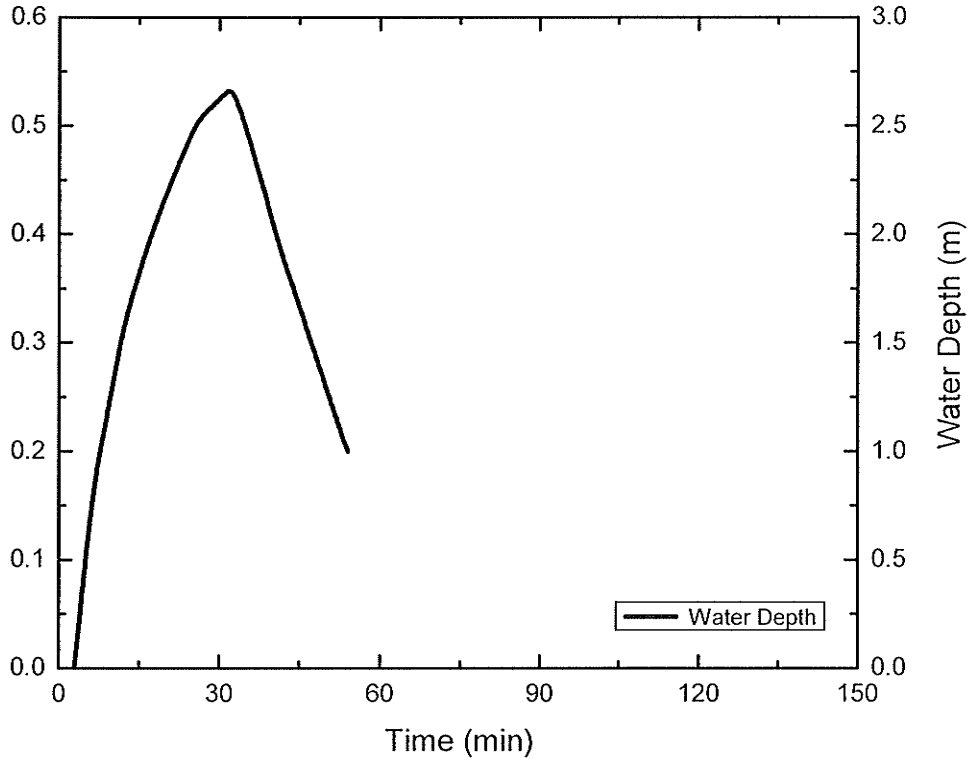

Figure 4.48 – Water Depth behind Dike B2, July 28, 2004.

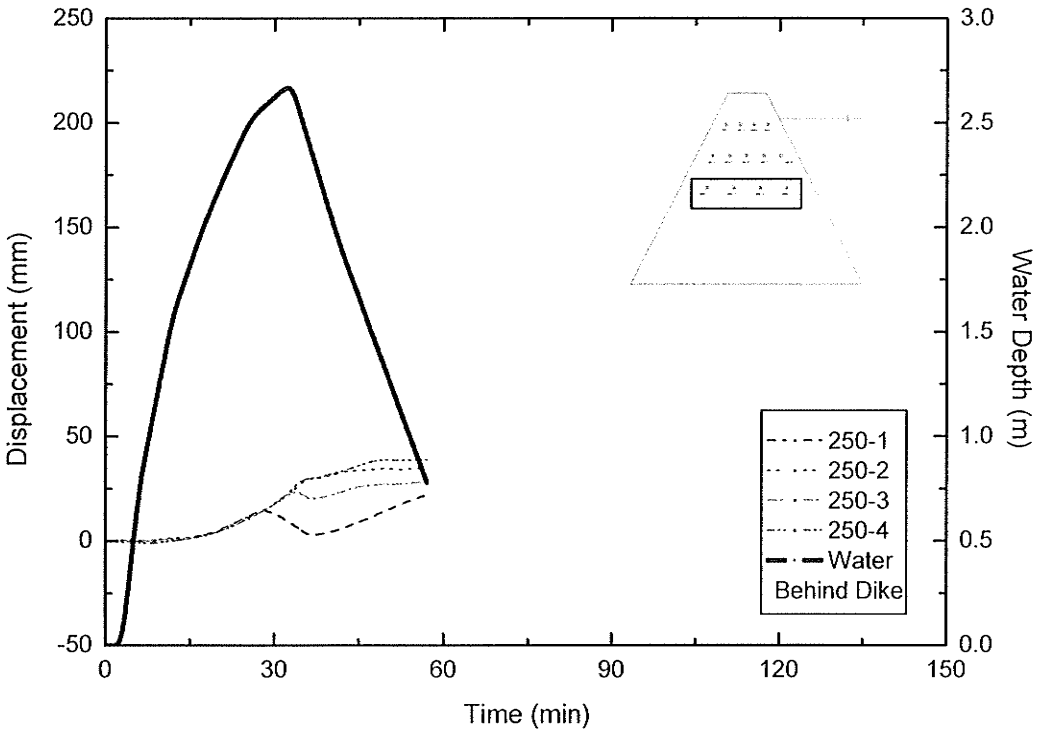

Figure 4.49 – Summary of Extensometers 1.55 m above base of Dike B2, Displacement and Water Depth vs. Time, July 28, 2004.

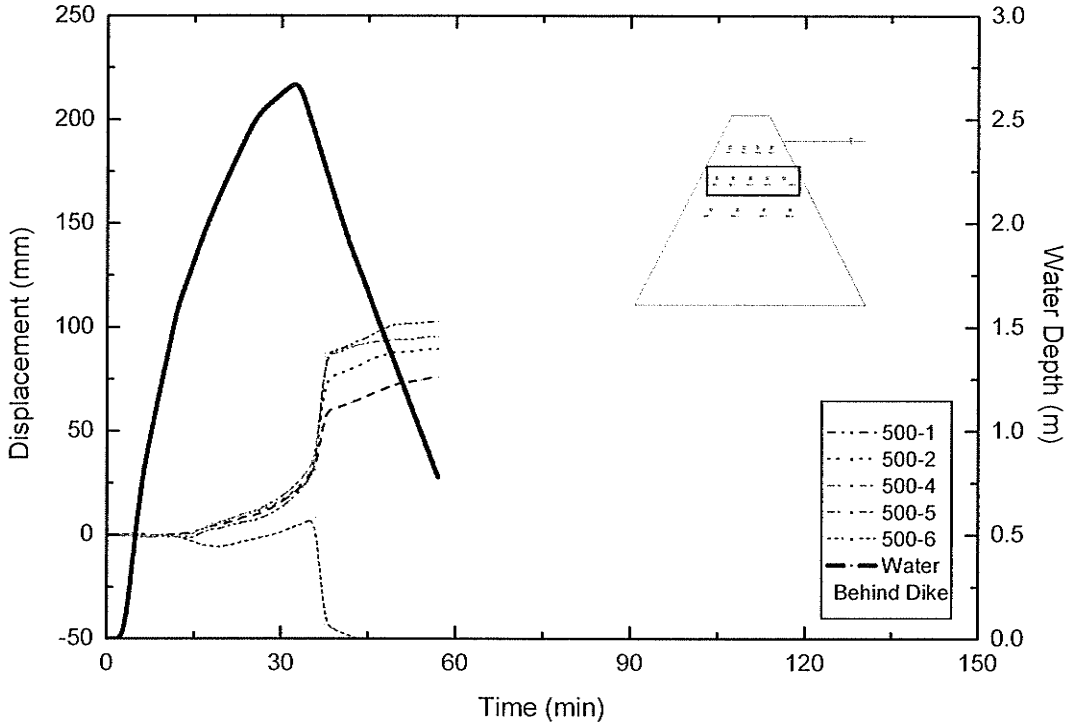

Figure 4.50 – Summary of Extensometers 2.05 m above base of Dike B2, Displacement and Water Depth vs. Time, July 28, 2004.

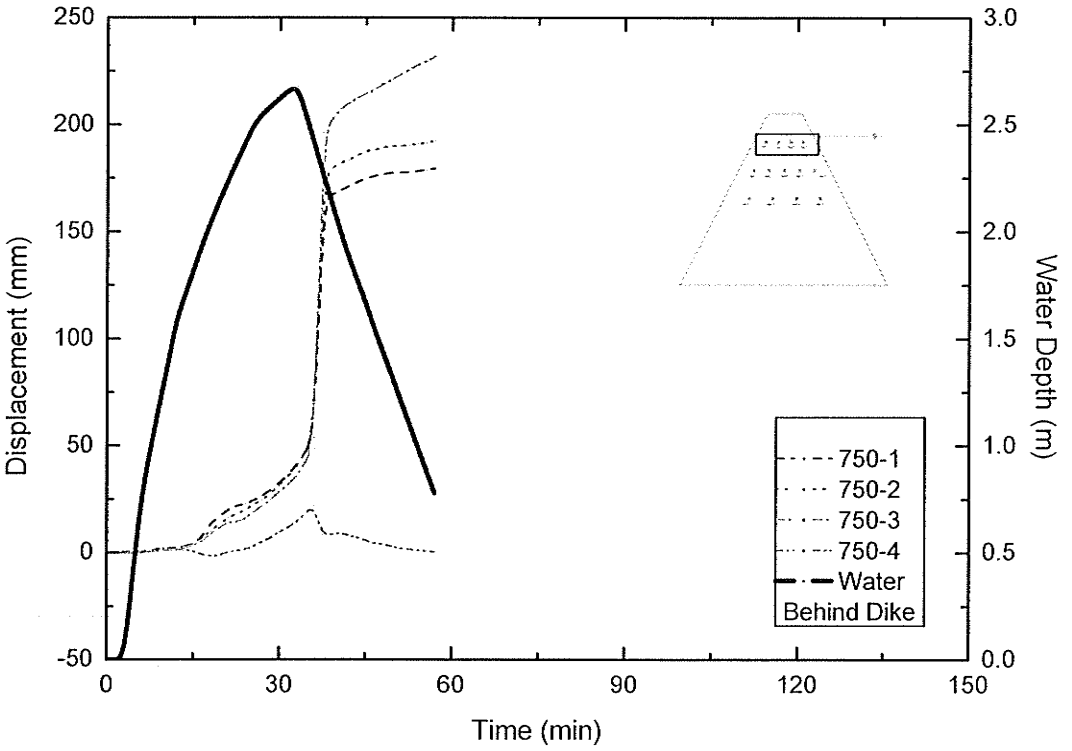

Figure 4.51 – Summary of Extensometers 2.55 m above base of Dike B2, Displacement and Water Depth vs. Time, July 28, 2004.

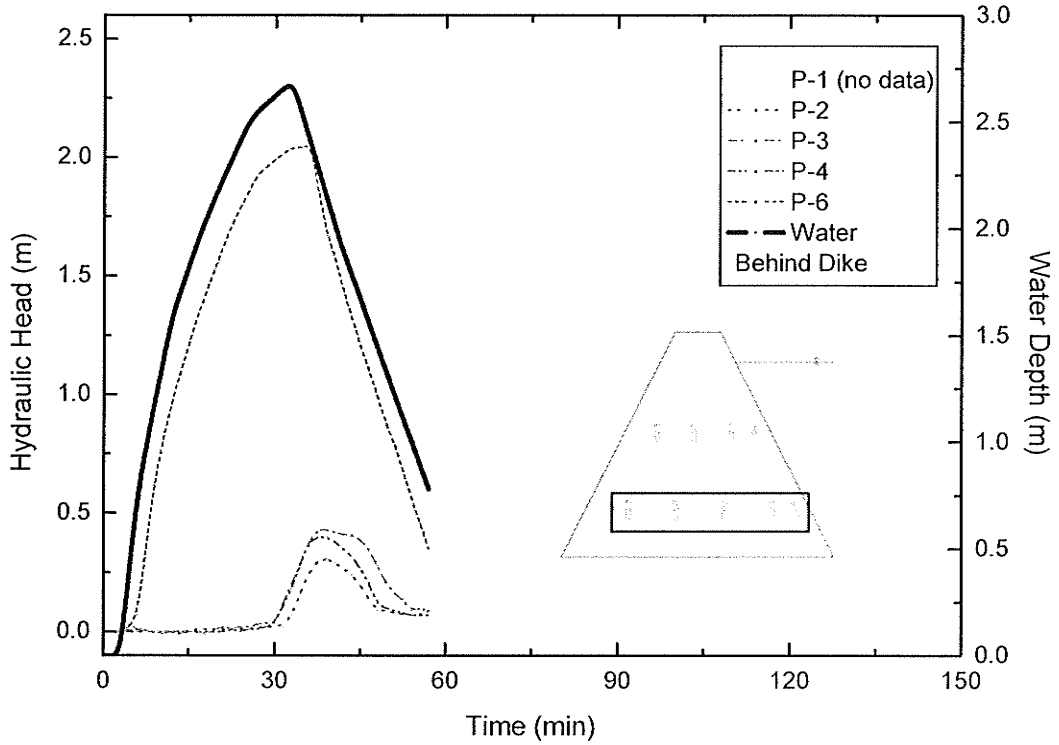

Figure 4.52 – Summary of Hydraulic Head readings by Piezometers 0.5 m above base of Dike B2, Time vs. Hydraulic Head, July 28, 2004.

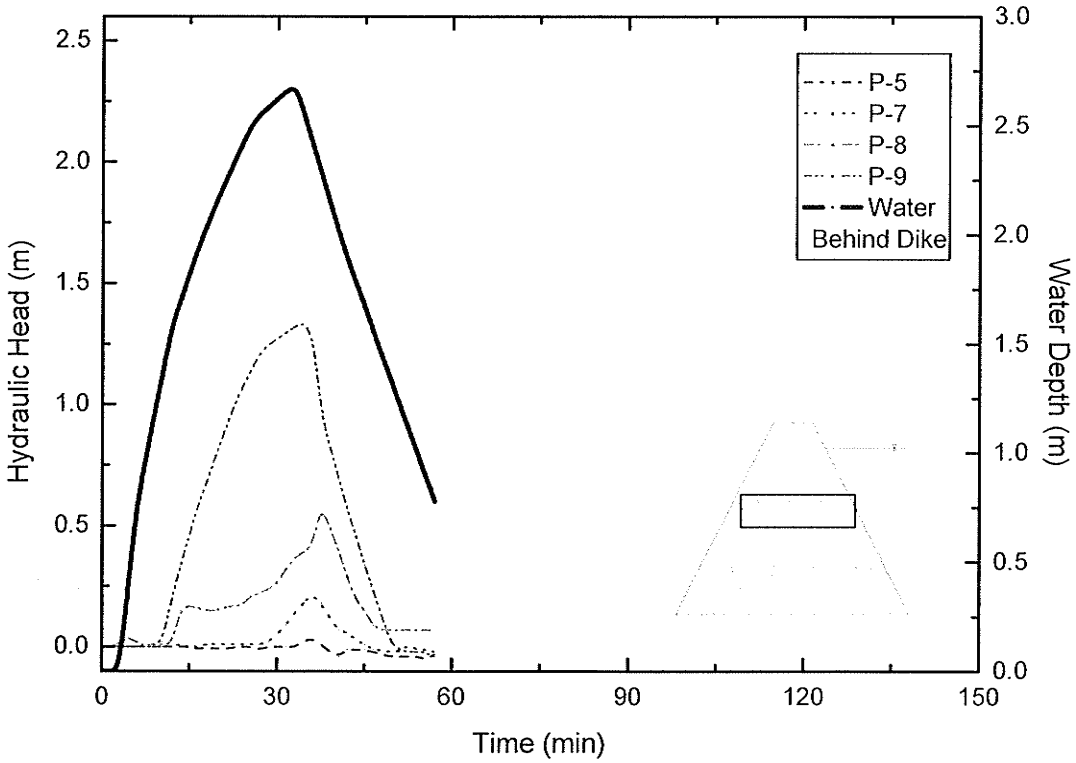

Figure 4.53 – Summary of Hydraulic Head readings by Piezometers 1.55 m above base of Dike B2, Time vs. Hydraulic Head, July 28, 2004.

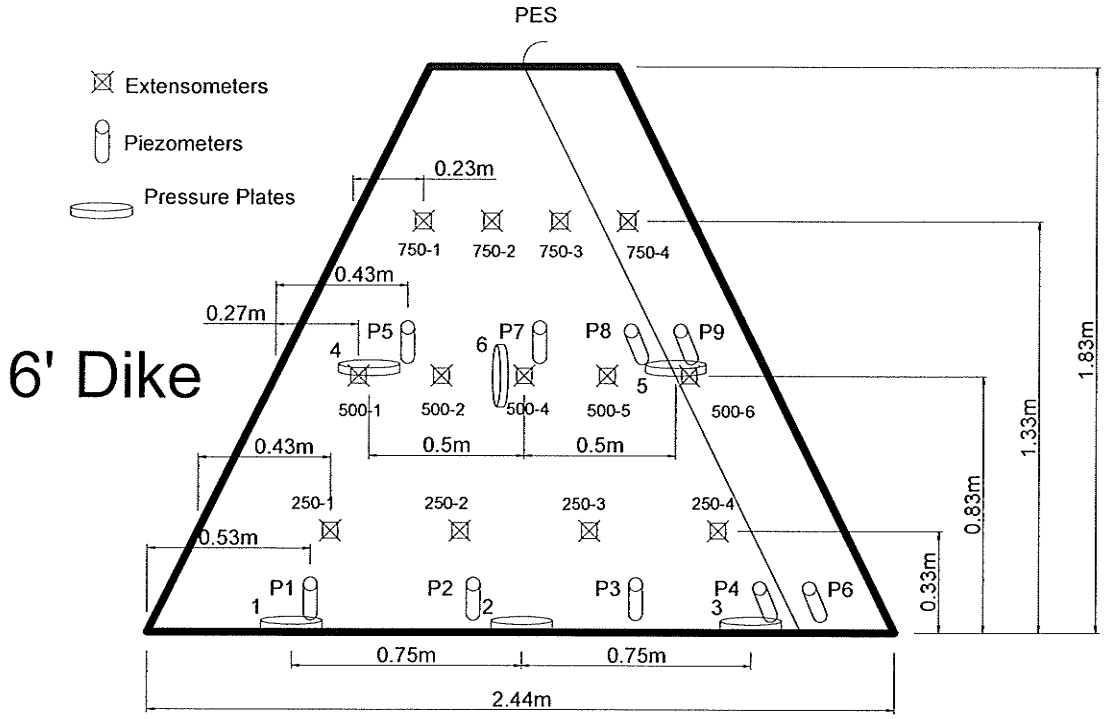

Figure 4.54 – Schematic of Internal Instrumentation Placement for Group C & E tests.

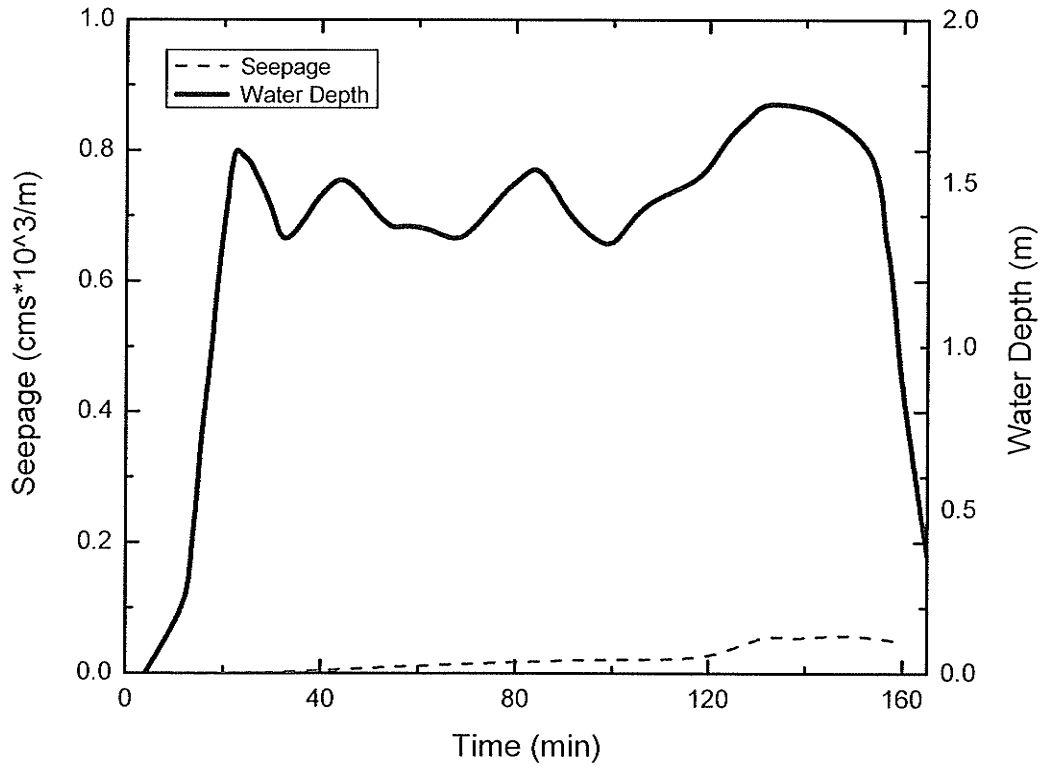

Figure 4.55 – Water Depth and Seepage through Dike C1, August 6, 2004.

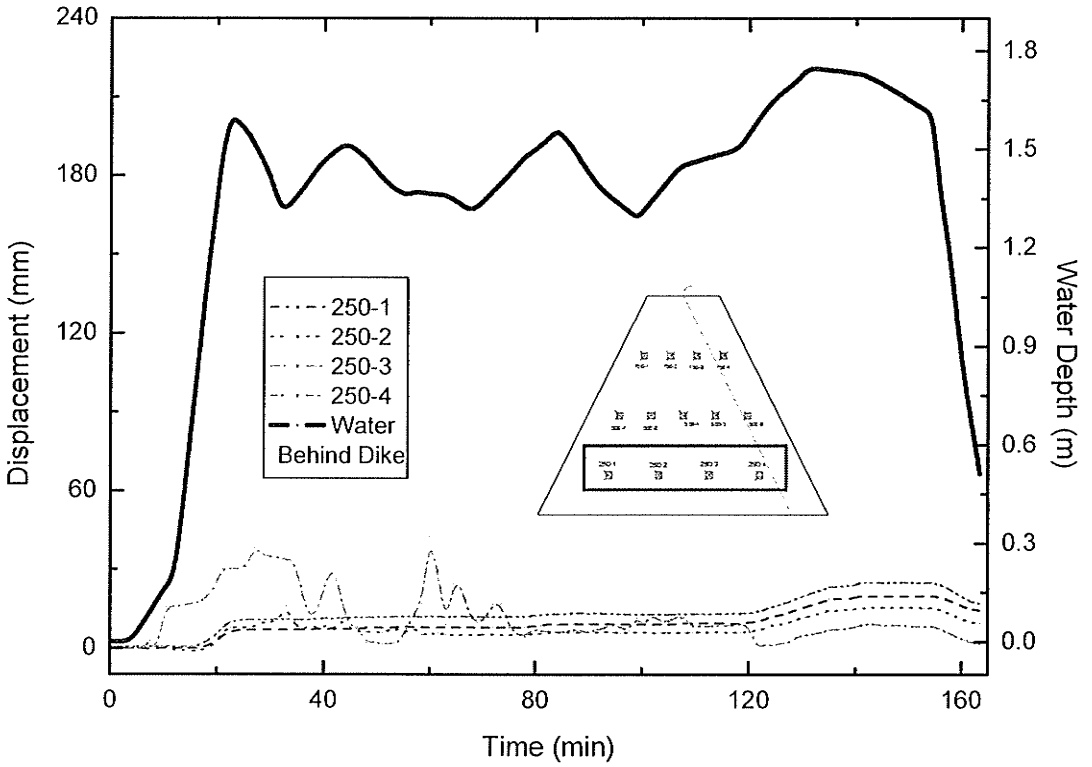

Figure 4.56 – Summary of Extensometers 0.33 m above base of Dike C1, Displacement and Water Depth vs. Time, August 6, 2004.

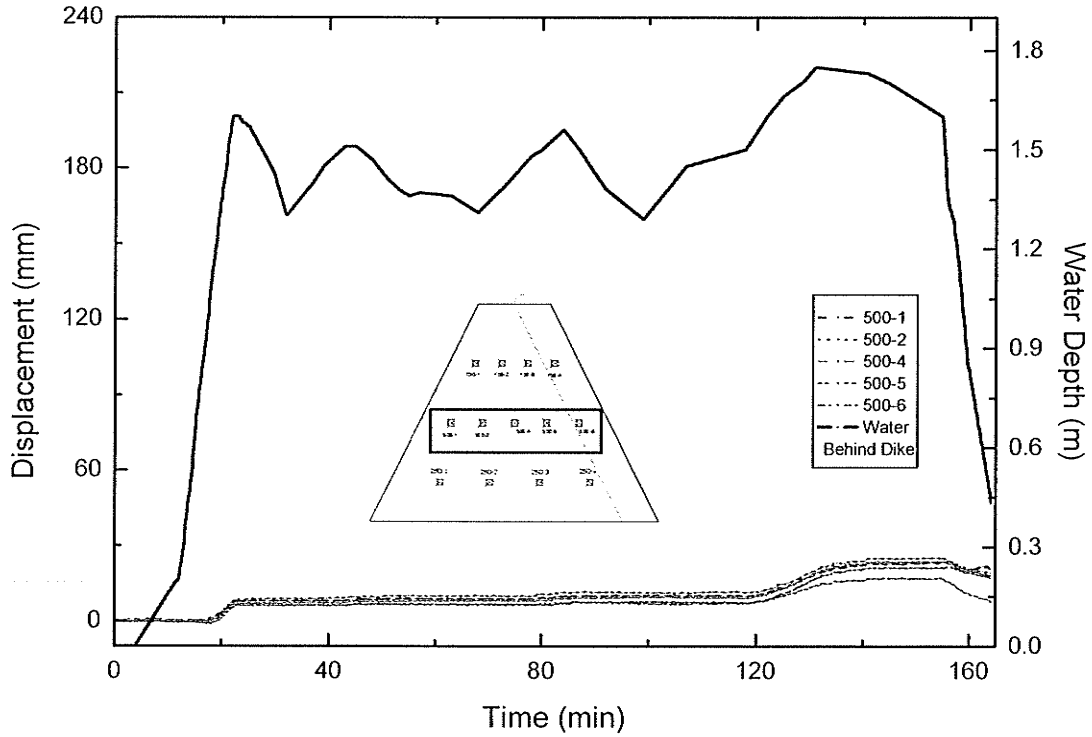

Figure 4.57 – Summary of Extensometers 0.83 m above base of Dike C1, Displacement and Water Depth vs. Time, August 6, 2004.

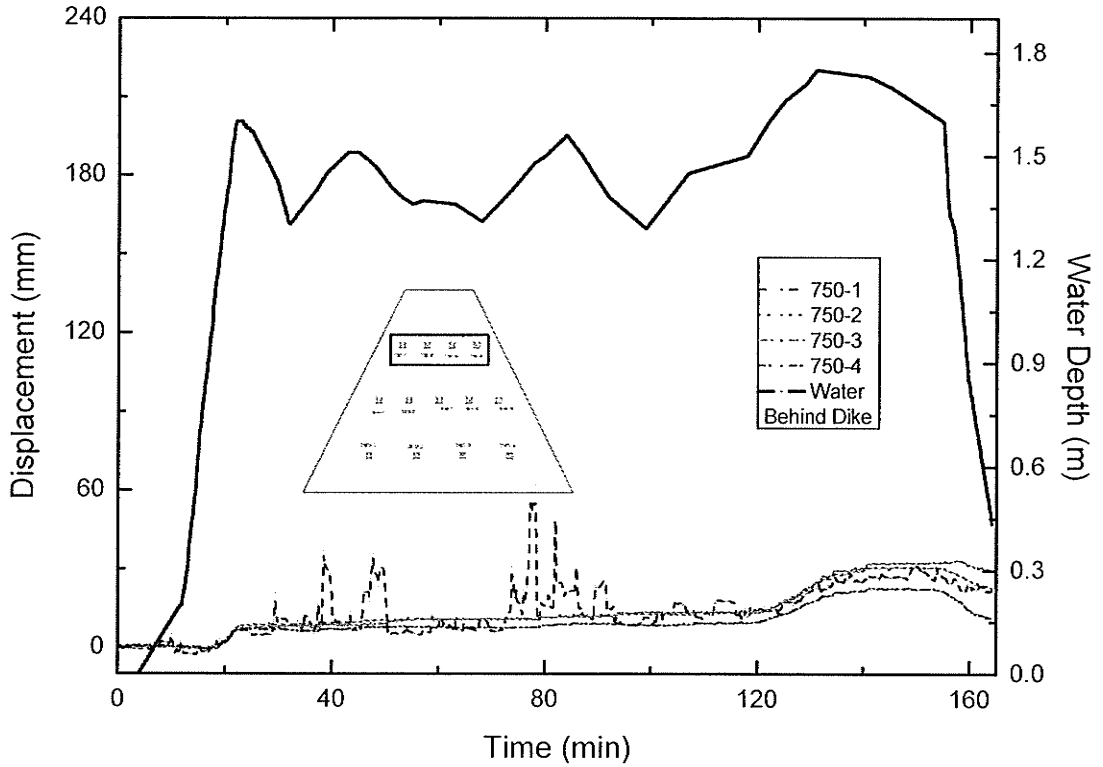

Figure 4.58 – Summary of Extensometers 1.33 m above base of Dike C1, Displacement and Water Depth vs. Time, August 6, 2004.

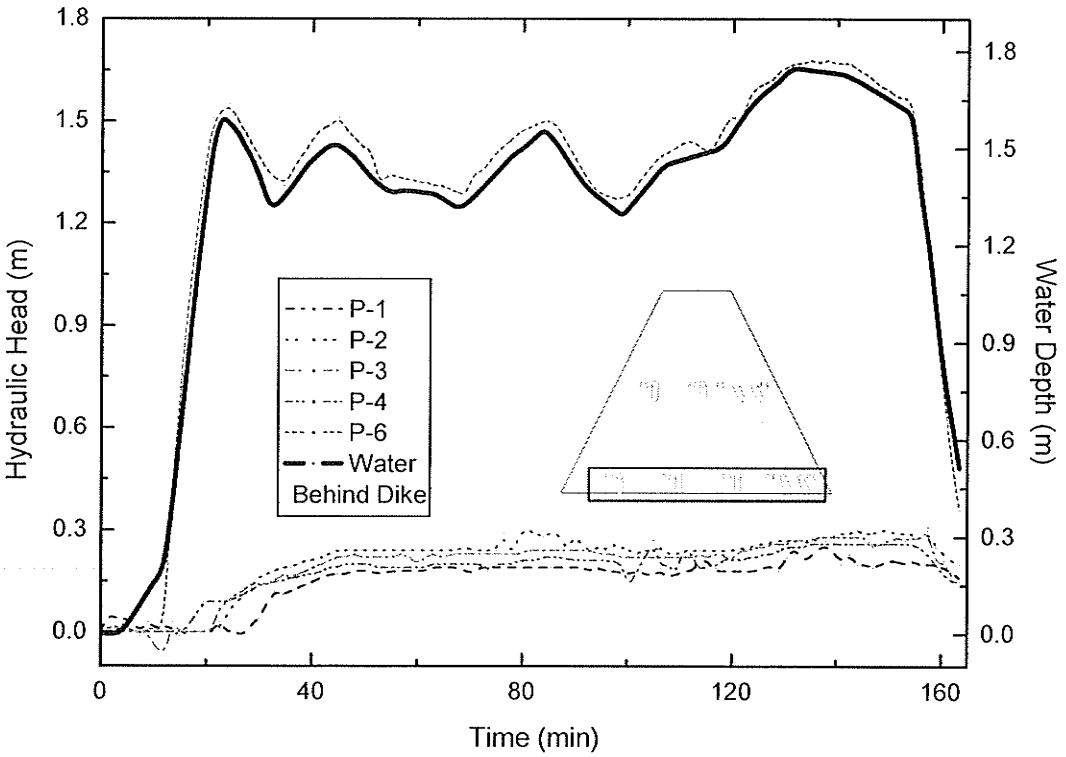

Figure 4.59 – Summary of Hydraulic Head readings by Piezometers at base of Dike C1, Time vs. Hydraulic Head, August 6, 2004.

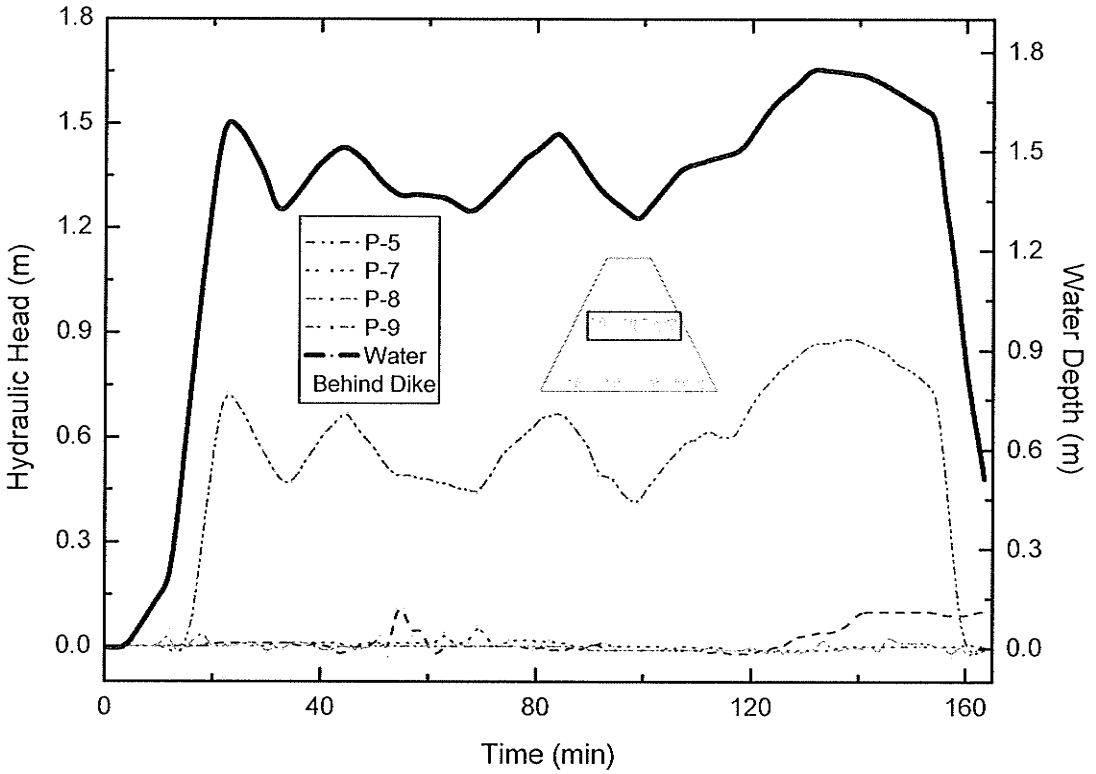

Figure 4.60 – Summary of Hydraulic Head readings by Piezometers 0.83 m above base of Dike C1, Time vs. Hydraulic Head, August 6, 2004.

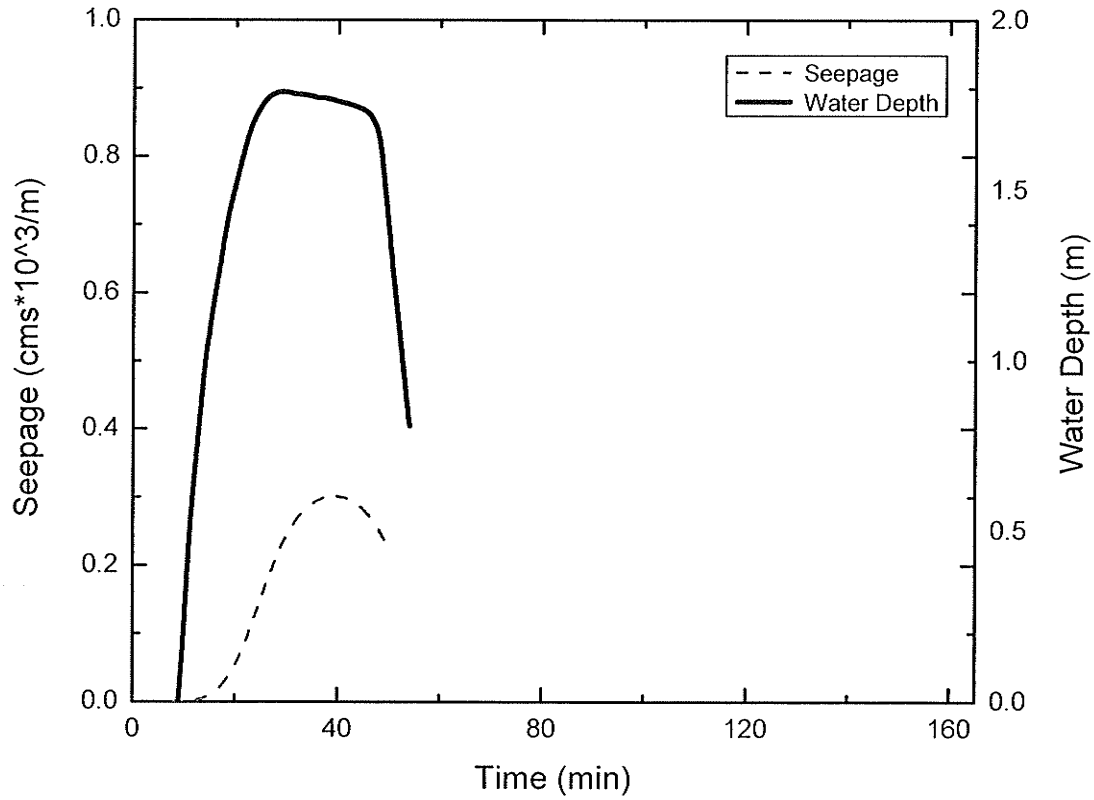

Figure 4.61 – Water Depth and Seepage through Dike C2, August 10, 2004.

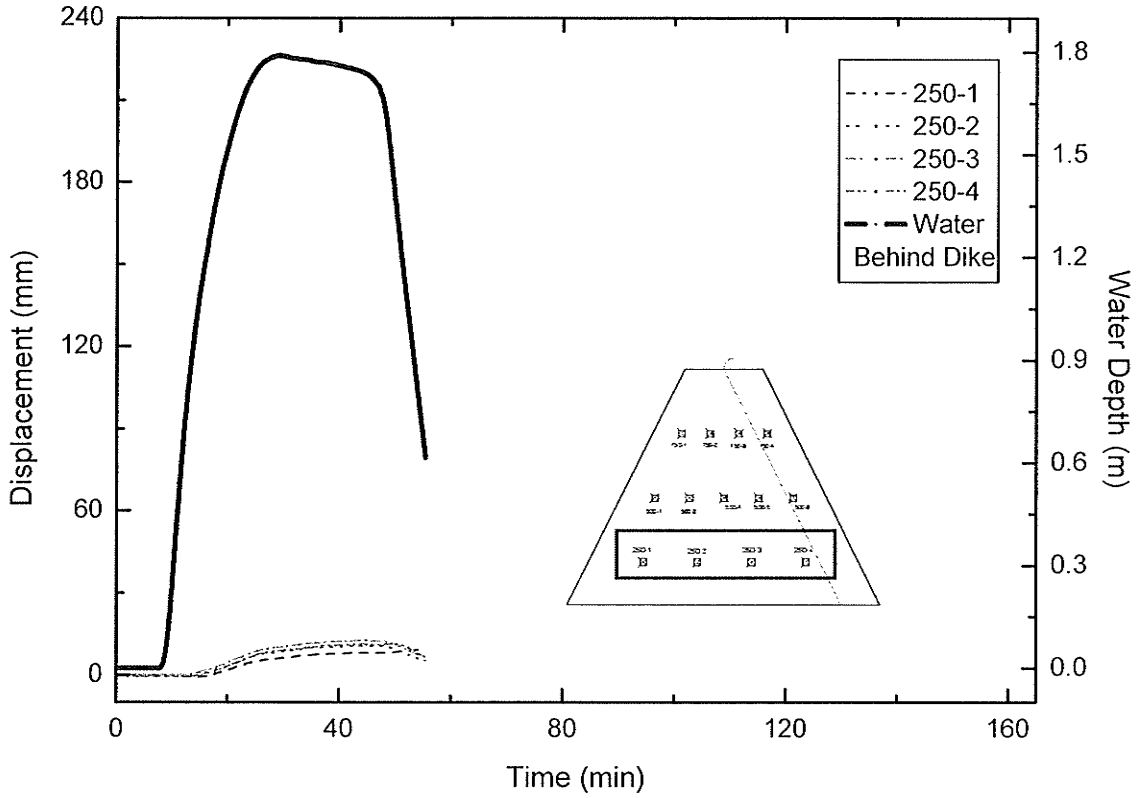

Figure 4.62 – Summary of Extensometers 0.33 m above base of Dike C2, Displacement and Water Depth vs. Time, August 10, 2004.

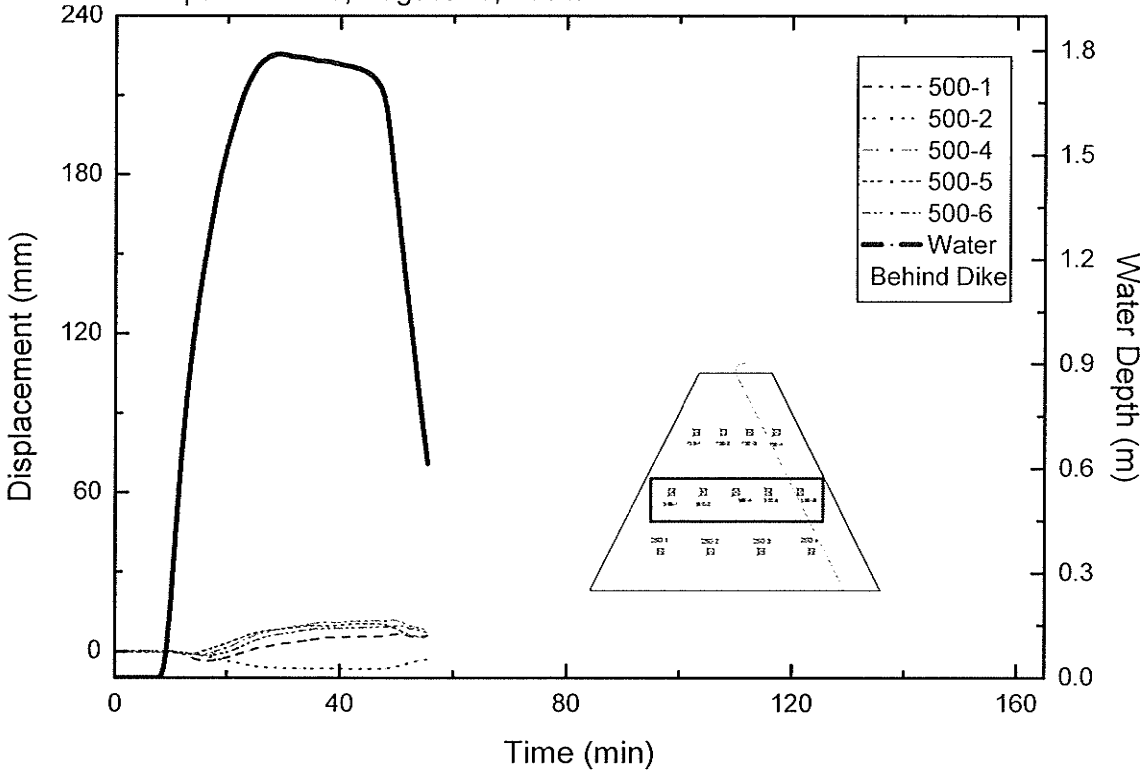

Figure 4.63 – Summary of Extensometers 0.83 m above base of Dike C2, Displacement and Water Depth vs. Time, August 10, 2004.

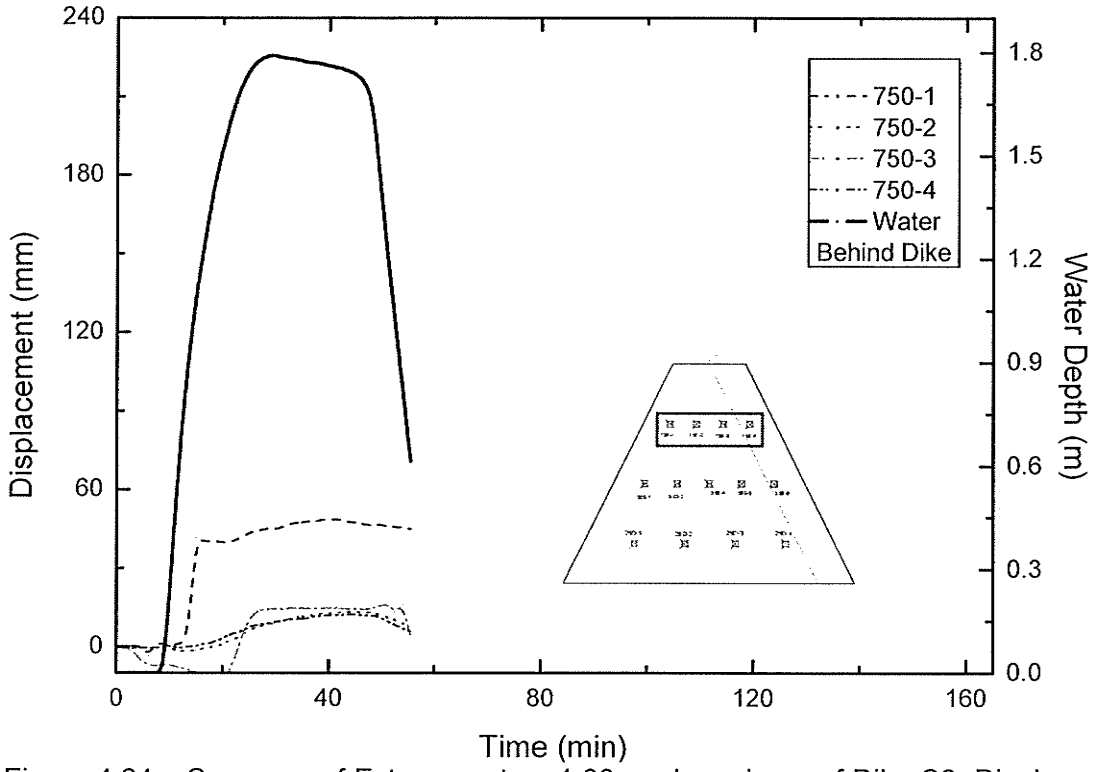

Figure 4.64 – Summary of Extensometers 1.33 m above base of Dike C2, Displacement and Water Depth vs. Time, August 10, 2004.

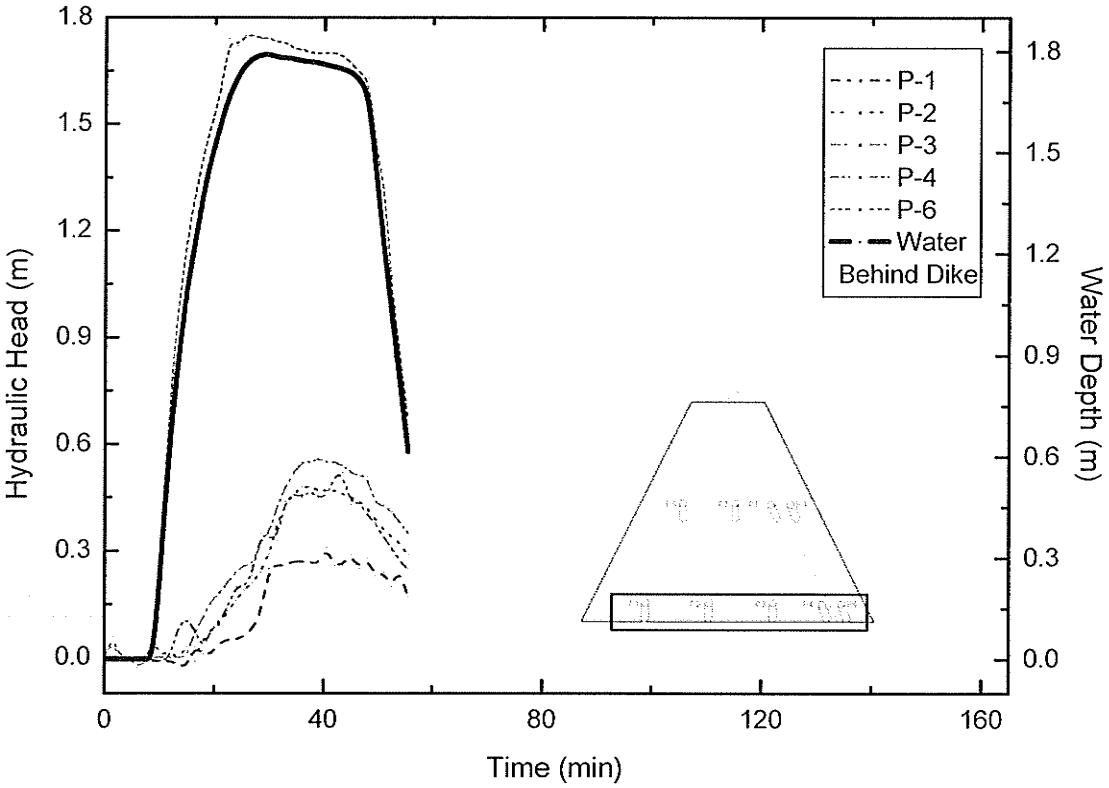

Figure 4.65 – Summary of Hydraulic Head readings by Piezometers at base of Dike C2, Time vs. Hydraulic Head, August 10, 2004.

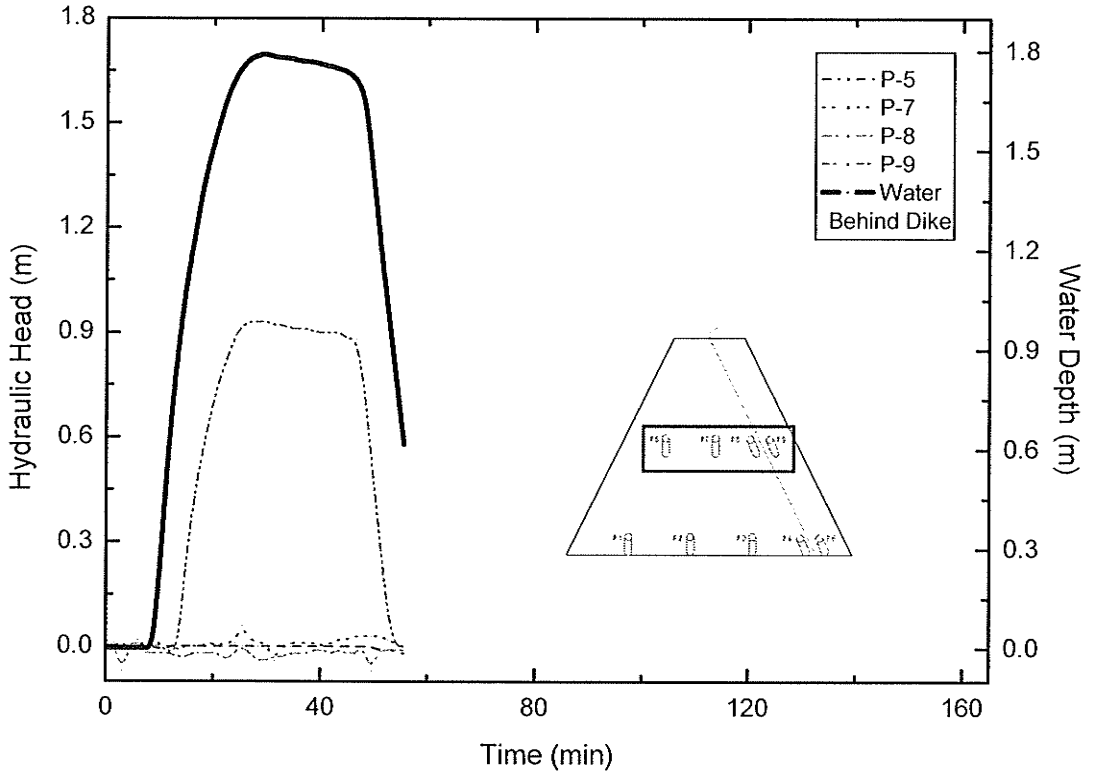

Figure 4.66 – Summary of Hydraulic Head readings by Piezometers 0.83 m above the base of Dike C2, Time vs. Hydraulic Head, August 10, 2004.

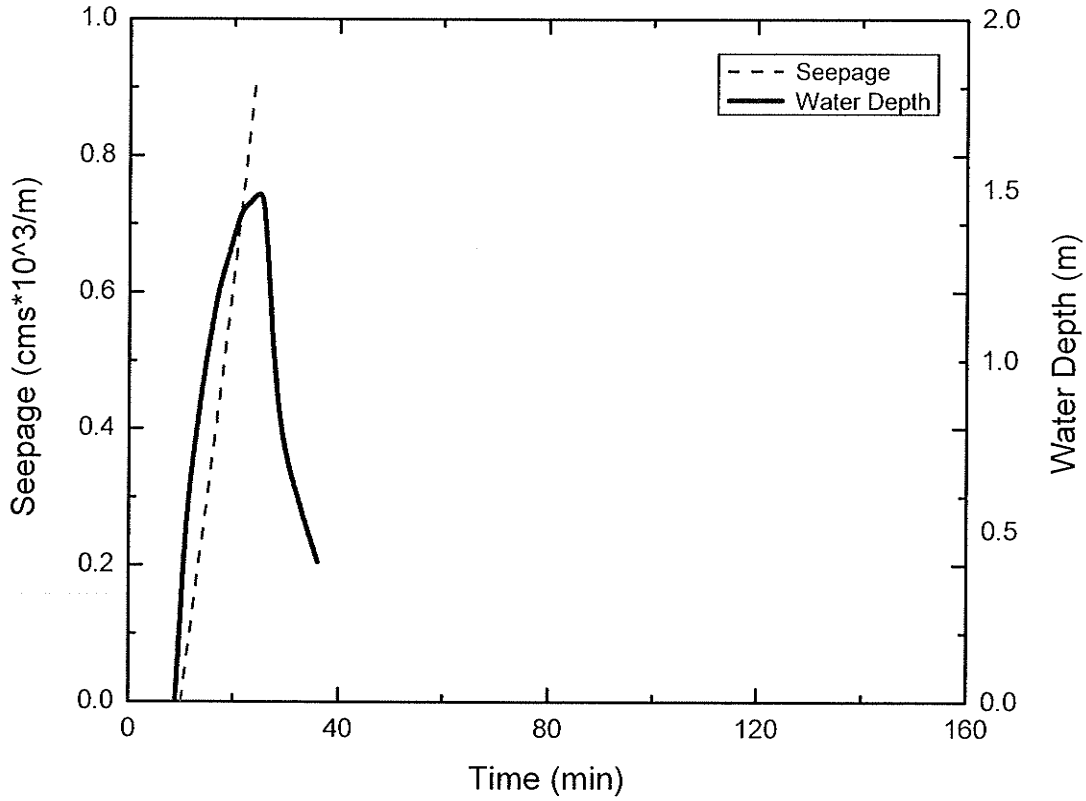

Figure 4.67 – Water Depth and Seepage through Dike C3, August 11, 2004.

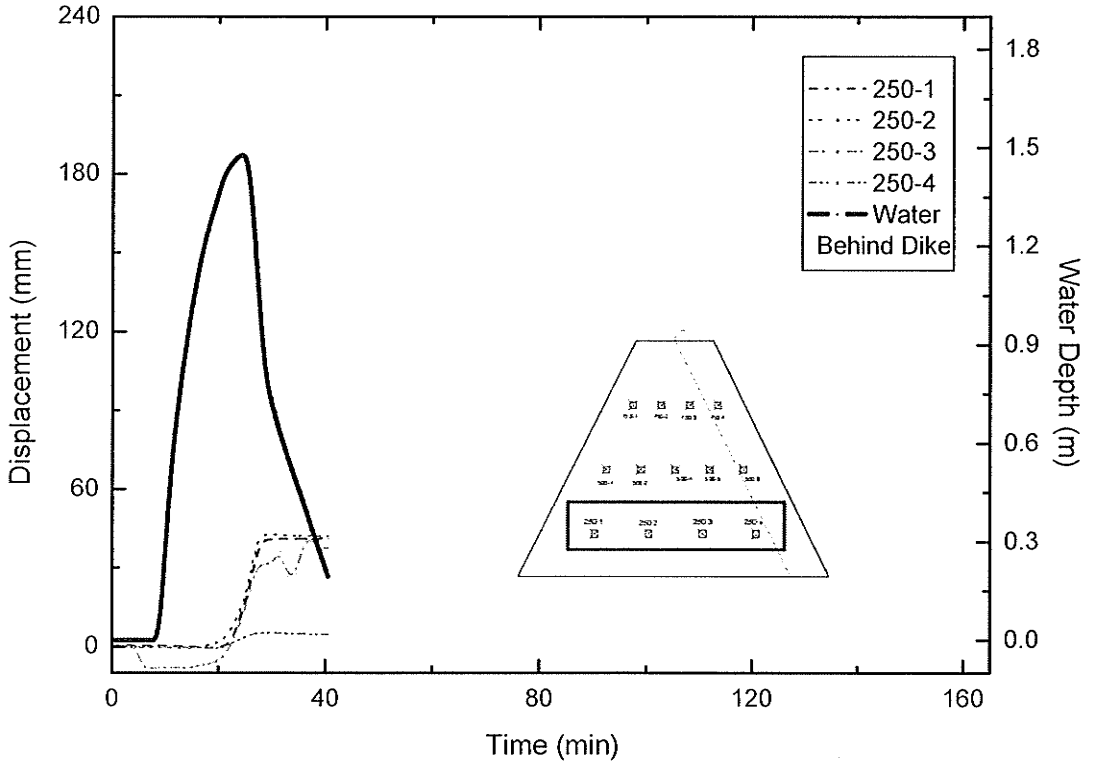

Figure 4.68 – Summary of Extensometers 0.33 m above base of Dike C3, Displacement and Water Depth vs. Time, August 11, 2004.

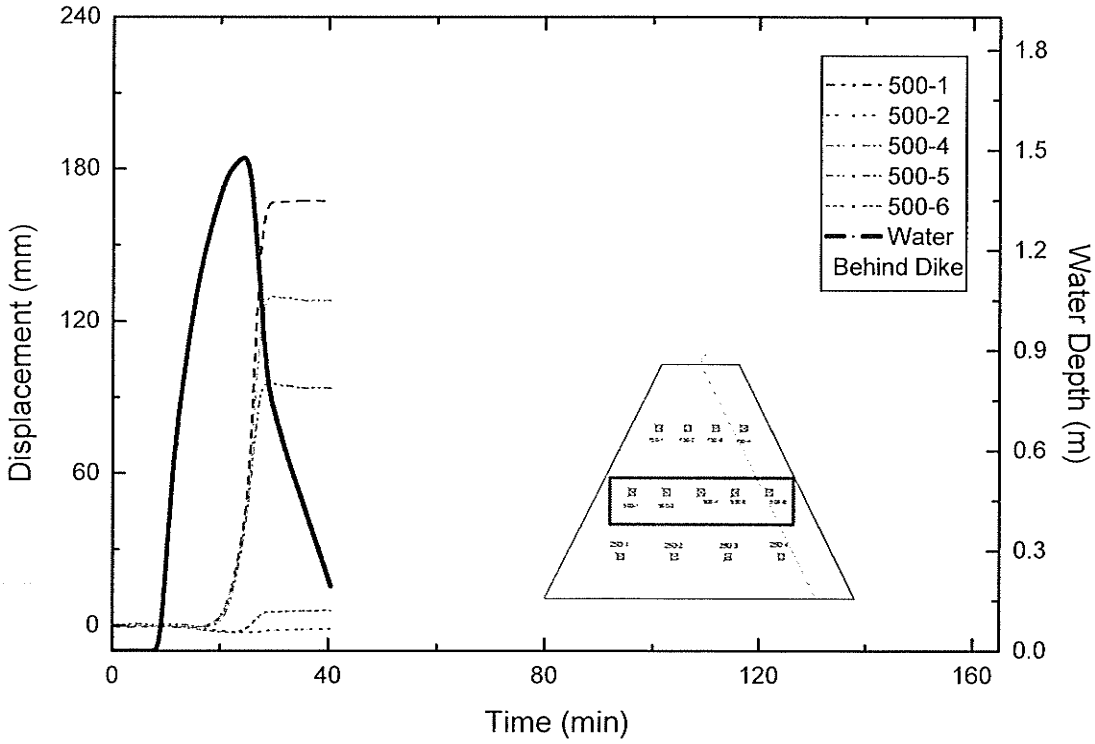

Figure 4.69 – Summary of Extensometers 0.83 m above base of Dike C3, Displacement and Water Depth vs. Time, August 11, 2004.

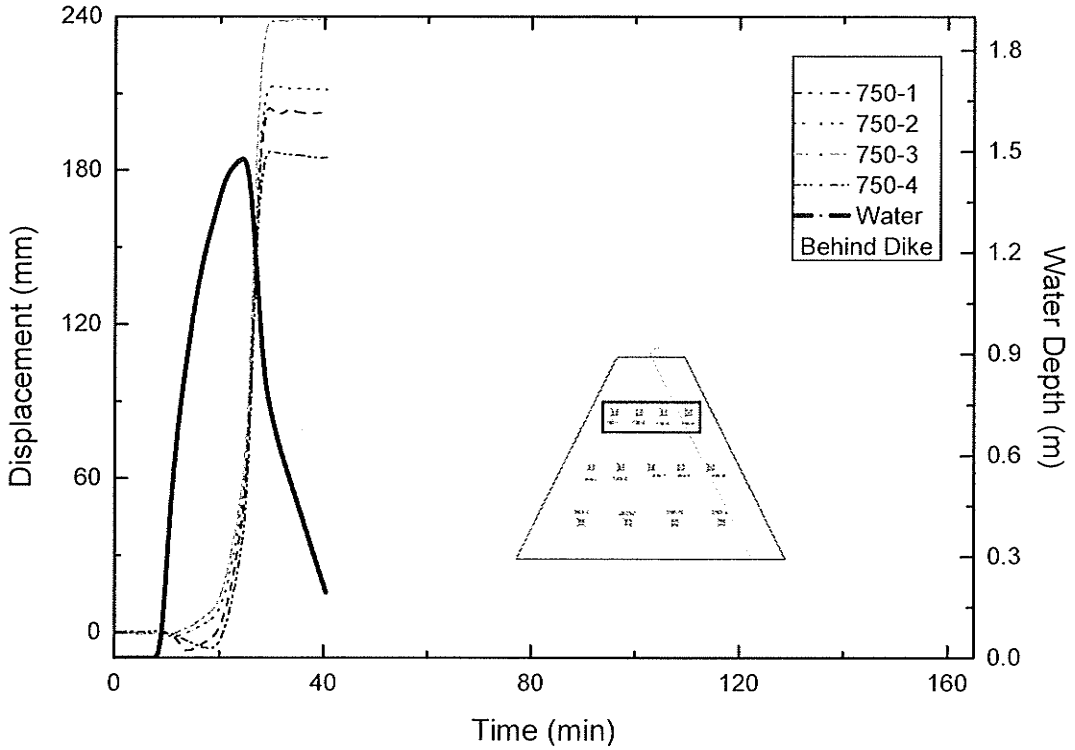

Figure 4.70 – Summary of Extensometers 1.33 m above base of Dike C3, Displacement and Water Depth vs. Time, August 11, 2004.

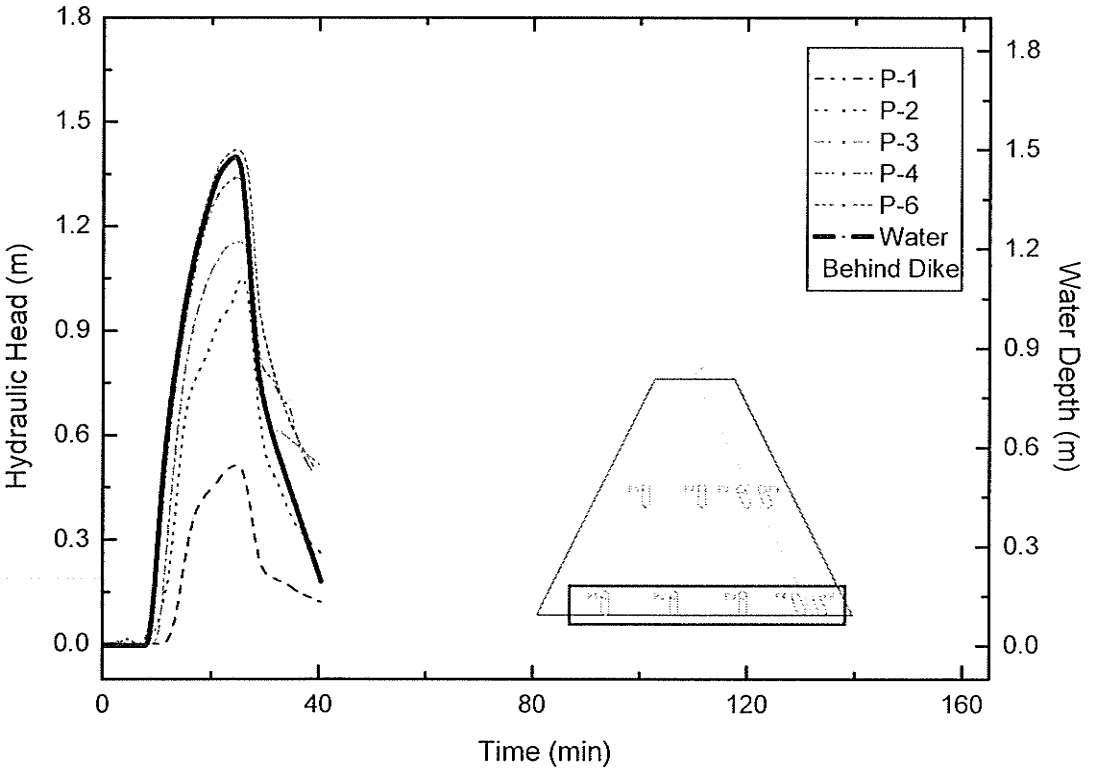

Figure 4.71 – Summary of Hydraulic Head readings by Piezometers at base of Dike C3, Time vs. Hydraulic Head, August 11, 2004.

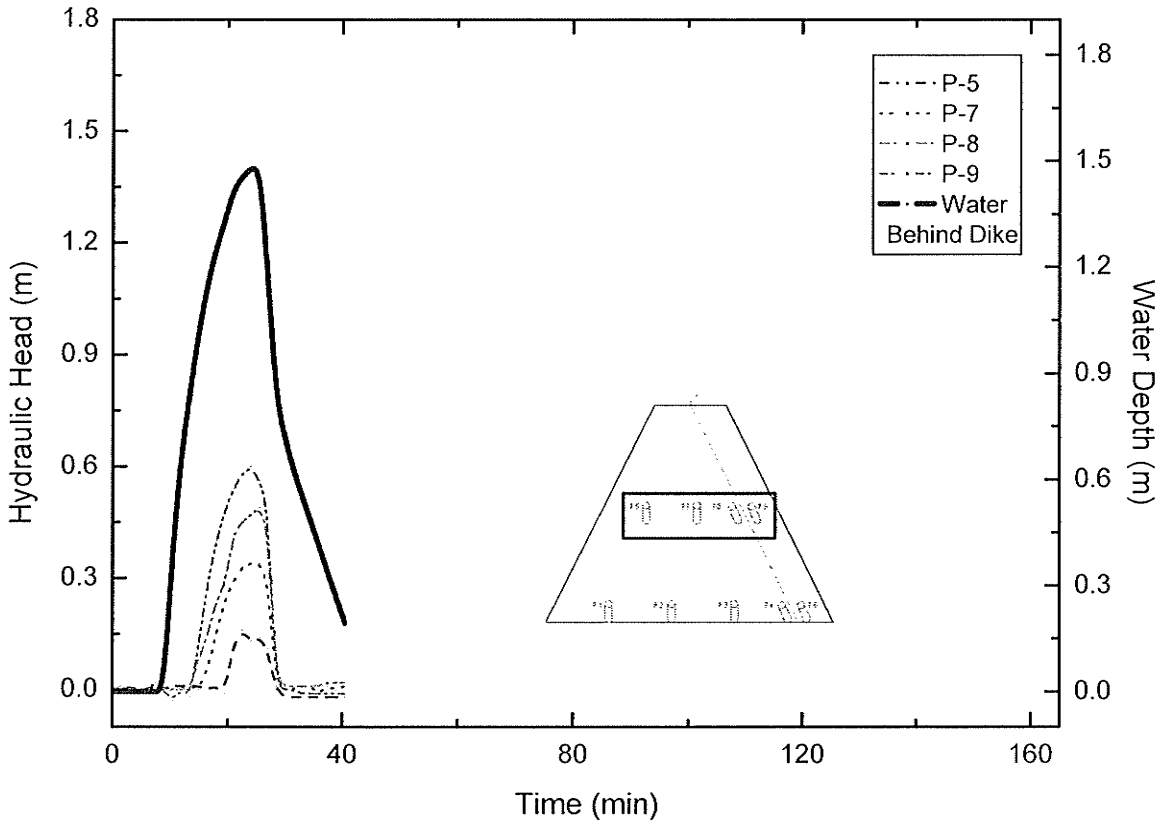

Figure 4.72 – Summary of Hydraulic Head readings by Piezometers 0.83 m above base of Dike C3, Time vs. Hydraulic Head, August 11, 2004.

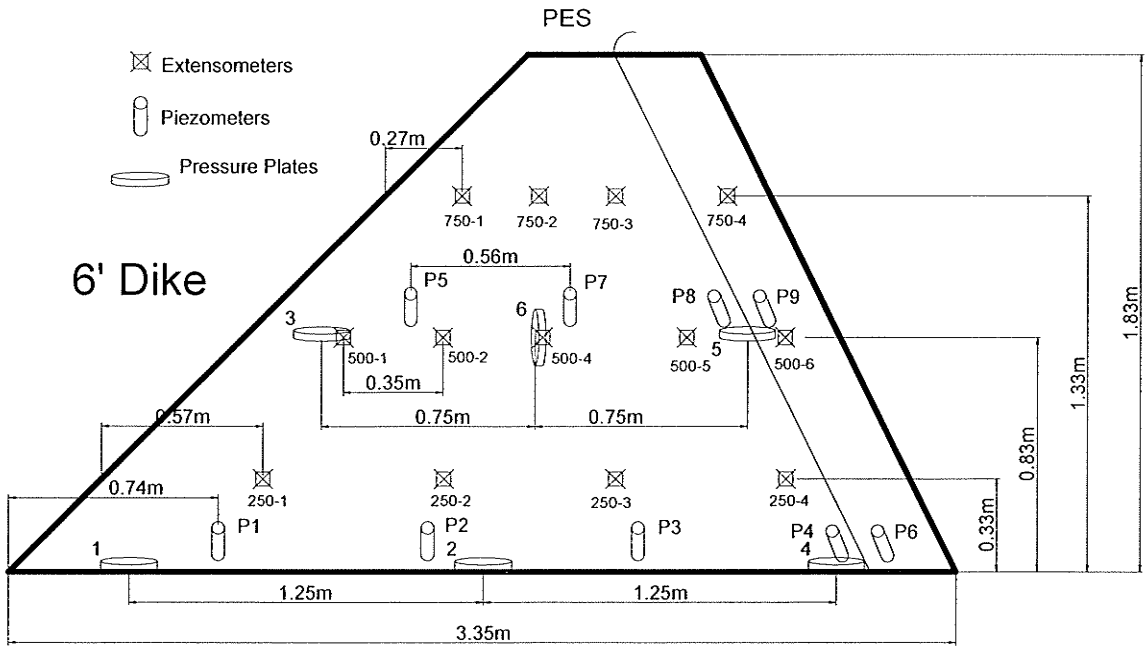

Figure 4.73 – Schematic of Internal Instrumentation Placement for Group D tests.

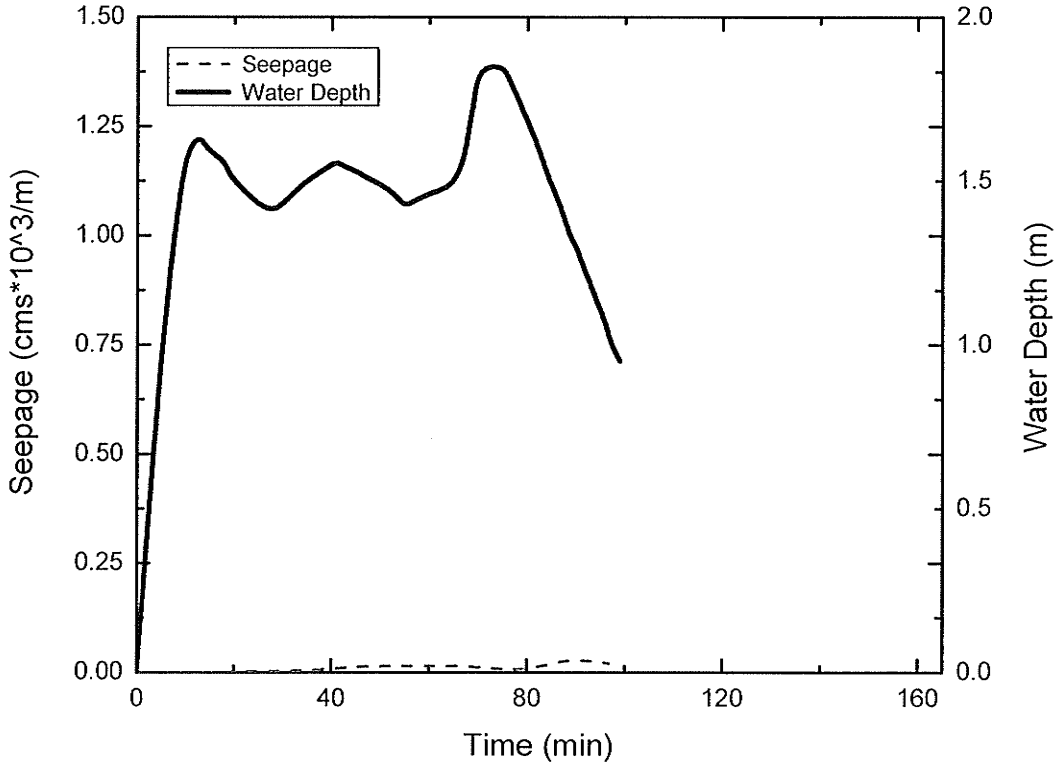

Figure 4.74 – Water Depth and Seepage through Dike D1, August 17, 2004.

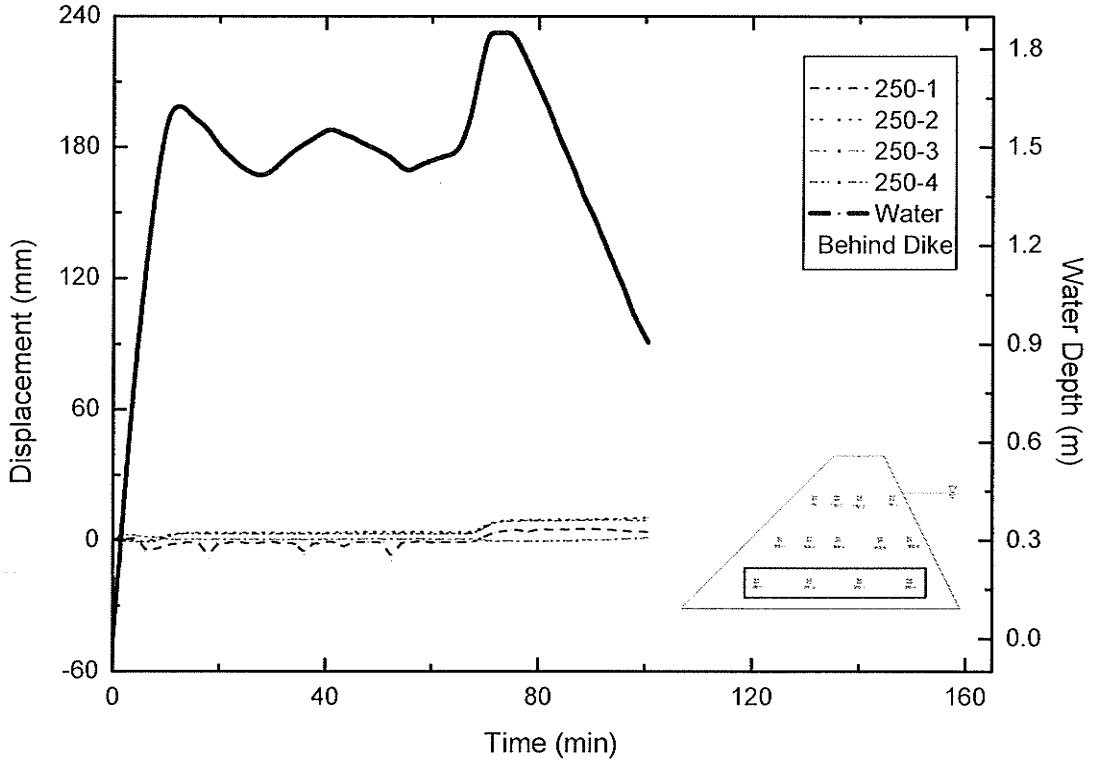

Figure 4.75 – Summary of Extensometers 0.33 m above base of Dike D1, Displacement and Water Depth vs. Time, August 17, 2004.

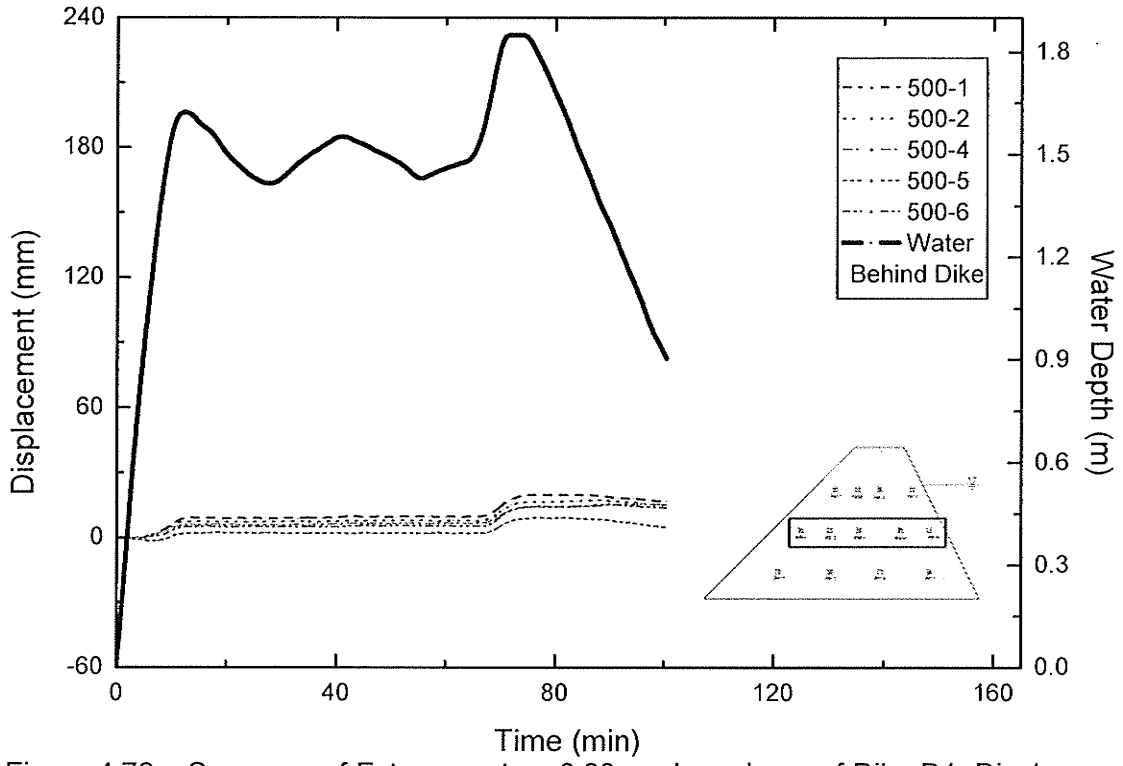

Figure 4.76 – Summary of Extensometers 0.83 m above base of Dike D1, Displacement and Water Depth vs. Time, August 17, 2004.

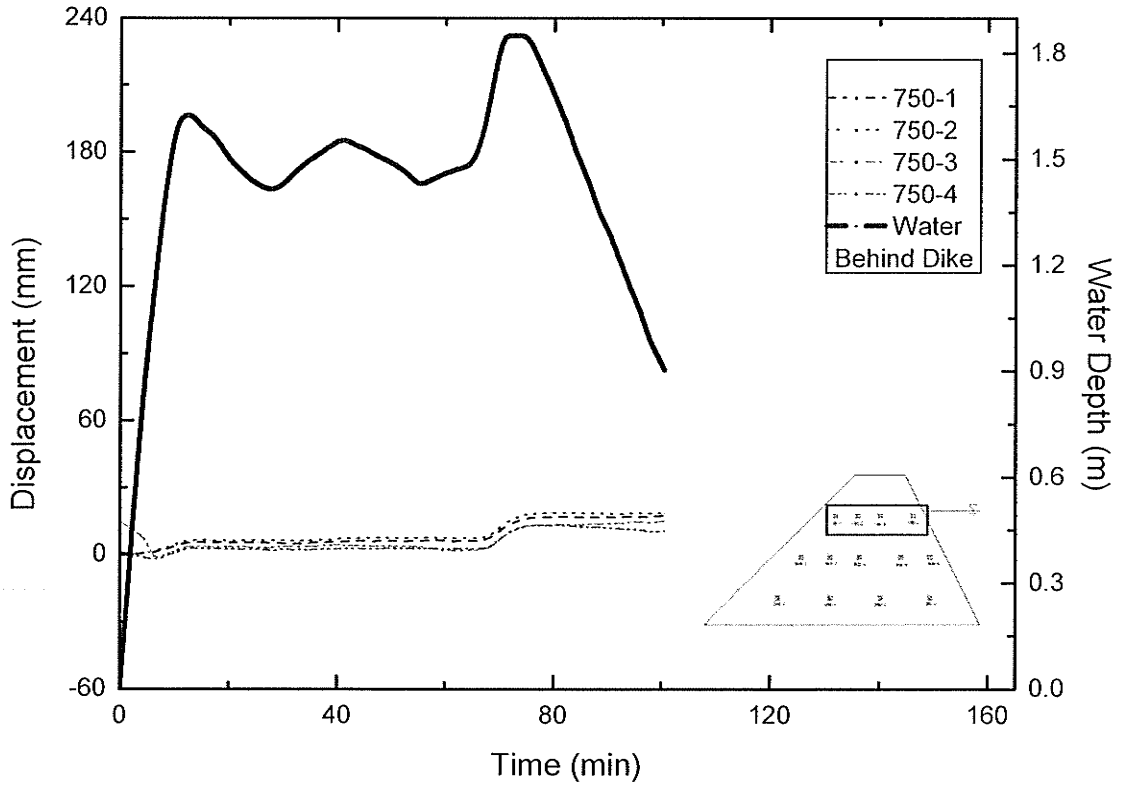

Figure 4.77 – Summary of Extensometers 1.33 m above base of Dike D1, Displacement and Water Depth vs. Time, August 17, 2004.

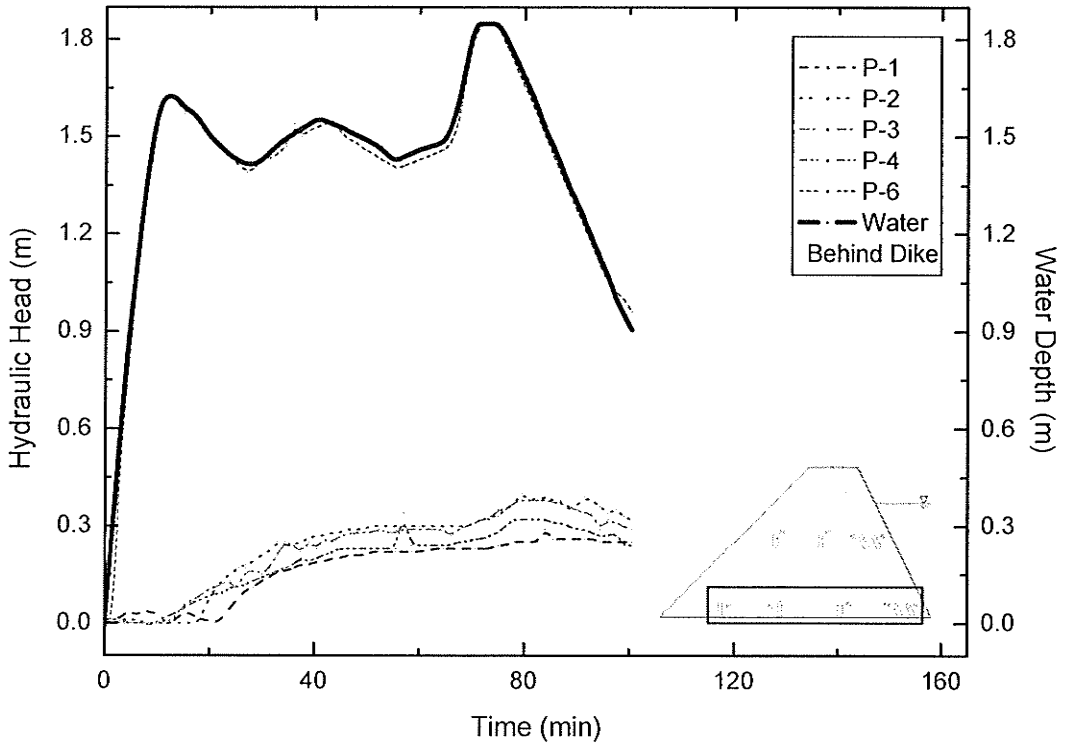

Figure 4.78 – Summary of Hydraulic Head readings by Piezometers at base of Dike D1, Time vs. Hydraulic Head, August 17, 2004.

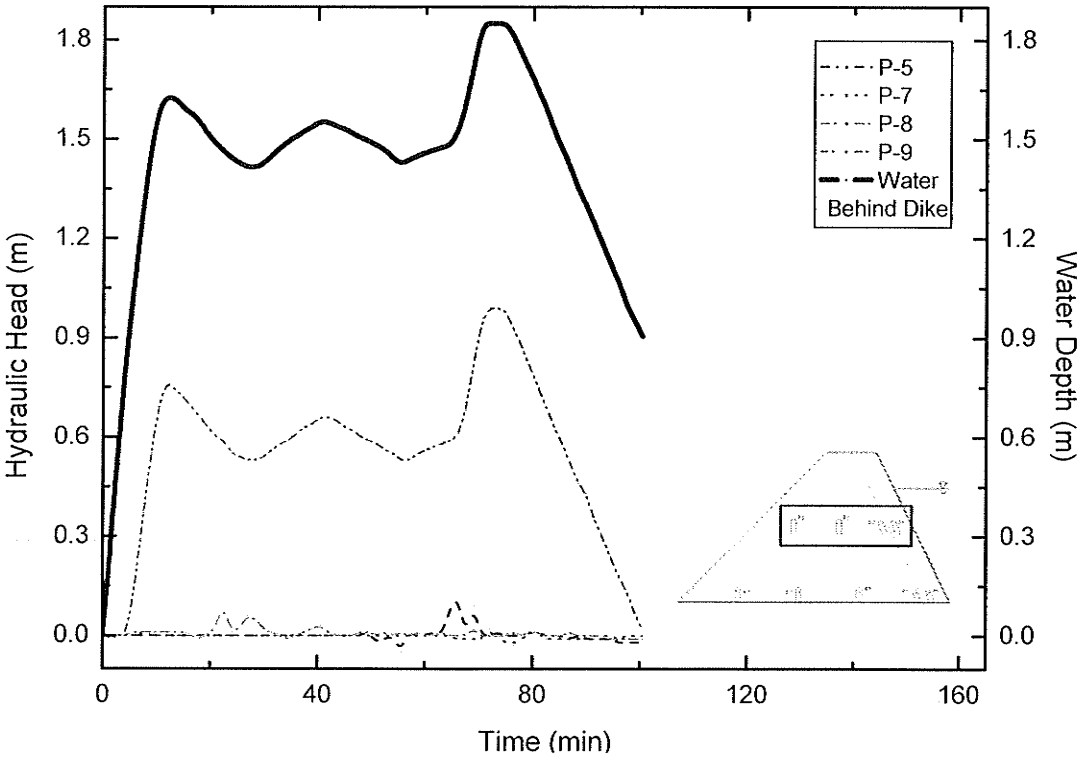

Figure 4.79 – Summary of Hydraulic Head readings by Piezometers 0.83 m above base of Dike D1, Time vs. Hydraulic Head, August 17, 2004.

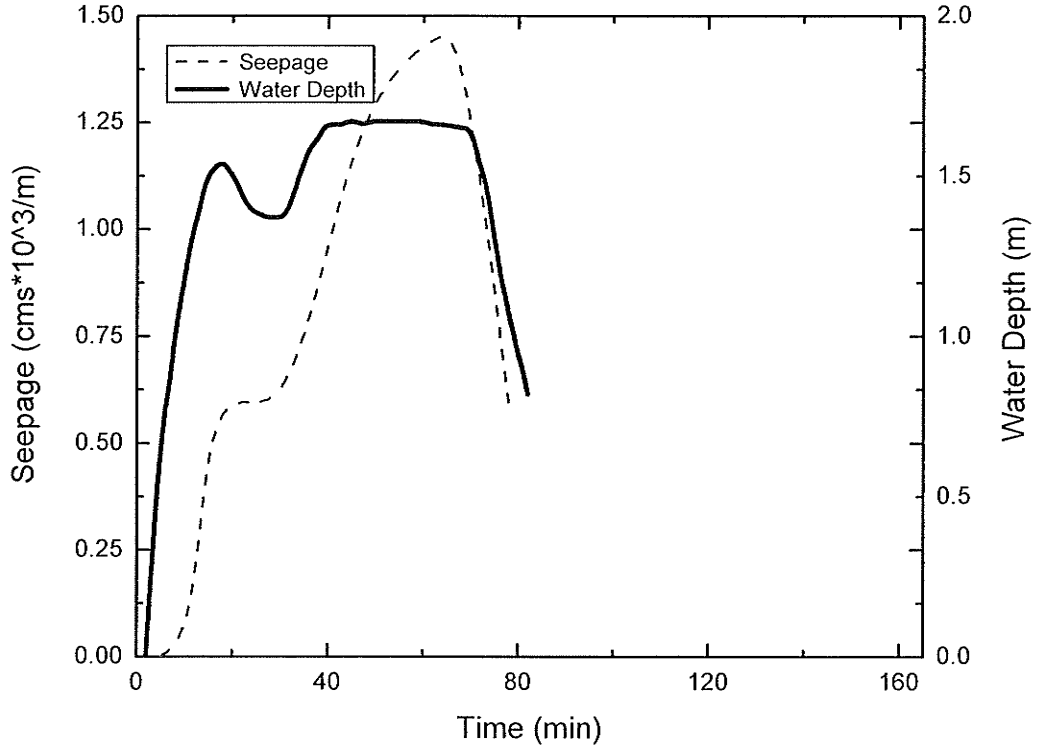

Figure 4.80 – Water Depth and Seepage through Dike D2, August 18, 2004.

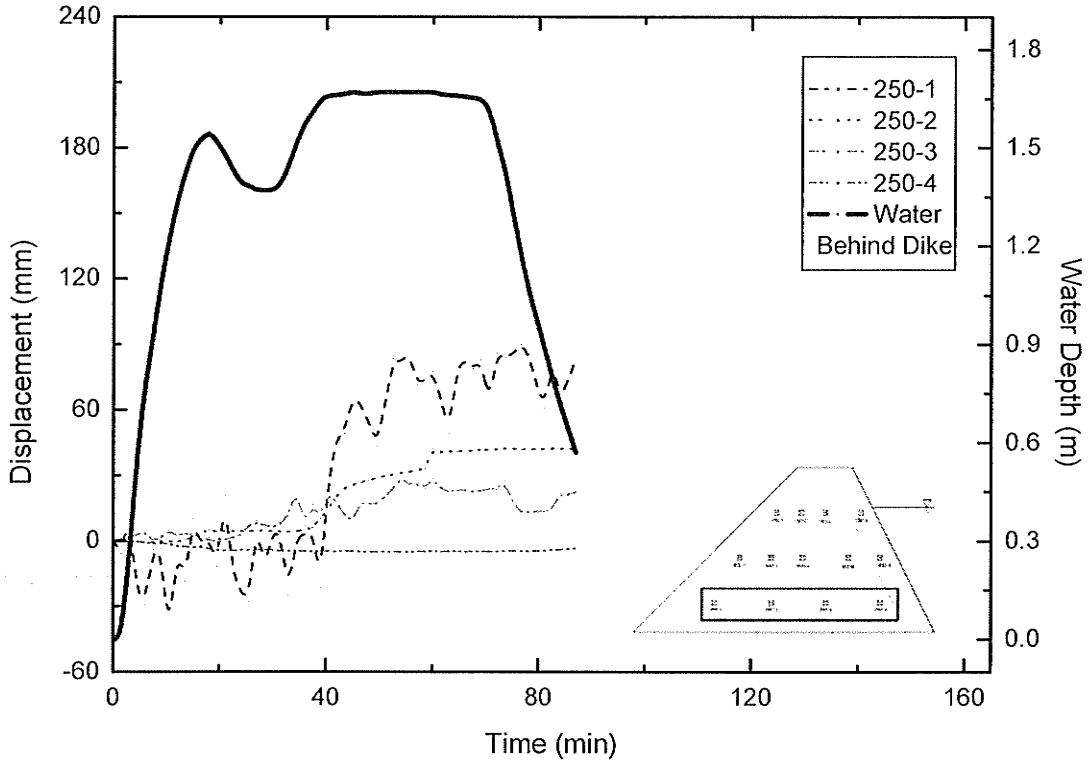

Figure 4.81 – Summary of Extensometers 0.33 m above base of Dike D2, Displacement and Water Depth vs. Time, August 18, 2004.

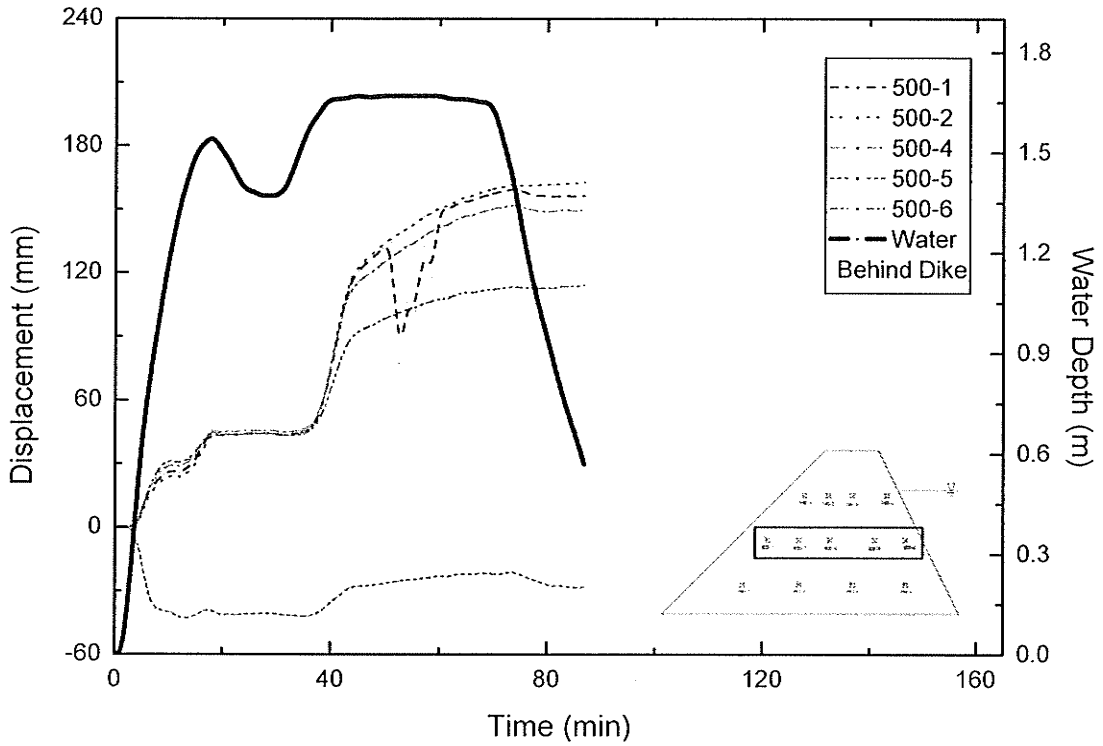

Figure 4.82 – Summary of Extensometers 0.83 m above base of Dike D2, Displacement and Water Depth vs. Time, August 18, 2004.

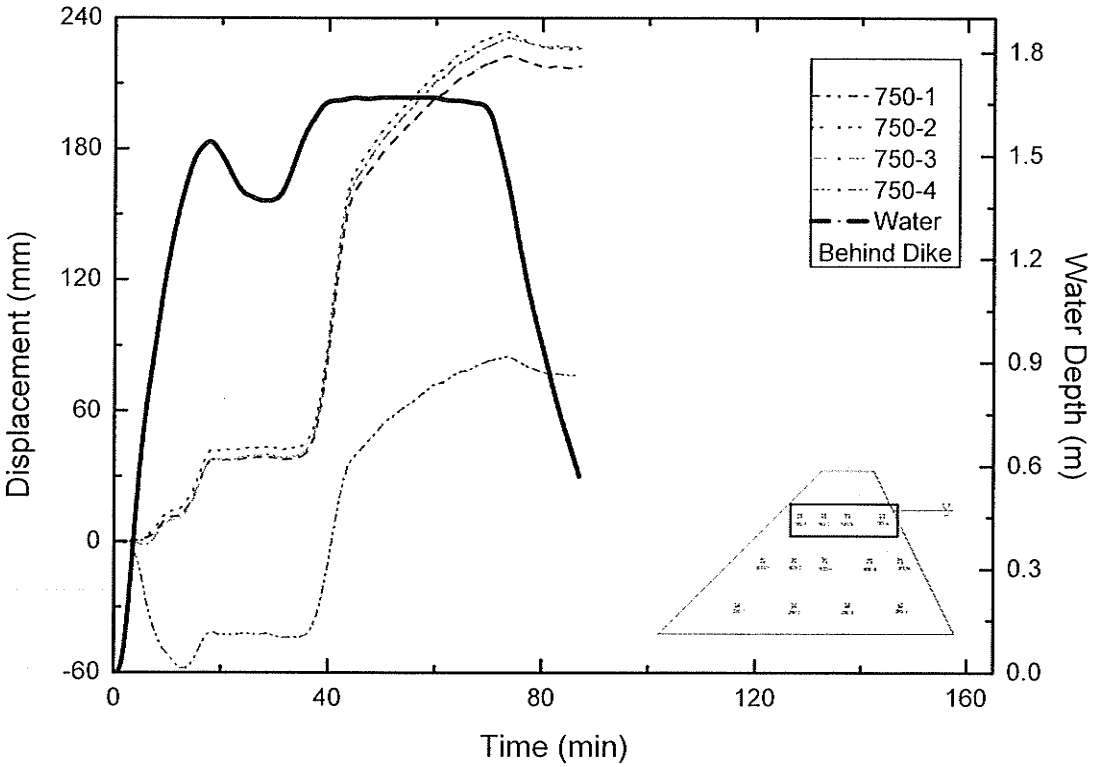

Figure 4.83 – Summary of Extensometers 1.33 m above base of Dike D2, Displacement and Water Depth vs. Time, August 18, 2004.

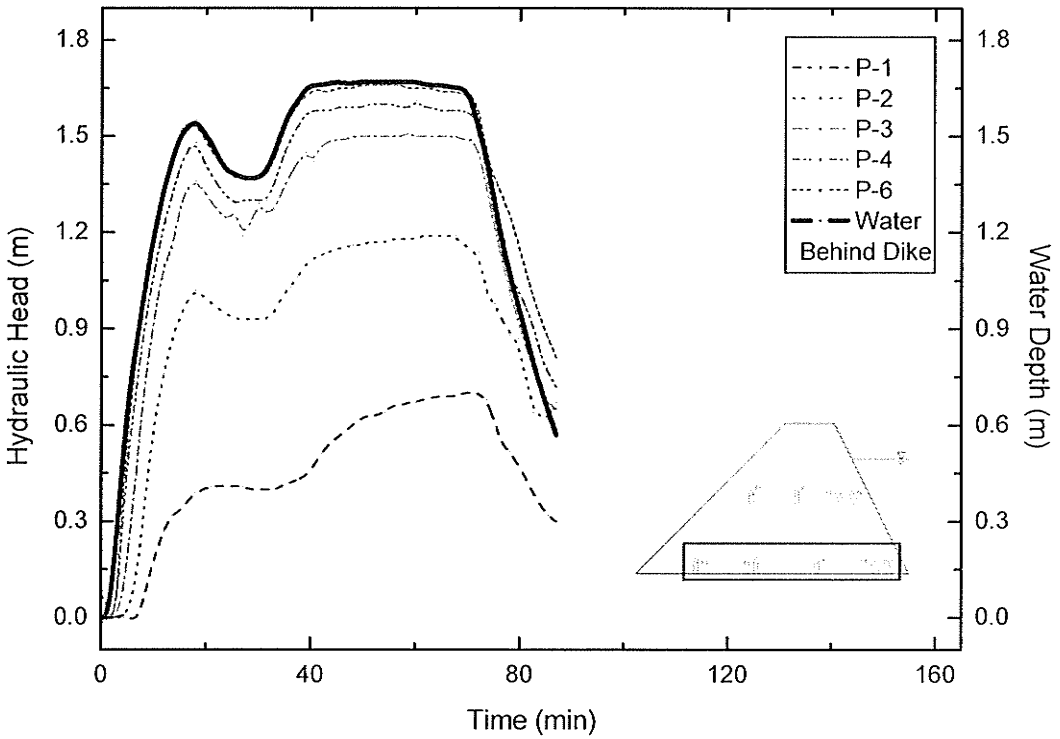

Figure 4.84 – Summary of Hydraulic Head readings by Piezometers at base of Dike D2, Time vs. Hydraulic Head, August 18, 2004.

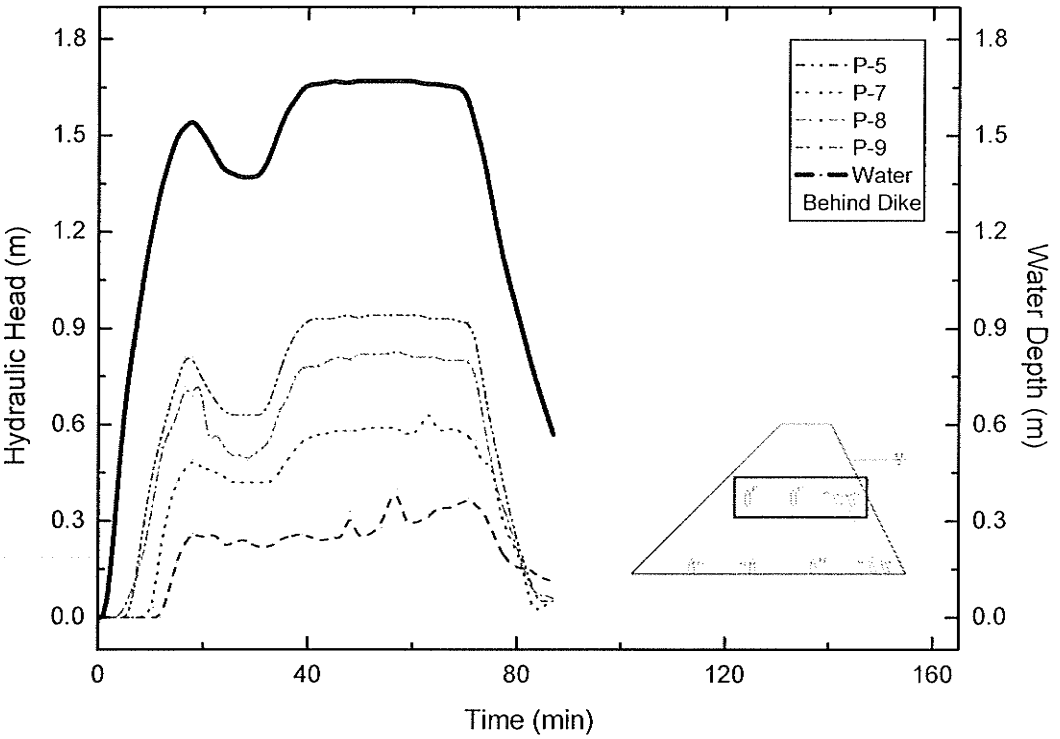

Figure 4.85 – Summary of Hydraulic Head readings by Piezometers 0.83 m above base of Dike D2, Time vs. Hydraulic Head, August 18, 2004.

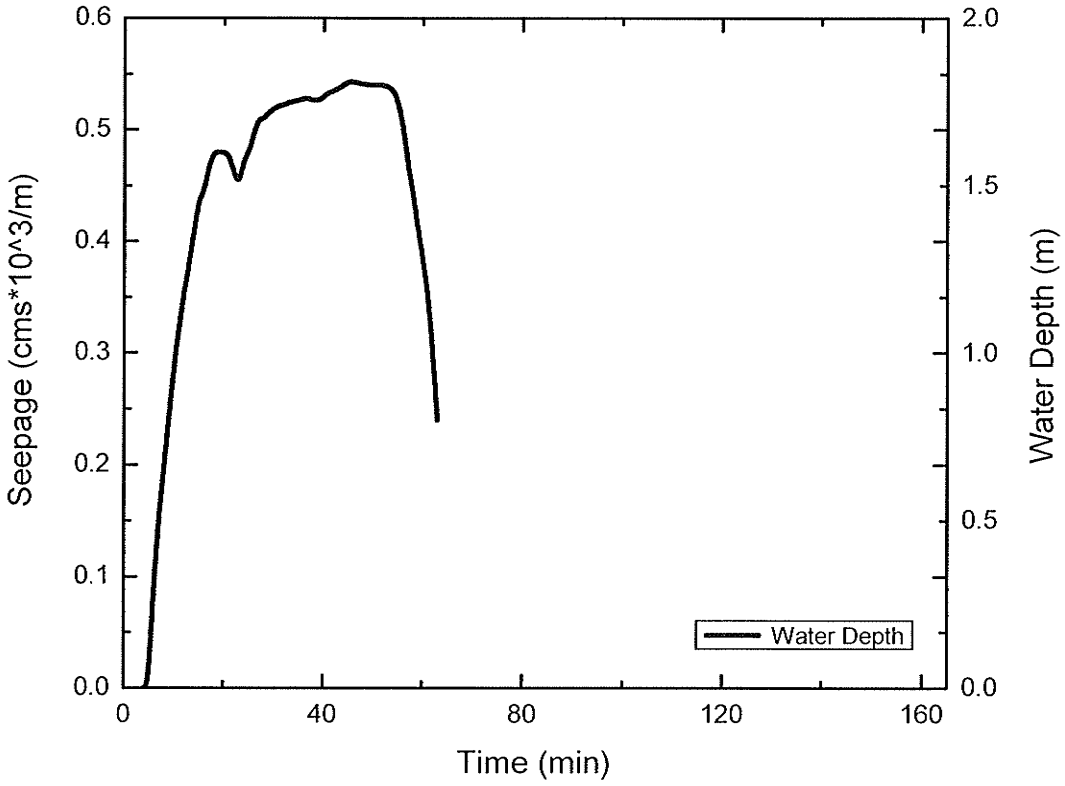

Figure 4.86 – Water Depth behind Dike E, August 21, 2004.

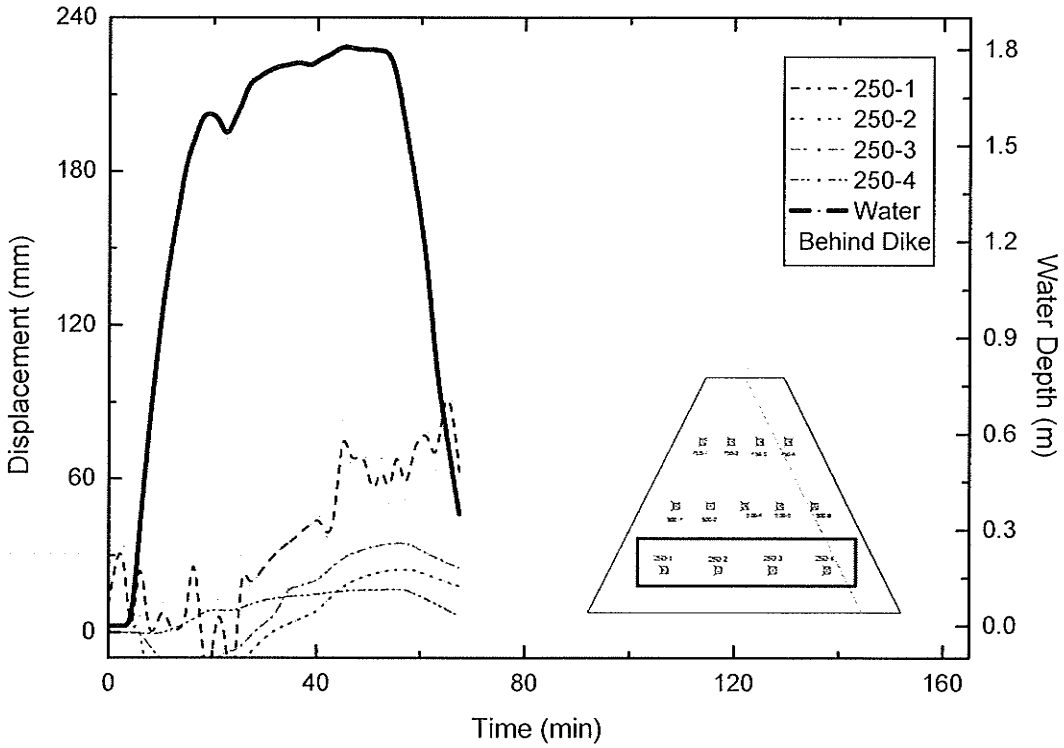

Figure 4.87 – Summary of Extensometers 0.33 m above base of Dike E, Displacement and Water Depth vs. Time, August 21, 2004.

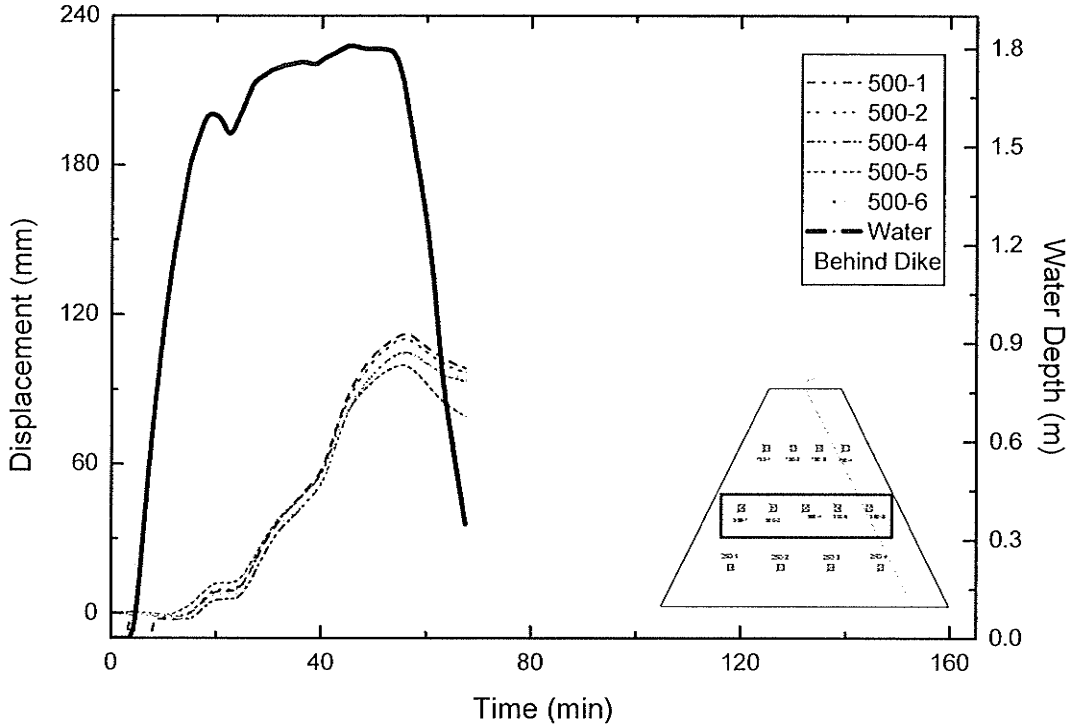

Figure 4.88 – Summary of Extensometers 0.83 m above base of Dike E, Displacement and Water Depth vs. Time, August 21, 2004.

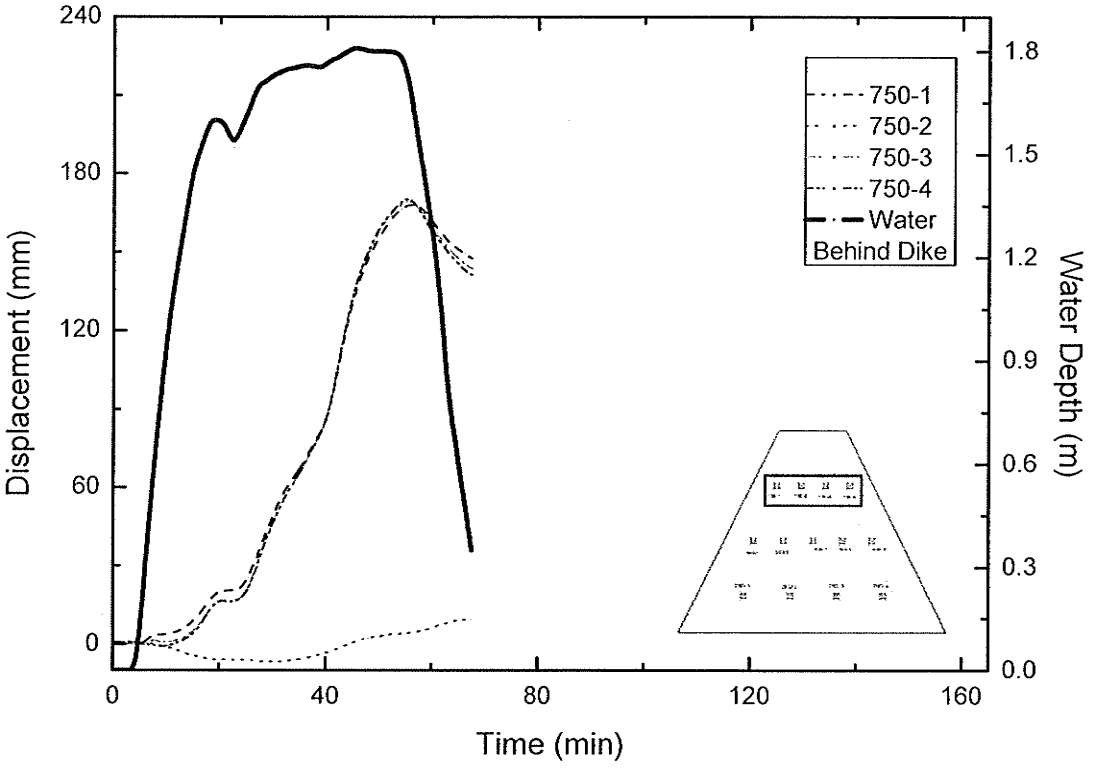

Figure 4.89 – Summary of Extensometers 1.33 m above base of Dike E, Displacement and Water Depth vs. Time, August 21, 2004.

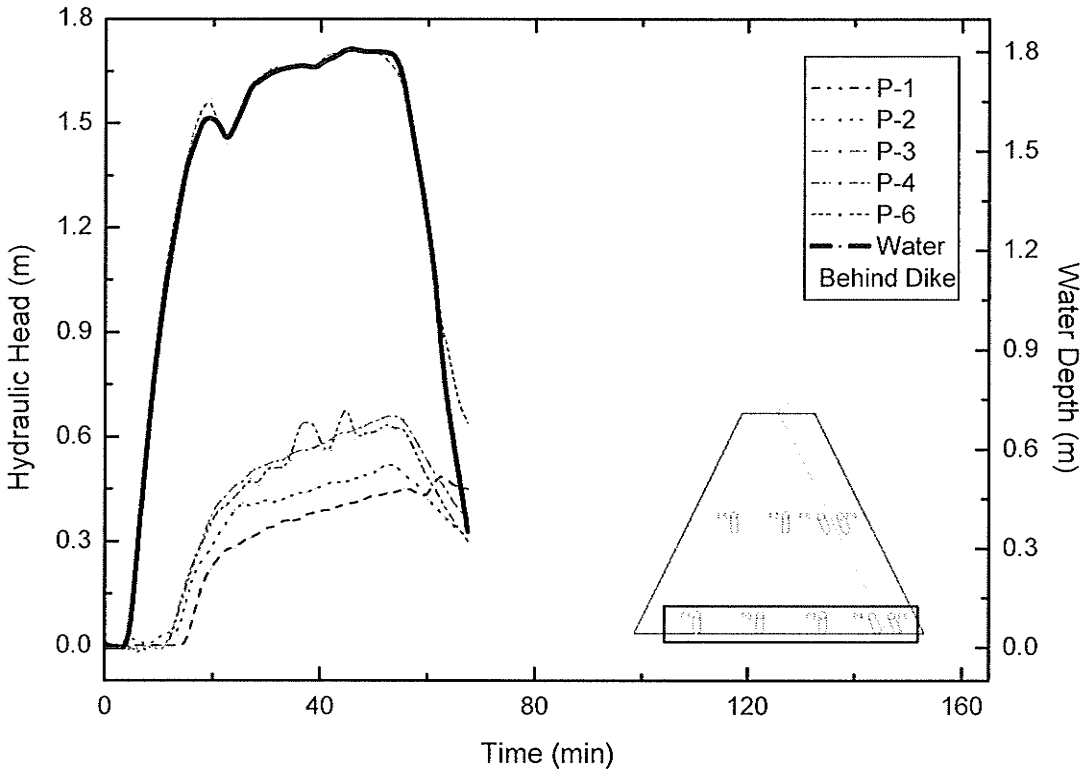

Figure 4.90 – Summary of Hydraulic Head readings by Piezometers at base of Dike E, Time vs. Hydraulic Head, August 21, 2004.

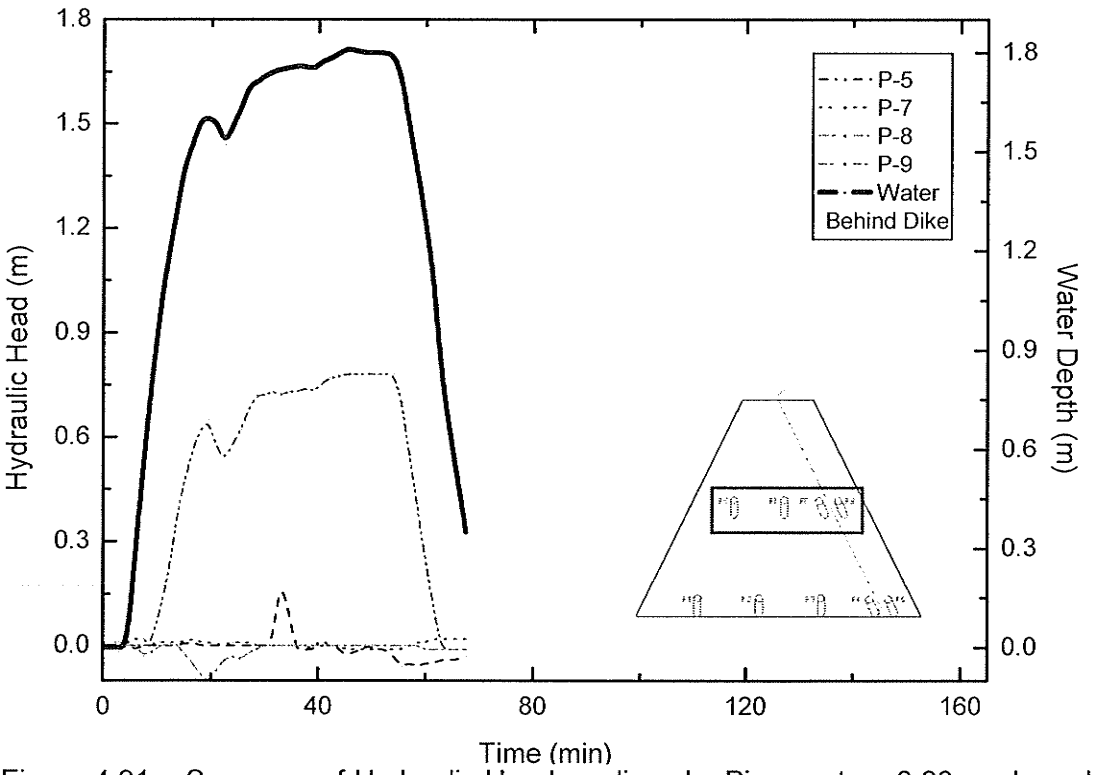

Figure 4.91 – Summary of Hydraulic Head readings by Piezometers 0.83 m above base of Dike E, Time vs. Hydraulic Head, August 21, 2004.

5 Discussion of Sandbag Dike Types

5.1 Introduction

The dikes tested in the full-scale testing facility in the summer of 2004 have been divided into five primary groups, as presented in Table 4.1. The divisions are based on similarities of dike height, geometry, materials used, and construction method.

Dikes in group A are eight feet in height and built by student researchers according to the City of Winnipeg template. Dikes in group B are ten feet in height built by student researchers according to the City of Winnipeg template. Dikes in group C are six feet in height built by student researchers according to the City of Winnipeg template using the materials recommended except that dike C3 was constructed without any PES layer. Dikes in group D are also built six feet in height by student researchers according to a geometry modified from the City of Winnipeg template, and dike D2 was constructed using the same geometry without any PES. Dike E was built six feet in height by volunteers provided with the City of Winnipeg template.

5.2 Group A Sandbag Dikes

These dikes were the first two dikes built in the full-scale testing facility. The height of 8 feet was chosen based on the desire to select a dike that might fail according to local expertise which suggested that an 8 foot dike was not stable at peak loading if built according to the City of Winnipeg 1997 template. The 8 foot dikes required fewer bags than the 10 foot dikes planned for subsequent testing, and therefore initial tests could be conducted more quickly at 8 feet than 10 feet to get a sense of the test duration from initial construction to decommissioning.

5.2.1 Displacement Data from Group A Dikes

Figures 5.1 and 5.2 are cross-sections of dike A1 cut through the centre of the dike with scaled vectors showing the direction and amount of movement measured by each row of extensometers at 87 and 171 minutes into test A1, respectively. The direction of the measured displacement is indicated by the point of the arrowhead in the figures. The distance between the centre of the round initial position marker and the back vertical end of the arrow head is the horizontal displacement measured by the extensometer indicated. Measurements of less than 1 mm (0.04") are not shown on the figures. When there was less than 1 mm of movement measured, the original location of the extensometer connection is indicated and no arrowhead is drawn.

Test A1 shows little difference in extensometer movement between the peak water level of 1.16 m (3.81') at 87 minutes into the test and the final reading taken at 1.1 m (3.61') of water 171 minutes after the start of loading. There is movement indicated by extensometers 500-6, 750-1 and 750-2 after 171 minutes that was not measured at 87 minutes, but the 500-6 extensometer read 1 mm and both of the 750s read 9 mm. These minimal movements measured at isolated positions in the dike are not considered significant for 84 minutes of loading. The measured displacement for each row of extensometers reached equilibrium approximately 120 minutes into the test.

Figures 5.3 and 5.4 are cross-sections of dike A2 cut through the centre of the dike with scaled vectors showing the direction and amount of movement measured by each row of extensometers at 62.5 and 75 minutes into test A2, respectively. There is a notable difference in extensometer movement between the measurements taken at the design water level of 1.82 m (5.97') at 62.5 minutes and the peak water level of 2.07 m (6.79') at 75 minutes into test A2. Figures 4.35 through 4.37 indicate that the measured

displacements for each row of extensometers did not reach equilibrium during the design loading or during the final over-top loading portions of the test. The displacements measured by the extensometers at each level in the dike continued to increase during all of the loading conditions in test A2. This means that the dike did not equilibrate under any of the loads applied, and continued to deform laterally throughout the duration of the test. This indicates that the dike was not stable under the applied loads.

5.2.2 Deformation Data from Group A Dikes

Figure 5.5 is a compilation sketch of the deformed dike shape 62.5 minutes into test A2 based on visual observations made during both tests A1 and A2, photographs taken during the tests, as well as extensometer and survey data. Figure 5.5 clearly shows the change in available freeboard caused by densification and deformation due to both wetting of the bags and the overall hydraulic loading, respectively. After one hour of loading on dike A2, the freeboard has been reduced from 0.61 m (2') to 0.38 m (1.25'), a 38% reduction.

Figures 5.6 through 5.9 are photographs of dike A2 during and after loading and the subsequent failure.

5.2.3 Pore Pressure Data from Group A Dikes

Figures 5.10 and 5.11 are cross-sections of dike A1 cut through the centre of the dike showing the initial positions of the vibrating wire piezometers in the dike and the hydraulic head measured at a given water depth and time interval from the beginning of the test. A line is drawn connecting the head levels for each row of piezometers, providing an estimate of the pore pressure profile through the dike at that elevation. Figure 5.10 shows the pore pressures present at 87 minutes into test A1, and Figure 5.11 shows the pore pressures at 171 minutes into the same test.

The piezometer data for test A1 shows little difference in the hydraulic head measured between the peak water level of 1.16 m (3.81') at 87 minutes into the test and the final reading taken at 1.1 m (3.61') of water 171 minutes after the start of loading. Figures 4.31 through 4.33 indicate that the measured pore pressures for each row of piezometers reached equilibrium approximately 90 minutes into the test.

Figures 5.12 and 5.13 are cross-sections of dike A2 cut through the centre of the dike showing the initial positions of the vibrating wire piezometers in the dike and the hydraulic head measured at a given water depth and time interval from the beginning of the test. Figure 5.12 shows the pore pressures present at 62.5 minutes into test A2, and Figure 5.13 shows the pore pressures at 75 minutes into the same test.

The piezometer data for test A2 shows a noticeable difference in the hydraulic head measured between the design water level of 1.82 m (5.97') at 62.5 minutes into the test and the reading taken at the peak water level of 2.07 m (6.79') of water 75 minutes after the start of loading. This indicates that the pore pressures through the dike were increasing under the design load. Figures 4.38 through 4.40 indicate that the measured pore pressures for each row of piezometers didn't quite reach equilibrium at 60 minutes into the test under the design load, and that they were increasing significantly when the dike was loaded to nearly over-top conditions at 75 minutes. Again, the indication is that the pore pressures were increasing and therefore the stability of the dike was decreasing nominally under the design load and significantly under the overtop load.

5.2.4 Seepage Data from Group A Dikes

Figures 4.27 and 4.34 superimpose the seepage rate per metre width and the water depth behind dikes A1 and A2 against time for tests A1 and A2 respectively. Figure 4.27 shows that seepage through dike A1 equilibrated to the loading rate about 80 minutes

into the test. Figure 4.34 shows that the seepage through dike A2 continued to increase throughout the test, both at the design load of 1.82 m (5.97') and the peak load of 2.07 m (6.79').

5.2.5 Summary of data from Group A Dikes

All of the data and visual observations during test A2 indicate that an 8' (2.44 m) sandbag dike built according to the City of Winnipeg 1997 template are not entirely stable at design loading levels of 6' (1.85 m). Both the sets of internal instruments showed increasing deformation and pore pressures under constant load. The geometry of the dike changed during loading due to densification by wetting and hydraulic pressures due to both the hydrostatic load and the reduced friction caused by flow through the dike. The seepage through the dike continued to increase throughout loading in test A2.

5.3 Group B Sandbag Dikes

These dikes were the second set of dikes built in the full-scale testing facility. The height of 10 feet was chosen in part to verify the first set of test findings that an 8 foot dike was not entirely stable according to the City of Winnipeg 1997 template. The 10 foot dike tests are approaching the height of the tallest sandbag dikes built and relied on in the flood of 1997. It is important to note that most observed sandbag dikes built to more than 8 feet in 1997 did not follow the City of Winnipeg template, but were generally more robust, using more bags than would have been required to follow the template, or were buttressed on the dry side with additional sandbags at regular intervals in order to support the loads anticipated at the crest level during the flood event (Doug McNeil, personal communication, June 2003).

5.3.1 Displacement Data from Group B Dikes

Figures 5.14, 5.15 and 5.16 are cross-sections of dike B1 cut through the centre of the dike with scaled vectors showing the direction and amount of movement measured by each row of extensometers at 94, 100 and 209 minutes into test B1, respectively. The direction of the measured displacement is indicated by the point of the arrowhead in the figures.

There is a noticeable increase in horizontal deformation of dike B1 in the 6 minutes between the end of 60 minutes of design depth loading (88 minutes into the test) at 2.44 m (8.0') and the peak water depth of 2.64 m (8.66') 94 minutes into the test. Figures 4.43 through 4.45 show the extensometer readings for test B1 equilibrating at the 250 level (1.55 m or 5.09' above the base of the dike) and increasing at the 500 and 750 levels (2.05 m (6.73') and 2.55 m (8.37') above the base of the dike, respectively) during design water depth loading. During peak water loading, all levels of instrumentation recorded motion that increased under steady hydraulic conditions. The extensometers recorded further deformation throughout unloading, suggesting that at this point the overall structure behaved with plastic rather than elastic behaviour. The strains that the overall structure had undergone under the hydraulic load had become permanent and that rather than recovering from the lateral deformations and rebounding even partially, the dike continued to deform even while the external load was being decreased.

Figures 5.17, 5.18 and 5.19 are cross-sections of dike B2 cut through the centre of the dike with scaled vectors showing the direction and amount of movement measured by each row of the extensometers at 33, 37 and 58 minutes into test B2, respectively. The direction of the measured displacement is indicated by the point of the arrowhead in the figures.

There is a considerable increase in horizontal deformation of dike B2 in the 4 minutes between the peak loading depth (33 minutes into the test) of 2.68 m (8.79') and the water depth of 2.48 m (8.14') just after failure caused by the peak load. Figures 4.49 through 4.51 indicate the extensometer readings for test B2 increasing at all levels during all hydraulic loading. As in test B1, the extensometers recorded further deformation throughout unloading, suggesting plastic rather than elastic behaviour.

5.3.2 Deformation Data from Group B Dikes

Figure 5.20 is a compilation sketch of the deformed dike shape 37 minutes into test B2 based on visual observations made during both tests B1 and B2, photographs taken during the tests, as well as extensometer and survey data. Figure 5.20 clearly shows the change in available freeboard caused by densification and deformation due to both wetting of the bags and the overall hydraulic loading, respectively. After 37 minutes of loading, the freeboard has been reduced from 0.61 m (2') to 0.3 m (1.0'), a 50% reduction.

Figures 5.21 through 5.23 are photographs of dike B2 during and after loading.

5.3.3 Pore Pressure Data from Group B Dikes

Figures 5.24, 5.25 and 5.26 are cross-sections of dike B1 cut through the centre of the dike showing the initial positions of the vibrating wire piezometers in the dike and the hydraulic head measured at a given water depth and time interval from the beginning of the test. Figure 5.24 shows the pore pressures present at 94 minutes into test B1, Figure 5.25 shows the pore pressures at 100 minutes, and Figure 5.26 shows the pore pressures at 126 minutes.

The piezometer data for test B1 shows some difference in the hydraulic head measured between the design water level of 2.44 m (8.0') at 94 minutes into the test and the peak water depth reading of 2.64 m (8.66') 6 minutes later. Figure 5.26 shows that the pore pressures in the dike increased further under sustained above design loading of 2.58 m (8.46'). Figures 4.46 and 4.47 show a slow but steady increase in measured pore pressures for both rows of piezometers throughout the test.

Figures 5.27, 5.28 and 5.29 are cross-sections of dike B2 cut through the centre of the dike showing the initial positions of the vibrating wire piezometers in the dike and the hydraulic head measured at a given water depth and time interval from the beginning of the test. Figure 5.27 shows the pore pressures present 33 minutes into test B2, Figure 5.28 shows the pore pressures at 37 minutes, and Figure 5.29 shows the pore pressures at 58 minutes.

The piezometer data for test B2 shows significant difference in the hydraulic head measured between the peak water level of 2.68 m (8.79') at 33 minutes into the test and the post-failure water depth reading of 2.48 m (8.14') 4 minutes later. Figure 5.29 shows that the pore pressures in the dike remained above atmospheric during unloading. Figures 4.52 and 4.53 show a steady increase in measured pore pressures for both rows of piezometers throughout the loading portion of the test.

5.3.4 Seepage Data from Group B Dikes

Seepage through dike B1, as shown in Figure 4.42, increased for the first 75 minutes of loading, then levelled off during the remainder of the test, decreasing during unloading. Unfortunately there were no seepage readings taken during test B2.

5.3.5 Summary of Data from Group B Dikes

The increase in horizontal deformation across the upper portion of dike B1 throughout the test indicates that the dike was not stable under design loading. Similarly the steady rate of horizontal deformation throughout the loading and unloading of dike B2 show that the 10' (3.05 m) dike was not able to sustain it's 8' (2.44 m) hydrostatic design load.

The corresponding jump in pore pressures and considerable horizontal deformation at the peak loading depth of 2.68 m (8.79') at 33 minutes into test B2 indicate a strong correlation between the two. The group B tests show that increased pore pressures inside the dikes lead to decreased stability of the dikes overall.

As with the group A tests, all of the data and visual observations during tests B1 and B2 indicate that a 10' (3.05 m) sandbag dike built according to the City of Winnipeg 1997 template is not stable at design loading levels of 8' (2.44 m). Both the sets of internal instruments showed increasing deformation and pore pressures under constant load. The geometry of the dike changed during loading due to densification by wetting and hydraulic pressures due to both the hydrostatic load and the reduced friction caused by flow through the dike. The seepage through the dike equilibrated during design depth loading in test B1, and no seepage data is available from test B2.

5.4 Group C Sandbag Dikes

This set of 6 foot (1.85 m) dikes were built and tested after recognising the relative instability of 8 and 10 foot dikes built according to the City of Winnipeg 1997 template. The height of 6 feet was chosen after discussion with the project's steering committee. The 6 foot dikes require significantly less bags than the 8 or 10 foot dikes and therefore more tests could be completed while the facility was in operation. The height of 6 feet is

close to the limit that was felt to be practical with the 1997 template geometry, and tests on this height of dike should prove to be very useful for future flood protection efforts.

Dike C1 and C2 were built in conformance with the 1997 template, and were loaded to design depth and over-top depth, respectively. Dike C3 was built with the same geometry as C1 and C2, but without the PES layer to prevent flow through the structure. Dike C3 was tested in the same manner as dike C1, but did not reach design depth for any sustained period of time.

5.4.1 Displacement Data from Group C Dikes

Figures 5.30 through 5.32 are cross-sections of dike C1 cut through the centre of the dike with scaled vectors showing the direction and magnitude amount of movement measured by each row of extensometers at 99, 137.5 and 154 minutes into test C1 respectively.

Every extensometer read less than 1" (25 mm) of movement after 70 minutes of design depth loading in test C1. After increasing the hydraulic loading to a peak level of 1.74 m (5.71') 38 minutes later, only the three outermost extensometers in the top row registered movement over 1" (25 mm). The extensometers did register a slight reduction of horizontal deformation during and after unloading. Figures 4.56 through 4.58 show the extensometer readings equilibrating at all levels within the dike and at all hydraulic loads applied in test C1.

Figures 5.33 and 5.34 are cross-sections of dike C2 cut through the centre of the dike with scaled vectors showing the direction and amount of movement measured by each row of extensometers at 35 and 43 minutes into test C2.

At a peak depth of 1.77 m (5.81') 35 minutes into the test, there was less than 1" (25 mm) of movement recorded by each extensometer except the outermost one at the highest elevation within the dike. There was very little change in the extensometer readings at 43 minutes into the test, following 30 minutes at over-topping load levels. Figures 4.56 through 4.58 show the extensometer readings equilibrating during all loading conditions in test C2.

Figures 5.35 and 5.36 are cross-sections of dike C3 cut through the centre of the dike with scaled vectors showing the direction and amount of movement measured by each row of extensometers at 25 and 36 minutes into test C3.

Due to excessive lateral and vertical deformation of Dike C3 during loading, the peak water level reached was 1.49 m (4.89'), at 25 minutes into the test. At this point in time, lateral deformations of well over 2" (50 mm) were observed at both of the upper levels of extensometers. Shortly after this, dike C3 failed dramatically and extensometer readings 36 minutes after the beginning of the test and at a water depth of 0.41 m (1.35') show considerable movement in the horizontal direction.

Extensometer 500-6 is particularly notable, showing a movement toward the water at 25 minutes into the test and then movement away from the load at 36 minutes. The initial movement toward the water load at this point in the dike is likely due to vertical deformations at higher levels in the structure causing spreading below. This movement was overcome and reversed by the flow through the dike which was unimpeded due to the lack of PES. Figures 4.68 through 4.70 show that the extensometer readings never equilibrated during test C3, increasing during loading at all levels.

5.4.2 Deformation Data from Group C Dikes

Figures 5.37 and 5.38 are compilation sketches of the deformed dike shape 43 minutes into test C2 and 27 minutes into test C3 based on visual observations made during tests C1, C2 and C3, photographs taken during the tests, as well as extensometer and survey data. Both figures clearly show the change in available freeboard caused by densification and deformation due to both wetting of the bags and the overall hydraulic loading. In test C2 after 43 minutes of loading, the freeboard has been reduced from 0.61 m (2') to 0.5 m (1.64'), a 17% reduction. In test C3 after 27 minutes of loading, the freeboard has been reduced to 0.23 m (0.75 m), a 62% reduction.

Figures 5.39 through 5.43 are photographs of dikes C1, C2 and C3 during and after loading.

5.4.3 Pore Pressure Data from Group C Dikes

Figures 5.44 through 5.46 are cross-sections of dike C1 cut through the centre of the dike showing the initial positions of the vibrating wire piezometers in the dike and the hydraulic head measured at a given water depth and time interval from the beginning of the test. Figure 5.44 shows the pore pressures present at 99 minutes into test C1, Figure 5.45 shows the pore pressures at 137.5 minutes, and Figure 5.46 shows the pore pressures at 154 minutes.

The piezometer data for test C1 shows a small difference in the hydraulic head measured between the peak water level of 1.74 m (5.71') at 137.5 minutes into the test and the design water depth reading of 1.29 m (4.23') 38 minutes earlier. Figure 5.46 shows that the pore pressures in the dike did not change significantly after 15 minutes of loading at well above design depth levels. Figures 4.59 and 4.60 show the measured

pore pressures for both rows of piezometers equilibrating at each loading stage of the test.

Figures 5.47 and 5.48 are cross-sections of dike C2 cut through the centre of the dike showing the initial positions of the vibrating wire piezometers in the dike and the hydraulic head measured at a given water depth and time interval from the beginning of the test. Figure 5.47 shows the pore pressures present at 35 minutes into test C2, and Figure 5.48 shows the pore pressures at 43 minutes.

The piezometer data for test C2 shows no significant difference in the hydraulic head measured between the peak water level of 1.77 m (5.81') at 35 minutes into the test and the water depth reading of 1.75 m (5.74') 8 minutes later, after 30 minutes of over-topping. Figures 4.65 and 4.66 show the pore pressures in the dike equilibrate during loading at over-topping levels.

Figures 5.49 and 5.50 are cross-sections of dike C3 cut through the centre of the dike showing the initial positions of the vibrating wire piezometers in the dike and the hydraulic head measured at a given water depth and time interval from the beginning of the test. Figure 5.49 shows the pore pressures present at 25 minutes into test C3, and Figure 5.50 shows the pore pressures at 36 minutes.

The piezometer data for test C3 shows a head profile that exits the dike well above grade on the non-loading side. Figures 4.71 and 4.72 indicate that the pore pressures in the dike did not equilibrate during loading. Figure 5.50 shows that the pressures in the dike did not dissipate immediately upon unloading, remaining almost 0.2 m (0.66') above the load water depth at 36 minutes into the test.

5.4.4 Seepage Data from Group C Dikes

Figures 4.55, 4.61 and 4.67 show the seepage rates with time through dikes C1, C2 and C3 respectively. The seepage rate in test C1 reached equilibrium at both design depth loading and at over-design depth loading. The seepage rate in test C2 stopped increasing during over-top loading. In test C3, the seepage rate continued to increase throughout the test, primarily due to the catastrophic failure of the dike and resulting deluge of water past the weir.

5.4.5 Summary of Data from Group C Dikes

Horizontal deformation data from tests C1 and C2 indicate that these dikes are relatively stable under both design and over-top loading conditions. The horizontal data from test C3 indicates that when the PES layer is removed from the dike the 6 foot dike is unstable.

The deformed shapes of dikes C2 and C3 show the relationship between deformation behaviour of a sandbag dike and pore pressure distribution within the same structure. Dike C2 did not deform significantly, even under over-topping load conditions. Dike C3 deformed catastrophically before reaching over-top load conditions.

Pore pressure distributions through dikes C1 and C2 show an equilibrium being reached at steady load conditions, both at the design and over-top water levels. The pore pressure distribution in dike C3 increased throughout loading and did not equilibrate due to failure of the dike.

The difference between the deformed profiles of dikes C2 and C3 is a further indication of the result of removing the PES layer on both the horizontal and vertical stability of the structure. Dike C3 deformed excessively under design load, failing catastrophically in

less than an hour from the start of the test. Dike C2 did not deform excessively and remained dimensionally stable under all loading conditions.

Seepage data from group C dikes give an indication of the kind of values that can be expected for stable and instable sandbag structures.

5.5 Group D Sandbag Dikes

These 6 foot (1.85 m) dikes were built as a direct result of discussions with the project's steering committee regarding the need to test alternative dike geometries. The change in geometry was minimal, simply making the dry side slope 1:1 instead of 2:1 (rise : run). The data from these tests is useful in terms of quantifying the change in stability and seepage rates for a known volume of sandbags and also because it represents possible results for modifications made to a dike after flood waters are already present on the wet side. Dike D1 was built with a PES layer and dike D2 was not.

5.5.1 Displacement Data from Group D Dikes

Figures 5.51 through 5.53 are cross-sections of dike D1 cut through the centre of the dike with scaled vectors showing the direction and amount of movement measured by each row of the extensometers at 65, 75 and 100 minutes into test D1, respectively.

The horizontal displacement was minimal at each level monitored by the extensometers in this test at all depths of loading. Four of the extensometers, two at the lowest elevation and one each at the two higher levels, did not record any significant movement in the dike after 50 minutes of loading at just above design depth 1.49 m (4.89'). Displacements remained below 1" (25 mm) at all recorded points throughout the test, even at over-top load conditions. There was no further deformation during the unloading portion of the test.

Figures 5.54 through 5.56 are cross-sections of dike D2 cut through the centre of the dike with scaled vectors showing the direction and amount of movement measured by each row of the extensometers at 30, 60 and 70 minutes into test D2, respectively.

Figure 5.54 shows displacements recorded by the extensometers after 20 minutes of loading at the design water depth for dike D2. As with dike C3, it is notable that the extensometers closest to the wet side of the dike recorded movement toward the load rather than away from it like the other extensometers in the dike. However, unlike dike C3, dike D2 stabilized under design load. After extensometer readings equilibrated, the water load was increased to approximately 1.65 m and held there for 30 minutes. This load level increased displacements throughout the dike, including the reversal of the upper extensometer that had originally recorded movement toward the water. Again, dike D2 stabilized under this load. Figures 4.81 through 4.83 show the extensometer measurements equilibrating for each loading condition in the test.

5.5.2 Deformation Data from Group D Dikes

Figure 5.57 is a compilation sketch of the deformed dike shape 70 minutes into test D2 based on visual observations made during both tests D1 and D2, photographs taken during the tests, as well as extensometer and survey data. Figure 5.57 clearly shows the change in available freeboard caused by densification and deformation due to both wetting of the bags and the overall hydraulic loading, respectively. After 70 minutes of loading, the freeboard has been reduced from 0.61 m (2') to 0.43 m (1.41'), a 30% reduction.

Figures 5.58 through 5.61 are photographs of dikes D1 and D2 during and after loading.

5.5.3 Pore Pressure Data from Group D Dikes

Figures 5.62 through 5.64 are cross-sections of dike D1 cut through the centre of the dike showing the initial positions of the vibrating wire piezometers in the dike and the hydraulic head measured at a given water depth and time interval from the beginning of the test. Figure 5.62 shows the pore pressures present at 65 minutes into test D1, Figure 5.63 shows the pore pressures at 75 minutes, and Figure 5.64 shows the pore pressures at 100 minutes.

The piezometer data for test D1 show a small difference in the hydraulic head measured between the peak water level of 1.85 m (6.07') at 75 minutes into the test and the above design water depth reading of 1.49 m (4.89') 10 minutes earlier. Figure 5.62 shows that the pore pressures in the dike did not change significantly after 50 minutes of loading at well above design depth levels. Figures 4.78 and 4.79 show the measured pore pressures for both rows of piezometers equilibrating at each loading stage of the test.

Figures 5.65 through 5.67 are cross-sections of dike D2 cut through the centre of the dike showing the initial positions of the vibrating wire piezometers in the dike and the hydraulic head measured at a given water depth and time interval from the beginning of the test. Figure 5.65 shows the pore pressures present at 30 minutes into test D2, Figure 5.66 shows the pore pressures at 60 minutes, and Figure 5.67 shows the pore pressures at 70 minutes.

There is a notable difference in the pore pressure distribution through the dike at design and peak water levels. The pore pressure distribution did stabilize at sustained loading well above the design depth, as demonstrated in the lack of change between Figures 5.66 and 5.67. Figures 4.84 and 4.85 show the piezometer readings equilibrating at both elevations at each load level during test D2.

5.5.4 Seepage Data from Group D Dikes

Figures 4.74 and 4.80 show the seepage rates with time through dikes D1 and dike D2. The seepage rate in test D1 reached equilibrium at both design depth loading and at over-design depth loading. The seepage rate in test D2 also stopped increasing during both design and over-top loading, although at a notably higher quantity than in test D1.

5.5.5 Summary of Data from Group D Dikes

Horizontal deformation data from tests D1 and D2 indicate that these dikes are stable under both design and over-top loading conditions. The horizontal data from test D2 indicates that stability can be achieved even when the PES layer is removed from the dike.

The deformed shape of dike D2 show the relationship between deformation behaviour of a sandbag dike and pore pressure distribution within the same structure. Dike D2 did not deform catastrophically, even under above design load conditions.

Pore pressure distributions through dikes D1 and D2 show an equilibrium being reached at steady load conditions, both at the design and above design water levels.

Seepage data from group D dikes give an indication of the kind of values that can be expected for stable sandbag structures with and without PES.

5.6 Group E Sandbag Dike

This 6 foot (1.85 m) dike was built as a direct result of discussions with the project's steering committee regarding the need to test dike construction quality. A group of volunteers from the community were solicited to attend the University of Manitoba on August 21, 2004 for the purposes of building a sandbag dike to be tested at the Sandbag Structures Research Facility in SmartPark. The volunteers were given a brief verbal

summary of the task before them as well as copies of the City of Winnipeg's 1997 sandbag dike design template. They were instructed to agree on a strategy for building the dike and to implement it under the supervision of an appointed volunteer who was to represent the potential homeowner whose home was to be protected by the dike. The researchers assisted the dike building activity only by helping to move bags from the stockpile to the volunteers placing the bags.

Instrumentation was installed in the dike at the same locations as in the dikes in group C. The installation periods were taken as time for the volunteers to get a drink of water and a break from the construction work. The entire exercise was supervised by a Manitoba EMO officer who acted as a safety officer for the activity.

There were several notable differences in the construction technique employed by the volunteers in comparison with the researchers. The volunteers did not interpret the 1997 template in the same way as the researchers. They placed bags at directions both parallel and perpendicular to the simulated flow in the flume.

The number of bags used in the volunteer dike appeared to be considerably less than the number used in the researcher built dikes. The relative number of bags used was determined by visual inspection of the stockpiles before and after the dikes were constructed. Although there is no numerical data to support this assertion, it is the opinion of the author that the volunteer built dike E was either of lower overall density or lower overall volume than the dikes built by the researchers.

The volunteers also used considerably more PES by weaving it excessively between the bags at the wet/dry interface in the dike. For the C1 and C2 dikes, which are the closest in comparison with the E dike, the researchers used one sheet of PES, therefore limiting

the horizontal joints in the dike to one at the base and one at the top. The volunteers used three sheets of PES in the construction of dike E, creating two additional horizontal joints in the dike.

5.6.1 Displacement Data from the Group E Dike

Figures 5.68 through 5.70 are cross-sections of dike E cut through the centre of the dike with scaled vectors showing the direction and amount of movement measured by each row of the extensometers at 45, 55 and 63 minutes into test E, respectively.

At a peak depth of 1.81 m (5.94') 45 minutes into the test, there was more than 3" (75 mm) of movement recorded by extensometers at each elevation within the dike. There was a noticeable change in the extensometer readings at 55 minutes into the test, following 30 minutes at above design load levels. Figures 4.87 through 4.89 show the extensometer readings increasing during all loading conditions in test E.

5.6.2 Deformation Data from the Group E Dike

Figure 5.71 is a compilation sketch of the deformed dike shape 55 minutes into test E based on visual observations and photographs taken during the tests, as well as extensometer and survey data. Figure 5.71 clearly shows the change in available freeboard caused by densification and deformation due to both wetting of the bags and the overall hydraulic loading, respectively. After 55 minutes of loading, the freeboard has been reduced from 0.61 m (2') to 0.56 m (1.83'), an 8% reduction.

Figures 5.72 and 5.73 are photographs of dike E during construction and when the structure is ready for loading.

5.6.3 Pore Pressure Data from the Group E Dike

Figures 5.74 through 5.76 are cross-sections of dike E cut through the centre of the dike with scaled vectors showing the direction and amount of movement measured by each row of the extensometers at 45, 55 and 63 minutes into test E, respectively.

There is a measured increase in the overall head indicated by the pore pressure distribution through the dike at sustained above design water levels. The pore pressure distribution did not stabilize during this sustained loading. Figures 4.90 and 4.91 show the piezometer readings increasing at the base of the dike throughout test E. The piezometers installed 0.83 m (2.72') above the base of the dike on the dry side of the PES did not record any increase in pore pressure above atmospheric during the test.

5.6.4 Seepage Data from the Group E Dike

No seepage readings taken during test E, due to local stockpiling of the bags to minimize volunteer efforts for building the dike.

5.6.5 Summary of Data from the Group E Dike

Horizontal deformation data from test E indicates that this dike was relatively unstable under above design loading conditions. The horizontal data from test E indicates that this dike continued to deform under steady loading conditions.

The deformed shape of dike E shows one of the variations of construction quality on a sandbag dike. Bags were witnessed falling off of the dry face of the dike during deformation under load, and the dike moved laterally significantly. Vertical deformation was not observed to the same extent in dike E as it was in earlier 6' (1.85 m) dikes tested in this research. This is probably due to the number of people working on the dike during construction, providing more compactive effort per unit area than in the dikes built

by the student researchers. It follows from this data and the previous observation that fewer bags were used in the volunteer built dike that the overall volume of the volunteer built dike was less than the volume of the researcher built dike of the same height and geometry.

Pore pressure distributions through dike E show a steady increase in flow through the dike under steady load conditions, both at the design and above design water levels. The pore pressure distribution in dike E increased throughout loading and did not equilibrate before the test was ended. This increase in seepage is partially due to the presence of two horizontal joints in the PES layer between the top and bottom of the wet side of the dike. The orientation of the some of the bags perpendicular to the water also contributed to the overall conductivity of the dike.

5.7 Summary of Seepage Data

Figure 5.77 is a ranking of the bulk conductivity per metre of dike for 10 of the structures tested. The seepage rate is dependent on the height of the dike and the depth of loading, and is strongly influenced by the presence or absence of a PES layer as well as the quality of the dike construction. In general, removing the PES layer causes the largest increase in bulk conductivity through the dikes as tested. The next most important factor is the depth of loading, followed by the overall height of the dike.

This ranking is presented in the discussion for interest sake only, as the elements of each test that affected seepage measurements were not controlled enough for an accurate comparison of all of the structures against each other. The bulk conductivity rates presented are appropriate for estimating relative pumping rates between dikes of different heights and construction materials and/or quality. These numbers should not be used as absolute conductivity values as the durations of the tests performed are

considerably shorter than the duration of an actual flood event and the long-term seepage characteristics of sandbag structures are still unquantified.

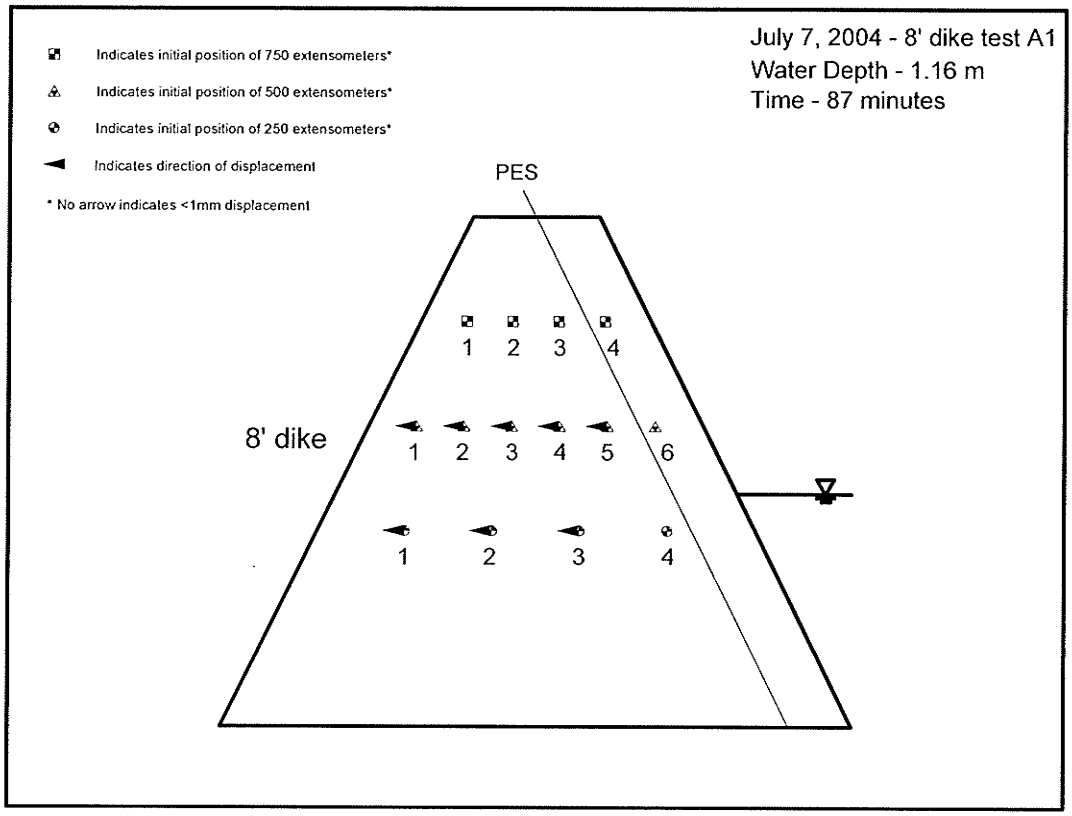

Figure 5.1 – Displacement of A1 Extensometers at Peak Water Level.

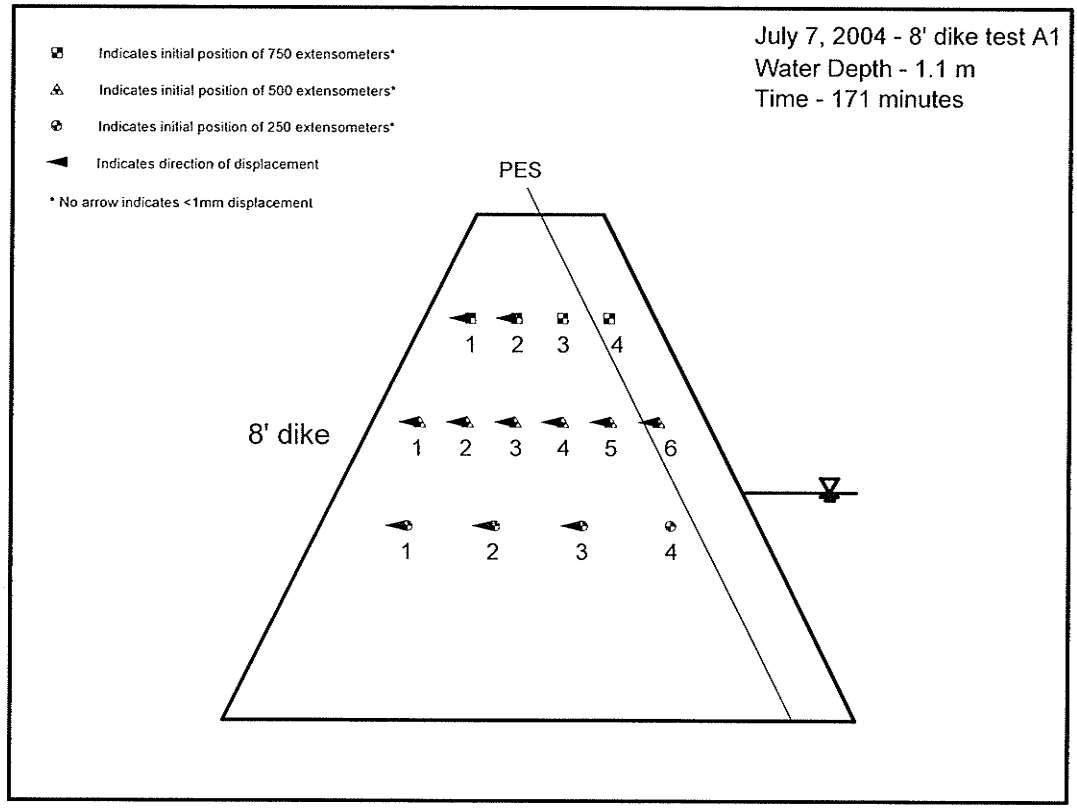

Figure 5.2 – Displacement of A1 Extensometers just before emptying Flume.

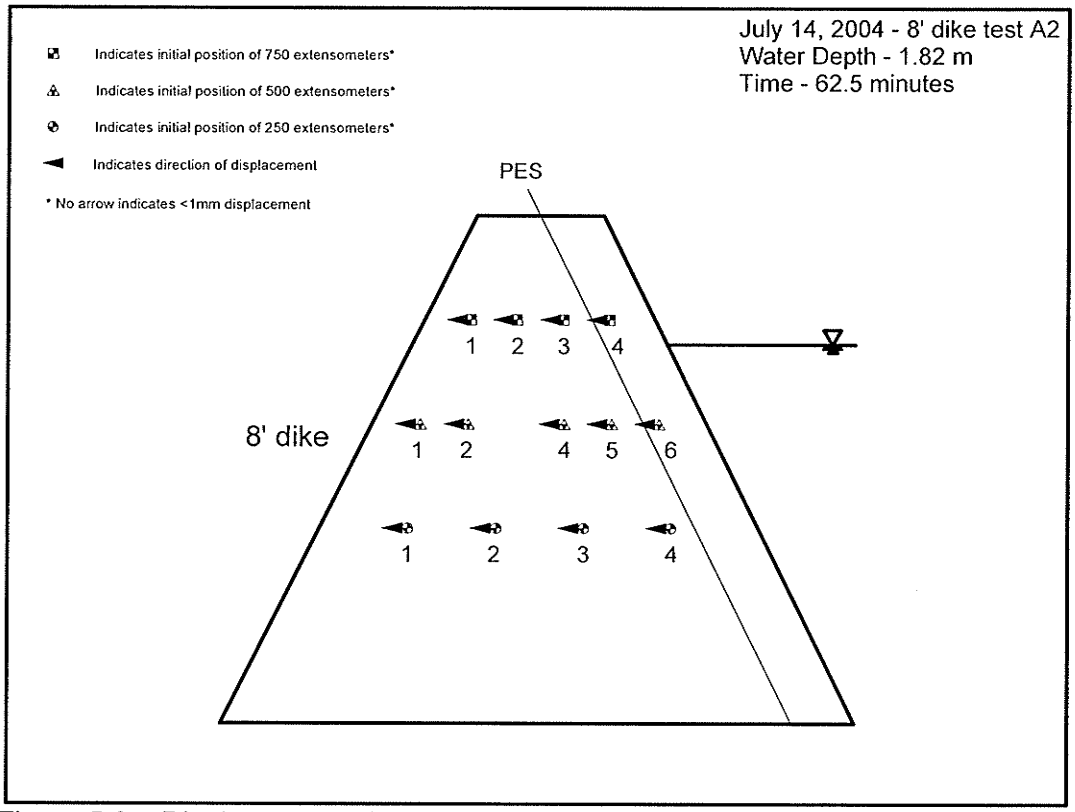

Figure 5.3 – Displacement of A2 Extensometers after 30 minutes at Design Water Level.

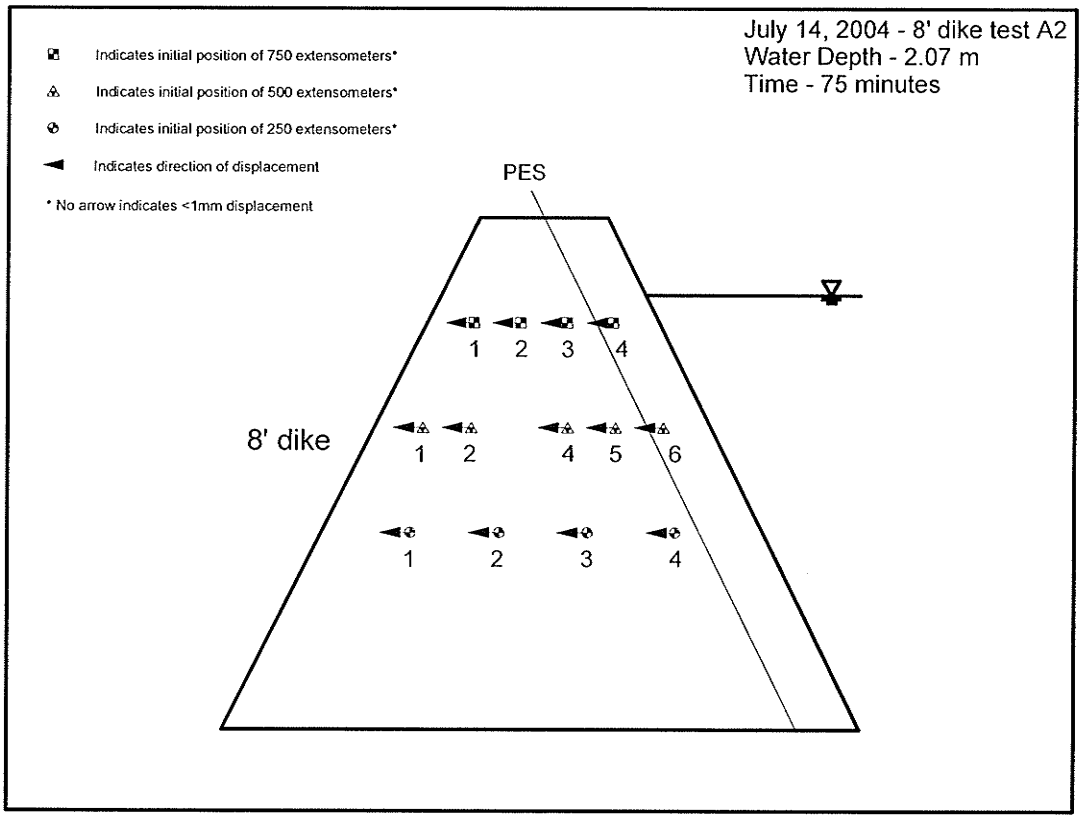

Figure 5.4 – Displacement of A2 Extensometers at Peak Water Level.

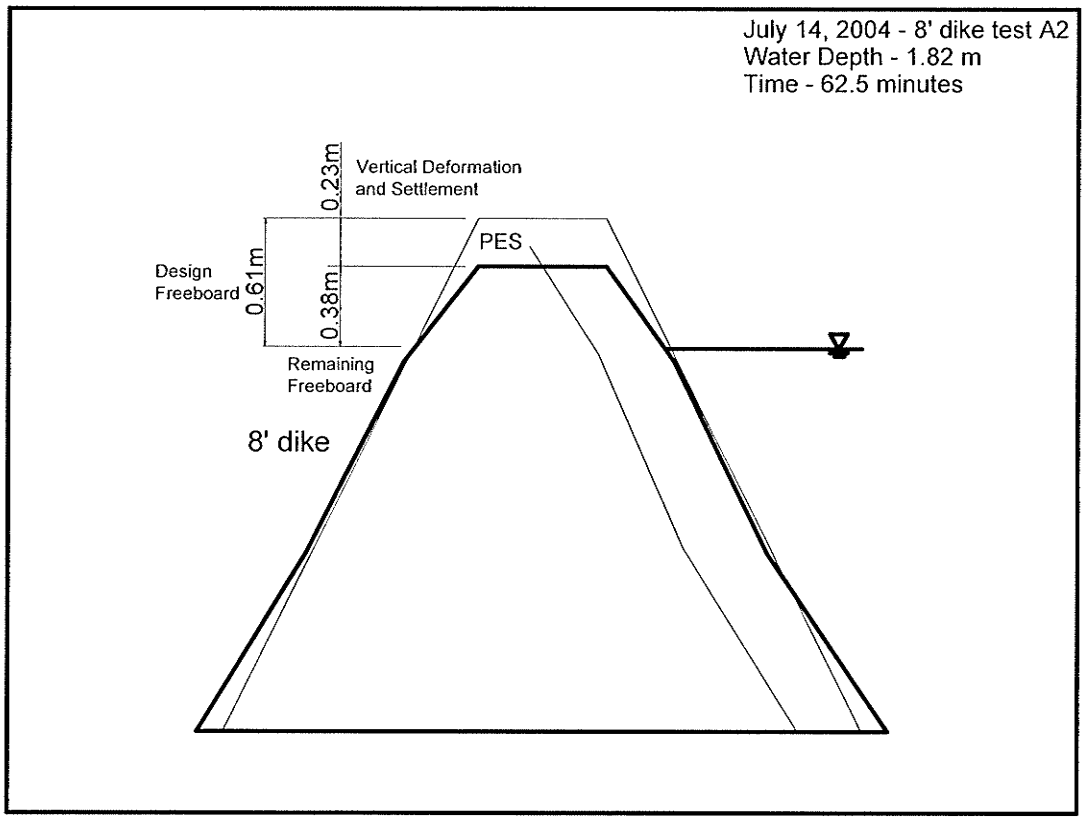

Figure 5.5 – Deformation, Dike A2 at Centre-line after 30 min at Design Water Level.

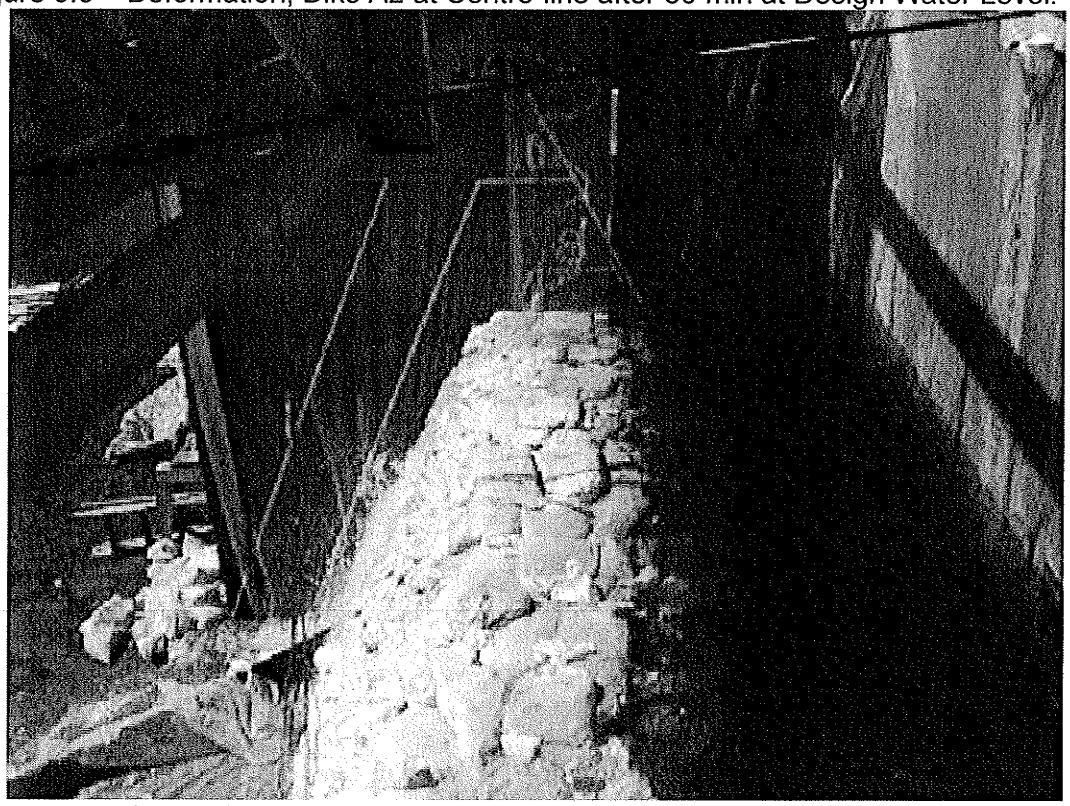

Figure 5.6 – Loss of Freeboard and Deformation Observed During Overtop Loading of Dike A2.

Figure 5.7 – Dike A2 Failing at Overtop Loading.

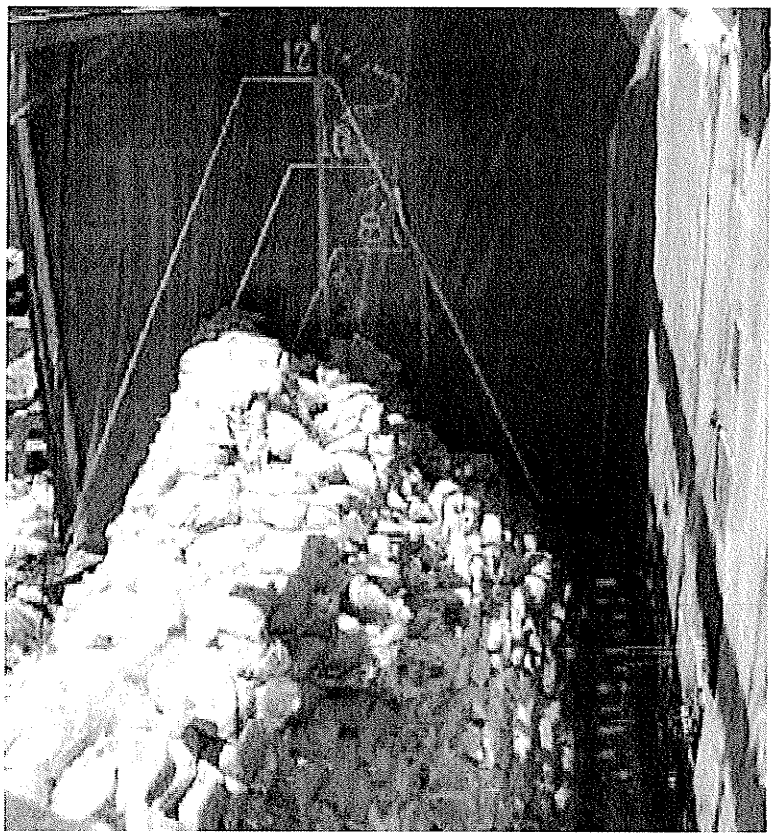

Figure 5.8 – Final Profile of Dike A2 against West Wall of Flume.

Figure 5.9 – Gap Between Sandbags Observed During Exhumation of Dike A2.

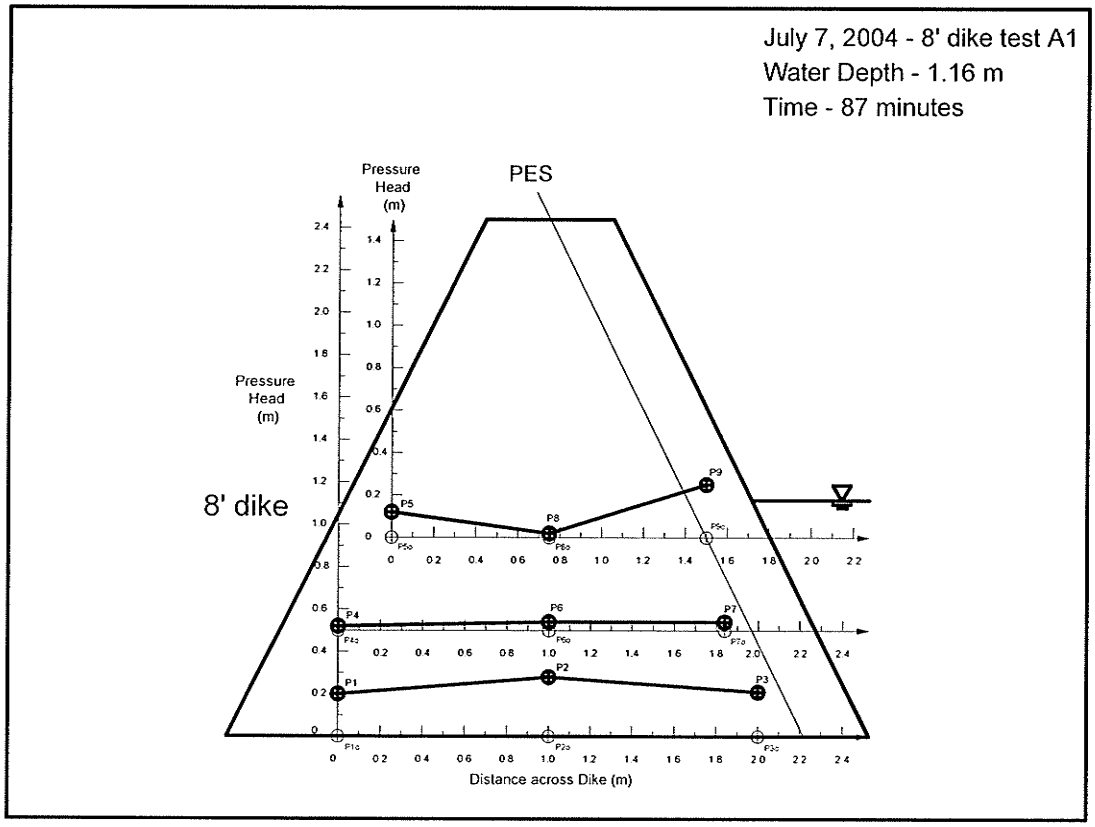

Figure 5.10 – Measured Pressure Head through Dike A1 at Peak Water Depth.

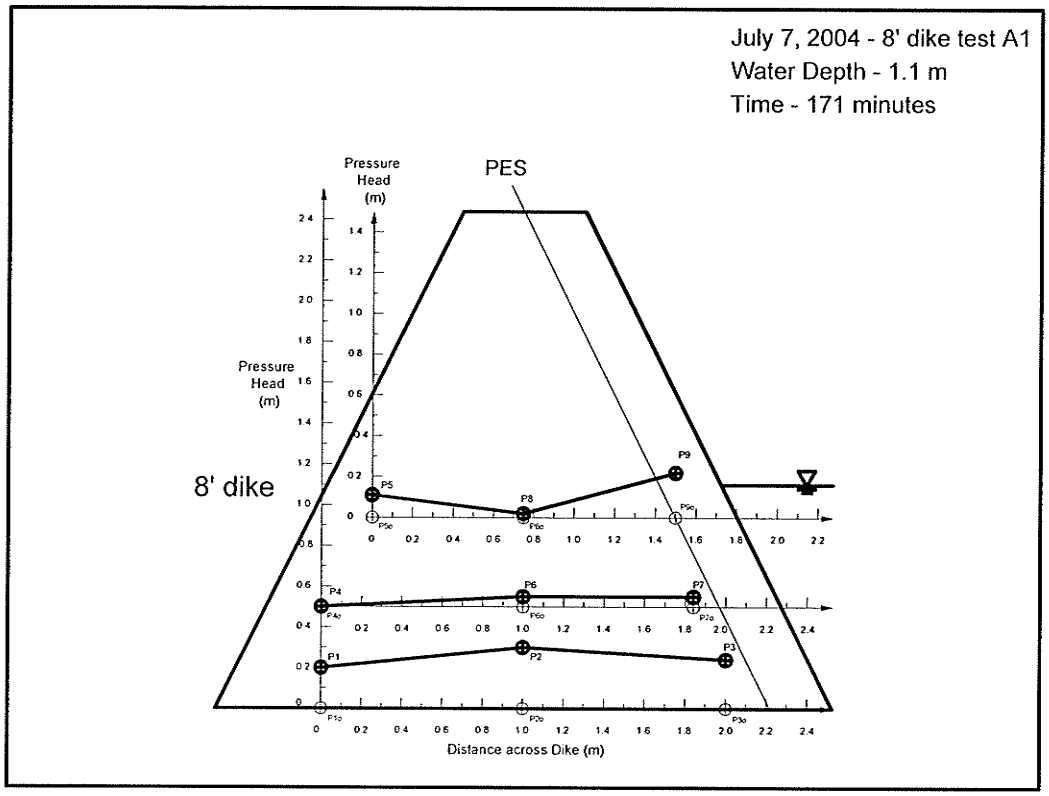

Figure 5.11 – Measured Pressure Head through Dike A1 before Emptying Flume.

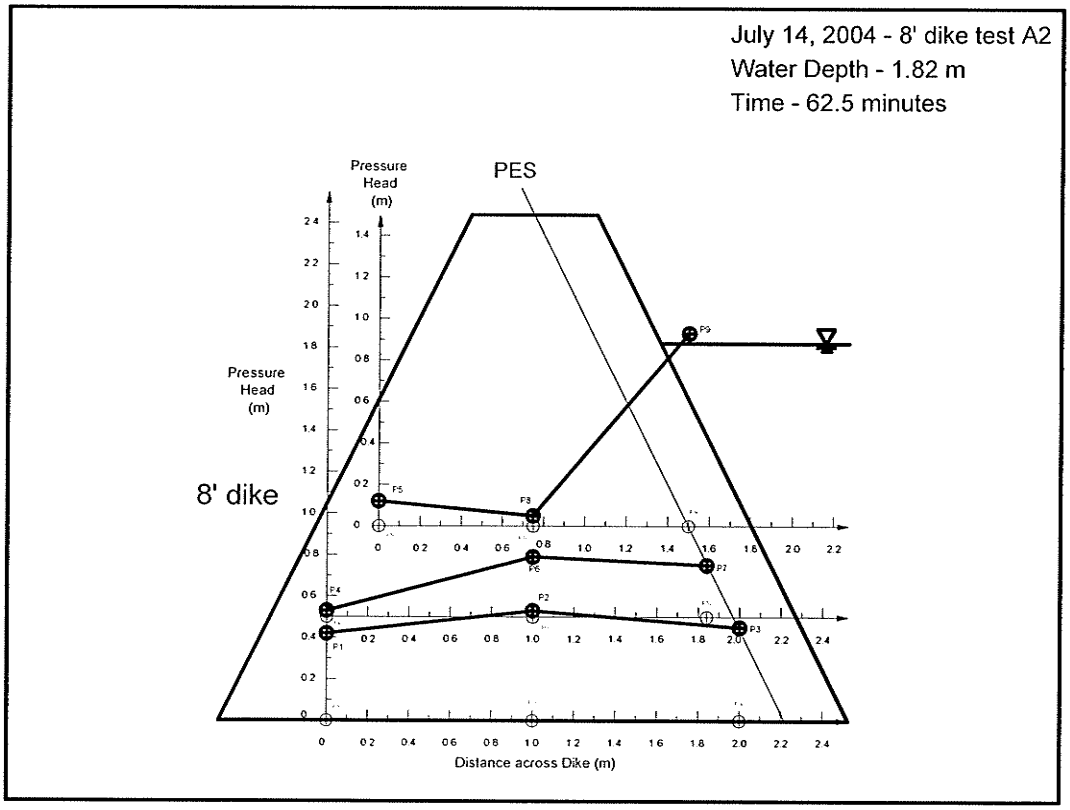

Figure 5.12 – Measured Pressure Head through Dike A2 at Design Water Depth.

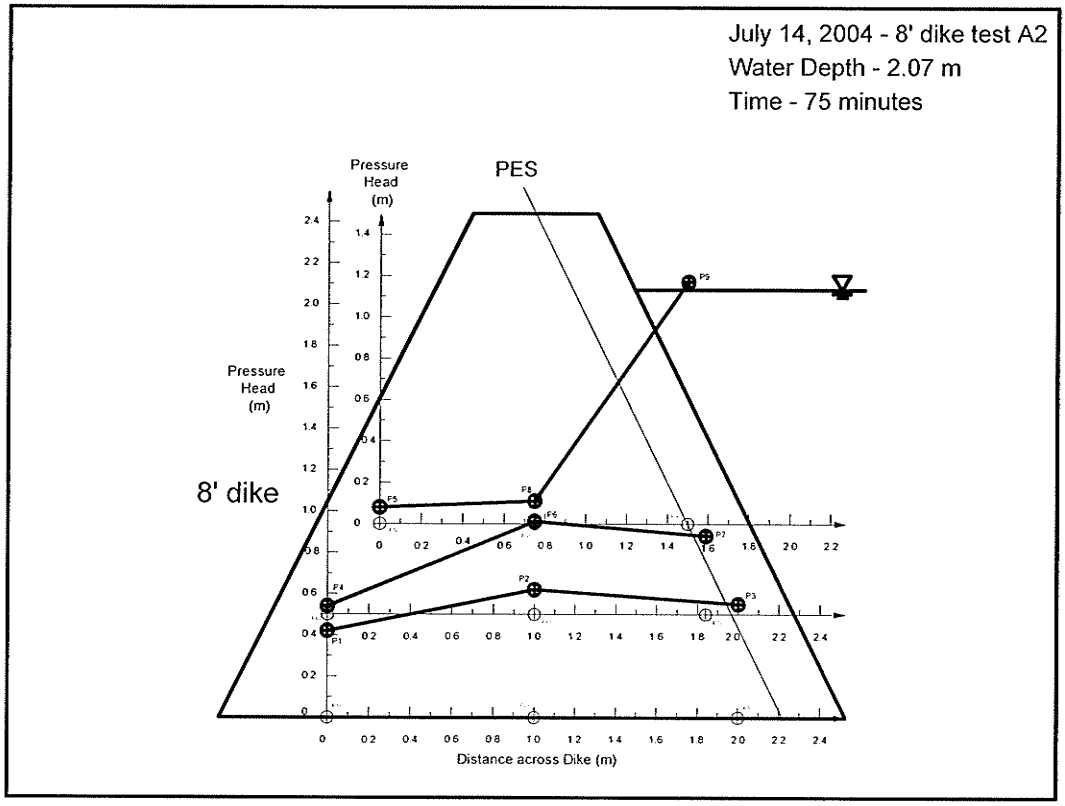

Figure 5.13 – Measured Pressure Head through Dike A2 at Peak Water Depth.

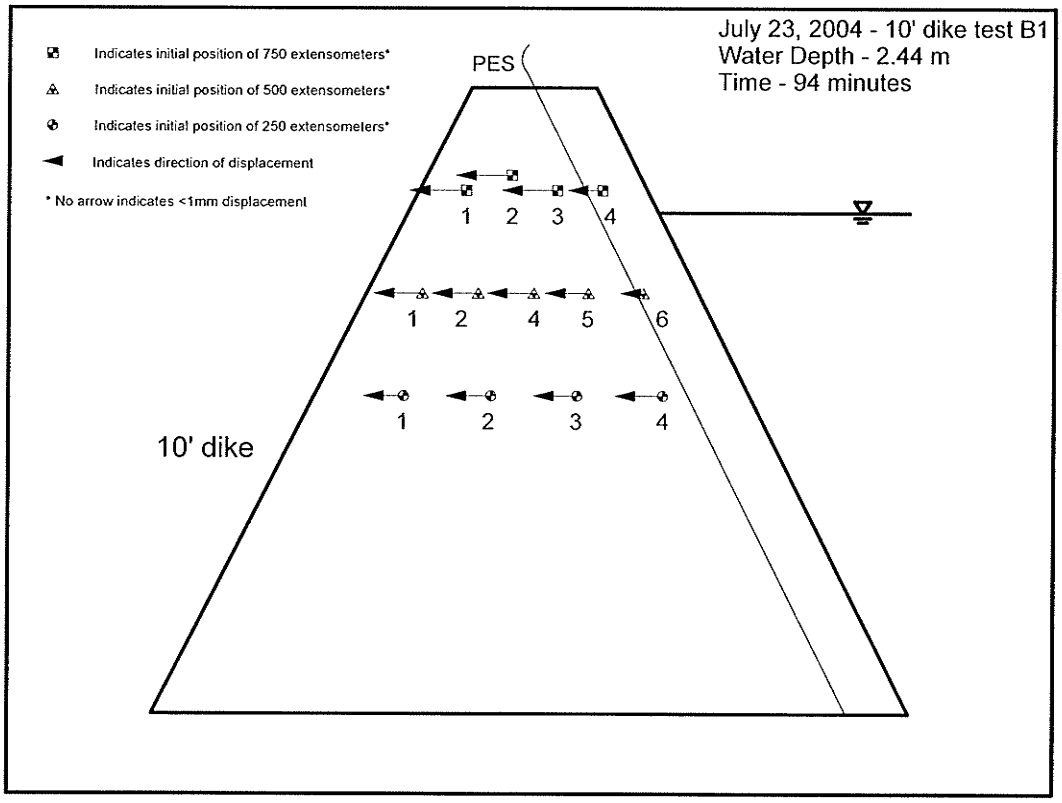

Figure 5.14 – Displacement of B1 Extensometers at Design Water Level.

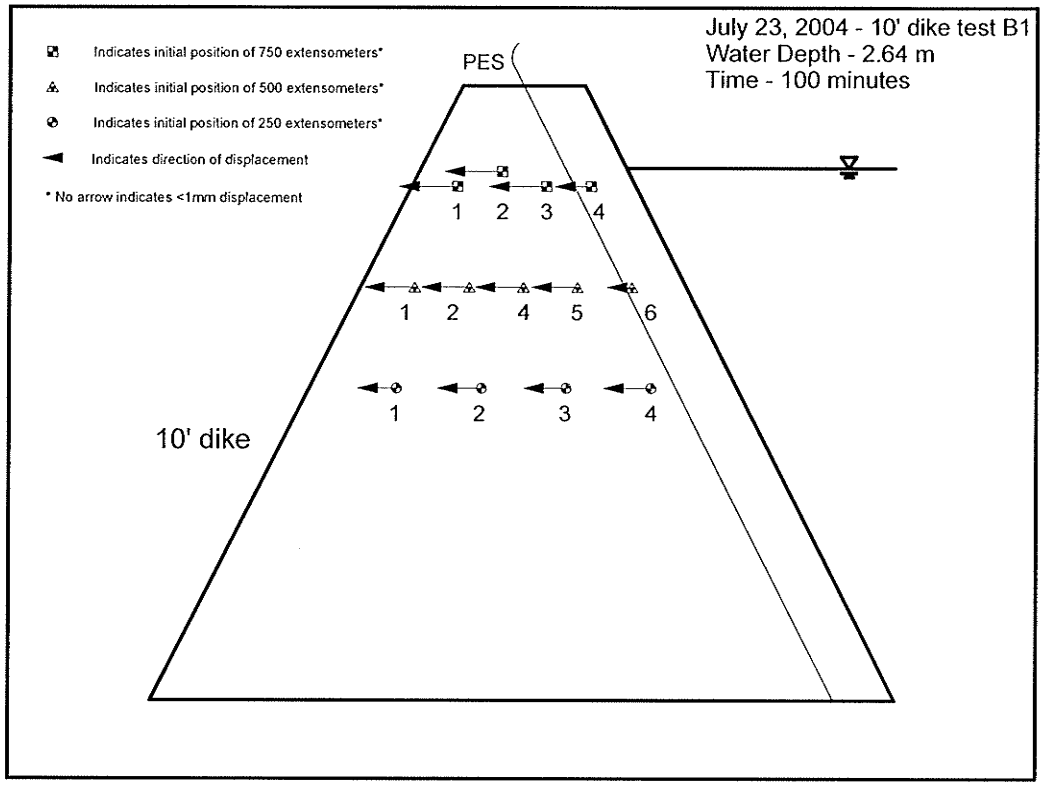

Figure 5.15 – Displacement of B1 Extensometers at Peak Water Level.

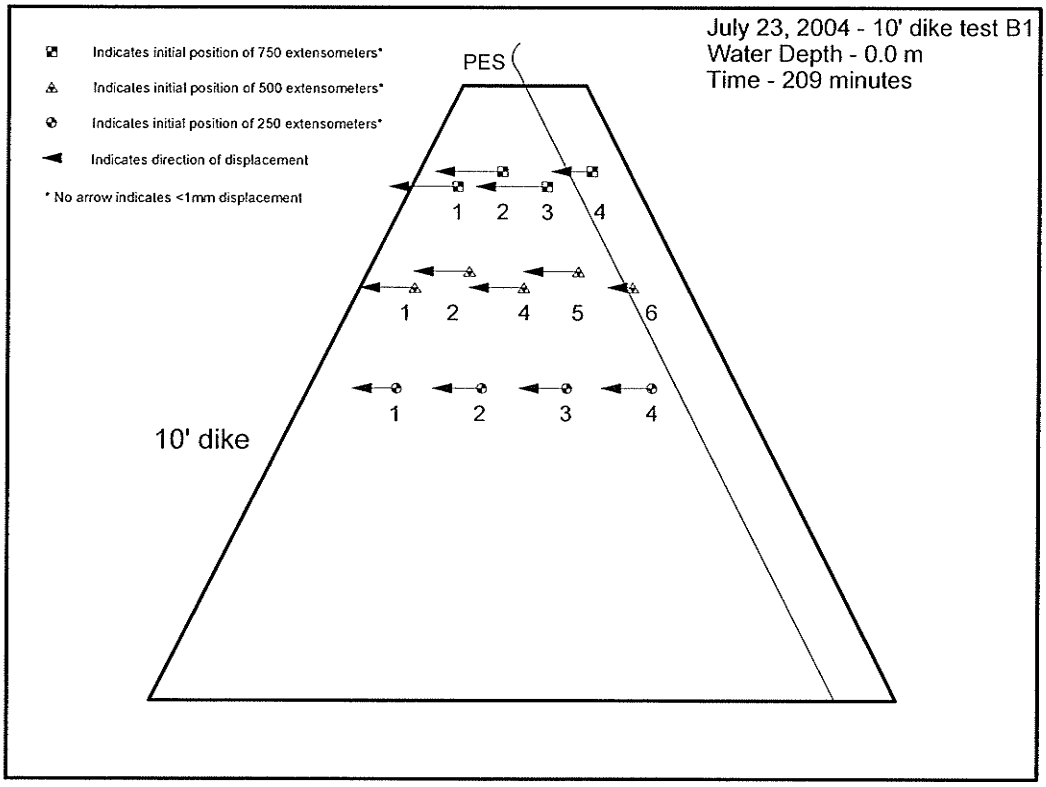

Figure 5.16 – Displacement of B1 Extensometers at End of Test.

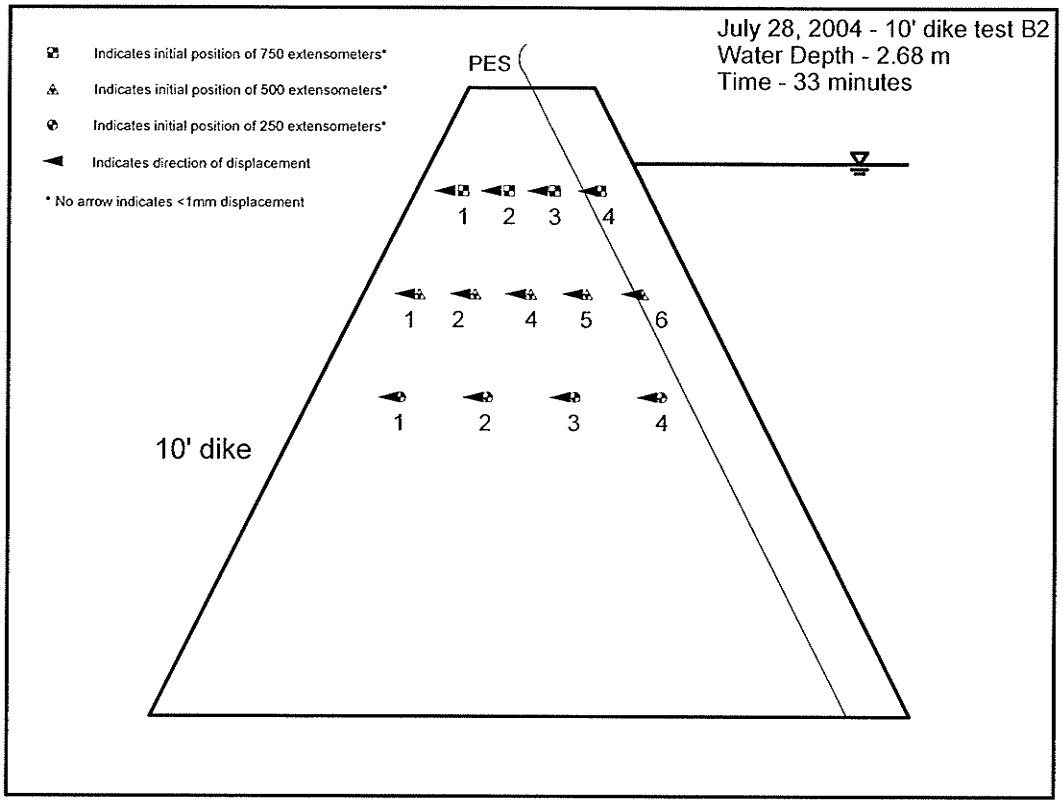

Figure 5.17 – Displacement of B2 Extensometers at Peak Water Level.

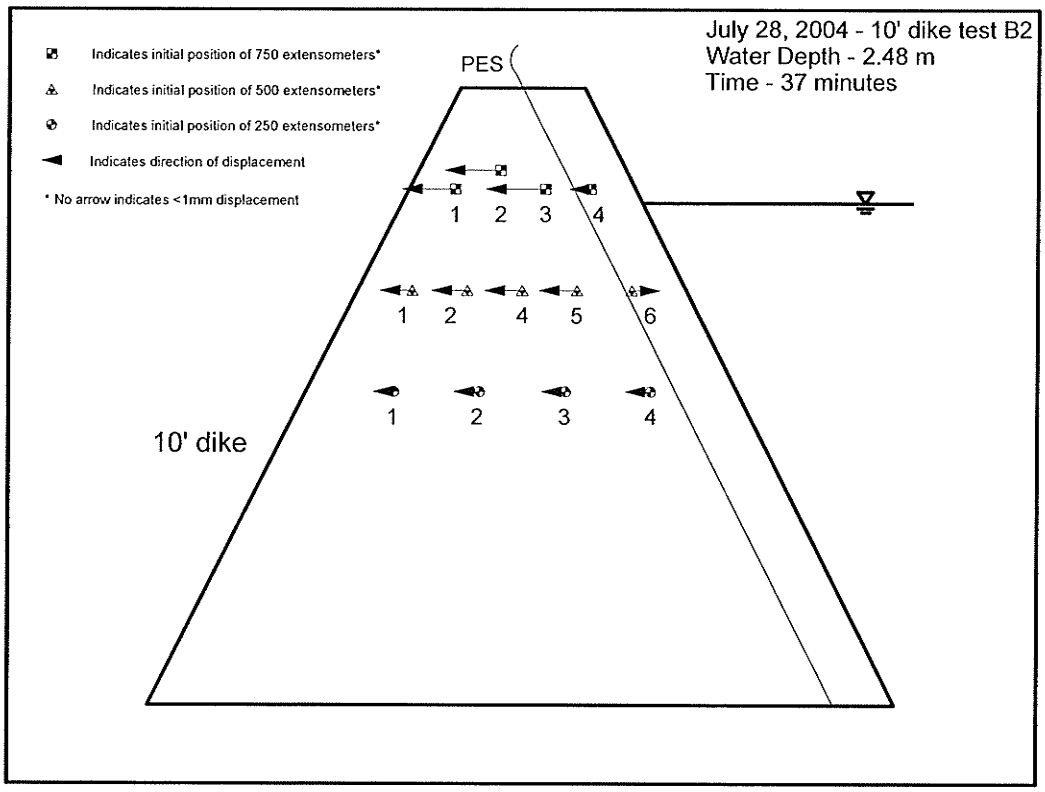

Figure 5.18 – Displacement of B2 Extensometers just after Peak Water Level.

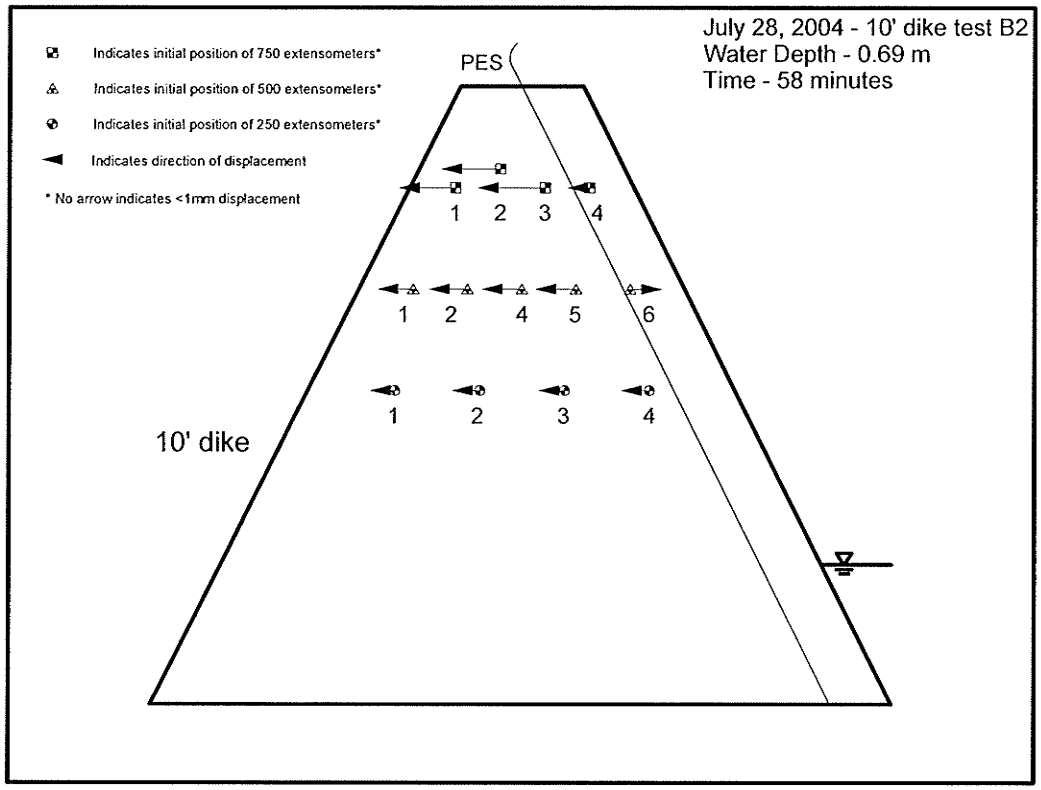

Figure 5.19 – Displacement of B2 Extensometers at Final Water Reading.

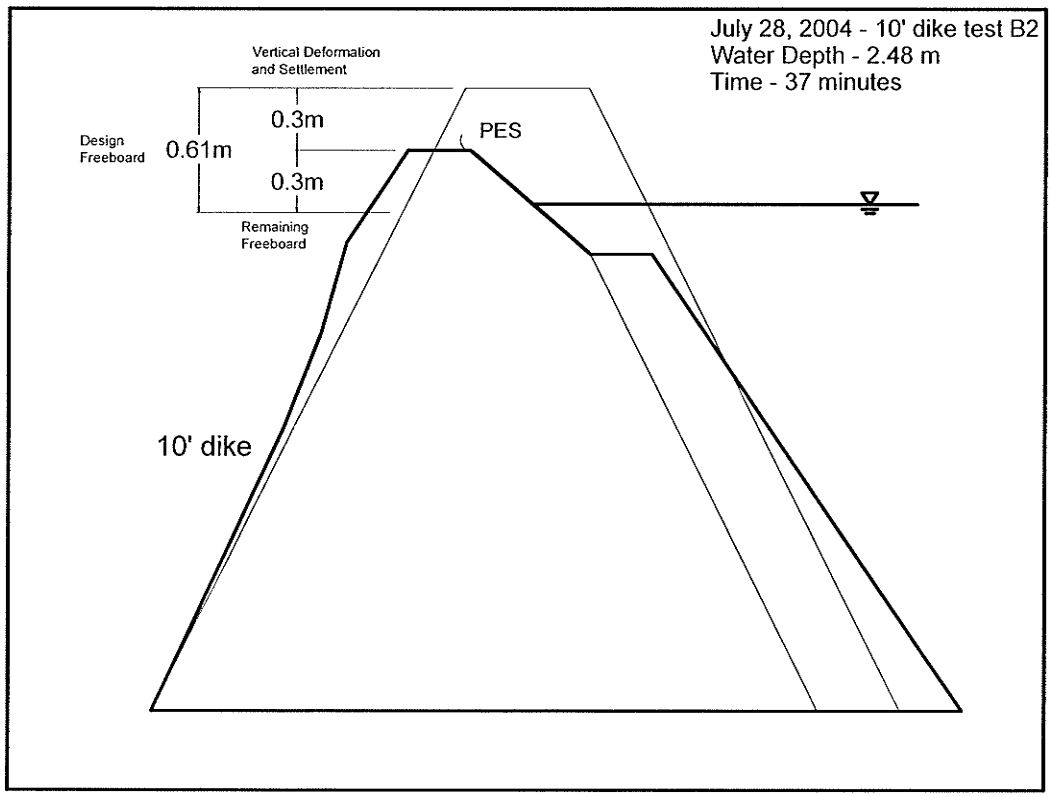

Figure 5.20 – Deformation at Centre-line of Dike B2 just after Peak Water Level.

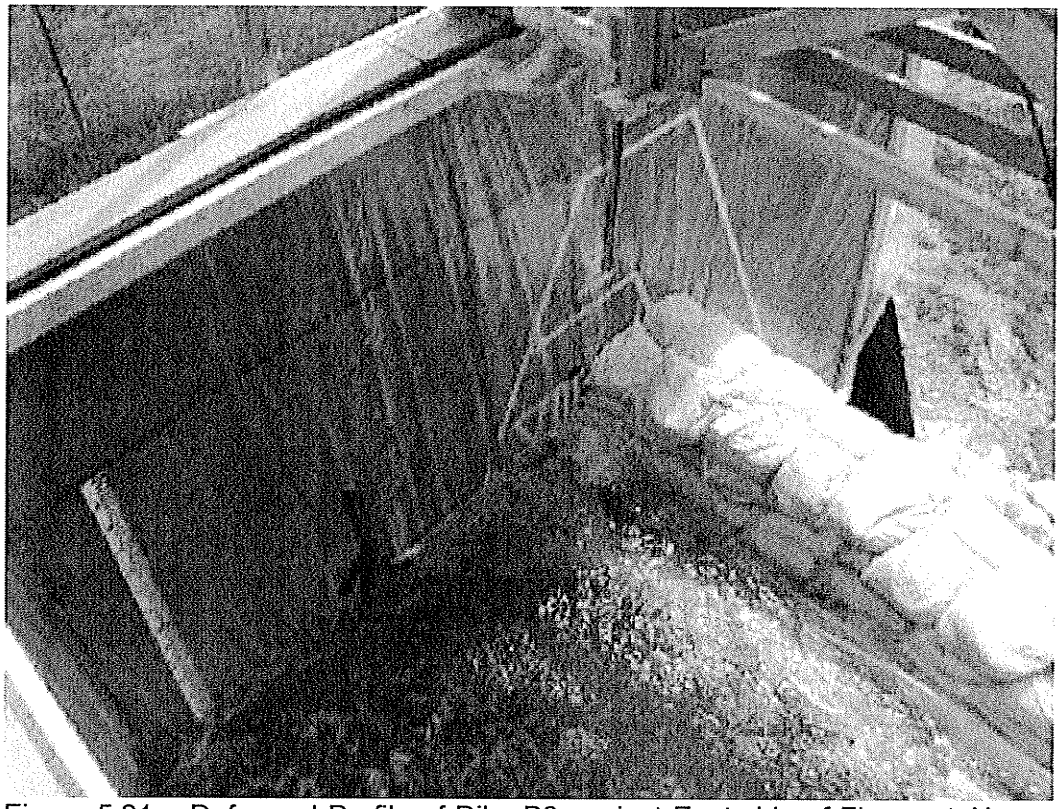

Figure 5.21 – Deformed Profile of Dike B2 against East side of Flume at Above Design Loading.

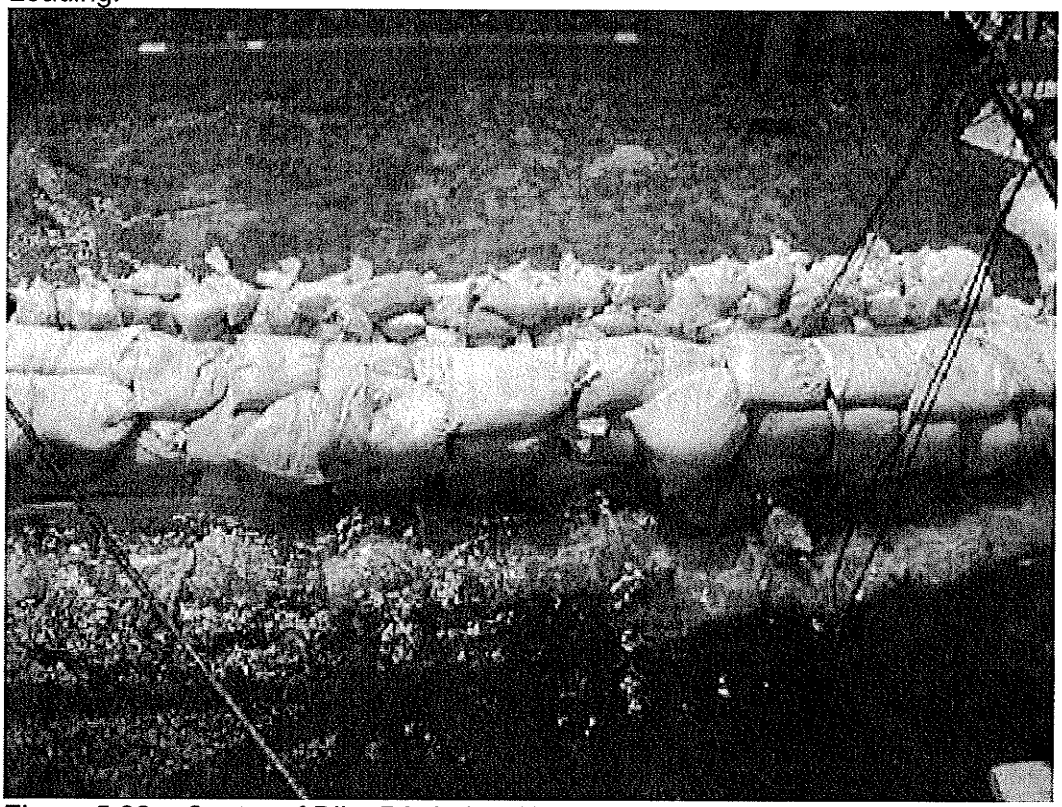

Figure 5.22 – Centre of Dike B2 during Above Design Loading (note submerged bags on wet side).

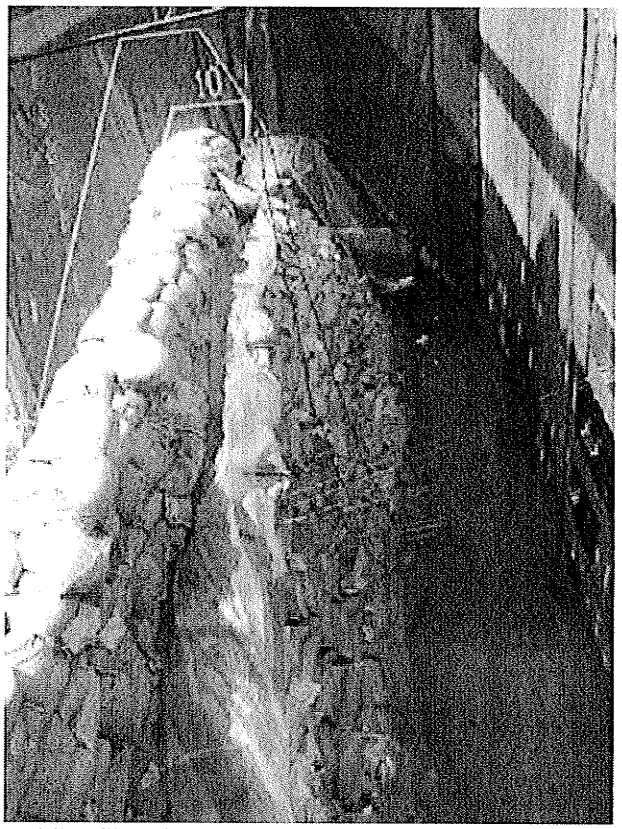

Figure 5.23 – Deformed Profile of Dike B2 against West side of Flume during Unloading.

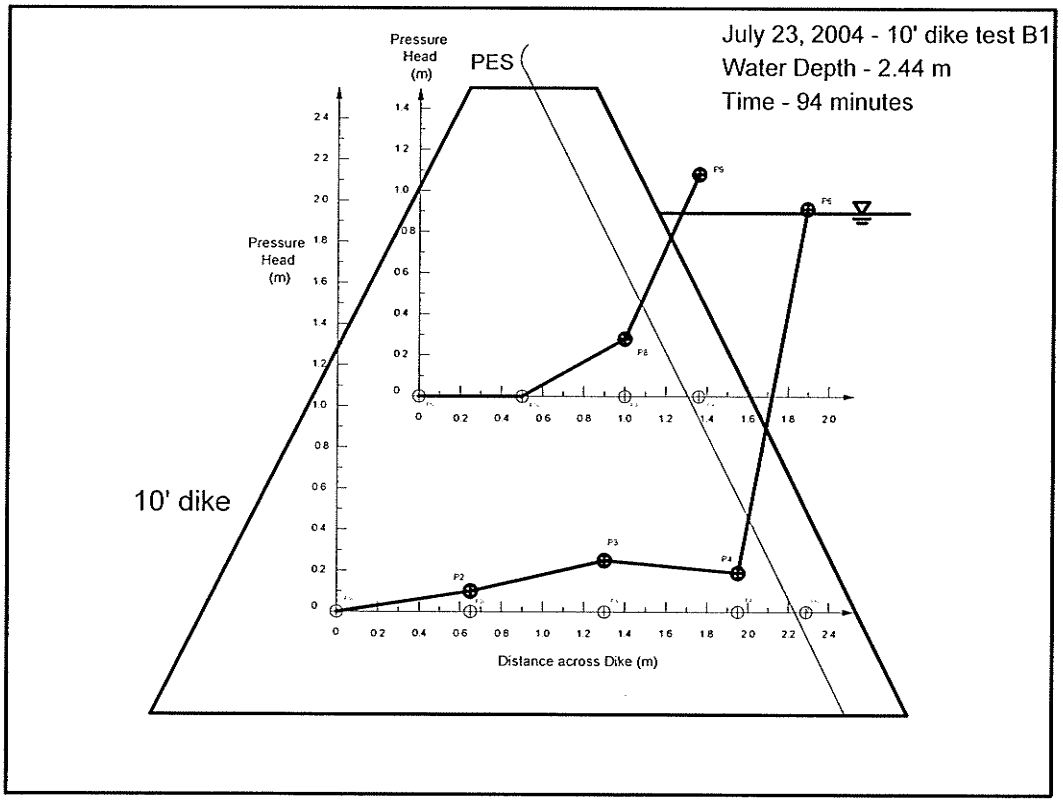

Figure 5.24 – Measured Pressure Head through Dike B1 at Design Water Depth.

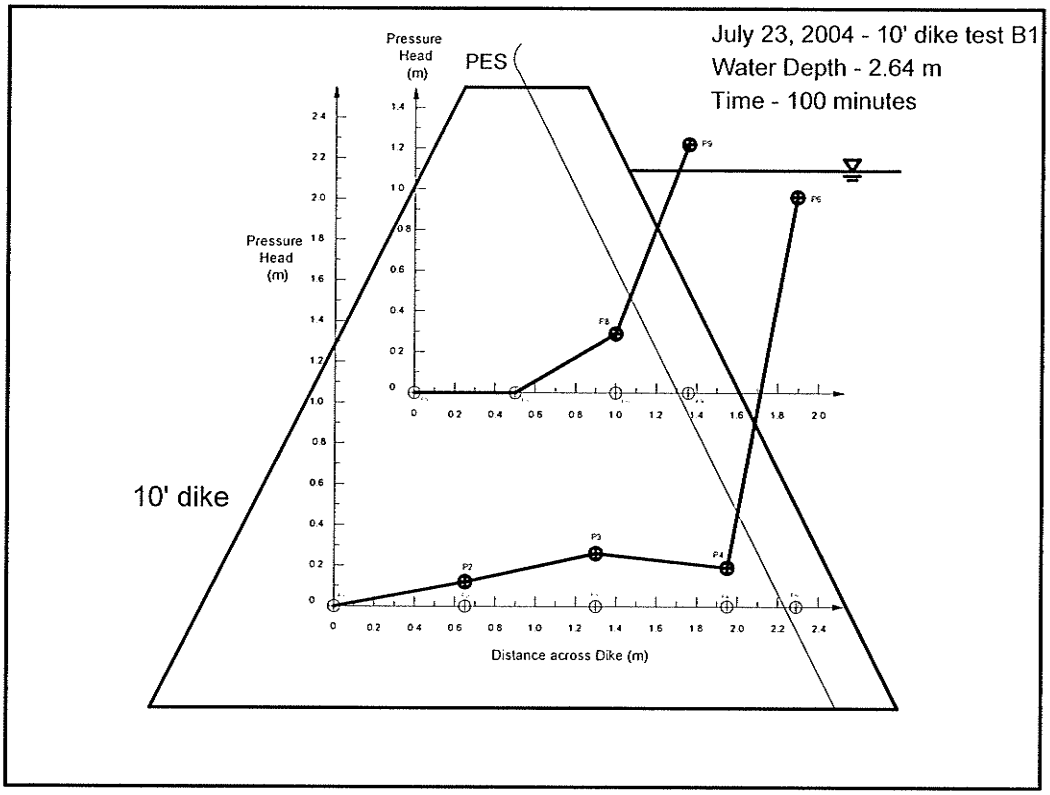

Figure 5.25 – Measured Pressure Head through Dike B1 at Peak Water Depth.

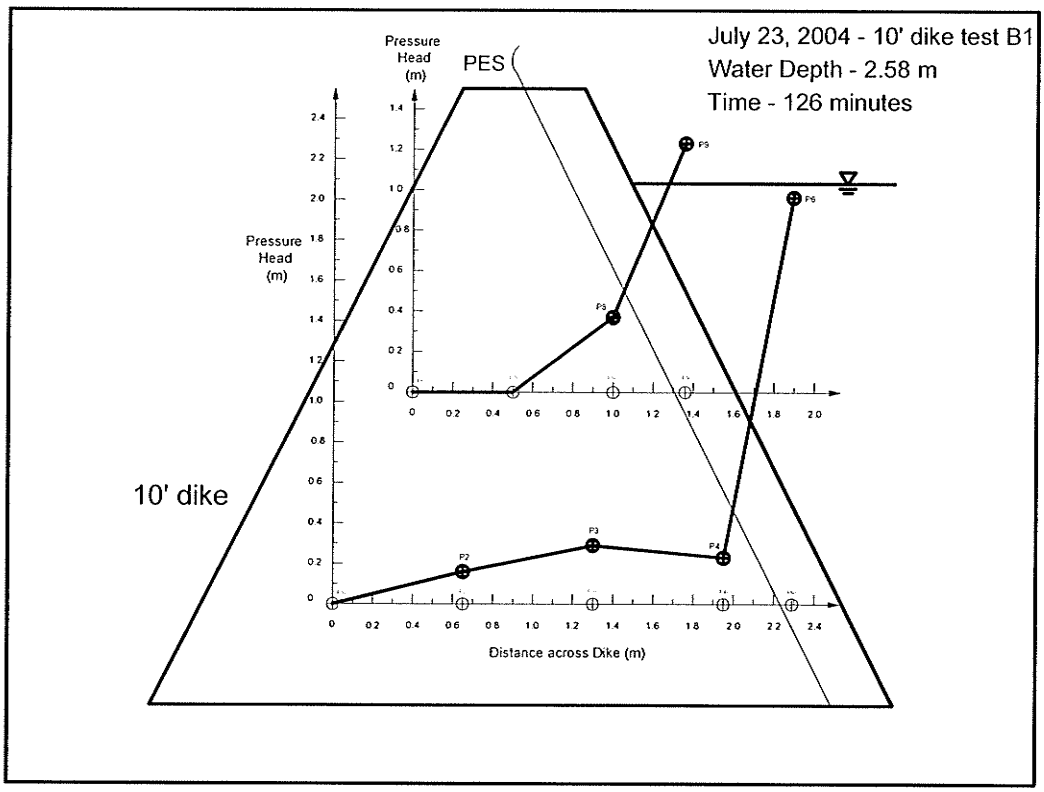

Figure 5.26 – Measured Pressure Head through Dike B1 during Peak Water Loading.

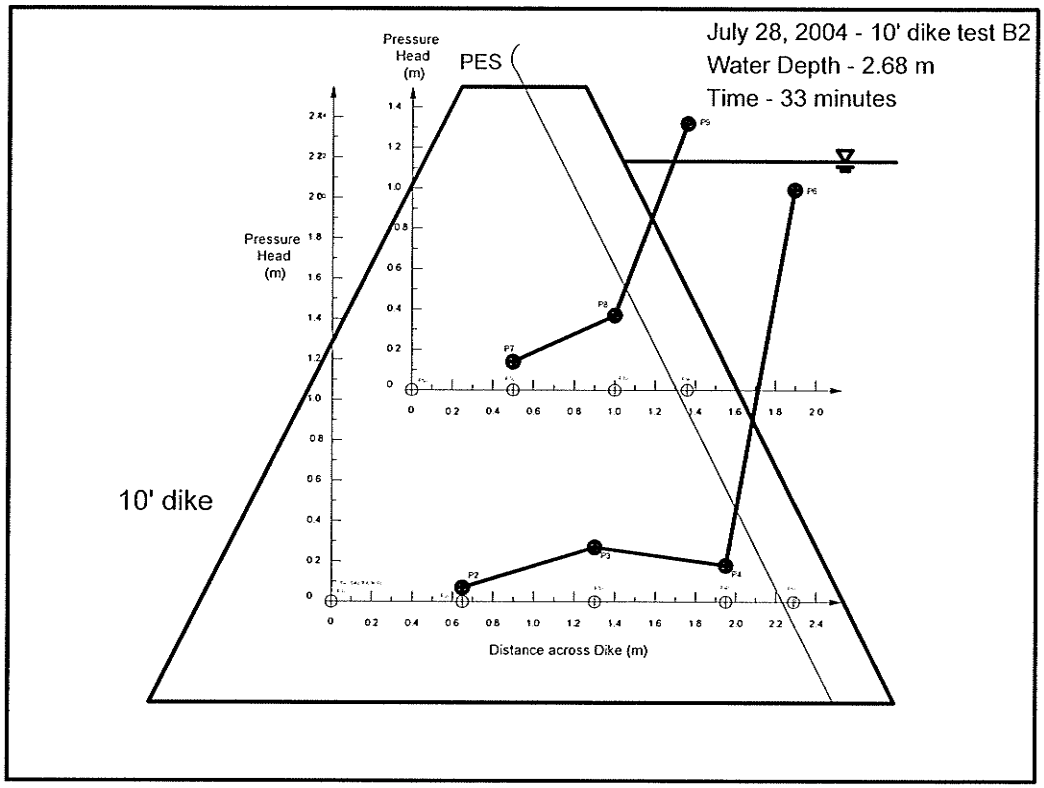

Figure 5.27 – Measured Pressure Head through Dike B2 at Peak Water Depth.

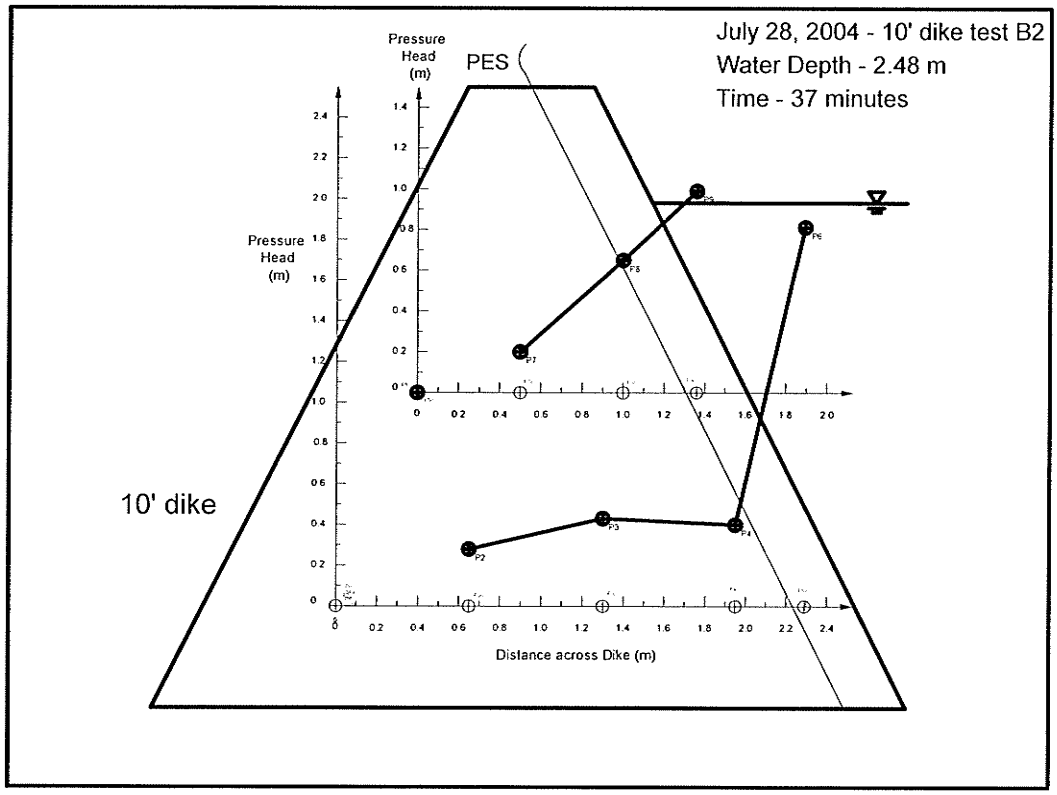

Figure 5.28 – Measured Pressure Head through Dike B2 just after Peak Water Depth.

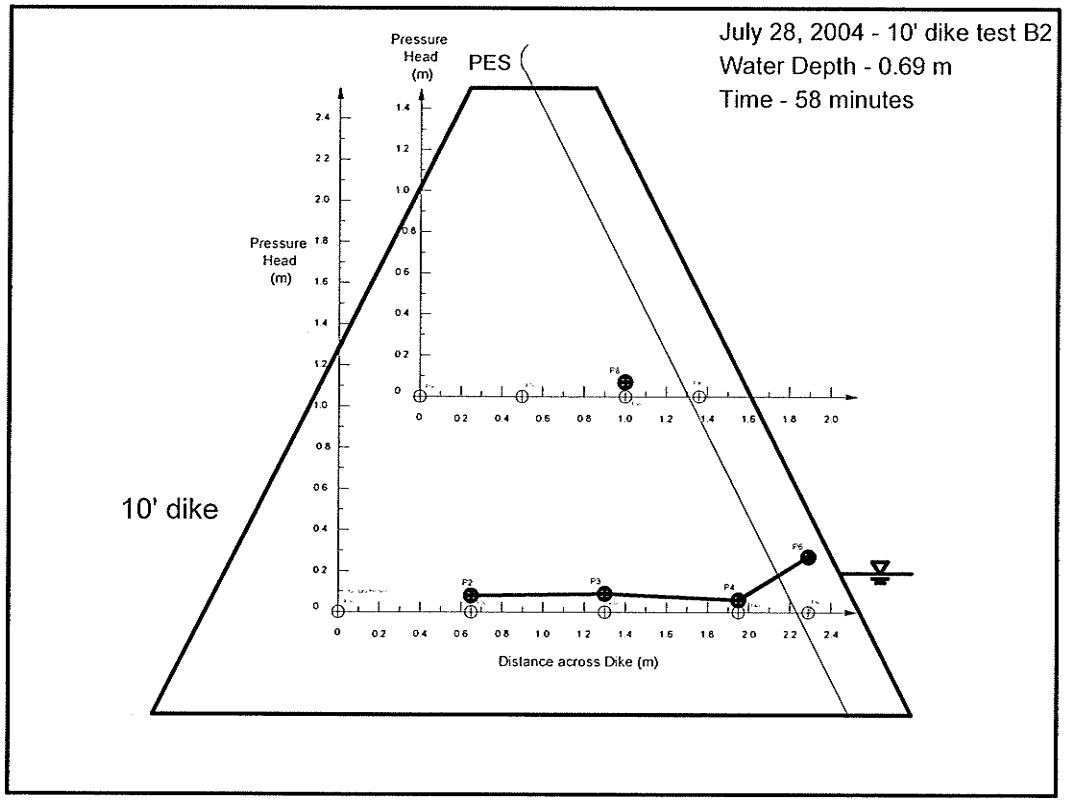

Figure 5.29 – Measured Pressure Head through Dike B2 while Emptying Flume.

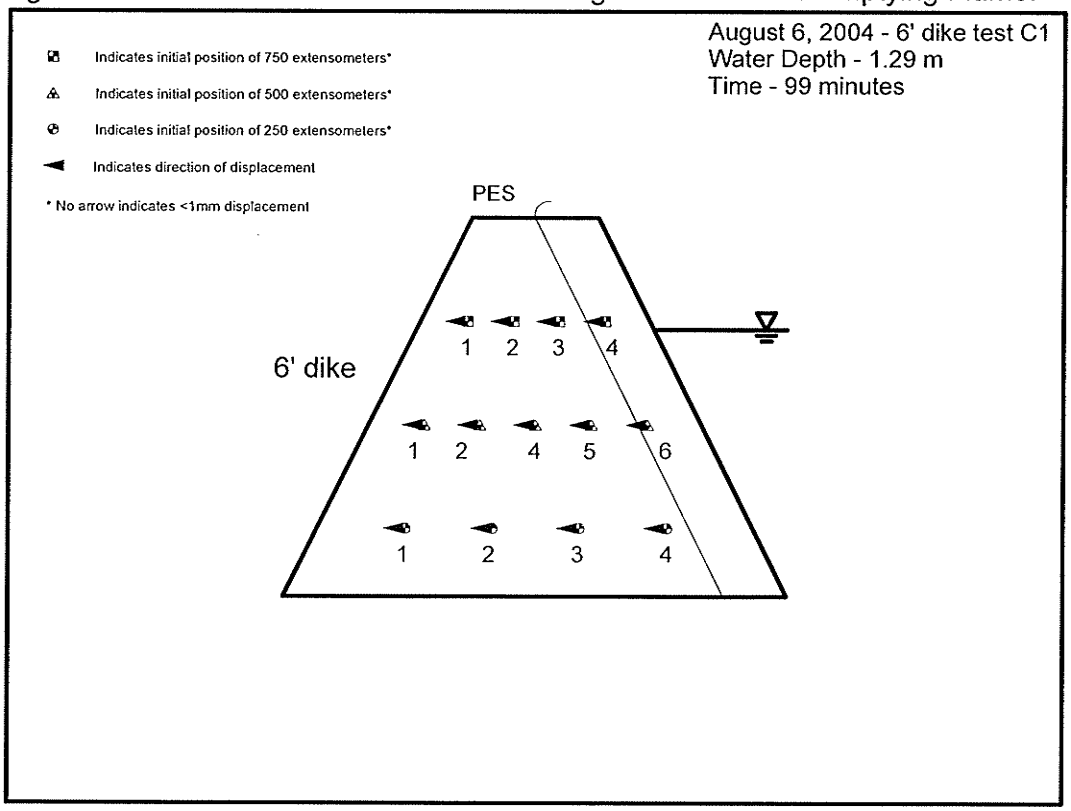

Figure 5.30 – Displacement of C1 Extensometers at Design Water Level.

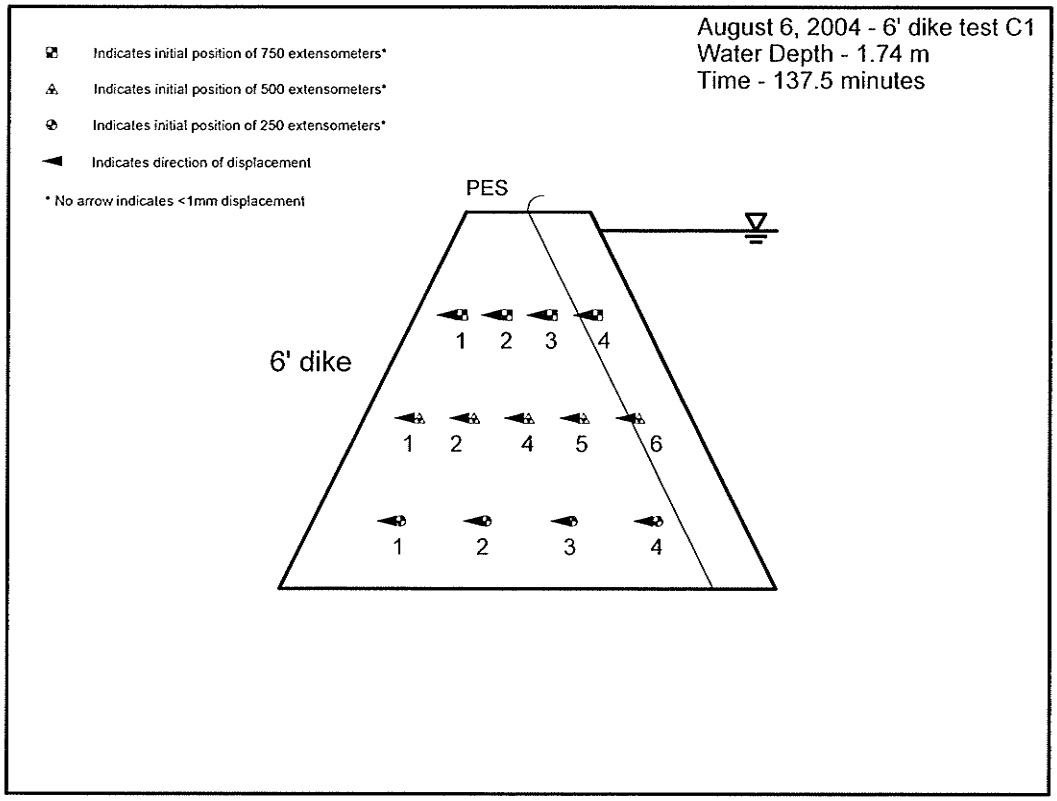

Figure 5.31 – Displacement of C1 Extensometers at Peak Water Level.

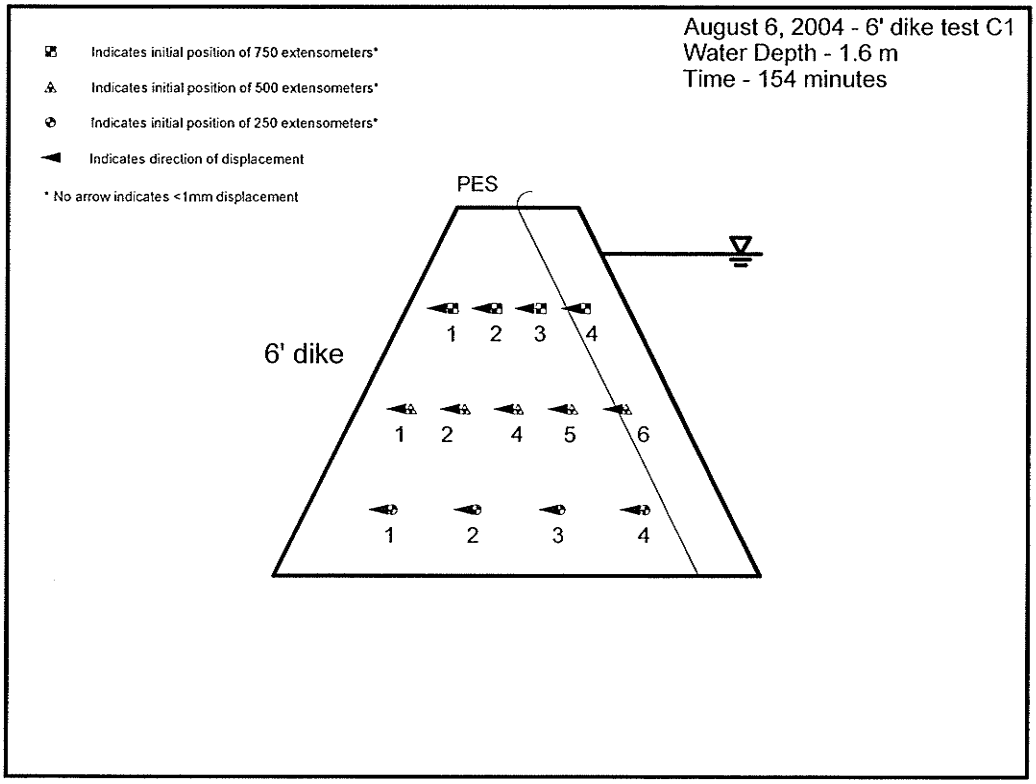

Figure 5.32 – Displacement of C1 Extensometers at Beginning of Unloading.

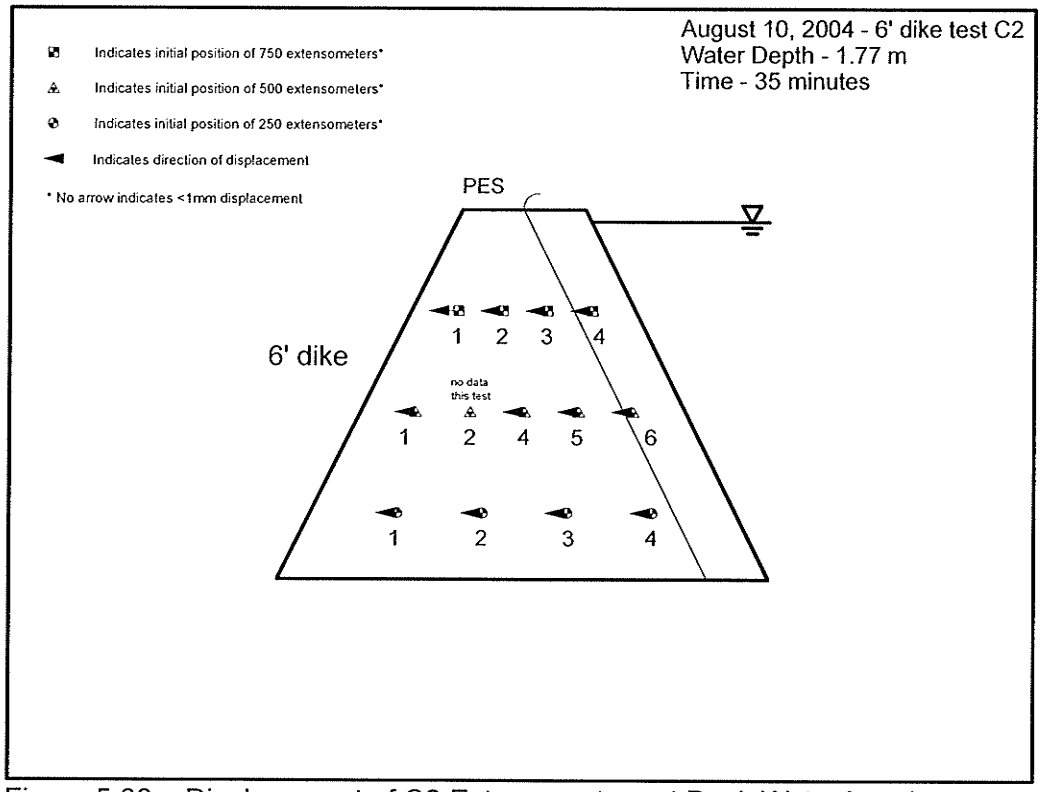

Figure 5.33 – Displacement of C2 Extensometers at Peak Water Level.

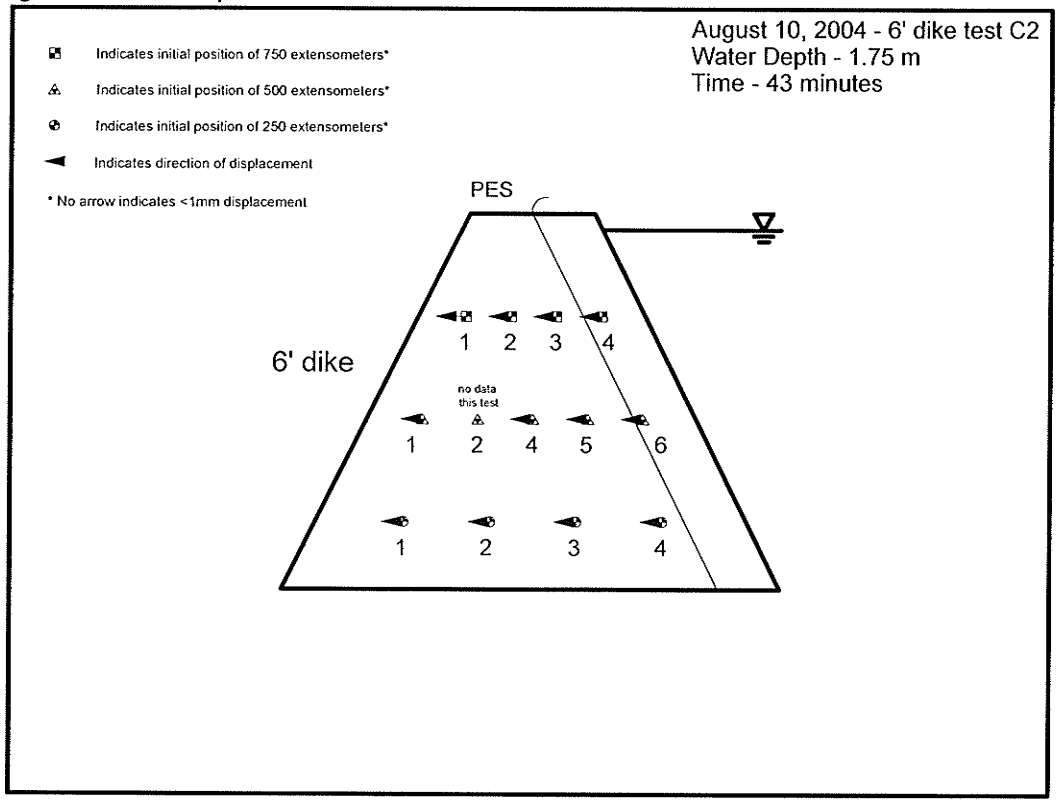

Figure 5.34 – Displacement of C2 Extensometers after 30 min at Peak Water Level.

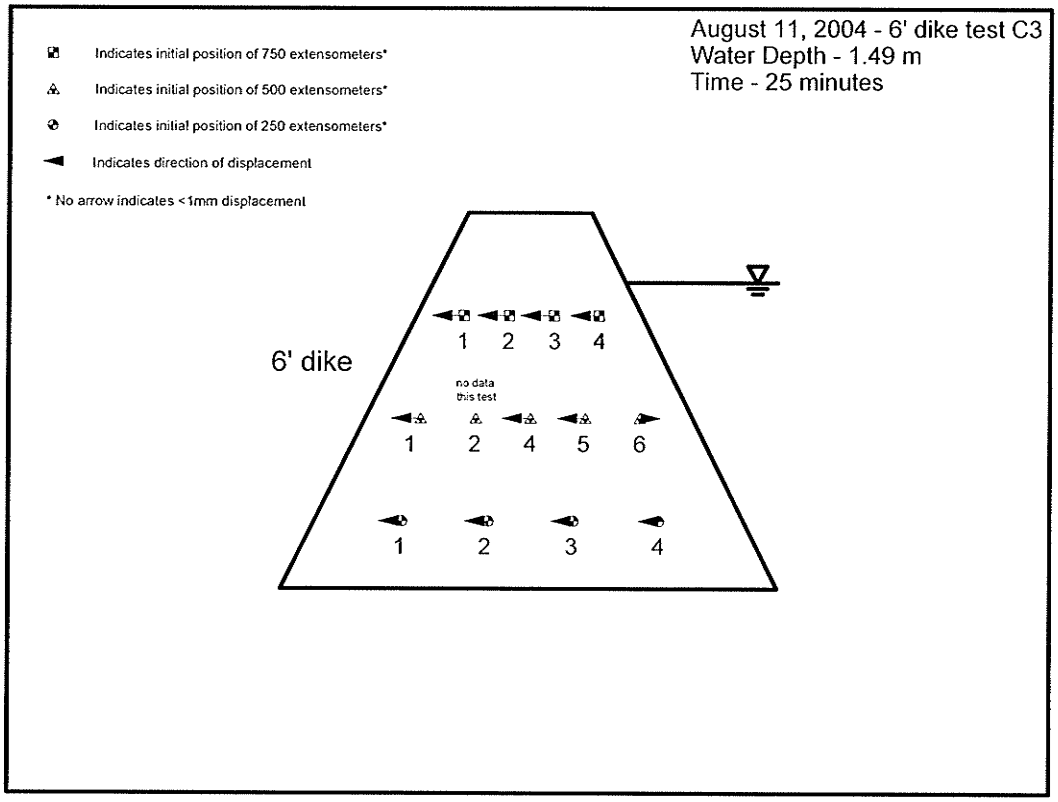

Figure 5.35 – Displacement of C3 Extensometers at Peak Water Level.

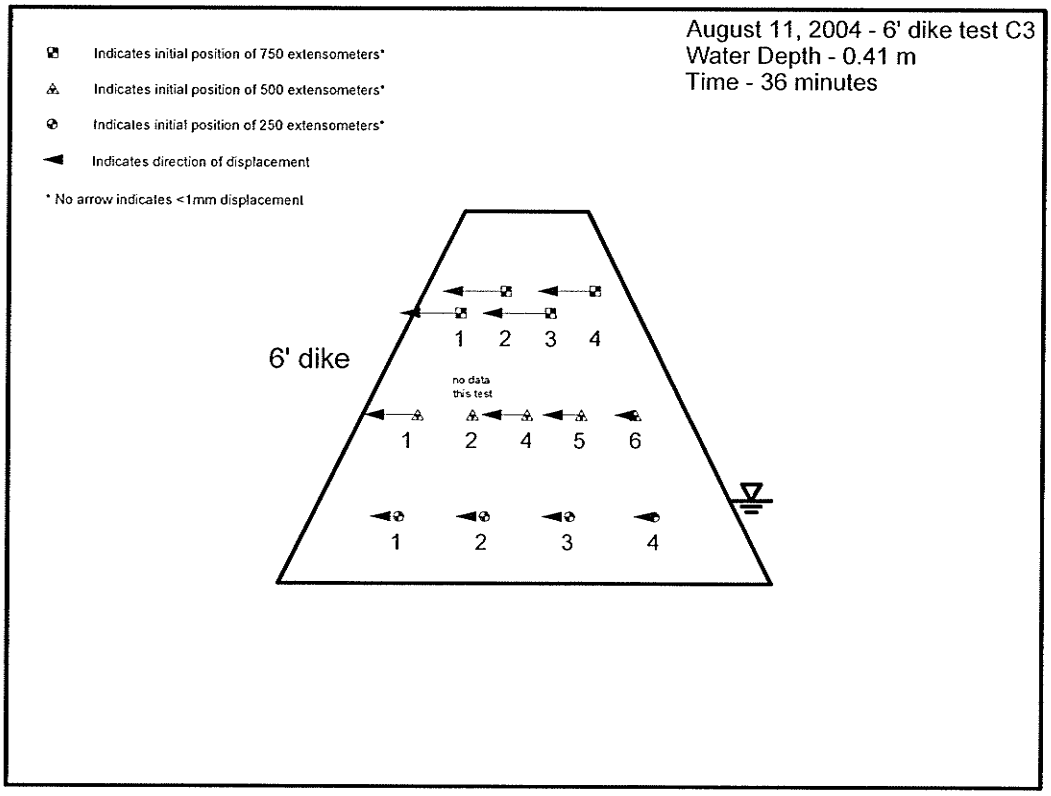

Figure 5.36 – Displacement of C3 Extensometers after Failure.

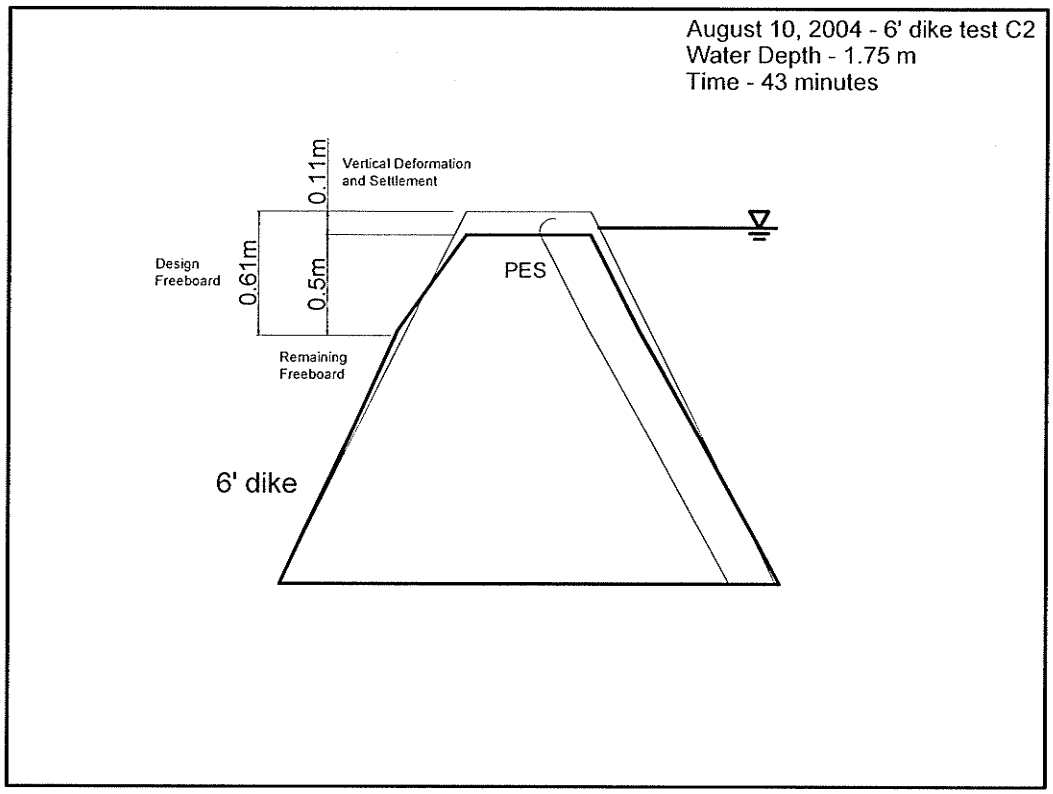

Figure 5.37 – Deformation at Centre-line of Dike C2 during Overtopping Water Levels.

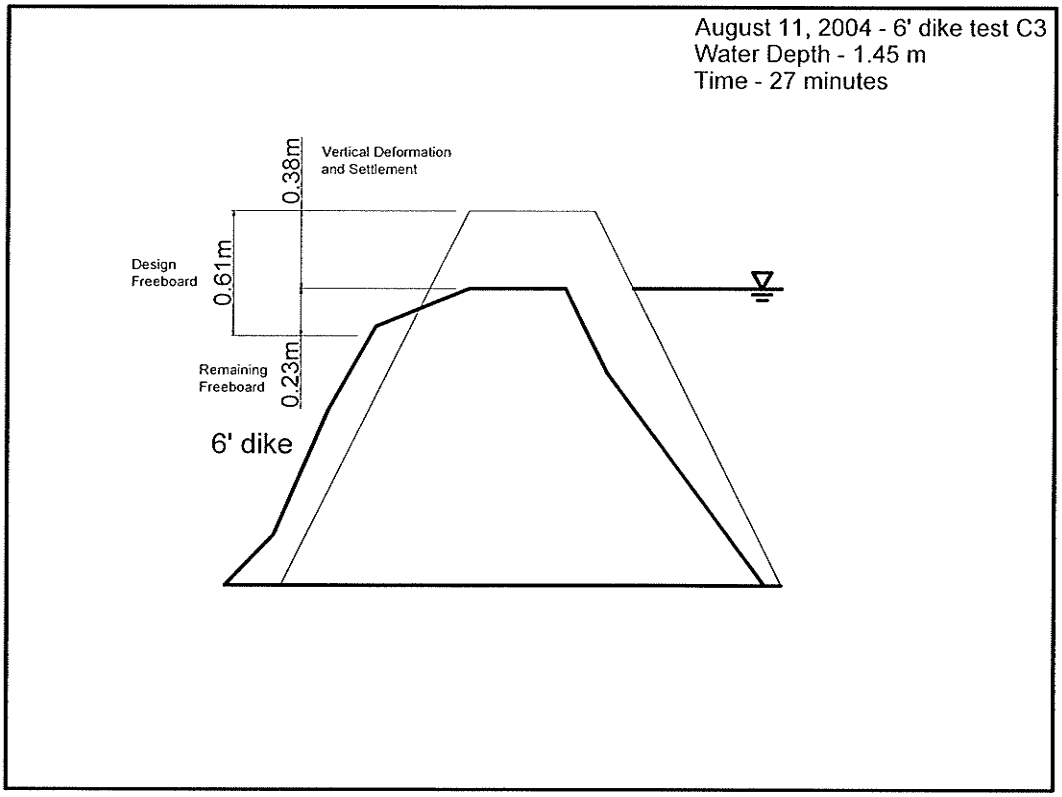

Figure 5.38 – Deformation at Centre-line of Dike C3 after Failure.

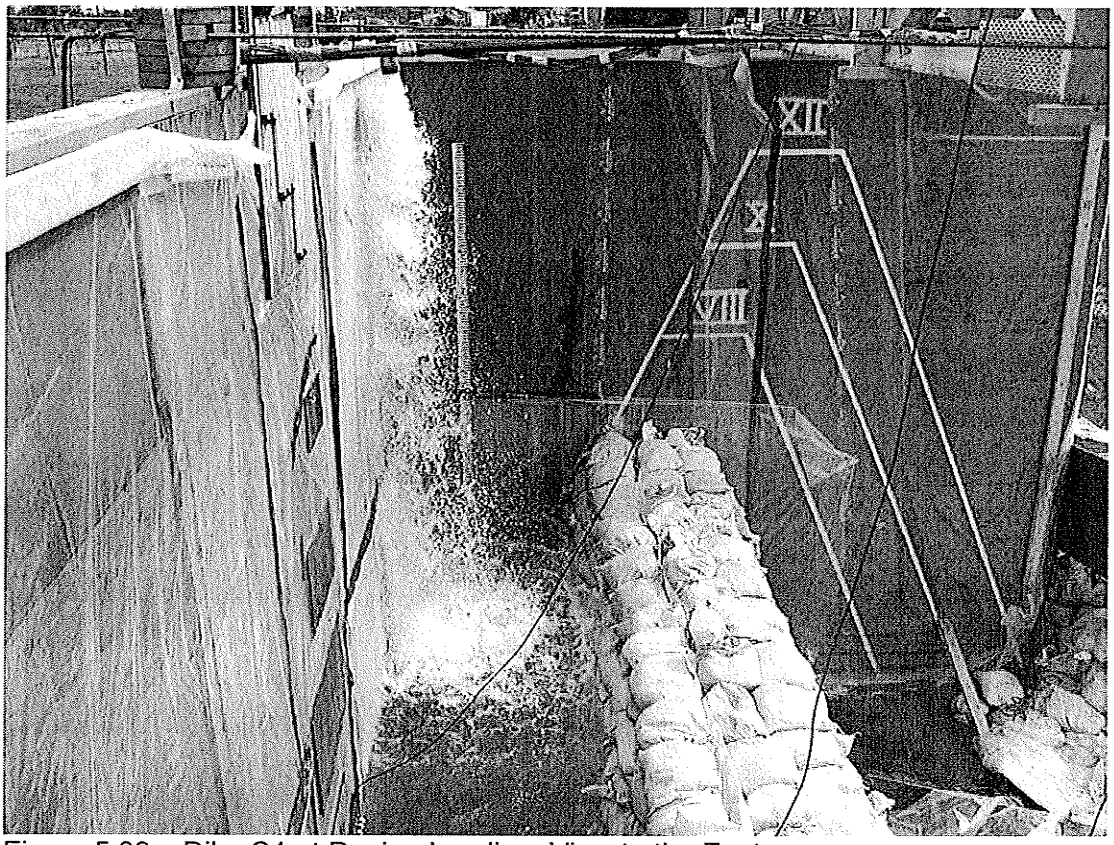

Figure 5.39 – Dike C1 at Design Loading, View to the East.

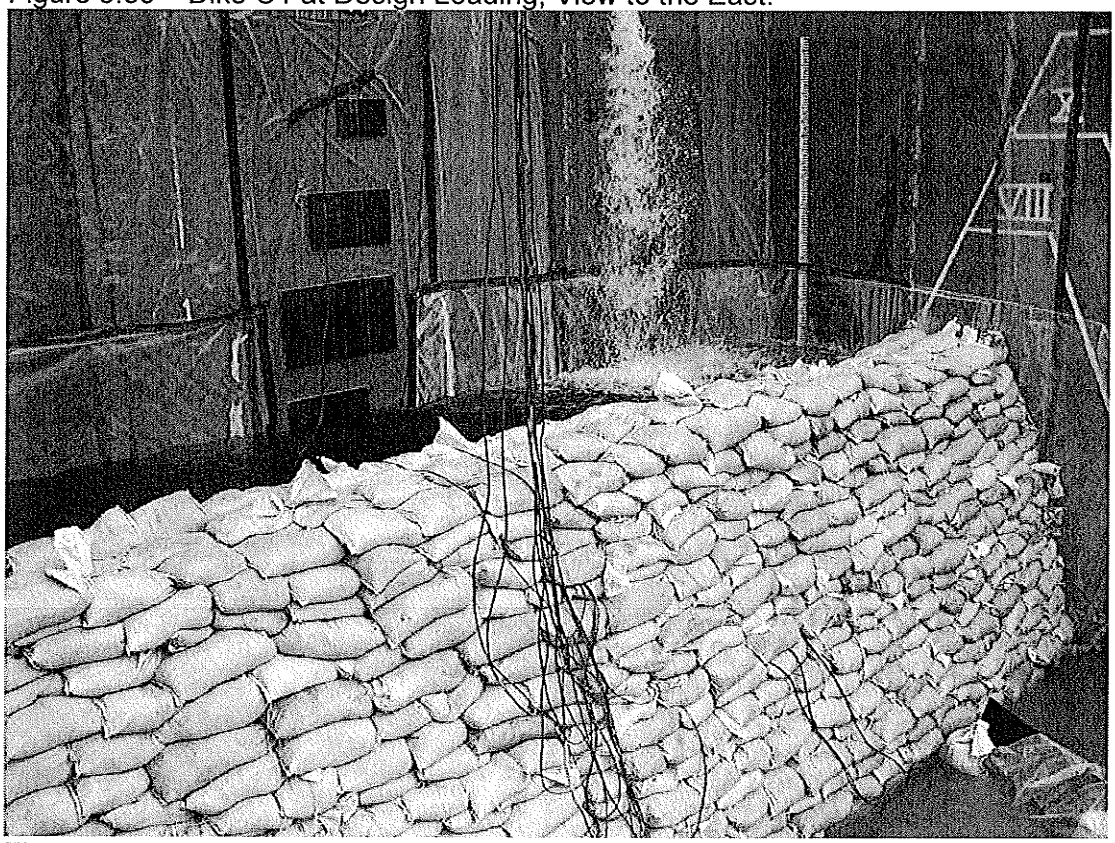

Figure 5.40 – Dike C1 at Above Design Loading, View to the East.

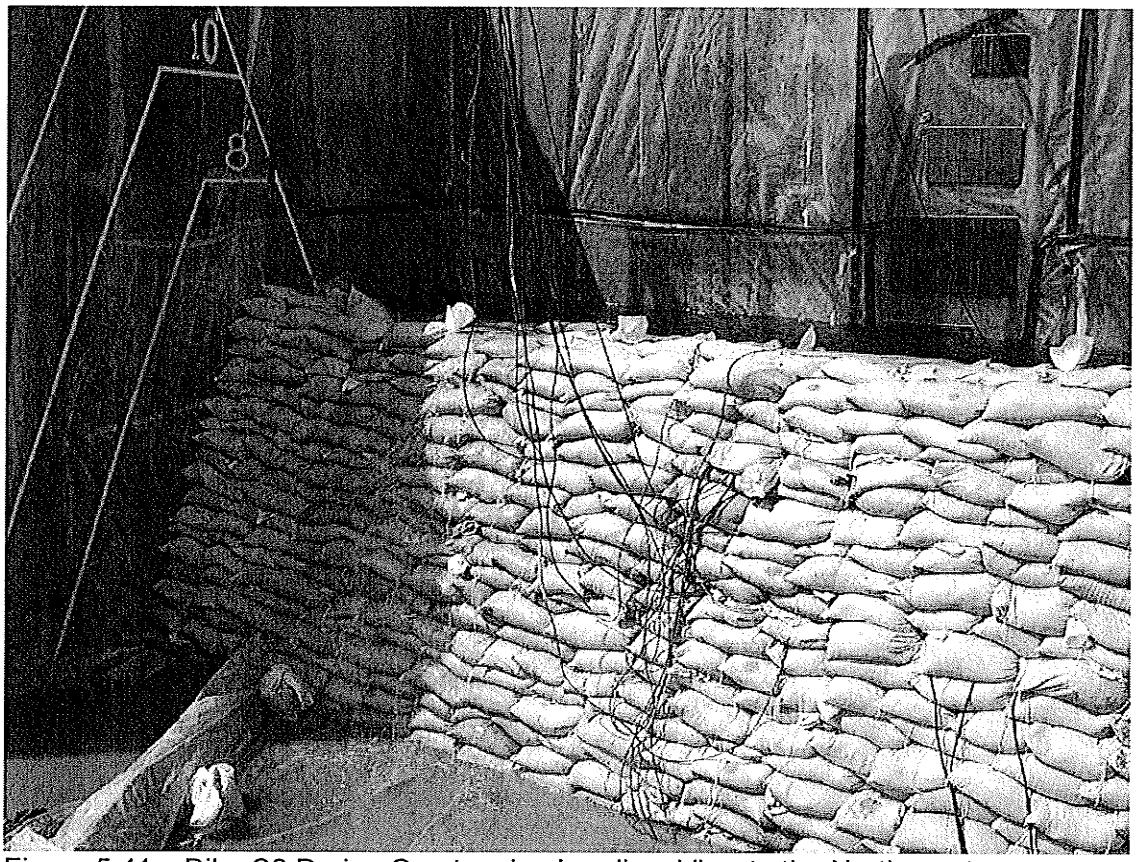

Figure 5.41 – Dike C2 During Overtopping Loading, View to the North-west.

Figure 5.42 – Dike C3 Final Deformed Shape, Front View.

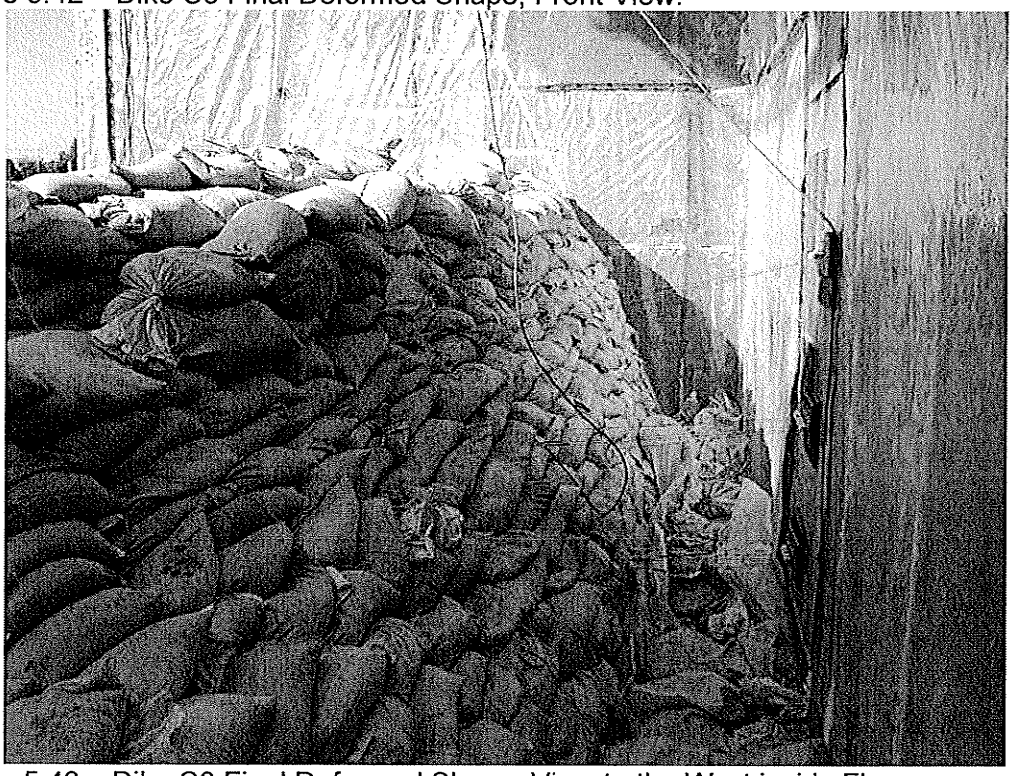

Figure 5.43 – Dike C3 Final Deformed Shape, View to the West inside Flume.

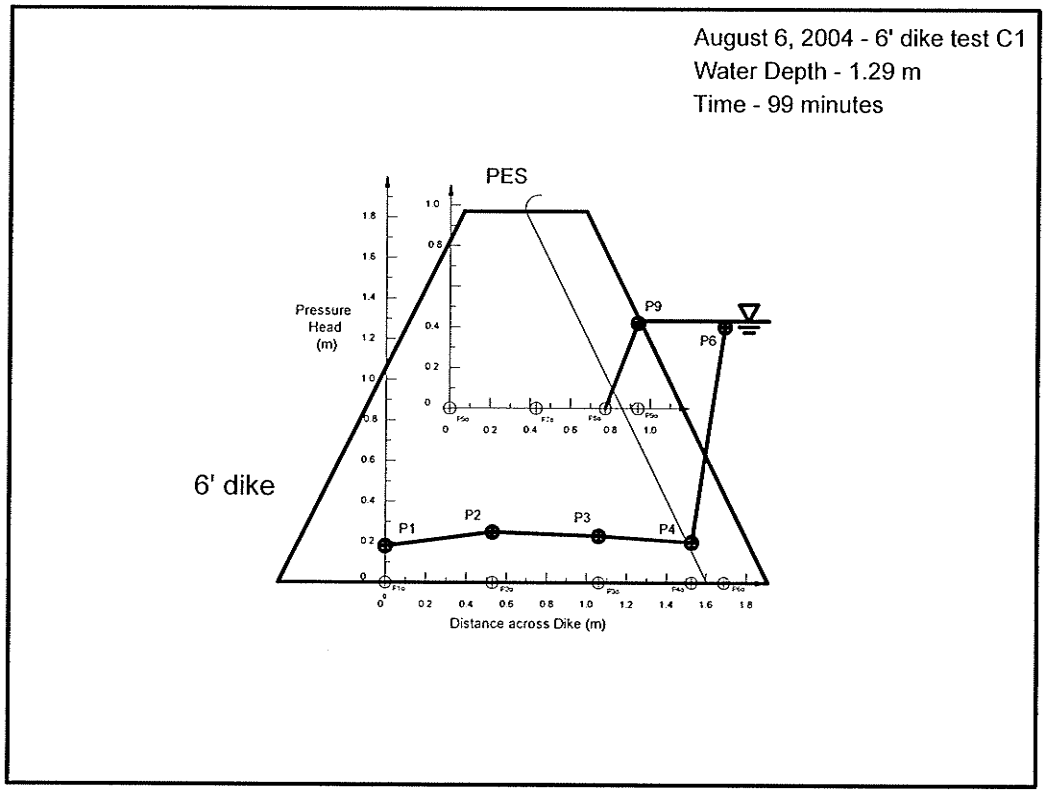

Figure 5.44 – Measured Pressure Head through Dike C1 at Design Water Depth.

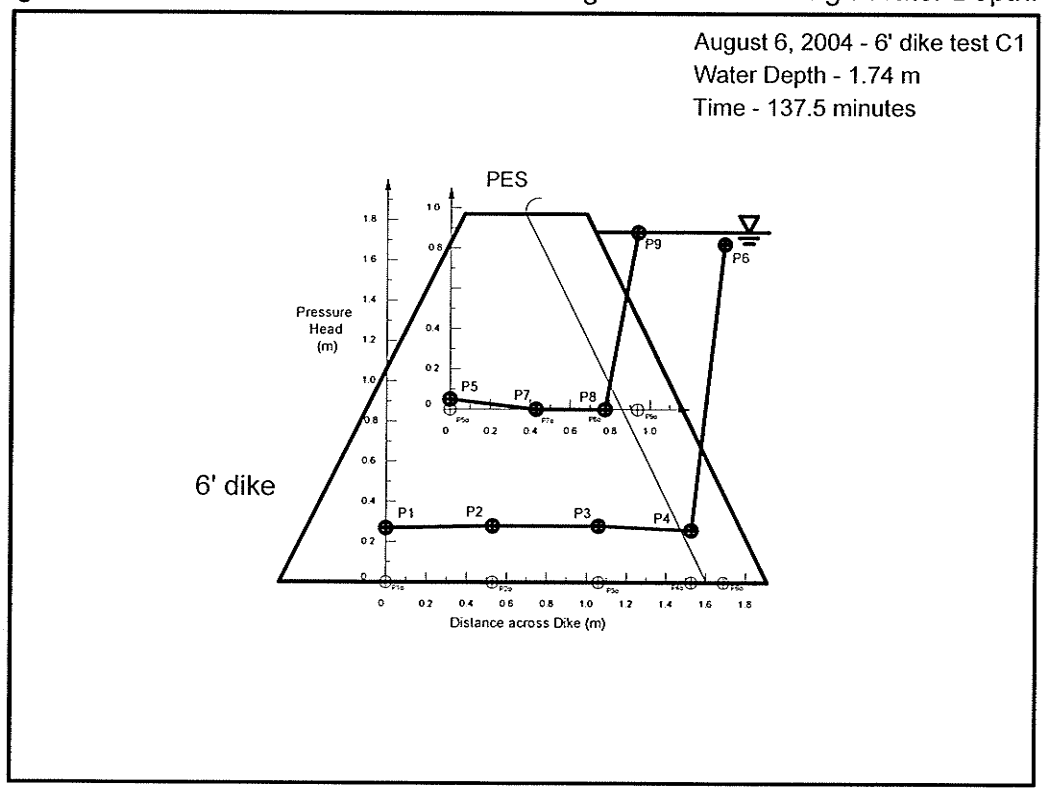

Figure 5.45 – Measured Pressure Head through Dike C1 at Peak Water Depth.

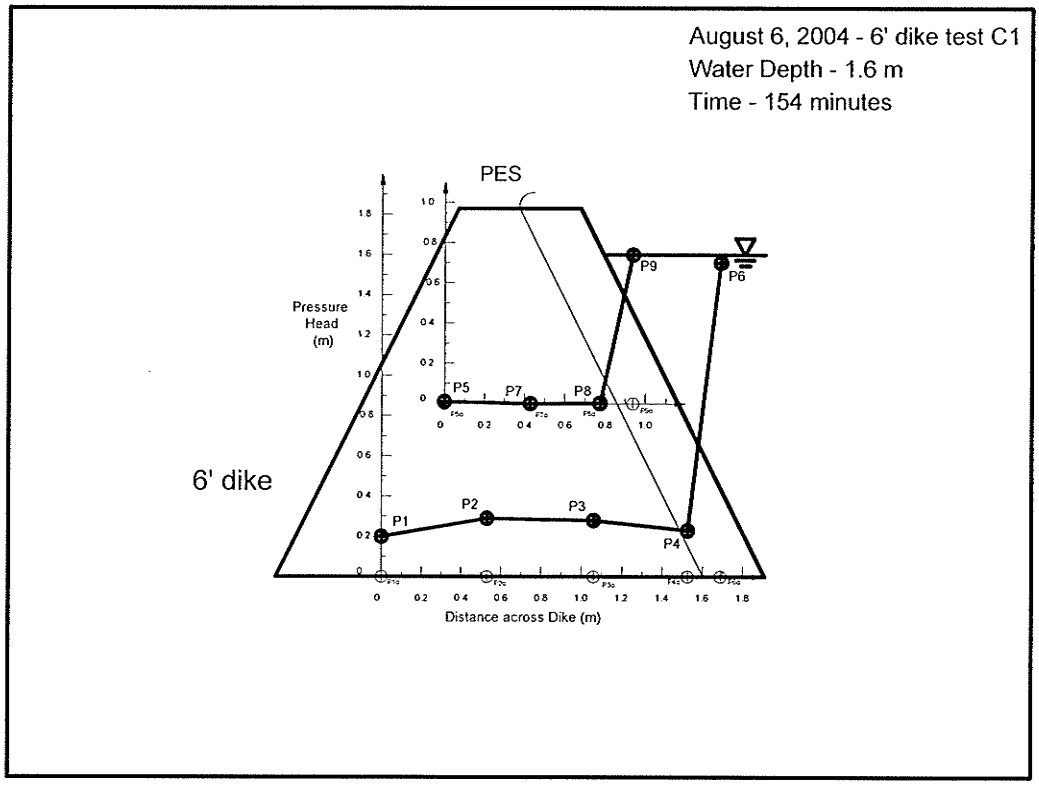

Figure 5.46 – Measured Pressure Head through Dike C1 at Beginning of Unloading.

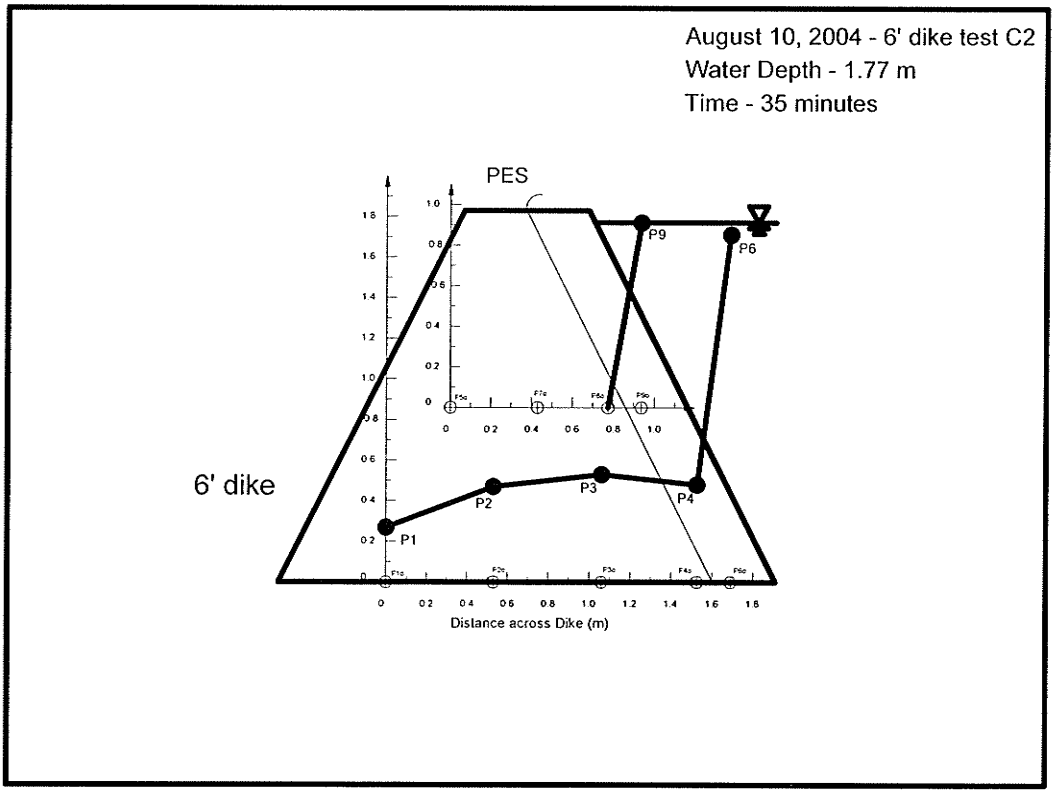

Figure 5.47 – Measured Pressure Head through Dike C2 at Peak Water Level.

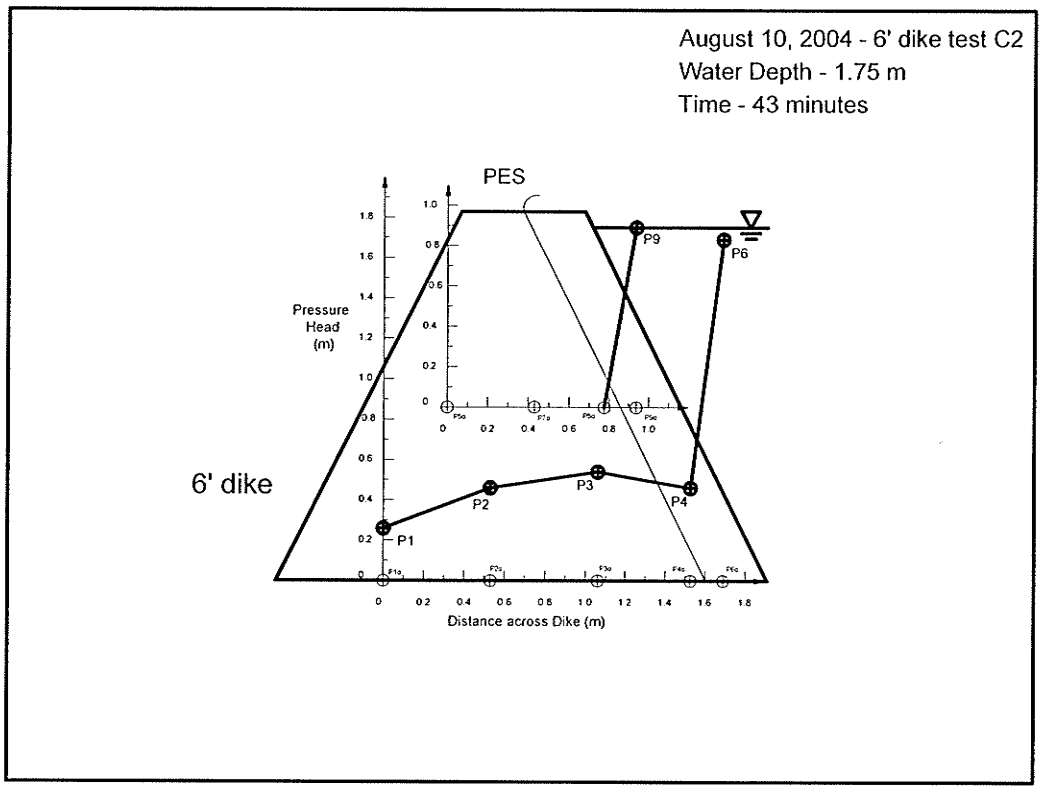

Figure 5.48 – Measured Pressure Head through Dike C2 after 30 min of Overtopping.

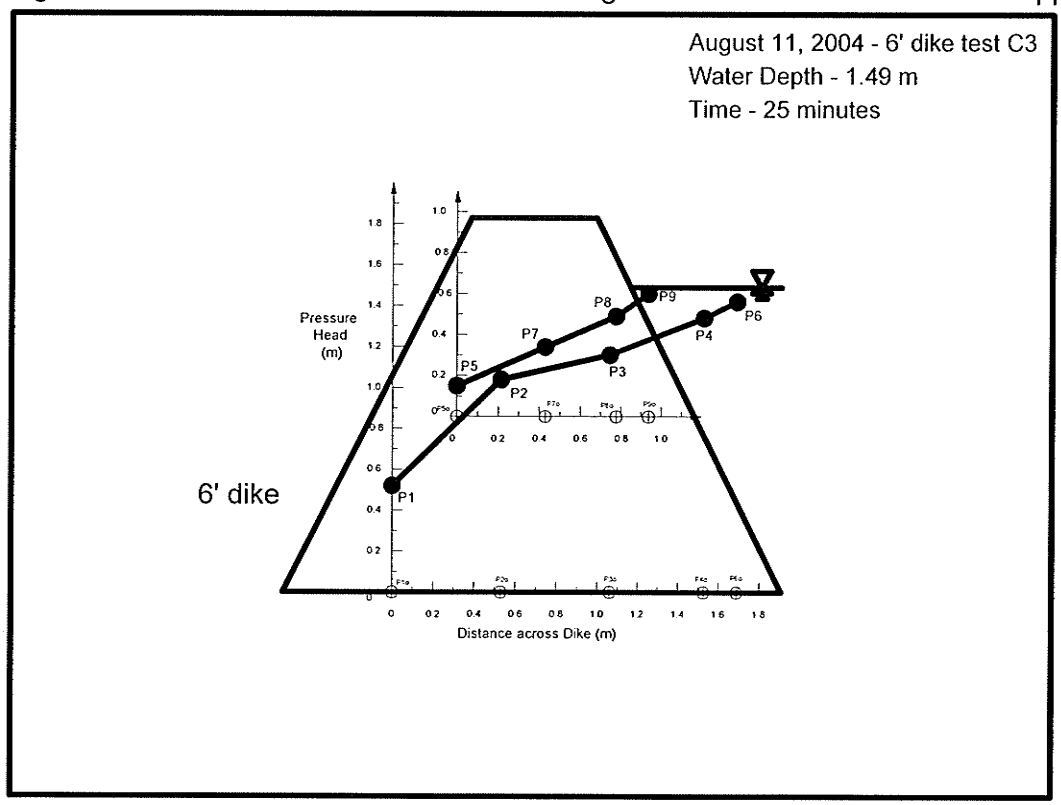

Figure 5.49 – Measured Pressure Head through Dike C3 at Peak Water Level.

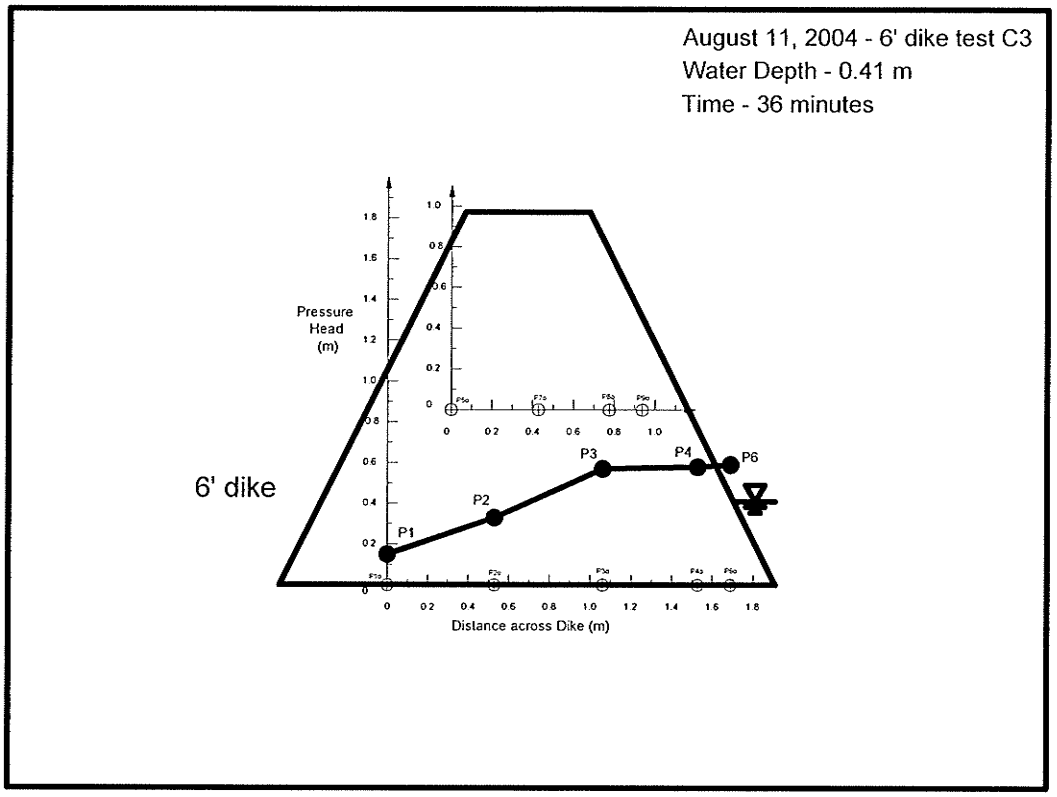

Figure 5.50 – Measured Pressure Head through Dike C3 after Failure.

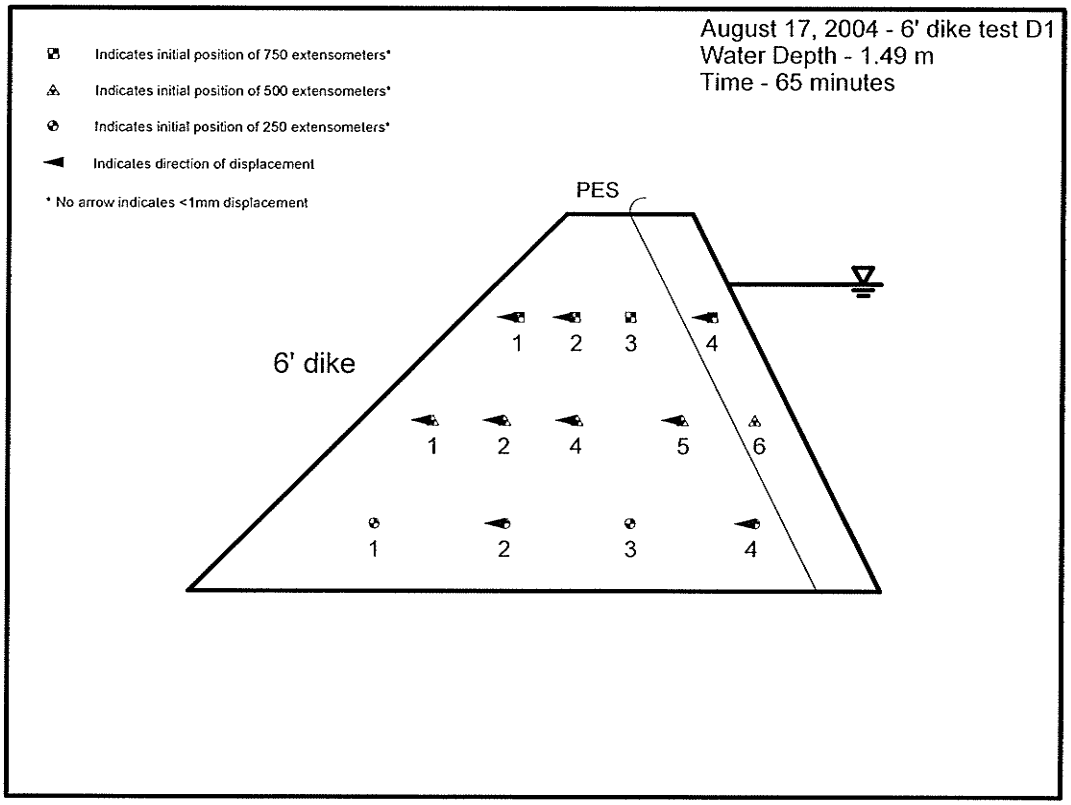

Figure 5.51 – Displacement of D1 Extensometers at Design Water Depth.

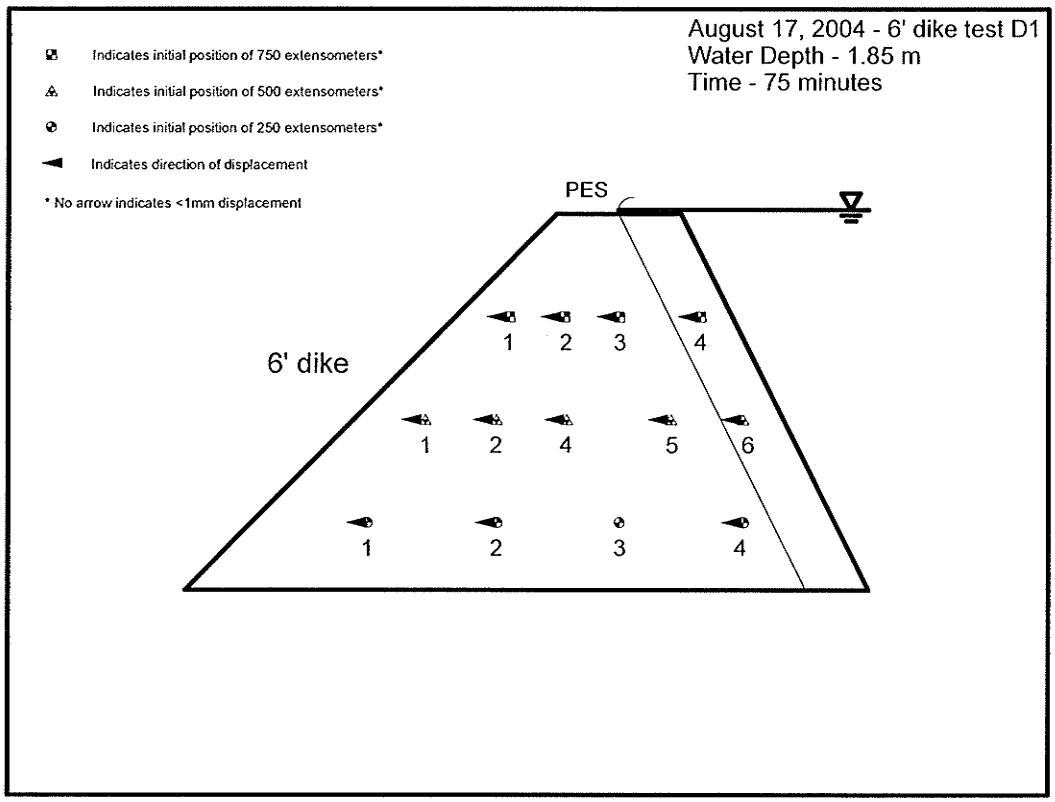

Figure 5.52 – Displacement of D1 Extensometers at Peak Water Depth.

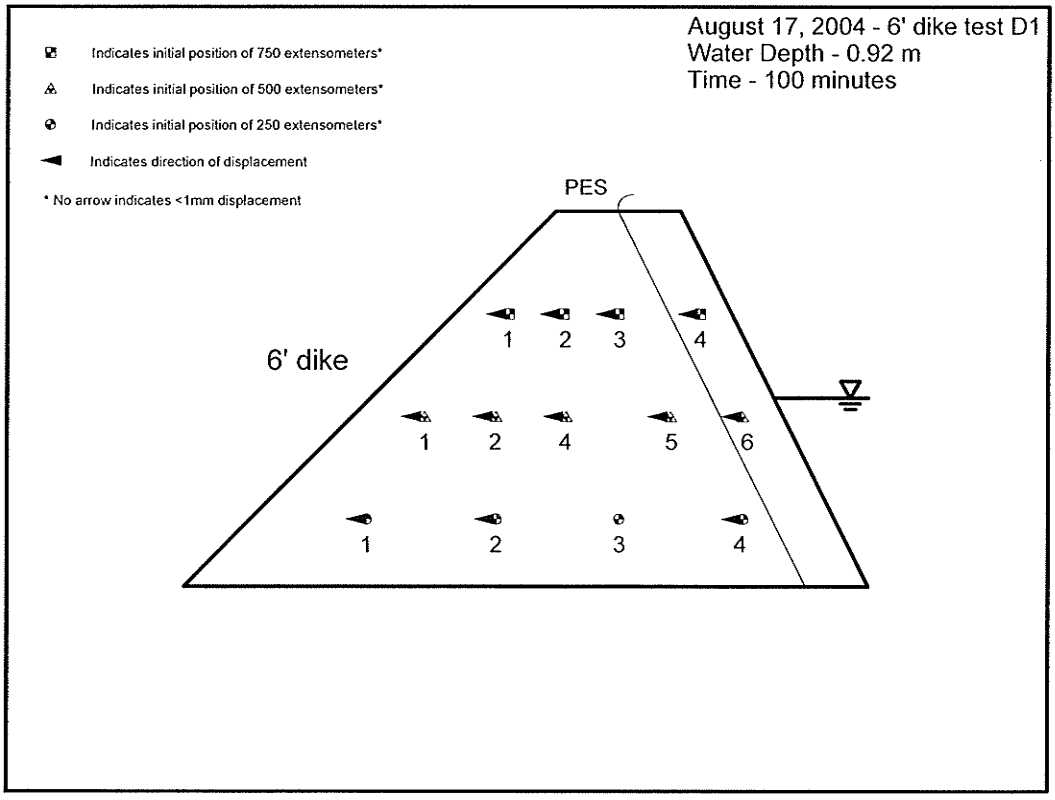

Figure 5.53 – Displacement of D1 Extensometers during Unloading.

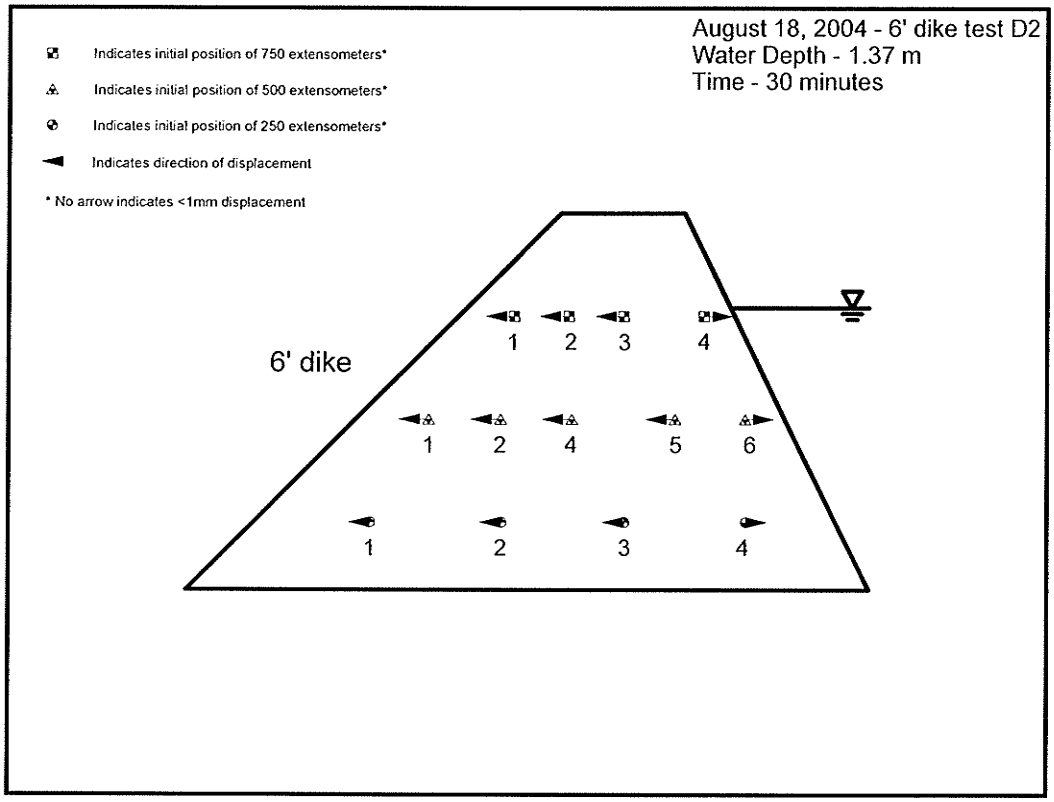

Figure 5.54 – Displacement of D2 Extensometers at Design Water Depth.

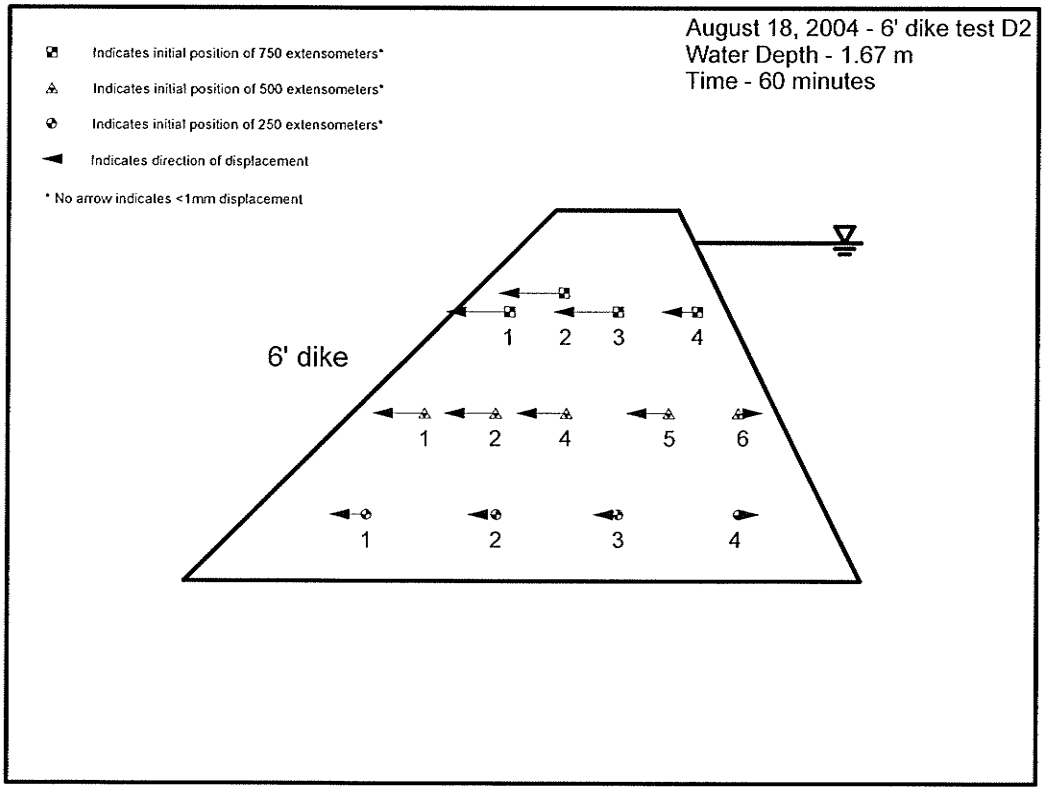

Figure 5.55 – Displacement of D2 Extensometers at Peak Water Depth.

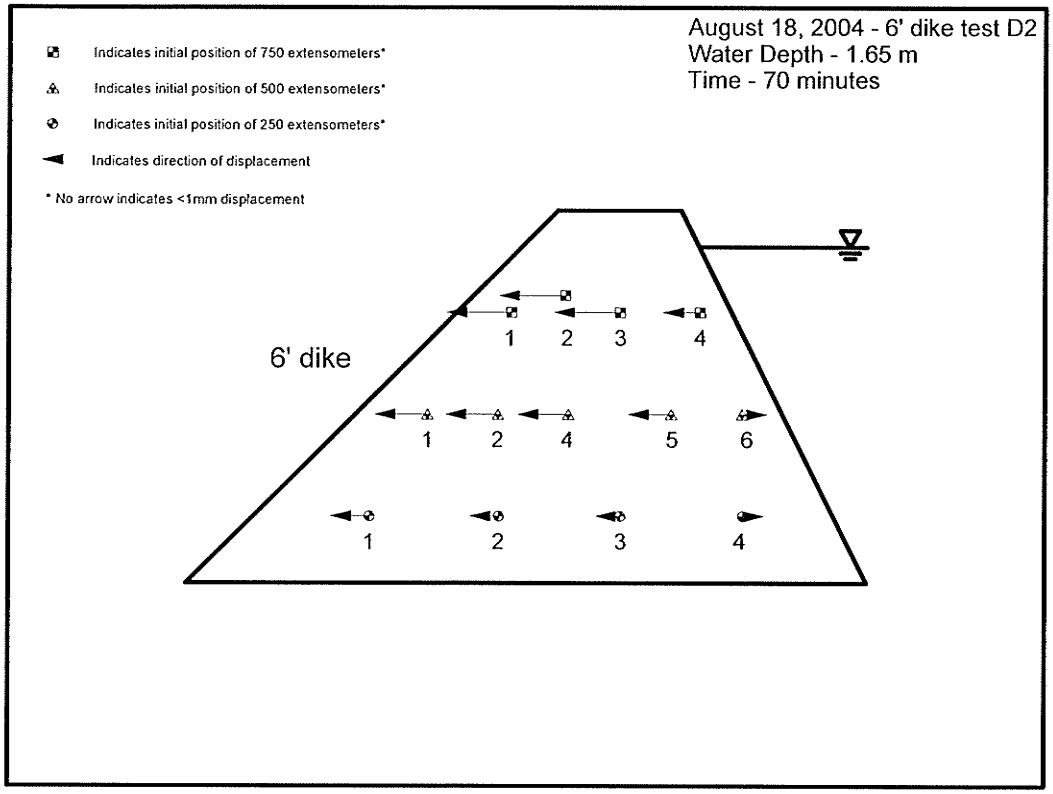

Figure 5.56 – Displacement of D2 Extensometers after Overtopping for 30 minutes.

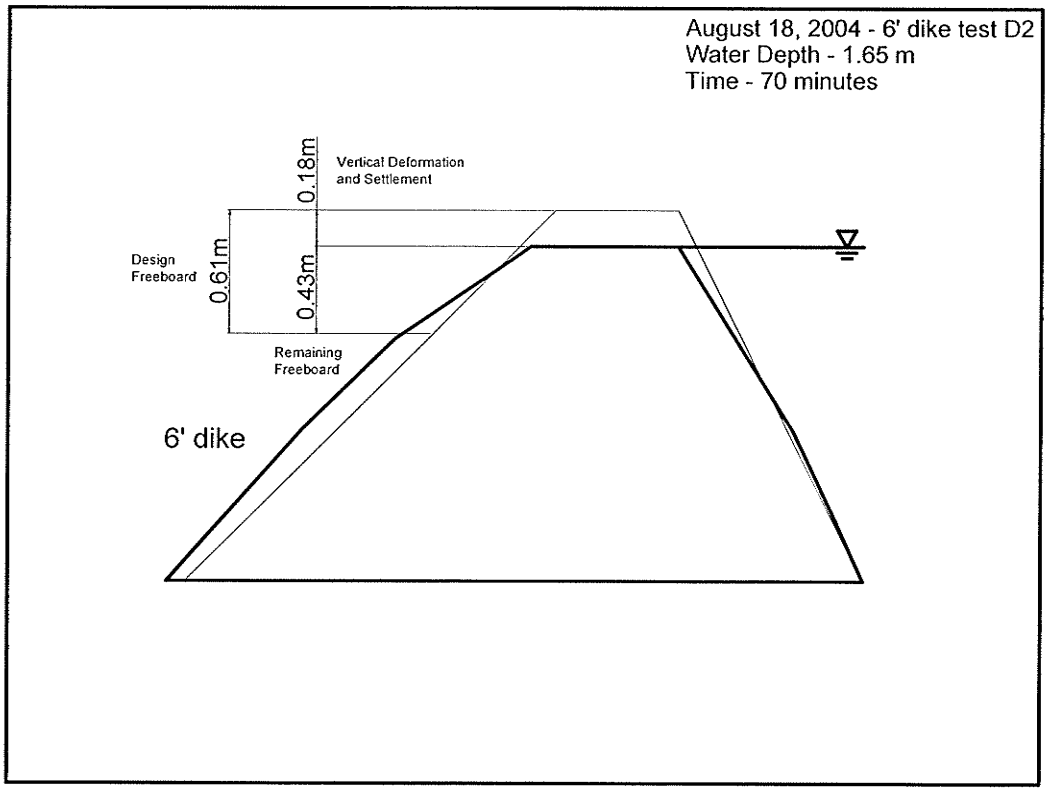

Figure 5.57 – Deformation at Centre-line of Dike D2 during Overtopping Water Levels.

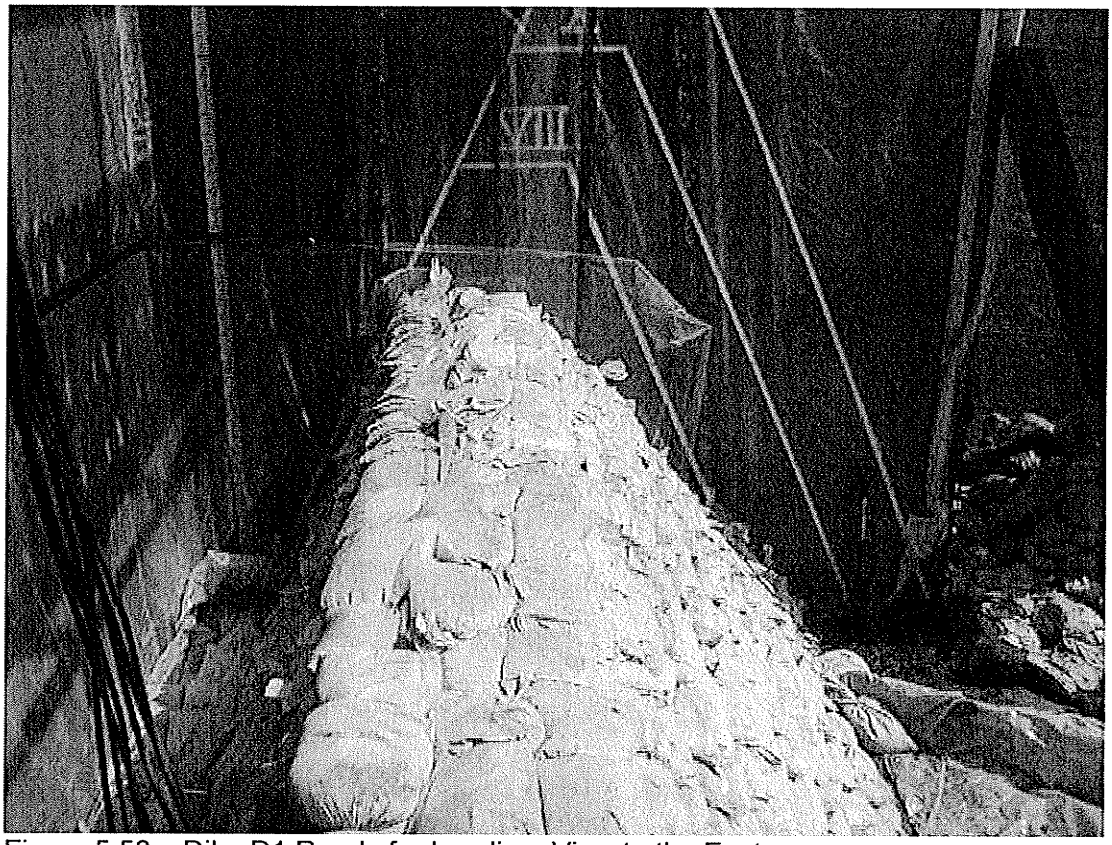

Figure 5.58 – Dike D1 Ready for Loading, View to the East.

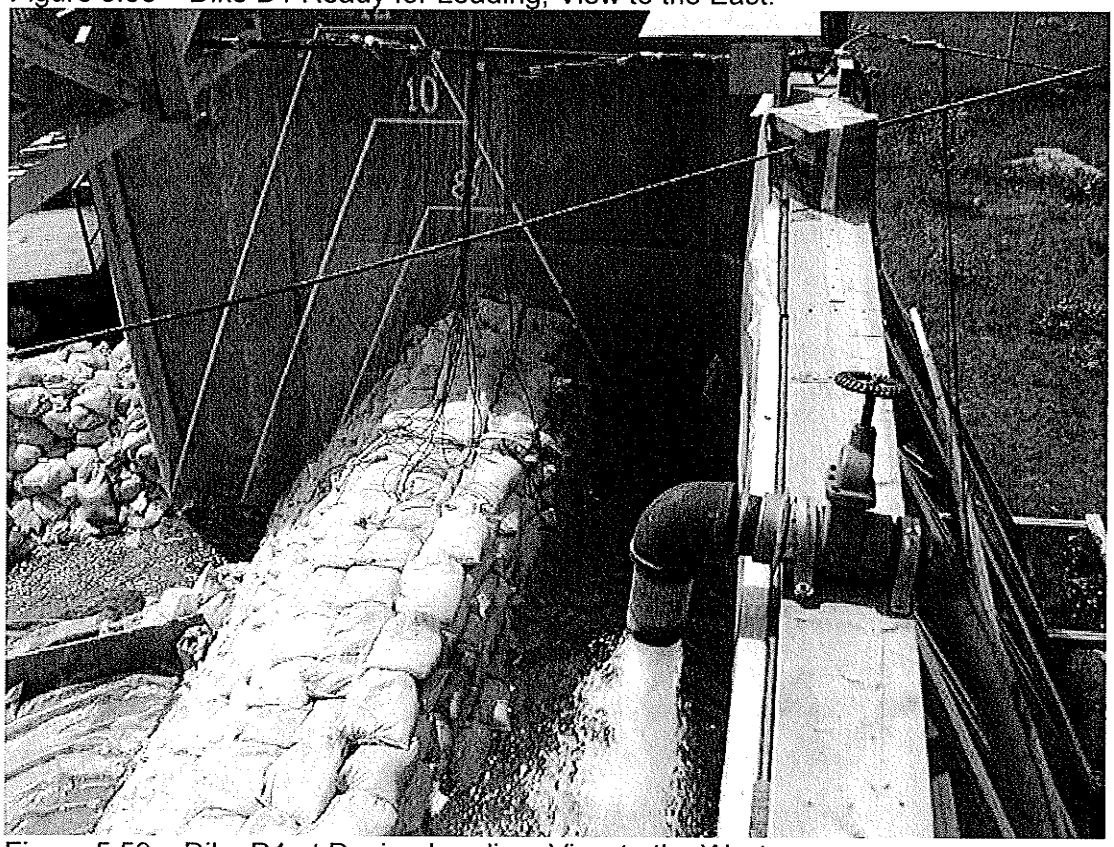

Figure 5.59 – Dike D1 at Design Loading, View to the West.

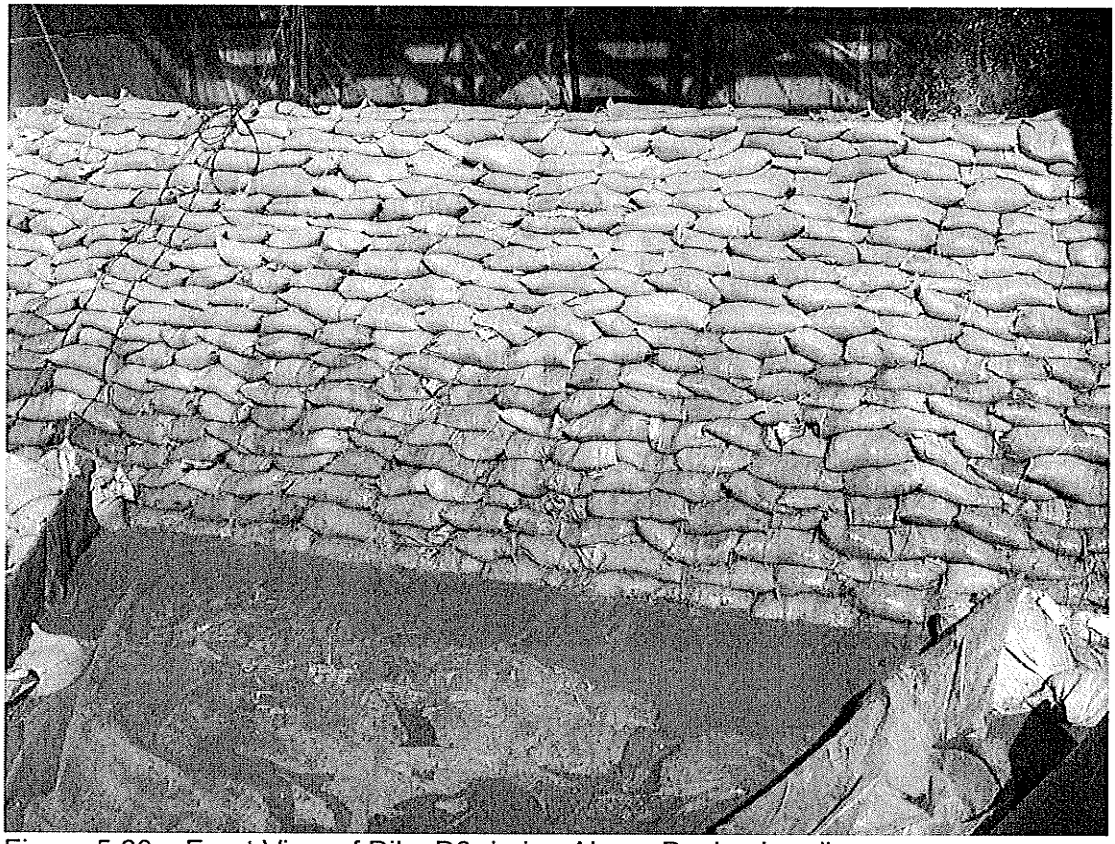

Figure 5.60 – Front View of Dike D2 during Above Design Loading.

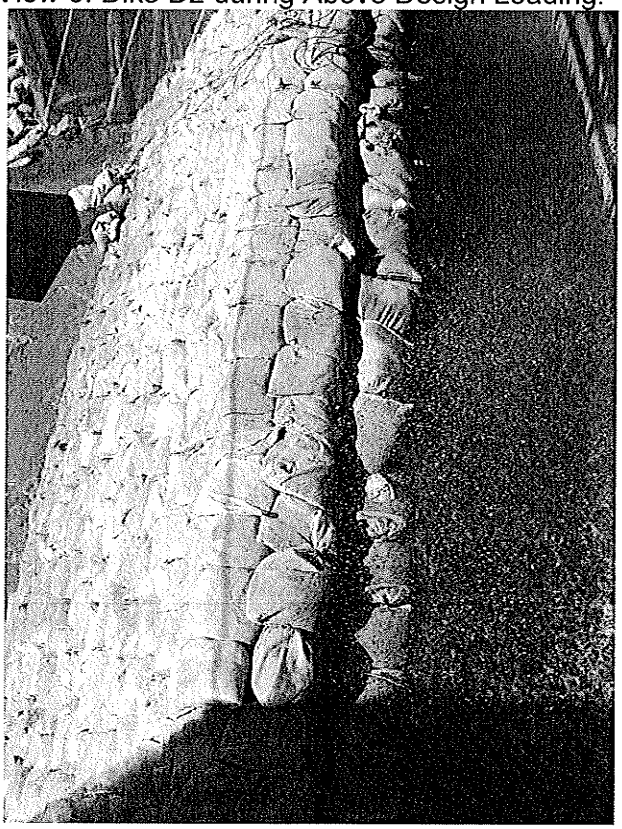

Figure 5.61 – Dike D2 during Above Design Loading, View from Above.

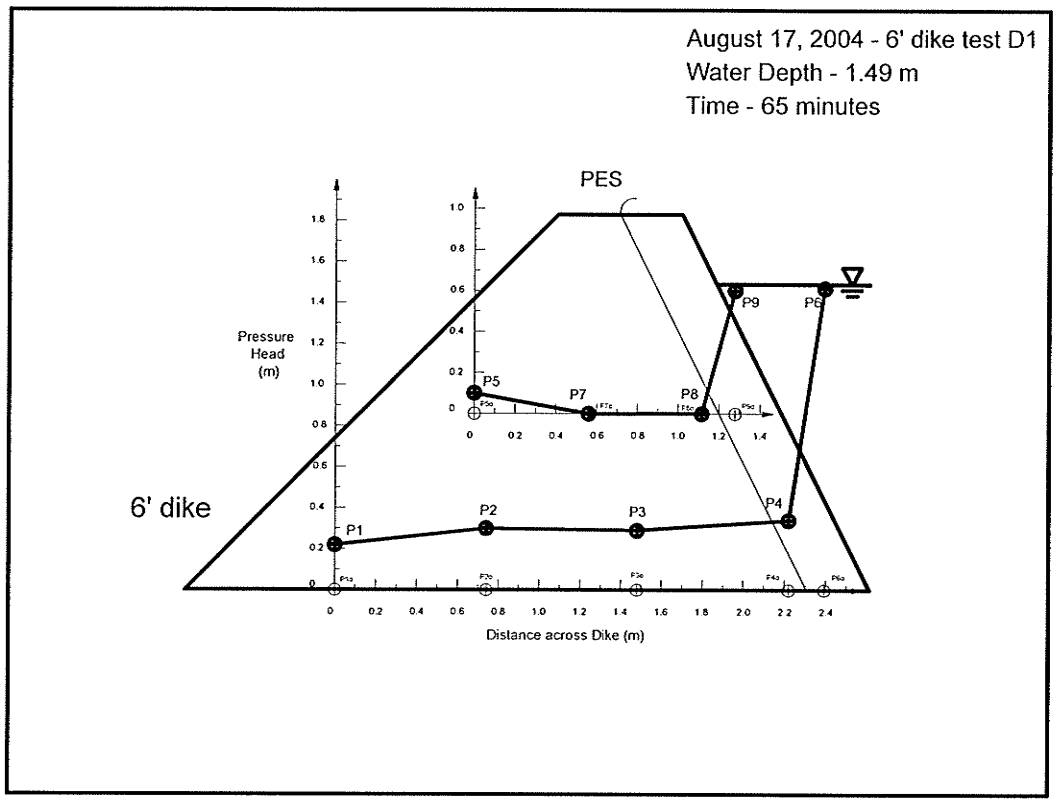

Figure 5.62 – Measured Pressure Head through Dike D1 at Design Water Depth.

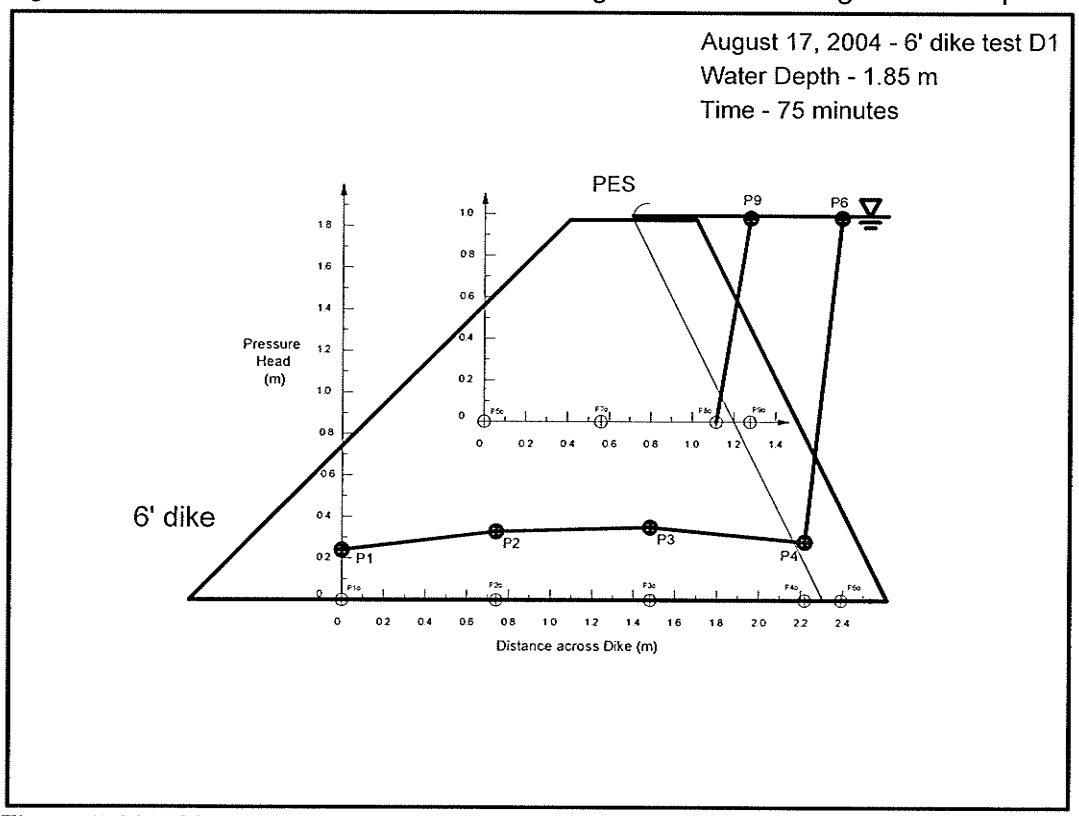

Figure 5.63 – Measured Pressure Head through Dike D1 at Peak Water Depth.

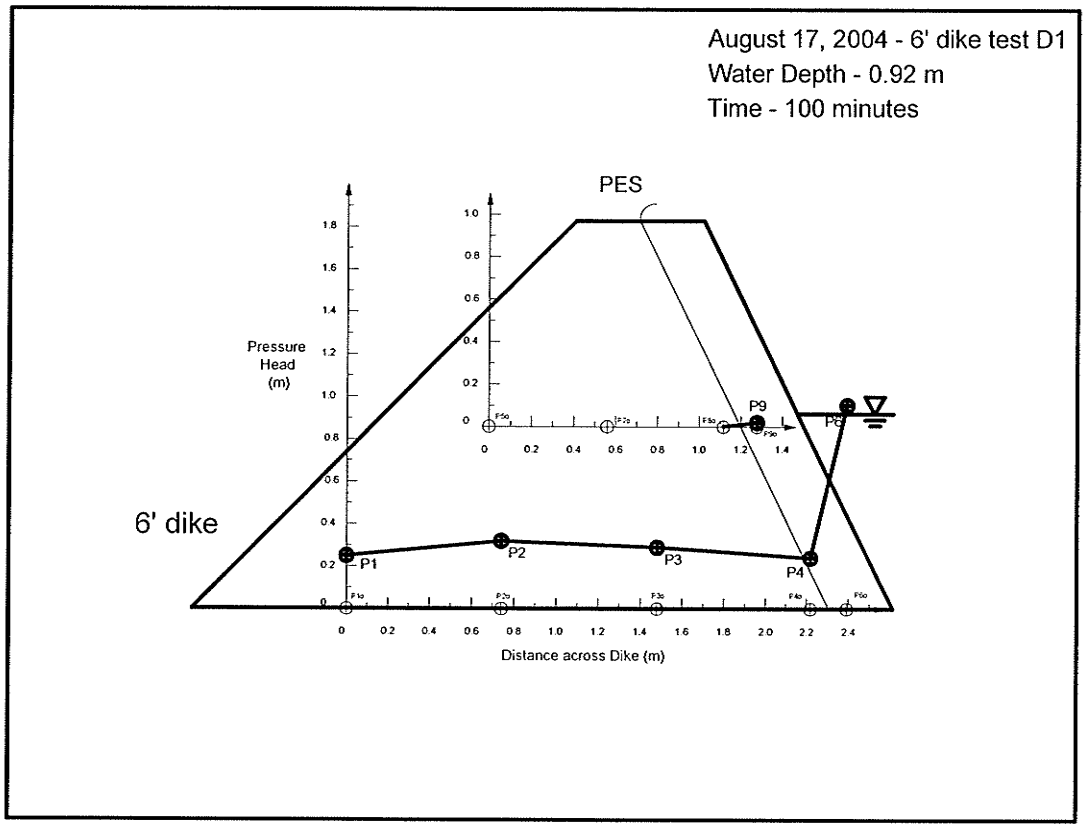

Figure 5.64 – Measured Pressure Head through Dike D1 during Unloading.

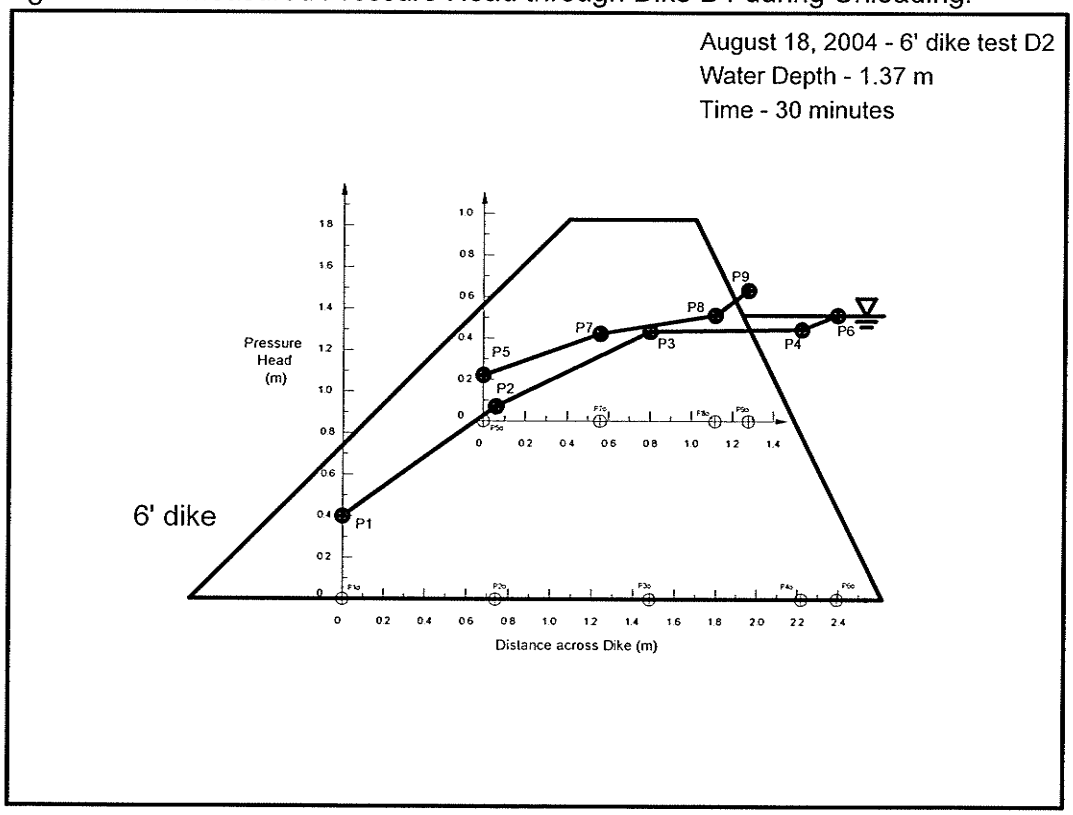

Figure 5.65 – Measured Pressure Head through Dike D2 at Design Water Depth.

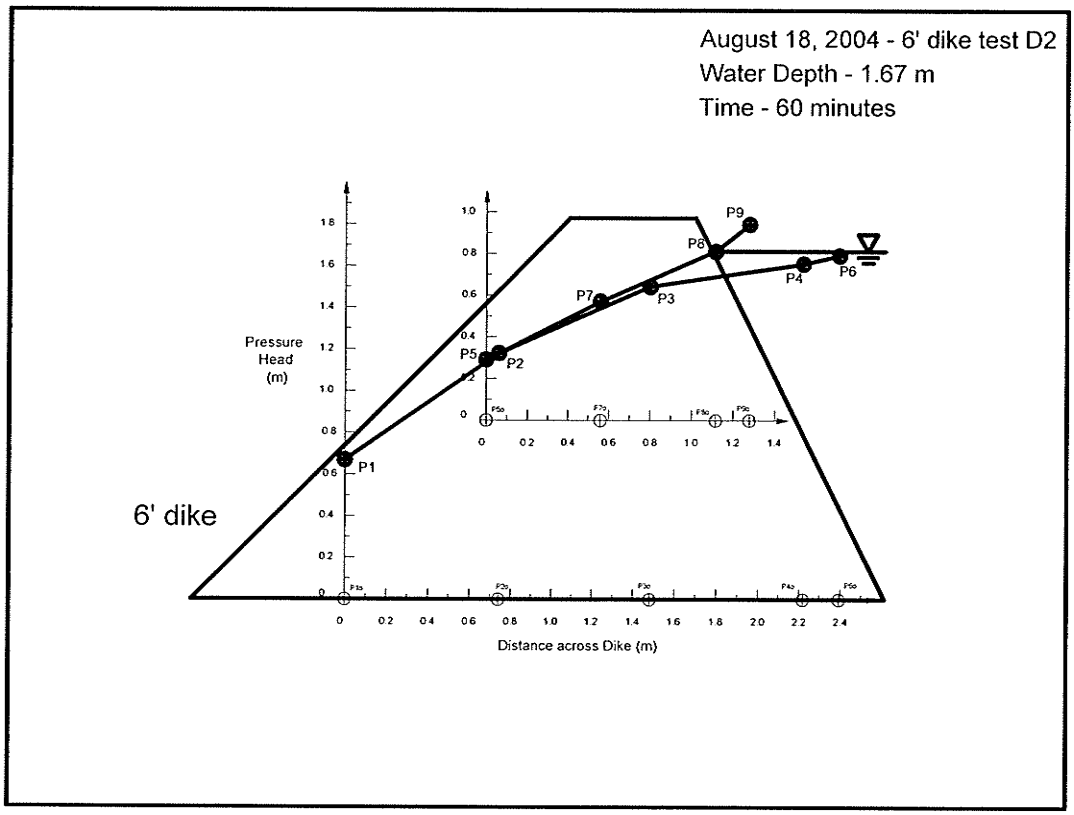

Figure 5.66 – Measured Pressure Head through Dike D2 at Peak Water Depth.

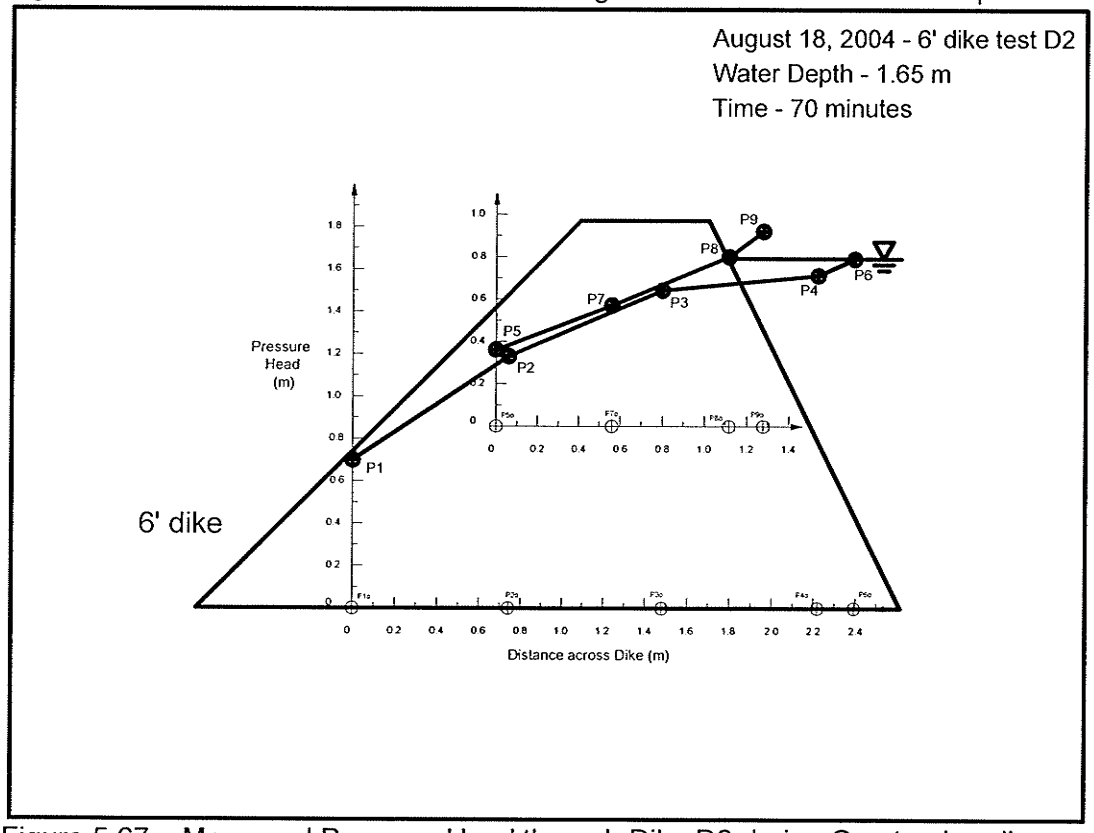

Figure 5.67 – Measured Pressure Head through Dike D2 during Overtop Loading.

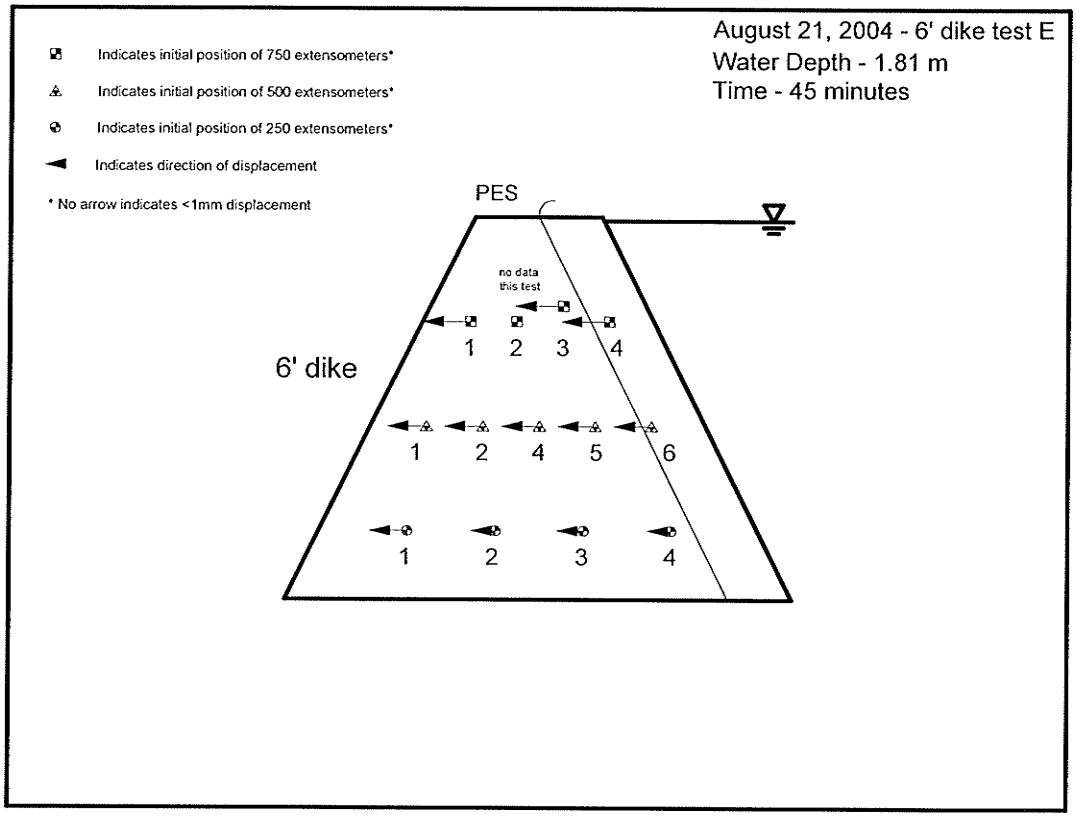

Figure 5.68 – Displacement of E Extensometers at Peak Water Depth.

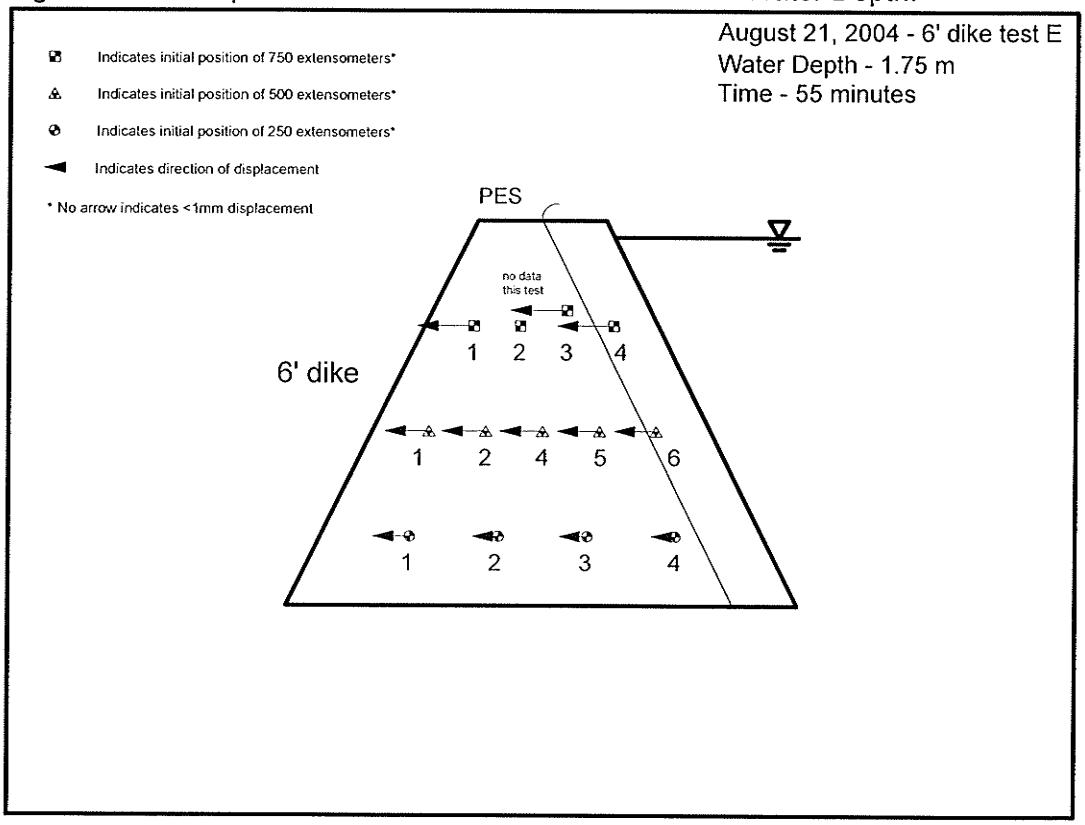

Figure 5.69 – Displacement of E Extensometers at above Design Water Depth.

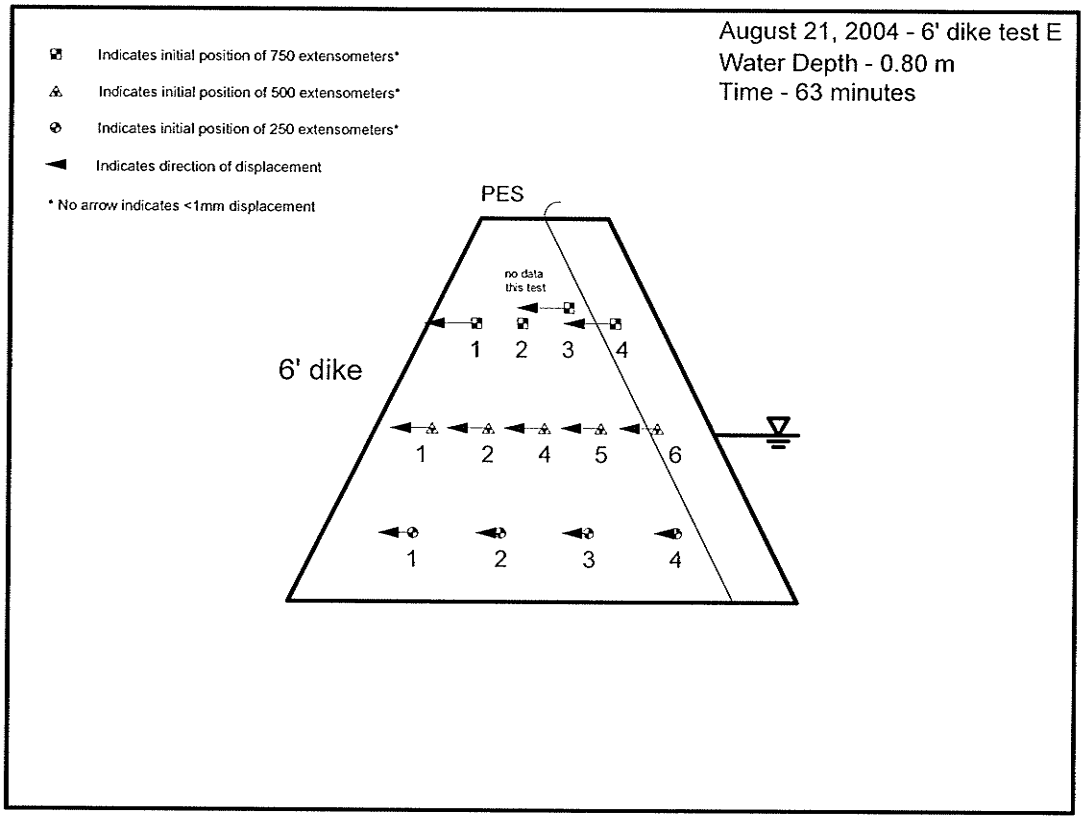

Figure 5.70 – Displacement of E Extensometers during Unloading.

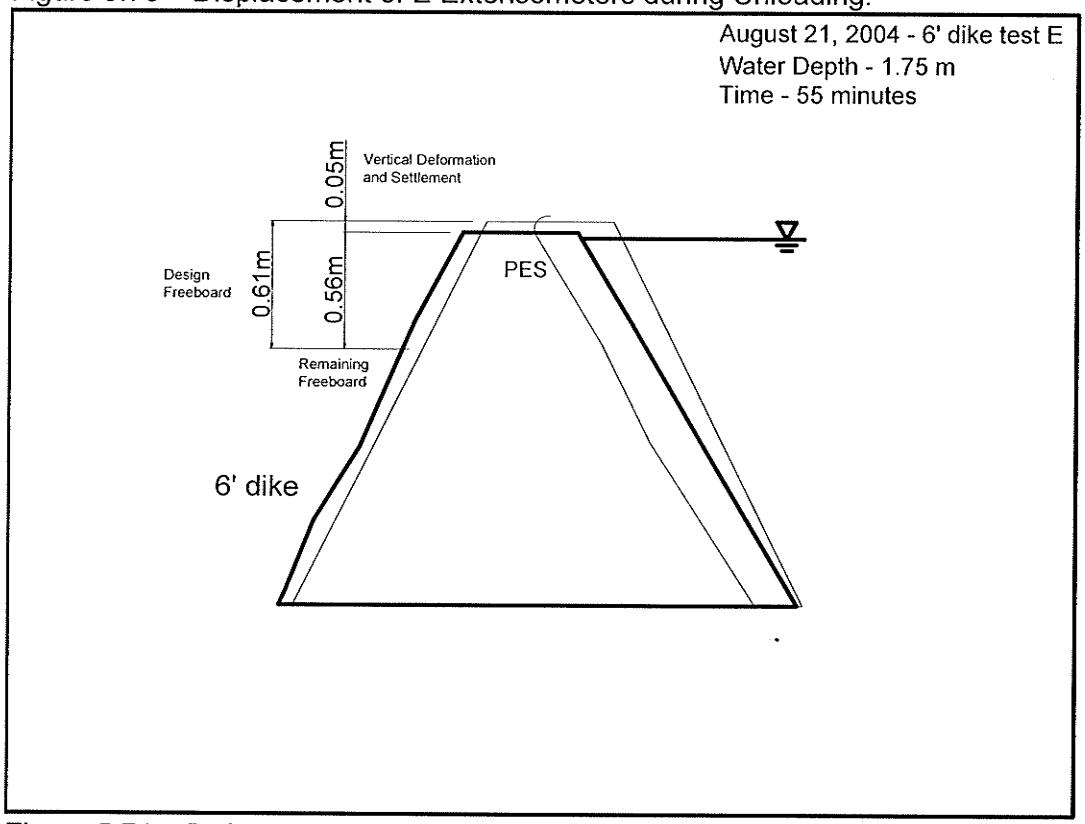

Figure 5.71 – Deformation at Centre-line of Dike E after 30 min of Above Design Loading

Figure 5.72 – Volunteers Weaving PES into Dike E, View to the North-east.

Figure 5.73 – Dike E Ready for Loading, View to the East.

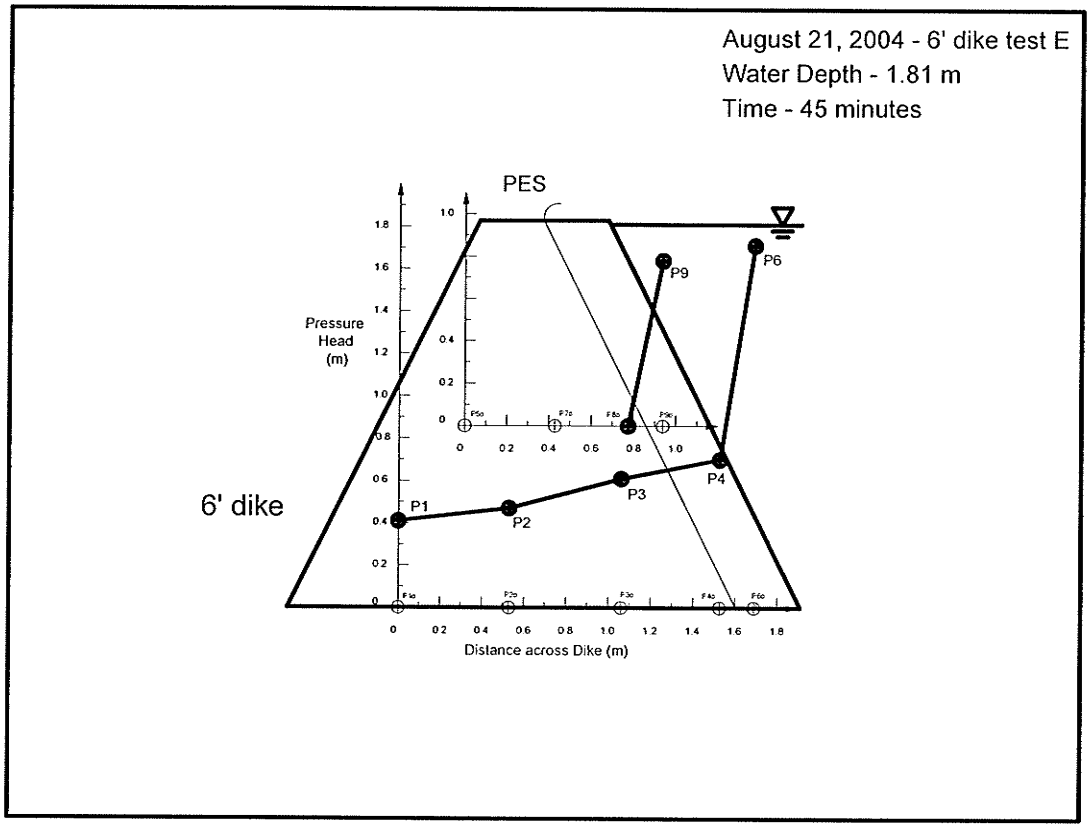

Figure 5.74 – Measured Pressure Head through Dike E at Peak Water Depth.

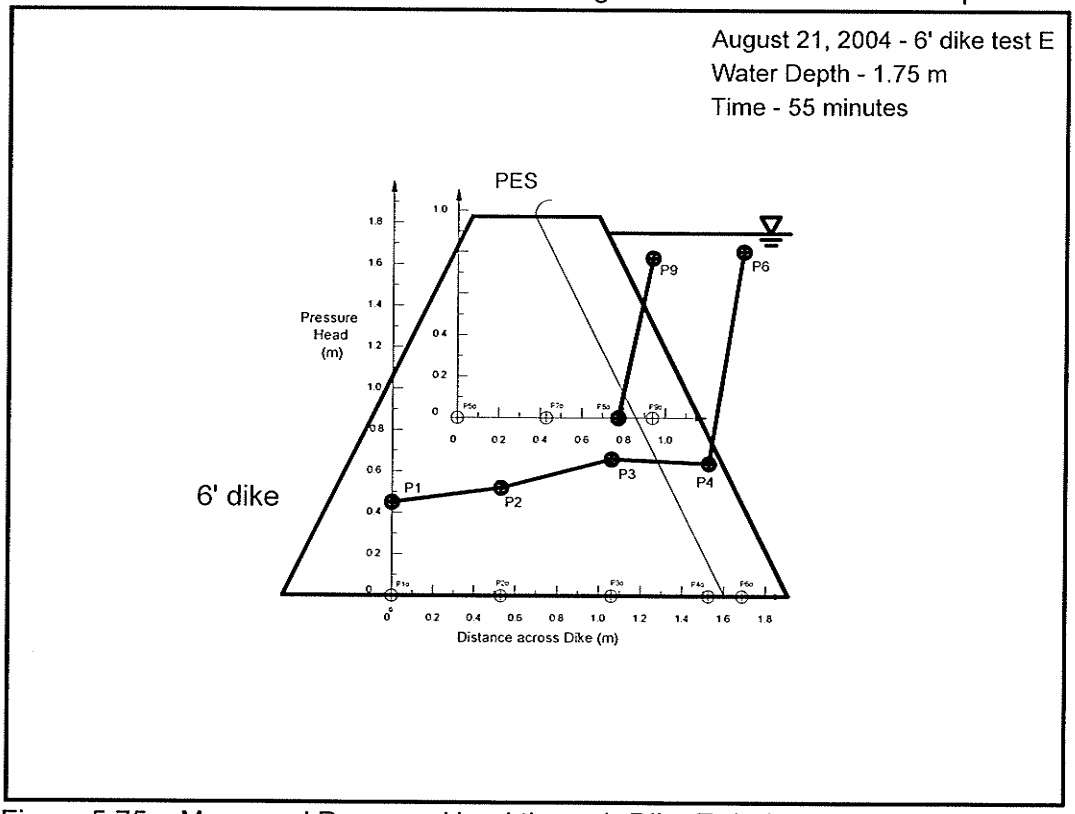

Figure 5.75 – Measured Pressure Head through Dike E during Above Design Loading.

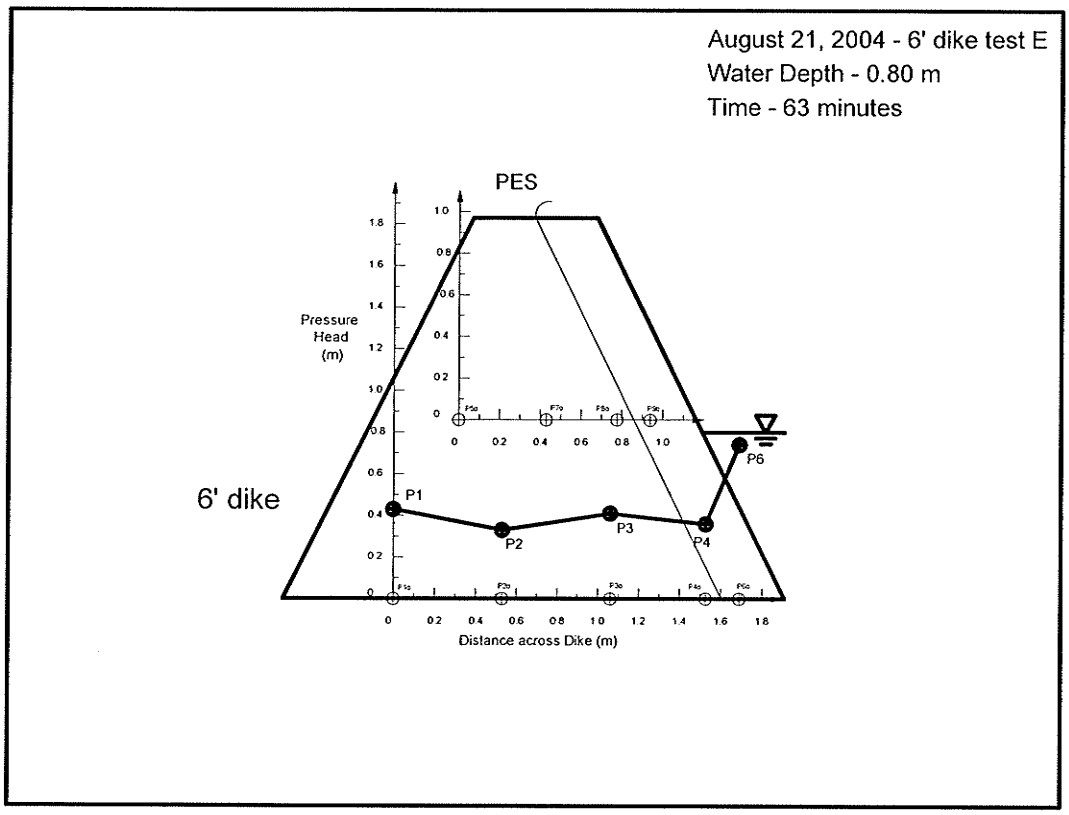

Figure 5.76 – Measured Pressure Head through Dike E during Unloading.

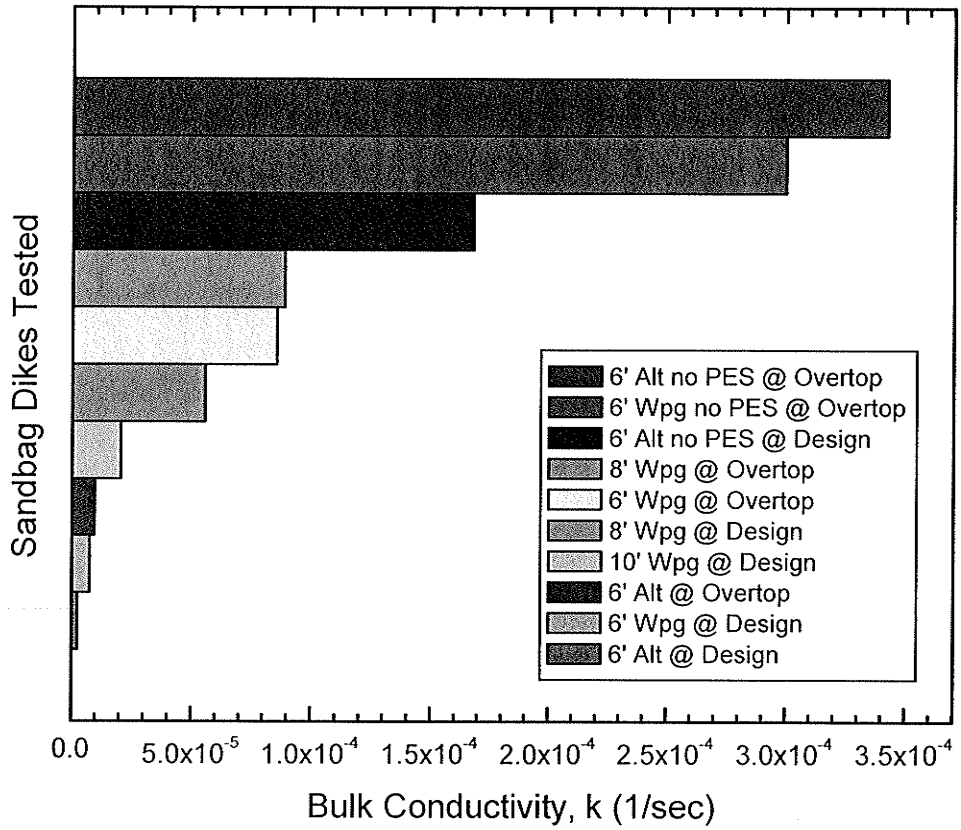

Figure 5.77 – Ranked Bulk Conductivity of Sandbag Dikes Tested.

6 Comparison of Sandbag Dike Types

6.1 Introduction

It is valuable to draw comparisons based on the test results that show some of the relationships between stability, deformability, conductivity, dike height, dike geometry, construction method, materials and quality. For testing purposes, the dikes were divided into groups A through E. For comparison purposes, they will be further divided into four sub-groups.

The first comparisons are between the set of dikes that share the same geometry, construction method, materials and quality and differ only in terms of height. The second comparisons are between two sets of dikes that share the same height, geometry, construction method and quality and differ in terms of materials used. The third comparisons are between two set of dikes that share the same height, construction method, materials and quality but differ in terms of geometry. The fourth comparison is between two dikes that have the same height, geometry and materials used, but differ in construction method and quality.

6.2 Comparison One – Effect of Varying Dike Height

One of the earliest goals of this research project was to define a maximum height of a safe sandbag dike that is practical to construct using the most commonly available materials following the 1997 template developed by the City of Winnipeg. The design of both the testing facility and the full-scale dike testing program revolved around the ability to differentiate between the stability and seepage characteristics of dikes of different heights, all built with the same geometry, construction method, materials and quality.

The tests that are compared to highlight the effect of a change of height are A, B and C. They represent the initial design loading of dikes 8, 10 and 6 feet (2.44, 3.05 and 1.85 m) in height, respectively. Comparisons of the dike's performance under design loading can be made in terms of horizontal displacement at three elevations, pore pressure distribution through a central cross-section, seepage rate and overall deformation.

6.2.1 Horizontal Displacement at Design Water Depth

The extensometer installations in all three of the tests had the uppermost row placed about 10 cm (4") above the design water depth for that dike, and the two lower rows placed 0.5 m and 1.0 m below, respectively. For example, the design water depth for 6' (1.83 m) dike C1 is 4' (1.22 m) and the uppermost row of extensometers is installed at 1.33 m (4.36').

Figure 6.1 is a plot of the average of the absolute extensometer measurements at each monitored elevation in the dikes with reference to the design water elevation. As expected, the horizontal displacement increases with increased dike height. The relative increase in displacement between dikes 8 and 10 feet tall (558%) is considerably larger than the increase in displacement between dikes 6 and 8 feet tall (94%). This suggests that there is some critical change in performance between dikes 8 feet and 10 feet in height subjected to comparable design load.

This agrees with observations that displacements decreased after unloading in dikes A2 and C1, but not dike B1. In broad terms, the 6 and 8 foot dikes retained some of their elasticity after sustained design loads, while it did not appear the same for the 10 foot dike.

6.2.2 Pore Pressure Distribution at Design Water Depth

The piezometer installations in the three tests featured a row near the base and a row near the mid-point of the dike. Figure 6.2 is a plot of the average piezometer readings for each row normalised as a percentage of their design depth versus their elevation within the dike as a percentage of dike height. There is a significant difference in the slopes of the lines connecting the two elevations of pore pressure measurements for each dike. The most striking difference is between the 6 foot dike and the 8 and 10 foot dikes. The 6 foot dike (C1) showed no wetting at its upper level of piezometers, and therefore the line connecting these two elevations for this dike has a negative slope. Conversely, the upper piezometers in both the 8 foot (A2) and 10 foot (B1) dikes recorded pore pressures and the lines joining their averages have positive slopes. The slope of the line for the 10 foot dike is steeper than the slope of the line for the 8 foot slope.

These trends support the assertion that increased pore pressures throughout a sandbag dike decrease the dike's stability. The 6 foot dike was found to be stable under design loading, but the 8 and 10 foot dikes were not.

6.2.3 Seepage Rate at Design Water Depth

The bulk conductivity per metre of sandbag dike is a function of the head driving the flow, the average length of available flow paths and the average porosity of the materials along that flow path. The conductivity of dikes C1, A2 and B1 when loaded at design water depth are compared in Figure 6.3 based on approximate estimations of bulk 'k' values. There is a general increase in conductivity with an increase in dike height, as is expected.

Dike A2 has the highest measured conductivity of these three dikes, which is likely an effect of two principal causes. The first is a less than perfect PES layer installation in this

first set of dikes tested. The second is measuring the flow across the entire width of the flume, a practise that was modified in later tests, as mentioned in chapter 4. Generally, an increase in bulk conductivity is expected with increasing dike height and the corresponding higher hydraulic gradient from the increased design loading elevation to the unchanged dry side base elevation. This is the overall trend observed in these tests.

6.2.4 Deformation under Design Water Depth

Figure 6.4 is a plot of the original and deformed dike profiles for tests C2, A2 and B2 respectively. In tests C2 and B2, the deformed profile is the result of loading above design levels. In test A2, the deformed profile shown is the result of design depth loading. The most striking difference between the three profiles is the reduction of available freeboard due to both densification of the dike by wetting and deformation of the dikes original geometry by loading. The reduction of available freeboard is greatest in the highest dike and least in the lowest dike.

The overall deformation is also greatest in the highest dike and least in the lowest dike. In test B2, the 10' (3.05 m) dike experienced excessive sliding along the PES layer. The occurrence of this sliding in the higher dikes agrees with the difference in measured Mohr-Coulomb friction values between dry PES and dry WSFPP and the values measured for saturated PES and WSFPP. The c' values for this interface went to zero in the saturated tests, indicating that saturation reduced the effective cohesion of the interface to very low values. In the large-scale tests, this translates into a reduction of the frictional stability of the PES layer during wetting and the overall stability of this portion of the dike is dependent on inter-weaving of the PES layer with the filled sandbags on each side. This inter-weaving serves to provide a connection to the surrounding sandbags so that the PES interface is not the weakest link in the dike and

the structure as a whole can be considered to have higher frictional resistance than the critical saturated PES-WSFPP interface.

6.2.5 Summary of Dike Height Comparison

From these comparisons it is evident that sandbag dikes built according to the City of Winnipeg's 1997 template are less stable, more conductive and more prone to deformation with increased height, particularly above 6' (1.83 m). These characteristics are closely tied to the pore pressure distribution through a given dike at its design load, and the normalised pore pressure distributions in the 8' and 10' (2.44 and 3.05 m) dikes tested were noticeably higher than in the 6' (1.83 m) dikes tested. Densification due to wetting is also magnified with increased dike height, as expected.

6.3 Comparison Two – Effect of PES layer

The PES layer is a key element in the City of Winnipeg's 1997 sandbag dike template. A survey of the materials present in a sandbag dike quickly reveals that the PES is the only component of the dike with any reasonable water-tightness. The other key materials, namely sand and WSFPP, are very porous and do little to impede flow through the dike under flood conditions.

The tests that will be compared to highlight the effect of the PES layer in a sandbag dike are tests C1 & C2 with C3 and test D1 with D2.

6.3.1 Horizontal Displacement at Design and Overtop Water Depths

Figures 6.5 and 6.6 are plots of the average absolute measured horizontal displacement at each extensometer elevation within dikes C1 & C3 and dikes D1 & D2 when loaded at design water depths, respectively. In both cases, the dikes with a PES layer show a small amount of displacement at each extensometer installation level, generally

increasing with an increase in elevation. The dikes without PES show much greater displacements, with dike C3 following the pattern of increasing displacement with increased elevation. Dike D2 exhibits the greatest displacements at its middle extensometer elevation, but they are not substantially larger than the displacements measured at its upper extensometer elevation. This can be partially attributed to the effect of using absolute values to average across the dike where there is relative motion between each of the monitored positions. It is also a function of the deformed shape that the loaded dikes tended to take, which featured less vertical deformation downwards through the cross-section and a lateral bulge towards the dry side in the upper two thirds of the profile.

Figures 6.7 and 6.8 are plots of the average absolute measured horizontal displacement at each extensometer elevation within dikes C2 & C3 and dikes D1 & D2 when loaded at overtop water depths, respectively. As in the design load case, there is more movement observed in the dikes without PES, C3 and D2, than in the dikes with a PES layer, C2 and D1. There is a considerable increase in the overall horizontal displacement at overtop water depths as compared to design loading.

6.3.2 Pore Pressure Distributions at Design and Overtop Water Depths

The piezometer installations in these tests also featured a row near the base and a row near the mid-point of the dike. Figures 6.9 and 6.10 are plots of the average piezometer readings at design depth loading for each row normalised as a percentage of their design depth versus their elevation within the dike as a percentage of dike height. There is a significant difference in the slopes of the lines connecting the two elevations of pore pressure measurements for each dike. The dikes with a PES layer did not register any excess pore pressures at their upper piezometer elevation, so the lines for these

readings have negative slope. The dikes without a PES layer did register excess pore pressures at both elevations, resulting in a positive slope for this particular plot.

Figures 6.11 and 6.12 are plots of the average piezometer readings at overtop loading for each row normalised as a percentage of their design depth versus their elevation within the dike as a percentage of dike height. At this loading level, pore pressures were measured at both piezometer elevations in both dikes C2 & C3. Dike D1 still did not register any excess pore pressures at its upper elevation of piezometers at overtop loading, but dike D2 did.

Generally, there is an increase in pore pressures through all of the dikes when going from design depth loading to overtop loading. There is also an increase in pore pressures when going from a dike with a PES layer to a dike with similar geometry without a PES layer. The increase in average measured pore pressures for dikes with PES to comparable dikes without PES is between 200 and 400%.

6.3.3 Seepage Rates at Design and Overtop Water Depths

Figure 6.13 is a comparison of the measured bulk conductivity per metre of dike in tests C1, C3, D1 and D2. As with the pore pressure measurements, the difference in conductivity between dikes with PES and dikes without PES is striking. Dikes C1 and C3 have measured bulk conductivities of 7.6×10^{-6} and 3.0×10^{-4} (sec^{-1}) per metre of dike respectively. Dikes D1 and D2 have measured bulk conductivities of 2.5×10^{-6} and 1.7×10^{-4} (sec^{-1}) per metre of dike respectively. In both dike geometries this is an increase in conductivity of two orders of magnitude, based solely on the removal of the PES layer.

6.3.4 Deformed Dike Shapes at Overtop Water Depth

Figure 6.14 is a side by side comparison of the deformed shapes of dikes C2 and C3 after sustained overtop loading. There is considerably more deformation evident in dike C3 than in dike C2. Dike C2 sustained overtop loading for 30 minutes and the extensometer and piezometer readings for this dike reached equilibrium despite the water flowing over its top. Dike C3 did not maintain its shape for any length of time at overtop loading levels.

The freeboard available for these dikes after loading is also telling about the influence of the PES layer. In dike C2, the freeboard was reduced by 18% after overtop loading, and in dike C3, it was reduced by 62%.

6.3.5 Summary of the Effect of the PES layer

Video data and visual observations of group C tests also demonstrate the difference in dikes with and without a PES layer. In test C3, where there is no PES layer, water flows through nearly half-way up the face of the 'dry' side of the dike. This is in agreement with the piezometer data, which indicates a head profile through dike C3 that is between 0.4 and 0.8 m (1.31' and 2.62') at the dry side.

It is clear that the PES layer plays an instrumental role in the stability and seepage characteristics of sandbag dikes. The PES slows the rate of flow through the dikes under hydraulic loading, which reduces the pore pressures inside the dikes which maintains the stability of the overall structure and holds back the floodwaters with a maintainable rate of seepage. In the absence of the PES layer, the geometry of the City of Winnipeg 1997 template is not stable. An increase in dike volume of more than 25% is required for stability without PES, but even with this configuration, seepage rates are more than can be reasonably addressed by pumping systems in flood conditions.

6.4 Comparison Three – Effect of Dike Geometry

The City of Winnipeg's 1997 template is based on an evolution of sandbag dike geometry that is motivated by a need to protect as much flood area as possible using the least number of bags while maintaining a reasonable level of safety. The idea for testing a 1:1 dry side slope as opposed to the standard 2:1 slope was brought forward by the steering committee. The rationale was that a dry side modification represents a practical solution in a mid-flood crisis situation such as the discovery of a dike missing the PES layer. The tests that will be compared to highlight the effect of a change of geometry are C1, C2 & C3 with D1 & D2.

6.4.1 Horizontal Displacement at Design and Overtop Water Depths

Figure 6.15 is a plot of the average absolute measured horizontal displacement at each extensometer elevation within dikes C1 and D1 when loaded at design water depth. There is a noticeable decrease in movement in dike D1 when compared to dike C1, although both dikes had average horizontal deformations of less than 12 mm (1/2") under design loading.

Figure 6.16 is a plot of the average absolute measured horizontal displacement at each extensometer elevation within dikes C2 and D1 when loaded to overtop water depth. There is more horizontal deformation measured under overtop loading than under design depth loading, but in this case dike D1 recorded more deformation at the middle extensometer elevation than dike C2. This is evidence of different deformation behaviour due to different dike geometry.

The general shape of the plots for the C dikes and the D dikes are consistent between both tests. The trend of increased horizontal displacements with increased water depths is also maintained.

6.4.2 Pore Pressure Distributions at Design and Overtop Water Depths

Figure 6.17 is a plot of the average piezometer readings for dikes C1 and D1 at design loading for each row normalised as a percentage of their design depth versus their elevation within the dike as a percentage of dike height. The pore pressure distributions in the dikes are very similar. Neither dike experienced excess pore pressures at the higher piezometer elevation. Dike C1 has a slightly higher pore pressure reading at the base level than D1.

Figure 6.18 is a plot of the average piezometer readings for dikes C2 and D1 at overtop loading for each row normalised as a percentage of their design depth versus their elevation within the dike as a percentage of dike height. At overtop loading, the pore pressure distributions in the dikes are noticeably different. Excess pore pressures are measured at the higher elevation of piezometers in dike C2 but not in dike D1. This gives a positive slope to the plot for dike C2, and a negative slope for dike D1. Both of the dikes show an increase in pore pressures from design to overtop loading conditions.

The difference in measured pore pressures from design to overtop loading that is observed in dike C1 and C2 is not observed in dike D1. This difference is largely attributable to the increased area and corresponding increase in flow-paths through the dike cross-section.

6.4.3 Seepage Rates at Design and Overtop Water Depths

Figure 6.19 is a comparison of the measured bulk conductivity per metre of dike in tests C1 at design load, C2 at overtop load, and D1 at both design and overtop loads. The difference in bulk conductivity between dikes built to the City of Winnipeg 1997 template and dikes built with a 1:1 slope on the dry side is noticeable. Dikes C1 and D1 have measured bulk conductivities of 7.6×10^{-6} and 2.5×10^{-6} (sec^{-1}) per metre of dike at design loads, respectively. Dikes C2 and D1 have measured bulk conductivities of 8.6×10^{-5} and 9.7×10^{-6} (sec^{-1}) per metre of dike at overtop loads, respectively.

The noticeable decrease in measured bulk conductivity in the dikes with the 1:1 dry side slope is due to the increased length of flow-paths from the 2:1 side slope dikes.

6.4.4 Deformed Dike Shapes at Overtop Water Depth

Figure 6.20 is a side by side comparison of the deformed shapes of dikes C3 and D2 after sustained overtop loading. These are both dikes built without a PES layer in place, but dike D2 has about 25% more sandbags in its cross-section. There is considerably more deformation evident in dike C3 than in dike D2. Dike D2 sustained overtop loading for 30 minutes and the extensometer and piezometer readings for this dike reached equilibrium despite the water flowing over its top. Dike C3 did not maintain its shape for any length of time at overtop loading levels.

The difference between these two test results is effectively the difference between stability and catastrophic failure of a flood protection structure. The only difference between dikes C3 and D2 is the amount of sandbags installed on the dry side of the dike. While the seepage rates through a dike with no PES may be higher than it is practically possible for the average homeowner to pump back, they are still considerably lower than the seepage rates over a totally failed dike.

6.4.5 Summary of effects of Dike Geometry

The geometry of a sandbag dike's cross-section is instrumental to the stability and seepage characteristics of that dike. It also influences the constructability of the structure from both a material supply and expertise perspective.

These tests demonstrate that the loss of stability due to excessive flow through a dike constructed without a PES layer can be overcome with additional bags on the dry side. This provides a dry side solution for dikes that are already loaded or may be suspected of not having sufficient PES installed. It also confirms the practise of 'buttressing' dikes on their dry side that was relied on in several cases in Manitoba's flood of 1997.

6.5 Comparison Four – Effect of dike construction and quality methods

It is important to recognise that the majority of sandbag dikes constructed during a flood event are built by volunteers. The amount of training and experience in any given group of volunteers will be highly variable. Given the same materials and basic information, there will be an appreciative difference between dikes built by different groups of people. This is of absolute importance given that flood protection efforts are subject to the 'weakest link' causing failure. It doesn't do very much good for a length of dike to be built to high standards if it is attached to and therefore dependent on a poorly built section. The water will simply go around strong sections of dike and through or over weak ones.

The tests that will be compared to highlight the effect of a change of construction method and quality are C1 & C2 and E.

6.5.1 Horizontal Displacement at Design and Overtop Water Depths

Figure 6.21 is a plot of the average absolute measured horizontal displacement at each extensometer elevation within dikes C1 and E when loaded at design water depth. There is only a small increase in movement in dike E when compared to dike C1, and both dikes had average horizontal deformations of less than 25 mm (1") under design loading.

Figure 6.22 is a plot of the average absolute measured horizontal displacement at each extensometer elevation within dikes C2 and E when loaded to overtop water depth. There is considerably more horizontal deformation measured under overtop loading than under design depth loading in dike E. The volunteer built dike did not appear to be stable under overtop loading. This is in direct contrast to the 6' dikes built by student researchers (containing a proper PES layer).

6.5.2 Pore Pressure Distributions at Design and Overtop Water Depths

Figure 6.23 is a plot of the average piezometer readings for dikes C1 and E at design loading for each row normalised as a percentage of their design depth versus their elevation within the dike as a percentage of dike height. The pore pressure distributions in the dikes are very similar, both decreasing from the base level to the higher elevation of piezometers.

Figure 6.24 is a plot of the average piezometer readings for dikes C2 and E at overtop loading for each row normalised as a percentage of their design depth versus their elevation within the dike as a percentage of dike height. Again, the distributions in the dikes are similar, but in overtop loading dike C1 and E both registered excess pore pressures at the higher piezometers. The volunteer built dike has higher pore pressures at the base level but both dikes are more or less equal at the higher elevation.

6.5.3 Deformed Dike Shapes at Overtop Water Depth

Figure 6.25 is a side by side comparison of the deformed shapes of dikes C2 and E after 30 minutes of sustained overtop loading. The dikes deformed similarly, with the volunteer built dike showing more horizontal displacement and the researcher built dike showing more vertical settlement. The available freeboard in dike C2 was reduced by 18% as compared with an 8% reduction in dike E.

The difference in deformation between the two dikes is likely related to differences in construction method. The volunteers placed bags at alternating orientation with respect to the central axis of the dike and the researchers did not. The alternating bag placement could be responsible for the increased horizontal deformation in the volunteer dike.

There were more people involved in the volunteer dike building exercise than in the research built dikes, and more people physically on the dike during construction. This should have resulted in better compaction during construction. The superior compaction is likely responsible for the minimal vertical deformation in the volunteer dike.

The volunteers used three sheets of PES in their dike, creating two horizontal joints. The researchers used one sheet of PES in their dikes, limiting the seam to the base of the dike.

6.5.4 Summary of effects Construction Quality Methods

The most striking difference between the dikes built by researchers and the dike built by volunteers is that the volunteer built 6' dike continued to deform under constant overtop load while all of the research built 6' dikes equilibrated under both design and overtop loading conditions. This indicates that a reduction construction quality can significantly compromise the stability of a given dike. Where the research built dikes pointed to the

limit in seepage and stability for the City of Winnipeg 1997 template being somewhere in the 8' range, the volunteer built 6' dike showed instabilities that would not be acceptable in a flood event.

The exercise also proved to be an excellent example of the need for clear communication between flood control authorities and the volunteers who will be building sandbag dikes in a flood situation. The difference in interpretation of the same information sheet by the volunteers and the researchers highlights the ambiguities with regard to bag orientation and PES placement.

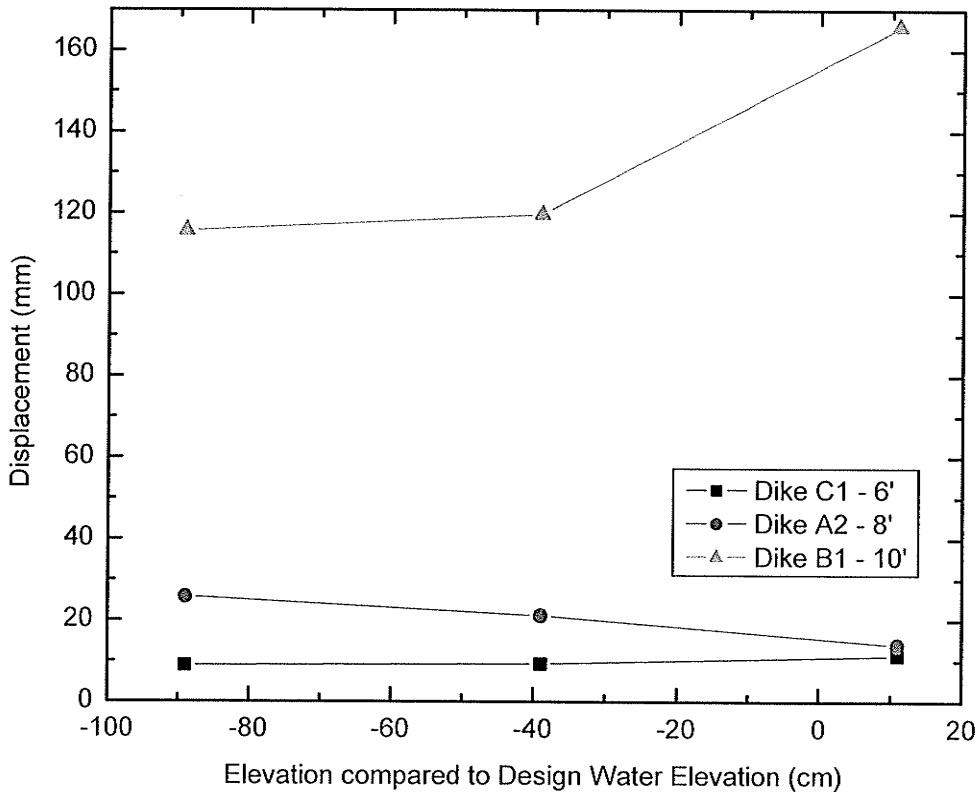

Figure 6.1 – Average Extensometer Data Comparison for Dikes C1, A2 and B1.

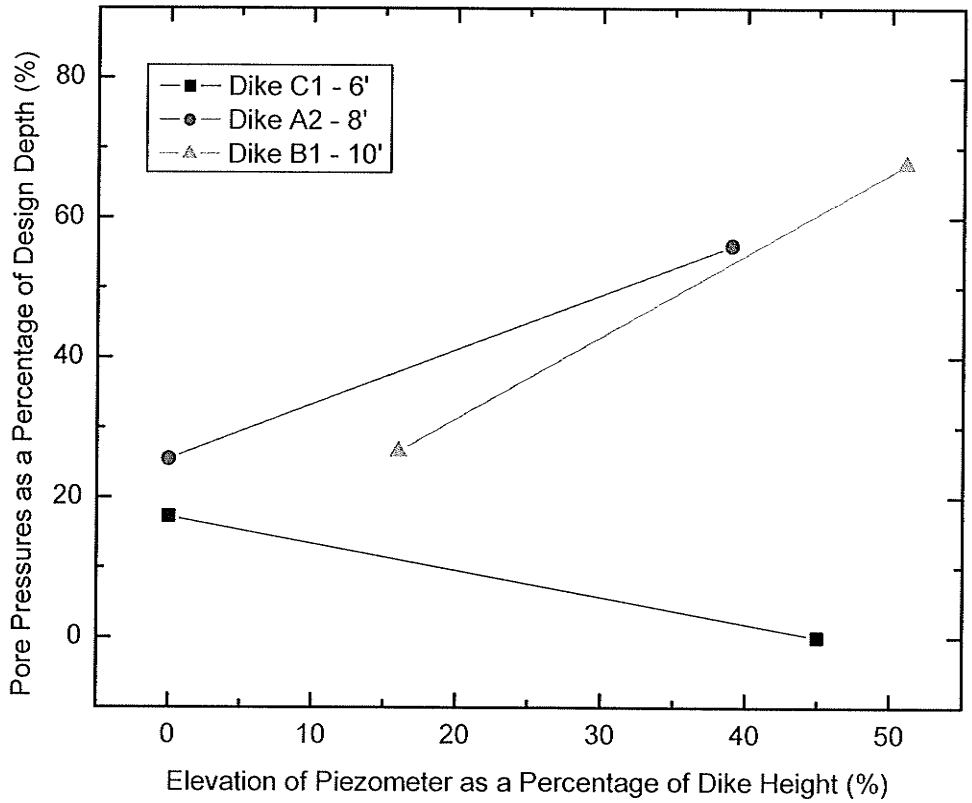

Figure 6.2 – Normalised Pore Pressure Data Comparison for Dikes C1, A2 and B1.

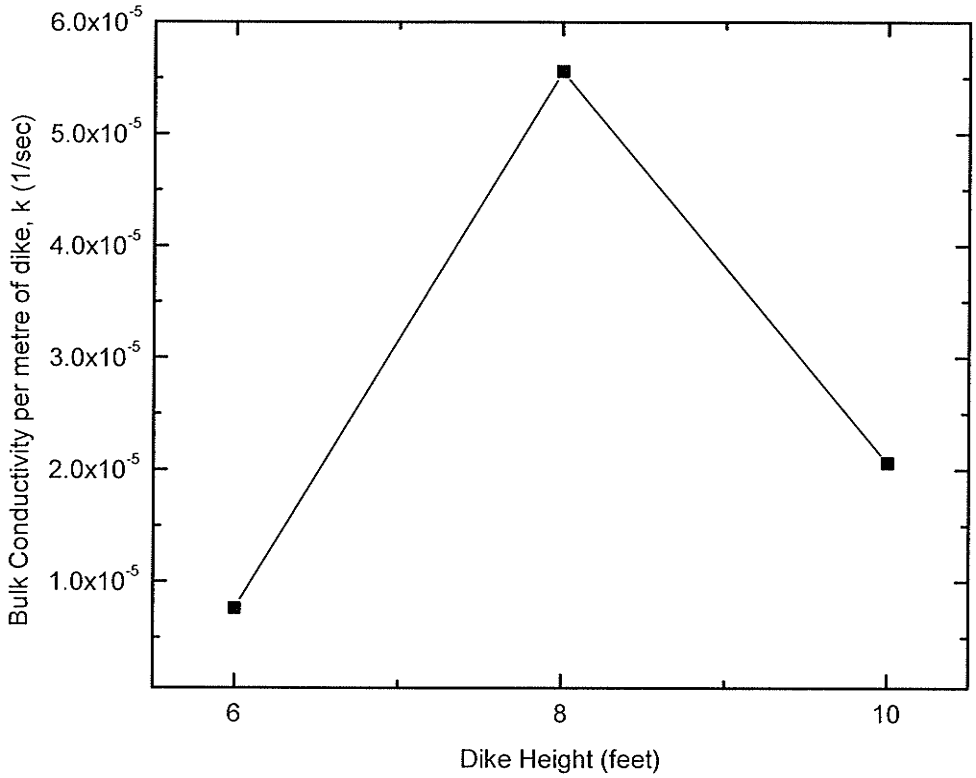

Figure 6.3 – Bulk Conductivity Comparison for Dikes C1, A2 and B1.

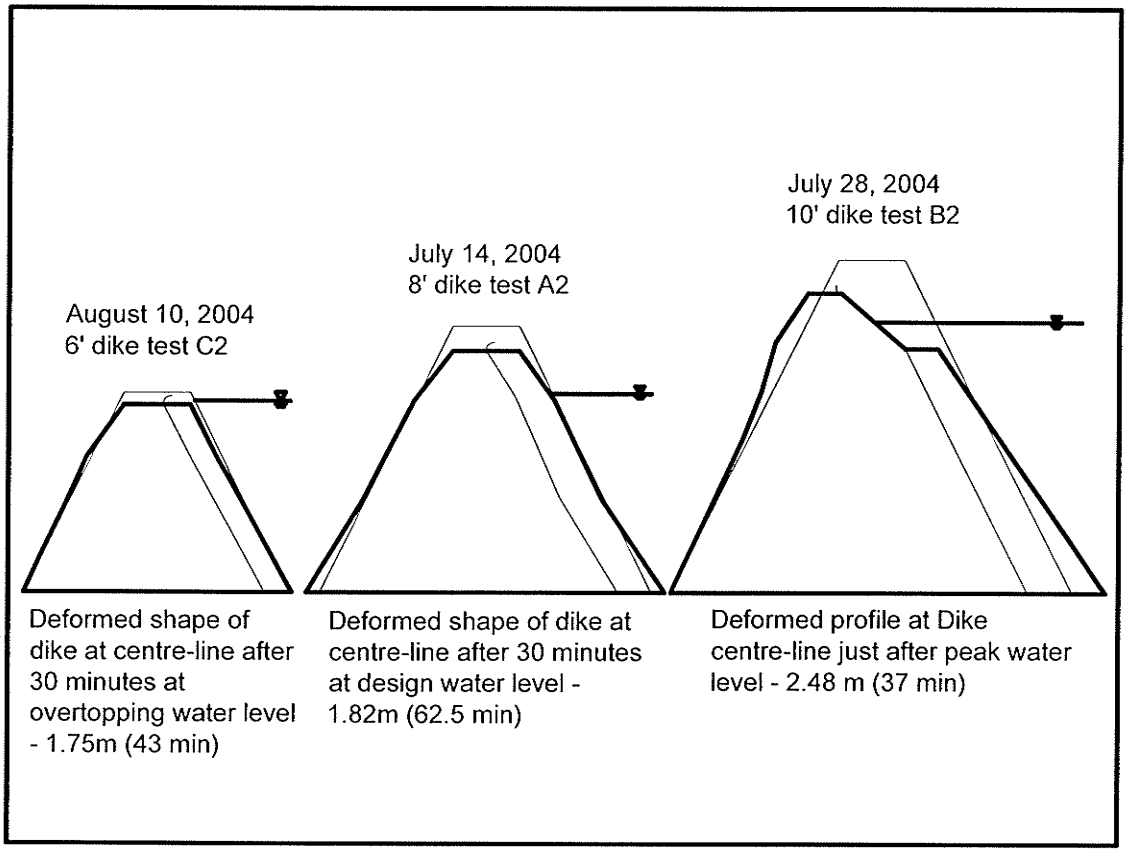

Figure 6.4 – Deformed Shape Side-by-side Comparison for Dikes C1, A2 and B1.

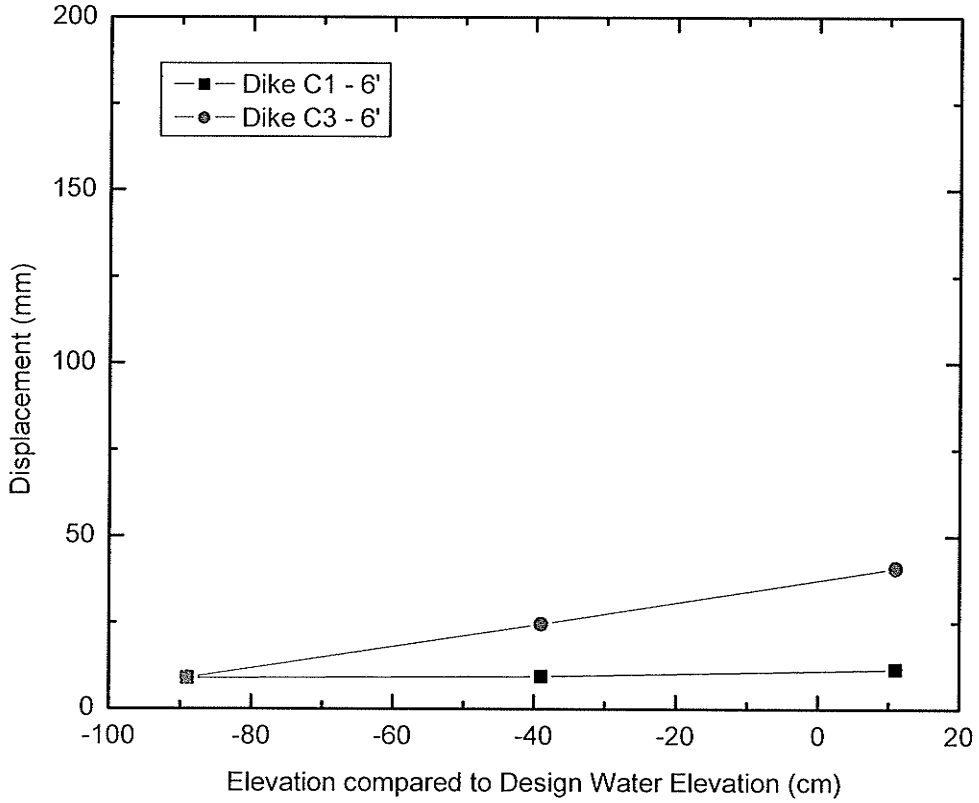

Figure 6.5 – Horizontal Deformation at Design Load, Dikes C1 (PES) & C3 (no PES).

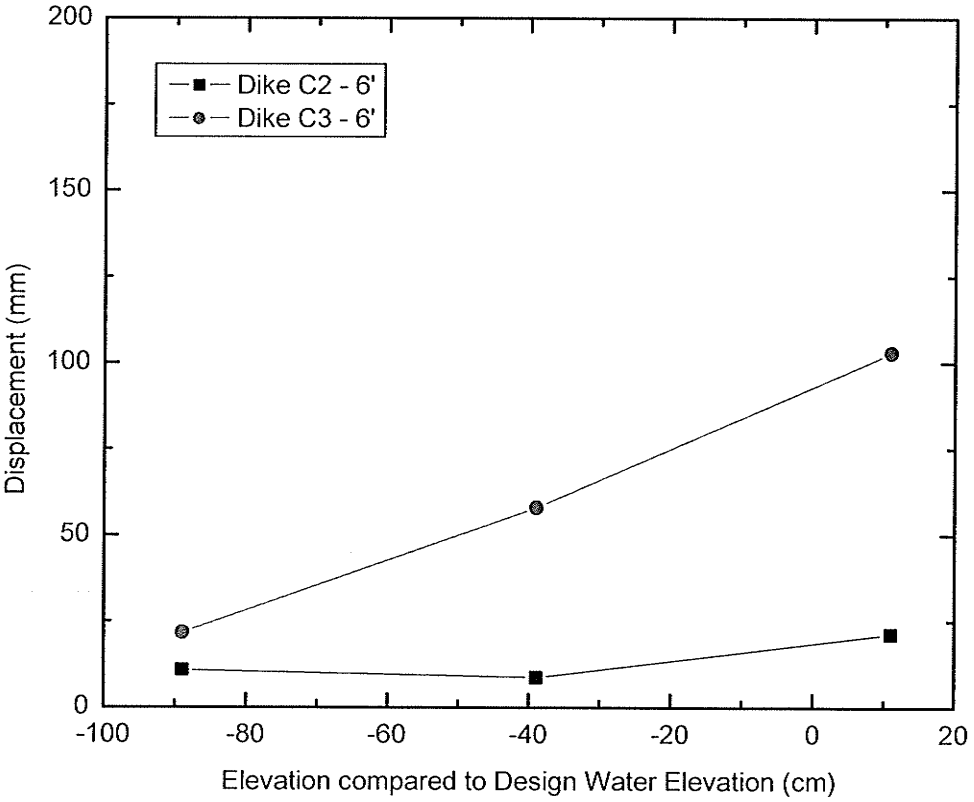

Figure 6.6 – Horizontal Deformation at Overtop Load, Dikes C1 (PES) & C3 (no PES).

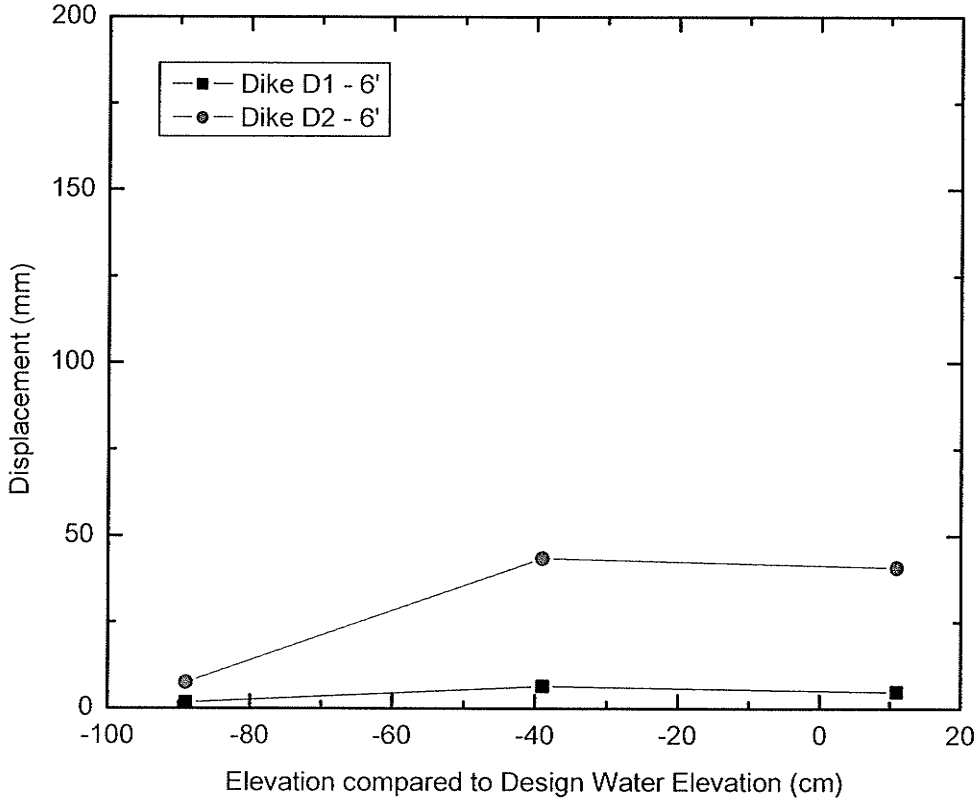

Figure 6.7 – Horizontal Deformation at Design Load, Dikes D1 (PES) & D2 (no PES).

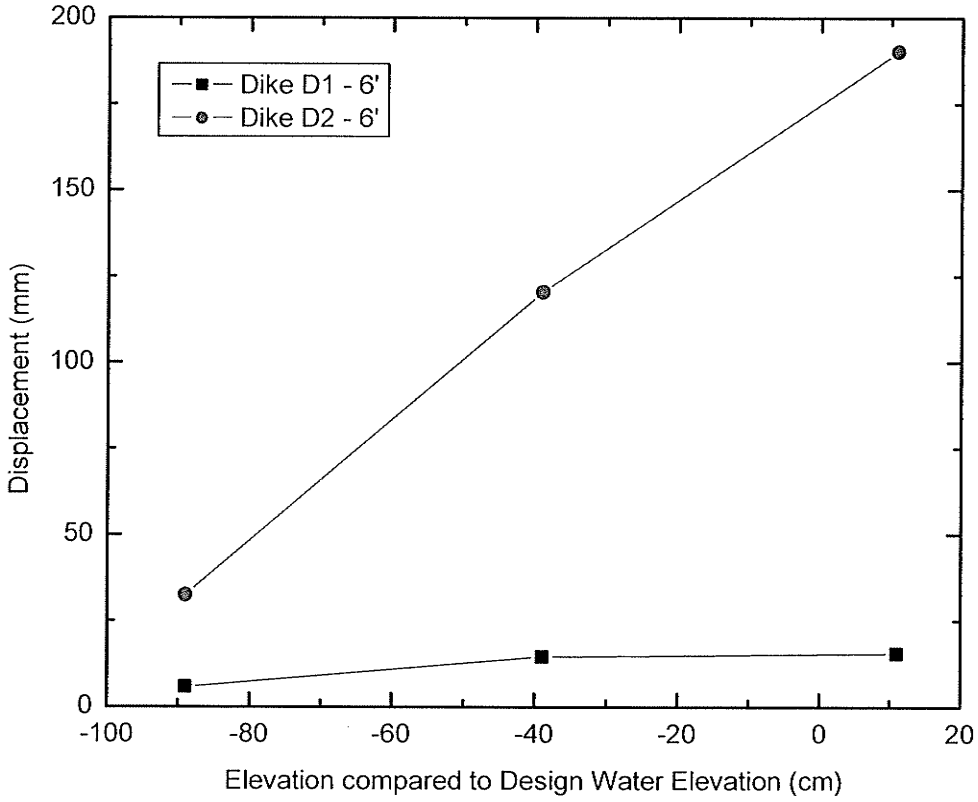

Figure 6.8 – Horizontal Deformation at Overtop Load, Dikes D1 (PES) & D2 (no PES).

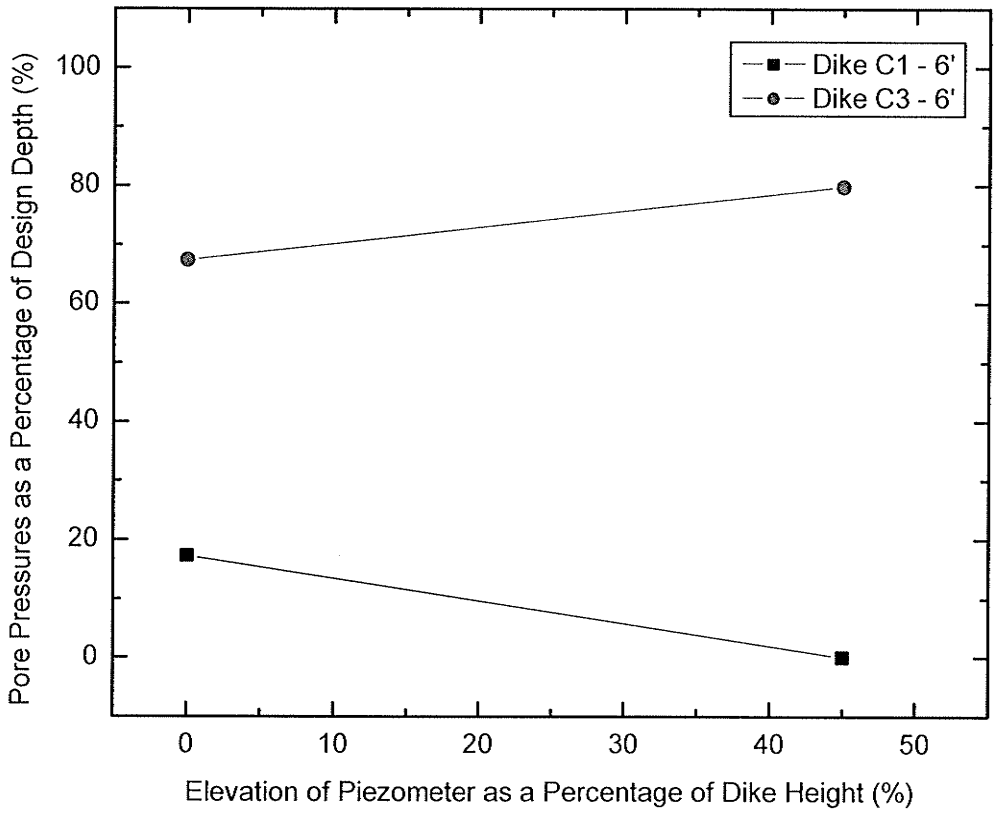

Figure 6.9 – Pore Pressure Data at Design Load, Dikes C1 (PES) & C3 (no PES).

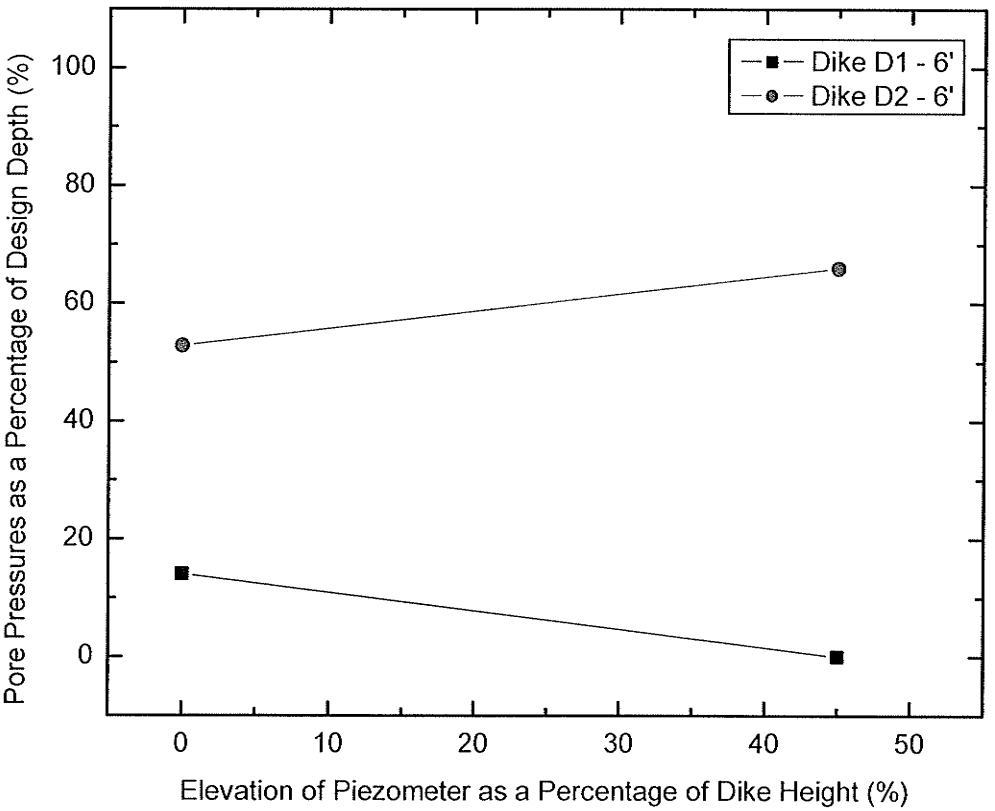

Figure 6.10 – Pore Pressure Data at Design Load, Dikes D1 (PES) & D2 (no PES).

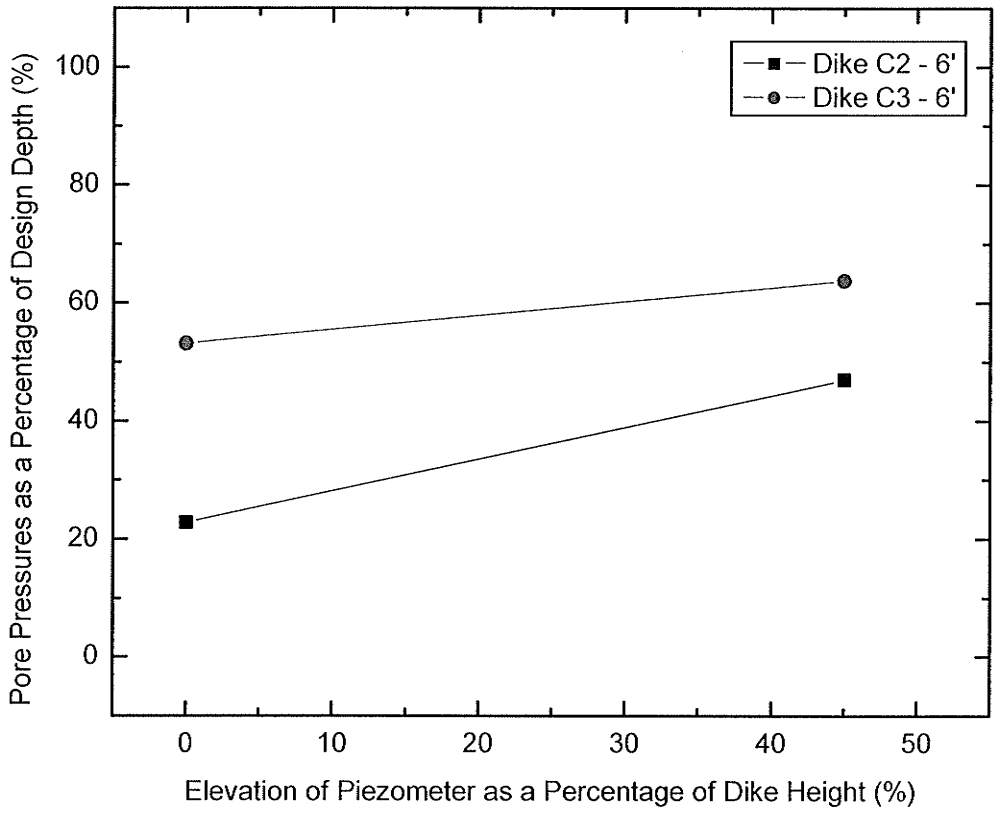

Figure 6.11 – Pore Pressure Data at Overtop Load, Dikes C1 (PES) & C3 (no PES).

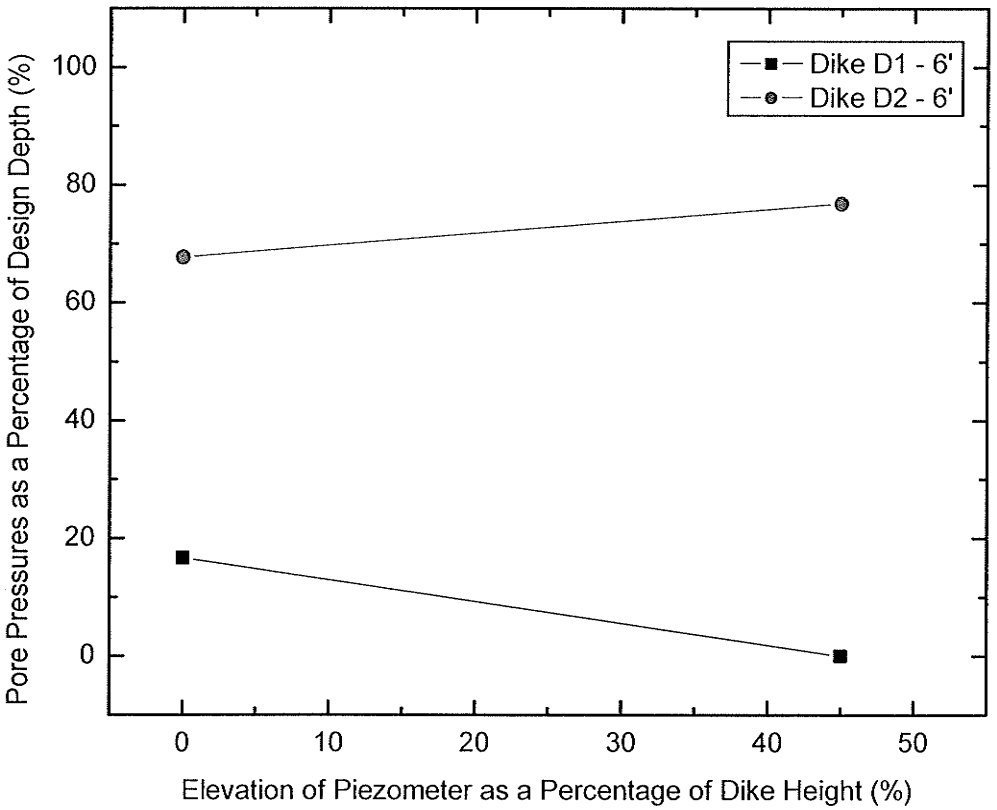

Figure 6.12 – Pore Pressure Data at Overtop Load, Dikes D1 (PES) & D2 (no PES).

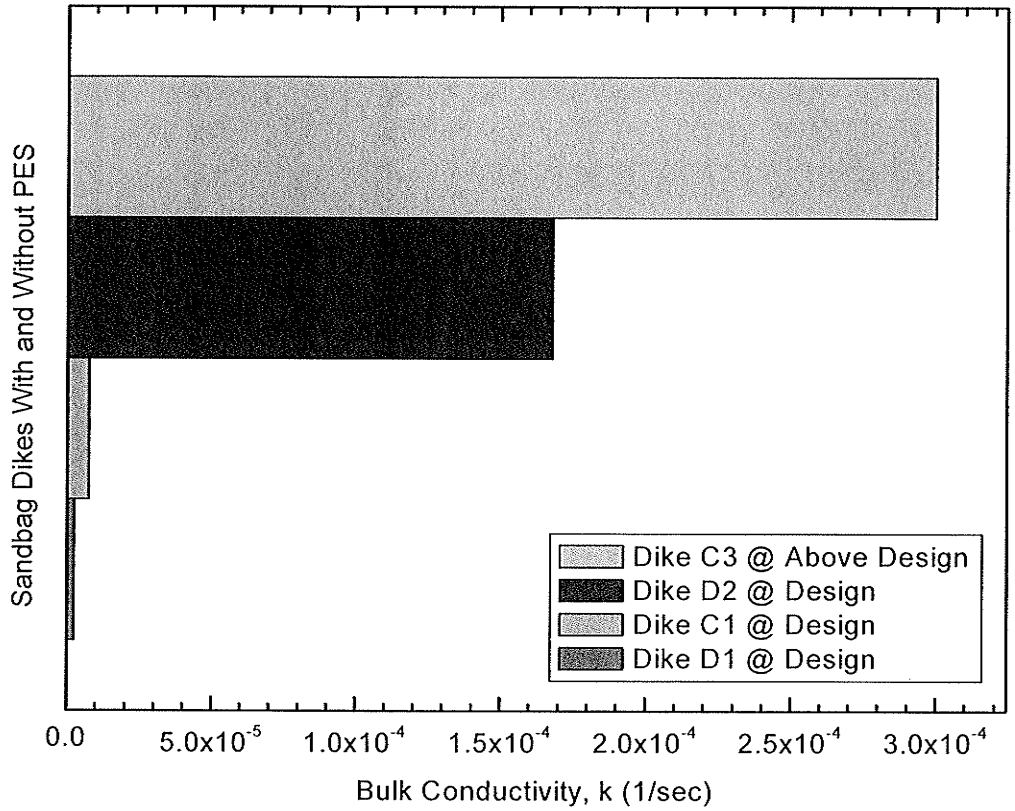

Figure 6.13 – Bulk Conductivity Comparison for Dikes C1, C3, D1 and D2.

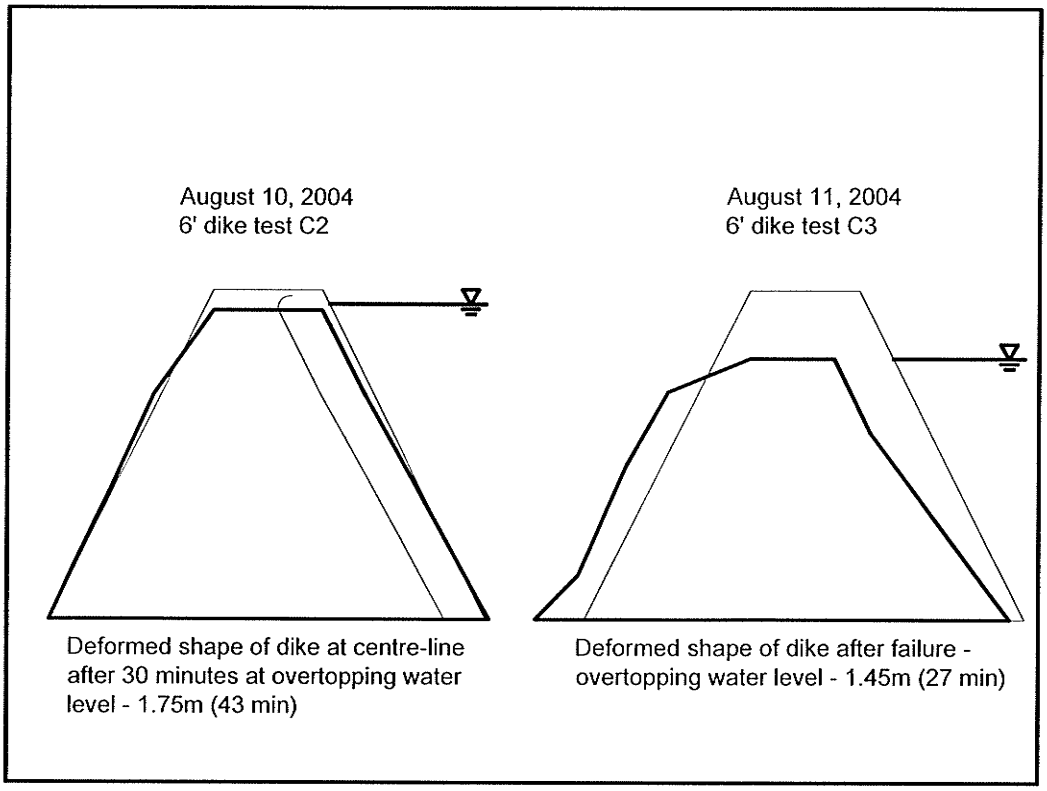

Figure 6.14 – Deformed Shape Side-by-side Comparison for Dikes C2 and C3.

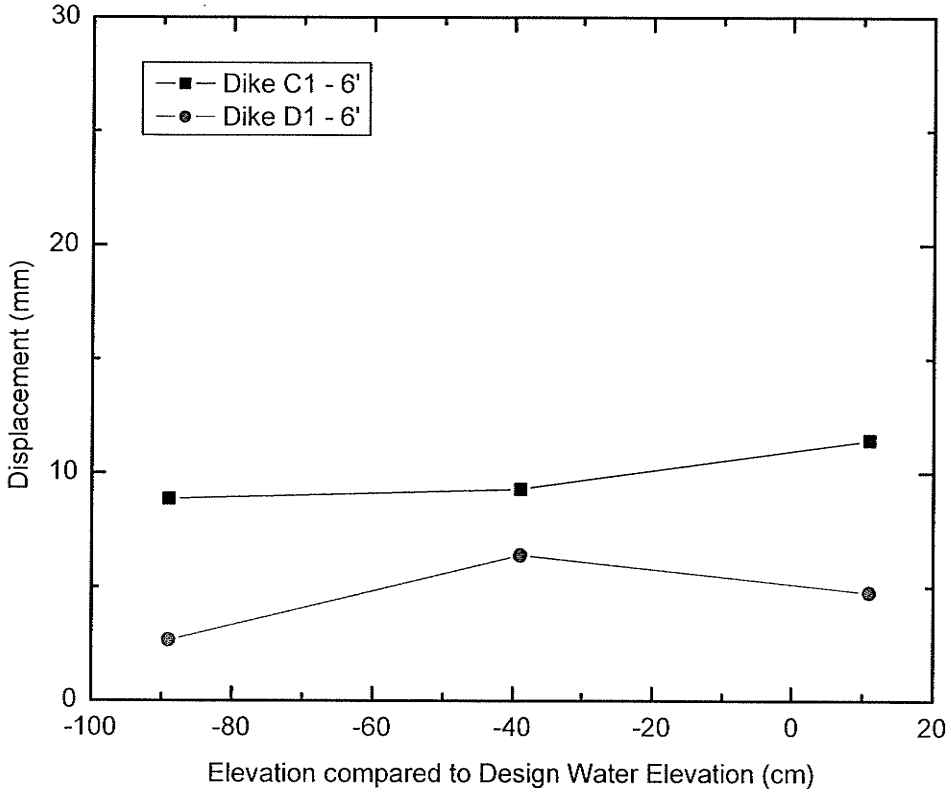

Figure 6.15 – Horizontal Deformation at Design Load, Dikes C1 (Wpg) & D1 (Alt).

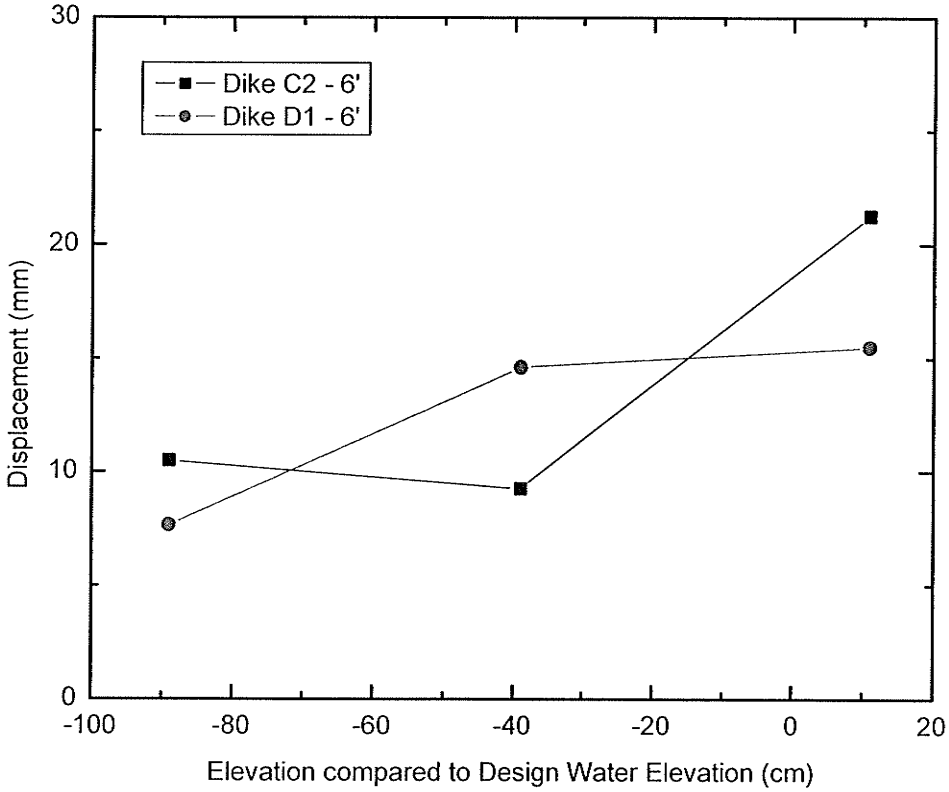

Figure 6.16 – Horizontal Deformation at Overtop Load, Dikes C2 (Wpg) & D1 (Alt).

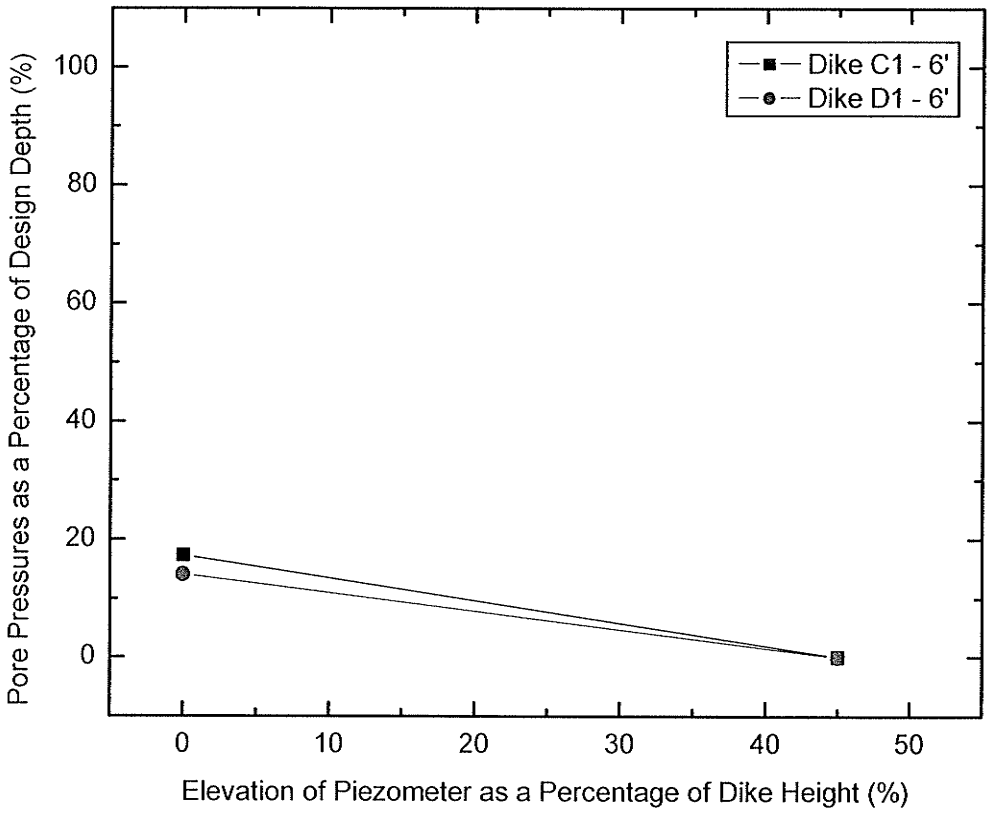

Figure 6.17 – Pore Pressure Data at Design Load, Dikes C1 (Wpg) & D1 (Alt).

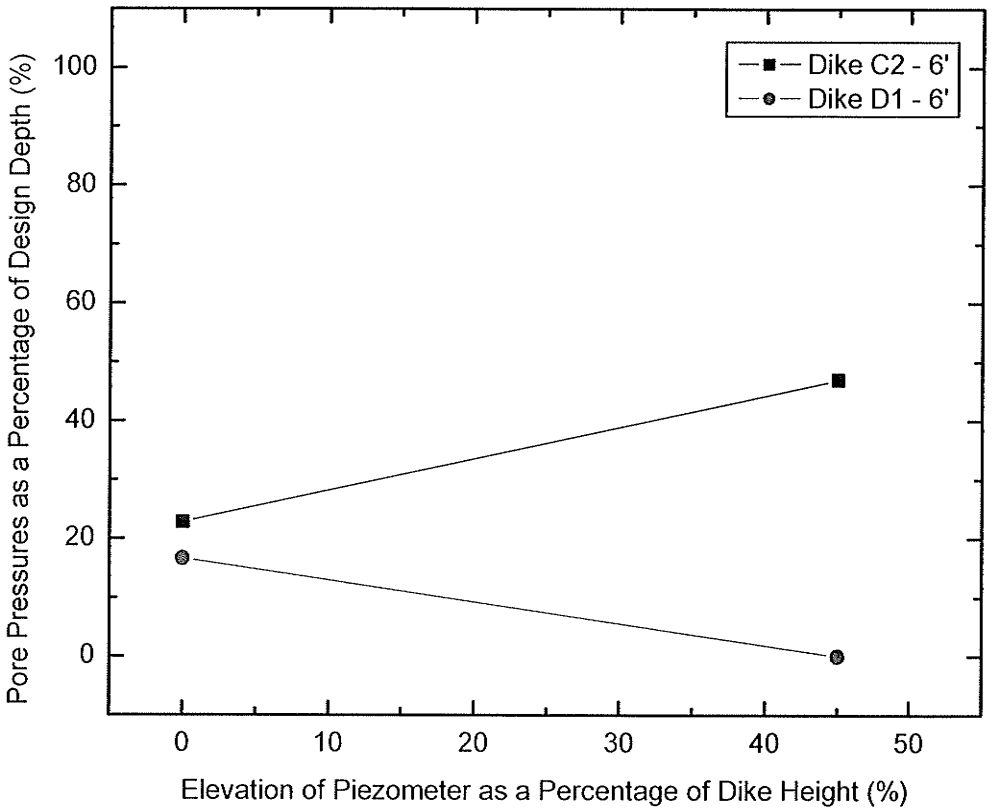

Figure 6.18 – Pore Pressure Data at Overtop Load, Dikes C1 (Wpg) & D1 (Alt).

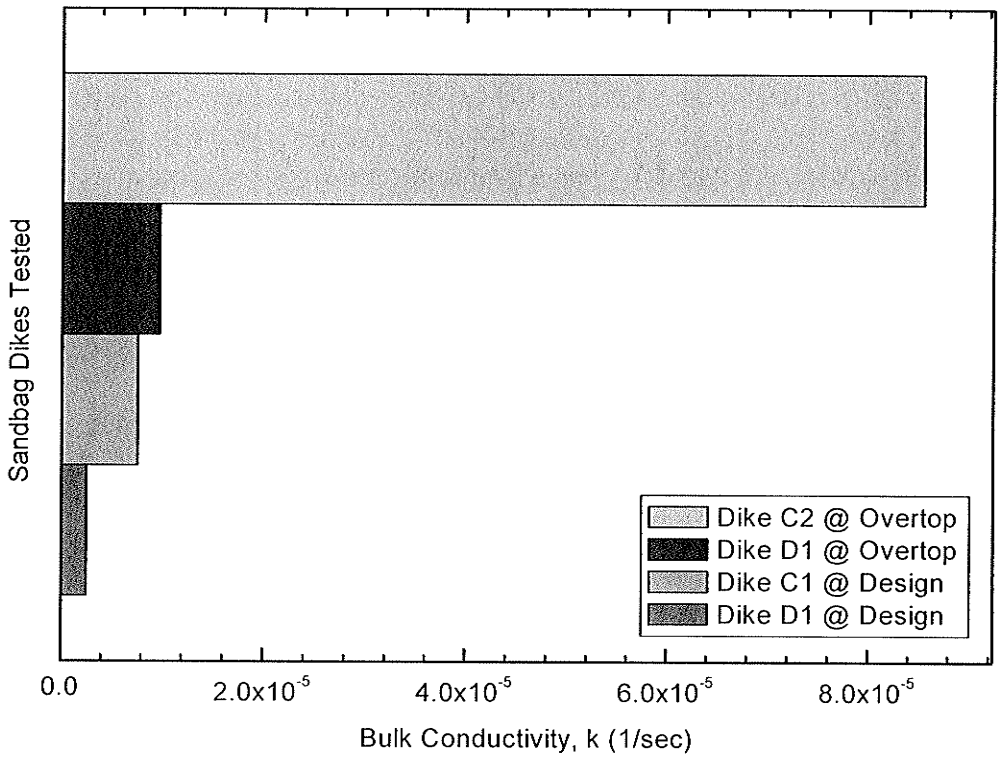

Figure 6.19 – Bulk Conductivity Comparison at Different Loads for Dikes C1, C2 and D1.

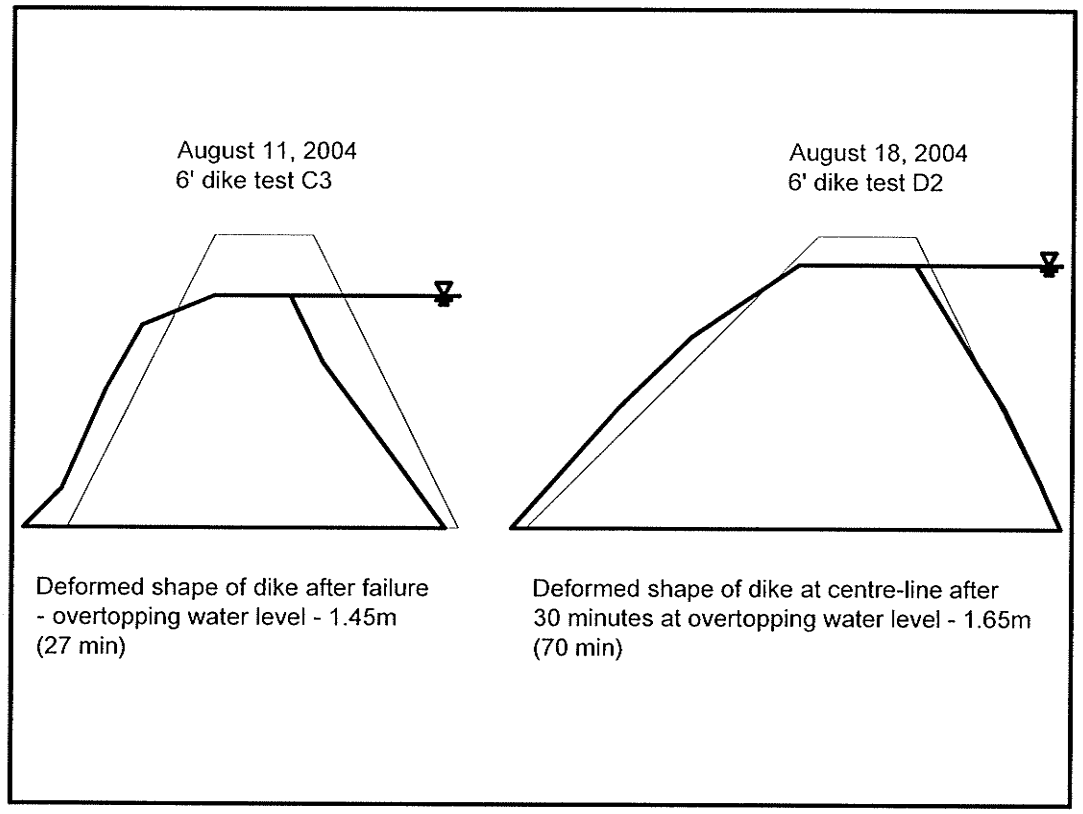

Figure 6.20 – Deformed Shape Side-by-side Comparison for Dikes C3 and D2.

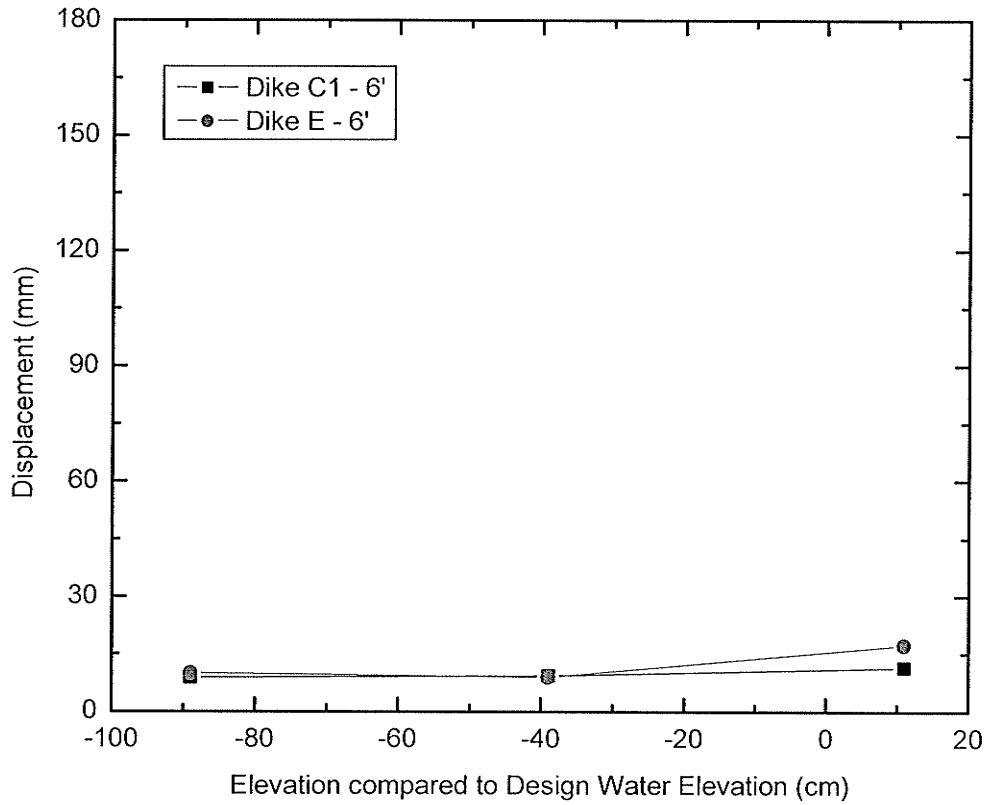

Figure 6.21 – Horizontal Deformation at Design Load, Dikes C1 (UM) & E (Volunteer).

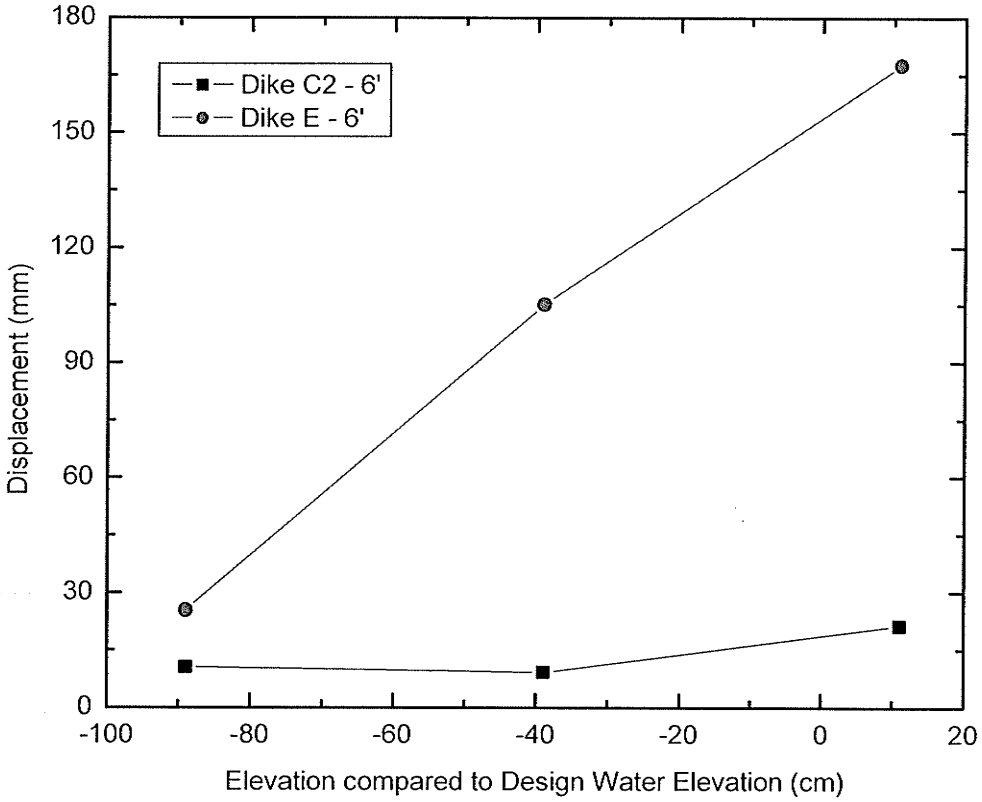

Figure 6.22 – Horizontal Deformation at Overtop Load, Dikes C1 (UM) & E (Volunteer).

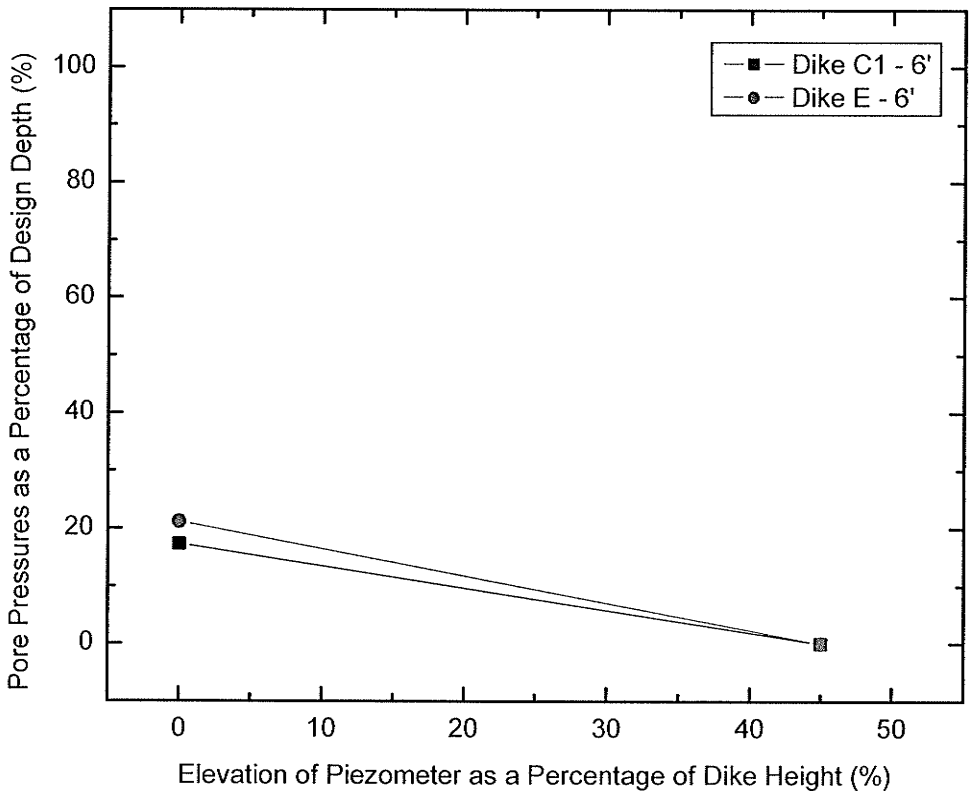

Figure 6.23 – Pore Pressure Data at Design Load, Dikes C1 (UM) & E (Volunteer).

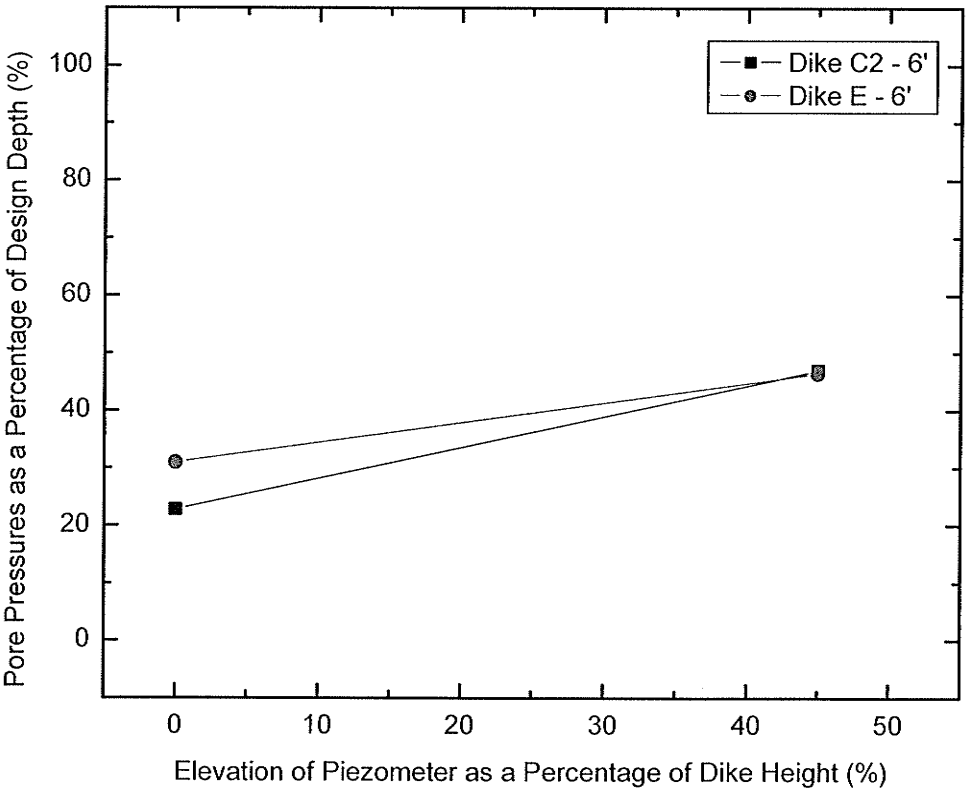

Figure 6.24 – Pore Pressure Data at Overtop Load, Dikes C1 (UM) & E (Volunteer).

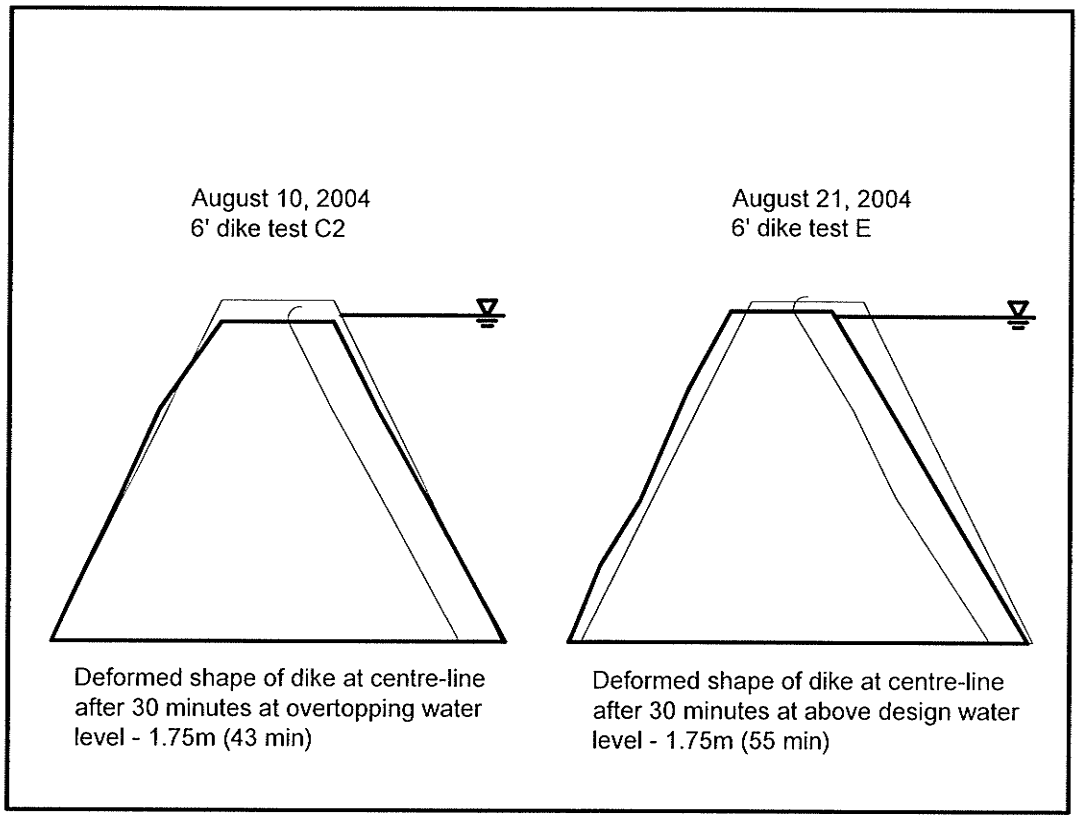

Figure 6.25 – Deformed Shape Side-by-side Comparison for Dikes C2 and E.

7 Conclusions and Recommendations

7.1 Introduction

The research documented in this thesis has provided some answers to key questions about sandbag dike performance in Manitoba, illuminated some aspects of temporary flood protection that were previously limited to anecdotal evidence, and raised a set of questions for future research.

Quantitative data is now available that describes the frictional characteristics of all of the materials and interfaces present in a sandbag dike built to the City of Winnipeg's 1997 template. There is now evidence justifying a limit to the height which it is safe to build a sandbag dike according to this template, and provisions for modification to design dikes of greater heights. The importance of the PES layer for maintaining stability and reducing seepage has been verified and measured. An alternative geometry has been tested to provide a dry side solution to dikes that may be compromised by their construction and loading conditions. Similar dikes in terms of materials and geometry were tested with different construction methods and construction quality.

An unexpected result of this testing has been the documentation of the effects of densification by wetting on sandbag structures. Where this was previously observed in the field during flood events, there was a lack of measurement ability during floods to quantify this behaviour due to the constraints of an emergency situation. Now there is a set of data for designing sandbag dikes to maintain their necessary freeboard under predicted loading conditions.

Questions not addressed and arising from this research include but are not limited to: the effect of frozen ground on dike stability and seepage along the base, the effect of varying sandbag orientation, the effect of horizontal seams and overlap width on both

seepage and stability, the effect of wave action and debris collision(s), and the effects of further geometric variations.

7.2 Conclusions

7.2.1 Safe Limit to Height of Dikes built to 1997 Template

The field tests conducted on sandbag dikes in the flume during the summer of 2004 showed that dikes built according to the 1997 template to a height of 6' (1.83 m) and loaded to their design depth of 4' (1.29 m) appear relatively stable. It is possible that with exceptional construction quality dikes of 8' (2.44 m) may be stable up to their design load of 6' (1.83 m), but it is not recommended that heights above 6' be attempted without the consultation of qualified personnel during all stages of construction and most notably during initial dike placement.

7.2.2 The Importance of the PES Layer

The PES layer in a sandbag dike is absolutely instrumental to minimise the seepage rate through the structure and to limit excessive pore pressures throughout the dike. In doing this, the PES is also instrumental in maintaining the stability of the structure. Elevated pore pressures and flow rates through sandbag dikes greatly reduce the frictional resistance of the material interfaces in the dike, and lower the effective stresses present in the sand itself, thereby lowering the strength of the dike.

7.2.3 The Effect of Change in Geometry

Changing the dry side of the 1997 dike template to a 1:1 slope from a 2:1 slope increased the stability of the dike and reduced the seepage rates through the dike. This 25% increase in bags was found to be enough to stabilize a 6' (1.83 m) dike built without any PES under design and above design loading conditions. The quantitative

information available from these tests confirms the past practise of 'buttressing' and represents a starting point for further testing on geometrical variation in sandbag dikes.

7.2.4 The Effect of Construction Method and Quality

The exercise of having volunteers construct a 6' (1.83 m) dike with a minimum of instruction and interference gives a clear indication of both the need for consistency and quality in dike construction as well as the need for clear and concise communication tools for educating and training flood protection workers, both officials and volunteers.

7.2.5 The Effect of Densification by Wetting

Because sandbag dikes are built by hand and cannot be mechanically compacted in most situations, the sand in each bag is subject to densification by wetting during initial flood loading. Both full-scale and in-isolation tests were carried out and showed that a 10' (3.05 m) dike can be expected to settle by up to 1' (0.3 m) as a result of wetting. This is extremely significant in light of the design freeboard of 2' (0.61 m) applied to these structures.

7.3 Recommendations for Further Testing

The following are several suggestions for future testing, divided into two groups. The first are actual aspects of the dikes themselves. These represent issues that are important to the stakeholders in the research. The second group are improvements to the research method itself. These are issues primarily of concern to the tests themselves.

7.3.1 Sandbag Dike Aspects for Future Consideration

7.3.1.1 Base Conditions

Spring flooding conditions in Manitoba often involve frozen ground. This change in conditions needs to be quantified both in laboratory in-isolation tests and in full-scale

field tests of sandbag dikes built on frozen ground. The flume designed and built for this research can easily be adapted for this purpose. It simply must be erected in the fall and allowed to go through the winter so that it will be ready for tests in the spring.

The effect of varying the base material from sod to a surface like asphalt is also unquantified at this point. Tests on various base materials could be conducted in the full-scale flume.

7.3.1.2 Alternative Geometries

There are many changes to the dike geometry that are possible, and a set of comparison tests would yield information on the best use of materials for a given height of temporary flood protection. Expanding on the alternative geometry tested in this research by examining the effect on dikes of different heights built with a 1:1 dry side slope would be a natural place to start.

7.3.1.3 Alternative Materials and Innovative Flood Protection Systems

There are alternative materials available for building sandbag dikes, ranging from higher quality WSFPP bags to additional stabilization plates to combat base sliding. These materials need to be tested in order to measure their efficiency and economy in improving the performance of sandbag dikes.

There are also many alternative flood protection structures available, some of which are presented in chapter 2. The flume built for this set of tests is capable of testing many of these structures alongside sandbag dikes in order to build a set of data accurately comparing their performance.

7.3.1.4 Variation of Bag Orientation

The volunteers who built dike E placed the majority of the bags in their dike parallel to the long axis of the dike, which corresponds to the direction of flow in actual flooding conditions. Every third or fourth lift of bags, however, they placed the bags perpendicular to the long axis of the dike, in the same manner as a mason places a soldier course every fourth or fifth course of bricks in a structural brick wall. This practise is consistent with the anecdotal experience of several people involved with flood protection efforts in Winnipeg in the past.

Members of this research project's steering committee pointed out that this method of placing the bags can create preferential flow paths across the dike. However, the amount that these flow paths would actually impact the performance of the dike would likely depend on the condition of the PES layer.

Tests on dikes with bags placed perpendicular to the flood water flow direction would shed some light on the magnitude of the effect of this practise.

7.3.1.5 Variation of PES Installation

In watching the volunteers build their dike, it became apparent that there are many possible configurations of PES installation in a sandbag dike. Variation of seam location, overlap width and overall number could easily be tested, and would be very valuable for designers.

7.3.1.6 Wave and Debris Loading

Flood conditions subject sandbag structures to wave and debris loading. The Hydraulics Research Testing Facility at the University of Manitoba has a wave-generation

apparatus that could be implemented in the full-scale testing facility in order to simulate some of these conditions.

7.3.2 Improvements in Research Method

7.3.2.1 Duration of Tests

The overall length of time that water can be held in the flume is determined by safety factors and the research agreement signed by all of the stakeholders. Recognising this, it is not practical to recommend long term testing in the flume unless future research takes this into account and satisfies all relevant safety concerns.

One element of testing that could be done on a longer term basis is the collection of electronic data from extensometers and piezometers until they cease to change after each loading.

7.3.2.2 Stiffness of Flume

Future erections of the full-scale testing facility should implement corner stiffening at the base as well as the top of the walls, as well as across the front face at both the foundation and the top of the structure. This would go a long way to reducing seepage through the corners of the structure and allow more precise testing with the use of less water.

7.3.2.3 Water-Tightness of Flume

The walls of the flume need to be installed in a trench that is free of porous material and backfilled with a compacted clay material on both sides. This flow path proved to be critical in one of the tests in the summer of 2004, and while there was no catastrophic failure, a significant amount of water was wasted and the planned overtop test of the 10' (3.05 m) dike was not completed.

References

Allan, J. C., Komar, Paul D., Hart, Roger (2003). A dynamic revetment and reinforced dune as 'natural' forms of shore protection in an Oregon State Park. Coastal Structures 2003, Portland, Oregon, American Society of Civil Engineers.

ASCE (1968). Final Report of the Committee on Backfilling in Public Rights-of-way. St. Louis, Missouri, ASCE: 1-57.

ASTM (1963). Standard Test Method for Particle-Size Analysis of Soils. D 422 - 63. West Conshohocken, PA, American Society of Testing and Materials. **4:** 10 - 17.

ASTM (1999). Standard Test Method for Direct Shear Test of Soils Under Consolidated Drained Conditions. D 3080 - 98. West Conshohocken, PA, American Society for Testing and Materials. **4:** 324-329.

ASTM (2000). Standard Test Method for Determining the Coefficient of Soil and Geosynthetic or Geosynthetic and Geosynthetic Friction by the Direct Shear Method. D 5321 - 92. West Conshohocken, PA, American Society of Testing and Materials. **4:** 953 - 958.

Biggar, K., Srboljub Masala (1998). Alternatives to sandbags for temporary flood protection. Edmonton, AB, Alberta Transportation and Utilities Disaster Services Branch & Emergency Preparedness Canada: 1-71.

Blatz, J. A., Bathurst, Richard J. (2003). "Limit Equilibrium analysis of large-scale reinforced and unreinforced embankments loaded by a strip footing." Canadian Geotechnical Journal **40**(6): 1084-1092.

Bove, J. A. (1990). Direct Shear Friction Testing for Geosynthetics in Waste Containment. Philadelphia, PA, ASTM.

Collios, A., P. Delmas, J-P. Gourc & J-P. Giroud (1980). Experiments on soil reinforcement with geotextiles. 1980 ASCE National Symposium, Portland, Oregon, ASCE.

Craig, R. F. (1998). Soil Mechanics. London, UK, E & F Spon.

Criley, K. R., D. Saint John (1997). Variability analysis of soil vs. geosynthetic interface friction characteristics by multiple direct shear testing. Geosynthetics '97, Long Beach, CA, Industrial Fabrics Association International.

Duncan, J. M., James K. Mitchell, Christian Lovern, James Coffey (1997). Innovative Alternatives to Conventional Levees for Flood Protection. Blacksburg, VA, Virginia Tech University, USACE: 1-102.

Finch, H. A. (1939). "Earth-cement mixture in sacks used for river-bank revetment." Engineering News-Record **122**(19): 659.

Hanson, G. J., Cook, K. R., Hahn, W. (2000). Preliminary results of earthen embankment breach tests. Milwaukee, Wisconsin, American Society of Agricultural Engineers: 1531-1543.

Jewell, R. A., C.P. Wroth (1987). "Direct shear tests on reinforced sand." Geotechnique **37**(1): 53-68.

Juran, I., Christopher, B. (1989). "Laboratory model study on geosynthetic reinforced soil retaining walls." Journal of Geotechnical Engineering **115**(7): 905-926.

Kalumba, D., F. Scheele (1999). Friction characteristics of sand/geotextile interfaces for three selected sand materials. Geotechnics for developing Africa; proceedings of the Twelfth regional conference for Africa on Soil mechanics and geotechnical engineering, Durban, South Africa, Jones & Wagener, Rivonia, South Africa.

Kerr, J. (1978). Foundations and Fills. Edmonton, AB, Hardy Associates: 1-19.

Koerner, R. M. (1998). Designing with Geosynthetics. Upper Saddle River, New Jersey, Prentice Hall.

Laba, J. T. (1983). "Cohesive soil compaction by water jetting." Canadian Geotechnical Journal **20**: 394-405.

Lopes, P. C., M.L. Lopes, M.P. Lopes (2001). "Shear behaviour of geosynthetics in the inclined plane test - Influence of soil particle size and geosynthetic structure." Geosynthethics International **8**(4): 327-342.

Matsouka, H. S. L. (2001). Mechanical properties of soilbags and their applications to earth reinforcement. Landmarks in Earth Reinforcement. e. a. Ochiai, Swets & Zeitlinger: 587-592.

O'Rourke, T. D., S.J. Druschel, A.N. Netravali (1989). "Shear Strength Characteristics of Sand-Polymer Interfaces." Journal of Geotechnical Engineering **116**(3): 451-469.

Tan, S. A., S.H. Chew, W.K. Wong (1998). "Sand-geotextile interface shear strength by torsional ring shear tests." Geotextiles and Geomembranes **16**: 161-174.